456

Background of Technical Specifications for Substation Equipment exceeding 800 kV AC

Working Group

A3. 22

April 2011

CIGRÉ WORKING GROUP A3.22

BACKGROUND OF TECHNICAL SPECIFICATIONS FOR SUBSTATION EQUIPMENT EXCEEDING 800 KV AC

Members:

H. Ito (Convenor), A. Janssen (Secretary), J. Amon F., S-W. Bahng, M. C. Bhatnagar, J. Brunke, E. Colombo, R. Diaz, W. Due, D. Dufournet, P. C. Fernandez, Y. Filion, A. Giboulet, J. Jäger, S. Kale, A. Keri, T. Kobayashi, M. Kosakada, E. Kynast, Z. Liu, A. Lokhanin, C. van der Merwe, M. de Nigris, V. Rashkes, D. Peelo, U. Riechert, B. Shperling, R. Smeets, L. Stenström, G. Sun, S. Wang, Y. Yamagata, Yao Sili, J. Yesuraj, R. Yeckley

Coordination with

M. Waldron (Coordination chair, SC A3), P. Boss, Y. Shirasaka (SC A2), A. Wiersma (SC B3), M. de Nigris (WG A3.21), B. Richter (WG A3.17), T. Yokota (WG B3.22), E. Zaima (WG C4.306)

ISBN: 978-2-85873-145-9

Abbreviations

1LG	Single-phase line fault to ground
2LG	Two-phase line faults to ground
3LG	Three-phase line faults to ground
4LG	Four-phase line faults to ground in case of double circuit tower
ACSR	Aluminium Conductor Steel Reinforced
AF	Amplitude Factor, k_{af}
AIS	Air Insulated Switchgear
AN	Audible-Noise
ATP	Alternative Transients Program
CB	Circuit Breaker
CCGT	Combined Cycle Gas Turbine
CISPR	International Special Committee on Radio Interference
COV	Continuous Operating Voltage
CP line	Constant Parameters Line
CSS	Controlled Switching System
CT	Current Transformer
CVT	Capacitive Voltage Transducer
DS	Disconnecting Switch
EHV	Extra High Voltage
EMI	Electromagnetic Immunity
EMTP	Electro Magnetic Transient Program
ES	Earthing Switch
ESDD	Equivalent Salt Deposit Density
ESKOM	Electricity Supply Commission
FACTS	Flexible AC Transmission Systems
FFO	Fast Front Overvoltage
FPCF	First Pole to Clear Factor, k_{pp}
FPD	Fast Protective Device
GCB	Gas Circuit Breaker
GIS	Gas Insulated Switchgear
GMR	Geometrical Mean Radius
Hybrid-IS	Hybrid Gas Insulated Switchgear
HPL	High Power Laboratory
HQ	Hydro Quebec

HSES	High Speed Earthing Switches
HSGS	High Speed Grounding Switches
HVDC	High Voltage Direct Current
IEC	International Electrotechnical Commission
IEEE	The Institute of Electrical and Electronics Engineers
ITRV	Initial Transient Recovery Voltage
KEPCO	Korea Electric Power Corporation
LIPL	Lightning Impulse Protection Level
LIWV	Lightning Impulse Withstand Voltage
LLF	Long Line Fault
MOSA	Metal Oxide Surge Arrester
MOV	Metal Oxide Varistor
MTS	Mixed Technology Substation
OH-line	Over head line
OP	Out of Phase
PD	Optical potential devices
PIR	Pre-Insertion Resistor
PSS/E	Power System Simulation for Engineering
RI	Radio Interference
RIV	Radio Interference Voltage
RRRV	Rate of Rise of Recovery Voltage
RTDS	Resistance Temperature Detector simulation
RV	Recovery Voltage
SA	Surge Arresters
SC	Series Capacitor
SFO	Slow-Front Overvoltage
SIPL	Switching Impulse Protection Level
SIWL	Switching Impulse Withstand Level
SIWV	Switching Impulse Withstand Voltage
SLF	Short Line Fault
SOV	Switching Overvoltage
SPAR	Single-Phase Rapid Auto-Re-closing
SPS	Single Phase Switching
SR	Shunt Reactor
SVC	Static Var compensator

TD	Test Duty
TEV	Transient Ground (Earth) Potential Rise
TCSC	Thyristor-Controlled series Capacitor
TEPCO	Tokyo Electric Power Company
TFF	Transformer Fed Faults
TLA	Transmission Line Arrester
TLF	Transformer Limited Fault
TNA	Transient Network Analyzer
TOV	Temporary Overvoltage
TPAR	Three-Phase Rapid Auto-Re-closing
TRV	Transient Recovery Voltage
UHV	Ultra High Voltage (exceeding 800 kV)
VFTO	Very Fast Transient Overvoltage
VT	Voltage Transformer

1 Introduction

The increasing demand for electric energy in countries with an increasing economy, like China, India and Brazil, and the continuing transfer to electricity as energy source in more mature economies, as in Japan, Europe and North America, go hand in hand with the worldwide need for sustainable power. Both sustainable power sources and conventional power plants, including hydro-power and nuclear plants, are more and more constructed at locations far from load centres. This leads to long overhead (OH)-lines for the transmission of bulk power. Furthermore, large scale implementations of sustainable power plants at distributed and/or distant locations require a strong interconnecting infrastructure for exchange of the fluctuating power output. Worldwide and on European scale it can hardly be accomplished to integrate fluctuating green power sources without the backbone of a so-called "Super-grid", like, for instance, an UHV AC system with voltages as high as 1100 or 1200 kV.

After on-site commissioning tests during December 2008 in China, the first commercial operation of an UHV-system with a rated voltage of 1100 kV AC started successfully on January 6th, 2009. Since then the UHV AC and DC networks are steadily extended. Also in India, plans to start commercial operations of a 1200 kV AC system within a number of years are formed, while in Japan commercial operation of their 1100 kV system is foreseen to take place in the next decade. At this moment, in Brazil experts are considering to exploit the hydropower potential of the Amazon River by transporting the electric energy along a distance of 2500 km by UHV AC and/or DC systems. Commercial operation is foreseen to start at the end of the next decade. Together with the 1200 kV network in Russia (temporarily operated at EHV), all these projects indicate the growing maturity of UHV technology.

Plans for new commercial developments have created a real demand for standardization in the field of UHV technologies. Effective UHV standardization requires that up to date experiences, from the planned and operated installations in China, as well as from the major work carried out in Japan, Italy and Russia during the past verifications, should be drawn together and "best practice" should be identified. In October 2006, CIGRÉ SC A3 established the WG A3.22 "Technical Requirements for Substation Equipment exceeding 800 kV" in order to review the state-of-the-art of technical specifications for substation equipments ($\geq$ 800kV) in various projects from all over the world. The WG was requested to provide the technical background of all aspects of the available specifications and to come up with recommendations for the future standards of UHV substation equipments. WG A3.22 completed the first survey by collecting the available information and presenting Technical Brochure 362 [1] which includes various field experiences obtained from the national projects. The second stage of investigations in order to provide back-ground information for standardization was based on the Technical Brochure 362 and the results are now presented in this second Technical Brochure.

In order to minimize the costs and visual impact of UHV transmission lines and substations as much as possible, advanced technological solutions and analytical optimization techniques are required. Here CIGRÉ WG A3.22 plays an important role, as it stimulates the application of such techniques as well as the harmonization and standardization of equipment requirements and the coordination between the bodies involved in similar studies. Furthermore, the outcome of the studies in the field of reduced insulation coordination requirements and requirements for other transients (e.g. TRVs, ITRVs, VFTOs) at UHV will, without any doubt, also have an impact on

the insulation coordination requirements (distances, dimensions, insulation thickness) for EHV voltages (800 kV, 550 kV, 420 kV).

CIGRÉ WG A3.22 has published preliminary results at a number of events, each time focussing on different aspects of transient phenomena in UHV systems [2] [3] [4] [5] [6] [7]. As the results presented were not yet final, small differences between the preliminary conclusions of the publications do exist.

During the second stage of investigations WG A3.22 counted 44 experts from 17 countries including the coordination participants from other WGs and Study Committees.

References

[1] CIGRÉ Technical Brochure 362, December 2008, "Technical Requirements for Substation Equipment exceeding 800 kV AC"

[2] CIGRÉ SC A3 Session 2008, Report A3-211 "Technical Requirements for Substation Equipment exceeding 800kV"

[3] Électra 241, December. 2008, "Technical Requirements for Substation Equipment exceeding 800kV AC"

[4] Second International IEC/CIGRÉ Symposium on Standards for Ultra High Voltage Transmission, New Delhi, January 2009, "System Impacts on UHV Substation Equipment"

[5] Second International IEC/CIGRÉ Symposium on Standards for Ultra High Voltage Transmission, New Delhi, January 2009, "UHV Equipment Requirements: state of the art & prospects for equipment"

[6] CIGRÉ SC A2/A3/B3 Colloquium and Regional Conference 2009, South Africa "Comparison of UHV and 800 kV Specifications for Substation Equipment"

[7] 2009 International Conference on UHV Power Transmission, Beijing, May 2009, "Switching Transients in UHV Networks"

2 System Requirements

2.1 Insulation levels (LIWV, SIWV, SFO, VFTO)

2.1.1 Introduction

UHV technology is characterized by a stringent need to reduce as far as possible the sizes, weights, costs and environmental impacts of the OH-lines and substations, in order to get projects which are feasible from an economic, societal and technical point of view. The present UHV voltages in the process to be standardized by IEC, are 50% higher than those for system voltages that fall under the 800 kV class, but as insulation strength per metre decreases with the length of the air gap, certainly for switching impulses under wet conditions, straight forward extrapolation of the dielectric requirements would lead to disproportional large structures. Therefore, by means of the application of a number of new technologies and new analysis techniques, utilities are able to reduce the dielectric requirements to values that lead to much smaller structures. This results in insulation levels that are not far from the levels applied at the voltage class of 800 kV, as can be seen in figure 2.1.1. The first column shows the IEC values for 800 kV and the last column shows the values for TEPCO's 1100 kV-project, which might fall within the range of values applied for 800 kV [1]. In Japan the towers of the UHV OH-lines are only 77% of the size that would be necessary when insulation levels would have been extrapolated from the lower voltage classes (See figure 2.1.9).

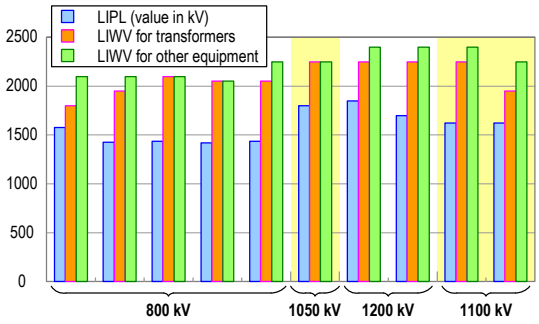

Figure 2.1.1 (a) LIPL/LIWV

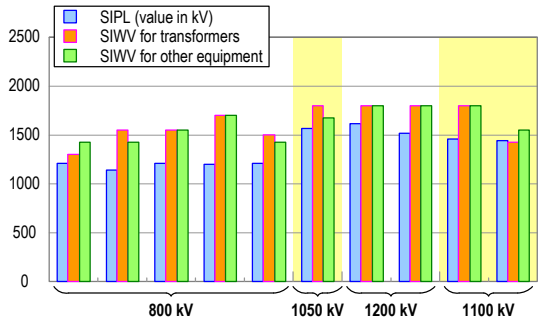

Figure 2.1.1 (b) SIPL/SIWV

A technology used to reduce the insulation levels are the application of "high performance" surge arresters that show a steeper curvature than conventional arresters and therefore a lower ratio between the Protection Levels (LIPL and SIPL) and the Continuous Operating Voltage (COV). This ratio can be further decreased by applying multi-column arresters. Closing resistors are used to control slow front overvoltage (switching overvoltages, SFO) due to closing and re-closing of OH-lines. Switchable shunt reactors, fast protection schemes, single-phase auto-re-closing (SPAR), three-phase auto-re-closing (TPAR) and 4-legged shunt reactors are applied to achieve stable power supply when a fault occurs on the lines. Closing resistors are used to control slow front overvoltage (SFO) by closing and re-closing of OH-lines. With respect to SFO generated in the healthy lines at the source side of the CB when clearing a fault, it depends on the fault conditions and tends to be larger in multi-phase line faults to ground such as 2LG, 3LG. Although the probability of the occurrence of these faults is comparatively low in UHV systems, opening resistors are used to reduce the opening SFO for the purpose of avoiding successive breakdowns that may affect the availability of the whole system. Other options are the application

of transmission line arresters (TLA) and controlled switching, but at present, these technologies are not applied in UHV systems. The application of TLA can be expected to reduce SFO to less than ground fault overvoltage levels in a healthy phase (typically 1.6 to 1.7 p.u.). Shielding of OH-lines, improved earth return conditions and other countermeasures against back-flashover lead to an improved lightning withstand performance. When necessary damping resistors in GIS disconnectors reduce the amplitude of VFTO, which can otherwise exceed the LIWV level.

As can be seen in figure 2.1.1, thanks to the use of "high performance" surge arresters reduced margins between LIWV and LIPL, on one hand, and between SIWV and SIPL on the other hand, form another reason why insulation levels for UHV are not far from those for 800 kV. Advanced calculation and simulation techniques are developed and used which offer the possibility to get an overview about the stresses of the network, the combinations of events and conditions to be considered. By such a systematic approach utilities will be able to offer transparency with respect to their risk policy and their design margins.

There is no technical reason why similar techniques and policies could not be applied to 800 kV networks and even for lower system voltages. However, there may be difficulties since, in an existing network, it may be difficult to adapt the insulation coordination as consistently as it is possible for new networks.

2.1.2 Utilities' policies on insulation level

Utilities generally use both analytical and simplified IEC approaches to evaluate LIWV levels. For the UHV systems of 1050 kV, 1100 kV and 1200 kV, the specified LIWVs ranges from 1.25 to 1.49 times the LIPL value (see figure 2.1.2 (a)).

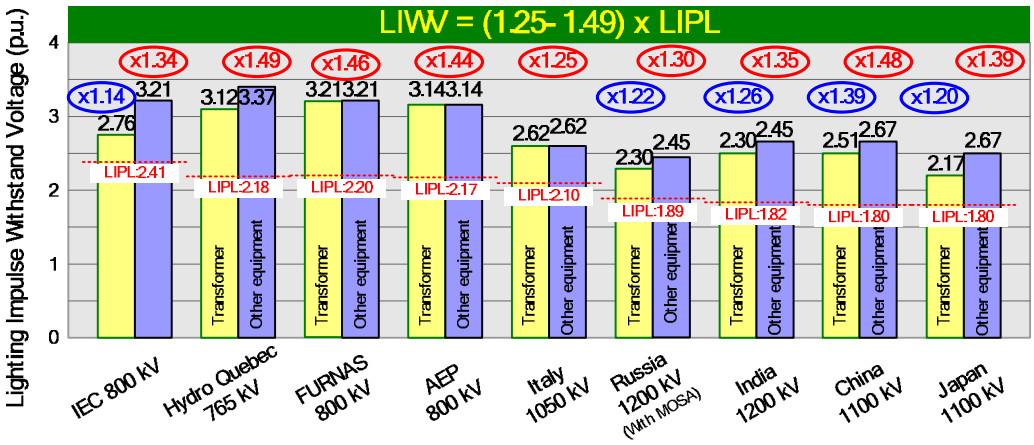

Figure 2.1.2 (a) LIWV specifications for transformers and substation equipment

On the other hand, suppressing switching overvoltages as much as possible is a prerequisite for insulation clearances in air to reduce the heights of transmission towers and the dimensions of open-air parts in substations. Therefore, the specified switching overvoltages will determine the dimensions of the OH-lines and will strongly affect the UHV construction costs. The applications of mitigation measures can reduce the SFO level. Figure 2.1.2 (b) shows the SIWV of the EHV and UHV networks.

Another important aspect for insulation coordination is the utility's policy with respect to the withstand margins for severe lightning or switching conditions with a

very low probability of occurrence and precise computer simulations will accurately show the impact of such severe conditions.

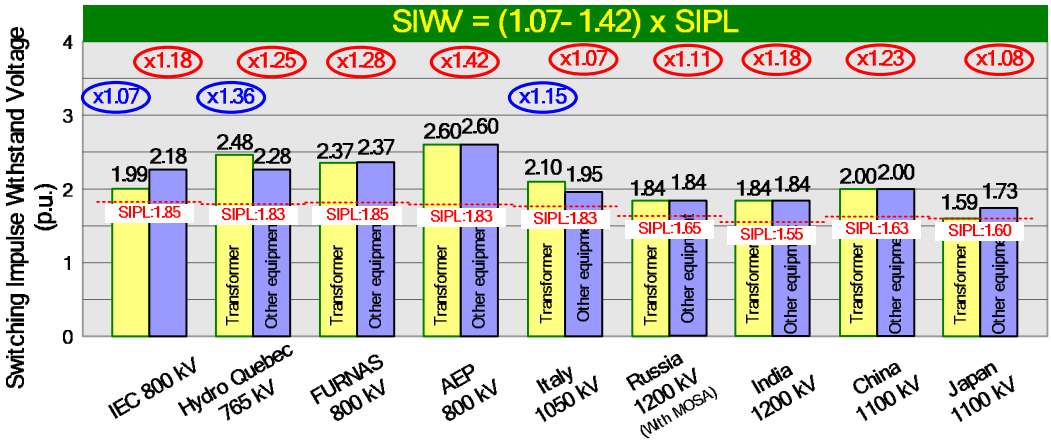

Figure 2.1.2 (b) SIWV specifications for transformers and substation equipment

The general procedure of the insulation coordination is defined by IEC 60071-1 and the application guide IEC 60071-2. Figure 2.1.3 illustrates the flow chart given by IEC 60071-1 for the determination of the rated or standard insulation level.

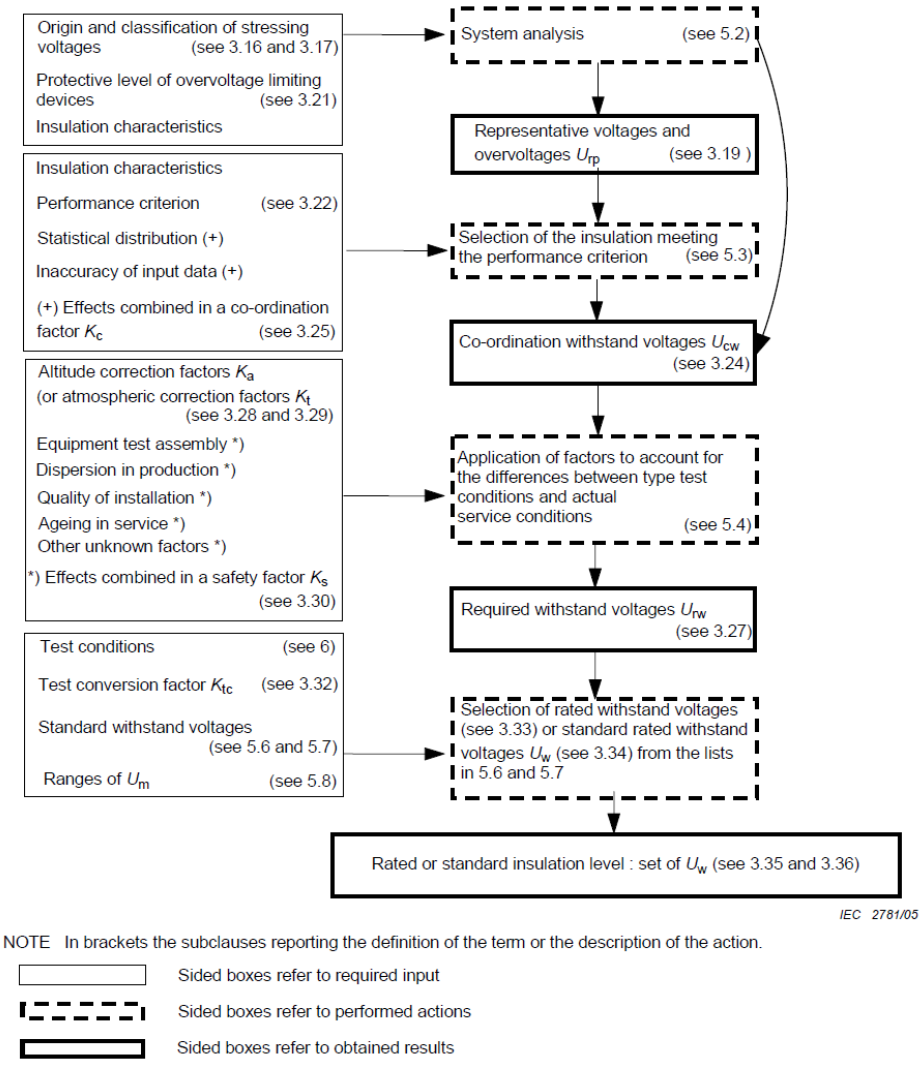

Figure 2.1.3 Flow chart for the determination of rated or standard insulation level (IEC60071-1)

The general process for deciding the basic insulation level can be systematically decided according to the flow chart from IEC 60071-1 in figure 2.1.3. However, the insulation withstand level is dependent on the applied insulation coordination technologies such as the application of switching surge suppression resistors or the designed protection levels of arresters and also upon the severity that users assume (especially in case of UHV systems). Furthermore, the safety factor that considers the applicable failure rate and the margin of the insulation performance are different depending on user' policies.

A comparison of these processes for different countries is roughly illustrated in figure 2.1.4. If a point of a factor is plotted in upper section of the figure, the factor for LIWV is higher. On the other hand, a plotted point in the lower section indicates a lower LIWV. For example the South Korean 800 kV system has strict protection specifications - an increased number of arresters with a lower LIPL are applied. However a higher OH-line outage rate was evaluated by considering an aging effect of the insulation, which leads to a slightly higher margin and safety factor as well as to a higher LIWV. Conversely, the Canadian specifications for LIPL are less strict and a lower OH line outage rate was chosen.

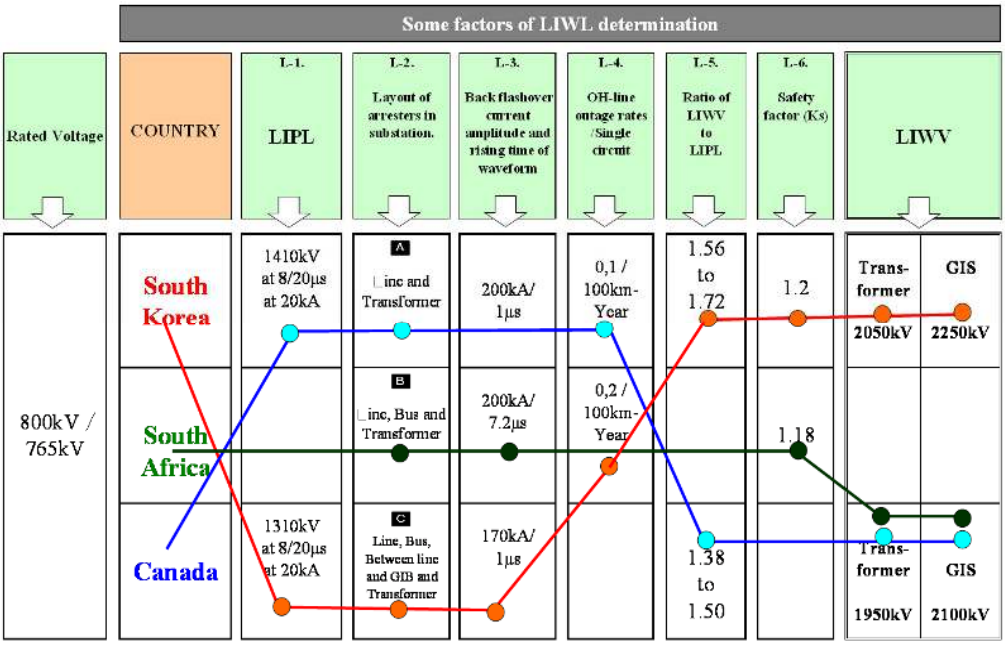

Figure 2.1.4 Comparison of 800kV LIWV related factors from different countries

Table 2.1.1 Example of Determination process for LIWV

Country	South Korea 800 kV	China 1100 kV (pilot)
LIPL	1310 kV (2.0 p.u.) at 20 kA	1620 kV (1.8 p.u.) at 20 kA
MOSA layout	1 unit for line entrance 1 unit for busbar 1 unit for transformer	1 unit for line entrance 2 units for busbar 1 unit for transformer
Maximum calculated overvoltage	---	1796 kV for transformer 2040 kV for GIS
OH line outage rate	0.4 faults/100 km-line-year/ double circuit	0.112 faults/100 km-line-year/ Single circuit
Safety factor	---	1.15 for internal insulation
LIWV for transformer	2050 kV (3.14 p.u.)	2250 kV (2.51 p.u.)
LIWV for other equipment	2250 kV (3.44 p.u.)	2400 kV (2.67 p.u.)
LIWV / LIPL	1.72	1.48

Table 2.1.2 Example of Determination process for SIWV

Country	South Korea 800 kV	China 1100 kV (pilot)
SIPL	1200 kV (1.85 p.u.) at 2 kA	1460 kV (1.63 p.u.) at 2 kA
Resistance for GCB	1000 Ω for closing	600 Ω for closing
Calculated overvoltages at substations (2% value)	1124 kV for Grounding fault 999 kV for Closing 1186 kV for opening	1400 kV for closing
Maximum line length	160 km	420 km (tentative)
Safety factor	---	1.15 for internal insulation
SIWV for transformer	1500 kV (2.30 p.u.)	1800 kV (2.0 p.u.)
SIWV for other equipment	1425 kV (2.18 p.u.)	1800 kV (2.0 p.u.)
SIWV / SIPL	1.25	1.23

In case of 800kV systems, typical policies of insulation coordination are as follows.

2.1.2.1 Hydro Quebec policies of insulation coordination

The protection level for lightning surge offered by the MOSA depends on the V-I characteristics of the MOSA and is more or less related to the service voltage (Maximum COV) and TOV specified. The basic design criteria for the lightning performances of the 765kV lines and substations were decided by the occurrence of fault rate calculated from simulations. If the risk of failure calculated is too high, the location and number of MOSA in the substation can be modified to obtain the desired risk of failure. Switching overvoltage (SOV) on the lines is basically determined by EMTP studies and the highest values are generally obtained during a re-closing sequence of the line in presence of a trapped charged on the line. For series-compensated lines, MOSA are installed at the line entrance for suppression of SOV. Closing resistors were used on the air blast CBs during the first stage of the 765 kV network.

2.1.2.2 Eskom policies of insulation coordination

The maximum tower earthing resistance of the transmission line towers is designed to 50 Ω. With this value for tower earthing resistance a lightning current higher than 130 kA is required to cause a back-flashover event. The lightning overvoltage analysis for a 800 kV GIS therefore conclude that even severe atmospheric discharges of low probabilities does not pose a risk to the GIS equipment, power transformers and shunt reactor insulation when utilizing 612 kV rated MOSAs, positioned at the GIS entrance and close to the transformer and reactor bushings.

2.1.2.3 KEPCO policies of insulation coordination

Insulation Levels of the substation equipment is determined by the protective levels offered by the MOSA and by the location of the MOSA in the substation. The LIWV specified for the 765 kV power transformers is 2050 kV giving a maximum safety margin of about 20%. This safety margin is needed to take into account the ageing of insulation system of EHV equipment (paper/oil for power transformers).

SOV on the 765 kV lines are basically determined by TNA & EMTP studies. The highest values are generally obtained during a re-closing sequence of the line in presence of a trapped charged on the line. Closing resistors are used for the suppression of closing overvoltage.

2.1.3 Background of technical requirements

Figure 2.1.2 (a) and (b) illustrate switching and lightning impulse withstand voltages for existing projects. UHV specifications including insulation levels should not be extrapolated from EHV systems, because most UHV systems can realize a reduction of insulation level, maintaining high reliability and cost reduction using some additional technologies. This chapter will introduce some practical technologies, which affect the insulation level.

2.1.3.1 Surge arrester protection

In case of impulse overvoltages, the V-I characteristic and arrangement of the MOSA in the substation are important factors. Figure 2.1.5 illustrates the V-I characteristics of a high performance surge arrester. Optimal insulation coordination can be achieved based on high-performance MOSAs, as demonstrated in UHV projects of the 1990s and later in Japan, Italy and China. Table 2.1.3 shows characteristics of MOSAs which are applied to 800kV systems and UHV systems. The ratios of protection levels, LIPL and SIPL, for the UHV systems are lower than those for 800kV systems and can contribute to reduce the LIWV and SIWV.

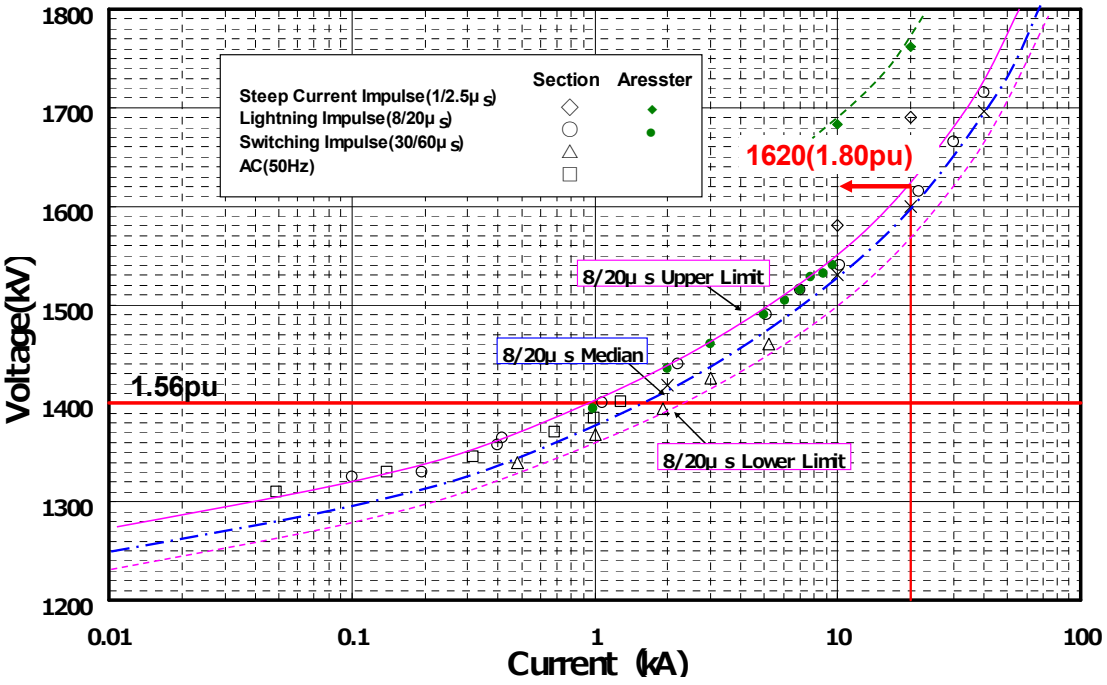

Figure 2.1.5 Example of V-I characteristics of high-performance surge arrester

Table 2.1.3 Specification of MOSAs Characteristics

	800kV system				UHV system				
	Hydro Quebec	KEPCO	AEP	ESCOM	ITALY	RUSSIA	JAPAN	CHINA	INDIA
Rated voltage	----	612 kV	----	612 kV	750 kV	800 kV	826kV	828kV	850kV
SIPL (30/60us) at 2kA	1140 kV 1.83 p.u.	1200 kV 1.85 p.u.	1197 kV 1.83 p.u.			1570 kV 1.60 p.u. at 2.8 kA	1400 kV 1.56 p.u. at 1.0 kA	1460 kV 1.62 p.u.	1500 kV 1.53 p.u.
L IPL (8/20us) at 20kA	1410 kV 2.26 p.u.	1310 kV 2.01 p.u.	1420 kV 2.17 p.u.		1750 kV 2.04 p.u.	1764 kV 1.80 p.u. at 15 kA	1620 kV 1.8 p.u.	1620 kV 1.8 p.u.	1700 kV 1.74 p.u.
Very Steep Front Wave (1us) at 20kA	1620 kV 2.59 p.u.	1440 kV 2.20 p.u.							

Table 2.1.4 illustrates a study of several arrangements of high performance MOSA with the corresponding costs and withstand voltages in Japan. It shows the arrangement composed by two surge arresters per circuit at the line entrance, two per quarter bus and one per transformer bank as one of the most favourable applications (highlighted).

Table 2.1.4 Relationship between LIWV and MOSA layouts

(:kV)

Layout of Surge Arrester	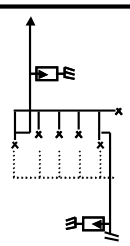	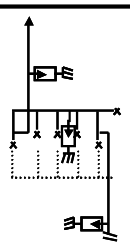	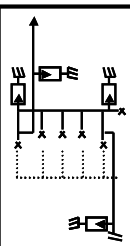	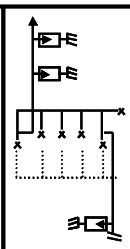	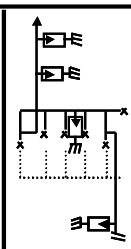	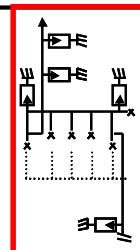
Transformer Overvoltage LIWV	1950 1950	1943 1950	1895 1950	1943 1950	1938 1950	1896 1950
GIS Overvoltage LIWV	2898 2900	2854 2900	2730 2900	2628 2700	2506 2550	2208 2250
Cost	102 %	105 %	109 %	103 %	103 %	100 %

2.1.3.2 GCB with closing/opening pre-insertion resistor

UHV systems demand more insulation clearance than current EHV systems, especially in case of the clearance for switching impulse voltage in air under rain condition. Equipments' size and total costs may be larger according to the increasing insulation level. The application of a closing and opening pre-insertion resistor is one of the effective technologies to solve this issue.

Figure 2.1.6 shows the comparison of maximum values of switching overvoltages (SOV) in two exemple 800 kV transmission systems calculated using EMTP. The simulations have been performed without mitigation, with a circuit breaker's closing resistor as well as with a MOSA at the ends or at the middle of the transmission line. In case of the Canadian transmission system, a closing resistor of 300Ω was applied and for the Korean system 400Ω has been used. According to the simulation results shown in the figure 2.1.6, the closing resistor can reduce the maximum value of the SOV by 36%. MOSAs could reduce the SOV's peak by 14% to 28% depending on its position and system components. A combination of the closing resistor and the MOSAs would lead to a further decrease of the SOV's maximum amplitude.

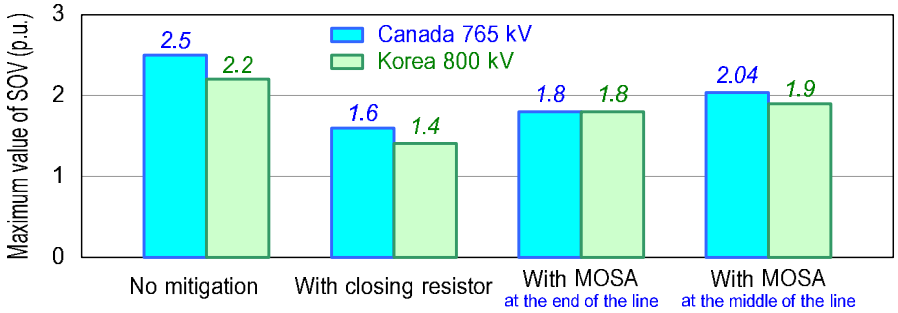

Figure 2.1.6 Reduction of SOV by closing resistor or MOSA in 800kV systems

A combination of mitigation technologies, like the application of closing and opening resistors, optimized V-I characteristic of MOSA and the optimized placement of arresters in the substation or the application of controlled switching could reduce the switching overvoltage more effectively. The influence of the value of a closing resistor on the maximum overvoltage is illustrated in the following two figures. Figure 2.1.7 shows the influence of the closing resistor on the overvoltage in the 1100 kV system of China (2 % probability value). Figure 2.1.8 shows an example of the overvoltage at healthy lines during the fault interruption by a CB with closing and opening resistor and with high performance lightning arrester in the Japanese 1100 kV system. Both cases indicate an optimal resistance value depending on the additional damping elements.

It has to be mentioned, that the dissipated energy of the resistor depends on the resistance. Therefore, the decision about the resistance value shall be balanced between mitigation effect and required energy dissipation of the resistor itself.

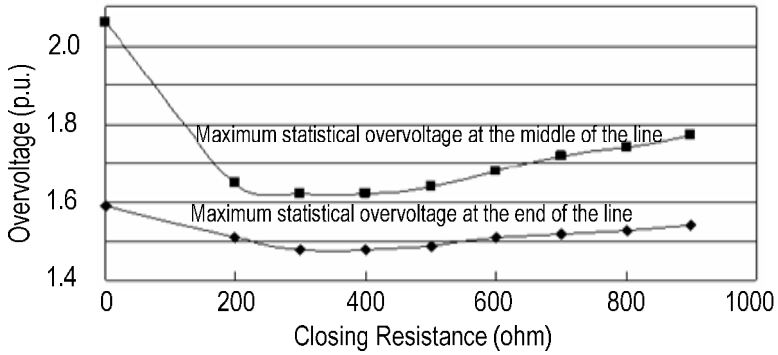

Figure 2.1.7 Typical closing overvoltage with different resistance in 1100 kV system

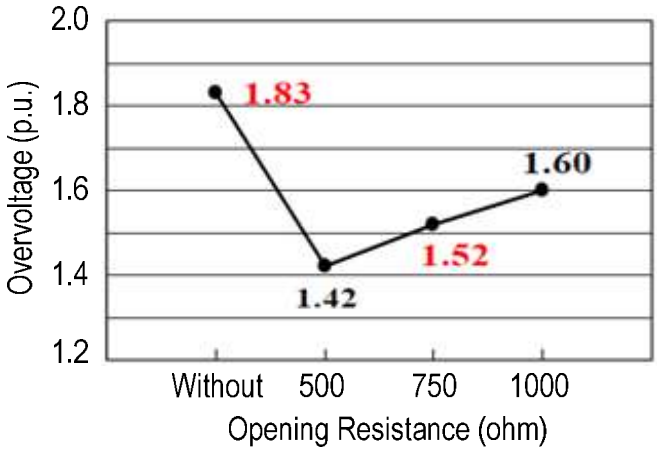

Figure 2.1.8 Typical opening overvoltage during a fault interruption in 1100 kV system

Table 2.1.5 shows the switching overvoltage depending on the suppression techniques from different UHV transmission lines in Italy, Japan, China and India. The closing resistor value ranges from 500 Ω to 700 Ω.

Table 2.1.5 Switching overvoltage level and measures for overvoltage suppression

Country	Italy	Japan	China	India
Highest Voltage	1050kV	1100kV	1100kV	1200kV
Suppression of switching overvoltage	MOSA Closing &Opening Resistor 500Ω	MOSA Closing &Opening Resistor 700Ω	MOSA Closing Resistor 600Ω	MOSA Closing Resistor 600Ω
Switching overvoltage Insulation design level	1.7p.u.	1.6 / 1.7p.u.	1.7p.u.	1.7p.u.

Reducing the switching overvoltage will minimize design and overall costs of a transmission system. Figure 2.1.9 illustrates a comparison between a UHV transmission tower based on existing 550 kV technologies and an actual UHV transmission tower in Japan – The height is reduced from 143 m to 110 m.

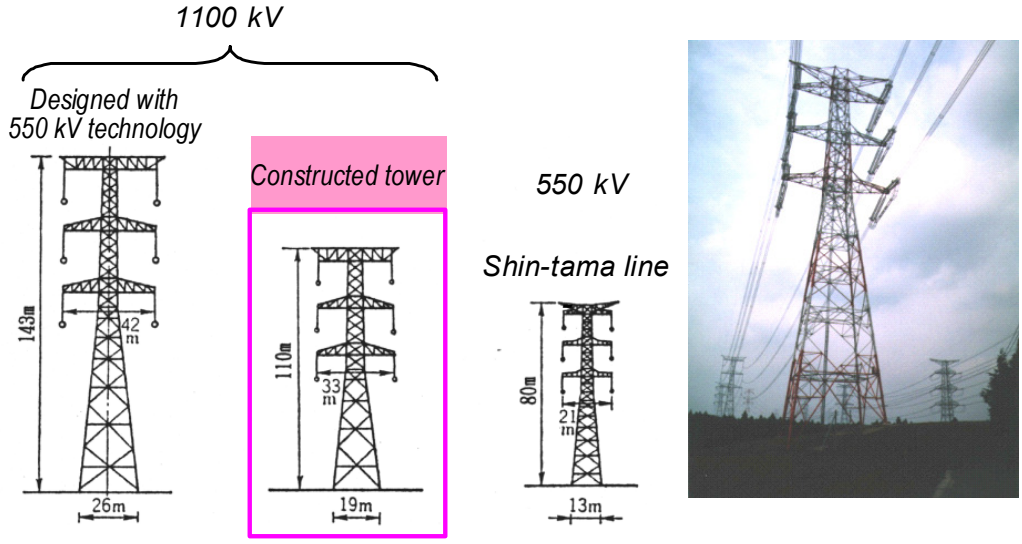

(a) Comparison of transmission tower designs (b) 1100 kV tower

Figure 2.1.9 1100kV tower design compaction

2.1.3.3 DS with resistor

Very fast transient overvoltages (VFTO) occur during switching operations of DS in GIS. The VFTO consists of frequencies up to 100 MHz and the maximum peak value of VFTO could be larger than lightning impulse withstand voltage (LIWV). Therefore, the transformer winding or GIS insulation could be overstressed. The peak value and frequency contents of VFTO depend on the GIS design [2] [3]. Chapter 4 describes the VFTO in detail.

The DS with a resistor can effectively decrease the peak value and high frequency contents of the VFTO. Figure 2.1.10 shows typical waveforms measured at transformer terminal during switching tests for 1100 kV GIS, where a transformer is directly connected to the GIS (DS) either with or without switching resistor. The measurements for both cases agree well with the EMTP simulations. The voltage change appearing at the wave-front that causes the internal voltage oscillation in a transformer winding is reduced from 1.35 p.u. to 0.3 p.u. by means of the switching resistor.

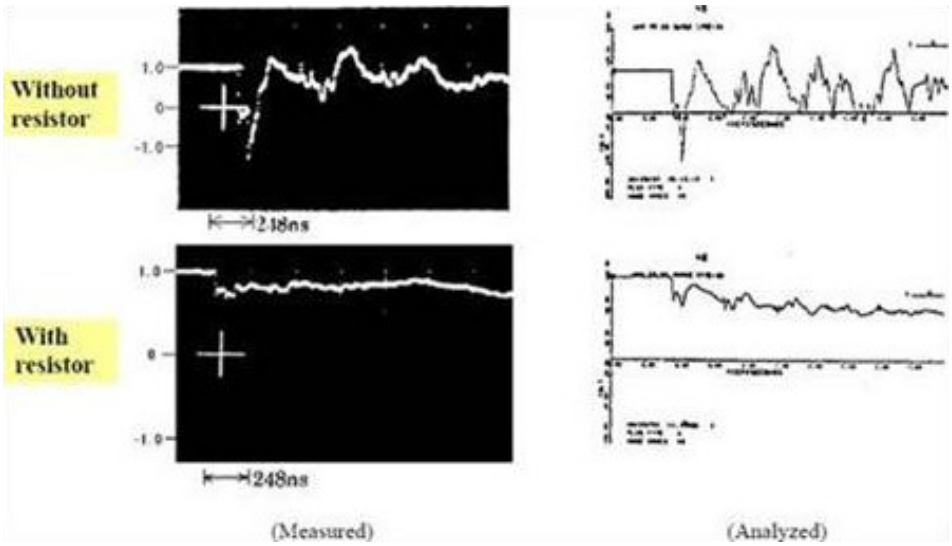

Figure 2.1.10 DS surge waveforms at transformer terminal

2.1.4 Recommendation for specifications

IEC Technical Committee 28: Insulation Coordination decided the standard lightning impulse withstand voltage (LIWV) and the switching impulse withstand voltage (SIWV) for UHV equipment in highest voltages of 1100 kV and 1200 kV.

Table 2.1.6 LIWV and SIWV of IEC TC28

(kV)	IEC TC28	
Highest voltage	1100	1200
Standard LIWV	1950, 2100, 2250, 2400, 2550	2100, 2250, 2400, 2550, 2700
Standard SIWV (Phase-to-earth)	1425, 1550, 1675, 1800,	1675, 1800, 1950,

Table 2.1.7 Insulation level for substation equipment and power transformers

Country		Italy	Russia/India	Russia	Japan	China
Highest voltage (kV)		1050	1200	1200	1100	1100
Type of arrester		MOSA	MOSA	Gapped arrester	MOSA	MOSA
Power Transformer	SIWV (p.u.)	1800 (2.10)	1800 (1.84)	2100 (2.14)	1425 (1.59)	1800 (2.00)
	LIWV (p.u.)	2250 (2.62)	2250 (2.30)	2550 (2.60)	1950 (2.17)	2250 (2.51)
Other Equipment	SIWV (p.u.)	1675 (1.95)	1800 (1.84)	2100 (2.14)	1550 (1.73)	1800 (2.00)
	LIWV (p.u.)	2250 (2.62)	2400 (2.45)	2900(2.96)	2250 (2.51)	2400 (2.67)

Lightning overvoltages dominate the non-self-restoring internal insulation design of substation equipment and it is important to suppress lightning overvoltages effectively by arranging MOSAs at appropriate locations such as at line entrances, busbars and transformers. VFTO could be reduced by the switching resistors. A typical example of the reduction of VFTO is less than 1.3 p.u. obtained using the disconnector with a 500 Ω switching resistor. This mitigation measure is also effective for suppression of electromagnetic interferences in the secondary system.

2.2 Temporary Overvoltages (TOV)

2.2.1 Introduction

TOV in large systems is mainly caused by Ferranti effect, (ferro)-resonance phenomena and single-phase faults. One special resonance phenomenon in relation to shunt reactors is that during SPAR (single-phase auto-re-closing), the reactor may be energized by capacitive coupling from the healthy phases. Another special resonance phenomenon is caused by large power transformer or shunt reactor energisation in a weak network, as may occur during the initial stage of UHV network or during system restoration. TOV up to 1.45 p.u. and 1.55 p.u. for some seconds has been reported following line to ground fault interruption [4] [5]. Ferro-resonance overvoltages at second harmonic were observed during one-side switching of 750 kV lines even from powerful feed networks where they were generated by nonlinearity of shunt reactor and/or transformer magnetization curves. These TOV could be especially harmful for EHV/UHV equipment if protective overvoltage relays operate on effective, not peak, voltage values and are not able to detect the TOV.

As suitable countermeasures are available such as transformer controlled switching taking into account residual flux and pre-insertion resistors, it is assumed that resonance and ferro-resonance phenomena will be anticipated and prevented or at least limited in magnitude and/or duration. The two remaining causes of TOV are single-phase faults and Ferranti effect.

2.2.2 Background of technical requirements

In the case of single-phase faults, the relationship between TOV and k_{pp} (first-pole-to-clear factor) results in an overvoltage of 1.27 p.u. for $k_{pp} = 1.3$, of 1.16 p.u. for $k_{pp} = 1.2$ and of 1.06 p.u. for $k_{pp} = 1.1$. Only in cases of relatively high k_{pp}, the TOV reaches a certain importance.

The Ferranti effect is normally controlled by shunt reactors and series capacitor banks, when applied. Some utilities switch on the shunt reactors before the OH line is energized and switch them off at high loads or, sometimes, after switching off the OH line. Depending on utility operating practices, series-capacitors can be connected to the line before energizing the line or during a re-closing sequence which did not require the by-pass of the series capacitor. In the case of sudden load rejection at a heavily loaded long line, the voltage jump due to Ferranti effect will lead to a TOV, which lasts until either the OH line is tripped at both sides or the shunt reactors are switched on. (See figure 5 in the Ref. [6])

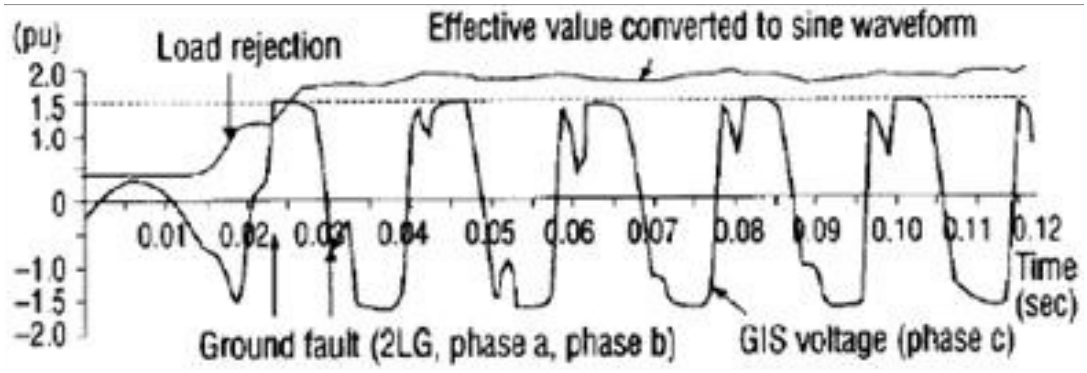

Figure 2.2.1 TOV at load rejection followed by ground faults [6]

Furthermore, UHV systems often operate in conjunction with HVDC links and with other power systems as well. In the case of a sudden voltage drop due to a fault occurrence, the HVDC converter will momentarily block and the synchronous generators and FACTS will try to compensate this voltage drop. The effects of these operations will remain in service to raise the voltage and avoid a complete trip of the HVDC installation. When the fault is cleared, the system will be exposed to a large power oscillation (TOV) lasting more than 100 milliseconds. Simulation studies have to be performed considering the effect of the power transformer saturation curves and the dynamic behaviour of these power electronics apparatus.

2.2.3 Summary of utilities practices

Table 2.2.1 summarizes TOV and MOSA energy absorption study results for the UHV systems in China, Japan, Russia and India. The amplitude of TOVs ranges from 1.3 to 1.5 p.u. depending on the system conditions. The TOV of 1.5 p.u. is reported in Japan, considering a load rejection followed by grounding faults. The arrester energy is analysed considering the short-circuit impedance seen from the arrester during TOVs. TOVs will require detailed and ongoing study as the UHV systems evolve from the initial and mostly radial (weak) configurations to the ultimate meshed (strong) systems. Remedial action schemes may be necessary in order to limit TOV durations to acceptable values. As the amplitude and the duration of TOV should be determined by the system requirements in different projects, a test method of MOSA capability should be considered for wide applications.

Table 2.2.1 TOV and MOSA energy absorption study results

Country	India	Russia		Japan	China
Highest voltage	1200	1200		1100	1100
Type of arrester	MOSA	MOSA	Gapped SA	MOSA	MOSA
TOV (p.u.)	1.4	1.3 [1.35] 1)	1.3 2)	1.5 3)	1.4
Duration (sec.)	0.44	3 [0.15] 1)	5 2)	0.17 3)	0.4 – 0.5
Energy absorption, calculations (MJ)	35	---	---	55	8.6
Energy absorption, specifications (MJ)	55	40 5)		55	40 (20) 4)

Note: The TOVs are calculated with the prospective overvoltages without the MOSAs except in Japan.

1) The voltage and duration in the parenthesis [ ] are equivalent to the values of 1.3 p.u. and 3 seconds.

2) For gapped arresters the permissible duration of TOVs is determined by the performance of auxiliary resistors shunting its gaps for proper voltage distribution, not by that of arrester main non-linear resistors.

3) The duration is equivalent values corresponding to the energy absorption of 55 MJ.

4) The maximum energy absorption for MOSA in the China's UHV pilot project is required to be 20 MJ by the analysis and specified as 40 MJ in two switching events.

5) Estimated from a specified current impulse withstand capability of 2.8 kA with a wave shape of 3/8 ms.

2.3 Secondary Arc Extinction

2.3.1 Introduction

The use of 4-legged shunt reactor schemes to enable single-pole autore-closing (SPAR) was proposed by Knudsen [7] and Kimbark [8] in the early 1960s. The basic principle is as follows. When a single-phase line-to-ground (1LG) fault occurs on a transmission line, the line circuit breakers are single-pole tripped to clear the fault, i.e. interrupt the so-called primary fault current. However, due to inductive and capacitive coupling to the sound phases, a much lower secondary arc current occurs in the previous arc channel of the primary fault current. Successful single phase switching relies on self-extinction of the secondary arc before the circuit breaker poles re-close. The 4-legged reactor scheme compensates for the capacitive and inductive coupling to the sound phases and thereby promotes extinction of the secondary arcs within desired re-closing times generally less than one second.

The secondary current arc is a free burning arc in atmospheric air but with a difference. In principle, a free burning arc is sustained and continues to propagate provided that the arc power input exceeds the arc power loss. If the two quantities become equal, the arc will stall; and if the power loss exceeds the power input, the arc will collapse and extinguish [9]. The extinction process associated with secondary current arcs is more complex and is due mainly to non-uniformity within the arc itself as discussed later. The magnitude of the secondary arc current depends on a number of factors including the line design, the primary fault current and its asymmetry, possible current injection from other sources such as an in-service series capacitor bank and ambient conditions, principally air temperature and wind velocity.

The physical behaviour of the arc also contributes to its survival or collapse. Anjo et al describe this behaviour as follows [9]:

“When the primary arc current has magnitude of 8 kA and duration of 5 cycles as in the present experiment, the bottom of the luminous part of post-arc gas moves upward with the speed of about 5.3 m/s being apart from the lower electrode; here it is assumed that the wind velocity is less than 1 m/s. The post-arc gas is highly conductive. Hence the secondary arc is ignited inside the post-arc gas. The temperature of this post-arc gas is not uniformly distributed because of its convection and diffusion. Therefore the spatial distribution of ion density is also not uniform.

A secondary arc stretches along the path when the ion density is comparatively high. This is the reason why the secondary-arc path is so winding. Once it begins to bend, the path is bent more strikingly by the electromagnetic force due to the arc current itself. Thus the arc is stretched more and simultaneously subject to much larger electromagnetic force. It is well known that the arc path can be stretched by a comparatively small electromagnetic force.”

Furthermore, “the self-extinction time becomes longer and longer as the secondary-arc current increases and the maximum arc power also becomes larger and larger. Thus, the arc length can be stretched more easily than when the secondary-arc current is small. This makes the self-extinction time long.

On the other hand, when the arc voltage is subject to considerable fluctuation, the self-extinction time also becomes long. The fluctuation of the arc voltage is due to the reduction of the arc path or the short-circuiting of stretched arc path. Therefore, the

arc path begins to renew its stretching and the self-extinction time is also made longer. This self-extinction time is not uniformly distributed because of irregular stretch of the arc path and random occurrence of its short-circuiting."

These observations in laboratory testing are supported by later actual laboratory and field fault testing as discussed in the next section. As it has been already noted, the main reason for extinction of the secondary arc column is its non-uniformity. This non-uniformity becomes more pronounced with time and increases with increasing column length.

2.3.2 Review of laboratory and field fault testing

Field fault testing to verify the performance of secondary arc current extinction measures have been carried out by a number of utilities. The results of these tests on 550 and 800 kV lines are summarized in Table 2.3.1. All of the tests were performed on single-circuit lines. Key observations from the results are as follows:

The waveform of the steady-state secondary arc current is quite convoluted and quantifying it by means of its calculated power frequency component seems a good approach.

Power flow has an influence on the secondary arc current and its extinction time.

Intuitively, the primary fault current and its asymmetry will influence the secondary arc current and its extinction. However, the data is insufficient to be able to derive any definitive relationship between the quantities.

Ambient conditions, air temperature and wind velocity, are factor factord but again the data is insufficient to quantify relationships.

The various laboratory and field test results (diamond-shaped points) show a wide scatter and indicate no doubt of the wide ranging circumstances involved.

Test results in the 330 kV and 750 kV systems were used to predict the recommended dead-time values with 90% probability, as shown in figure 2.3.1.

Data from the only 1200kV field tests (Figure 4 in [10]) are shown to the right of Figure 2.3.1. The round points represent instances where the secondary arc self-extinguished within the allowed time. The triangular points show the results where arc did not extinguish within the allowed time, because the faulted phase was shunted to ground before arc extinction.

Artificial single-phase grounding test was conducted during commissioning on the pilot 1100 kV systems with 4 legged shunt reactor in China (see chapter 8). The measured durations of the secondary arcs were 118 ms in the one case and 42 ms in the other.

The comparisons of the 750 to 765 kV test data with those from the UHV tests appear to show that in the latter larger gaps the arc extinguishes faster for a given secondary arc current value.

The empirical relationship proposed by Haubrich et. al., [11]: $t_p = 0.25 \times (0.1\ I_B + 1)$ is shown in figure 2.3.1, where t_p is the deadtime in seconds and I_B is the secondary arc current in amperes.

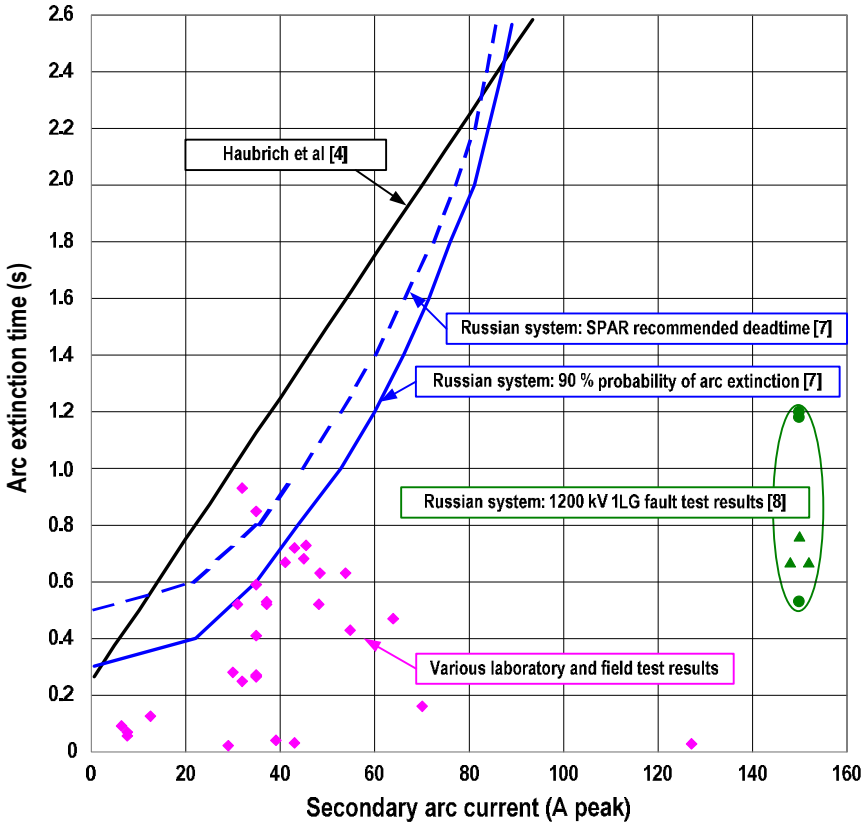

Figure 2.3.1 Secondary arc extinction time as a function of secondary arc current

Table 2.3.1 Laboratory and field test results

Utility/laboratory system voltage year published	Power flow MA	Primary fault current		Secondary arc				Atmospheric conditions	Comments
		kA rms	d.c. component	Current, A rms	Extinction time, seconds	TRV, kV peak	TRV, kV/μs		
Toshiba HPL [9], 1968	NA	8	NA	12.7 - 31.5	0.3 - 0.9 sec	(1)	(1)	1 bar, 0.5°C, wind 0 - 1 m/s	(1) Arc voltages up to 75 kV at extinction were measured
FQH HPL [11], 1974	NA	3 - 18	NA	20 - 40	≤ 1 sec	40 (2), 70 (3)	NA	Wind 2.5 m/s and 5 m/A	(2) 3 m gap, (3) 5 m gap
TVA [12], 500 kV, 1971	710, 905, 525, 945	8 (4)	NA	6.5, 7.5, 7.5, 12.5	0.092, 0.058, 0.070, 0.125	24.5, 28.5, 37, 59	NA	(Ambient temperature for this test: -18°C (5)	(4) Primary fault current about 8 kA; circuit breaker had opening resistors reducing the fault current to less than 1000 A
Russian System [10,13,14] 750 kV (7), 1978	0 to 1280	NA	NA	18, 60, 80 (6)	< 0.1 to 0.9	56, 303, 87	(8)	Wind 0 - 5 m/s	(6) Line lengths 87, 334 and 525 km, respectively, (7)Three-legged reactors , (8) Rise time range of 5 to 110 ms measured
Manitoba Hydro , 550 kV, 1982 [15]	0 320 320 0 510 0 520 500 500	6.37 (11) 8.63, 7.64 2.93 3.77 4.17 5.76 6.22 6.89	57 47 26 7 10 9 64 71 50	- - 127 (13) - - 29 (13) - - 43 (13)	 - 0.028 0.008 0.008 0.021 0.042 0.039 0.030	37 - 61 35 37 29 34 33 30	3.2 - 1.6 1.9 2.3 1.3 1.1 1.9 1.2	NA	(11) Opening resistors of 600 ohms on CB at MH line end , (12) All peak values, (13) Magnitude of final peak before arc extinction
Minnkota Power Co-op, Inc. and Otter Tail Power Company, 345 kV, 1982 (Discussion to [15])	NA	NA	NA	32 (14)	0.25 - 0.93 (14)	104 (14)	NA	NA	(14) Not clear if these results are based on an actual test
BPA, 500 kV, 1982	NA	NA	Asymm. Sym. Sym. Asymm. Sym. Asymm. Asymm. Sym.	31 (16) 37 39 - 30 45 51 37	0.52 0.52 0.042 0.93 0.28 0.68 0.67 0.53	49 49 51 49 49 48 48 48	NA	Wind calm to 1.4 - 1.7 m/s	(16) First three tests line length 122 km followed by five tests line length 148 km
BC Hydro [16], 550 kV, 2004	0 (17)	7.4	34 < 20 < 20 28 20	35 (18) 35 35 35 35	0.41 0.85 0.59 0.27 0.26	(19)	(19)	Calm, -5°C	(17) Line charging current of approximately 170 A due to line being open-ended (18) Estimated 60 Hz component (19) Not measured

All of the tests except one summarized in table 2.3.1 on 550 and 800 kV lines were performed prior to 1984. The one recent test was that performed by BC Hydro in 2004. The secondary arc current was measured with an optical CT with a bandwidth of 6 kHz and a sampling rate of 100,000 per second. A trace of the measured primary arc (10 kA peak) followed by the secondary arc is shown in figure 2.3.2. As shown, the current has two phases: a quasi steady-state phase followed by a reignition phase leading to arc extinction. Although the test consisted of only five shots, the shorter the quasi steady-state phase or the shorter the time to the first reignition, the longer the total arcing time as shown in figure 2.3.3.

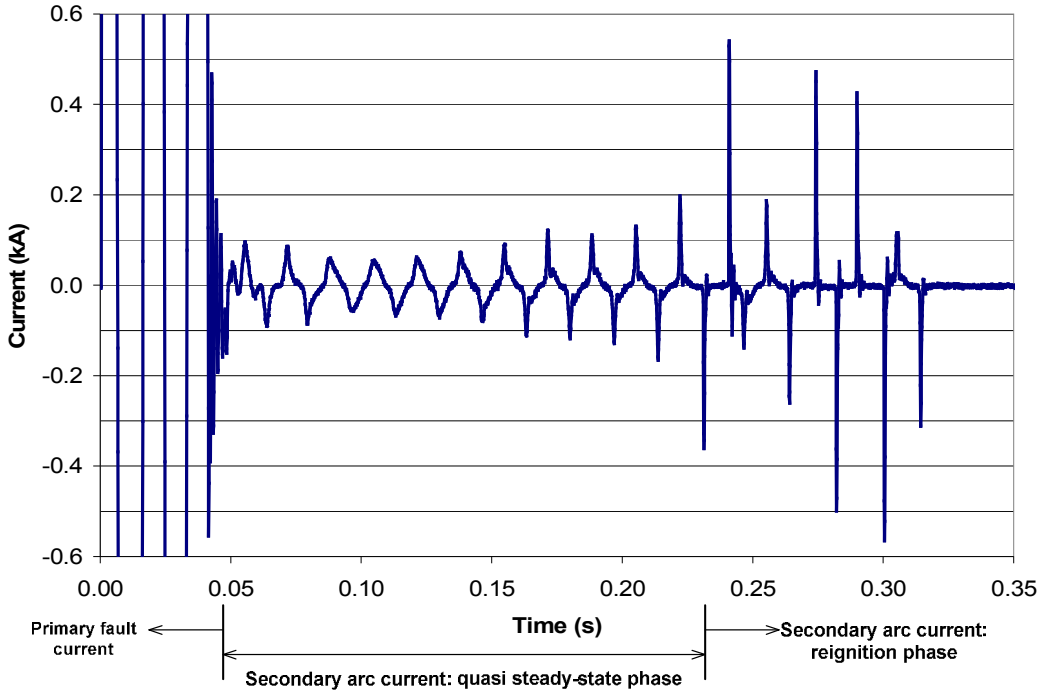

Figure 2.3.2 Secondary arc current trace

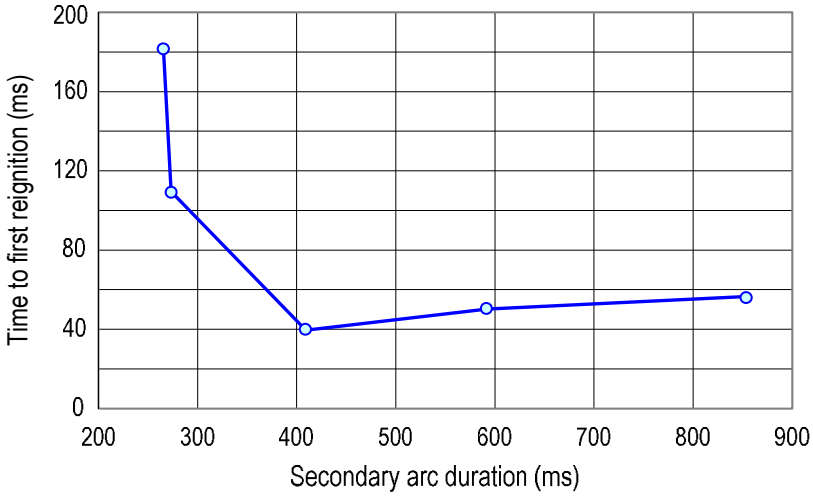

Figure 2.3.3 Time to first reignition versus secondary arc extinction time

2.3.3 Utility practices and experiences

Utility practices and experiences are shown in Table 2.3.2 based on the referenced literature.

Table 2.3.2 Utility practices and experience

Utility system voltage	Line Length	Degree of compensation	Deadtime trip to re-close	Success rate (%)
German [11], 220 kV, 380 kV	NA	60%	1 - 1.5 sec	85%
TVA [12], 500 kV	150 km	50%	0.5 sec	NA
Russian System 750 kV	87– 525 km	NA	0.7-1.5 sec w/o neutral reactors 0.5-1 sec with neutral reactors	52%
New Brunswick Electric Power Commission (Discussion to [15]), 345 kV	317 km	NA	0.7 sec, Based on TNA studies giving expected secondary arc currents 22 to 40 A	100% Based on three SLF faults up to time of publication
Manitoba Hydro [15] 500 kV	528 km	73%	1.5 sec	SPAR discontinued in 1999 due to HVDC commutation failure concerns and addition of series compensation, will be reinstated in 2009
Minnkota Power Co-op, Inc. and Otter Tail Power Company, [Discussion to [15]), 345 kV	194 km	NA	Initially 1 s and later increased to 2 s	55%
Brazilian Utilities 500 kV, 345 kV, 230 kV	≤300 km, > 300 km in special cases	78%	0.8 - 1.2 sec Design secondary arc value ≤ 50 A rms	NA
ESKOM, 800 kV	NA	70%	NA	NA
Powergrid India, 400 kV	NA	55-60%	1 sec, Secondary arc current limited to 40 A	NA
BC Hydro [16], 500 kV	150-300 km	30 (reactor one line end), 80 (reactors both line ends)	1 sec	80-90% for longer lines with neutral reactors; 50-75% for shorter lines with no neutral reactors
TEPCO, Japan, 550 kV	Around 150 km, double circuit	NA	1 sec (Multi phase re-close)	90% (95% in case of lightning)
TEPCO, Japan, 1100 kV, [17]	200 km, double circuit	NA	1 sec (HSGS applied, Multi phase re-close)	NA

The influences of line length and circuit arrangement are shown in figure 2.3.4.

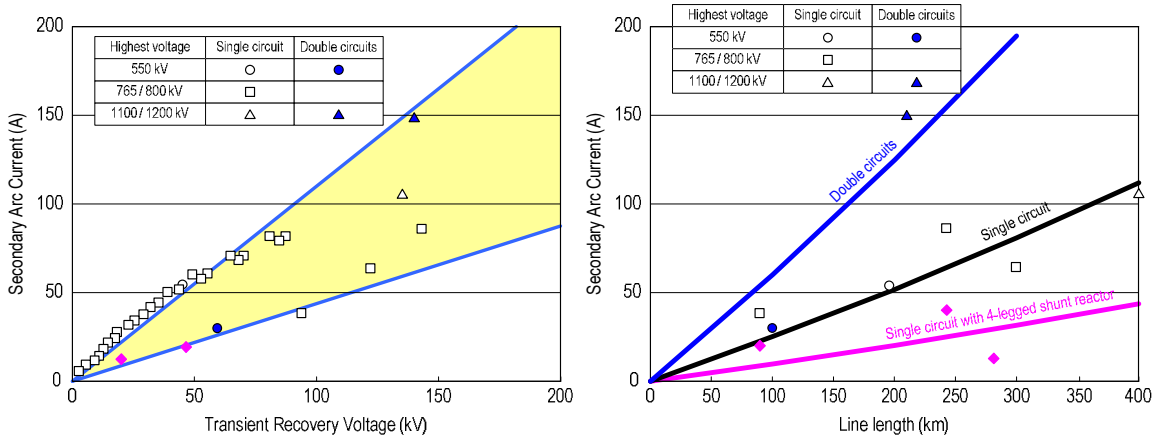

Figure 2.3.4 Secondary arc current as a functions of line lengths and circuit arrangement

The secondary arc current due to electro-static induction increases with the line length and can be significantly reduced by the application of 4-legged shunt reactors, especially in the case of single circuit transmission line.

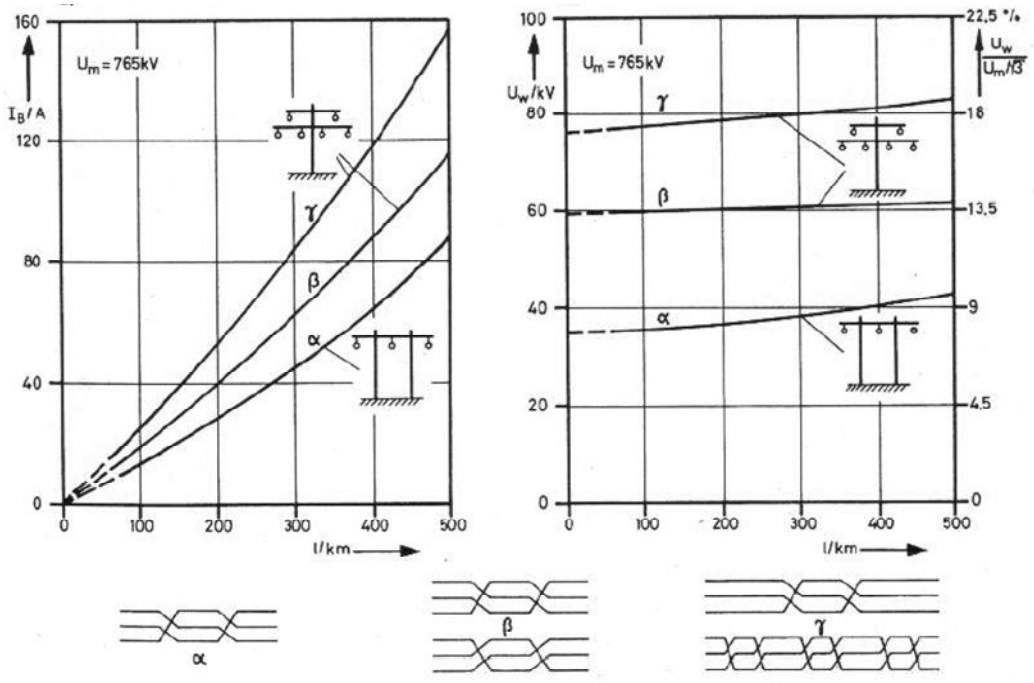

Figure 2.3.5 Influence of line configuration and transposition type on secondary arc current for 765 kV lines [11]

For double circuits at 765/800 kV, the secondary arc current magnitudes more than double over those for single circuits at the same voltage. This increase in secondary arc current is also observed by Haubrich et al as shown in figure 2.3.5 for transposed lines and a triangular phase configuration [11]. The difference in magnitude of the single to double circuit is as great in this case and is possibly attributable to different phase configurations and transposition practices. In Japan, secondary arc currents of 150 A with an extinction time of 4 seconds were estimated based on experimental data and the decision was made to use high speed ground switches (HSGS) as discussed later [17] [18].

2.3.3.1 Experience with SPAR schemes in Brazil

Shunt compensated EHV overhead transmission lines are normally very long, with an important bulk transmission function, playing an important role with respect to the transmission grid's reliability.

The single-phase scheme causes relatively small switching overvoltages. However, the extinction of the secondary arc due to a failure from phase to ground demands greater dead times in the auto-re-closing scheme (in the range of 0.8 to 1.5 seconds). On the other hand, the three phase auto-re-closing scheme generally causes much greater switching transient overvoltages than in the prior condition, but the duration of idle time can be greatly reduced in the case of the 3 phase auto-re-closing feature (around 300 to 700 milliseconds), since the capacitive couplings among phases observed in the single-phase scheme do not exist.

Application of fast TPAR schemes (idle-times below 500 ms) is important in power systems where stability problems occur, due to the disturbance caused by the fault

application and the tripping of the faulted line (during the idle-time of the auto-re-closing scheme operation). Also, due to the same reason, the SPAR schemes can be successfully used in such cases, or in poor-meshed transmission systems. Attention must be given to SPAR application in the vicinity of HVDC links, due to the unbalances imposed upon voltage and current during the opening of the faulted phase.

Secondary arc extinction is the most important concern on single-phase auto-re-closing. Due to its complex behaviour characteristics, it is quite often analyzed by extremely generalized criteria or simplified methods that may lead to mistaken conclusions or non-optimized solutions for single-phase re-closing implementation.

In Brazil, the maximum RMS value of the secondary arc current considered in the planning evaluation studies for applying single phase auto-re-closing is below 50 A. This criterion for secondary arc limiting value is used to determine the ohmic value of the neutral reactor's impedance during the design stage of the transmission line under planning investigation.

It is worth to mention here that this secondary arc current RMS value is always considered as a compromise with the generated TRV after the clearing of the secondary arc current in the location of the phase-to-ground fault. This compromise is related to a high probability of success in clearing the short-circuit only opening the faulted phase and takes into account the relationship between the secondary arc current RMS value versus the first peak of the generated TRV. This relationship is defined by means of a reference curve, calculated considering a conservative approach obtained by means of typical single-phase auto-re-closing performance tests (Refer to figure 2.3.6).

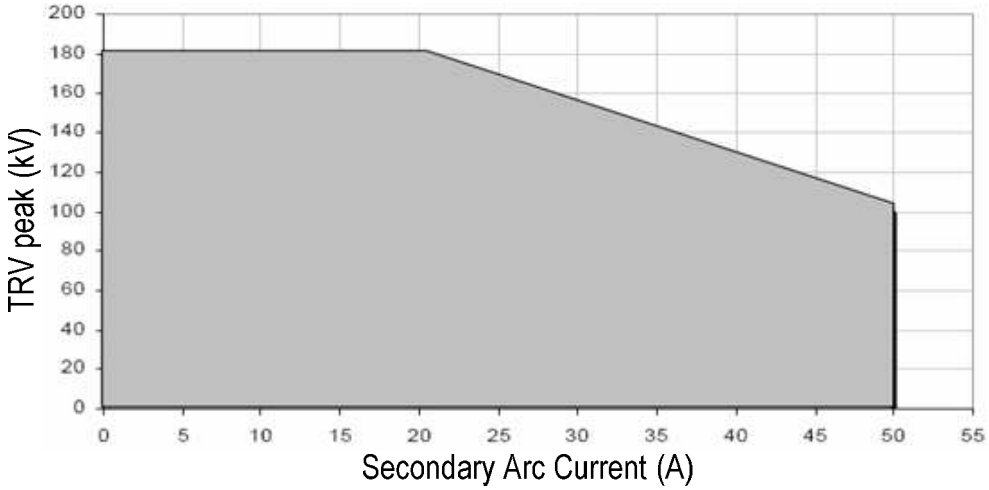

Figure 2.3.6 Correlation between the secondary arc current (RMS value) versus the first peak of the generated TRV in the EHV system from 230 kV upon 800 kV

Therefore, if during the planning studies 50A is considered as the value for the maximum secondary arc current, the accepted TRV peak value is lower. If one considers the maximum value for the secondary arc current to be below this value of 50 A the accepted TRV first peak value may be higher, according to the curve shown above in figure 2.3.6.

Generally the Brazilian overhead transmission lines using single-phase auto-re-closing at voltage levels of 230 kV, 345 kV and 500 kV, consider 40 A as the maximum value for the secondary arc current for planning purposes. This limited value is ensured by definition of the ohmic value for the neutral reactor impedance.

Regarding the dead time (idle-time) for re-closing the faulted phase, it is considered to be in the range of 0.8 to 1.2 seconds. This definition is obtained during the planning studies using suitable tools for proper electromagnetic performance evaluation analysis (such as EMTP, ATP or RTDS).

For fully transposed transmission lines, when clearing phase-to-ground faults without opening the other two non-faulted phases, as stated in the first TB 362, conventional 4-legged shunt reactors are often used to limit the secondary arc current maximum values during the operation of single phase auto-re-closing schemes. The 4-legged shunt reactor is very reliable in terms that the recovery voltage at the faulted point will not cause the reignition of the arc, resulting in auto-re-closing failure.

In the Brazilian national grid, all lines using the single-phase auto-re-closing feature are fully transposed and, therefore, the usage of the conventional 4-legged shunt reactor is quite sufficient to provide the proper conditions for clearing line-to-ground faults.

The conventional 4-legged shunt reactor is the normally used shunt reactor bank (a three phase unit or a bank of three single phase units) with the addition of a 'neutral reactor', as it is usually called in Brazil. In this application, beyond the normal roles of the shunt reactor (control of steady state voltage profile, mitigation of transient and temporary overvoltages), it plays an additional role, with the crucial help of the neutral reactor, for limiting the secondary arc current maximum values during the operation of single- phase auto-re-closing schemes.

The only difference in terms of the shunt reactor used in such 4-legged configuration, compared to the common one used only for voltage control purposes, is related to the insulation of its winding. The insulation level of the 4-legged one has to be higher in comparison with the common shunt reactor, since the introduction of the fourth reactor leg (neutral reactor) demands the increase of LIWV and SIWV of the neutral point of the shunt reactor connected to the line phases, from near zero to a value in the range of few hundreds of kV (depending on the nominal voltage level and other parameters related to the transmission line design).

2.3.3.2 AEP experience of modified shunt reactor

As stated before, when a single line-to-ground (1LG) fault occurs on a transmission line, the line circuit breakers are single-pole tripped to clear the faulted phase.

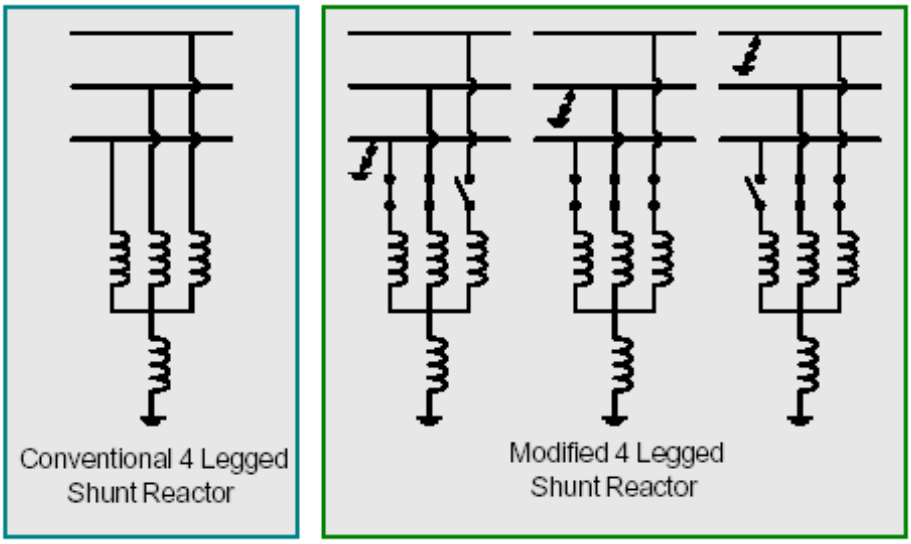

Figure 2.3.7 Schematic diagrams of a conventional 4-legged shunt reactor bank and the modified 4-legged shunt reactor bank used on AEP non-transposed lines

A modified 4-legged shunt reactor for untransposed transmission lines was proposed and installed on AEP 765 kV lines in late 1970s [19]. This shunt reactor configuration, shown in Figure 2.3.7, effectively compensates unequal phase-to-phase line capacitances of the untransposed lines. It should be also mentioned that such technique [19] can also be utilized for double-circuit transmission lines, if necessary.

Field tests, by applying line-to-ground faults, have been conducted in order to analyze the secondary arc current behavior including its extinction process. The actual field test results obtained by AEP on the 765 kV lines and by Russia (former Soviet) on the 750 kV and 1200 kV transmission lines are presented in figure 2.3.8 [14, 20-22]. The secondary arc currents in this figure are given in *rms* values except for the 1200 kV test data which are identified by the peak values (their *rms* values are unknown). The data presented in this figure allow estimation of the re-closing time as a function of the secondary arc current. At the same time it should be stated that the number of the reported field tests with higher secondary arc currents is very limited especially when the dispersion of the secondary arc extinction time is considered.

The main observations from the mentioned above field tests are summarized below.

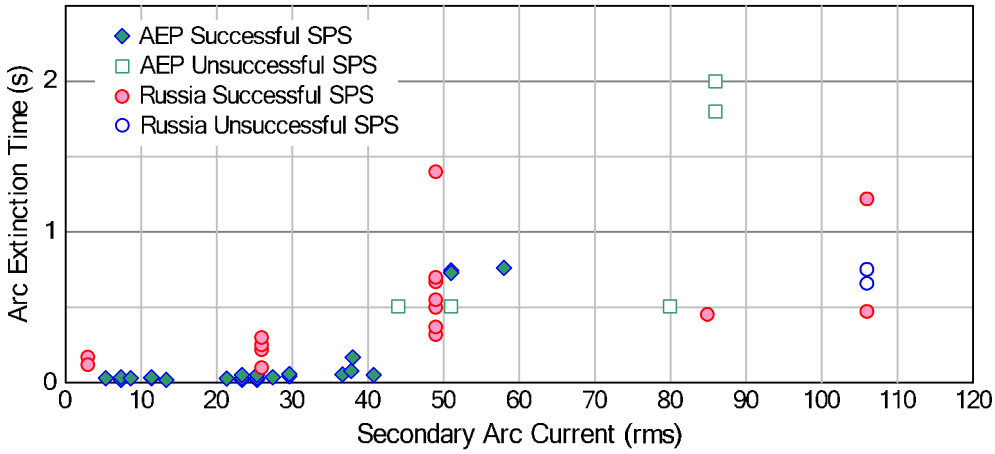

Figure 2.3.8 Secondary arc extinction time versus secondary arc current for 750 kV, 765 kV and 1200kV transmission lines

The waveform of the secondary arc current changes during the arc burning process and usually is quantified by its calculated ***rms*** value at the fundamental frequency component. The secondary arc current ***rms*** values during the AEP and Russia tests including unsuccessful re-closings reached 86 A ***rms*** and 49 A ***rms*** respectively [20, 22]. The single-phase re-closing tests on a 1200 kV UHV line (500 km long) were performed without and with neutral reactors. Without neutral reactors the secondary arc current was 106 A ***rms***. In four of these tests the arc extinction time varied from 0.48 second to 1.22 seconds. In three of other tests, the arc did not extinguish in 0.67 through 0.76 seconds, because that the line was shunted to ground before arc extinction [10]. With the neutral reactors the secondary arc current was 64 A ***rms*** and the arc extinguished in about 0.47 second [14].

The recovery voltage and its rate of rise after the secondary arc interruptions might significantly affect the arc sustainability and therefore its extinction time.

Primary fault current seems to influence the arc extinction. For example, there is a large dispersion in the extinction time (0.33 to 1.42 seconds) for the 49 A ***rms*** current in the Russia tests. That may be explained by the fact that the secondary arc was initiated with wires, dropped on an already opened phase (i.e. without primary fault current). The extinction time is different with the presence of the metal particles in the 49 A ***rms*** arc path, as opposed to normal cases, starting with thousand of amperes of primary fault currents.

The recovery voltage on the faulted phase, after the secondary arc extinctions, influences the secondary arc extinction process as well. The recovery voltage for a shunt reactor compensated line builds up in a beat, oscillating process and usually can be described by a combination of two main transient frequency components: one close to system frequency and another one, namely the modulating frequency around a few Hertz. Figure 2.3.9 shows the secondary arc current I_s and the recovery voltage V_r for a single-phase re-closing test on a 765 kV shunt compensated line [21]. The secondary arc current in this test was equal to 70 A ***rms***, where the faulted phase re-closing in 0.5 seconds was unsuccessful. During this test the secondary arc interrupted and re-struck twice, the first time after 8.7 ms at 90 kV and the second time in 10.5 ms after the second interruption at 110 kV flashover voltage.

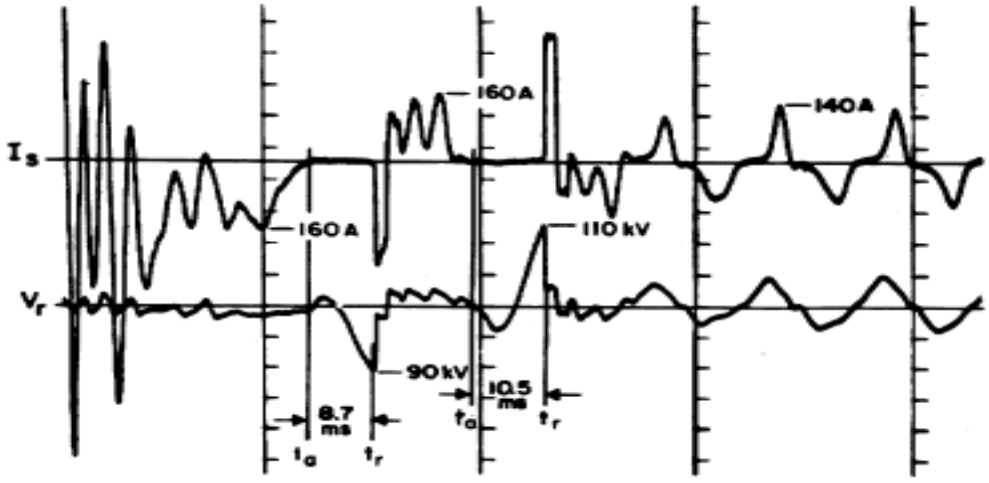

Figure 2.3.9 Secondary arc current and recovery voltage during an unsuccessful single-phase re-closing test on a 765 kV line

The arc re-strikes allow to estimate the air gap withstand voltage capability as a function of time from the last secondary arc current interruption. The re-strike voltage V_r as well as withstand voltage V_g during the secondary arc extinction process for two series of tests on 765 kV lines are presented in figure 2.3.10.

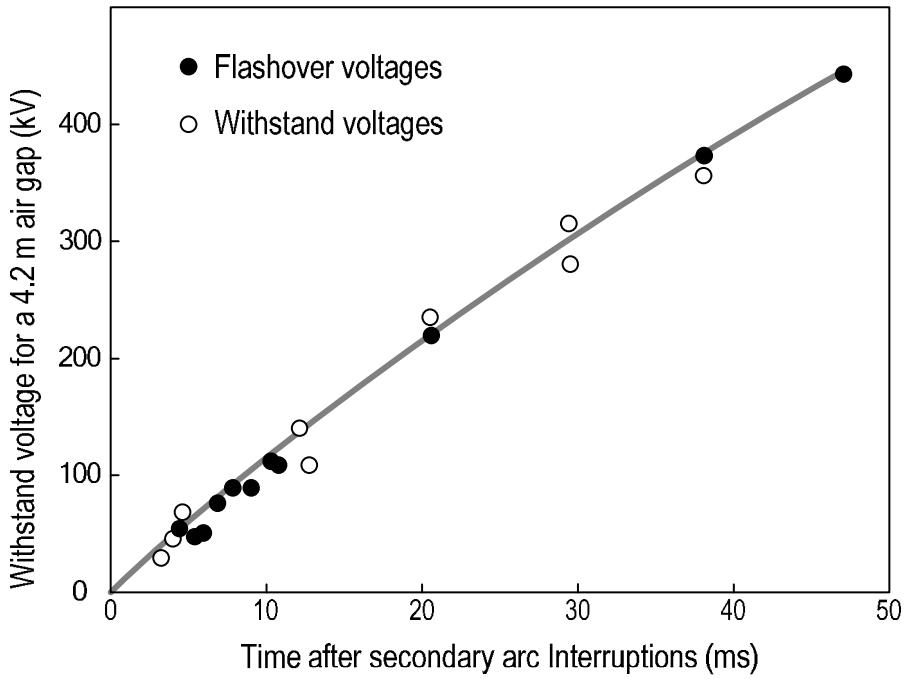

Figure 2.3.10 Withstand voltage characteristic for a 4.2 m air gap after secondary arc Interruptions: Solid dots - flashover voltages, Circles - withstand voltages

The test data in this figure illustrate relatively small deviation of the gap re-strike voltage V_r in respect to the recorded gap withstand voltage Vg for up to 50 ms from the arc interruptions. The results of these tests suggest that the dependency of the average between V_r and Vg voltages versus time shown in figure 2.3.10 might be treated as a 50% air gap flashover voltage characteristic following the secondary arc current interruptions. The rate of increase of the mentioned above air gap withstand capability for this series of tests equals approximately 10 kV/ms for the first 40 ms.

In summary, the presented data on the secondary arc extinction time for the 750 kV – 765 kV and 1200 kV transmission lines might be used as a guide for single-phase switching application on UHV lines.

2.3.3.3 Eskom 800 kV Auto Re-close Philosophy

If the fault is single-phase, the circuit-breakers will trip the affected phase and will re-close after 1 second. If the fault is not cleared when the circuit-breakers close, the circuit- breakers will trip all 3 phases. After about a further 10 seconds (circuit-breaker spring rewind or recharge time), the circuit-breakers will re-close (stronger end first and weaker end after synchronism has been confirmed). If the fault is still not cleared the circuit-breakers will trip and will lock out.

If the fault is a multi phase fault, the circuit-breakers will trip all 3 phases. After 3 seconds the circuit-breakers will re-close. If the fault is not cleared the circuit-breakers will trip and lock out.

In addition to this philosophy the following sequences also exist

If the system is selected to “3 pole” then the sequence is as follows:

The circuit-breakers will trip all 3 phases for all fault types and will re-close after 3 seconds (stronger end first and weaker end after synchronism has been confirmed). If the fault is still not cleared, the circuit-breakers will trip and will lock out.

If the system is selected to "1 pole" then the sequence is as follows:

If the fault is a single-phase fault, the circuit breakers will trip the affected phase and will close after 1 second. If the fault is not cleared when the circuit-breakers close, the circuit-breakers will trip all 3 phases and will lock out. If the fault is a multi phase fault, the circuit-breakers will trip all 3 phases and will lock out.

All of Eskom's 800 kV lines are shunt compensated by single phase reactors with the compensation factor being approximately 70 % to manage reactive power flow. Extensive simulation studies are done to optimise the neutral grounding reactor needed to limit the secondary arc current and recovery voltage to values that will generally allow a high rate of successful single-phase re-closing operation.

Figure 2.3.4 includes the simulation results for the recovery voltage and the secondary arc current on an 800 kV line for single-phase faults on the different phases and at different locations on the line. The neutral reactor was varied and the optimum size was found to be 1.1 H. For this neutral reactor the secondary arc current and recovery voltage are kept to a minimum, which greatly increases the chances for a successful single-phase auto re-close.

2.3.3.4 Discussion

As noted earlier, the secondary arc extinction process is complex and is related to its non-uniformity as explained by Rashkes [23]:

"*Non-uniformity of the secondary arc affects its extinguishing process. If an extinguishing were reached through the elongation of uniform arc column, unsuccessful attempts of extinguishing would not be observed, only the final single extinguishing. In numerous field tests we observed unsuccessful attempts of extinguishing impossible for uniform columns.*

In addition to usual recording of current and voltages we used in these tests speed filming that revealed spots with different brightness along the arc column at each extinguishing attempt that could be explained by internal exchange of energy between parts of the column. As a result, the temperature and conductivity drop in some short parts of column whereas other parts still are hot. The number and length of dark spots fast increase with time, and if the attempt is unsuccessful the current flows again and the channel becomes bright.

Elongation of the arc column with time also helps to reach the extinguishing, so at strong wind the extinguishing time drops. But from this filming it became evident also that the elongation observed was less than it would be necessary to extinguish current through the uniform arc column."

Since the field experience of secondary arc extinction in UHV lines is rather limited, working groups within SC A3 will continue to collect information on secondary arc extinction time and its dependence on the arc current and the recovery voltage as well as the effects of relevant parameters such as line design, the primary fault current, wind velocity and air temperature.

Figure 2.3.11 shows a secondary arc at the instant of extinction. The fault was initiated across a post insulator and between two hoops, the lower of which can be clearly seen. The non-uniformity discussed above is very evident.

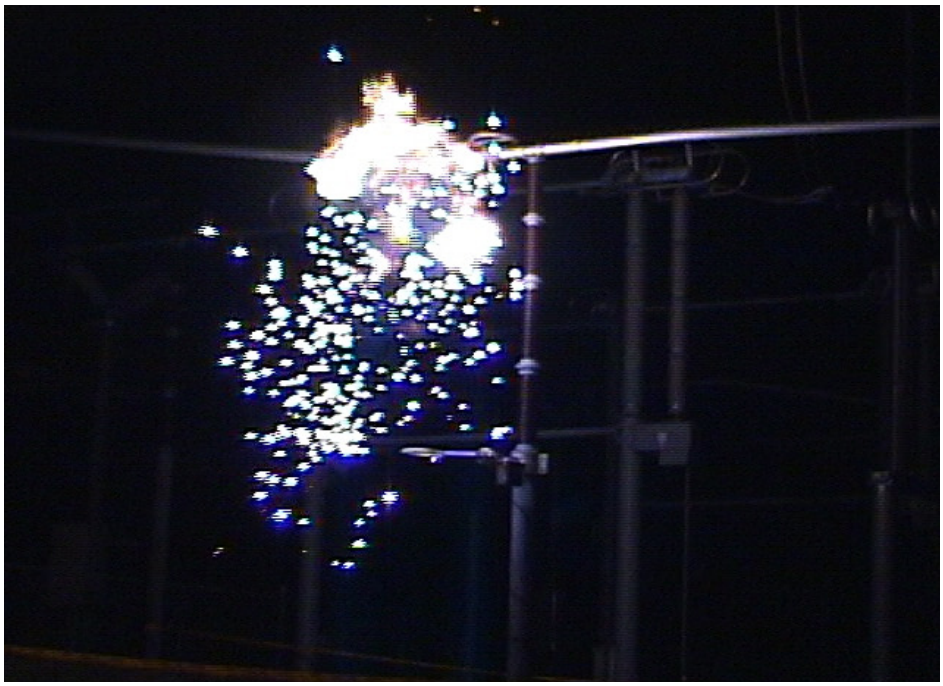

Figure 2.3.11 Secondary arc at instant of extinction (Courtesy of BC Hydro)

Present design practices have a history of success and the same principles can be extended to UHV applications. Simulation using EMTP is acceptable to determine the prospective secondary arc current, however, accurate determination of the arc extinction time remains elusive. Calculation of the arc extinction has been attempted but does not address the statistical nature of the events [24]. Also a further complication is the effect of reignitions given the conclusions from the BC Hydro tests in this regard.

2.3.4 Background of technical requirements for HSGS

High Speed Grounding Switches (HSGS) or High Speed Earthing Switches (HSES) were applied on both ends of 550 kV transmission line in the USA and successfully demonstrated secondary arc extinctions in the field with imposed duties of 700 A (inductive) for first switch to open and 120 A (capacitive) for the second switch to open [25].

In Korea, HSGS are installed on both ends of 800 kV double-circuit transmission lines with a line length longer than 80 km (single end of lines with a line length shorter than 80 km) and 22 successful high-speed multi-phase re-closings for the period of 2003-2007 have been experienced.

UHV systems with vertical tower configurations of double-circuit OH-lines in Japan are equipped with HSGS to achieve high-speed single and multi-phase re-closing considering various faults conditions such as 1LG, 2LG, 3LG and 4LG.

2.3.4.1 BPA specifications for HSGS

The specifications of induced current interrupting conditions for HSGS installed in BPA 550 kV transmission lines are shown in Table 2.3.3. The first switch to open has a small inductive current interruption duty with TRV peak time of 1 ms, while the second switch to open has a small capacitive interruption duty with TRV peak time of 8 ms [25].

Table 2.3.3 BPA specifications for 550 kV HSGS

	First Switch to Open (Inductive)	Second Switch to Open (Capacitive)
Interrupting Current	700 A	120 A
Peak Recovery Voltage, E2	200 kV peak	260 kV peak
Time to E2	1 ms	8 ms

2.3.4.2 TEPCO specifications for HSGS

Untransposed, double-circuit OH-lines with vertical tower configuration are commonly applied in Japan. A high-speed multi-phase re-closing scheme is used for power systems such as a 500 kV system in order to achieve a secure stable power supply when a fault occurs on the lines. This scheme treats the double-circuit line as one system. If at least two different phase lines are healthy among the six phases (2 circuits, each with three phases), only the faulted phases are tripped and re-closed separately as shown in figure 2.3.12.

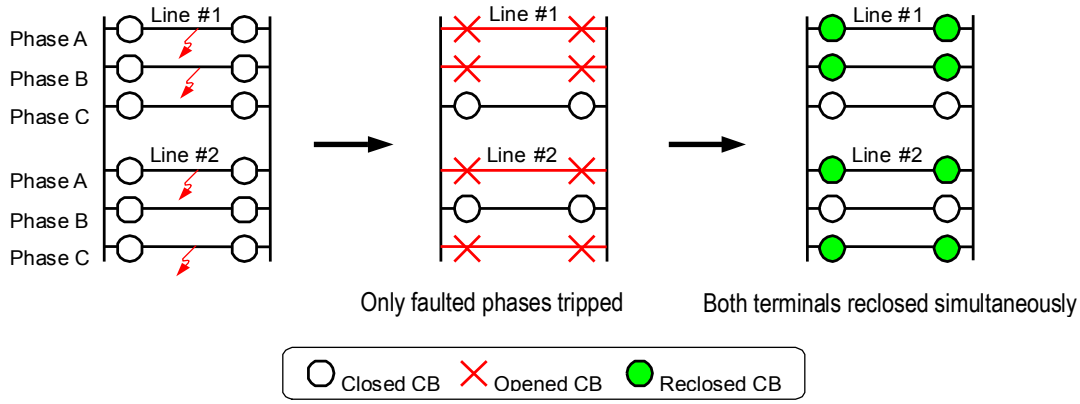

Figure 2.3.12 Example of a trip-re-close sequence by high-speed multi-phase re-closing scheme

This high-speed multi-phase re-closing scheme with the re-closing time around one second is also indispensable for the UHV system to secure the system stability. However, the secondary arc current induced from healthy phases is sustained for longer due to higher voltage and larger capacitance of the UHV lines and either 4-legged shunt reactor schemes or HSGS are employed to minimize the duration of the secondary arc in UHV systems.

In the case of double circuit transmission lines, it is difficult to choose an optimal reactor to effectively minimize the secondary arc extinction time for various fault conditions and so it was decided to employ HSGSs that can extinguish the secondary arc quickly. Furthermore, the UHV systems in Japan do not have any shunt reactors to control the system voltage, which also leads to the conclusion to choose the HSGS for multi-phase re-closing scheme. HSGS specifications are summarized in Table 2.3.4. [17] and the technical background for the specifications is described below.

Table 2.3.4 Specifications for HSGS in Japan

		Basic interruption		Delayed current zero interruption	
		(1)	(2)	(3)	(4)
Electromagnetic induction current interruption	Interruption current (A)	5780 (rms)	6940 (rms)	3500 (mean)	7830 (mean)
	TRV peak value (kV)	640	410	170	65
	Rate of rise of TRV (kV/μs)	0.79	1.15	0.26	0.46
	Arcing time (ms)	-	-	80 +Ta_{min}	80 +Ta_{min}
Electrostatic induction current interruption	Interruption current (A)	1160 (peak)	520 (peak)	3500 (mean)	7830 (mean)
	TRV peak value (kV) (1 – cos) waveform	900	700	570	390
	Arcing time (ms)	-	-	80 +Ta_{min}	80 +Ta_{min}
Reference (Corresponding line length)		70- 200 km	40-70 km	200 km	40 km

(Note) Ta_{min}; Shortest arcing time in basic electromagnetic induction current interruption.

(A) Analytical conditions (See table 2.3.5 and figure 2.3.13)

Line lengths of 40 km to 200 km are considered, corresponding to the minimum and maximum lengths planned in Japan. The power flow of 13 GW is considered as approaching the maximum level that can be transmitted regarding the system stability. As for the fault conditions, single-phase line fault to ground cases of the double circuit lines (1LG, 2LG, 3LG and 4LG) are considered, since the multi-phase re-closing scheme is applied as described before.

Furthermore, as interruption failures of HSGSs would take transmission lines out of service for a long time, a successive ground fault due to multiple lightning was also considered. The condition considers a 1LG fault followed by another 1LG fault during an HSGS operation interrupting the first 1LG. The successive fault was limited to this "1LG + 1LG" whose probability of occurrence is small but which cannot be discounted.

Table 2.3.5 Analysis conditions

	Analysis conditions
Line length/ Power flow	Line length; 40 - 200 km (Untransposed, double-circuit, The maximum length was changed from 210 km at the initial stage to 200 km), Power flow; 13 GW
Back system	Simulated by a lumped impedance that makes a short-circuit current of the UHV side bus to be 50 kA.
Fault condition	Single fault; 1LG, 2LG, 3LG and 4LG, Successive fault; 1LG + 1LG

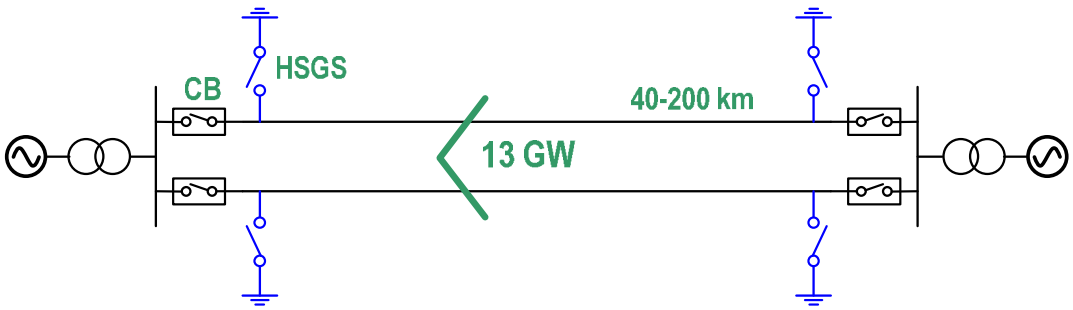

Figure 2.3.13 UHV double circuit system with HSGSs

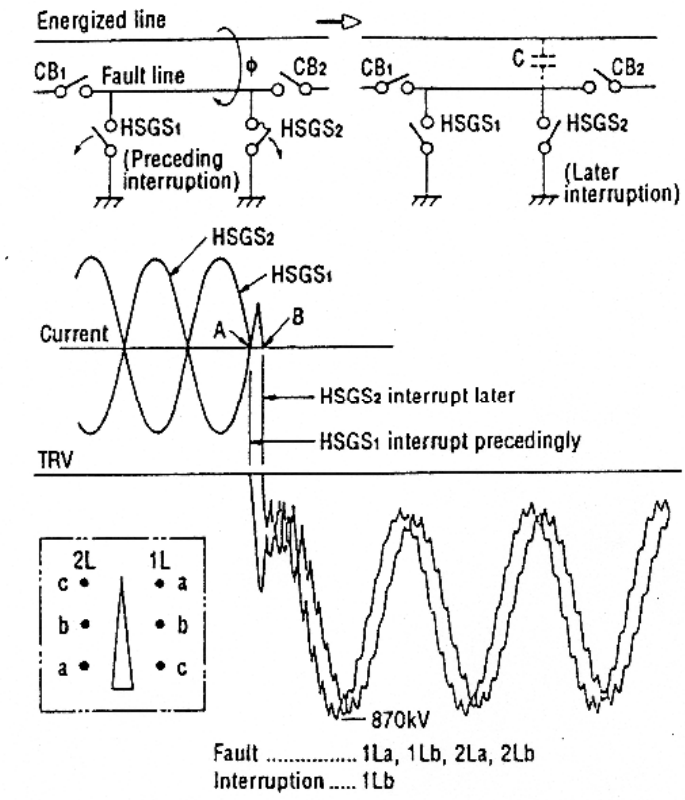

Figure 2.3.14 Example of interruption waveforms by HSGS

(B) Normal interruption duties (without the delayed current zero interruption)

Figure 2.3.14 shows a typical example of current and voltage behaviour of HSGS interruptions at each end of the line.

Figure 2.3.15 summarizes the analytical results of the line length dependence of TRVs and induced currents including a successive ground fault case. It is assumed that a successive ground fault occurs at the remote end of the line, which corresponds to the case with the largest electromagnetic induction current.

<Electromagnetic induction current interruption>

In the case of the successive ground fault, the electromagnetic induction current and TRV, affected by the fault current, become roughly twice those of single fault case. Even though this tendency cannot be seen from figure 2.3.15, it can be obtained from the analytical results for 250 km lines with 13 GW condition at the first stage planning.

As the line length increases, the primary fault current becomes smaller resulting in the induction current (I_m) and the rate of rise of TRV $(dV/dt = Z \times d(I_m)/dt)$ becoming smaller. However TRV peak voltage (TRV_m) becomes larger because it takes more time until the travelling wave returns. In the case of 1LG, the effect of the line length is relatively small.

<Electrostatic induction current interruption>

As the line length increases, electrostatic induction current (I_c) and voltage (TRV_c) become larger. The influence of the successive ground fault is limited.

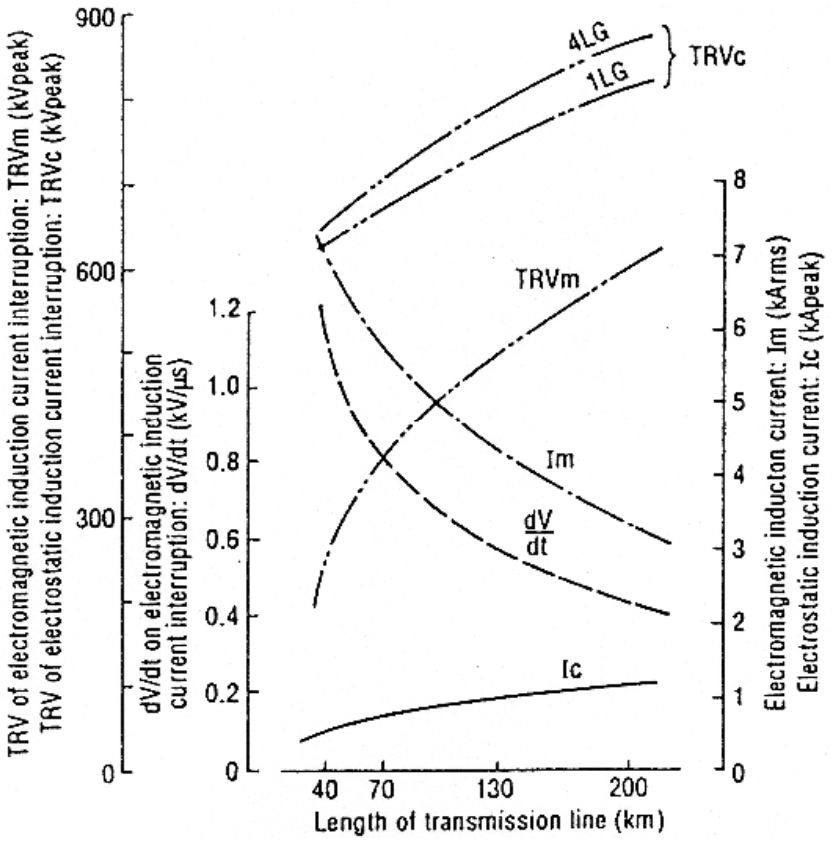

Figure 2.3.15 Analytical results of TRV and induced current as a function of line length

Figure 2.3.15 (See also tables 2.3.5 and 2.3.6) can provide two different interruption duties corresponding to line lengths of 70-200 km and 40-70 km. The line length boundary of 70 km was selected considering the severity of the TRV and the currents.

Table 2.3.5 Analysis results: Electromagnetic induced current interruption

Line length (km)	Interruption current (Arms)	TRV	
		Rate of rise (kV/μs)	Peak value (kV)
200	3,350	0.45	636
130	4,310	0.58	533
70	5,780	0.79	406
40	6,940	1.15	282

Table 2.3.6 Analysis results: Electrostatic induced current interruption

Line length (km)	Interruption current (A peak)	TRV peak value (kV)
200	1,160 (375kHz)	870
130	930 (580kHz)	800
70	710 (1,070kHz)	690
40	515 (1,870kHz)	656

(Note) Frequency in the bracket shows that of the interruption currents

The duties for an electromagnetic induced current interruption are specified in table 2.3.7 and those for an electrostatic induced current interruption are specified in table 2.3.8.

Table 2.3.7 Specifications of electromagnetic induced current interruption duties

Test condition	Interruption current (Arms)	TRV	
		Rate of rise (kV/μs)	Peak value (kV)
Duty (1)	5,800	0.79	640
Duty (2)	7,000	1.15	410

Table 2.3.8 Specifications of electrostatic induced current interruption duties

Test condition	Interruption current (A peak)	TRV peak value (kV)
Duty (1)	1,200	900 (1- cos)
Duty (2)	520	700 (1- cos)

(Note)Interruption current for (1) Maximum case (large arcing time) and (2) minimum case (small arcing time) were selected.

2.3.4.3 Delayed current zero interruption

When a successive ground fault occurs, there is a possibility of delayed current zero phenomena depending on the fault timing, fault location, and power flow condition. The difference between phase angles of the induced current from the load current of the healthy phase and that from the short-circuit current of the second fault is roughly 180 degrees as shown in figure 2.3.16. In the worst case, this delayed current zero phenomena continue until the circuit breaker clears the successive fault. For this reason it was specified that the HSGS should withstand a long arcing time up to 80 ms without a current zero.

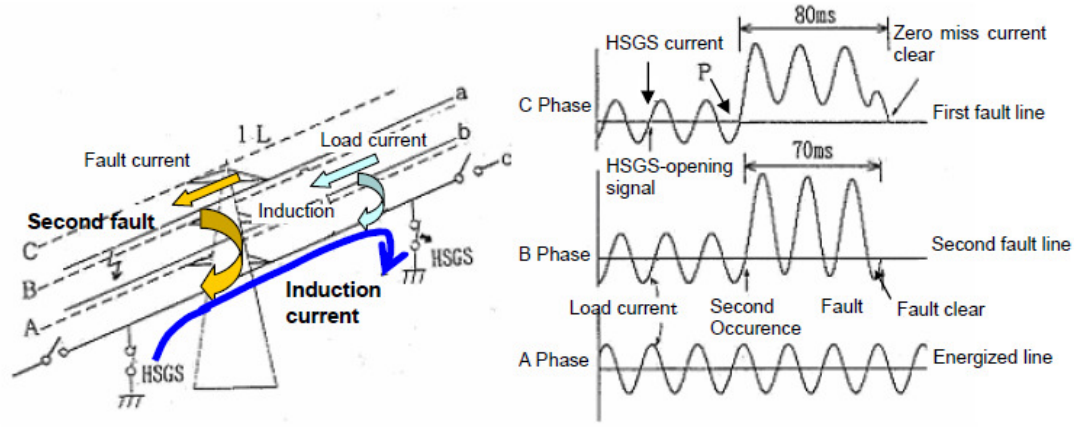

The severest case for HSGS in which a second fault follows just before HSGS breaks the electromagnetic induction current at point P.

Figure 2.3.16 Delayed current zero phenomena in HSGS

For delayed current zero interruption duties, (as summarized in Table 2.3.4) the severest condition for the maximum line length of 200km (3) and for the minimum line length of 40 km (4) were determined. The interruption currents were derived from the following equation as mean value. (Compare figure 2.3.17.)

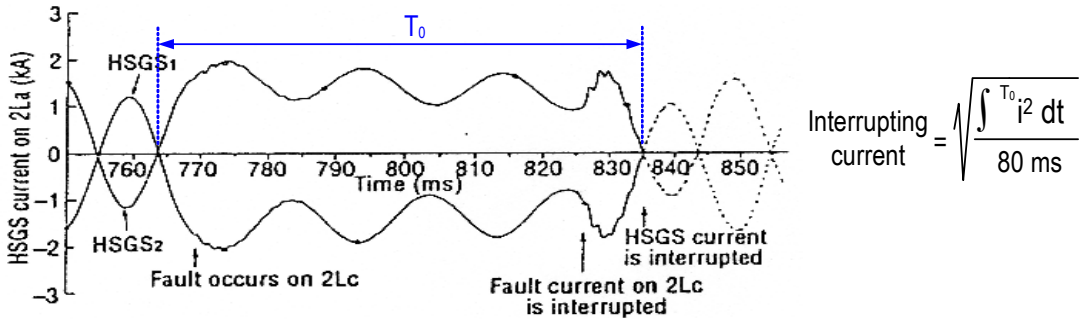

Figure 2.3.17 Definition of the interruption current for delayed current zero phenomena

2.3.5 Summary of technical requirements (HSGS)

Table 2.3.9 summarizes the technical requirements for HSGS applied to the UHV and EHV systems in the US, Korea and Japan.

Table 2.3.9 HSGS requirements

	USA	Korea	Japan	Japan*
Highest voltage	550	800	1100	1100
Interrupting current (A)	700	8000	7000	7830
TRV peak (kV)	260	700	900	570
RRRV (kV/μs)	0.1	1.3	1.15	0.46

*Duty for delayed current zero interruption with the arcing time of 80ms+minimum arcing time

2.4 Out-of-phase

2.4.1 Introduction

CIGRE WG A3.22 in cooperation with Study Committees B5 and B3 have explored (a) CIGRE experience on the out-of-phase conditions, (b) system stabilization schemes used to avoid the out-of-phase conditions and (c) detection methods of out-of-phase condition and timing of opening command for out-of-phase interruption by a protection relay.

CIGRE Session paper B5-207 (2006) [26] shows some experience on power system blackouts. Some out-of-phase (out-of-step) conditions seem to have occurred even though the details of these events are unknown. However, Japan has never experienced out-of-phase interruption, because system stabilization schemes (special protection systems) are employed to avoid out-of-phase conditions before protection relays detect the out-of-phase angle larger than 180 deg.

Table 1 of [26] shows time of the slip interval from normal to 180 deg and time from 180 deg to 360 deg. Values range from 0.20 to 0.54 s during a 180 deg change of the phase angle. (The slip interval is about 400 to 1080 ms per turn.) The out-of-phase angle can be evaluated as 126-160 deg when the out-of-phase interruption is completed 60 ms after the detection. The values are expected to be larger than 105 deg, which corresponds to the specified recovery voltage (2E) under out-of-phase condition in effectively earthed neutral system.

Since out-of-phase phenomena is not peculiar to only UHV systems a wider analysis of this topic within CIGRE may be warranted.

2.4.2 Background of technical requirements

In the case of out-of-phase interruption a severe TRV is generated since the voltage oscillation of source and load side cause large voltage difference across the contacts. In the case of switching at substations with long overhead lines of similar length the TRV may become particularly severe.

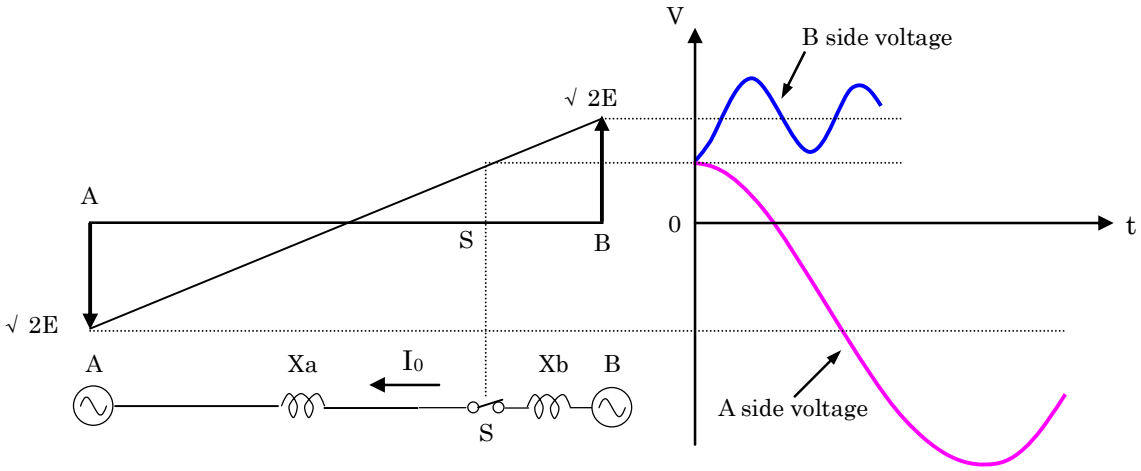

Io =2E*sin(½θ)/ (Xa + Xb)

=2E/ (Xa + Xb) (When θ=180 degree)

Figure 2.4.1 Concept of out-of-phase interruption

Without opening resistors, the phase difference between breaking current and voltage is 90 degree and AC voltage at the moment of interruption is at its peak. At the time of transient voltage peak after interruption, the AC component of voltage is after its peak. With large back impedances (in other words a network of small short circuit current) the frequency of oscillation of TRV tends to be low and therefore the AC component becomes small at the time of TRV peak. This means the TRV peak itself becomes small.

2.4.3 Utilities' policies on out-of-phase duties

In the Italian network, switching operations under out-of-phase angles higher than 40 degrees are seldom experienced. This range of synchronism is kept under control by the out-of-step protection. Where this protection is not active the CB can operate only under the condition that no voltage is applied at one of the terminals.

Three 230 kV lines and one 500 kV line connect Manitoba with the U.S. transmission system. Out-of-step relays on these lines are set to trip for severe contingencies and island or isolate Manitoba from the U.S. network (e.g. double HVDC bipole trip in Manitoba resulting in more than 3000 MW generation loss). The relays are typically double blinders and are set to trip either for an out-of-step swing entering the blinders (from the right hand side) or leaving the blinders (left hand side). At these points, the angle across the breakers is not at the maximum 180 degree level. Despite this situation, a PSS/E case was built where the angle is 180 degrees and the resulting TRV, for inclusion in the 230 kV and 500 kV breaker specifications, was calculated using EMTP . This has resulted in a stronger than normal breaker being installed. The incremental cost of the stronger breaker is not significant. This approach assumes that proper islands will be created and breakers will be able to cope with such stresses.

This avoids random islands being created via zone 1 relay operation and minimises the risk of circuit-breaker damage.

At AEP, the out of step relays are generally set at 40 degrees with some exceptions that are at 65 degrees. However, for a proposed 765 kV line, AEP calculations show a requirement for operation up to 95 degrees out of phase meaning the relays may be set for 120 degrees in order to have a margin. In this case the main problem becomes the closing resistor energy dissipation requirement due to the large duration of prestrike. This, in combination with the resistor insertion time, makes the resistors good for only one operation before a long cool down time is required. This is not acceptable and there are ongoing investigations on this issue including the possible use of alternatives to switching resistors.

2.4.4 Interim reports and future investigation on out-of-phase

Preliminary conclusions from WG A3.22 studies relating to system separation on an UHV-line are as follows:

- I_{op} and RV are dependent on the out-of-phase angle that, for long distance transmission, may approach 180°.

- RRRV decreases with numbers of lines connected to the busbar.

- U_c is proportional to RRRV and to the line length and is thus proportional to I_{op} and is dependent on the number of circuits connected to the busbar.

- RRRV and U_c may reach values larger than the standard specification to IEC 62271-100, for instance when I_{op} is higher than 5 kA and/or the number of circuits is less than 3, and/or the line length is higher than 350 km.

- For an identical configuration an angle of, for example, 105° will lead to vakues of I_{op}, RRRV and U_c which are 20% lower than those for an out-of-phase angle of 180°,

- Since, in UHV-systems, k_{pp} will normally be close to 1.0 (with a maximum around 1.2), the voltage factor of 2.0 as specified in the Standards covers an out-of-phase angle close to 180°.

- I_{op} is defined to be 25% of the rated short-circuit current, while type tests are specified with a current of 25% and of 5%. For actual and foreseen system configurations 25% seems to be rather high and is to be considered as a maximum value or even beyond that.

- Not enough information is available yet to draw preliminary conclusions with respect to the amplitude factor of the TRV under out-of-phase switching condition

2.5 DC time constants

2.5.1 Introduction

Large power generators and large-capacity power transformers have high X/R ratios, which contribute to the increase in DC time constant in fault currents. EHV and UHV transmission lines employ multi sub-conductor bundles (sub-conductor with large-diameter) in order to reduce corona noise as well as increase transmission capacity. For example, UHV transmission lines use 8 conductors, 400–810 mm^2, depending on the allowable level of corona noise. The application of large multi sub-conductor

bundles increases the DC time constant (τ= L/R) because the reduction in resistance (R) exceeds the reduction in inductance (L).

2.5.2 Background of technical requirements

Table 2.5.1 summarizes analytical results of DC time constants calculated using various tower designs with different multi sub-conductor bundle used in different projects. The constants were obtained by a ratio of positive-sequence inductance to positive-sequence resistance of the lines. Special case time constants, in excess of the standard value of 45ms, were added in IEC 62271-100 based on a survey conducted by CIGRE WG 13.04. The special case time constant is 75 ms for rated voltages 550 kV and above which corresponds to the medium value of the constants, surveyed for 800 kV lines.

Table 2.5.1 DC time constant of short-circuit currents in EHV / UHV transmission lines

Maximum voltage (kV)	Conductors		DC time constant (ms)
	Size (mm^2)	Bundle	
Canada, 765 kV	686	4	75
USA, 800 kV	572	6	89
South Africa, 800 kV	428	6	67
Brazil, 800 kV	603	4	88
China, 800 kV	400	6	75
Russia, 1200 kV	400	8	91
Italy, 1050 kV	520	8	100
China, 1100 kV	500	8	120
Japan, 1100 kV	810	8	150
India, 1200 kV	774	8	100

2.5.3 Recommendations for specifications

It is expected that the DC time constant for UHV systems will be higher than the standard values due to utilization of multi sub-conductor bundles with a larger diameter besides the existence of large power generators and large capacity power transformers. The influences of the high DC component on test-duty T100a can be evaluated by the energy of the last major loop before the interruption, slope of current at the time of interruption and TRV characteristics and the results do not show any significant difference when the constant exceeds about 120 ms. Therefore, it is recommended to use a time constant of 120 ms for rated voltages higher than 800 kV.

References

[1] Second International IEC/CIGRÉ Symposium on Standards for Ultra High Voltage Transmission, New Delhi, January 2009, “System Impacts on UHV Substation Equipment”

[2] L. Jiming, C. Weijang, W. Shaowu, B. Lian-geng, X. Zutao, W. Xiaogang, H. Bin, Z. Bin; “Analysis on Overvoltages Related to the UHV AC Systems”,

Second International Symposium on Standards for Ultra High Voltage Transmission, Jan. 2009, India

[3] R. Hemmi, et. Al., “Evaluation of VFTO and its reduction by parallel resistor during switching operation of disconnecting switch in future UHV GIS insulated substations”, International Conference of UHV Power Transmission Technology, pp.460-466, 2006, Beijing China

[4] CIGRÉ Technical Brochure 336, December 2007, “Changing Network Conditions and System Requirements, Part II, The impact of long distance transmission”, CIGRE WG A3.13

[5] A. K. Lohkanin, V. S. Rashkes, et al., "Temporary Overvoltage and their Influence upon the Insulation Level of Equipment”, CIGRE SC 33 Session 1990, Report 33-209

[6] E. Zaima, et al., “System Aspects of 1100 kV AC Transmission Technologies in Japan: Solutions for Network Problems Specific to UHV AC Transmission System and Insulation Coordination”, IEC/CIGRE UHV Symposium 2007, Beijing, Report 2-1-1

[7] N. Knudsen, “Single Phase Switching of Transmission Lines Using Reactors for Extinction of the Secondary Arc” CIGRE Paper No. 310, 1962

[8] E.W. Kimbark, “Suppression of Ground-Fault Arcs on Single-Pole-Switched EHV Lines by Shunt Reactors” IEEE Transactions on Power Apparatus and Systems, March 1964

[9] K. Anjo, H. Terase and Y. Kawaguchi, “Self-Extinction of Arcs Created in Long Air Gaps” Electrical Engineering in Japan, Vol. 88, No. 4, 1968

[10] I.M. Bortnik, V.S. Rashkes et al, “1200 kV Transmission Line in the USSR: The First Results of Operation” CIGRE Paper No. 38-09, 1988

[11] H. Haubrich, G. Hosemann and R. Thomas, “Single-Phase Autore-closing in EHV Systems” CIGRE Paper No. 31-09, 1974

[12] L. Edwards, J.W. Chadwick, H.A. Riesch and L.E. Smith, “Single-Pole Switching on TVA’s Paradise-Davidson 500-kV Line Design Concepts and Staged Fault Test Results” IEEE Transactions on Power Apparatus and Systems, November/December 1971

[13] N.N. Belyakov, A.N. Komarov and V.S. Rashkes, “Results of Internal Overvoltages and Electrical Equipment Characteristics Measurements in the Soviet 750 kV Networks” CIGRE Paper No. 33-08, 1978

[14] N.N. Belyakov, V.S. Rashkes et al, “Application of Single-Phase Autore-closing in a Complex EHV Network Containing 1200 kV Transmission Lines” CIGRE Paper no. 34-207, 1990

[15] J.G. Kappeman, G.A. Sweezy, V. Koschik and K.K. Mustaphi, “Staged Fault Tests with Single Re-closing on the Winnipeg-Twin Cities 500 kV Interconnection” IEEE Transactions on Power Apparatus and Systems, March 1982

[16] F. Rahmatian, D. Peelo, G. Polovick, B. Sunga and J. Lehtimaki, “Optical Current and Voltage Sensors in EHV Series Capacitor Bank Application.” CIGRE SC A3 and B3 Joint Colloquium, Tokyo, 2005

[17] Y. Yamagata, et al, “Specifications and development of high speed grounding switch” Colloquium of CIGRE SC13, Report 1.3, September 1995, Florianopolis

[18] H. Mizoguchi, et al, “Development of an interrupting chamber for 1000 kV high-speed grounding switches” IEEE Transaction on Power Delivery, Vol. 13, No. 2, April 1998

[19] B. R. Shperling and A.J. Fakheri (A. J. F. Keri), “Single Phase Switching Parameters for Untransposed EHV Transmission Lines”, IEEE Transactions on Power Apparatus and Systems, Mar/Apr. 79

[20] A. J. Fakheri (A.J.F. Keri), T.C. Shuter, J.M. Schneider and C.H. Shih, "Single Phase Switching Tests on the AEP 765 kV System - Extinction Time for Large Secondary Arc Currents", IEEE Transactions on Power Apparatus and Systems, August 1983

[21] B. R. Shperling, A.J. Fakheri (A.J.F. Keri), C.H.Shih, B.J.Ware “Analysis of Single-Phase Switching Field Tests on the AEP 765 kV System”, IEEE Transactions on Power Apparatus and Systems, April 1981

[22] H. N. Scherer, Jr., B. R. Shperling, J. W. Chadwick, N. N. Beliakov, V. S. Rashkes, K. V. Khoetsian, “Single Phase Switching tests on 765 kV and 750 kV Transmission Lines”, IEEE Transactions on Power Apparatus and Systems, June 1985

[23] Chief Editor M.L. Levinshtein, “Processes at Single-Pole Reclosures in HV Lines” (Book in Russian), Energoatomizdat Publishing House, Moscow, 1991

[24] A. T. Johns, R. K. Aggarwal and Y. H. Song, “Improved Techniques for Modelling Fault Arcs on Faulted EHV Transmission Systems”, IEE Proceedings Generation, Transmission and Distribution, March 1994

[25] R.M. Hasibar, A.C. Legate, J. Brunke and W.G. Peterson “The Application of High-Speed Grounding Switches for Single-Pole Re-closing on 500 kV Power Systems”, IEEE Trans. On Power Apparatus and Systems, Vol. PAS-100, No. 4, April 1981

[26] D. Z. Meng, “Maintaining System Integrity to Prevent Cascading Blackout”, CIGRE Paper. B5-207, 2006

3 Equipment Requirements (Circuit Breakers)

This Chapter deals with the technical requirements for the switching duties of UHV circuit-breakers. Terminal faults, transformer limited faults (TLF), long line faults (LLF), short line faults (SLF), un-loaded line switching and opening resistors are discussed in order to provide enough background information for IEC standardization purposes.

3.1 Terminal Faults

The most relevant technical aspect for the specifications of short-circuit breaking tests is the inherent transient recovery voltage (TRV) that a circuit-breaker has to withstand. In the next sections, background information is given on the standard specification of TRVs for EHV circuit-breakers (3.1.1), on the particularities for UHV (3.1.2) and the recommendations for standard specifications (3.1.3). Some of the considerations given in 3.1.2 could also be applied at 800 kV and even below 800 kV, but this aspect is not further addressed.

3.1.1 Introduction

In the international standards, TRVs are described by two- or four-parameter envelopes with a number of characteristics, which form the basics of the TRV specifications. Under service conditions, the prevailing TRV envelopes should be less severe than those specified in the Standards, while for type tests the envelopes of the applied TRV wave-shapes should be not less severe than those specified in the Standards. In IEC Standard 62271-100 the characteristics have been specified for rated voltages up to and including 800 kV, but not yet for UHV voltages. In view of typical UHV network topologies and system parameters, the characteristics to specify TRVs will be addressed individually.

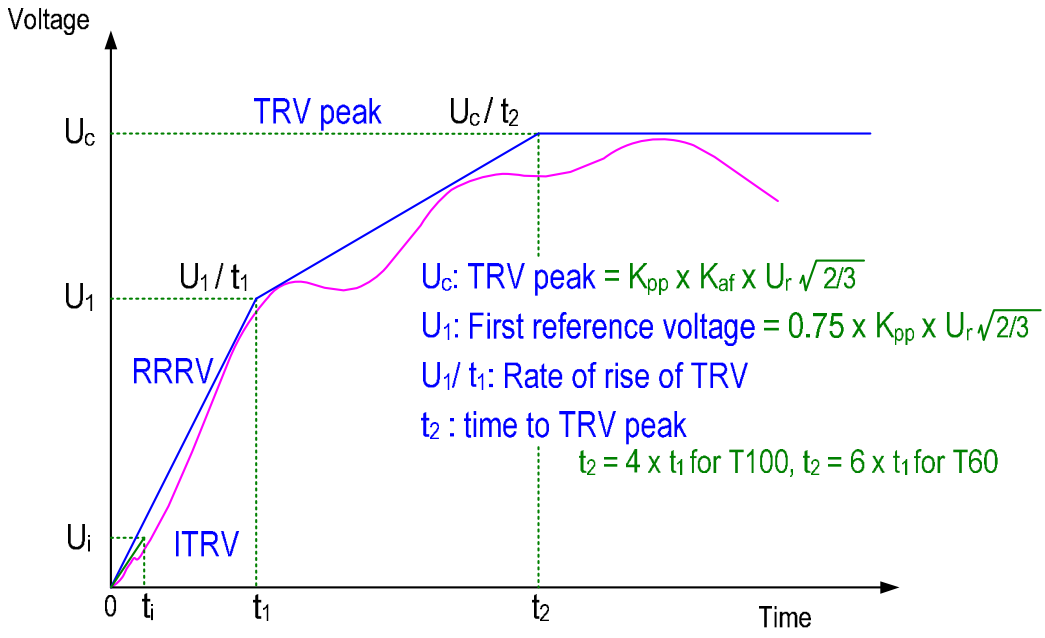

Figure 3.1.1 TRV by four-parameter expression

3.1.1.1 RV

The recovery voltage (RV) is the power frequency voltage that stresses the contact gap of each pole, after clearing the short-circuit current. A terminal fault is considered to be when one side of the circuit-breaker is short-circuited and connected to earth, while at the other side the system power frequency voltage will appear, including a shift of the system neutral voltage, caused by an unbalance in the short-circuit currents per phase. After short-circuit interruption of the first clearing pole, the remaining two-phase short-circuit current will cause a RV as large as $K_{pp} \times U_r / \sqrt{3}$ with k_{pp} being the first-pole-to-clear factor. This RV last until the second pole clears the short-circuit current, which normally occurs 3 to 5 ms after the first pole. Within a few ms the third pole will clear the remaining single phase to earth fault current and will bring back the balance between the phases of the system: the RV of the last clearing pole is Ur/√3, as, from this moment on, it is for the other two poles as well. The RV is an important characteristic to define other voltage related characteristics, but is also an important parameter for type testing as it is used to verify the dielectric performance of the circuit-breaker during the time interval after the clearing process. IEC 62271-100 stipulates that the RV has to be withstood during 300 ms after clearing.

According to IEC 62271-101 (Synthetic testing), clause 4.1, deviations from the requirements put forward in IEC 62271-100 are acceptable under the conditions that (a) during the first 2.0 or 2.5 ms (for 60 Hz or 50 Hz resp.) the instantaneous recovery voltage is higher than 0.95 k_{pp} p.u. and that (b) during the first 100 ms the instantaneous peak value of the recovery voltage is higher than 0.5 p.u.

The k_{pp} is depending on the power frequency system parameters X_0 and X_1 as follows: $k_{pp} = 3X_0/(X_1+2X_0)$ or $3k/(1+2k)$ with $k = X_0/X_1$. For OH-lines X_0 is roughly 3 times X_1 and for large power transformers X_0 is less than X_1, so that k_{pp} depends on the ratio of short-circuit current flowing through the OH-lines versus current flowing through the transformers. For networks with an effectively earthed neutral of the transformers, to the IEC Standard $k_{pp} = 1.3$ (in case of clearing a grounded three-phase fault).

3.1.1.2 RRRV, u_1, t_1

The initial part of the TRV envelope is a ramp function with certain steepness, known as the Rate of Rise of Recovery Voltage (RRRV). According to the IEC Standard 62271-100, the ramp function rises to a voltage equal to $0.75 \times RV = 0.75 \times K_{pp} \times U_r / \sqrt{2/3}$ (i.e. u_1). Physically, as long as OH-lines are involved, the initial part of the TRV is an over-damped response to the suddenly disappeared short-circuit current, which can be described by dI/dt. The response looks like a 1-exp function with an initial increase equal to $Z_{eq} \times dI / dt$; Z_{eq} being the equivalent surge impedance of the system at that location, thus determined by the number of OH-line circuits. IEC indicates the RRRV is standardized to 2 kV/µs for the terminal fault test duty T100 and to 3, 5 and 7 kV/µs for the test duties T60, T30 and T10 respectively.

The 1-exp function runs to an asymptote up to $K_{pp} \times E_0$ with an initial steepness equal to the RRRV. The 4-parameter envelope is defined by three parts, as shown in figure 3.1.1: the first part up to the point u_1/t_1, and the third part after u_c/t_2 and the second part in between. In figure 3.1.2, the envelopes belonging to an 1-exp function ($k_{af} = 1.0$) and belonging to $k_{af} = 1.4$ are given (the last one to be discussed later on).

Although E_0 depends on the contribution of the local and remote sources, in the Standards E_0 is chosen to correspond to the maximum system voltage U_r:
$E_0 = k_{pp} \times U_r \times \sqrt{2/3}$

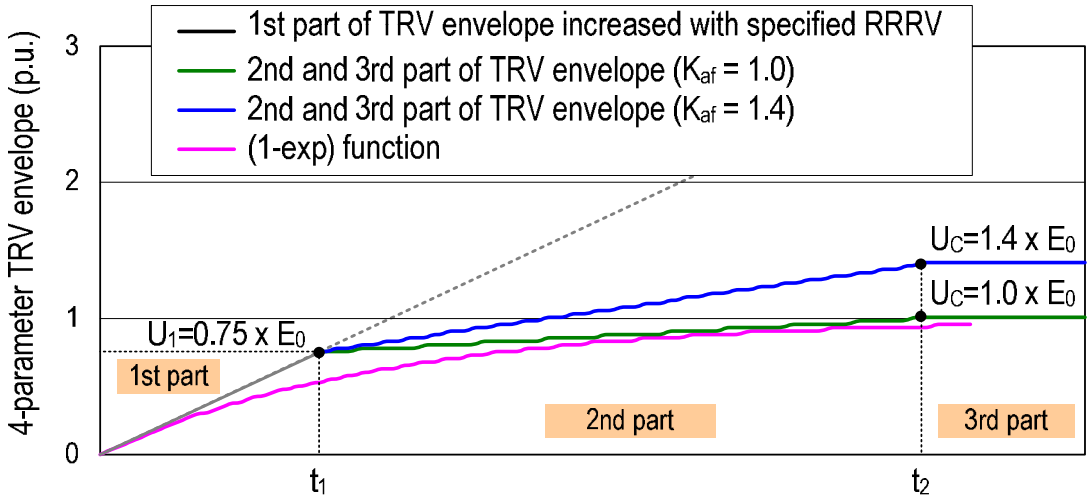

Figure 3.1.2 Four-parameter envelope

3.1.1.3 t_d, u', t'

At the very beginning of the TRV wave-shape there are some physical phenomena that have to be considered in addition to the 4-parameter description. Due to the capacitance of the busbar in the substation where the circuit-breaker that has to clear the terminal fault is located, a retardation in the ramp function, being the system response to the interruption of the fault current in that pole, will occur. This time delay t_d is defined as $Z_{eq} \times C'$ with C' as the capacitance of the busbar and all connected apparatus. For system voltages up to 800 kV it is specified as 2 µs.

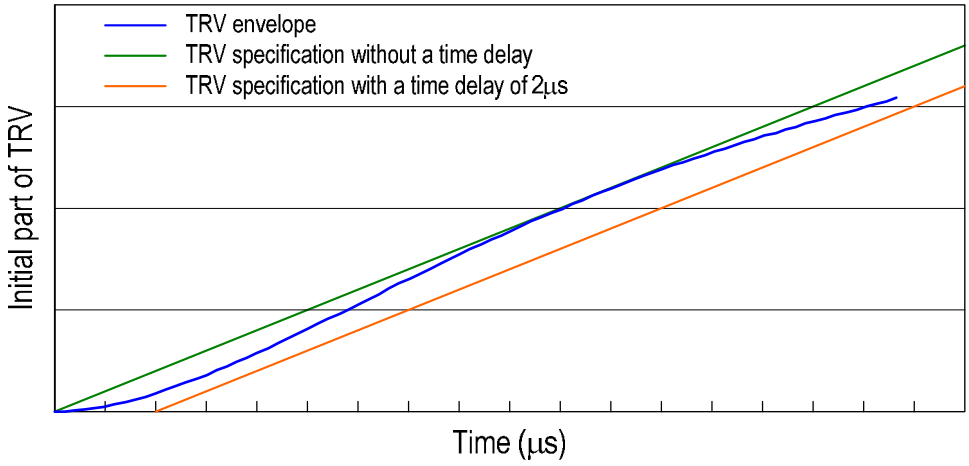

Fig. 3.1.3 ITRV

In terms of the envelope this means that the TRV is allowed to lag behind for 2 µs with respect to the first part of the envelope. This is allowed for a small part of the TRV and the TRV may not lag more than 2 µs. Therefore in addition to the three parts of the 4-parameter envelope a delay line is given, which may not be crossed by the TRV wave-shape. The delay-line starts at 2 µs and runs until u'/t' with u'= ½ u_1 and t'= ½ t_1+2 µs. See figure 3.1.3.

The 2-parameter TRV, as applied for T30 and T10, gives the envelope of an 1-cos function with a time delay of 15% of t_3, which is inherent to a damped 1-cos function.

3.1.1.4 ITRV, f_i , t_i

Another phenomenon is related to the fact that the busbar is to be considered as an extended structure with initially travelling waves. Like on OH-lines the triangular voltages that result from the travelling waves are characterized by surge impedances and travelling time (time to peak = twice travelling time). As long as the fault current is low (< 25 kA to the Standards), the surge impedance is low (only air insulated busbars have to be considered) and the dimensions are relatively small (voltages < 100 kV) the travelling waves on the busbars do not have to be taken into account. Indirectly the surge impedance has been specified to be 260 Ω for rated voltages up to 800 kV, while for 800 kV a value of 325 Ω has been specified. Indirectly, because a factor f_i (Multiplying factor, see the clause 4.102.4 in IEC62271-100) has been specified, this takes into consideration the surge impedance as well as the rated short-circuit current. The first ramp of the zigzag pattern of the TRV, as caused by the travelling waves is called the ITRV (initial TRV). The time to peak t_i is standardised per rated voltage and happens to be more or less proportional to ln (U_r). For 800 kV t_i is specified to be 1.1 μs.

The time delay and the ITRV have a counterbalancing effect on the arcing time, as they influence the arc extinction process during the so-called thermal phase of current interruption. As similar effects play a role at SLF-test duties, the Standards allow to neglect the requirements put forward with respect to the ITRV, when SLF-test are performed without any appreciable time delay at the line-side.

3.1.1.5 U_c , t_2

After the first part of the TRV with essentially an over-damped response from the system to the interrupted short-circuit current, the 1-exp function will appear as a travelling wave along the connected OH-lines and reflect at discontinuities in the network. Travelling waves that reflect at a substation with lower surge impedance will return as negative voltage waves and lead to a reduction of the TRV, while travelling waves that reflect at a substation with higher surge impedance (for instance only transformers) will lead to an increase of the TRV. The last category leads to the most onerous TRV wave-shapes and are taken into account in the Standards. So, after twice the travelling time to such a discontinuity a second 1-exp function will be superimposed to the original 1-exp function, albeit with a lower amplitude.

Due to the many reflections in a meshed system, the length of the smaller OH-lines are usually taken into account. In case of a network with a more radial structure an equivalent line length has to be taken into account. Because average line lengths increase proportional to the rated voltage, the time of arrival of the reflected wave will increase proportional to the voltage as well. The sum of the original wave-form and the reflected waveform will lead to the peak value of the TRV, since damping and distortion will generally prohibit further reflected waves leading to substantially higher peak values. It is the form of an 1-exp function that gives a time to peak somewhat later than the moment of arrival of the first reflected wave; typically t_2 is about 2T/0.85 or longer, with T being the travelling time in one direction: length of the OH-line divided by the propagation speed. To IEC, for test duty T100, t_2 has been standardized to t_2=4 x t_1. The same absolute value for t_2 is used for the other test

duties. However, to the draft IEEE Standard C37.06 (D10), t_2 is defined as 3 x t_1, with t_1 belonging to T60.

The TRVs at breaker terminal faults in situations where the source side is dominated by transformers, show a single frequency response and are specified as 2-parameter TRVs: T10 and T30. In that case td = 0.15 t_3 (see former paragraph).

The ratio between the peak value of the TRV, U_c, and the peak value of the 1-exp function, $k_{pp} \times E_0 = k_{pp} \times U_r \times \sqrt{2/3}$, is known as the amplitude factor k_{af}. To the IEC Standard 62711-100 k_{af} is specified as 1.4, 1.5, 1.54 and 0.9*1.7 for T100, T60, T30 and T10 respectively (rated voltage of 100 kV and above). For rated voltage above 245 kV k_{pp} is specified to be 1.3, except for T10, where k_{pp} = 1.5. The total value of U_c becomes therefore 1.82, 1.95, 2.00 and 2.30 E_0 for T100, T60, T30 and T10 respectively.

The values mentioned are for three phase terminal faults. Other applications, like transformer limited faults, long line faults, short-line faults and single-phase faults have to be compared with these values, but will be discussed in another chapter.

In previous IEEE Standards, instead of a 4-parameter envelope the Ex-Cos method was used to specify the TRV wave-shapes, based on similar considerations. The main difference between the IEEE Standards and the IEC Standards is caused by the policy to apply a first-pole-to-clear factor equal to 1.5 for all test duties, in order to cover situations where an ungrounded three-phase fault has to be cleared. In countries where the IEEE Standards are applied this factor 1.5 can be encountered.

In the former IEC Standards the amplitude factors have been 1.4, 1.5, 1.5 and 0.9×1.7 for T100, T60, T30 and T10 respectively. Further the first-pole-to-clear factor for T10 has been specified as 1.3, so that, when reference is made to IEC, utilities may have specified their circuit-breakers slightly different depending on the edition and amendment of IEC 62271-100 used at that time.

3.1.2 Background of technical requirements

With the slight changes in the amplitude factors and first-pole-to-clear factor in mind, it can be stated that Hydro Québec, KEPCO, ESKOM and China have specified the TRVs for terminal faults for their 800 kV circuit-breakers in accordance with the IEC Standard, while Furnas and AEP have specified their 800 kV circuit-breakers to the IEEE Standard.

For UHV, China has based the TRV specifications on the IEC approach, apart from the RRRV for T10 that has been increased from 7 kV/µs to 10 kV/µs. Also India is considering to apply the IEC Standards for the future 1200 kV-system. However, in Italy and in Japan the experts have used the IEC approach, but modified the requirements to the particular system conditions. Also in Russia the GOST-Standards have been modified with respect to the original IEC Standards. The main question is whether the extensive studies, as carried out for instance in Japan, are representative for other parts of the world as well, taking into consideration that Chinese experts are following the IEC approach to a large extent.

3.1.2.1 RV

For the TEPCO UHV system k_{pp} is less than 1.2 in all cases and, similarly, in the 800 kV system of HQ k_{pp} is less than 1.2 in 90% of cases. Information from systems with lower rated voltages seems to confirm this trend, but typical for the highest system voltages are the long trunk lines for the transmission of electrical energy along far distances. In such systems it may be expected that the long OH-lines have a limited contribution to the total short-circuit current, and that large transformers are always connected to the substations, thus contributing a relatively large part of the total short-circuit current. It is the ratio of the short-circuit current flowing through the OH-lines to the current flowing through the transformers that determine the overall X_0/X_1 ratio and therefore k_{pp}. The higher the contribution through transformers the lower k_{pp}. As already stated in CIGRÉ Technical Brochure 362 [1], it is recommended for UHV-applications to specify k_{pp} as 1.2, for all terminal fault duties.

To IEC 62271-101 (Synthetic testing), clause 4.1, deviations from the requirements put forward in IEC 62271-100 are acceptable under the conditions that (a) during the first 2.0 or 2.5 ms (for 60 Hz or 50 Hz resp.) the instantaneous recovery voltage is higher than 0.95 k_{pp} p.u. and that (b) during the first 100 ms the instantaneous peak value of the recovery voltage is higher than 0.5 p.u.. It should be investigated whether such a requirement is applicable and/or sufficient for UHV technologies, where the large volumes of the interrupter chambers and surroundings will lead to large time intervals before the hot exhaust gases are reflected into the dielectrically most stressed areas. However, it is expected that the prescribed minimum rate of decrease of the test voltage is sufficient to demonstrate the dielectric withstand strength during the phase with hot gases, that lasts up to maximum 10 ms. Based on an exponential decrease of the applied voltage, the requirements (a) and (b) of IEC 62271-101 can be extrapolated to the residual voltage after 10 ms: An exponential decrease from k_{pp} to 0.95 × k_{pp} within 2 ms (60 Hz) will give $0.95^{5} \times k_{pp} = 0.93$ after 10 ms, while an exponential decrease from k_{pp} to 0.5 within 100 ms will give a decrease to $(0.50/k_{pp})^{0.1} = 0.92$ after 10 ms and $k_{pp} = 1$. Therefore, the residual voltage will be larger than $0.95^{5} \times k_{pp} = 0.93$ p.u. (a) and larger than $(0.50/k_{pp})^{0.1} = 0.92$ p.u. (b), for k_{pp}=1.2 and for 60 Hz.

3.1.2.2 RRRV, u_1, t_1

The initial response of an UHV-system to the interruption of a short-circuit current is identical to the response at lower rated voltages and is a function of the equivalent surge impedance at the busbar in relation to the interrupted short-circuit current.

The rate of rise of the TRV is deduced from the minimum number of OH-lines that are connected to the busbar, thus forming together the equivalent surge impedance at the busbar side of the circuit-breaker. Values are standardized at 2, 3, 5 and 7 kV/μs for the test duties T100, T60, T30 and T10, respectively (first clearing pole; ≥ 100 kV). For n lines, the RRRV is determined by

$$RRRV = Z_{eq} / n \times dI / dt$$

And with 50 Hz and an equivalent surge impedance of 450 Ω and fault current I (kA), the RRRV is given by

$$RRRV = I \times 0.2 / n \quad \text{kV/μs}$$

The equivalent surge impedance for UHV is less than 450 Ω, certainly for the first clearing pole, and is estimated to be maximum 330 Ω. The minimum number of OH-line circuits connected to the busbar can be calculated with 330 Ω.

Typical surge impedances for UHV OH-lines in the frequency range of switching overvoltages are shown in the table 3.1.1. For the relatively low frequency range belonging to long travelling times of the travelling waves, the equivalent surge impedances calculated at power frequency are more appropriate. Apart from the 800 kV-lines in South Africa, 330 Ω is a little large for the first clearing pole. However, 330 Ω seems to be appropriate in general, including the 3rd pole.

Table 3.1.1 Surge impedance of transmission lines

Highest voltage (kV)	Conductors		TRV Frequency (conditions)	Z0 (Ω)	Z1 (Ω)	Equivalent surge impedance(Ω)		
	Size (mm2)	Bundle				1st pole	2nd pole	3rd pole
550 (Japan)	410	6	60 Hz (Normal span)	509	228	279	294	322
			60 kHz (Normal span)	444	226	270	281	299
800 (South Africa)	428	6	50 Hz (Normal span)	561	258	315	331	359
			27.5 kHz (Normal span)	403	254	290	296	304
1,100 (Italy)	520	8	50 Hz (Normal span)	485	211	260	275	302
			25 kHz (Normal span)	406	210	250	260	275
1,100 (Japan)	810	8	50 Hz (Normal span)	504	236	287	301	325
			25 kHz (Normal span)	476	228	276	289	311

Note) China's constants are presumed to be nearly same as these values, because they adopt same 8-bundle conductors and clearances are not so different from Japan's ones.
Note) The positive and zero sequence surge impedances give average values for the three phase conductors. By modal analysis where for each involved conductor the self and mutual impedances are calculated, depending on the conductor's position with respect to all other conductors, relative large deviations from these "average" values can be found.

The TRV envelope has to cover the RRRV of the 1st and the 3rd clearing pole. Under the condition that the standard values for the RRRV are specified for UHV as well, the minimum number of OH-lines, necessary to give a steepness of the TRV below the specified RRRV can be calculated. For example for T100, 50 kA, 50 Hz, the minimum number of connected OH-line circuits (n) is:

$RRRV = 330 / 450 \times 0.2 / n \times 50$ kV/μs, $RRRV = 7.33 / n$ kV/μs ≤ 2 kV/μs → n > 3 (for T100)

And for T60 and T30, respectively:

$RRRV = 330 / 450 \times 0.2 / n \times 30 = 4.4 / n$ kV/μs ≤ 3 kV/μs → n > 1 (for T60)

$RRRV = 330 / 450 \times 0.2 / n \times 15 = 2.2 / n$ kV/μs ≤ 5 kV/μs → n = 1 (for T30)

So, with a certain minimum number of OH-line circuits connected to the busbar (at the moment of fault clearing), the RRRV will be less than the steepness specified in the Standards. But for the future 1100 kV-system of TEPCO, situations are feasible, where only one OH-line circuit is connected (while a fault occurs in the other UHV circuit) under conditions of a high short-circuit current. For instance such a severe

case with a short-circuit current of 28 kA has been simulated. The above calculations give a RRRV of 4.1 kV/μs for a current close to that of T60.

A closer look into this case reveals that the RRRV is slightly less, as Z_{eq} is 300 Ω in stead of 330 Ω. Further, due to the slow 1-exp function the RRRV will further decrease. Conversely, as the part of the short-circuit current delivered through the OH-line (17 kA) is larger than the part delivered through transformers (10 kA), k_{pp} will be relatively large (but still smaller than 1.2) and so will be $k_{pp} \times E_0$. Moreover, in general, when a large part of the short-circuit current is delivered through OH-lines, E_0 tends to increase, as $E_0 = \omega L_1 \times L_{sc} \times \sqrt{2}$; L_1 being the short-circuit inductance belonging to the local source (i.e. the transformers and the sources behind the transformers). Normally the local part of the short-circuit current ($k \times I_{sc}$; see figure 3.1.4) will lead to $E_0 = U_r \times \sqrt{2/3}$ and the remote part $((1-k) \times I_{sc})$ to an extra increase in E_0, so that the 1-exp function will reach quite a high value. Fortunately, before reaching such values, reflecting waves interfere and reduce the wave-shape, at least in the case described.

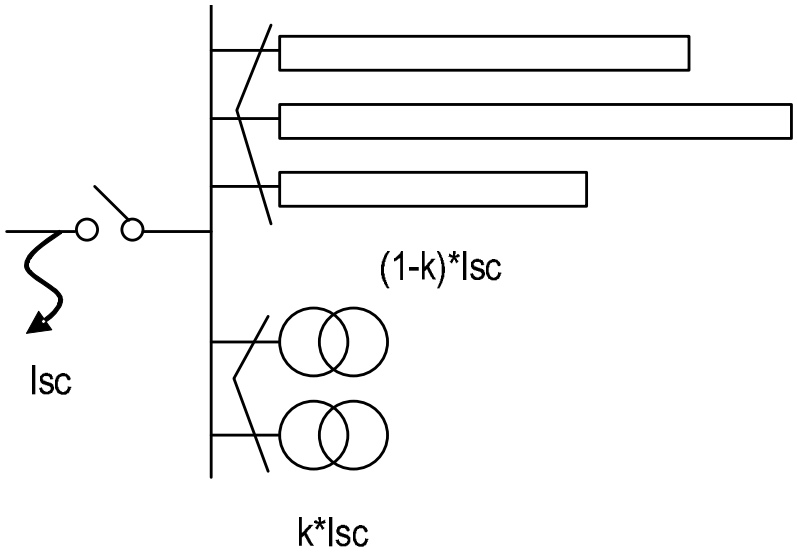

Figure 3.1.4 Short-circuit current

For this case, that is most severe with respect to the initial part of the TRV, the simulations and calculations show it to be nearly covered by T60, when k_{pp} = 1.2 is applied, and completely covered by T60, when k_{pp} = 1.3 is applied (u_1 being $0.75 \times k_{pp} \times U_r \times \sqrt{2/3}$).

In the next figures the information given will be illustrated, first of all by means of a case where a moderate short-circuit flows through the single OH-line circuit (case A). The step by step increasing short-circuit current (figure 3.1.5) leads to proportionally increasing values of E_0 in the calculated 1-exp TRV wave-shapes (figure 3.1.6).

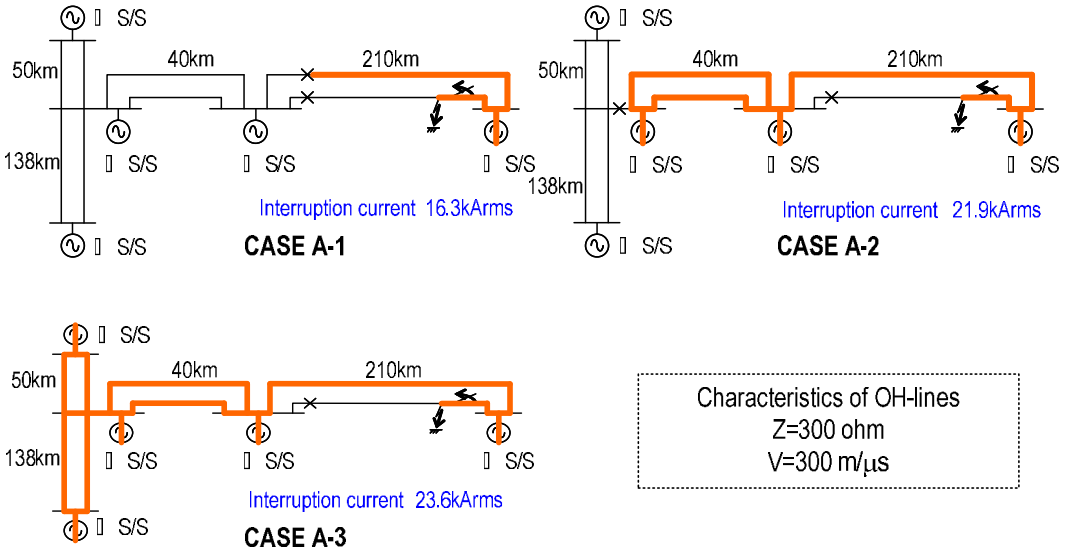

Figure 3.1.5 Step by step increasing short-circuit current

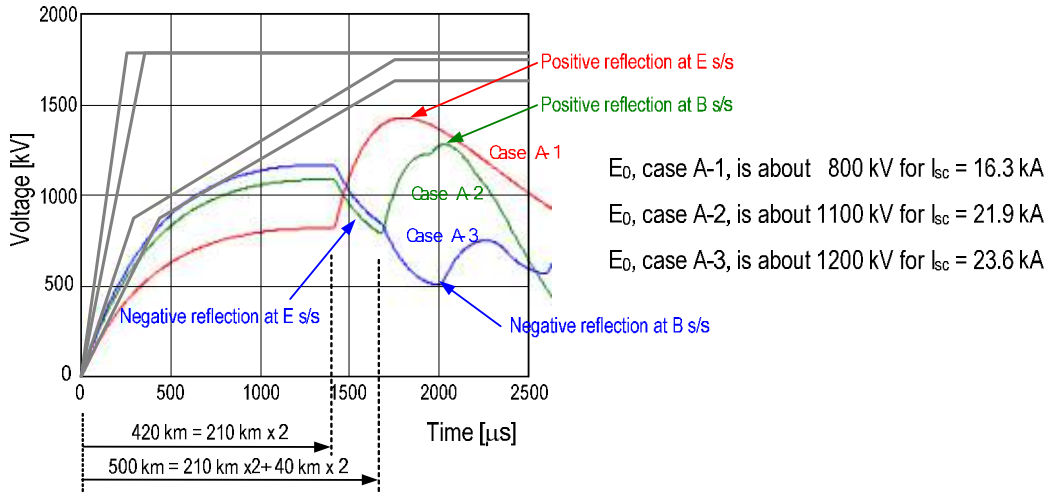

Figure 3.1.6 TRV for different cases in figure 3.1.5

The most severe case is given in the figures 3.1.7 and 3.1.8: D-4, with the breaking current of 27.7 kA and only one OH-line connected to the substation D.

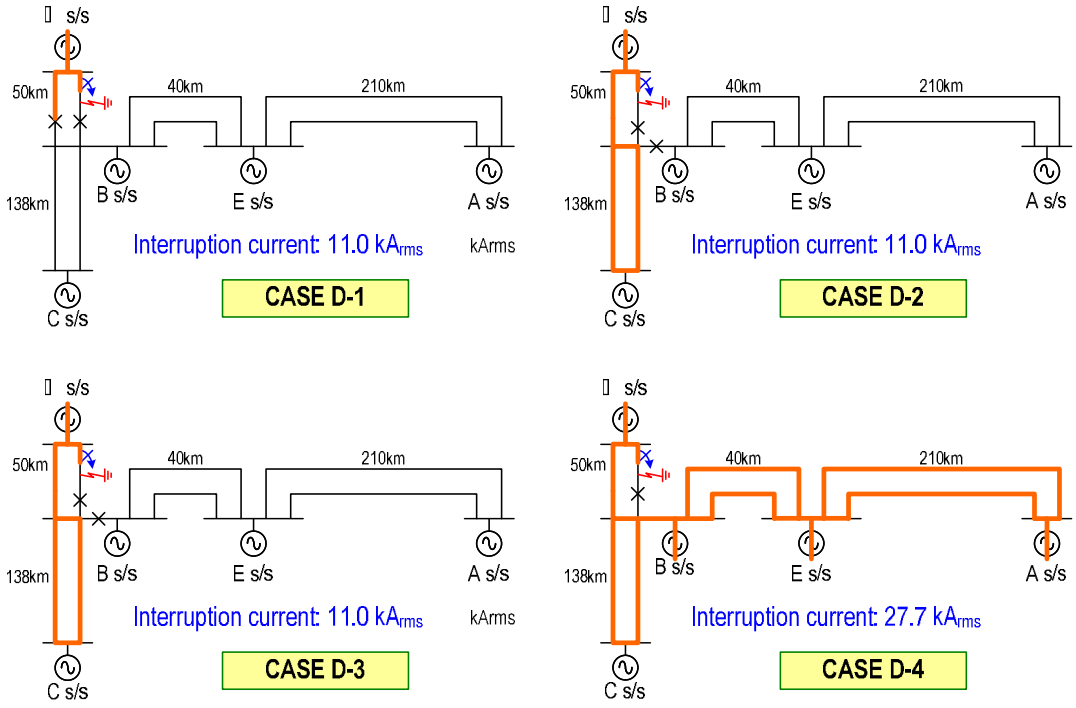

Figure 3.1.7 network cases for bus terminal faults at D substation

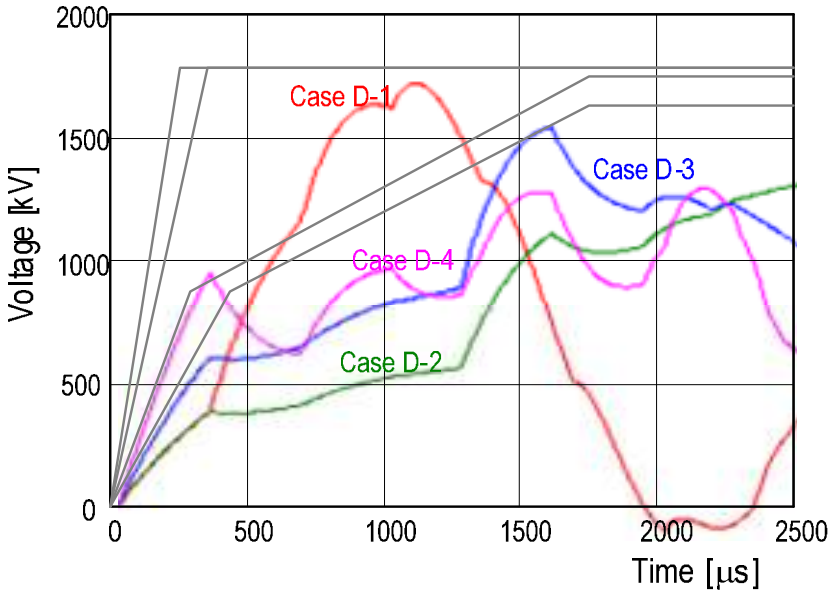

Figure 3.1.8 TRV results for different cases in figure 3.1.7

The initial part of the TRV for case D-4 just exceeds the envelope of T60.

However, the case is rather exceptional when considering the terminal faults only, because an UHV substation (connected by 2 OH-line circuits only) is located very close to another UHV substation with a large short-circuit-power, so that a misbalance exists between short-circuit power and the number of connected OH-lines. As a conclusion it can be stated that the values of 2, 3, 5 and 7 kV/µs for the RRRVs as specified for T100, T60, T30 and T10, respectively, can be applied for UHV as well. Also u_1 and t_1 can be specified to the usual method prescribed in the IEC Standard.

3.1.2.3 t_d, u', t'

The initial part of the TRV applied for terminal faults consists of a ramp function with a time delay. The ramp function is defined by the RRRV and specified as 2 kV/μs for T100 and 3 kV/μs for T60. These values are applicable for all rated voltages of 100 kV and above and are also proposed for the UHV range of voltages.

The time delay is, in principle, fixed as well: 2 μs for all rated voltages of 100 kV and above, for both T100 and T60. Its value depends on the local capacitance of the substation in combination with the equivalent surge impedance of the connected OH-lines.

The local capacitance, at least a minimum value, can be deduced from the information collected by CIGRÉ WG B3.22 [2]. It consists of the capacitance of the conductors of a phase to earth plus the capacitance of bushings, capacitive voltage transducer / divider (CVTs), MOSAs, earthing switches, transformers and shunt reactors, when applied. According to the information collected by WG B3.22 the capacitance to earth of a phase conductor in GIS is 35 pF/m, while for AIS the capacitance is 12.7 pF/m (based on data for 800 kV in India). As the dimensions of an UHV AIS substation are more than triple the dimensions of an UHV GIS substation, minimum values of the total capacitance to earth can be expected with GIS substations. For both the layout of a double busbar 1100 kV GIS substation (Japan) and a rather small 1100 kV breaker and a half scheme in GIS (China) the length of the conductors per phase and the capacitance of the involved equipment can be calculated as follows.

Double busbar, 4 line bays, 4 transformer bays, 2 section bays (1 per busbar) with a total length of $4\times(24m+18m)+4\times(24m+18m)+2\times 26m+2\times 24m = 428$ m × 35 pF/m = 15 nF. Equipment connected is (per bay) a bushing, CVT and an earthing switch (300+150+150 = 600 pF), together 5 nF. Further a number of transformers, each with at least 5 nF. Let us assume that at least 2 transformers are connected, so that the total capacitance is 30 nF.

Four OH-line circuits with each a surge impedance of 330 Ω gives an equivalent surge impedance of 82.5 Ω, so that the time delay td becomes $82.5\times 30 = 2.5$ μs, close to 2 μs. Less OH-lines or more transformers will lead to higher values of td.

In a similar way a rudimentary breaker and a half scheme may consist of 1 line bay, 1 transformer bay, 1 busbar with a total of about 200 m GIS, giving 7 nF. Equipment connected is (per bay) a bushing, CVT, earthing switch and a transformer or shunt reactor (300+5000+150+5000 = 10.5 nF). In total 28 nF.

One OH-line of 330 Ω results into a td of 9 μs, far more than 2 μs.

In conclusion a reasonable minimum value for the source side time delay is the standard value also applied for lower rated voltages: 2 μs. There is no reason alter the definitions as used at lower rated voltages for u'and t'.

3.1.2.4 ITRV, f_i, t_i

At rated voltage of 800 kV and below no ITRV has been specified for GIS circuit-breakers because of the low surge impedance of the GIS busbars. Also, at UHV the surge impedance is 90 Ω for GIS technology in comparison to about 300 Ω for AIS technology and the capacitance of UHV equipment connected to the GIS-busbar gives a considerable time delay to the otherwise very fast travelling waves. Thus, a similar consideration can be applied for UHV: no ITRV is to be specified for GIS substations.

For AIS and MTS or Hybrid-IS substations (See IEC Std. 62271-205 for the definitions of Hybrid-IS and MTS), values for the busbar surge impedance of 266 Ω (800 kV, India) to 360 Ω (UHV Hybrid-IS, China) have been given by CIGRÉ WG B3.22 [2]. The value specified in the Standards is 325 Ω for 800 kV and no specification is yet given for UHV applications. Note that to the IEC-Standard dead-tank breakers, including MTS-technologies are to be treated in a similar way as live-tank breakers.

A first estimation of the surge impedance of a conductor above earth is 60 ln(2*h*/*r*) with an height of *h* m and a radius of *r* m and for UHV air insulated bay connections a height of about 20 m can be assumed. In case of a bundled conductor the diameter is estimated to be 1 m, so that the radius is equal to 0.5 m. These values lead to a surge impedance of 263 Ω which is very close to surge impedance values applied for rated voltage below 800 kV (260 Ω). The height of conductors in the bays, busbars and OH-line connections of a proposed 1200 kV substation in India is foreseen to be 18m, 38m and 50m respectively. The diameter of the octagonal bundle conductors is foreseen to be 1.17 m and the related surge impedances become 247, 292 and 308 Ω. However, it is seriously considered to apply at the bay level (i.e. 18m) a double Al tube (D=114.5 mm, distance 450 mm) that corresponds to a surge impedance of 322 Ω.

From simulations of travelling waves within substations it can be learnt that the effect of small stray capacitances, such as those from support insulators, bushings and AIS-CTs (e.g. SF_6-gas insulated), can be regarded as an addition to the stray capacitance of the conductors, that is itself about 10 pF/m. Support insulators give about 20 pF and add about 10% to the capacitance per m of the conductors. A low value for the bushing- and CT-capacitance is 300 pF; as will be shown later, one CT on a length of 220 m adds 14% to the capacitance per m. Large capacitances (>1000 pF) have to be treated separately, as they initially can be regarded as a short-circuit for the travelling waves. Both the surge impedance and the propagation speed are inverse proportional to the capacitance per m, so that they both decrease by 12% due to the capacitance of the supporting insulators and of the bushings or CTs.

This is shown in figure 3.1.9 with examples of ITRV simulations for an 800 kV substation. The black line gives the specified ITRV parameters for 800 kV. The coloured lines show the simulated ITRVs for a substation with a 1½ breaker scheme with a terminal fault at the middle circuit-breaker in a bay. The pink line gives the ITRV, including the effect of supporting insulators, CTs, bushings and the connection to a transformer between the middle and the outer breaker (Z=146 Ω). The blue line shows the same situation, but without the connection to the transformer (Z=203 Ω). The distance from the circuit-breaker to the busbar is 91 m and the capacitance of the 2 connected CTs (each 800 pF) and the 5 supporting insulators leads to an additional 18.7 pF/m. Knowing that the surge impedance of the bay conductor was 350 Ω, the reduction by the additional capacitance leads to a surge impedance of 207 Ω, close to the simulated 203 Ω. The green line shows the effect of the 7 supporting insulators only, giving Z=329 Ω, a little above the 326 Ω calculated by 1.5 pF/m in addition to 10 pF/m.

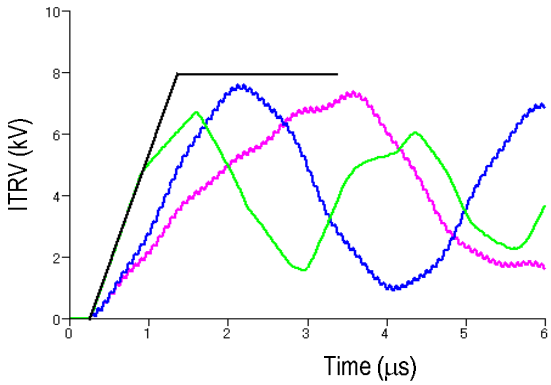

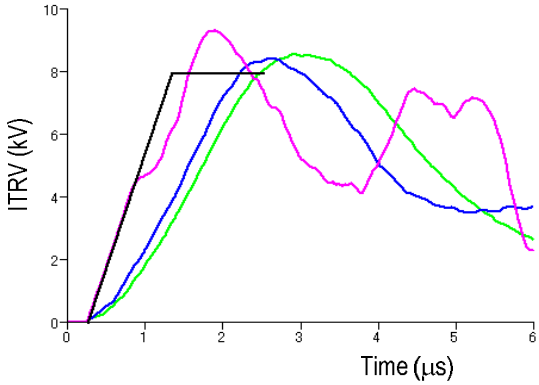

Figure 3.1.9 ITRV in 800 kV AIS substation *Figure 3.1.10 ITRV in 1100 kV Hybrid-IS substation*

For an 1100 kV-substation, 1½ breaker scheme, the ITRVs have been simulated as well; see figure 3.1.10. The black line again gives the ITRV parameters for 800 kV. The green and blue lines present the ITRV in case of a Hybrid-IS substation with and without connection to a transformer or OH-line respectively. The effect of the connection is minimal and the surge impedances are relatively low: 163 and 186 Ω. Such low equivalent surge impedances are caused by the long bay connections in GIS technology and give reason to apply similar ITRV-conditions for Hybrid-IS as for GIS. The AIS situation, where only supporting insulators are considered (4×20 pF) over a bay length of 65 m, leads to the pink line with a reduction of the surge impedance from 350 Ω to 332 Ω (330 calculated).

These examples show that the reduction of the surge impedance by small capacitance can be calculated in a simple way, also at UHV level, and confirm the conclusions put forward in [4]. Note that to the IEC-Standard dead-tank breakers, including HIS-technology, are to be treated in a similar way as live-tank breakers, as the type test conditions have been specified at the terminals of the circuit-breaker. In case of UHV, and maybe also at 800 kV, the connections in GIS busbar technology between circuit-breaker and air terminal are relatively long and give reason to reconsider the need to test HIS-circuit-breakers for ITRV. As the blue and green lines in figure 3.1.10 show, the ITRV waveshapes are moderate in comparison to AIS circuit-breakers. This is mainly caused by the additional capacitance of the busbar in GIS technology. Beyond 15 m of such a GIS-busbar connection, it is recommended to delete the ITRV requirement for HIS technology, as with 45 pF/m and a bushing of 300 to 600 pF the total capacitance reaches up to 1000 pF.

The sharp increase of the TRV wave-shape during the first µs or less (the ITRV) is caused by the travelling waves within a substation, opposite to the sharp increase of the TRV during the first tens of µs, known as short-line fault (SLF), caused by the travelling waves on an OH-line.

Within a substation the configuration of the phase conductors is different from that on OH-lines and so is the surge impedance. A further difference is the number of discontinuities in the surge impedance due to many apparatus with a lumped capacitance (> 1000 pF) or a lumped inductance (line traps), and the number of connections to the line bays and busbars. Taking into consideration, as shown above, that the many smaller capacitances can be taken into account in the surge impedance and propagation speed of the travelling waves and that those connections smaller than roughly 10 m can be neglected, the surge impedance for ITRV in UHV AIS substations is 300 Ω.

(Notes)

Supporting insulators (1200 kV AIS) give an estimated capacitance of a sphere with a diameter of 1 m, 18 m above ground. This is equal to the capacitance between two spheres at a distance of 36 m; in formula 2.5 $\pi\varepsilon_0 r$, leading to 40 pF with r=450+115 mm, being the overall dimension of the twin Aluminium tubes. As a sphere is probably not the proper configuration to simulate the support insulator, the capacitance is arbitrarily halved to 20 pF. Post insulators are applied for each 22 m, unless other equipment is installed to support the bay connections.

The capacitance of twin Aluminium tubes per m. can be calculated as follows. GMR of two tubes (centreline distance 450 mm, diameter 114.5 mm) is 321/2 mm. By $C=2\pi\varepsilon_0/\ln(2h/GMR)$ F/m, it becomes 55.64/5.4 =10.3 pF/m. The supporting insulators add about 10% per m.

In an 1½ breaker scheme, at each side of a circuit-breaker a CT is installed. An free-standing CT gives a capacitance of at least 300 pF, based on an internal insulation by SF6-gas. On a bay connection of 220 m (as will be discussed later), the CT gives an additional capacitance of 1.4 pF/m, at least. Dead-tank breakers will not have separate free-standing CTs, but, on the other hand, smaller bay dimensions.

Therefore, the reduction in Z for life tank breakers is about 11% and for dead-tanks about 5%, with respect to 322 Ω gives 290 and 305 Ω respectively. Phase to phase distances are larger than phase to earth distance, so that Zs = 60 ln (2h/GMR) is applicable.

[4] indicates that the travelling waves inside a substation result in a rather complicated waveform of the ITRV after the arrival of the first reflected wave. As the first reflected wave will introduce a reduction of the steepness of the ITRV and maybe even a decrease of the ITRV, the part up to this first peak is considered to be the relevant part that influences the interruption characteristics of the circuit-breaker involved.

The time t_i to the peak value is determined by the length of the conductors from the circuit-breaker up to the first discontinuity in the connections. A discontinuity can be formed by the connection of the bay with the circuit-breaker involved and the busbar, where the travelling wave can propagate in two directions and a negative voltage wave of ⅓ is reflected (as the travelling wave will be split into two more or less equal parts and one reflected wave: ⅓ negative) or by each bay connected to the same busbar. These negative reflected waves double their amplitude when they hit the terminal of the circuit-breaker, thus reducing sharply the steepness of the ITRV; see green curve in figure 3.1.9 and the pink curve in figure 3.1.10. A CVT with a capacitance of between 2 and 5 nF will initially lead to a full reflection of the voltage wave. The reflected wave diminishes with a time constant of ZC, say $300\,\Omega \times 3nF \approx 1\,\mu s$.

The length of connections between a circuit-breaker and the first discontinuity can be taken from an example of an AIS substation, as collected by CIGRÉ WG B3.22: a 1200 kV substation with a 1½ CB-scheme in India. Substation schemes such as 2-breaker and 1½ breaker schemes will be applied at UHV level, at least in AIS technology.

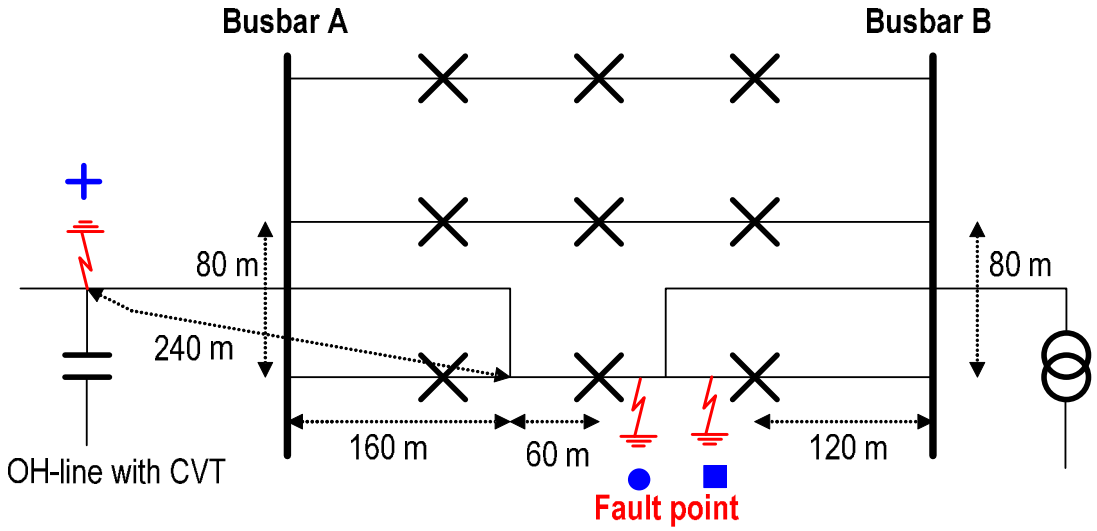

Figure 3.1.11 1200 kV AIS substation in India

The following situations have to be studied in greater detail. In the Indian 1200 kV AIS substation with a 1½ CB-scheme, two situations with a breaker terminal fault and another with a close fault can be foreseen, as shown in figure 3.1.11.

The first situation is denoted by the terminal fault indicated by the square, the other by the circle. From the first circuit-breaker to the source, we will find a distance to the first discontinuity of 120 m. The travelling time forwards plus backwards is 0.8 µs. The travelling wave on the busbar will also be reflected at the next bay at 80 m. By the second reflection the ITRV will reach its first peak value; i.e. after 1.3 µs.

The second situation is more complicated, but the first distortion will already occur after 60 m (reflection of -⅓, reduction of ITRV-steepness with ⅔), so that the first situation is to be considered as more severe. However, the situation changes, if for instance, the connection to the OH-line does not (yet) exist. In that case the first discontinuity is at a distance of 60 m + 160 m = 220 m, leading to a travelling time of 1.5 µs.

(Note) In both situations it has to be considered that a diameter connected as the last one to a busbar, is not exactly located at the end of the busbar, as usually certain equipment is connected at the far end: MOSA, ES or CVT at a location of 40 m or more further.

The 1½ CB-scheme is quite often applied at 800 kV and foreseen in UHV substations. Also the situation where one connection is failing in a diameter (a configuration of 3 circuit-breakers and two bays) happens quite often.

The third situation, indicated by the cross, is rather severe for the last breaker clearing the fault. At the source side as well as at the line side an ITRV will occur, doubling the effect of a single ITRV. The double-side ITRV has to be compared with L90, taking into consideration the somewhat lower surge impedance within the substation. This situation is more or less neglected at lower rated voltages where the line surge impedance is nearly double that of the substation surge impedance, so that SLFmay cover the phenomena.

One has to consider that it is not realistic to assume that the double-side ITRV will occur with 100% of the rated short-circuit current, as, at least, the contribution from the connection with the nearby fault has to be withdrawn from the total substation fault level. Furthermore nearby reflections will reduce the ITRV steepness. In figure 3.1.11 the first reflection is at the T-off for the OH-line connection, at a distance of 40

m from the left breaker and 60 m from the middle breaker. In this case the double ITRV will last for 0.3 to 0.4 μs, falling back to about 1.3 times a single side ITRV for another 0.4 to 0.5 μs.

One may argue that both circuit-breakers will share and clear the fault current, so that each breaker sees, say, 60% of the short-circuit current. But, a condition, not to be disregarded, is the fault after maintenance or at re-closing, when the circuit-breakers are closed one by one, so that only one circuit-breaker sees the full short-circuit current and has to clear this current, including its ITRV. Suppose that this circuit-breaker is faced with a short-circuit current of 75%, then an ITRV surge impedance of 300 Ω will be covered by L90 (with 330 Ω) without time delay at the line side, apart from the first 0.3 to 0.4 μs.

In conclusion:

- For a single side ITRV it is recommended to specify t_i as 1.5 μs, thus covering also the case of the middle breaker to interrupt a terminal fault, when the diameter is not (yet) fully extended
- To take a busbar surge impedance of 300 Ω as a base to define f_i
- To regard the single side ITRV as being covered by SLF without line side time delay, as the steepness of the ITRV (100% short-circuit current with 300 Ω) is about that of L90 (90% short-circuit current with 330 Ω).
- To pay attention to the fact that a double side ITRV is not covered by L90 since, unlike the situation at lower rated voltages, the equivalent line surge impedance is relatively low for UHV and the substation dimensions very large. At the lower rated voltages 260 Ω is about 60% of 450 Ω, so that L90 covers a double side ITRV up to 80% of the rated short-circuit current. But at UHV L90 will cover a double side ITRV only up to 75% of the rated short-circuit current, apart from the first 0.3 to 0.4 μs. Standardization bodies will have to consider whether the probability of having such a situation is to be covered.
- Dead-tank breakers are to be treated in a similar way as live tank breakers, but it is recommended to treat HIS breakers as GIS-breakers, as the additional capacitance shows to be rather high, due to the long bay connections in GIS-technology.

3.1.2.5 t_{dL}

It is expected that UHV circuit-breakers will be designed to be applied for OH-lines making SLF a mandatory test duty. Performing the SLF tests without any time delay at the line side (t_{dL} specified to be 0.5 μs for rated voltages ≥ 245 kV) could offer a possibility to by-pass the precise ITRV requirements. But this has to be decided after careful judgment of the possible situations in UHV AIS substations. For Hybrid-IS substations the situation is less critical since distances reported so far are shorter than those in AIS substations, so that ITRV is less severe.

The connections and equipment at the line-side of the circuit-breaker determine the time delay to be specified for SLF-tests. According to the information prepared by WG B3.22 the smallest capacitance can be deduced from the double busbar scheme in GIS technology (Japan). The following length of GIS-connections between circuit-breaker and OH-line is given: 11.5+3+3+3 = 20 m (from line to circuit-breaker) at 35 pF/m gives 700 pF. The equipment connected is a bushing, CVT and earthing switch (300+150+150 = 600 pF), in total 1300 pF.

Together with the line surge impedance of 330 Ω, 1300 pF leads to a line-side time delay of 0.43 μs, close to the 0.5 μs, given in the Standards.

Note that minimum values have been used and external connections as well as the capacitance of equipment like disconnectors and MOSA has been disregarded.

Note that for testing purposes the capacitance of the test object (between circuit-breaker and test line) has to be subtracted from the capacitance that can be deduced from the specified line surge impedance and line-side time delay.

3.1.2.6 u_c, t_2

For systems with long lines, the time of travelling waves forward and backwards is so long that it approaches the time of a quarter cycle of the system's natural frequency. This especially has to be taken into account for UHV. Therefore the relatively late time of the TRV peak tends to be dominated by the oscillation characteristic of the whole network. The equivalent circuit can be roughly described by lumped elements as in figure 3.1.12, where the remote power source is omitted.

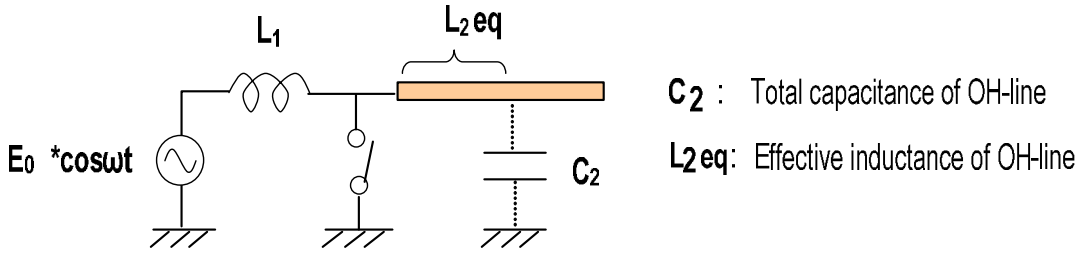

Figure 3.1.12 Equivalent circuit for the total characteristics of TRV

In the case where the fault current from the remote end is negligible, the impedance seen from the circuit-breaker terminals and the fault current are given by:

$$ZT(s) = 1/\left[1/sL_1 + 1/\left(sL_{2eq} + 1/sC_2\right)\right]$$

$$i(s) = \left(E_0 / L_1\right)/ s^2$$

The total TRV is given by:

$$V(s) = i(s) \times ZT(s) = \omega_0^2 \times E_0 /\left[s \times \left(s^2 + \omega_0^2\right)\right] + C \times E_0 \times L_{2eq} \times \omega_0^2 \times s /\left(s^2 + \omega_0^2\right)$$

Therefore,

$$V(t) = E_0 \times \left(1 - \cos \omega_0 t\right) + [E_0 \times L_{2eq} /\left(L_1 + L_{2eq}\right) \times \cos \omega_0 t = E_0 \times \left(1 - k \times \cos \omega_0 t\right), with\ k = L_1 /\left(L_1 + L_{2eq}\right)$$

$$\omega_0 = 1/\sqrt{(L_1 + L_{2eq}) \times C_2}$$

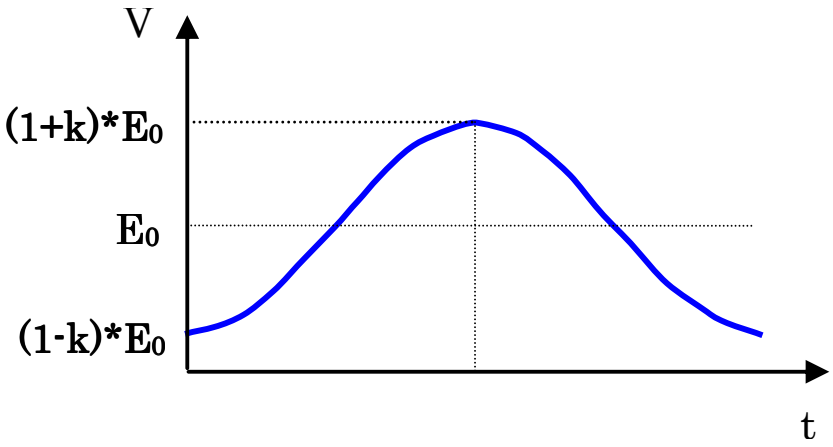

Figure 3.1.13 Total TRV waveform

The TRV waveform is a 1-cosine shape (See figure 3.1.13). To understand the TRV trend practically, hand-calculations were carried out with open end OH-line as shown in figure 3.1.14. The loss in the network is neglected in the calculation, and RRRV and U_c are defined as shown in figure 3.1.15. The figures 3.1.16, 3.1.17 and 3.1.18 give calculated results including the initial part of the TRV.

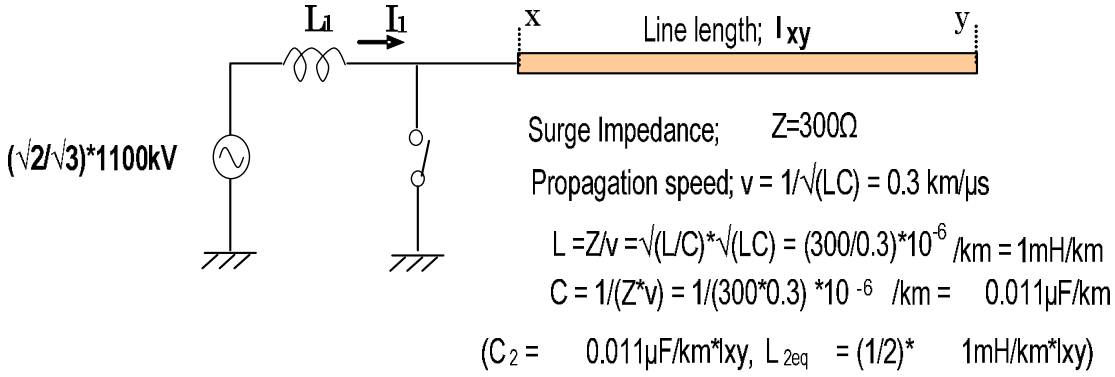

Figure 3.1.14 Hand-calculation model of total TRV waveforms

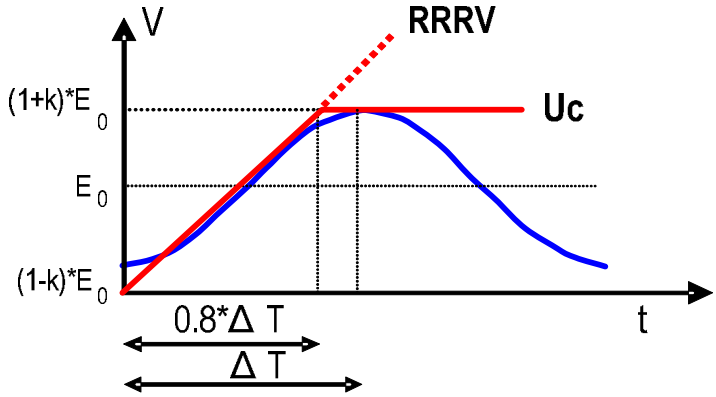

Note 1) $\Delta T = \pi * \sqrt{[L_1 + L_{2eq}] * C_2}$, $RRRV = U_c/(0.8 * \Delta T)$

Figure 3.1.15 Definitions of RRRV and U_c

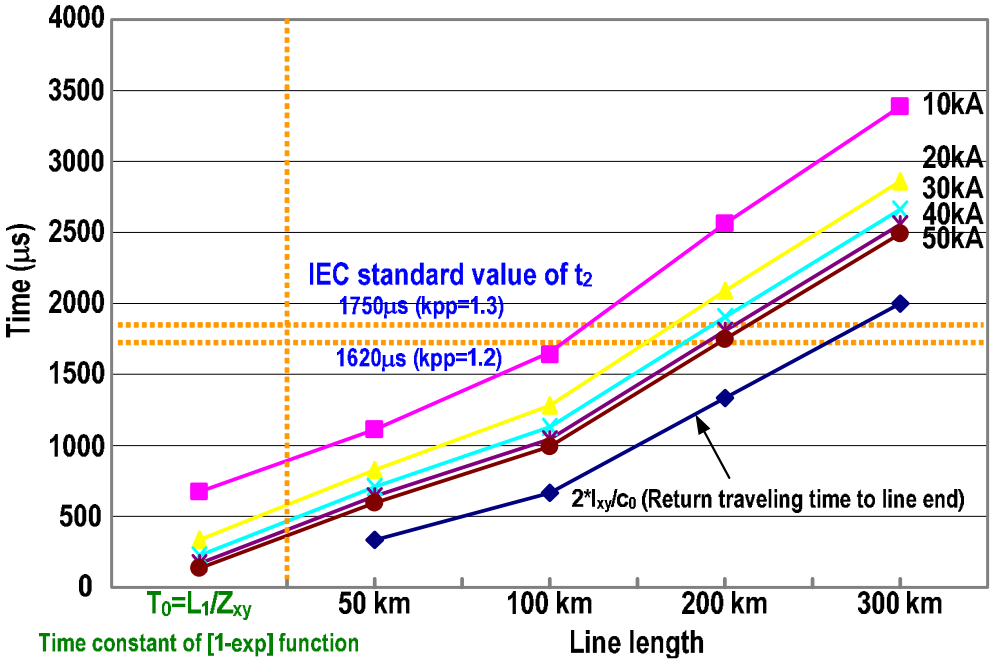

Figure 3.1.16 Calculated results of time to TRV peak ΔT

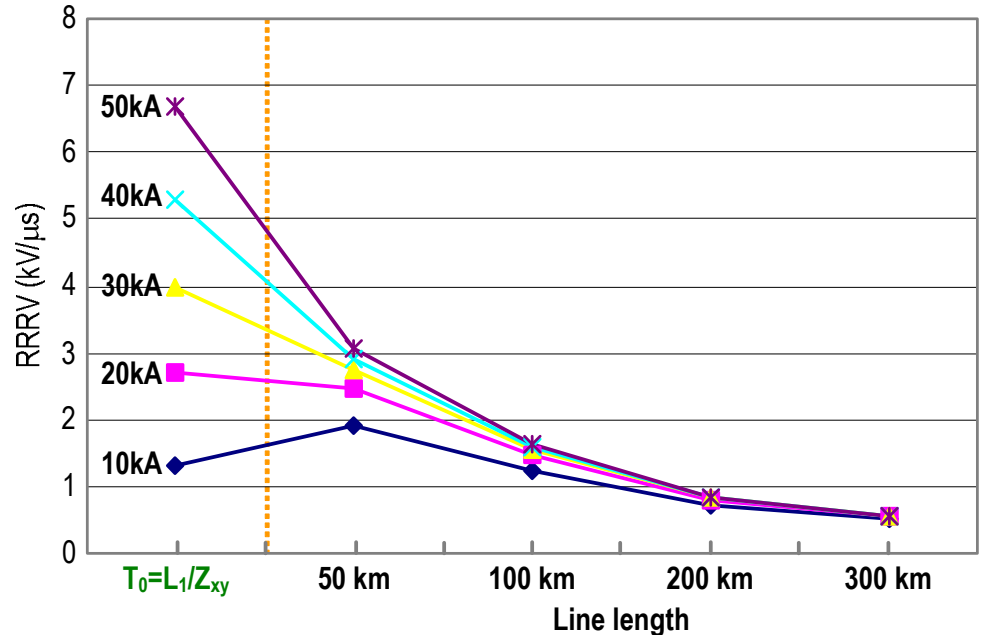

Figure 3.1.17 Calculated results of RRRV

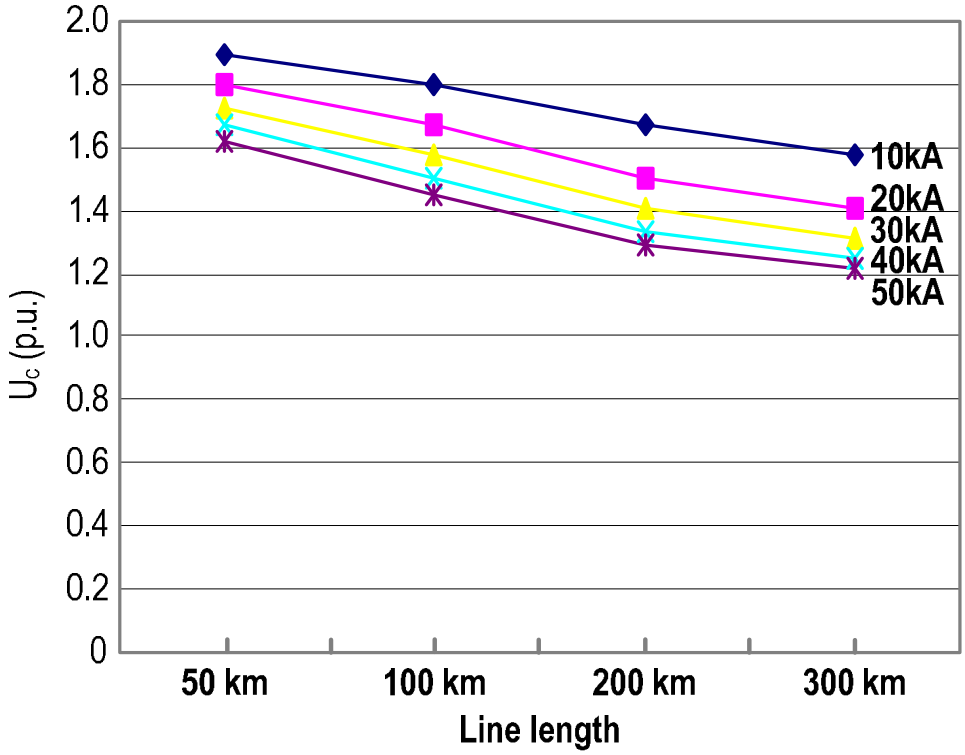

Figure 3.1.18 Calculated results of TRV peak voltage U_c

These estimations are done based on a single-phase circuit, so it is necessary to consider k_{pp} to estimate the TRV for a three-phase circuit. However, from these figures the following trends can be identified:

- The time to TRV peak becomes longer as the OH-line length becomes longer. This can be explained as the oscillation frequency of the network decreasing due to the increase of the total capacitance.
- The time to TRV peak becomes longer and RRRV becomes lower as the fault current fed from the transformer is smaller (power source side inductance is larger) under the same conditions for the line.
- The time to TRV peak is larger than the return travelling time to the open-end (See figure 3.1.15).
- TRV peak voltage becomes smaller as the line length become longer and as the fault current fed from the transformer becomes larger (power source side inductance is smaller).

The followings are results of EMTP calculations, which are rather comparable with the simplified calculations discussed before.

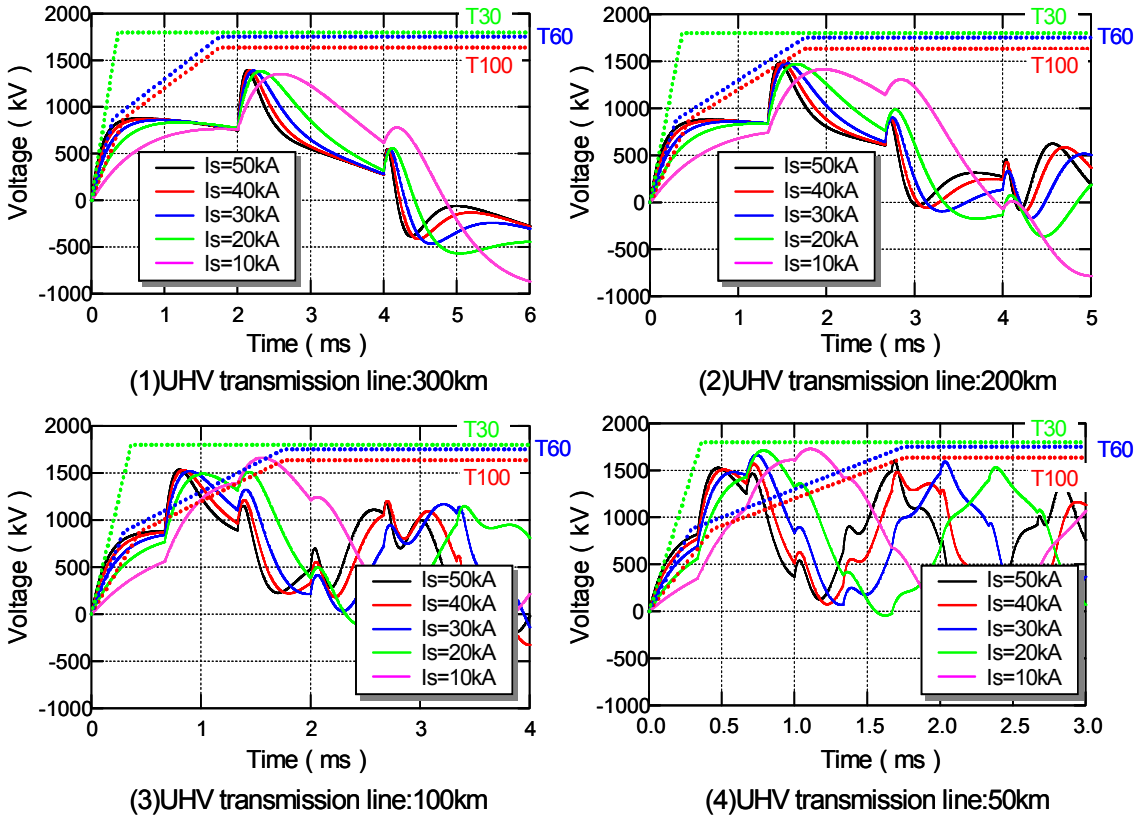

Figure 3.1.19 Results of EMTP calculations

The above EMTP calculations are based on the condition of an OH-line with open end. In case remote sources are considered (figure 3.1.20), the TRV waveforms are slightly different as shown in figure 3.1.21. Especially the initial part of the TRV waveform is different and the RRRV in case of a remote source is higher than in the case without remote source.

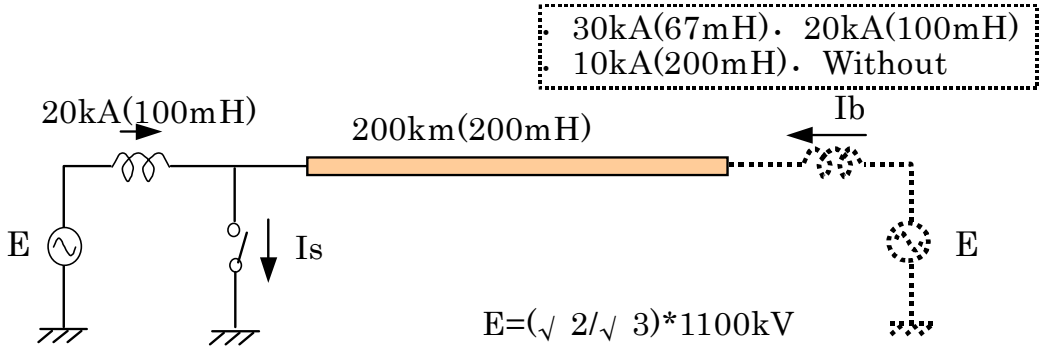

Figure 3.1.20 Effect of remote power source to TRV

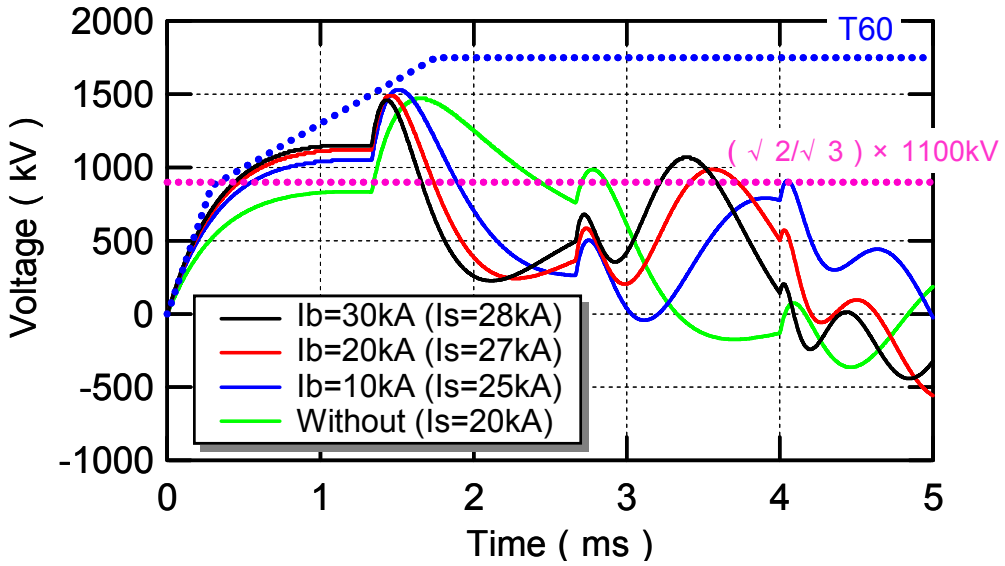

Figure 3.1.21 Effect of remote power source to TRV

From the simplified calculations and the comparison with the more complex 3-phase EMTP- simulations, it can be concluded that:

(1) In case of a simple network configuration, the time to TRV peak is determined by the return travelling time to open end (including the case that there are only transformers connected and no transmission lines). In this study, the time to peak will be the sum of the return travelling time plus about 200 µs to reach the peak of the TRV.

(2) In the centre of a simple network or in meshed networks, the TRV waveform is complicated by overlapping of the positive and negative reflected travelling waves. Even in the case of TEPCO's UHV network, where the UHV line lengths are relatively short, time to peak is around 1500 – 2000 µs, as the equivalent line length is more than 200 km (figures 3.1.12 and 3.1.14).

(3) Today's IEC standard values for t_2 of T60 and T100 are 876 µs for 550kV and 1272 µs for 800 kV. To the existing IEC Standard t_2 is 4 times t_1 and for 1100 kV systems this will give 1620/1750 µs in case of k_{pp}=1.2/1.3. As the time to peak is about 20 % larger than t_2 (figure 3.1.15), the corresponding values for ΔT are 1940 and 2100 µs respectively. These values would be a little too high for an UHV network with an equivalent line length of 200 km. A value as high as t_2 =3 x t_1 (T100) would fall into the proper range considering the above results for UHV systems. Such a value of t_2 is also applicable for T60, as the equivalent line length will not essentially vary with the short-circuit current. As t_1 for T60 is 1.5 times shorter than t_1 for T100, due to the 50% higher RRRV of T60, t_2 for T60 has to be specified as 4.5 times t_1 of T60.

(4) The time to TRV peak will be shorter with short (equivalent) OH-line lengths. This implies that the calculation results for the Japanese UHV systems can be considered as being more severe than the results for other UHV systems.

A remark to be made is that the rather simple topology of UHV networks leads to situations not foreseen at the lower rated voltages, although similar situations may also occur at 800 kV. For instance: calculations and simulations show that clearing a line fault at the same time at both line ends, will give a TRV that contains three components: the well known component of the TRV at the line-side, the component at

the busbar side (standardized by the 4-parameter envelopes, that takes into consideration the reflection of the travelling waves generated by the circuit-breaker itself) and a third component generated by the switching overvoltage due to the circuit-breaker clearing at the other end. As modern protection systems are so fast that both circuit-breakers will receive a tripping command at more or less the same time, modern fast operating mechanisms may cause the current zero used for clearing to be the same for both breakers. The travelling waves from the switching operation at the other end will arrive at the breaker terminal during the development of its own TRV, which takes a rather long time for UHV. See knee-point in TRV of figure 3.1.22, after about 800 μs. Figure 3.1.22 relates to the figures 3.1.5 and 3.1.6, where the network and simple calculation results are given. This phenomenon is further discussed in the Chapter on LLF.

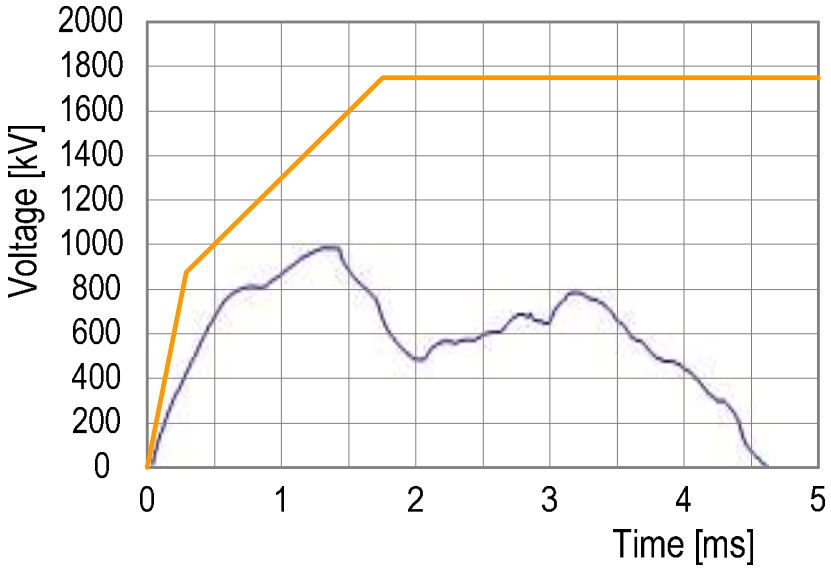

Figure 3.1.22 Simulation of Case A-3

The peak value of the TRV, as calculated theoretically in figure 3.1.18, is reached without taking into consideration phenomena as damping, distortion and multiple reflections. The information on the amplitude factor k_{af} is relatively poor, but simulations by experts from Japan indicate for T100, that k_{af} should be between 1.45 and 1.50. In other sources values of 1.44 (based on general IEEE-studies) and 1.46 (India) have been mentioned. Furthermore one could expect less damping due to the large conductor sizes in UHV systems, so that it seems to be reasonable to increase k_{af} for T100 from 1.4 to 1.5. For T60 a similar amplitude factor is proposed, meaning the same amplitude factor as already specified in the Standards. Also for T30 the standard amplitude factor is followed: 1.54. As T10 is to be considered as a test duty to cover transformer limited faults (TLF) and LLF (long line faults) rather than bus terminal faults, the discussion on amplitude factors is treated in the next sections.

Table 3.1.2 shows peak values in kV and in p.u., based on U_r = 1100 kV for combinations of k_{pp} = 1.2 or 1.3 and k_{af} = 1.5 or 1.55 result into.

Table 3.1.2 TRV peak

U_c	k_{pp} = 1.2		k_{pp} = 1.3	
k_{af}	1.5	1.55	1.5	1.55
(kV)	1616	1670	1750	1810
(p.u.)	1.8	1.86	1.95	2.02

3.1.2.7 The impact of MOSA

MOSAs may, depending on their rating and application, clip the peak value of the TRV. Of course there is a complicated interaction between network, switching overvoltage and MOSA, but a straight forward approach is to assume that the current absorbed by the MOSA will influence the instantaneous TRV waveshape in the same way as the injected current (simulated by superposition the effect of the short-circuit current interruption) excites a TRV-response in the system. In other words the $RRRV = Z_{eq} \times dI/dt$ and $TRV(t) = Z_{eq} \times I(t)$ responses of the system to the injected current can be applied as well to the current diverted by the MOSA: $I_a(t)$.

The time interval between a noticeable current absorption by a MOSA and the peak value of the TRV is relatively small. It is comparable with the duration of the initial part of the TRV, where the TRV can be regarded as proportional to the time: $TRV(t) = Z_{eq} * I(t)$. Thus, a simple model for the reduction of the instantaneous TRV-value as function of the diverted current I_a can be used: $\Delta TRV(t) = Z_{eq} * I_a(t)$ with $I_a(t)$ seen as a negative current. To find the intersection with the MOSA-characteristic, as in figure 3.1.23, the curve to assess the residual TRV peak value (i.e. TRV – ΔTRV) is drawn through the point where ΔTRV=0 and thus $I_a=0$ (TRV = U_c, without any influence of MOSAs) and the point where TRV=0, $\Delta TRV=U_c$ and $I_a=U_c/Z_{eq}$. (For T100 (50 kA, 50 Hz), Z_{eq} = 90 Ω and U_c = 1616 kV, thus I_a = 18 kA.) In this case the maximum value of the residual TRV will be at the intersection of the straight line and the MOSA-characteristic.

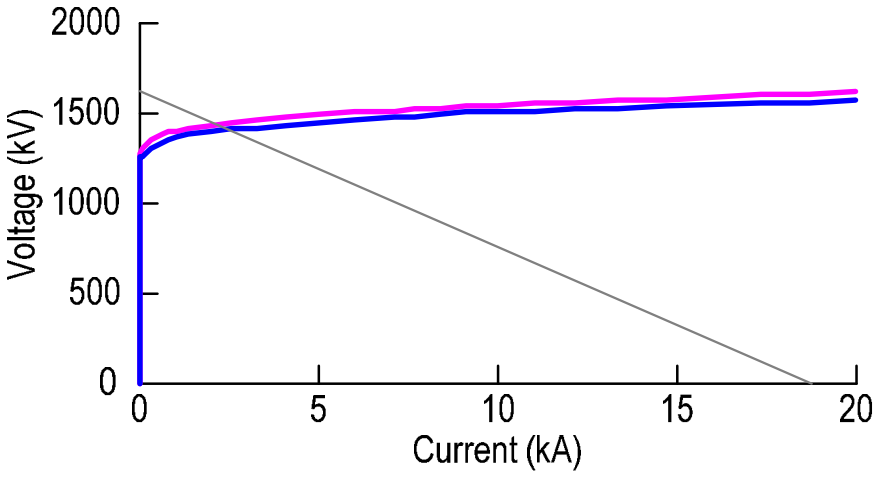

Figure 3.1.23 Intersection between different MOSA-characteristics and system response

For T60, the equivalent surge impedance is much higher (230 Ω) and the line steeper, leading to a lower intersection point on the MOSA-characteristic. In case the number of connected OH-lines to a substation is higher than the number assumed to define the type tests, the equivalent surge impedance will decrease and the line become flatter, leading to a higher intersection point. On the other hand the current I_a has to be divided over all MOSAs connected in the same substation. Since each OH-line has one or more MOSAs, the general trend is that the line (applicable to I_a/n with n the number of MOSAs) will become steeper again.

Similar considerations can be given for switching overvoltages, assuming that the most severe case is limited to one OH-line with one MOSA connected. Knowing that the intersection point with the MOSA characteristic will be at SIPL with 2 kA, and that the equivalent surge impedance is 330 Ω, a line representing switching

overvoltages can be drawn. With respect to the TRV-lines it can be concluded that all lines, based on the number of OH-lines and the number of MOSAs, will be below the switching overvoltage line, so that SIPL forms a good indicator for the maximum value of the clipped TRV-peak.

The SIPL is not an internationally fixed value and may even vary within a certain system, depending on the utility's policy and specifications. Some variation in SIPL has therefore to be considered. Suppose, for instance, that the switching overvoltage is just limited to 1. 6 p.u. = 1440 kV (based on 1100 kV system). A variation of 5 % will give a limitation of the clipped peak value to SIPL = 1510 kV and that moreover a certain margin between circuit-breaker performance and MOSA protection level will be necessary (for example: 5 %). Thus, in case of terminal faults in a system with k_{pp} = 1.2, a SIPL of 1440 kV would lead to a specified TRV level of 1588 kV. This is close to the inherent peak value for T100 (1616 kV). By applying such margins (some utilities might even apply larger margins, comparable to SIWL/SIPL, while others will allow lower margins), the effect of the MOSA on the specified TRV peak value is negligible. The effect on the actual or simulated TRV waveform is still clear as can be seen in figure 3.1.24.

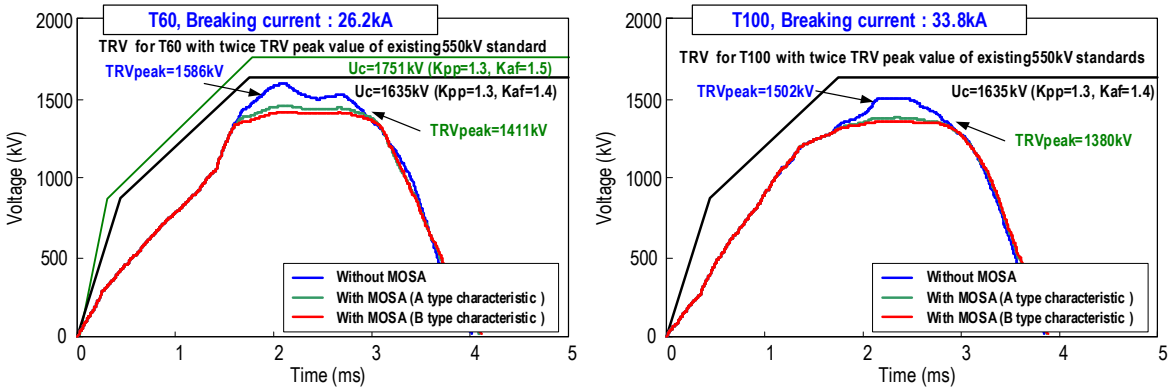

Figure 3.1.24 Effect of MOSA on TRV wave-shape

Note that 33.8 kA is just above T60 but that 26.2 kA is within T60

However, in case of T30/T10 the application of MOSA will reduce the peak value, at least in case of terminal faults. Here, however, other cases where T30 and T10 have to cover TRVs that occur in the system, have to be taken into consideration as well, especially the cases where the TRV partly appears at the load-side of the circuit-breaker: TLF and LLF. In the latter cases MOSA (phase to ground) will be less efficient in reducing reduce the peak values of the TRV.

3.1.3 Recommendations

3.1.3.1 RV

k_{pp} = 1.2 for UHV systems.

RV should be kept for 300 ms for type tests or, for synthetic testing > 0.95 k_{pp} p.u. for the first 2.5 ms and > 0.5 p.u. for 100 ms. Such criteria are relevant especially for UHV circuit-breakers as the back-flow of the hot gases will show some retardation due to the large dimensions of UHV circuit-breakers.

3.1.3.2 RRRV, u_1 , t_1

From the point of view of terminal faults, RRRV can be specified as for the lower rated voltages: 2, 3, 5 and 7 kV/μs for T100, T60, T30 and T10, respectively.

The first knee-point of the 4-parameter TRV envelope u_1/t_1 can be specified in accordance with the regular IEC procedure (u_1 being $0.75 \times k_{pp}$ p.u. and t_1 being $u_1 / RRRV + td$)

3.1.3.3 t_d , u', t'

Based on the information collected on substation dimensions, there is no reason to deviate for UHV from the policy applied to lower rated voltages for t_d, u'and t'.

3.1.3.4 ITRV, f_i , t_i

The value for the equivalent surge impedance for UHV busbar systems and bay connections, based on the information available, is proposed to be 300 Ω, including the effect of the capacitance of insulating supports and CTs or bushings. ITRV is applicable for live tank and dead-tank circuit-breakers, but for Hybrid-IS substations the conditions are less severe than for AIS substations and for GIS substations there are no needs to specify an ITRV. It is recommended to treat Hybrid-IS the same as GIS.

The time to the first knee-point of the ITRV is proposed to be 1.5 μs, based on a 1200 kV 1½ CB- scheme and considering the middle circuit-breaker in a bay where one connection is missing.

ITRVs are more or less covered by SLF-test duties without time delay at the line-side. This applies also for double-side ITRV up to 75% of the rated short-circuit current, but not for the first 0.3 to 0.4 μs.

3.1.3.5 t_{dL}

To be specified as for the lower rated voltages: 0.5 μs.

3.1.3.6 U_c , t_2

TRV in UHV systems can be covered, taking into account a first pole-to-clear factor of 1.2 and without considering possible effects by MOSA, by the values that can be calculated with k_{af} to be specified as at the lower rated voltages, but not less than 1.5. This means: 1.5, 1.5 and 1.54 and 0.9×1.7 for terminal faults T100, T60, T30 and T10 respectively, as given in table 3.1.3.

Note that to the IEC Standard, in order to cover TLF, k_{pp} for T10 is higher than for T100, T60 and T30, however for UHV k_{pp} = 1.2 is recommended, based on the large influence of the transformer with the secondary fault on the overall k_{pp} (it is the transformer that reduces k_{pp}). To cover LLF the Standard offers as an alternative a higher amplitude factor, while keeping k_{pp} identical for all test duties: k_{af} = 1.76 for T10.

Further it is recommended to define t_2 as being 3 × t_1, for T100 and as being 4.5 × t_1 for T60, meaning that t_2 has the same absolute time value for T100 and T60. This recommendation seems reasonable since the equivalent length of the network should be the same value between T100 and T60; see figure 3.1.25, red lines.

Table 3.1.3 TRV as a function of Amplitude factors based on the existing standard

Duties	1100 kV	k_{pp}= 1.2	1200 kV	k_{pp} = 1.2
	k_{af}	TRV (kV)	k_{af}	TRV (kV)
T10	1.76 1.53	1897 1649	1.76 1.53	2069 1799
T30	1.54	1660	1.54	1811
T60	1.50	1617	1.50	1764
T100	1.50 1.40	1617 1509	1.50 1.40	1764 1646
Out-of-phase	1.25	2245	1.25	2450

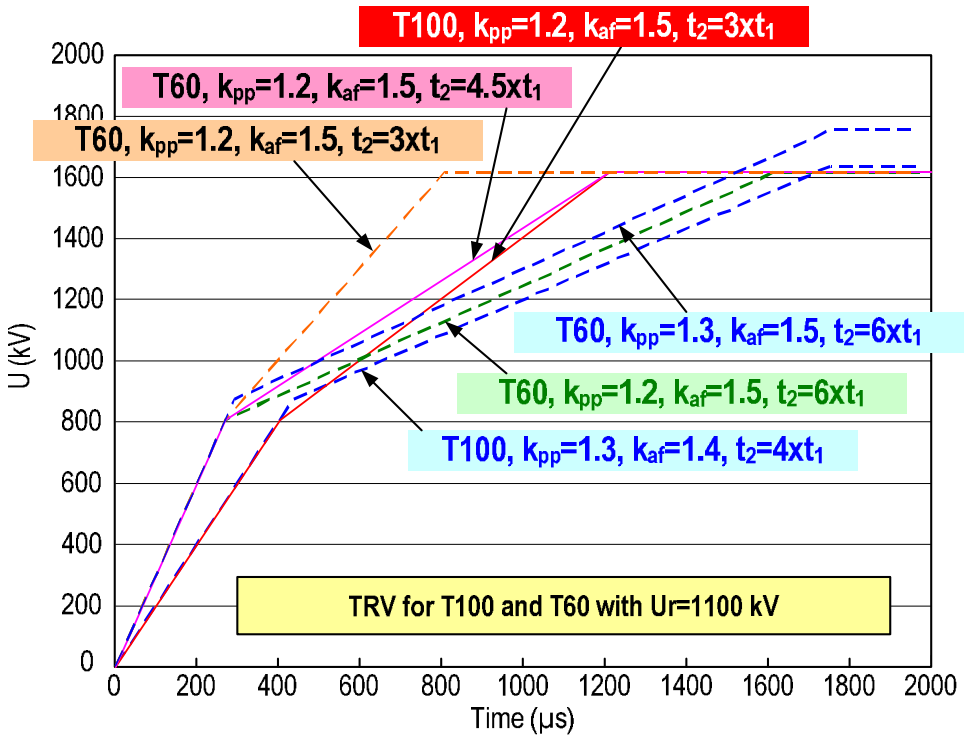

Figure 3.1.25 reduction of t_2 for T100 and T60

Table 3.1.4 summarizes the recommendation for UHV TRV requirement in comparison with 800 kV requirements. Table 3.1.5 also summarizes the difference in the TRV-parameters for 1100 kV in comparison to extrapolation from those based on the existing IEC standard. Time t_3 for TLF is based on the following relationship, where U_r is the rated voltage and I is the TLF current. Factor *k* of 6 is suggested for UHV applications. See the section 3.2.

$$t_3 = \frac{k \times \sqrt{U_r}}{I^{0.21}} \qquad (*)$$

Table 3.1.4 UHV TRV requirements in relation to 800 kV requirements

UHV	RRRV	k_{pp}	k_{af}	t_2	t_3
T100	2	1.3 -> 1.2	1.4 -> 1.5	$4*t_1$ -> $3*t_1$°	
T60	3	1.3 -> 1.2	1.5	$6*t_1$ -> $4.5*t_1$°	
T30	5	1.3 -> 1.2	1.54		t_3 -> t_3°
T10	7	1.3 -> 1.2	1.76		t_3 -> t_3°
TLF	(*)	1.5 -> 1.2	0.9*1.7		(*)

t_1° and t_3° are based on k_{pp}=1.2

Table 3.1.5 Differences in TRV-parameters for 1100 kV

UHV	u_1	t_1	Uc	t_2 or t_3
T100	876 -> 808 kV	438 -> 404 µs	1634 -> 1617 kV	1752 -> 1212 µs
T60	876 -> 808 kV	292 -> 269 µs	1751 -> 1617 kV	1752 -> 1212 µs
T30	-	-	1798 -> 1660 kV	360 -> 332 µs
T10	-	-	2061 -> 1897 kV	294 -> 271 µs
TLF	-	-	1786 kV	(*)

3.1.3.7 SLF

To be specified in a similar way as for lower rated voltages, but with adapted surge impedance at the line side: 330 Ω.

For AIS applications: no time delay at the line side to cover ITRV.

3.1.3.8 Others

Make test, operating sequence, arcing window, electrical endurance, mechanical endurance, full pole tests, synthetic tests, tests with an opening resistor (when applied): there is no reason not to follow the requirements and procedures specifies for lower rated voltages.

3.2 Transformer Limited Faults (TLF)

3.2.1 Introduction

Severe TRV conditions may occur when there is a fault immediately after a transformer without any appreciable capacitance between the transformer and the circuit breaker. The fault and the circuit breaker can be on the same side of the transformer or on opposite sides. In such cases, the rate-of-rise of transient recovery voltage (RRRV) may exceed the values specified in the standards for terminal fault test duty T10.

The system TRV can be modified by a capacitance or a resistor and then be within the standard TRV capability envelope. As an alternative, the user can choose to specify a circuit breaker that can withstand a faster TRV than specified for terminal fault test duties.

Taking into account the actual characteristics of power transformers for rated voltages 800 kV and higher, i.e. its short-circuit reactance and power, the fault current for transformer limited faults is usually between 10 % and 16 % of the rated short-circuit current of the circuit breaker (a typical value of 10 kA corresponds to 20% of the rated short-circuit current for a 50 kA circuit breaker and 16% for a 63 kA circuit breaker). However higher value of the TLF current are possible e.g. in the case of the 800 kV system of AEP in which the 765 kV / 500 kV transformers that connect AEP system to the neighbouring systems have impedances as low as 6.35%, leading to fault currents up to 17.2 kA. Conversely, the maximum TLF current for the 735 kV system of Hydro-Quebec is only 6 kA.

As the TLF current varies over a wide range, depending on the characteristics of the transformer, it is recommended to choose a TLF breaking current value in the R10 series, the closest to the actual value calculated for the application, but in order to standardize it is considered to define 10 kA and 12.5 kA as standard ratings (for UHV).

As a theoretical example, considering a 3000 MVA, 1100 kV transformer with a short-circuit impedance of 14% and a 90% voltage drop across the transformer, the TLF current is 11.2 x 0.9 = 10.1 kA. In this case the closest value in the R10 series is 10 kA.

The tables of TRVs for TLF in the IEEE Guide C37.06.1 are based on the following relation between time t_3, the rated voltage (Ur) and the TLF current (I):

$$t_3 = \frac{k \times \sqrt{U_r}}{I^{0.21}} \qquad (1)$$

The value of the k-factor is 3.18 in draft D10 of IEEE C37.06 (based on t3 values taken from ANSI C37.06.1-2000) for rated voltages 123kV to 800kV. This value was determined from data of transformers up to 550kV [3].

3.2.2 Background information

The TRV parameters can be calculated from (1), assuming that there is 90% voltage drop across the transformer (as in IEC 62271-100).

As an example the 3000 MVA transformers in Japan (nominal voltage 1050 kV, 18%) can be given. Applied in a substation with a maximum short-circuit current of 50 kA, a TLF would give a short-circuit current of 8 kA at the 1100 kV-side. A typical surge capacitance (at the UHV-side) of 10 nF together with a typical capacitance of 3 nF between transformer and UHV circuit-breaker gives a typical total capacitance of 13 nF. Minimum values of the surge capacitance and between transformer and circuit-breaker would result in a total capacitance of about 9 nF.

Based on the calculation of the natural frequency of the transformer ($1/2\pi/\sqrt{LC}$) a typical value for t_3 ($0.85 \times \pi\sqrt{LC}$) is 140 µs and a minimum value is 116 µs. By applying a k-factor of 3.18, the IEEE-formula would give 68 µs. In order to fit for t_3, the k-factor has to be 5.5 to 6.5.

The question, however, is whether the IEEE-formula has to be adapted or whether a minimum value for the equivalent surge capacitance has to be given, for example 9 nF. As the IEEE formula forms a detour to calculate t_3, it is proposed to define a minimum value for the equivalent surge capacitance. Assuming that the TRV is due only to the voltage variation across the transformer, the peak value of the TRV depends on the amplitude factor, the first-pole-to-clear factor and the voltage drop across the power transformer. The IEC Standard defines an amplitude factor of 1.7 and a voltage drop of 90% for transformer limited faults at rated voltages up to 800 kV.

These values are considered to be conservative but there is no evidence so far that would justify a deviation from this policy for UHV. The first-pole-to-clear factor for the lower voltages is specified to be 1.5, also in cases where for T100, T60 and T30 k_{pp} is defined to be 1.3. For 800 kV and above a careful examination of k_{pp} is necessary.

At the source side of the circuit-breaker k_{pp} will increase with respect to breaker terminal faults (where k_{pp} is proposed to be 1.2), as the number of transformers supplying a part of the short-circuit current is reduced by one (i.e. the transformer at the load side of the circuit-breaker). The main part of the short-circuit impedance is at the load-side, being this transformer with short-circuit at the secondary side. The

X_0/X_1 ratio is small for UHV-transformers where the neutrals at both sides are directly connected to earth and, therefore, k_{pp} at the load side will be less than 1.0. Thus the overall first-pole-to-clear factor will be close to 1.0 and there is no reason to propose that k_{pp} is higher for TLF than for breaker terminal faults. It would be more reasonable to propose that k_{pp} is less, for instance 1.1 or even 1.0. The same conclusion is applicable for TFF (transformer fed faults, where the UHV transformer is at the source side of an UHV circuit-breaker with a terminal fault).

Neglecting the voltage variation on the source side and considering an amplitude factor of 1.7 and a first-pole-to-clear factor of 1.2, the peak TRV in an 1100 kV system is given by

$$u_c = \frac{Ur}{\sqrt{3}}\sqrt{2} \times 0.9 \times 1.7 \times 1.2 = 1649\ kV \qquad (2)$$

The RRRV is then given by: $\frac{1649}{116} = 14.2\ kV/\mu s$ (3),

i.e. double the value for the standard test duty T10.

TLF duties were studied based on the actual data of TEPCO's transformers supplied by the manufacturers. Table 3.2.1 shows the rating and number of investigated transformers that have surge capacitances measured by the second Kyodai method described in section 3.2.2.3. Several transformers shown in section 3.2.2.3 are included in this table.

Table 3.2.1 Rating and number of investigated transformers

	Rated voltage	Capacity per Bank	Number of bank *	
UHV transformer	1050/ 525 kV	3,000 MVA	3*	
500 kV transformer	525 or 500/ 275 kV	1,500 MVA	8	18
		1,000 MVA or below	7	
	512.5 or 500/ 147kV	750 MVA	3	
275 kV transformer	275/ 147 kV	450 MVA, 300 MVA	6	10
	275/ 66 kV	300 MVA	4	

* Data were provided as per phase for UHV and per bank for 500kV and 275kV.

3.2.2.1 Relation between surge capacitance and short-circuit current

For rated voltages 123kV to 800kV, TRV values for TLF in ANSI Guide C37.06.1 and a draft D10 of IEEE C37.06 are based on the following relation between t_3, rated voltage (U_r) and TLF short-circuit current (I_s).

$$t_3 = \frac{k \times \sqrt{U_r}}{{I_S}^n} \quad \text{(n= 0.21, k= 3.18 for lower voltage)} \quad (1)$$

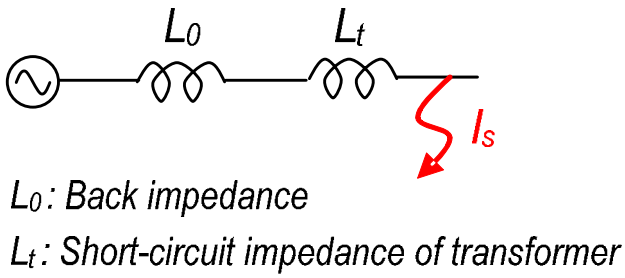

Figure 3.2.1 Model circuit of transformer limited fault

On the other hand, I_s is determined by back impedance and the impedance of transformer.

$$Is = \frac{U_r}{\sqrt{3} \times \omega \times (L_o + L_t)} \quad (2)$$

As $L_t \approx 0.9 \times (L_0 + L_t), I_s \propto U_r / L_t$ (3)

And considering that t_3 is determined by natural frequency of the circuit ($1/2\pi/\sqrt{L_tC}$), then

$$t_3 \propto \sqrt{L_t \times C} \propto \sqrt{U_r \times C} / \sqrt{Is} \propto \sqrt{U_r} \times C^{0.5} / Is^{0.5} \quad (4)$$

Here, C is the equivalent surge capacitance of the transformer with all other terminals short-circuited. Since C becomes larger as the transformer's capacity increases, the following relation could be assumed and applied.

$C \sim I_s^{\,m}$ (5)

Then equation (4) can be modified to,

$$t_3 \propto \frac{\sqrt{U_r}}{Is^{0.5-0.5m}} \quad (6)$$

Equation (6) is the same as equation (1) by replacing "0.5 - 0.5m" with n. Therefore, it could be concluded that the formula proposed by IEEE is basically correct, and in the case of m= 0.58, that is, $C \sim I_s^{\,0.58}$ ($\rightarrow \ln C = const. + 0.58 \times \ln(I_s)$), it becomes $t_3 \sim 1/ I_s^{\,0.21}$.

Figure 3.2.2 shows the relation between I_s and C, where Is was calculated by equation (2) assuming the back impedance (L_o) has the value corresponding to a short-circuit current of 50 kA at UHV and 275 kV system, and 63 kA at 500 kV system respectively.

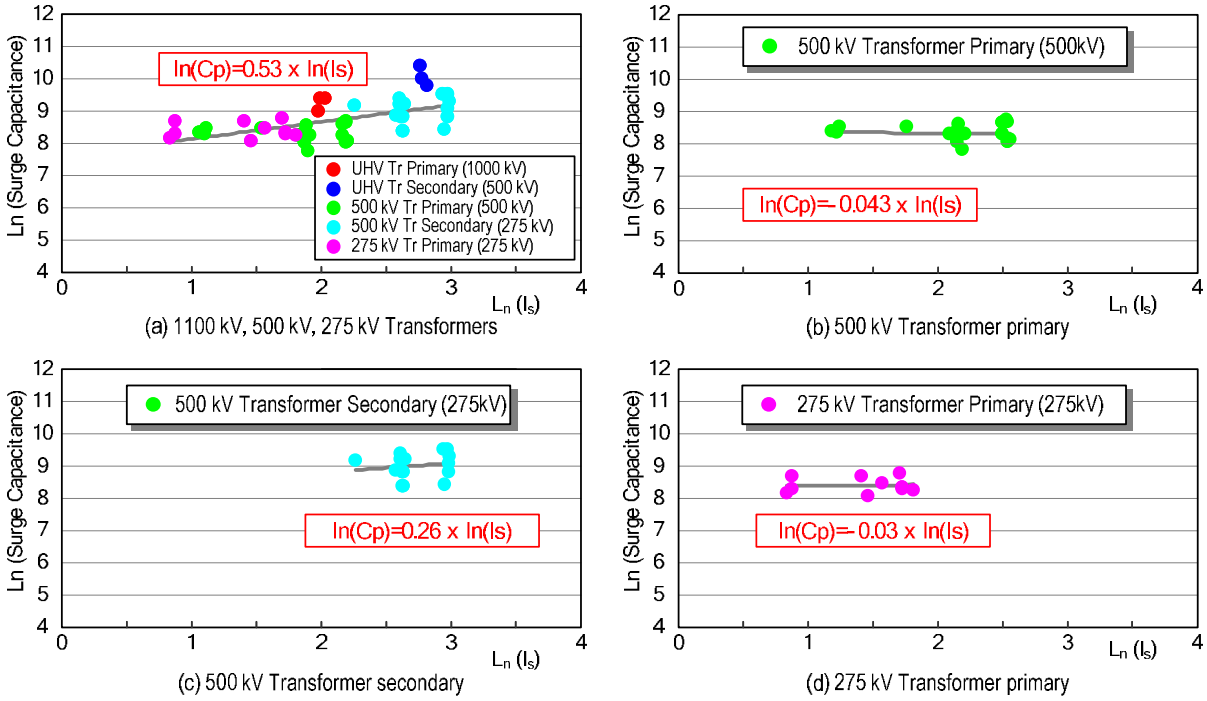

Figure 3.2.2 Transformer surge capacitance dependence on the short-circuit current

From Figure 3.2.2, the following relations can be obtained

Overall: $ln(C) = 0.53 \times ln(Is)$ → $C \sim I_s^{0.53}$ → $t_3 \sim 1/I_s^{0.24}$

500kV Primary (500kV): $ln(C) = 0.043 \times ln(Is)$ → $C \sim I_s^{0.043}$ → $t_3 \sim 1/I_s^{0.52}$

500kV Secondary (275kV): $ln(C) = 0.26 \times ln(Is)$ → $C \sim I_s^{0.26}$ → $t_3 \sim 1/I_s^{0.37}$

275kV Primary (275kV): $ln(C) = 0.03 \times ln(Is)$ → $C \sim I_s^{0.03}$ → $t_3 \sim 1/I_s^{0.49}$

For different voltage classes, the coefficient m of $C \sim I_s^m$ is smaller than 0.58, which means that the surge capacitance is not changed greatly with the capacity, and coefficient n of $t_3 \sim 1/I_s^n$ is 0.37 to 0.52, slightly larger than 0.21. However, in general, it can be said that the IEEE formula of $t_3 \sim 1/I_s^{0.21}$ is well matched since the overall coefficient n is 0.24.

3.2.2.2 Relation between RRRV and short-circuit current

The RRRV was calculated by hand assuming following equations.

$$U_c = \frac{\sqrt{2}U_r}{\sqrt{3}} \times 0.9 \times 1.7 \times 1.2 \quad (7)$$

$$t_3 = 0.85\pi \times \sqrt{L_t \times C} \quad (8)$$

$$RRRV = U_c / t_3 \quad (9)$$

Figure 3.2.3 shows calculated results of RRRV values for TLF with 1000 kV, 500 kV and 275 kV transformers.

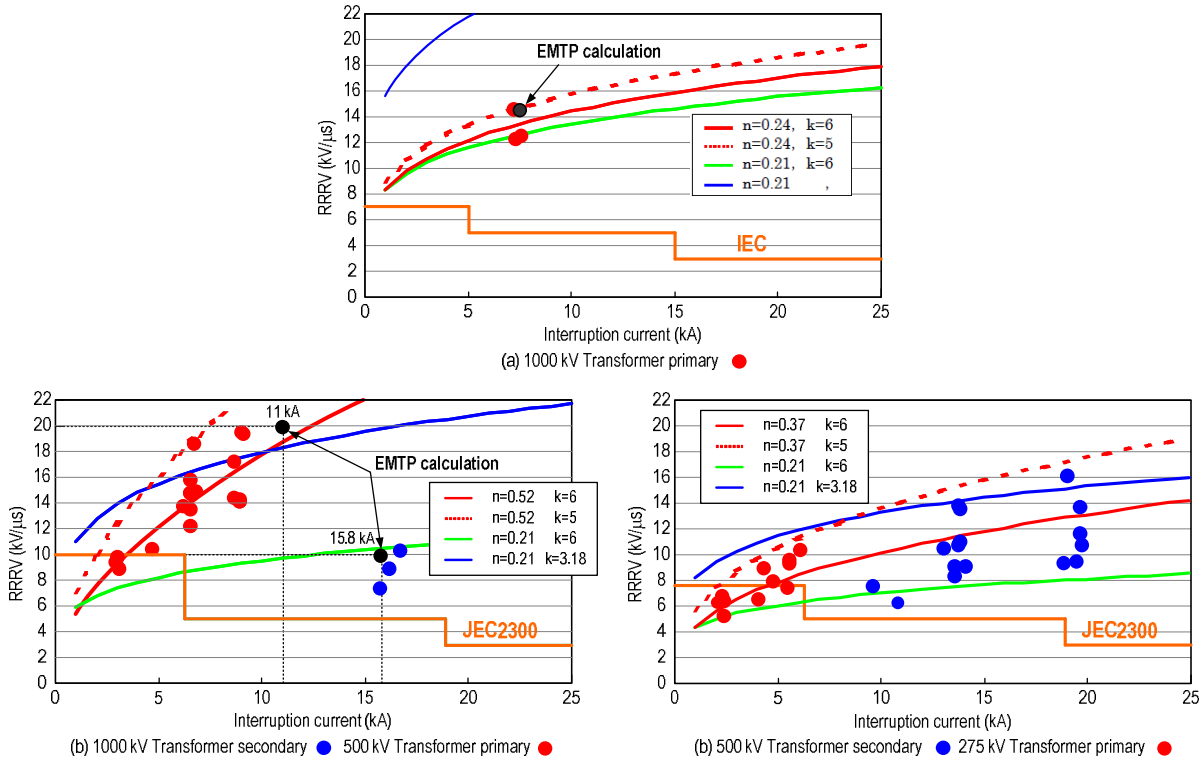

Figure 3.2.3 RRRV for TLF dependence on the short-circuit current

Up to 500 kV, the IEEE-formula with n= 0.21 and k= 3.18 can cover almost all data, though larger values of n and k give a better fit.

In Japan, as described in CIGRÉ Technical Brochure 362, type tests of 550kV GCBs, whose interrupters have been used for one unit of two-break UHV GCBs, were done following TEPCO's specifications that were derived by detailed EMTP calculation.

Terminal fault for 500kV transformer primary circuit: Is= 11 kA, RRRV=20 kV/μs

Terminal fault for UHV transformer secondary circuit: Is= 15.8 kA, RRRV=10 kV/μs

For UHV, the RRRV is lower than that from the IEEE-formula with n= 0.21, k= 3.18. It can be covered with n= 0.24, k= 5, which corresponds to 15 kV/μs at 8 kA.

Since the surge capacitances of UHV transformers are larger than the values extrapolated from lower voltages (because the average internal electric field stress increases for size reduction and series capacitance of windings becomes larger to suppress transient internal voltage oscillation) the k-factor of the IEEE-formula tends to be larger than that of lower voltage.

3.2.2.3 Comparison of two different measurements on surge capacitance

There are two typical measurements for surge capacitance, C, of a power transformer shown in Table 3.2.2: frequency response method and step wave (Daini-Kyodai) method. The frequency measurement can calculate the capacitance with the measured resonant frequency value and the evaluated inductance L of a transformer. The Daini-Kyodai method can measure constants such as C, L and resistance R of a transformer directly.

In Japan, the surge capacitances are evaluated by Daini-Kyodai method. Table 3.2.2 shows a testing circuit to measure the surge capacitances for a primary and a secondary winding.

Table 3.2.2 Comparison of frequency measurement and Daini-Kyodai method

	Method1: Frequency measurement	Method2: Daini-kyodai method
Test circuits and procedure	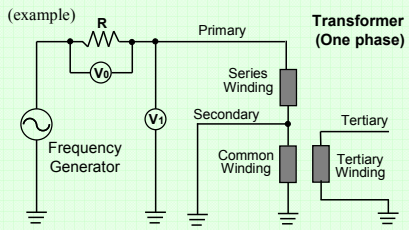 Typical test circuit is shown to measure the frequency characteristic for a power transformer. The capacitance of a power transformer is calculated from the measured resonant frequency and the inductance L of the power transformer.	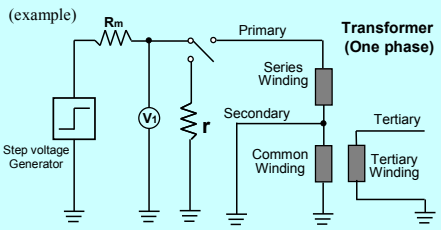 As a step wave is applied to a power transformer, follow oscillation waveform depending on resonant frequency of a power transformer is observed at V1 in the figure. Constants such as C, R and L of transformer's impedance Zx can be calculated from the frequency and voltage magnitude of the waveform.
Example of measurement results	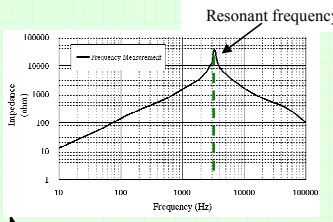 Constants C is calculated from fx and L	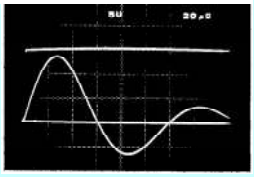 Constants C, R and L are calculated

Figure 3.2.4 shows a comparison of measurement results from a UHV transformer. The resonant frequency, f_x , calculated based on the parameters (C, L,R) evaluated by Daini-Kyodai method is identical to the value of f_x measured by the frequency measurement. Based on this evidence, both methods are considered to be equivalent in measuring the surge capacitance of a transformer.

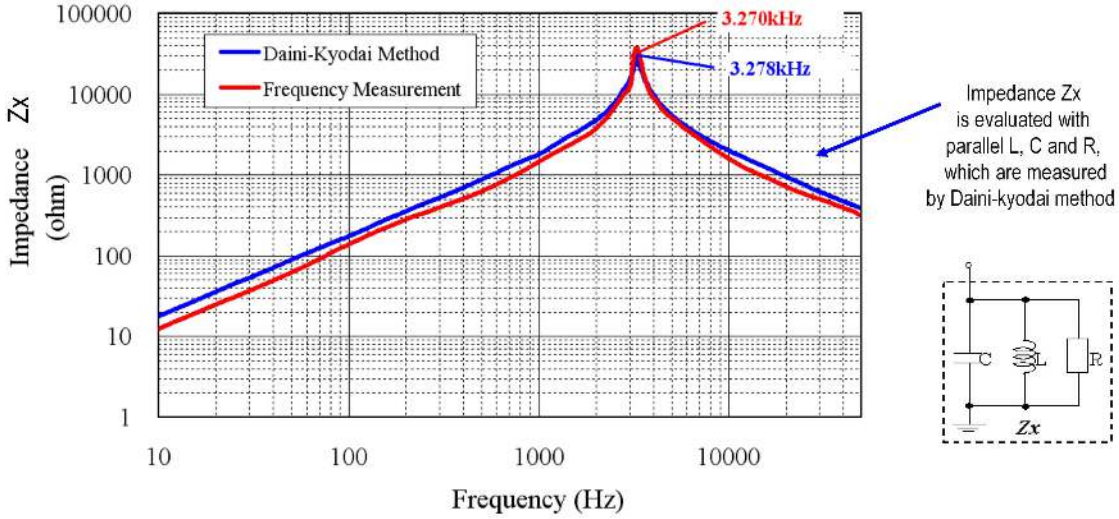

Figure 3.2.4 Comparison of measurement results with UHV transformer

3.2.2.4 Measurements of amplitude factor of power transformers

Figure 3.2.5 illustrates the relation between TRV and the damping constants derived from TRV measurement. Figure 3.2.6 summarizes the amplitude factor k_{af} derived from the damping constants measured by the step wave (Daini-Kyodai) method for various types of TEPCO's transformers. It can be obtained that k_{af} is almost always 1.8 or less.

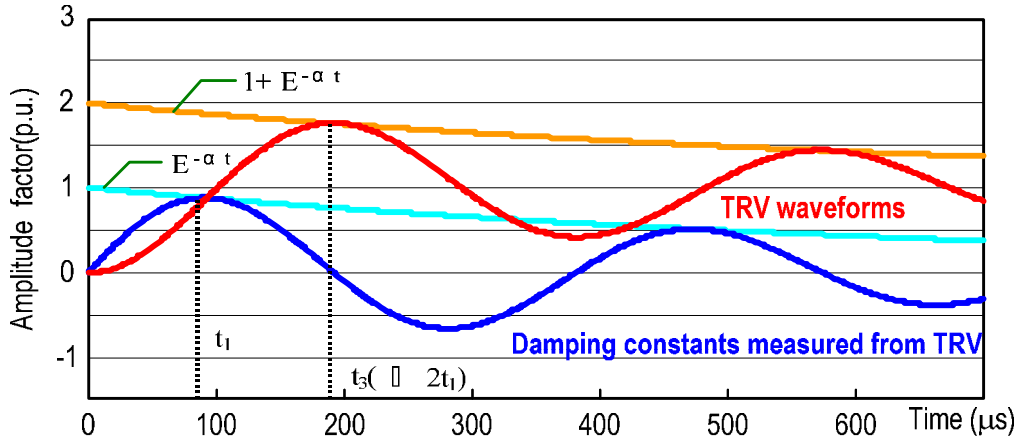

Figure 3.2.5 Relation between surge constants measured waveform and TRV waveform

Since the current used for surge constant measurement is very small (in the order of mA) and losses possibly increase in the range of actual short circuit current, the IEC standard value of 1.7 seem to be adequate, especially for UHV. In the UHV system in Japan, the voltage distribution of a transformer can also be covered by the standard value of 0.9.

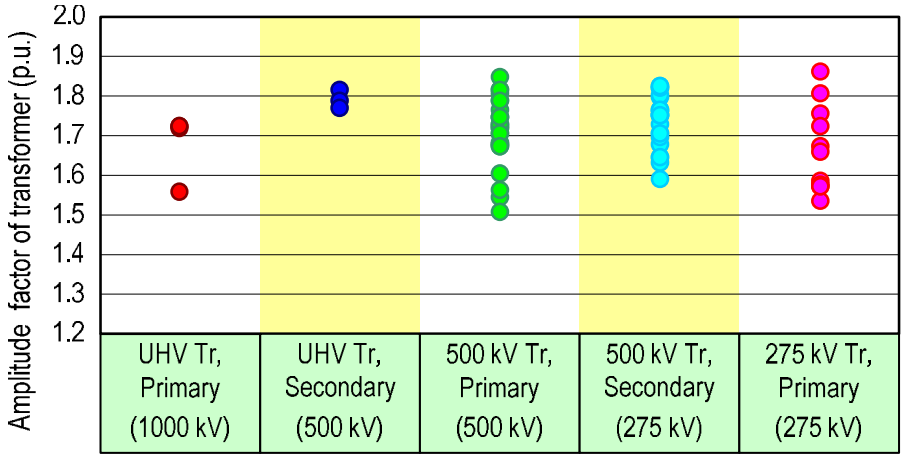

Figure 3.2.6 Typical measurements of the amplitude factors of different transformers

3.2.2.5 Measurements of transformer surge capacitance

Figure 3.2.7 shows examples of the surge capacitances for a primary winding and shows that the surge capacitance of a transformer depends on the rated capacity.

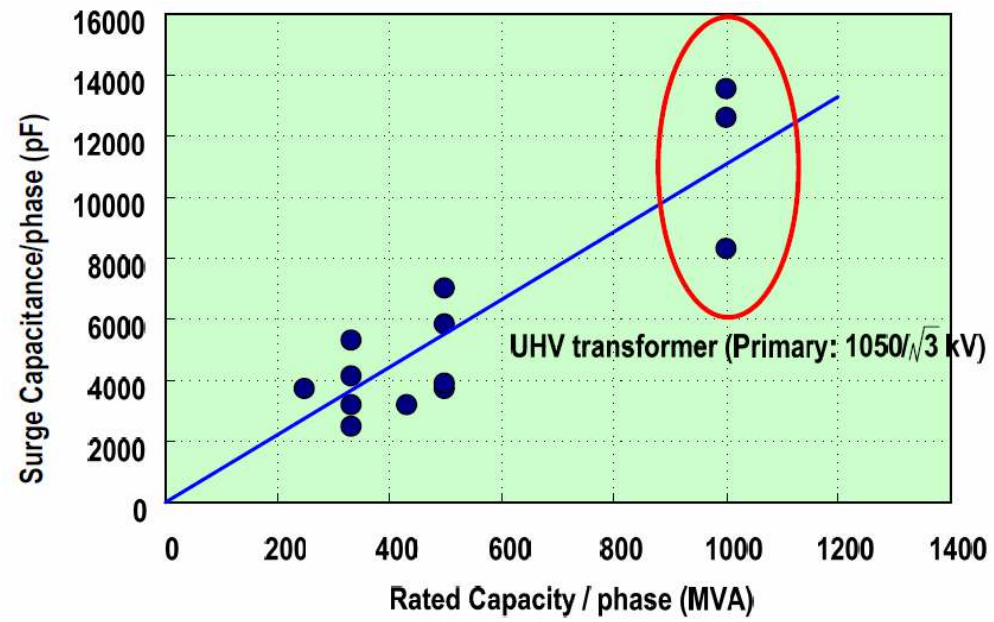

Figure 3.2.7 Examples of surge capacitance or transformer primary

3.2.3 Recommendations

The TRV peak for transformer limited faults (TLF) are defined by:

$$u_c = \frac{Ur}{\sqrt{3}}\sqrt{2} \times 0.9 \times 1.7 \times 1.2$$

With k_{pp} = 1.2 and an inherent amplitude factor for the transformer of k_{af} = 1.7 (assuming that the quality-factor of very large capacity transformers is comparable with that of large transformers in EHV systems. Here the quality-factor is an index to determine the qualitative behaviour of simple damped oscillator). As shown in the figure 3.2.6, k_{af} of UHV transformers is the same level as those of 500 kV and 275 kV transformers. The source side impedance is supposed to be 10 % of the transformer impedance and the peak value of the TRV at the source side is supposed not to coincide with the peak value of the TRV at the transformer side.

The TLF current is taken from the R10 series, with 10 kA and 12.5 kA as standard values. As the current is usually close to the values specified for test duty T10 (or T30), in most cases it could be possible during testing to combine the TLF test duty and one of the terminal fault test duty.

For the RRRV or t_3 it is recommended to apply a minimum value of the equivalent surge capacitance not less than 9 nF. By means of the power frequency inductance of the transformer and this capacitance the natural frequency (with short circuited secondary side), the time to peak and the time coordinate t_3 can be calculated in a rather straight forward way. An alternative method would be to use the IEEE-formula with an adapted k-factor:

$$t_3 = \frac{6 \times \sqrt{U_r}}{I^{0.21}}$$ with t_3 in µs, U_r in kV and I in kA

The impact of MOSAs is, when any, limited to the peak value of the TRV at the transformer side, where the TRV wave-shape may be clipped to a value of about 1400

kV. It is recommended to take some margin around this clipping level, due to some variation in MOSA characteristic, depending on specification and application, etc. Suggested is a margin of 5 %, besides a margin of 5 % for the TRV to ensure that the circuit-breaker can withstand the clipping level of the MOSA. Together this leads to a TRV peak value, clipped by a MOSA, of 1540 kV. In that case, however, it seems to be reasonable to consider the source side peak value as well, due to the flattened peak of the TRV. Just to give an idea, for the case where the source side impedance is only 10 % (but clipping will also be possible in other cases, with a larger share at the source side to the total TRV):

$$u_c = \frac{Ur}{\sqrt{3}}\sqrt{2} \times 0.1 \times 1.5 \times 1.3 = 175 \text{ kV},$$

so that the total TRV peak value becomes 1715 kV, well above 1649 kV specified without the impact of a MOSA.

3.3 Long-Line Faults (LLF)

3.3.1 Introduction

The first description of long line faults (LLF) was introduced by experts from Japan at the CIGRÉ SC 13 Session in 2002 [5]. Clearing such faults gives transient phenomena across the terminals of the circuit-breaker that are of a similar physical nature as those that appear at clearing short-line faults (SLF), but unlike the TRV wave-shape at SLF, the RRRV is less steep, while the peak value can reach quite large values.

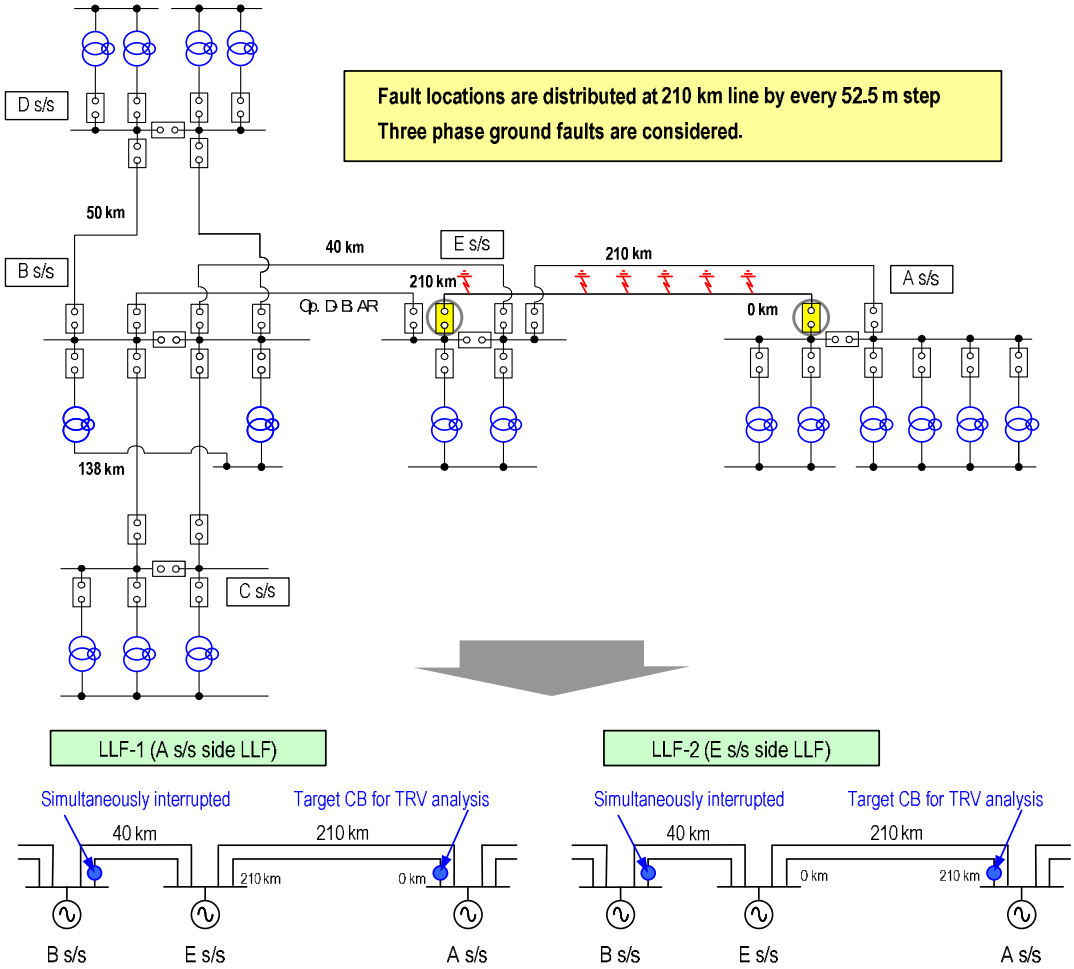

Figure 3.3.1 Analysis circuit for LLF

To study LLF-phenomena the EMTP-simulation of the future UHV network in Japan has been used, and the longest line has been subjected to 3-phase grounded short circuit faults at different locations, as shown in figure 3.3.1. In section 3.3.2 background information for the simulation results is given in order to understand the phenomena and to extrapolate the results to wider applications. Analytical formulas for some particular phenomena are given in detail in the sections 3.3.4 and 3.3.5. (3.3.3).

For UHV systems a rather simple network topography is expected: more radial than meshed. This means that some typical effects may occur, such as the influence of the circuit-breaker clearing the fault current at the other end of the double circuit OH-line. The switching overvoltage generated by that circuit-breaker may influence the busbar side part of the TRV of the circuit-breaker under consideration. This effect will be further elaborated in section 3.3.4, and the TRVs for the circuit-breakers at both sides of the faulty circuit will be calculated.

Both EMTP simulations and simplified calculations to understand the phenomena will be presented. Table 3.3.1 and 3.3.2 show the simulation results for both circuit-breakers.

Table 3.3.1 Calculated results for LLF-1 （A s/s side LLF）

Fault location	Phase	Interrupting current I (kA) *	Peak voltage Up (kV)	Time to peak voltage Tp (μs)	Up/Tp (kV/μs)	Clearing pole
0km (A s/s)	A	24.0 (100%)	1102	586	1.88	3rd
	B		1057	506	2.09	2nd
	C		991	703	1.41	1st
52.5km	A	15.6 (65%)	1139	307	3.71	3rd
	B		1161	384	3.02	2nd
	C		1334	478	2.79	1st
105.0km	A	11.1 (46%)	1341	657	2.04	3rd
	B		1280	613	2.09	2nd
	C		1293	663	1.95	1st
157.5km	A	8.0 (33%)	1290	838	1.54	3rd
	B		1519	993	1.53	2nd
	C		1600	1046	1.53	1st
210.0km (E s/s)	A	5.1 (21%)	1359	1441	0.94	3rd
	B		1647	629	2.62	2nd
	C		1670	1325	1.26	1st

Table 3.3.2 Calculated results for LLF-2 （E s/s side LLF）

Fault location	Phase	Interrupting current I (kA)	Peak voltage Up (kV)	Time to peak voltage Tp (μs)	Up/Tp (kV/μs)	Clearing pole
0km (E s/s)	A	30.5 (100%)	1585	2331	0.68	3rd
	B		1057	714	1.48	2nd
	C		1385	1194	1.16	1st
52.5km	A	18.7 (61%)	1063	320	3.32	3rd
	B		1306	510	2.56	2nd
	C		1438	513	2.80	1st
105.0km	A	13.0 (43%)	1425	770	1.85	3rd
	B		1302	739	1.76	2nd
	C		1396	767	1.82	1st
157.5km	A	9.5 (31%)	1321	847	1.56	3rd
	B		1583	936.9	1.69	2nd
	C		1629	1058	1.54	1st
210.0km (A s/s)	A	6.6 (22%)	1268	886	1.43	3rd
	B		1619	650	2.49	2nd
	C		1684	1276	1.32	1st

The difference of the calculated values by the clearing pole might be influenced by the characteristics of the OH-lines, since the self and mutual impedance of each conductor are slightly different, as they are un-transposed.

For each location of the fault along the OH-line, the most severe TRV is plotted in the figures 3.3.2 and 3.3.3 for each side of the OH-line. A comparison is made between the EMTP-simulations and the rough calculations that will be elaborated in the next section.

It is clear that LLFs generate rather high peak values of the TRV. Moreover, in comparison to a bus terminal fault, the RRRV is rather high as well.

Note that due to the estimation of k_{pp}, the rough calculations show higher peak values than the simulations do. The rough calculations lead, for the lowest short-circuit currents calculated (about T10), to a total peak value of near 1900 kV, i.e. 2.1 p.u. But, because the peak value for T10 is specified as $k_{pp}*k_{af}$, with k_{af} = 1.76, as

explicitly specified in edition 2 of IEC 62271-100 to cover LLF, with k_{pp} = 1.2 the nearly 1900 kV or 2.1 p.u. can be considered to be covered.

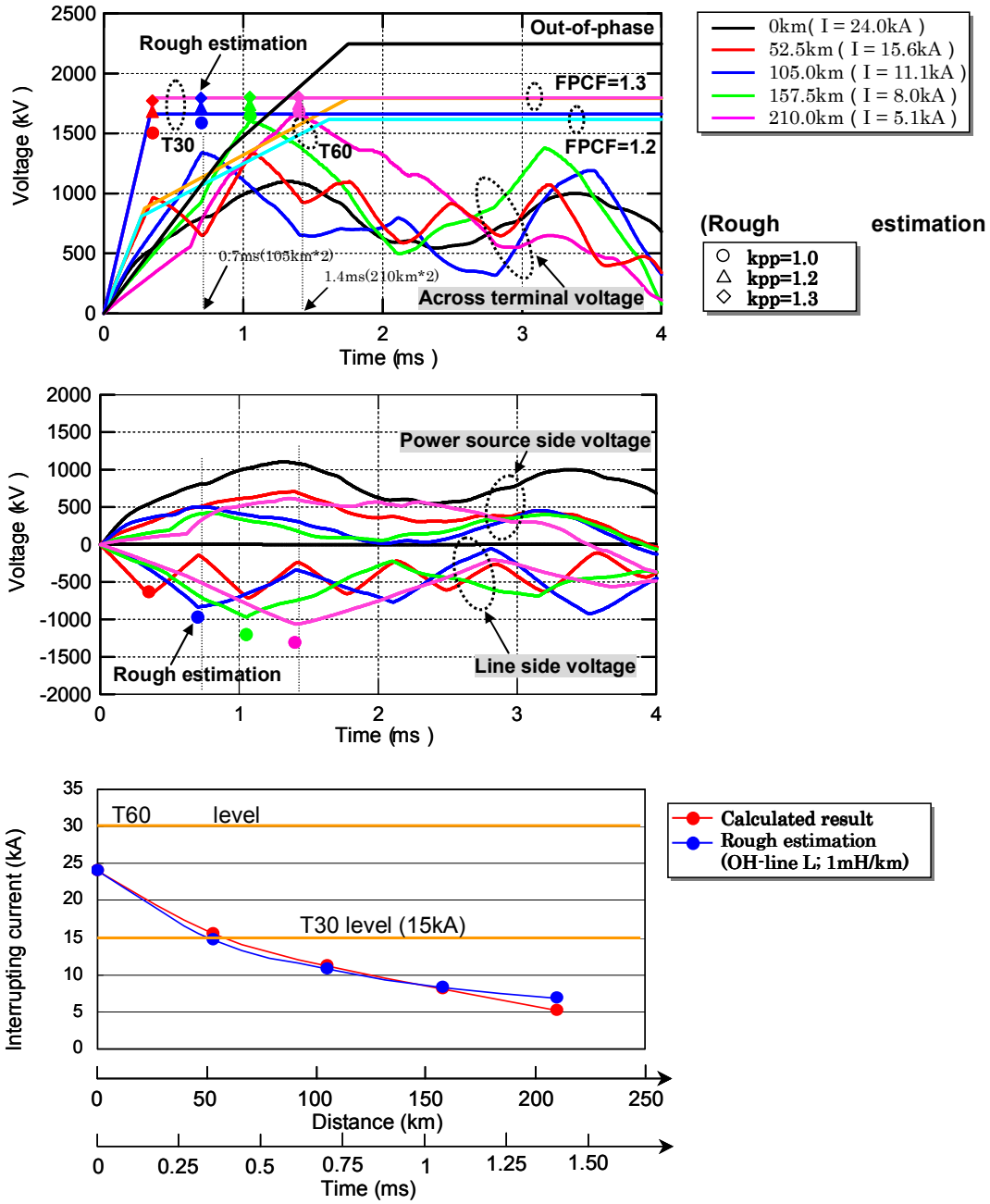

Figure 3.3.2 Calculated results for LLF-1 (As/s side LLF)

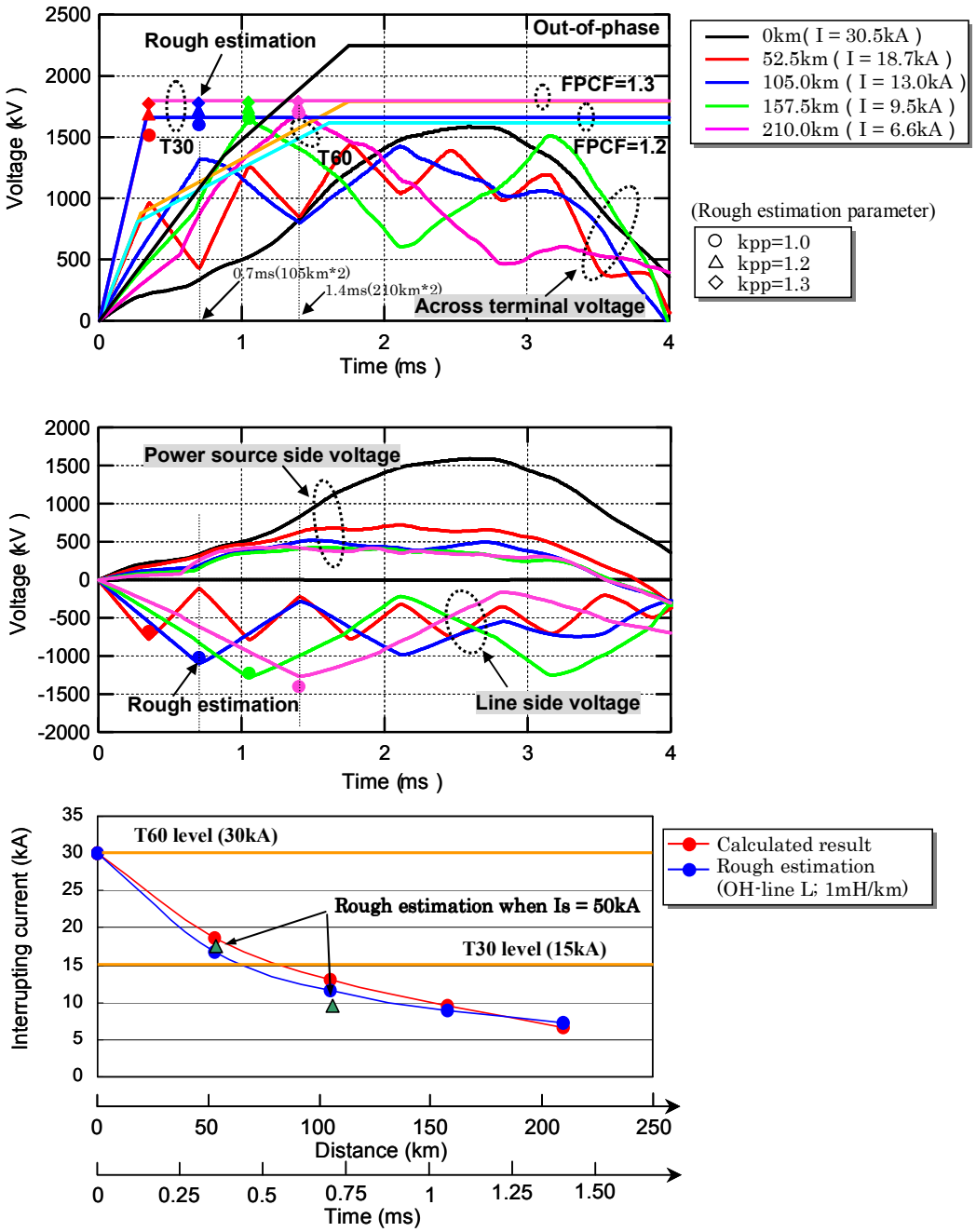

Fig.3 Calculated results for LLF-2 (E s/s side LLF)

Figure 3.3.3 Calculated results for LLF-2 (E s/s side LLF)

3.3.2 Background

3.3.2.1 Generalization of the TRV of LLF

The estimations of TRV waveforms shown in Figures 3.3.2 and 3.3.3 are derived from the following equations.

Line side peak voltage; $U_p = U_m \times (1 - I / I_s) \times 2$. (Note that for d_3 a factor 2.0 is applied rather than 2.4, as proposed by CIGRÉ WG A3.19 in the section 3.3.5.)

Time to reach U_p; $T_p = 2 \times L / C_0$ (C_0; light velocity, assuming that the propagation speed is equal to light)

Across terminals peak voltage; $U_p = U_m \times (1 - I/I_s) \times 2 + U_m \times k_{pp} \times k_{af} \times I/I_s$

TRV at both the line side and the power source side are considered. At the source side several values are applied for k_{pp} = 1.0, 1.2, 1.3 while k_{af} = 1.5 (as the values of I_s are almost in the range of T60, IEC standard value for k_{af} of T60 is adopted.)

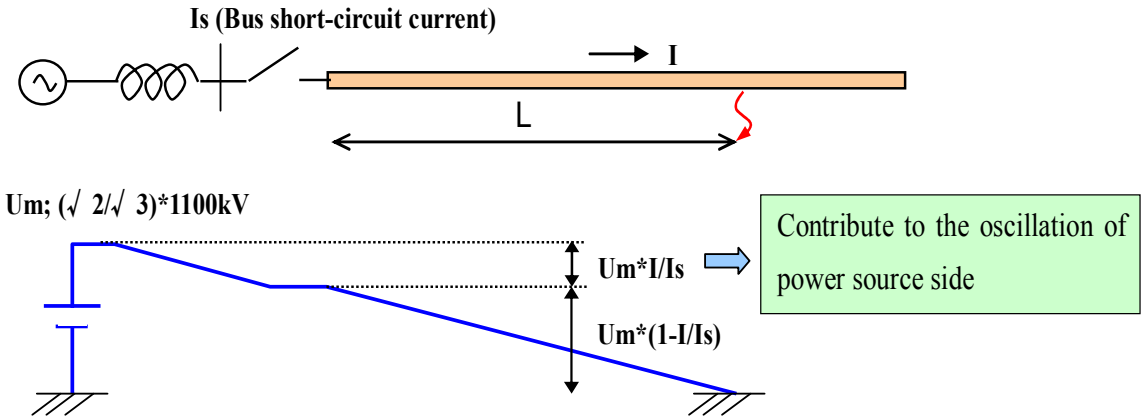

Figure 3.3.4 Voltage distribution at a line fault

As shown in Figures.3.3.2 and 3.3.3, these rough estimations for the line side peak voltages agree well with the EMTP calculation results whilst the across terminals peak voltages cover EMTP calculation ones. However, for the power source side with a parallel OH-line, there is an effect of the other side CB's fault clearing. The effects of the travelling waves generated by the other side CB's fault clearing appears to be prominent in the case of comparatively long distance faults.

Since these estimations cannot provide an accurate TRV for systems with a parallel OH-line, it seems to be difficult to generalize the TRV for LLF duty by this method. However, the power source side voltage, including the effect of the switching overvoltage generated by the circuit-breaker at the other line-end and transmitted through a parallel OH-line circuit, can be explained by the simple calculations as described in section 3.3.4. These estimations can provide the following conclusions.

(1) The line side peak voltage becomes larger as the bus short-circuit current increases.

(2) The power source side voltage tends to decrease with increasing bus short-circuit current because the increase of the bus short-circuit current means a decrease of the back impedance seen from the fault clearing CB. In such a case there has to be an increase of the number of OH-lines connected to the bus and/or a decrease of the source side inductance, leading to a reduction the TRV peak voltage (see also section 3.1.2.2).

(3) The voltage across a circuit breaker does not change so much with an increase of the bus short-circuit current due to the combination of the above effects.

3.3.2.2 Comparison with the standard value

In the range of T30 (15kA or less), typical results of TRVs can be covered by TRV representations for T30 and out-of-phase duties having respectively an amplitude factor k_{af} = 1.54 and 1.25 and a first-pole-to-clear factor k_{pp}= 1.2.

In the range of T60 (15kA-30kA), where the distance to the fault location is smaller than several tens of km, typical TRVs slightly exceed a TRV representation for T60 duty having an amplitude factor of 1.5 and k_{pp}= 1.2. In the range of currents near 60% of rated breaking current, the short-line-fault breaking capability L60 demonstrates the capability of a circuit-breaker to handle values of RRRV than are higher than those specified by the T60 duty. This SLF breaking capability demonstrates the withstand capability for TRV that reaches up to almost 800 kV within less than 100 µs.

The RRRV withstand demonstrated by a SLF test duty with 60% of rated short-circuit current and a surge impedance of 330 Ω is 4.4 kV/µs, which covers the RRRV obtained during LLF. Presently the SLF breaking capability is demonstrated in IEC by performing single-phase tests with TRV parameters relative to the first pole to clear i.e. the highest RRRV possible during a three-phase fault and considers that it covers in practical terms the interruption of all three poles.

Pending further studies this can be assumed to be true also in the UHV range, taking into account that when UHV circuit-breakers have either two chambers rated 550kV in series or four chambers rated 300kV in series, the fast TRV withstand on each chamber is significantly reduced compared to what it has to withstand when considered and tested a as single-unit pole 550/2 or 1100/4 kV.

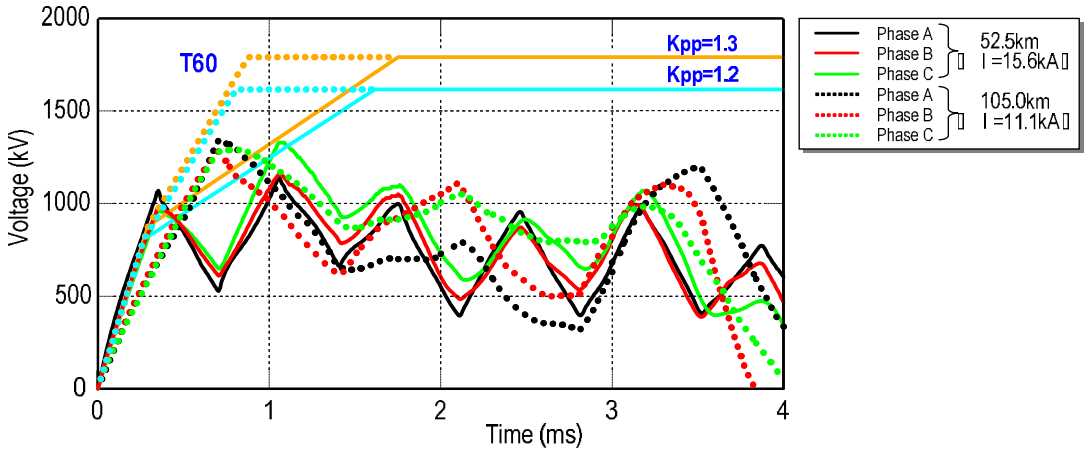

Figure 3.3.5 LLF-1 voltage across CB（E s/s side LLF）

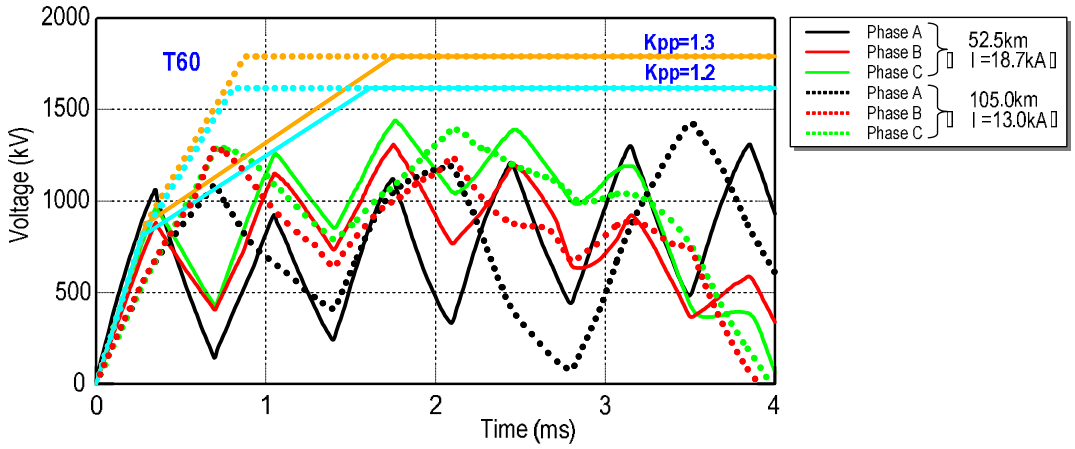

Figure 3.3.6 LLF-2 voltage across CB（E s/s side LLF）

3.3.3 Recommendation

TRV waveforms for LLF are covered by TRV representations for L60, T100, T60, T30, T10 and OP duties having peak values twice that of existing 550 kV standards, described in other chapters, even when k_{pp} = 1.2, but then for T10 k_{af} has to be specified as 1.76.

As discussed in section 3.1.2.6, it is recommended to reduce t_2 for T100 and T60 to become $t_2 = 3 \times t_1$ and $t_2 = 4.5 \times t_1$, respectively, considering a shorter equivalent line lengths than 200 km. Note that t_2 for T100 and T60 are identical, as the RRRV is specified to be 2 and 3 kV/μs, respectively.

There is no impact from MOSA on the TRV, as the parts of the TRV at each terminal of the circuit-breaker are relative low with respect to the clipping level of the MOSA applied.

3.3.4 Estimation of the effect of the other side CB's fault clearing

To evaluate the effect of LLF duties thefollowing remote end faults are studied.

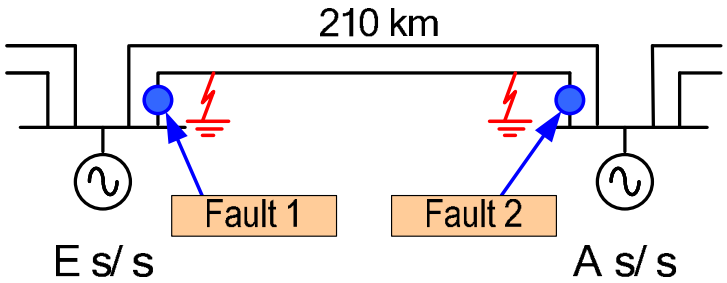

Figure 3.3.7 Estimation of TRV for TLF

(1) Fault 1; line fault near E s/s (LLF-1): LLF of 210km (at A s/s side)

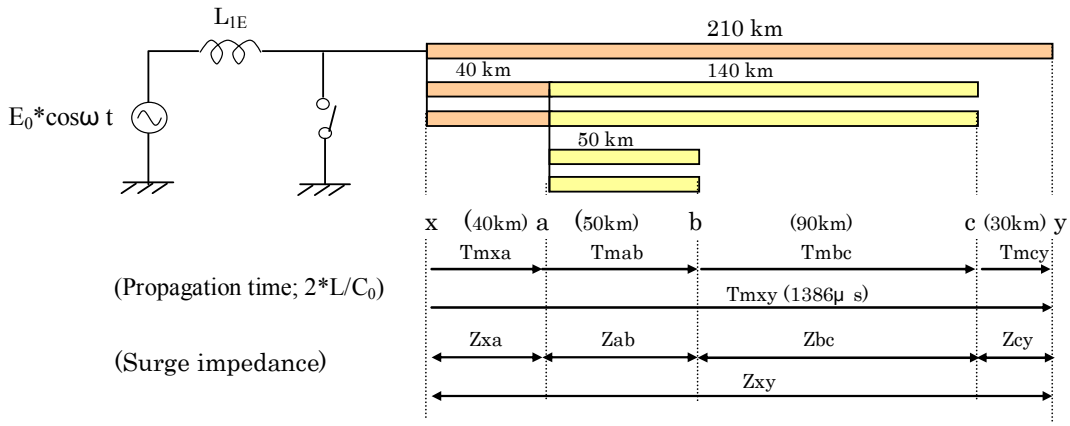

Figure 3.3.8 Simplified model for CB located at E substation

L_{1E} =200 mH (10kA) (a typical value), Here, surge impedances are assumed as 300Ω/1 per circuit. Therefore, equivalent surge impedance Z_{xy} is given by:

$$Z_{xy} = \left[Z_{xa} \times T_{mxa} + Z_{ab} \times T_{mab} + Z_{bc} \times T_{mbc} + Z_{cy} \times T_{mcy}\right] / T_{mxy} =$$

$$\left[(300/3) \times 264 + (300/5) \times 330 + (300/3) \times 594 + (300/1) \times 198\right] / 1386 = 119\ \Omega$$

Then, $T_0 = L_{1E} / Z_{xy} = 200 \times 10^{-3} / 119 = 1{,}667\ \mu s$

When the fault current from the power source at the remote end is neglected, the bus voltage V_E at E s/s side due to CB's clearing at E s/s side is given by:

$$V_E(t) = E_0 \times \left[1 - \exp\left(-t / T_0\right)\right] = E_0 \times \left[1 - \exp\left(-t / 1{,}667\right)\right] \ldots.(1)$$

The bus voltage V_{AE} at A s/s side due to the travelling wave generated by CB's clearing at E s/s side is given by:

$$V_{AE}(t - t_0) = k_A \times E_0 \times \left[1 - \exp(-(t - t_0)/1{,}667)\right] \ldots.(2)$$

Here t_0 = 210km/c_0 = 693 μs, and when $t < t_0$, V_{AE} =0

k_A is transmission coefficient at A s/s bus, and $k_A = 2 \times sL_{1A} / (sL_{1A} + Z_{xy})$

(2) Fault 2; line fault near A s/s (LLF-2): LLF of 210km (at E s/s side)

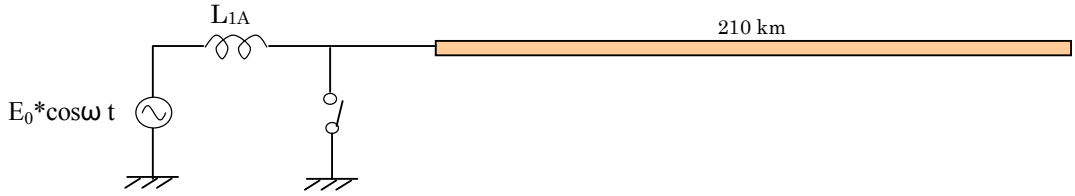

Figure 3.3.9 Simplified model for CB located at A s/s side

L_{1A} = 135 mH (15 kA) (a typical value), Z_{xy} = 300 Ω,

$$T_0 = L_{1A} / Z_{xy} = 135 \times 10^{-3} / 300 = 450\ \mu s$$

The bus voltage V_A at A s/s side due to CB's clearing at A s/s side is given by:

$$V_A(t) = E_0 \times \left[1 - \exp(-t / T_0)\right] = E_0 \times \left[1 - \exp(-t / 450)\right] \ldots.(3)$$

The bus voltage at E s/s side due to the travelling wave generated by CB's clearing at A s/s side is given by:

$$V_{EA}(t-t_0) = kE \times E_0 \times [1-\exp(-(t-t_0)/450] \quad \ldots. (4)$$

Here t_0 = 210 km / c_0 = 693 μs, and when t < t_0, V_{EA} =0

kE is transmission coefficient at E s/s bus. Since OH-line number increase 1 to 2 at E s/s and 2 to 4 at B s/s, equivalent kE is roughly 1/2.

(3) Estimation of the voltage at power source side

The power source side voltage for LLF due to remote end fault is roughly given by:

V(t) = (I/I_s) *the voltage for the bus terminal fault due to target CB [term A]+ the travelling voltage due to the terminal fault at the remote [term B]…(5)

For the voltage for LLF-1 of 210 km (fault near A s/s):

$$V(t) = (I/I_s) \times V_A(t) + V_A(t) + V_{AE}(t-t_0)$$

$$= (I/I_s) \times E_0 \times [1-\exp(-t/450)] + kA \times E_0 \times [1-\exp(-(t-693)/1{,}667)] \ldots (6)$$

For the voltage for LLF-2 of 210 km (E s/s TLF); $V(t) = (I/I_s) \times V_E(t) + V_{EA}(t-t_0)$

$$= (I/I_s) \times E_0 \times [1-\exp(-t/1{,}667)] + kE \times E_0 \times [1-\exp(-(t-693)/450) \quad \ldots (7)$$

Then the power source side voltages at 2×210 km / c_0 = 1386 μs which timing is that of the line side voltage reach to the peak voltage are calculated as following table.

Table 3.3.3 Estimation of the voltage at power source side

	[term A]	[term B]	[term A] + [term B]
LLF-1 (A s/s LLF)	(I/I_s) * E_0* [1 – exp (- t /450)] = 0.21*0.954* E_0= 0.2* E_0	kA * E_0* [1 – exp (- (t -693)/1,667)]= kA*0.34* E_0 = 0.41* E_0 (kA was assumed as 1.2)	0.61* E_0 *EMTP result; 0.68* E_0
LLF-2 (E s/s LLF)	(I/I_s) * E_0* [1 – exp (- t/1,667)] = 0.22*0.56* E_0 = 0.12* E_0	kE * E_0* [1 – exp (- (t - 693)/450)] = kE*0.79* E_0 = 0.40 * E_0 (k_E was assumed as 0.5)	0.52* E_0 *EMTP result; 0.5* E_0

These estimated values comparatively match to EMTP results, therefore it can be said the power source side voltage of LLF can be roughly estimated by these hand-calculation method.

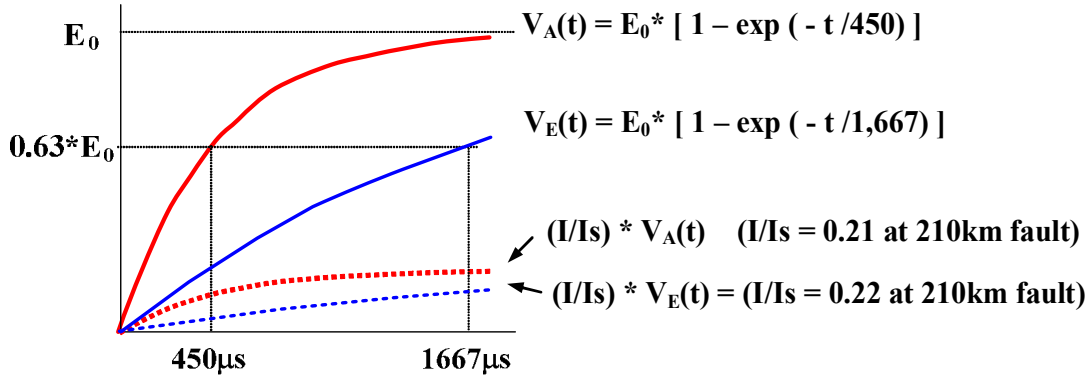

Figure 3.3.10 Estimated TRV of target CB

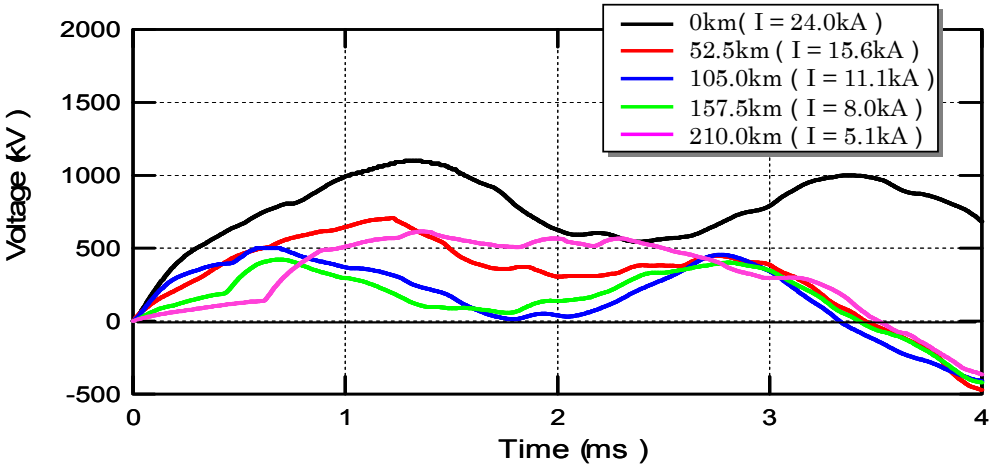

Figure 3.3.11 EMTP results of TRV for LLF-1at power source side (A s/s side LLF)

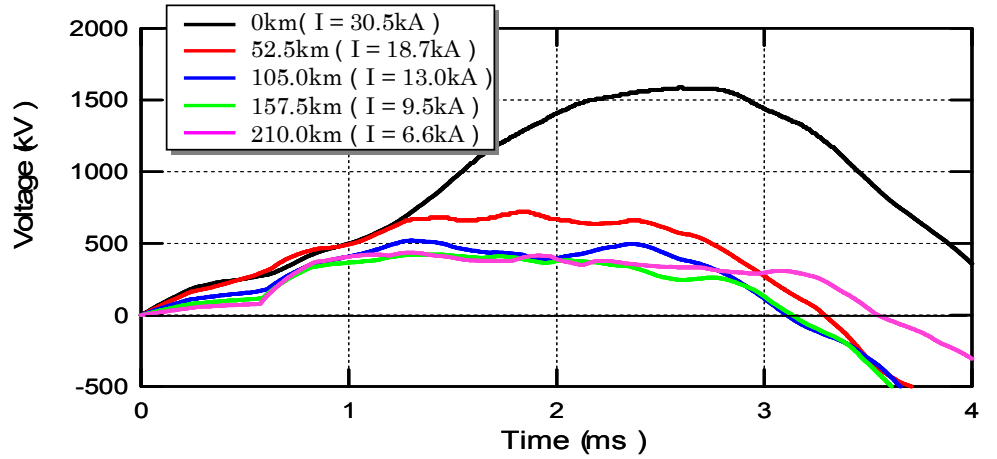

Figure 3.3.12 EMTP results of TRV for LLF-2at power source side (E s/s side LLF)

3.3.5 Line side peak factor for 3-phase versus 1-phase fault clearing

The following explanations are in line with the results published by CIGRÉ WG A3.19, but the final conclusion, based on EMTP-simulations, shows a factor d_3 to be 2.0 rather than 2.4, in comparison to d_1=1.6, a figure that is consistent with the EMTP-simulation results.

An important parameter is the X_0/X_1 ratio, which is dependent on the tower geometry, the line sag, the earth resistivity and the frequency of the travelling wave phenomena. With respect to X_0 and X_1 (f=50Hz) of the UHV-designed OH-line in TEPCO, table 3.3.4 shows the comparison between the simple calculations based on TEPCO tower design and parameters obtained by TEPCO experience. The calculated X_1 is almost equal to the experienced value while the X_0 value is about 30% smaller than the experienced value. Although the detailed comparison between measured values and calculations regarding fault currents etc. has not been done, as any problems have not been caused in the actual network operation, calculated X_0/X_1 of 2.64 is thought to be realistic.

Table 3.3.4 X_0/X_1 ratio for TEPCO

	Simple calculation	TEPCO experience
X_1	2.47*10^{-4} Ω/m (0.787 mH/km)	2.51*10^{-4} Ω/m (0.798 mH/km)
X_0	4.75*10^{-4} Ω/m (1.51 mH/km) - 4.91*10^{-4} Ω/m (1.56 mH/km) * Calculated by Carson's equation	6.63*10^{-4} Ω/m (2.11 mH/km)
X_0/X_1	1.92 – 1.99	2.64

**TEPCO experience values for Earthing resistivity ρ : 100 Ωm.*

The line side contribution to the TRV is equal to the instantaneous value of the line side voltage at current zero multiplied by the peak factor "d_1". The peak factor is defined in Table 4 of IEC 62271-100. This value is considered to be independent of rated voltage and to be equal to 1.6. This value is also suitable for UHV applications as shown in the following simplified calculation.

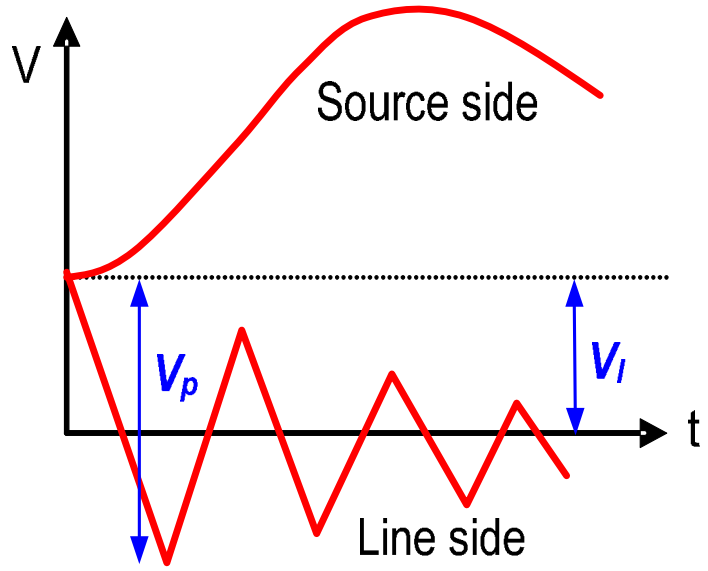

Figure 3.3.13 TRV for SLF duty

Peak factor (d_1) at single-phase fault or last pole clearing can be given by;

$$d_1 = \frac{V_p}{V_l} = \frac{(\omega Z_{last})I_1 \times \frac{2l_1}{c}}{(X_L l_1)I_1} = \frac{\omega \times \frac{2Z_1 + Z_0}{3} \times I_1 \times \frac{2l_1}{c}}{\frac{2X_1 + X_0}{3} \times l_1 \times I_1} = 2 \times \frac{(2 + \frac{Z_0}{Z_1})Z_1\omega}{(2 + \frac{X_0}{X_1})X_1 c} \quad \ldots. (1)$$

Where, l_1 : Line length to the single-phase fault point, I_1: Single-phase fault current, c : Propagation speed of light, Z_{Last} : Equivalent surge impedance for the third pole clearing (= $(2Z_1+Z_0)/3$), X_{L1}: Line reactance per unit length of power-frequency at single-phase fault (= $(2X_1+X_0)/3$)

If $Z_1 = \sqrt{L_1/C_1}$, $c = 1/\sqrt{L_1 C_1}$, $X_1 = \omega L_1$ are assumed, equation (1) is;

$$d_1 = 2 \times \frac{2 + Z_0/Z_1}{2 + X_0/X_1} \quad \ldots. (2)$$

In case of $X_0/X_1 = 3.0$, d_1 becomes a well-known equation as follows.

$$d_1 = 0.4 \times (2 + Z_0 / Z_1) \quad \ldots. (3)$$

When X_0/X_1=2.64 as per the TEPCO experience, and assuming Z_0/Z_1 = 476Ω/228Ω= 2.09 (Z_0, Z_1 are calculated values of Japan 1100kV case with 25kHz shown in Table 3.4.1 for UHV networks in Japan in the case of no bundle contraction), d_1 is equal to 1.76. In Italy a value of 1.57 is reported. The value in Japan is slightly higher than the standard value of 1.6 for SLF duty.

However, when peak voltage relaxation effects such as travelling losses and surge propagation of line-to-earth and line-to-line waves with different velocity are considered, d_1 is reduced. So it would be unnecessary to change the standard value of 1.6, though more study is desirable.

Peak factor (d_3) at three-phase faults or first pole clearing can also be given by;

$$d_3 = \frac{(\omega Z_{first} I_3) \times \frac{2l_3}{c}}{(X_{L3} l_3) \times I_3} = \frac{\omega \times \frac{3Z_1 Z_0}{Z_1 + 2Z_0} \times I_3 \times \frac{2l_3}{c}}{X_1 \times l_3 \times I_3} = 6 \times \frac{Z_1 Z_0}{Z_1 + 2Z_0} \times \frac{\omega}{X_1 c} = 6 \times \frac{Z_0 / Z_1}{1 + 2Z_0 / Z_1} \quad (5)$$

From equation (1) and (5), d_3 can be also given by;

$$d_3 = d_1 \times \frac{2 + X_0 / X_1}{3} \times \frac{Z_{first}}{Z_{last}} \ldots. (5)'$$

Where, l_1 : Line length to the three-phase fault point, I_3 : three-phase fault current, Z_{first} is: equivalent surge impedance for the first pole clearing (= $3Z_1Z_0/(Z_1+2Z_0)$). X_{L3} : Line reactance per unit length of power-frequency at three-phase fault (= X_1). When the fault current and the reactance at source side are equal for three-phase and single-phase fault, the ratio of the peak voltage becomes the same as that of the peak factor as follows.

$$\frac{V_{p3}}{V_{p1}} = \frac{d_3 \times V_{l3}}{d_1 \times V_{l1}} = \frac{d_3 \times X_{L3} l_3 I_3}{d_1 \times X_{L1} l_1 I_1} = \frac{d_3 \times l_3 X_1}{d_1 \times l_1 (2X_1 + X_0)/3} = \frac{d_3}{d_1}$$

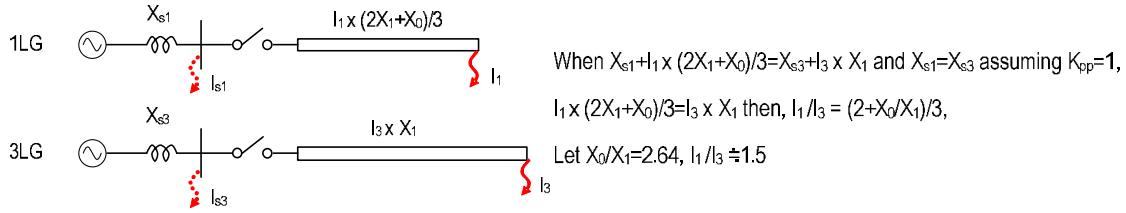

Figure 3.3.14 Consideration of single and three phase fault

When Z_0/Z_1 =2.09 (this value is at 25 kHz, so in the frequency range of LLF, it becomes slightly higher due to the frequency dependency of Z_0), from equation (5), d_3 becomes 2.4.

However, EMTP simulations of LLF for the TEPCO network show that an estimation of peak factor = 2.0 is relatively well matched with the calculated line side TRV, which can be seen in figures 3.3.2 and 3.3.3 in the section 3.3 LLF.

It seems that peak voltage relaxation effects are relatively large, and consequently the peak factor d_3 becomes a not so large value as derived by equation (5) or (5)'.

3.4 Short-Line Faults (SLF)

3.4.1 Introduction

IEC 62271-100 requires type tests to demonstrate the capability of circuit breakers directly connected to overhead lines to interrupt short-line faults (SLF). These faults are considered to occur on transmission lines at a distance that ranges from 100 m to a few kilometres along the line. Two test duties, L90 and L75, are stipulated with a current equal to 90% and 75% of the rated short-circuit breaking current, respectively. A third test duty is required if the minimum arcing time obtained during test duty L75 is a quarter of a cycle or more greater than the minimum arcing time determined during test duty L90.

The severity of the SLF test duties depends mostly on the rate of rise of recovery voltage that is the product of the line surge impedance and the slope of the fault current at current zero.

3.4.2 Line surge impedance

The equivalent line surge impedances (Z) for each pole-to-clear are given by equations (1), (2) and (3):

$$Z_{first\ pole} = \frac{3\,Z_1\,Z_0}{Z_1 + 2\,Z_0} \qquad (1)$$

$$Z_{second\ pole} = \frac{Z_1\,(Z_1 + 2\,Z_0)}{2\,Z_1 + Z_0} \qquad (2)$$

$$Z_{third\ pole} = \frac{(2\,Z_1 + Z_0)}{3} \qquad (3)$$

where Z_0 is the zero-sequence surge impedance and Z_1 is the positive-sequence surge impedance.

Some values of line surge impedances for UHV systems are given in Table 3.4.1 as well as values for EHV systems. It can be noted that in the case of three-phase line faults, the surge impedance is highest for the third pole to clear.

In IEC 62271-100, a single-phase test at phase-to-earth voltage is considered to cover all types of short-line fault. This is supported by the following considerations:

- In the case of three-phase faults, the line surge impedance is highest for the last pole to clear. Consequently, for single phase tests, the line surge impedance of the last pole to clear shall be used to get the highest RRRV. A single-phase fault interruption covers all SLF conditions if the highest value of the line surge impedance for the last pole to clear is taken from Table 3.

- A single phase short-line fault test demonstrates an arcing window of (180°−dα) that covers the requirements for all multi-phase fault cases in effectively-earthed and non-effectively earthed systems.

- The capability to withstand the peak value of TRV during a three-phase fault interruption is demonstrated by terminal fault test duty T100, whereas the highest RRRV is covered by SLF.

These considerations apply also in the case of UHV, therefore SLF are recommended to be performed single-phase with line characteristics defined hereafter for single-phase faults.

3.4.3 Background of technical requirements

For the line surge impedance, IEC 62271-100 and IEEE C37.04 have a standard value of 450 Ω, considering bundle contraction due to magnetic attraction caused by a large fault current, although the equivalent line surge impedance calculated without bundle contraction is less than 360 Ω (see IEEE C37.011-2005 and values in Table 3.4.1 for system voltages 500 kV and 765 kV). Besides the fault current, the actual values of line surge impedance depend on multi-bundle conductor designs (materials, cross-section, span and spacer size) and the mechanical tension applied on the conductors of the lines.

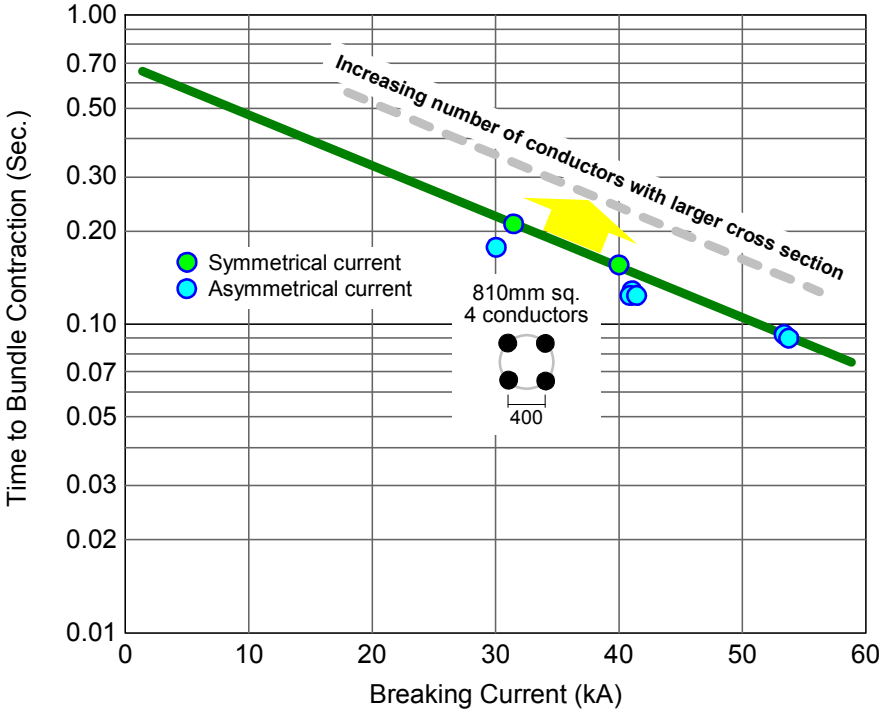

Figure 3.4.1 Collision time of multi-bundle conductors

Several studies including those of CIGRE WG 13.01 [6] have reported times for bundle contraction. For example, twin conductors with 686 mm^2 in cross-section carrying 40 kA collided at 50 ms after a fault occurrence and quadruple conductors with 810 mm^2 in cross-section carrying 30-50 kA collided at 100-200 ms as shown in Figure 3.4.1. A longer time for bundle contraction is expected for UHV lines due to the increased number of conductors and the larger cross section used.

Table 3.4.1 shows the line surge impedances for 500 kV, 765 kV and 1000 kV transmission lines (three-phase lines are transposed) evaluated using the constant parameter lines model (CP line) supported by the EMTP program. The TRV frequencies for L90 duty were 60 kHz, 27.5 kHz and 25 kHz respectively for these

system voltages. The TRV frequency depends on the line length and, for a given percentage of short-line fault, it is then dependent on the rated voltage and the rated breaking current of the circuit breaker.

The line surge impedance for the third pole-to-clear is highest when compared with the values for each pole under the condition that the breaking current is the same for each phase. The surge impedance is increased by approximately 20-30% when bundle contraction occurs.

For UHV transmission lines with 6-8 bundle conductors, bundle contraction is not completed when the fault current is interrupted (between 50 and 80 ms after a fault) due to the higher tension of lines and the fact that the lines have a large cross-section. In such cases, the line surge impedance for L90 and L75 duties can be reduced for the rated voltages of 1000 kV and above.

Table 3.4.1 Surge impedance of transmission lines

System voltage	Conductors		TRV Frequency (conditions)	Z0 (Ω)	Z1 (Ω)	Equivalent surge impedance (Ω)		
	Size	Bundle				1st pole	2nd pole	3rd Pole
500 kV (Japan)	410 mm^2	6	60 Hz (Normal span)	509	228	279	294	322
			60 kHz (Normal span)	444	226	270	281	299
			60 kHz (Bundle contraction)	580	355	408	417	430
765 kV (South Africa)	428 mm^2	6	50 Hz (Normal span)	561	258	315	331	359
			27.5 kHz (Normal span)	403	254	290	296	304
			27.5 kHz (Bundle contraction)	509	359	398	403	409
1,000 kV (Italy)	520 mm^2	8	50 Hz (Normal span)	485	211	260	275	302
			25 kHz (Normal span)	406	210	250	260	275
			25 kHz (Bundle contraction)	426	230	272	281	295
1,000 kV (Japan)	810 mm^2	8	50 Hz (Normal span)	530	229	282	299	329
			25 kHz (Normal span)	476	228	276	289	311
			25 kHz (Bundle contraction)	595	339	396	407	424

3.4.4 Recommendations for specifications

A value of 330 Ω is recommended for the surge impedance of lines in UHV systems.

3.5 Capacitive current switching

3.5.1 Introduction

Since capacitor banks and cables are not yet considered in UHV systems, capacitive switching requirements relate to unloaded line switching and the maximum capacitive currents (section 3.5.2) and the voltage factors (sections 3.5.3 and 3.5.4) are investigated based on the different line configurations in 800 kV, 1100 kV and 1200 kV systems in detail.

3.5.2 OH-line maximum lengths

Considering all technical aspects and issues that influence the determination of EHV/UHV OH lines maximum length (presented in table 3.5.1) it can be concluded that a value of the order of 400 km should be considered. Calculations show that for UHV, 400 km corresponds to roughly 1200 A at 1100 kV and 1300 A at 1200 kV; both calculated for 50 Hz. However, such long lines will be shunt compensated, which leads to lower capacitive currents meaning that even very long lines, as built for instance in Russia (up to 700 km), are covered by a capacitive current of 1300 A.

Most utilities that apply 800 kV or foresee to apply UHV, implement or will implement shunt reactors, connected to the OH-lines. Where the shunt rectors are switchable, they will be switched on before switching off the unloaded line. Also in case of single phase to earth faults, most utilities will switch on the shunt reactors before the healthy phase clearing. Despite the fact that shunt (and series) compensation will reduce the capacitive current and relax the TRV stresses, utilities commonly put forward requirements for the network condition without shunt reactors. No shunt compensation is applied in Japan (UHV) and Korea (800 kV). Series compensation is applied on 800 kV-lines in Brazil and Canada.

Most OH-lines in the considered voltage range are single circuit lines, with an exception for Japan (UHV), Korea (800 kV) and future lines in China (UHV), which are double-circuit lines. The 800 kV OH-lines in South Africa and Brazil are transposed as are the 800 kV and 1200 kV lines in Russia. 800 kV and UHV OH-lines in other countries are not transposed.

A few particularities are related to the early stage of development of the networks and to the radial structure of networks for 800 kV and above. For long distance transmission from large power plants to remote load centres, the OH-lines may have to be switched under severe conditions, such as TOVs and abnormal power frequencies related to system separation. In Brazil and in Canada special requirements have been put forward for instance with respect a 10% higher power frequency to be applied during the type test (Brazil) and with respect to the voltage factor to be applied during the type test.

A well-known special condition is switching an unloaded line with a single phase to ground fault, where higher voltage factors have to be applied, as will be discussed in the section 3.5.4. Another particularity is the network condition where two OH-lines in series have to be switched by a particular circuit-breaker. This is, for instance, the case when in an intermediate substation a circuit-breaker fails to clear a single phase to ground fault; see figure 3.5.1. The two lines in series lead to a further increased capacitive current beyond that due to the voltage asymmetry (because of the earth fault).

The given examples of particularities and special conditions are nowadays in the Standards treated as special cases, and are not covered by the recommended values for the capacitive currents.

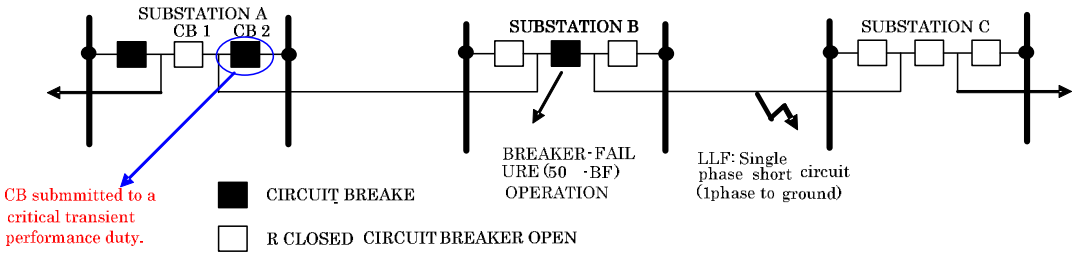

Figure 3.5.1 switching equipment withstand requirements derived from the possible condition of switching off two OH lines in series.

3.5.3 Background of technical requirements

The transient phenomena related to no-load line switching are more complex than presented in the Standards and described in several CIGRÉ Technical Brochures (305, 155, 47), certainly when the effect of different phenomena has to be quantified. Aspects to be addressed are for example: the effect of asymmetrical capacitances and induced voltages at the line side, the Ferranti-effect at long lines, the effect of line losses and consequential phase shift of line currents and ground return currents, the effects of phase shifting of the line currents after interruption of the first and of the second clearing pole, the effect of voltage jumps at the source side, the neutral shift at the source side, the neutral shift at the line side and finally the effects of testing three-phase phenomena in a single phase test circuit or even a synthetic test circuit.

In order to compare the requirements for no-load line switching, as specified in the Standards, between EHV and UHV network applications, it is important to be aware of these aspects, as the simulations at UHV cannot simply be compared with the requirements in the Standards, but should be compared with the phenomena as experienced on EHV OH-lines.

In section 3.5.4 the results from EMTP simulations, based on real line configurations, but with arbitrarily chosen system conditions (such as the rated voltage at the circuit-breaker terminals) are discussed. At first, however, the phenomena that occur under ideal circumstances with respect to symmetry and lossless lines are described. The relevant phenomena that influence the TRV are addressed, step by step and a comparison of the effects and the simulations of 800 kV and 1100 kV cases are given.

3.5.3.1 Source side

It is well known that switching of a no-load overhead line may cause a voltage "jump" on the source side due to the disappearance of the capacitive current through the source side impedance. However, in EHV and UHV networks the source side impedance is usually so low (the short-circuit power is so high) that the voltage jump may be disregarded. The voltage at the busbar will be affected by the capacitive current switched off to an extent of, at most, a few percent. In the simulations, as presented in section 3.5.4, a short-circuit power at the busbar corresponding to a short-circuit current of 40 kA has been assumed. Further, to simplify the calculations, at the source side it is assumed that no neutral shift will take place before, during or after the capacitive current switching process. Therefore the three phase voltages at the busbar can be treated as completely symmetrical and shifted by exactly 120°.

3.5.3.2 Line side neutral shift

For a completely symmetrical OH-line (i.e. a perfect and fully transposed line), the phase to phase and phase to ground capacitances for each pole can be expressed by two values: C_m and C_s respectively, or by two sequential components C_1 and C_0, with:

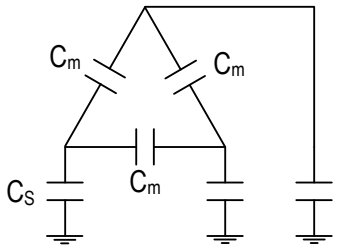

$C_1 = Cs + 3C_m$

$C_0 = Cs$

In this case the negative sequence capacitance is equal to the positive sequence capacitance C_1.

At the line side the positive sequence and zero sequence capacitances can be presented in several ways. For the purpose of further explanation, the so-called Neptune scheme is used to represent these capacitances, but this scheme can easily be transferred to other schemes. The following relationships can be calculated.

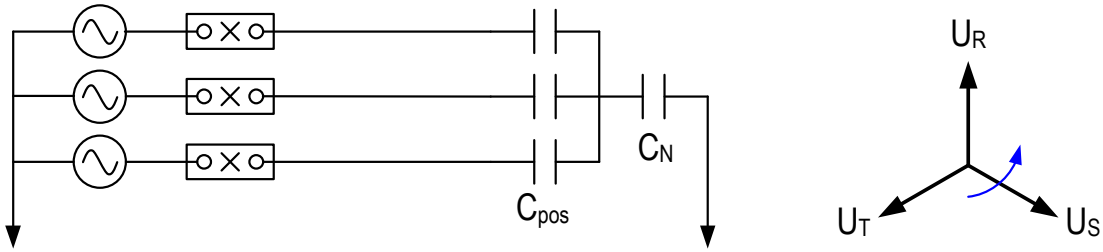

$C_{pos} = C_1$

$C_0 = 1/(1/C_1+3/C_N) = C_1C_N/(3C_1+C_N)$ (1)

$C_N = 3C_0C_1/(C_1-C_0)$ (2)

Figure 3.5.2 Relationship between C_0, C_1 and C_N

Before switching off the first phase of the OH-line, the neutral voltage at the line side will be zero. After clearing of the first pole (assumed to be phase R), the neutral voltage U_N changes, depending to the other phase voltages, as follows:

$$U_s = \frac{I_s}{j\omega C_1} + \frac{I_s + I_T}{j\omega C_N} \quad (3)$$

$$U_T = \frac{I_T}{j\omega C_1} + \frac{I_s + I_T}{j\omega C_N} \quad (4)$$

Adding equation (4) to (3),

$$U_s + U_T = -U_R = \frac{I_s + I_T}{j\omega C_N} \times \frac{2C_1 + C_N}{C_1} = U_N \times \frac{2C_1 + C_N}{C_1}$$

$$\therefore \quad U_N = (U_s + U_T)\left\{\frac{C_1}{2C_1 + C_N}\right\} = -U_R\left\{\frac{C_1}{2C_1 + C_N}\right\} \quad (5)$$

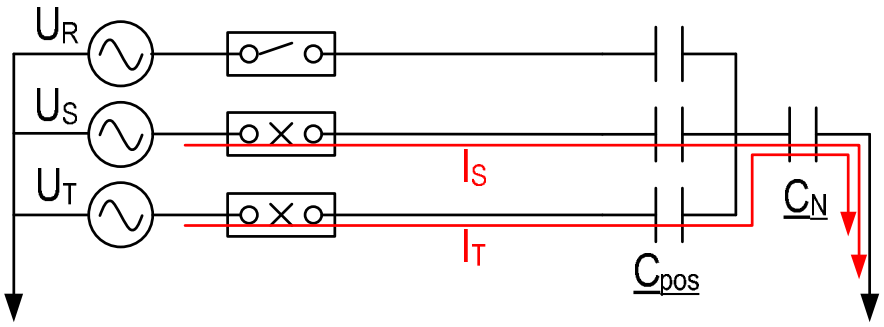

Figure 3.5.3 Neutral shift after clearing of first pole

In the time domain the equation for the neutral voltage becomes:

$$U_N(t) = -\left\{U_R(t) - U_{R(t=0)}\right\}\left\{\frac{C_1}{2C_1 + C_N}\right\} \qquad (6)$$

with t=0 at the moment of clearing of the first pole, i.e. phase R with the source voltage $U_R(t)$ has a voltage $U_R(t=0)$ at the moment of clearing. In the case of a lossless line $U_R(t=0)$ is the peak value of the phase to earth voltage.

The recovery voltage across the first clearing pole will consist of the source voltage versus the sum of the charged normal sequence capacitance of the R-phase conductor plus the neutral voltage:

$$U_{RV}(t) = U_R(t) - U_{R(t=0)} - U_N(t) = U_R(t) - U_{R(t=0)} + \left\{U_R(t) - U_{R(t=0)}\right\}\left\{\frac{C_1}{2C_1 + C_N}\right\}$$

$$= \left\{U_R(t) - U_{R(t=0)}\right\} \times \left\{\frac{3C_1 + C_N}{2C_1 + C_N}\right\} = \left\{U_R(t) - U_{R(t=0)}\right\}\left\{\frac{3}{2 + C_0 / C_1}\right\} \qquad (7)$$

Without current interruption in the 2nd and 3rd pole, the peak value of $U_{RV}(t)$ in p.u. will reach

$$U_{RV\ peak} = \frac{6}{2 + \frac{C_0}{C_1}} \qquad (8)$$

Figure 6 in the section 1.2.1.2 of CIGRÉ Technical Brochure 305 [7], shows U_{RV} as function of C_1/C_0.

In the case where the 2nd and 3rd pole interrupt after 90°, the peak value of $U_{RV}(t)$ in p.u. is

$$U_{RV\ peak} = \frac{3}{2 + \frac{C_0}{C_1}} + 1 = \frac{5 + \frac{C_0}{C_1}}{2 + \frac{C_0}{C_1}} \qquad (9)$$

The above and following considerations are based on lossless lines and lead to maximum values. Depending on the ratio C_1/C_0, the second pole will clear the capacitive current between 60° and 90° after the first clearing pole. To calculate exactly the moment of current zero for the second clearing pole, one has to calculate the current through pole S and pole T. Each current is the superposition of the current driven by U_S and the driven forced by U_T.

$$I_s = j\omega C_1 \times (U_s - U_N) = j\omega C_1 \times [U_s - (U_s + U_T)\left\{\frac{C_1}{2C_1 + C_N}\right\}]$$

$$= j\omega C_1 (U_s - U_T)\left\{\frac{C_1 + C_N}{2C_1 + C_N}\right\} + j\omega C_1 U_T \left\{\frac{C_1 + C_N}{2C_1 + C_N}\right\}\left\{\frac{C_N}{C_1 + C_N}\right\} \quad (10)$$

$$I_T = j\omega C_1 (U_T - U_S)\left\{\frac{C_1 + C_N}{2C_1 + C_N}\right\} + j\omega C_1 U_S \left\{\frac{C_1 + C_N}{2C_1 + C_N}\right\}\left\{\frac{C_N}{C_1 + C_N}\right\} \quad (11)$$

The first part of the last formula gives the 90° delay after the 1st clearing pole, while the second part gives some lagging phase angle, depending on $C_N/(C_1+C_N)$. Normal ratios for C_1/C_0 are from 1.5 to 3 and lead to $C_N/(C_1+C_N)$ being in the range of 0.86 to 0.6, meaning that the poles S and T will not clear around 90° after pole R and meaning that there is a substantial difference between pole S and pole T. Note that for pole T the shift will be backwards, while for pole S it will be forwards. The current through pole S will become zero before the current of pole T.

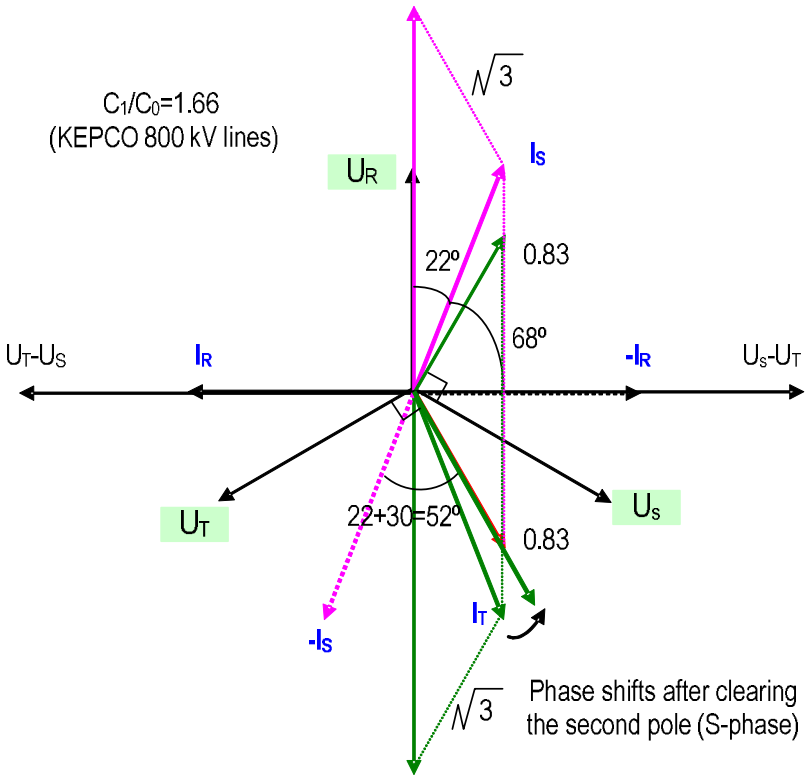

Figure 3.5.4 Vector diagram after first and second clearing pole

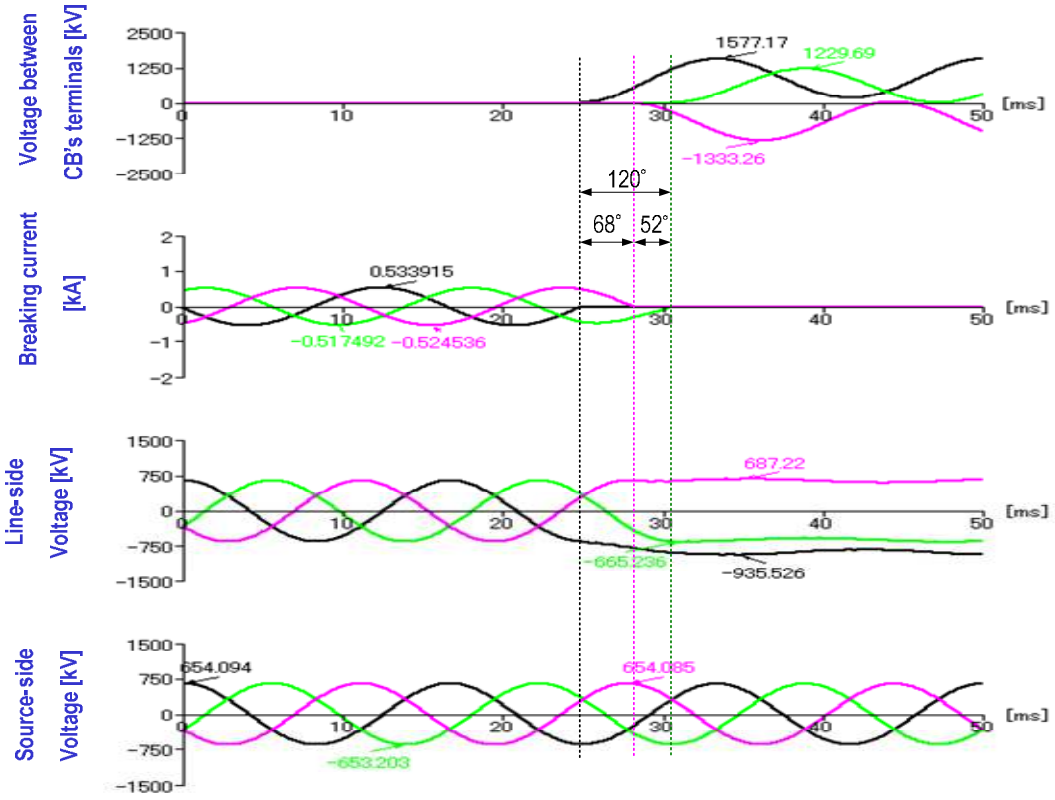

Figure 3.5.5 Example of phase shift after first and second clearing pole

This is explained in figure 3.5.5 and is visible in the simulations to be discussed in the next section such as KEPCO's 800 kV-line with C_1/C_0 = 1.66 (Table 3.5.1). Between the instants of clearing of the first and the second pole, the neutral will not complete a 90° sinusoidal swing, leaving a neutral voltage of about 63% (=1-cos (90°-22°=68°)) of $C_1/(2C_1+C_N)$ = 0.15 p.u., resulting into a neutral voltage of 0.095 p.u.

At clearing of the second pole (S), the last phase (T) voltage angle is -52° (i.e. 22° + 30°, with 22° being the lagging angle of I_T, and 30° being the angle between U_S-U_T and U_S). At clearing of the second pole, the voltage U_S corresponds to cos(-172°) ≈ -1.0 p.u.; and U_T corresponds to cos(-52°) = 0.6 p.u.. After 52° (i.e. 2.5 ms at 60 Hz), the last clearing phase (T) voltage will be 1.0 p.u. and the current will be 0.

At that last moment, the neutral voltage is the part of the total phase voltage (1 p.u.) that is proportionally divided over C_N and C_1. In this case C_1/C_0 being 1.66 and C_N/C_1 thus being 4.545, the voltage increase across the neutral capacitance will be 18% (=$C_1/(C_1+C_N)$=0.18) of 1-cos(-52°) = 0.38. Between the 2nd and 3rd pole interruption the neutral voltage was raised from 0.095 p.u. to 0.165 p.u. (=0.095+0.18×0.38). The recovery voltage of the first clearing pole will consequentially show a peak value of 2.17 p.u. (=2+0.165), when other phenomena are not considered.

The second clearing pole will show a recovery voltage peak of 1.93 p.u. (i.e. -2.0 p.u. + 0.07 p.u. due to the neutral shift between clearing of the 2nd and 3rd pole) and the last pole a peak of 2.0 p.u. exactly. The neutral shift and the recovery voltage for the first clearing pole are given in the following figures. The recovery voltage is compared with an 1-cos function with an amplitude of 1.08 p.u..

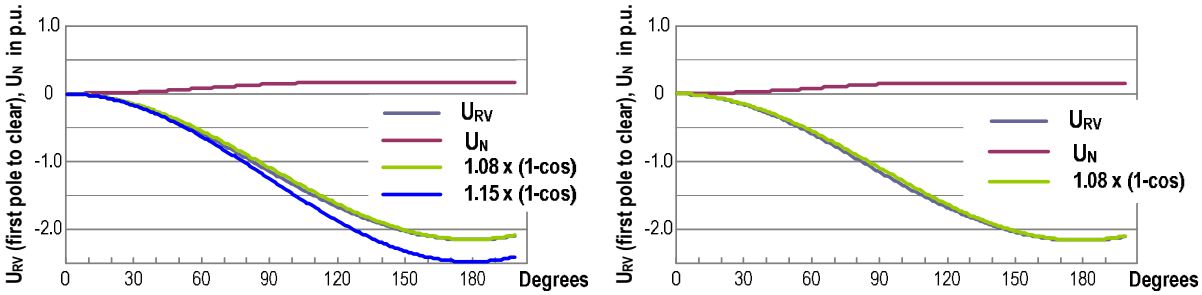

Figure 3.5.6 Recovery voltage of the first clearing pole

Other phenomena to be considered are, for instance, the mutual influence between systems on one tower, as is the case with the 800 kV-OH-line of KEPCO. From the voltage variation at the line side a clear 60 Hz superimposed voltage can be distinguished and the last clearing phase (T) gives a recovery voltage peak value of 1.88 p.u., thus leading to the conclusion that about 0.12 p.u. induced voltage is to be considered. 0.12 p.u. in addition to 1.93 p.u. for the second clearing pole gives 2.05 p.u. as peak value of the recovery voltage, very close to the simulated value, while 2.17 p.u. + 0.12 p.u. for the first clearing pole (R) is less than the simulated value of 2.4 p.u.. Note, however, that the induced voltage is not necessary the same for all phases and that the R phase (first clearing pole) seems to show a larger induced voltage. Simulations for a number of 800 kV and UHV OH-lines showed such effects. The next table gives some basic information of the no-load lines that have been simulated.

Table 3.5.1 Basic information of no-load lines switching

Utility	Voltage	Line length	C_1/C_0	# circuits	transposed
ESKOM	800 kV	440 km	1.68	1	yes
Hydro Quebèc	765	210, 400	1.66	1	no
KEPCO	800	39, 155	1.66	2	no
AEP	800	300	1.66	1	no
Furnas	800	266, 331	1.52	1	yes
TEPCO	1100	210, 250	1.92	2	no
China	1100	281, 358	1.62	1	no
China	1100	151, 327	1.60	2	no
India	1200	400	1.68	1	no

The shift of the clearing moments for the 2nd and 3rd pole with respect to 90° can be calculated from the C_1/C_0 ratios and these angles are 23° for a ratio of 1.52, 22° for a ratio of 1.66 and 20° for a ratio of 1.92. Figure 3.5.7 does not indicate much dependency on the C_1/C_0 ratio. The neutral shift and the peak values for the recovery voltages can also be calculated from this ratio.

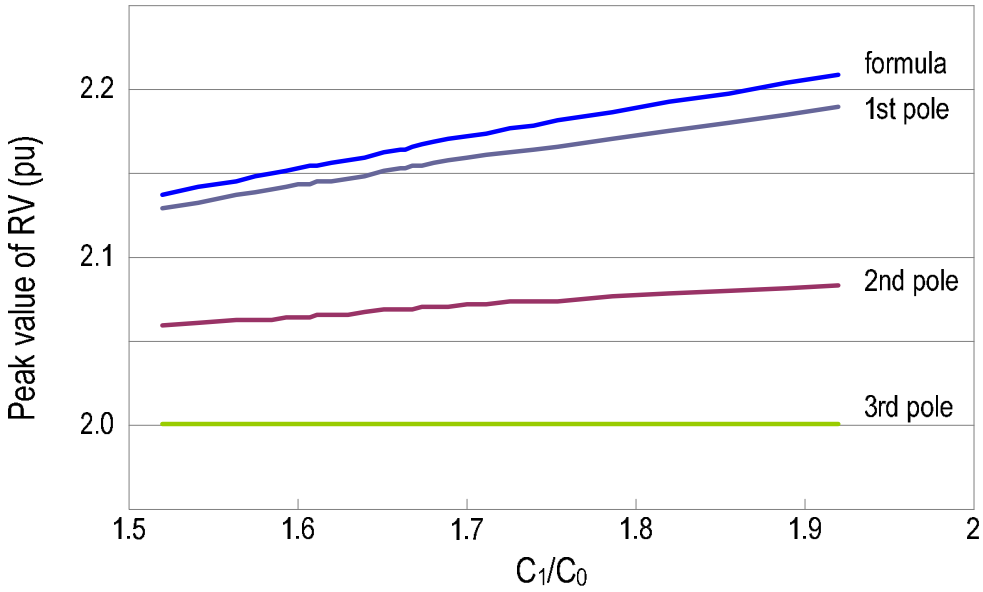

Figure 3.5.7 Peak values of the recovery voltage for the 1st, 2nd and 3rd clearing pole

From the calculations and simulations it is clear that the first clearing pole experiences the highest recovery voltage. Due to a rather limited voltage of the neutral, also after clearing of the second pole, the recovery voltage of the first pole (e.g. 2.17 p.u.) tends to a value relatively close to the hypothetical value for clearing of the second and third pole after 90° (e.g. 2.15 p.u.), which can easily be calculated by the formula (9) given before. It is evident that the mutual influence of another circuit on the same towers will be much larger than the inaccuracy introduced by that formula. Also the Ferranti-effect and the effect of non-ideal transposition are much larger.

3.5.3.3 Line side travelling waves

A phenomenon that plays an important role for longer OH-lines is the Ferranti-effect (in the above example the line length was only 155 km). Prior to interruption theflow of capacitive current will lead to an increase of the power frequency voltage along the OH-line. The longer the line the higher the Ferranti-effect voltage that is observed. The voltage along the OH-line due to the Ferranti-effect can be calculated by the formula:

$$U(x) = U_e \cos\{\beta(L - x)\} \qquad (12)$$

with U_e being the voltage at the open end of the line, L the length of the line in km, x the distance in km from the beginning of the line, and $\beta = \omega/c = 100\pi/300{,}000 = 0.001$ rad / km (at 50 Hz)

The following table and figure give some examples of the voltage rise at the line end due to the Ferranti-effect with V_s (sending end) = U(0) and V_r (receiving end) = U_e.

Table 3.5.2 Voltage rise at the line's end due to Ferranti effect

$(V_r-V_s)/V_s$	100 km	200 km	300 km	400 km
50 Hz	0.5 %	2.0 %	4.7 %	8.6 %
60 Hz	0.7 %	3.0 %	6.8 %	12.7 %

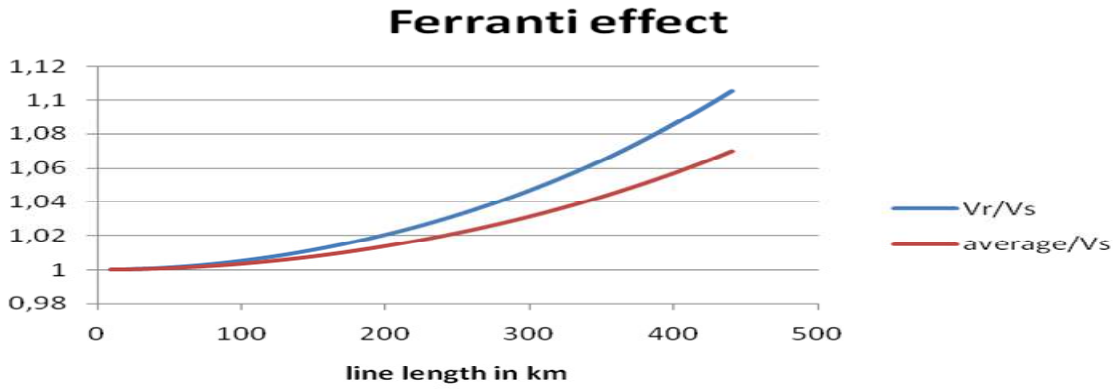

Figure 3.5.8 Ferranti effect and residual DC voltage

Immediately after current interruption travelling waves will equalize the high DC voltage at the line end with the 1 p.u. voltage at the beginning of the OH-line. The travelling waves will appear as a cosinusoidal wave-shape superimposed (with double amplitude) on the fore-mentioned DC and power frequency components of the recovery voltage. The wave-shape is shown in figure 3.5.9.

Over time, the Ferranti-effect will result in a somewhat higher DC voltage along the line: in principle up to the average value of the original voltage distribution. Integration of the cos-function gives the following:

$$U_{DC} = U_e \sin(\beta L)/\beta L = Vs \tan(\beta L)/\beta L \quad (13)$$

See also figure 3.5.8. For 440 km and 50 Hz this gives a residual DC-voltage of 1.07 p.u..

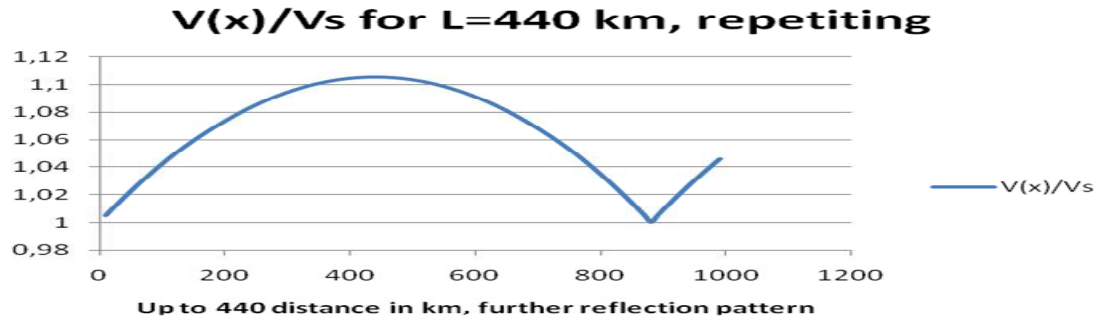

Figure 3.5.9 Voltage and reflection profile along a 440 km long line due to Ferranti effect

In the next section all the phenomena described above can be recognized. For instance, the simulation of a transmission line with a length of 440 km, fully transposed, single circuit, based on 800 kV towers from ESKOM, C_1/C_0 = 1.68, shows a voltage factor for the first clearing pole of 2.17 plus twice the amplitude of the Ferranti-effect: 2.17×653 kV + $2 \times 0.105 \times 653$ kV = 1554 kV versus 1559 kV as a simulated value.

In the next section, the results of simulations based on tower geometries from several utilities, both for 800 kV and UHV, will be given. The simulations are all performed for a simple theoretical network configuration, which is not in conformance with any specific network of the utilities involved. The purpose was only to compare several

tower geometries and conditions, such as single circuit and double circuit OH-lines, 800 kV and UHV OH-lines, shunt compensated and non-compensated lines, conditions with and without an earth fault.

Compensated lines will give a low frequency damped voltage at the line side, resulting in a recovery voltage across the breaker contacts that exhibits a slow beat pattern. This effect is also clearly visible in the next section.

3.5.4 Conclusions

- Based on the prevailing line lengths, the majority of UHV lines will show a line charging current of less than 1200 A at 1100 kV and 1300 A at 1200 kV.
- The power frequency recovery voltage at unloaded line switching is influenced by many factors, such as the voltage jumps at the source (depending on source impedance) and line side (depending on Ferranti-effect), the neutral shift at the line side, the induced voltage from another circuit (double circuit line), the asymmetry (unless fully transposed), the shunt and series compensation (when applied), the condition of an earth fault.
- The neutral shift at the line side, although complicated, can be approached by formula (9) for the situation where the second and third pole clear 90° after the first pole.
- Due to the fact that the neutral at the line side shifts in two distinct time frames and due to the fact that the C_1/C_0 ratio is relatively close to 1.7, the TRV of the first pole (i.e. the most stressed pole) follows closely a 1-cos shape. The voltage factor for single phase test circuits can therefore determined by the calculated peak factor of the recovery voltage, divided by 2.
- The Ferranti-effect at the line side gives a typical wave-form of the reflected travelling waves which follows the original cos-shape voltage distribution along the OH-line. The peak value of the Ferranti-effect can be calculated by formula (12). After the travelling waves have decayed a residual DC-voltage to formula (13) appears in the recovery voltage.
- The neutral shift at the line side gives a TRV peak value of 2.17 p.u.. As some utilities specify unloaded line switching without taking into consideration the shunt compensation, the Ferranti effect has to be added. For 440 km, 50 Hz, 0.21 p.u. has to be added, resulting into a TRV-peak of almost 2.4 p.u. or a voltage factor of 1.2.
- Other terms to be added come from the induced voltages from another circuit, asymmetry in case that incomplete transposition is applied and the occurrence of an earth fault (or TOVs). Apart from unloaded line switching under TOV conditions, the other aspects are treated in the next section.

3.5.5 Survey of simulated cases

3.5.5.1 Surveys of network conditions for capacitive current switching

Capacitive current switching under normal service and 1LG conditions were evaluated according to practical conditions of a transmission tower, multi-sub conductor bundle, normal current and line length. Typical tower designs and network conditions were investigated by WG A3.22 and are summarized in Table 3.5.3.

Table 3.5.3 Network conditions (CIGRE WG A3.22 survey)

Items	South Africa	Canada	Korea	United States	Brazil
Maximum Voltage	800 kV	765 kV	800 kV	800 kV	800 kV
Nominal Voltage	765 kV	735 kV	765 kV	765 kV	765 kV
Nominal current on the line	5000 A	3150 A	8000 A	2420 A	3150 A
Short-circuit current	50 kA	50 kA	50 kA	50 kA	40 kA
Shunt Reactor at line ends	400 MVA x 2	300 MVA x 2	None	300 MVA x 2	360 MVA x 2
Maximum Line length	440 km	400 km	155 km	300 km	331 km
Circuit	Single	Single	Double	Single	Single
Multi-conductor bundle	642 mm^2 x 6	686 mm^2 x 4	480 mm^2 x 6	520 mm^2 x 6	603 mm^2 x 6
Bundle spacing	320 mm	400 mm	400 mm	381 mm	457 mm
Line spacing	15.8 m	13.7 m	29 m x 2	15.24 m	15.85 m
Height of the grounding wire	50 m	45.2 m	93 m	41.6 m	43.5 m
Height of the lines	39 m	33 m	50-88 m	30.5 m	37.5 m

Items	Japan	China pilot	China	India
Maximum Voltage	1100 kV	1100 kV	1100 kV	1200 kV
Nominal Voltage	1000 kV	1000 kV	1000 kV	1100 kV
Nominal current on the line	8000 A	3150/4000 A	4000 A	5000 A
Short-circuit current	50 kA	50 kA	50 kA	50 kA
Shunt Reactor at line ends	None	960, 720 MVA	720 MVA x 2	660 MVA x 2
Maximum Line length	210, 250 km	358 km	327 km	400 km
Circuit	Double	Double	Double	Single
Multi-conductor bundle	810 mm^2 x 8	500 mm^2 x 8	630 mm^2 x 8	774 mm^2 x 8
Bundle spacing	400 mm	400 mm	400 mm	450 mm
Line spacing	15.5-16.5 m x2	22.2 m x2	30-36 m x2	15 m
Height of the grounding wire	120 m	62.3 m	97 m	77 m
Height of the lines	72.5-107.5 m	50 m	50-92 m	38-61m

3.5.5.2 Normal condition

Figure 3.5.10 shows the network parameters for South Africa shown in the table 3.5.3.

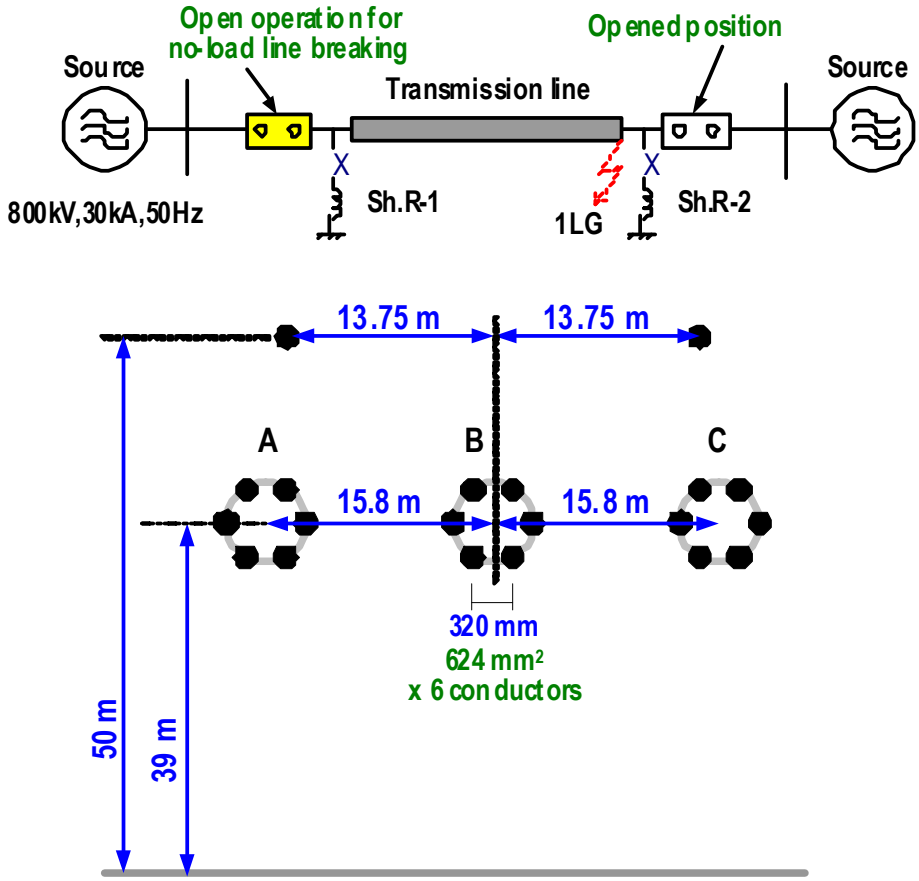

Figure 3.5.10 800 kV line configuration with single circuit of 440 km in South Africa

The voltage and current behaviour for capacitive current switching are calculated under normal service conditions based on 800 kV single circuit transmission lines with 440 km length in South Africa. Figure 3.5.11 (a) shows the typical results for the case with the voltage at the circuit breaker terminal set to the highest voltage in the power system. Figure 3.5.11 (b) shows results for the case when the voltage at the open-end of the transmission line is set to be the highest voltage in the power system.

For the lines without a shunt reactor, as shown in the figure 3.5.11 (a), the maximum breaking current is 969 A_{rms} and the maximum TRV peak is 1559 kV which corresponds to the voltage factor of 1.19. For the lines with 400 MVA shunt reactors connected at both line ends, the breaking current is reduced to 284 A_{rms} and the TRV peak is 727 kV showing that the application of the shunt reactors can effectively mitigate the severity of capacitive switching duties.

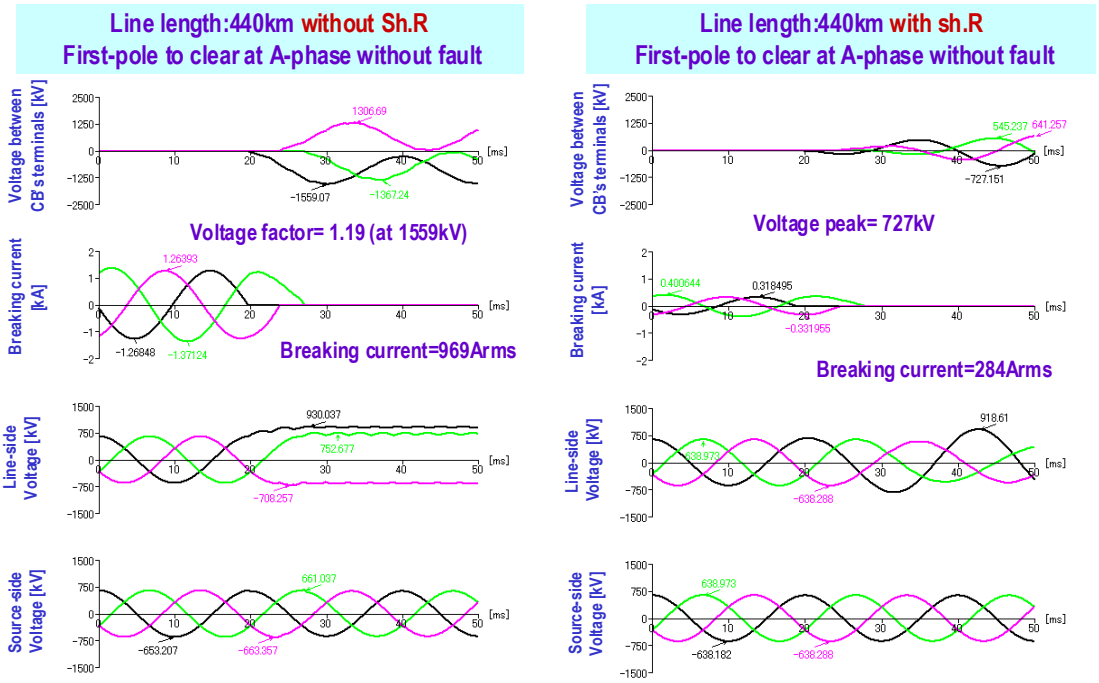

Figure 3.5.11 (a) Analytical results of no load 800 kV line breaking under normal service conditions (S. Africa), voltage at the circuit breaker terminal is the highest in power system

On the other hand, for the lines without a shunt reactor, as shown in the figure 3.5.11 (b), the maximum breaking current is 801 A_{rms} and the maximum TRV peak is 1392 kV which corresponds to the voltage factor of 1.06. For the lines with 400 MVA shunt reactors connected at both line ends, the breaking current reduced to 280 A_{rms} and TRV peak is 720 kV. TRV peaks based on the conditions that the voltage at the circuit breaker terminal is kept to be the highest voltage are 13% higher (440 km), 9% higher (300 km) or 5% higher (250 km) than those based on the conditions that the voltage at the line terminal is kept to be the highest voltage due to Ferranti effect. The voltage and current behaviour in section 3.5.5 is basically calculated based on the conditions that the voltage at the circuit breaker terminal is kept to be the highest voltage (the most severe cases).

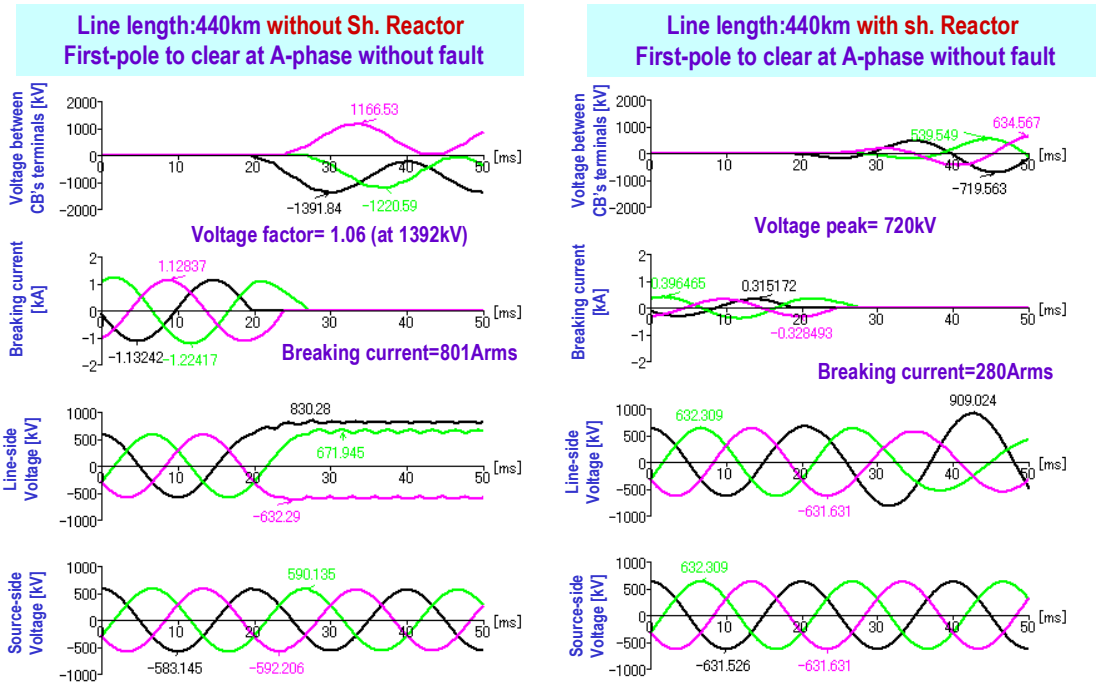

Figure 3.5.11 (b) Analytical results of no load 800 kV line breaking under normal service conditions (S. Africa), voltage at the open end of line is the highest voltage in power system

China's 1100 kV pilot project has a maximum line length of 358 km with 960 MVA and 720 MVA shunt reactors connected at the line ends. For this configuration, the calculation gives a breaking current of 143 A_{rms} and the TRV shows a prominent beat waveform that acts to mitigate the TRV peak and RRRV after line de-energisation, as shown in the figure 3.5.12.

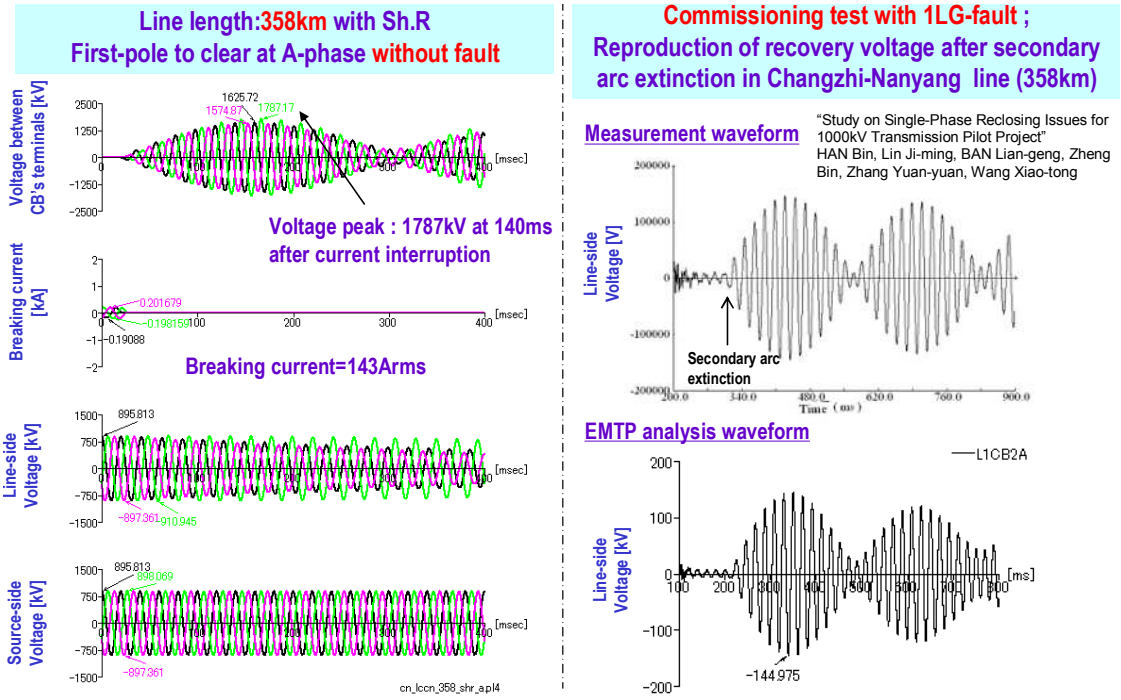

Figure 3.5.12 Analytical results of no load 1100 kV line breaking under normal service conditions (China pilot). Analytical voltage behaviour agrees with the experimental data well.

The TRV after the secondary arc extinction is also calculated and compared with the measurement of the TRV during the commissioning test. The analytical TRV shows a

good agreement with the measurement so validity of EMTP calculation on capacitive current switching is confirmed.

Figure 3.5.13 shows typical voltage and current behaviour in the case of capacitive current switching under normal service conditions based on 765 kV single circuit transmission lines with 210 km and 400 km length based on the conditions that the voltage at the circuit breaker terminal is kept to be the highest voltage in the power system. The breaking current increases and the TRV peak decreases with an increase of the line length.

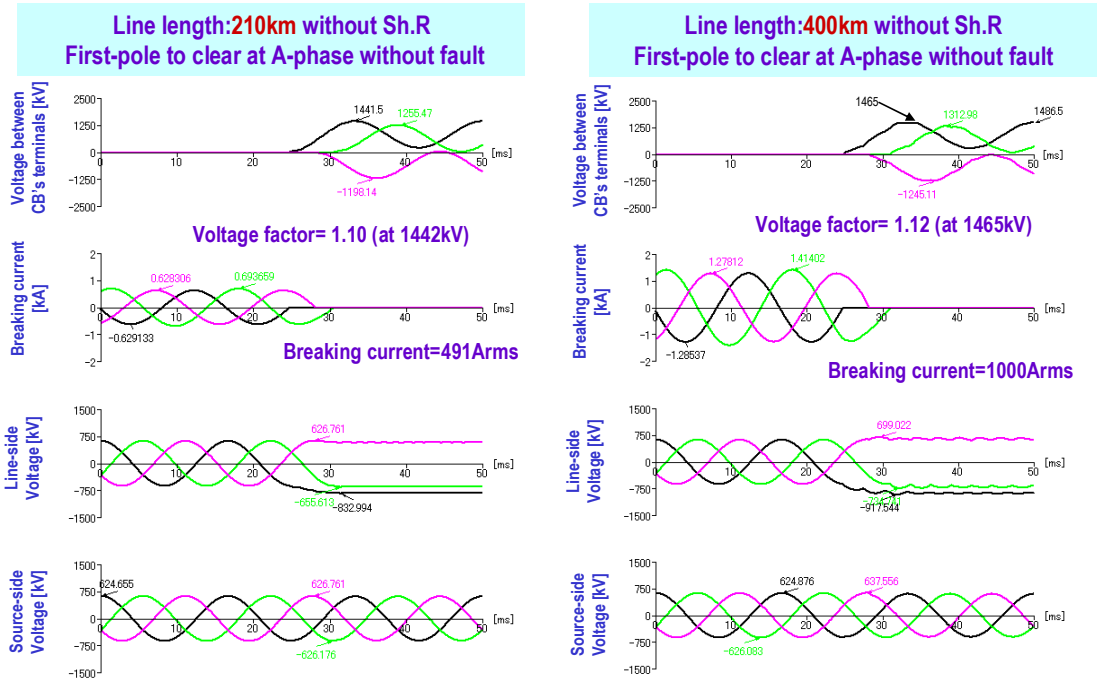

Figure 3.5.13 Analytical results of no load 765 kV line breaking without any faults (Canada)

Figure 3.5.14 shows 800 kV transmission lines of up to 155 km length with double circuits in South Korea.

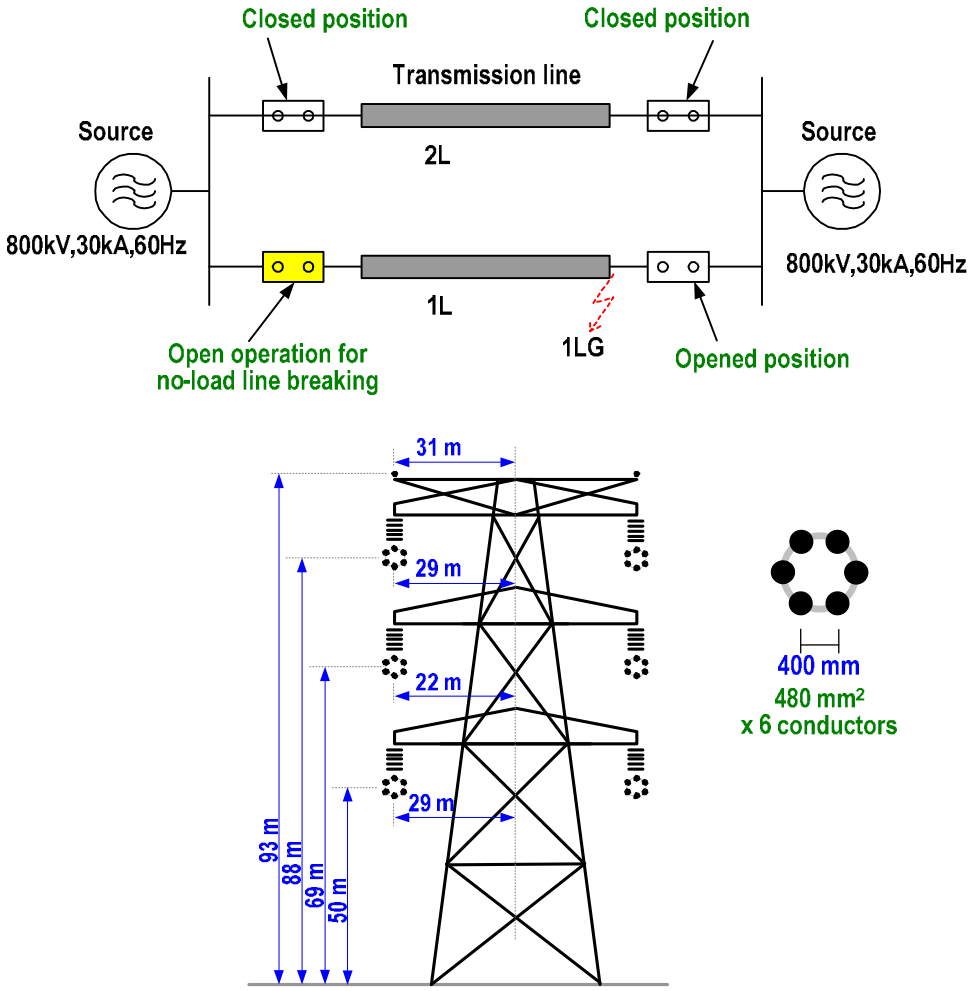

Figure 3.5.14 800 kV line configuration with double circuit of 155 km in South Korea

Figure 3.5.15 shows typical voltage and current behaviour in the case of capacitive current switching under normal service conditions based on 800 kV double circuit transmission lines with 155 km and 39 km length in South Korea.

For the lines with 39 km without a shunt reactor, the maximum breaking current is 94 A_{rms} and the maximum TRV peak is 1569 kV which corresponds to the voltage factor of 1.20. For the lines of 155 km without a shunt reactor, the breaking current is reduced to 378 A_{rms} and the TRV peak is 1577 kV which corresponds to the voltage factor of 1.21. The breaking current increases and the TRV peak decreases with an increase of the line length.

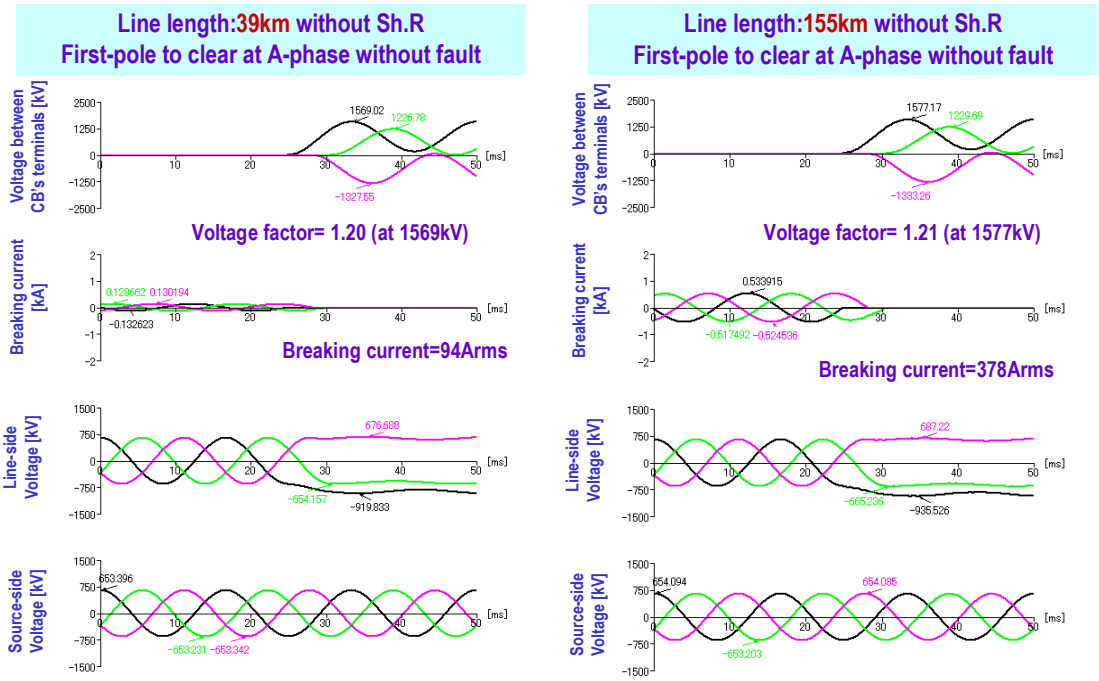

Figure 3.5.15 Analytical results of no load 800 kV line breaking without any faults (S. Korea)

Figure 3.5.16 shows typical voltage and current behaviour in the case of capacitive current switching under normal service conditions based on 1100 kV double circuit transmission lines with 210 km and 250 km length in Japan.

For the lines with 210 km without a shunt reactor, the breaking current is 665 A_{rms} and TRV peak is 2187 kV which corresponds to the voltage factor of 1.22.

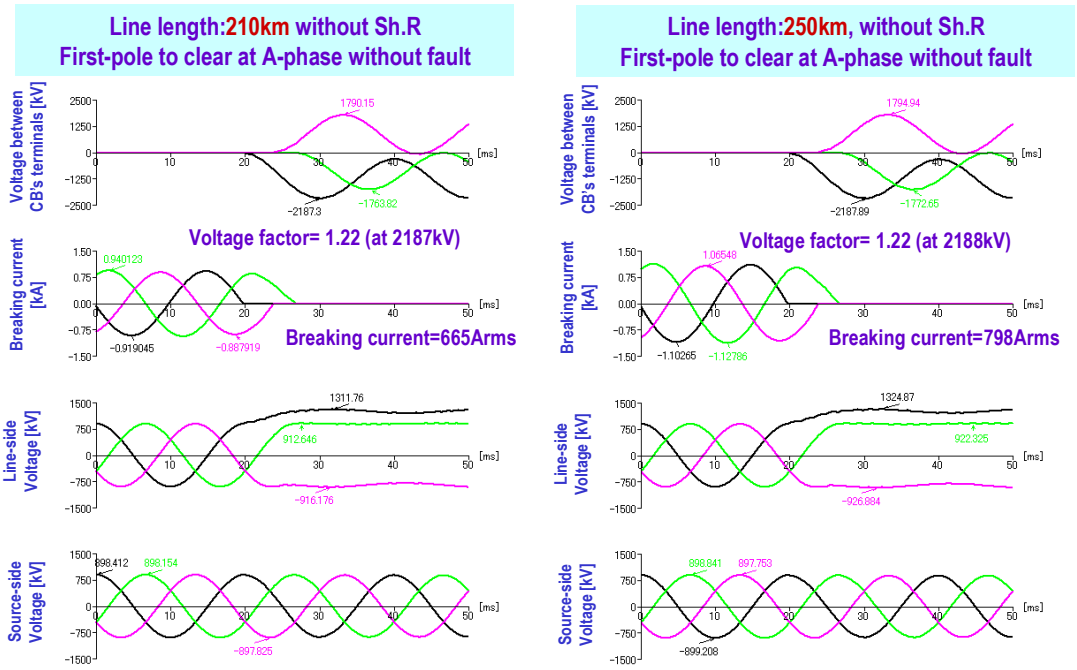

Figure 3.5.16 Analytical results of no load 1100 kV line breaking without any faults (Japan)

Figure 3.5.17 shows typical voltage and current behaviour in the case of capacitive current switching under normal service conditions based on 1100 kV double circuit transmission lines with 151 km and 327 km length in China. For the lines with 151

km without a shunt reactor, the breaking current is 443 A_{rms} and TRV peak is 2115 kV which corresponds to the voltage factor of 1.18.

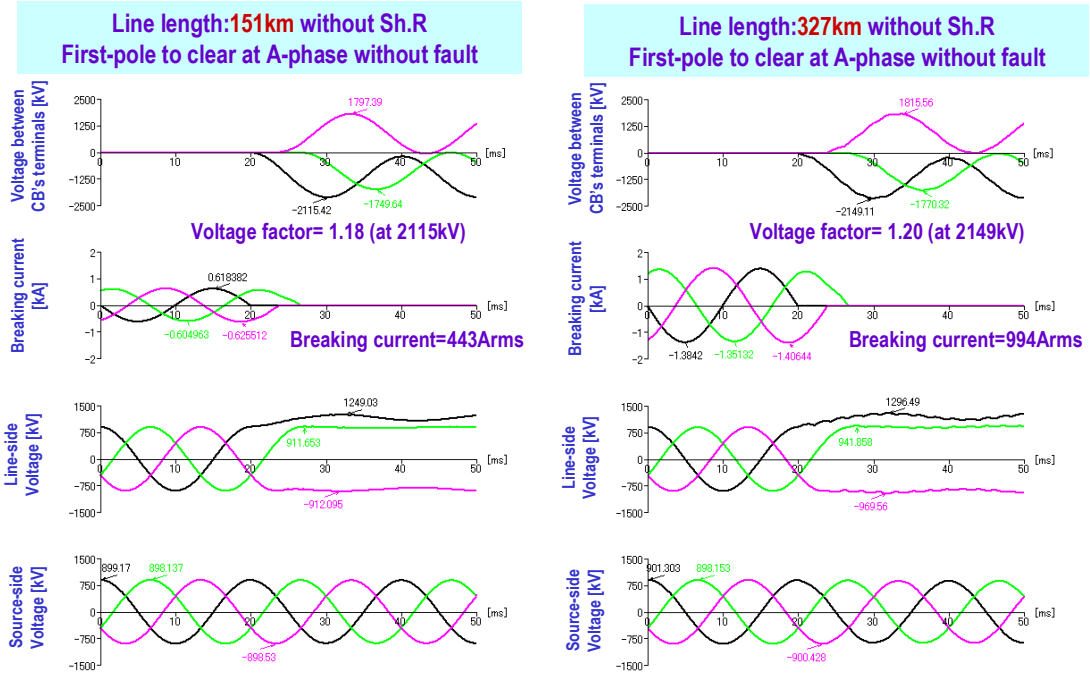

Figure 3.5.17 Analytical results of no load 1100 kV line breaking without any faults (China)

Theses results confirm that the voltage factor for capacitive current switching under normal service condition systems is less than 1.20 for 800 kV, 1100 kV and 1200 kV single and double circuit transmission lines.

3.5.5.3 Single phase line fault to ground (1LG) conditions

Figure 3.5.18 shows typical voltage and current behaviour in the case of capacitive current switching under single-phase line fault to ground (1LG) conditions based on 800 kV single circuit transmission lines of 440 km length in South Africa.

The maximum breaking currents are 1009 A_{rms} based on the conditions that the voltage at the breaker terminal is kept to be the highest voltage in the power system and 901 A_{rms} based on the conditions that the voltage at the open-end of the transmission line is kept to be the highest voltage in the power system (4.1% and 12.4 % larger as compared with normal service condition without any faults). The maximum TRV peaks are 1703 kV based on the conditions that the voltage at the breaker terminal is kept to be the highest voltage and 1520 kV based on the conditions that the voltage at the open-end of the transmission line is kept to be the highest voltage (9.1 % higher as compared with normal condition) which corresponds to voltage factors of 1.30 and 1.16.

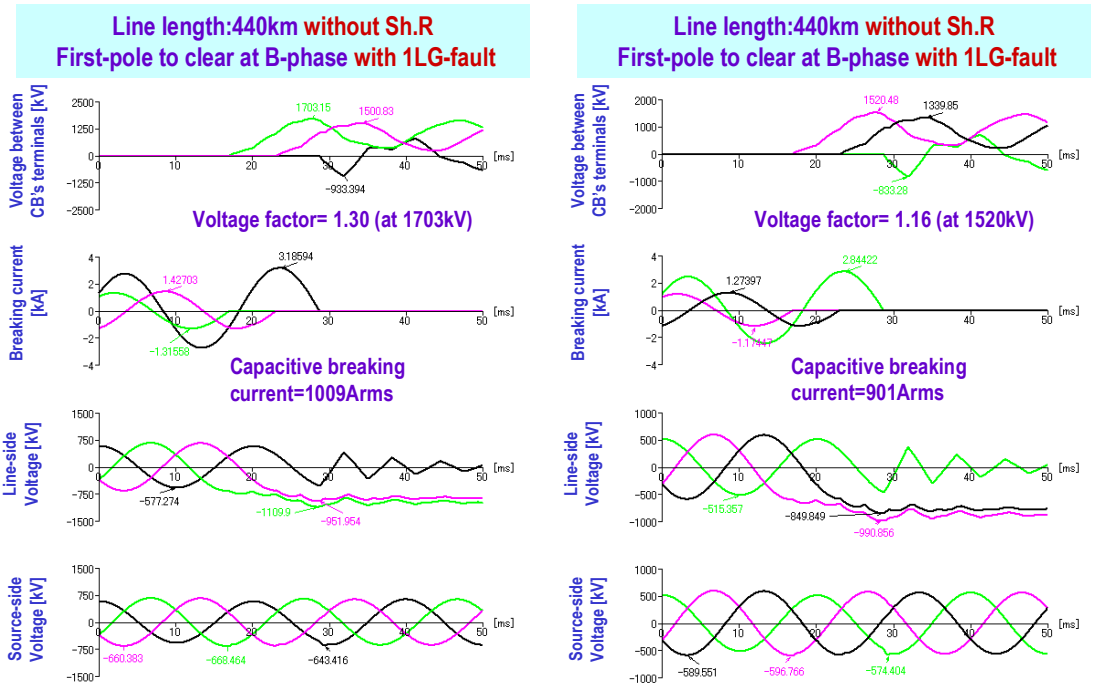

Figure 3.5.18 Analytical results of no load 800 kV line breaking with 1LG condition, left: the voltage at the circuit breaker terminal is the highest voltage, right: the voltage at the line terminal is the highest voltage (South Africa)

Figure 3.5.19 shows typical voltage and current behaviour in the case of capacitive current switching under 1LG conditions based on 765 kV single circuit transmission lines of 210 km and 400 km length in Canada based on the conditions that the voltage at the circuit breaker terminal is kept to be the highest voltage. For the lines with 210 km without a shunt reactor, the breaking current is 487 A_{rms} (the same level as compared with normal condition) and the maximum TRV peak is 1575 kV (9.2 % higher as compared with normal condition) which corresponds to a voltage factor of 1.20.

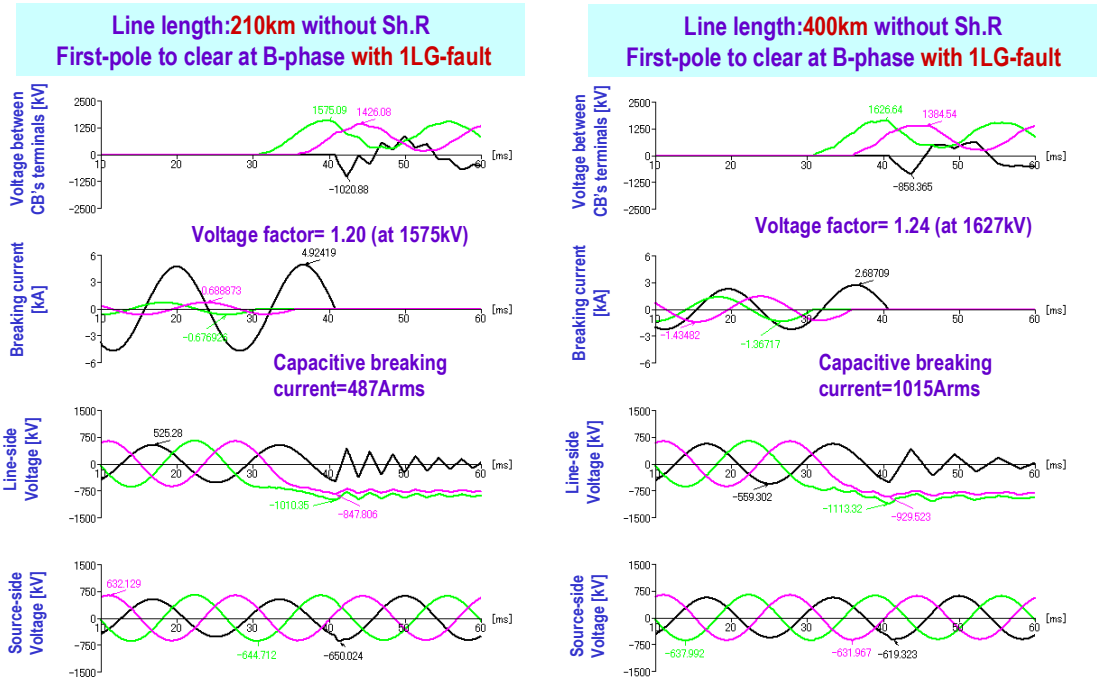

Figure 3.5.19 Analytical results of no load 765 kV line breaking with 1LG condition (Canada)

Figure 3.5.20 shows typical voltage and current behaviour in the case of capacitive current switching under 1LG conditions based on 800 kV double circuit transmission lines of 39 km and 155 km length in South Korea. For the lines with 39 km without a shunt reactor, the breaking current is 92 A_{rms} (the same level as compared with normal condition) and the maximum TRV peak is 1639 kV (4.5 % higher as compared with normal condition) which corresponds to a voltage factor of 1.25.

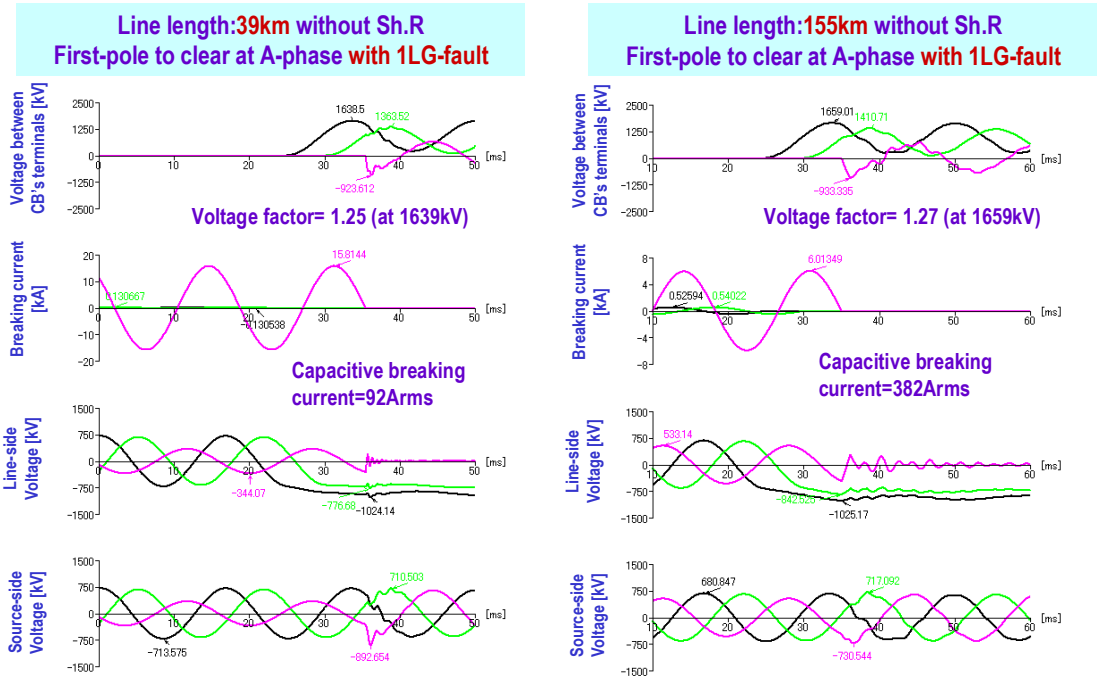

Figure 3.5.20 Analytical results of no load 800 kV line breaking with 1LG condition (S. Korea)

Figure 3.5.21 shows typical voltage and current behaviour in the case of capacitive current switching under 1LG conditions based on 1100 kV double circuit transmission lines of 210 km and 250 km length in Japan. For the lines with 210 km without a shunt reactor, the breaking current is 686 A_{rms} (the same level as compared with normal condition) and the maximum TRV peak is 2329 kV (6.5 % higher as compared with normal condition), which corresponds to the voltage factor of 1.30.

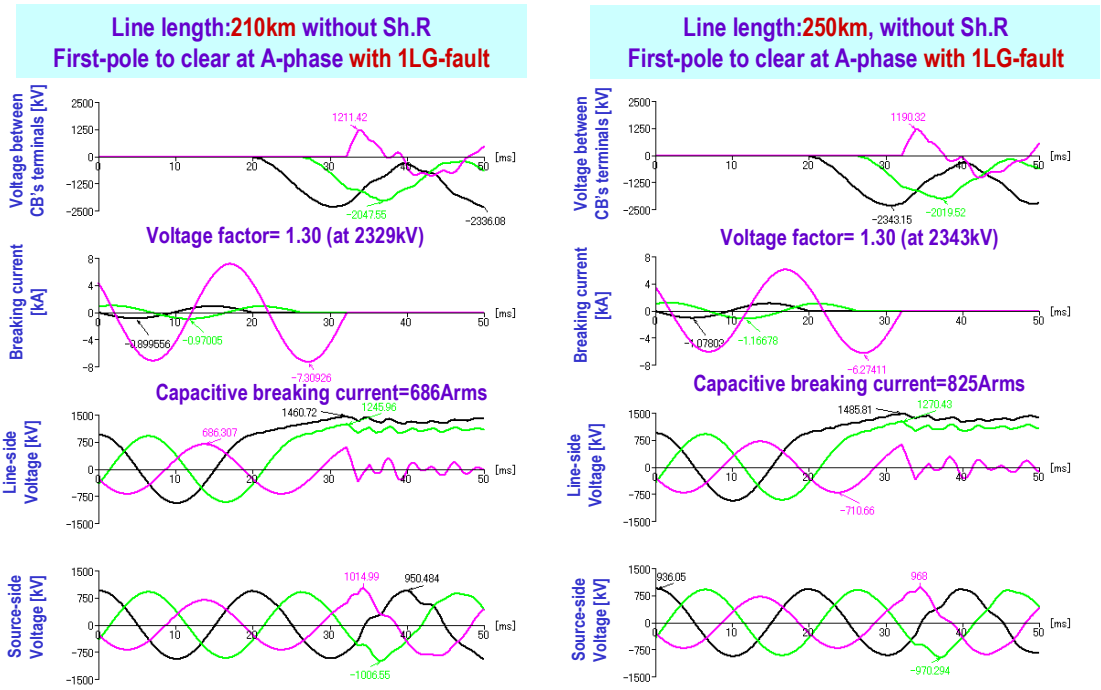

Figure 3.5.21 Analytical results of no load 1100 kV line breaking with 1LG condition (Japan)

Figure 3.5.22 shows typical voltage and current behaviour in the case of capacitive current switching under 1LG conditions based on 1200 kV single circuit transmission lines of 400 km length in India. The breaking current is 1474 A_{rms} (14% larger as compared with normal condition) and the maximum TRV peak is 2454 kV (10 % higher as compared with normal condition) which corresponds to a voltage factor of 1.25.

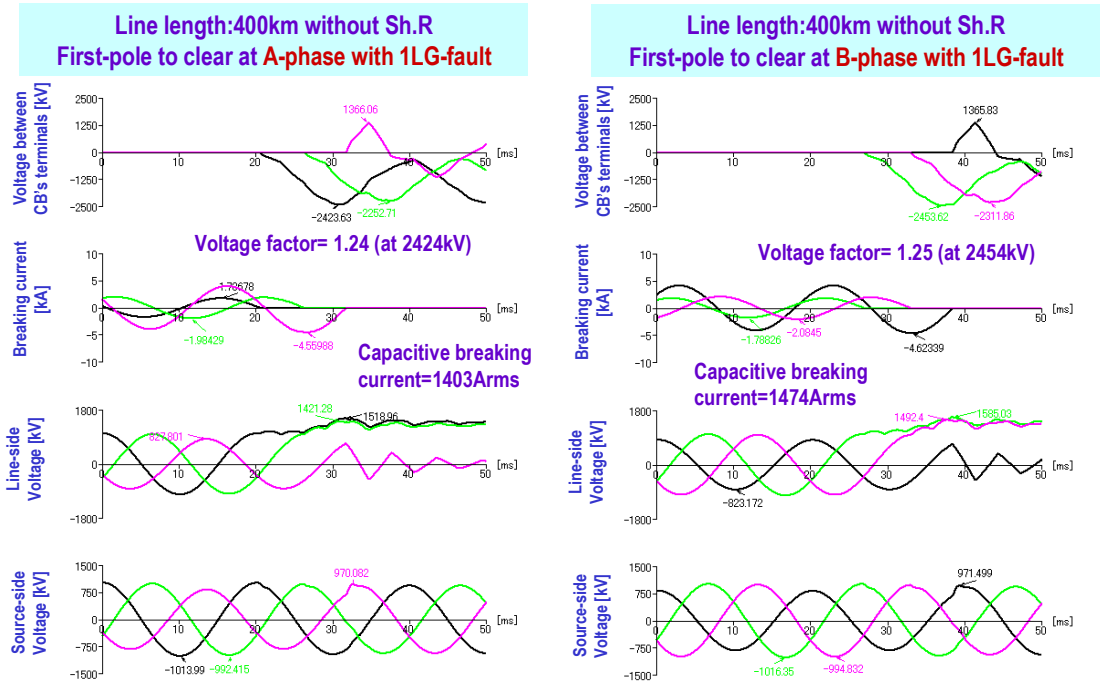

Figure 3.5.22 Analytical results of no load 1200 kV line breaking with 1LG condition (India)

3.5.5.4 *Initial part of TRV*

Figure 3.5.23 shows the initial part of TRV in the case of capacitive current switching for no load 800 kV line breaking in South Africa. Prominent super-imposed voltage increments are observed because the voltage increase due to Ferranti effect disappears immediate after the current interruption and causes an additional transient voltage. The ITRV is suppressed within a few milliseconds and the transient does not exceed 1/4 cycle (5 ms) after the interruption. Severe over-voltages would not be expected if re-ignitions occur in the ITRV region (less than 1/4 cycle) and the current can be interrupted at the next current zero. The TRV peak for healthy condition without a fault and 1LG condition can be covered by a (1-cos) waveform with a capacitive voltage factor (k_c) =1.2 and 1.4, respectively.

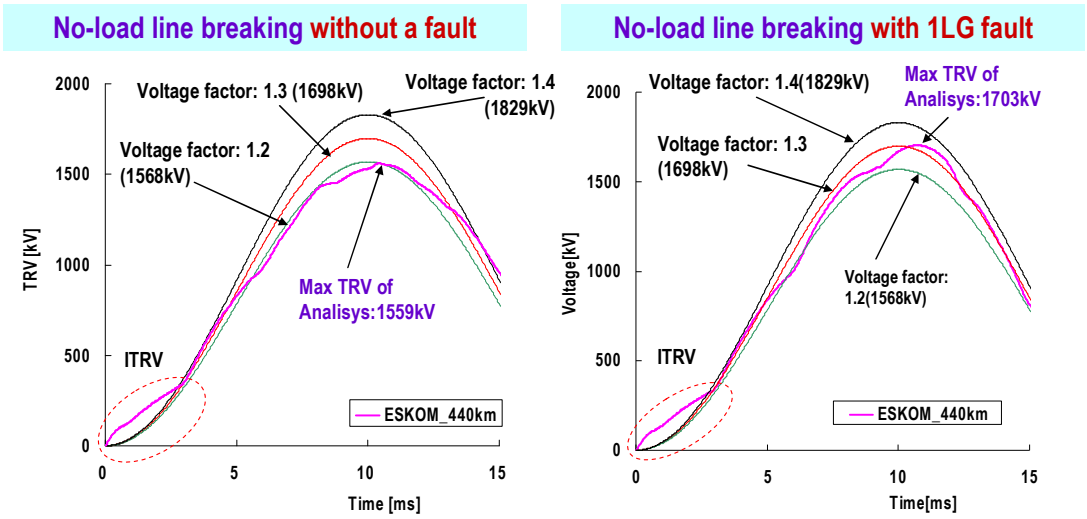

Figure 3.5.23 Initial part of TRV for no load 800 kV line breaking (South Africa, 50 Hz)

Figure 3.5.24 shows the initial part of TRV in the case of capacitive current switching for no load 1100 kV line breaking in Japan. The ITRV is suppressed within a few milliseconds and the transient does not exceed 1/8 cycle (2.5 ms) after the interruption. TRV peaks for healthy condition without a fault and 1LG condition can be covered by a (1-cos) waveform with a capacitive voltage factor (k_c) =1.3.

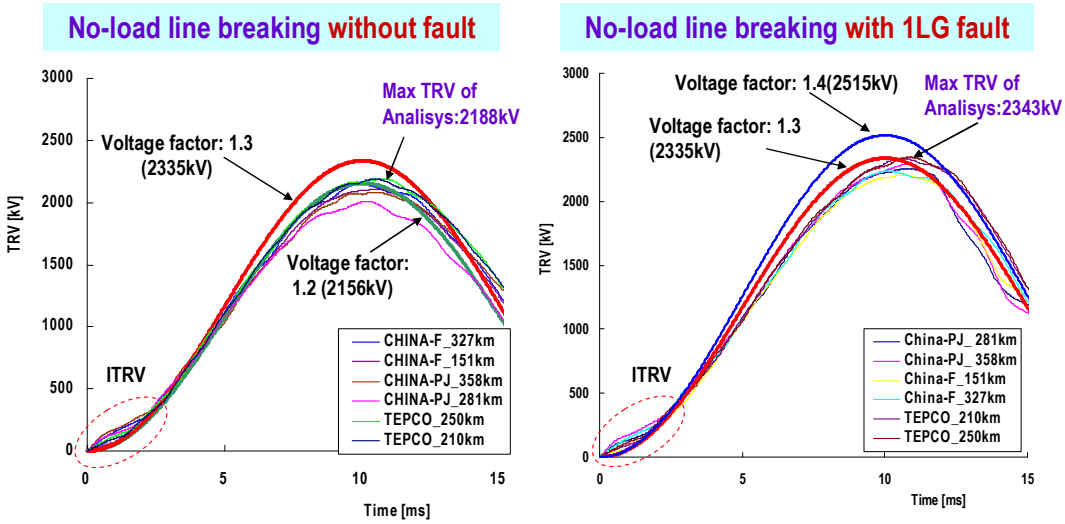

Figure 3.5.24 Initial part of TRV for no load 1100 kV line breaking (Japan, 50 Hz)

Figure 3.5.25 shows the initial part of TRV in the case of capacitive current switching for no load 1200 kV line breaking in India. The ITRV is suppressed within a few milliseconds and the transient does not exceed 1/4 cycle (5 ms) after the interruption. The TRV peak for healthy condition without a fault and 1LG condition can be covered by a (1-cos) waveform with a capacitive voltage factor (k_c) =1.2 and 1.3, respectively.

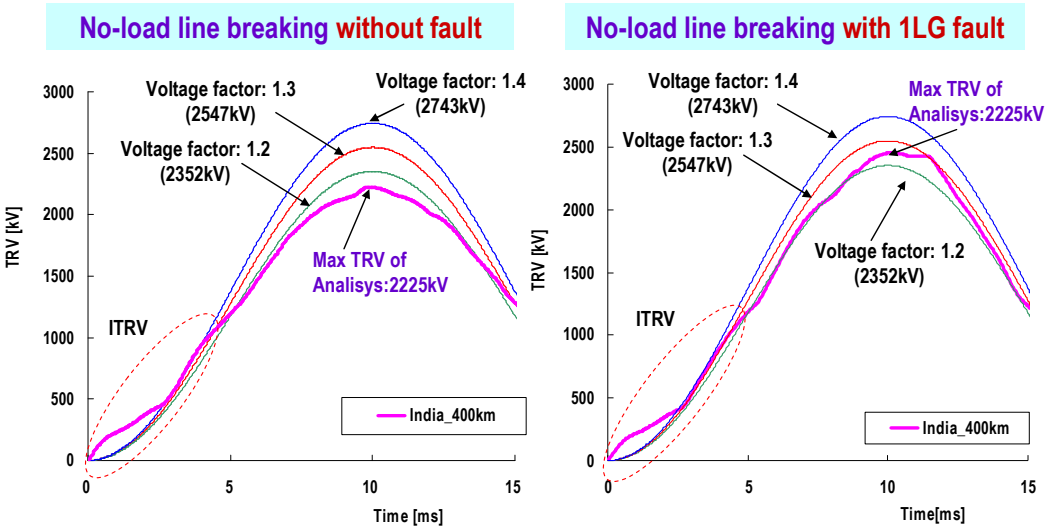

Figure 3.5.26 Initial part of TRV for no load 1200 kV line breaking (India, 50 Hz)

3.5.5.5 Summary of capacitive current switching

Table 3.5.4 summarizes the results of capacitive current switching under normal service and 1LG conditions. For line-charging current switching by circuit-breakers with rated voltages 800kV, 1100kV and 1200kV, the capacitive voltage factor (k_c) is covered by, or is close to, 1.2 under normal service conditions and is less than 1.3 under 1LG fault conditions.

Table 3.5.4 Summary of capacitive current switching (CIGRE WG A3.22 survey)

Highest Voltage	Power Frequency	Line Length	Without fault conditions				With fault (1LG) conditions			
			Capacitive breaking current		TRV peak (Voltage factor)		Capacitive breaking current		TRV peak (Voltage factor)	
			CB terminal: 2E	Line terminal: 2E	CB terminal: 2E	Line terminal: 2E	CB terminal: 2E	Line terminal: 2E	CB terminal: 2E	Line terminal: 2E
800 kV South Africa	50 Hz	440 km	969 A	801 A	1559 kV (1.19)	1392 kV (1.06)	1009 A	901 A	1703 kV (1.30)	1520 kV (1.16)
765 kV Canada	60 Hz	210 km	491 A	472 A	1442 kV (1.15)	1388 kV (1.11)	487 A	469 A	1575 kV (1.26)	1517 kV (1.21)
		400 km	1000 A	867 A	1465 kV (1.17)	1289 kV (1.03)	1015 A	880 A	1627 kV (1.30)	1411 kV (1.24)
800 kV Korea	60 Hz	39 km	94 A	93 A	1569 kV (1.20)	1567 kV (1.20)	92 A	92 A	1639 kV (1.25)	1636 kV (1.25)
		155 km	378 A	369 A	1577 kV (1.21)	1542 kV (1.18)	382 A	374 A	1659 kV (1.27)	1624 kV (1.24)
800 kV U.S.A	60 Hz	300 km	815 A	753 A	1527 kV (1.17)	1413 kV (1.08)	889 A	822 A	1688 kV (1.29)	1410 kV (1.08)
800 kV Brazil	60 Hz	266 km	643 A	606 A	1485 kV (1.14)	1400 kV (1.07)	670 A	632 A	1629 kV (1.25)	1535 kV (1.17)
		331 km	817 A	745 A	1526 kV (1.17)	1392 kV (1.06)	860 A	784 A	1638 kV (1.25)	1489 kV (1.14)
1100 kV Japan	50 Hz	210 km	665 A	647 A	2187 kV (1.22)	2131 kV (1.19)	686 A	668 A	2329 kV (1.30)	2276 kV (1.27)
		250 km	798 A	768 A	2188 kV (1.22)	2107 kV (1.17)	825 A	796 A	2343 kV (1.30)	2259 kV (1.26)
1100 kV China pilot	50 Hz	281 km	850 A	812 A	2082 kV (1.16)	1987 kV (1.11)	877 A	897 A	2253 kV (1.25)	2063 kV (1.15)
		358 km	1105 A	1024 A	2090 kV (1.16)	1938 kV (1.08)	1151 A	1143 A	2292 kV (1.28)	2030 kV (1.13)
1100 kV China future	50 Hz	151 km	443 A	434 A	2115 kV (1.18)	2076 kV (1.16)	450 A	446 A	2203 kV (1.24)	2177 kV (1.21)
		327 km	994 A	925 A	2149 kV (1.20)	1999 kV (1.11)	1025 A	967 A	2234 kV (1.24)	2105 kV (1.17)
1200 kV India	50 Hz	400 km	1293 A	1175 A	2225 kV (1.13)	2021 kV (1.03)	1474 A	1339 A	2454 kV (1.25)	2229 kV (1.14)

3.6 Requirements for CB opening resistors

3.6.1 Introduction

Suppression of switching over-voltages is a prerequisite for insulation clearances in air to reduce the heights of transmission towers and the dimensions of open-air parts in substations. Because lightning overvoltages dominate the non-self-restoring internal insulation design of substation equipment, it is important to suppress lightning overvoltages effectively by arranging MOSAs at adequate locations, such as at line entrances, busbars and transformers. To suppress switching overvoltages, in addition to the MOSAs, pre-insertion closing and opening resistors are often applied. The opening resistor can reduce the switching overvoltage and also have a considerable effect to reduce the amplitude of TRV oscillations.

3.6.2 General considerations for CB opening resistor

To achieve a compact and economic UHV infrastructure, various methods can be utilized to minimize the size of the OH-lines and substations. As the system voltage increases, the necessary insulation distance tends to become longer because of a "saturation" of insulating strength for large air gaps, certainly with respect to switching over voltages. To minimize the required corridor (and hence land occupation) for overhead lines and to minimize the height of the transmission towers, a minimization of switching over-voltages is essential. For that purpose, the application, appropriate allocation and consequential impact of "high performance" surge arresters is a key element for UHV system design. A further element is the suppression of switching over-voltages by resistor insertion during circuit breaker switching operations. Whilst the effects of closing resistors are well-known, the application of opening resistors should also be considered.

The most important effect of the application of opening resistors in UHV projects is a reduction of the switching surge which is generated in the healthy phases of the network at the source side of the circuit-breaker when clearing a line fault. If a successive breakdown would occur in a healthy phase, a multiple fault is introduced which can have a serious effect for the whole system.

In Japan the target is to reduce the switching surge level to that of the ground fault surge, 1.6 to 1.7pu, in order to design UHV transmission towers that are as compact as possible. To this end, in addition to closing resistors, opening resistors have been applied which also act to reduce the severity of TRV waveforms, as explained in the next paragraphs.

3.6.3 Effect of opening resistor on switching overvoltage

At the occurrence of a ground fault, the phase voltage changes to zero potential instantaneously which is the equivalent of inject a voltage which is equal and opposite to the phase voltage immediately before the ground fault. This voltage is induced to other phases (healthy phases) of the OH-line and, due to propagation and reflection within the system, overvoltages are superimposed on the AC voltage. Such a SFO (slow front overvoltage) is called a 'ground fault overvoltage' or 'earth fault overvoltage'.

The highest SFO is generated by a fault occurring near the peak value of the AC voltage since this is the largest voltage collapse and the maximum overvoltage tends to appear in the middle of an OH-line (See figure 3.6.1). After the transient phenomenon disappears the power frequency overvoltage remains (TOV as shown in figure 3.6.3)

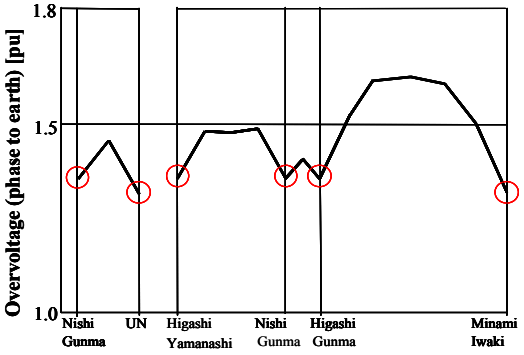

Figure 3.6.1 Ground fault overvoltage

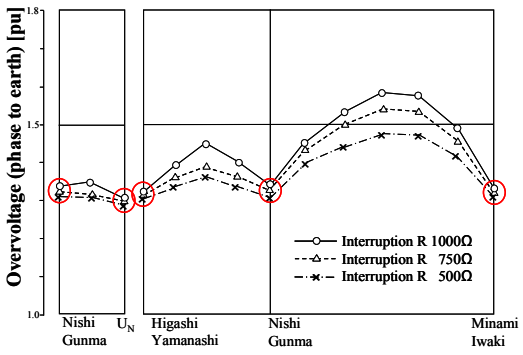

Figure 3.6.2 Overvoltage after clearing a fault

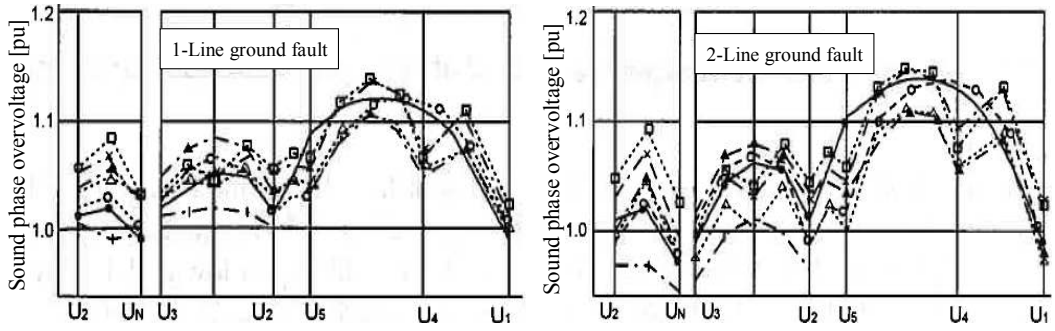

Figure 3.6.3 Temporary overvoltages (TOV) during ground faults

Figure 3.6.1 shows the maximum SFO for a ground fault anywhere in the system (not necessarily corresponding to those on the healthy phase(s) at the location of the ground fault). The analysis was carried out by simulating the whole network of TEPCO above 500kV in detail with fault locations, faulted phases, and voltage phases of fault timing, etc. as parameters.

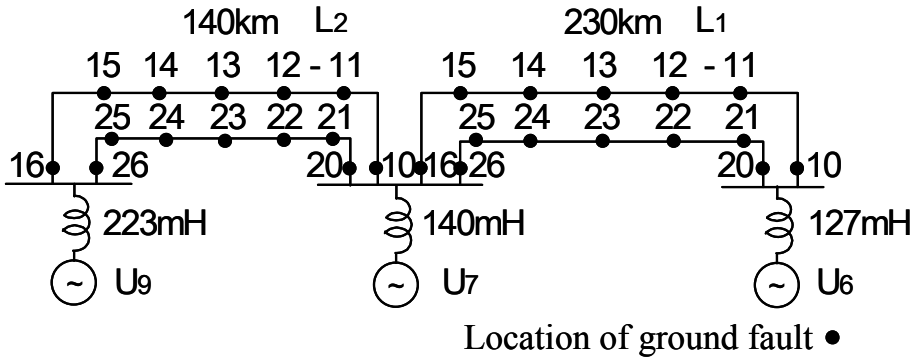

Figure 3.6.4 Analyzed system model for the ground fault

Table 3.6.1 Maximum SFO at the occurrence a ground fault

	Protection level of SA	
	V_{20kA} =1,620kV	V_{20kA}=1,800kV
Max. values at OH-lines	1,450kV (1.62pu)	1,480kV (1.65pu)
Max. values at 3 substations under above condition	1,210kV (1.35pu)	1,320kV (1.47pu)

* Protection level V_{20kA} =1,620kV (V_{1kA}≒1,400kV (1.56pu)) of SA is adopted in Japan.

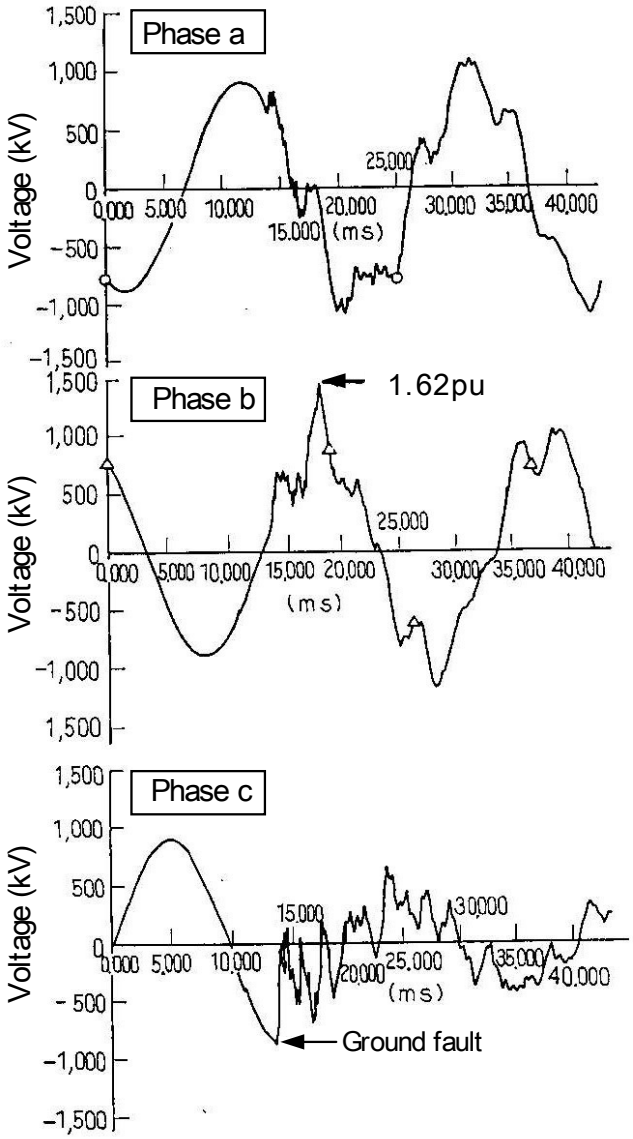

Figure 3.6.5 Analyzed waveform of maximum SFO at the occurrence of a ground fault (Fault location: near U6, SA protection level: V_{20kA}=1,620kV)

In the former stage the analysis was done for the system model as shown in figure 3.6.4, using two protection levels of the surge arrester. Maximum SFO is generated at a ground fault of the 230 km line near U6 substation (L1-11, voltage phase of fault timing is 70 degree), and the location where the maximum SFO appears is the healthy phase of the middle of the healthy line (L1-23). Maximum values are shown in table 3.6.1. Figure 3.6.5 shows the waveform of maximum value generated; 1.62 p.u.

From table 3.6.1 it can be seen that there are no effective measures to control ground fault overvoltages, except those near substations that can be reduced by surge

arresters. Therefore the ground fault SFO gives the lower limit for the determination of the suppression level by closing and opening resistors.

When a fault current is interrupted, overvoltages are generated at healthy circuits in the system. Figure 3.6.2 shows the maximum SFO for a single or multi-phase ground fault clearance anywhere in the system (not necessarily corresponding to that on the healthy circuit at the location of the earth fault). The analysis was carried out in detail with fault types, fault phases, and fault locations as parameters. Three-phase line fault to ground (3LG) were mainly calculated because the recovery voltages are the highest.

Similar to the ground fault occurrence, the analysis was done in the former stage for the system model as shown in figure 3.6.6, using protection levels of the surge arrester and with/without resistor of the circuit breaker as parameters.

The maximum SFO occurs on the middle of the 230 km healthy line during three-phase opening operations after three-phase line faults to ground generated at the location 3. Maximum values, the relationship between the locations of the fault and maximum SFO, and the waveform of maximum SFO are shown in table 3.6.2, figure 3.6.7 and figure 3.6.8, respectively.

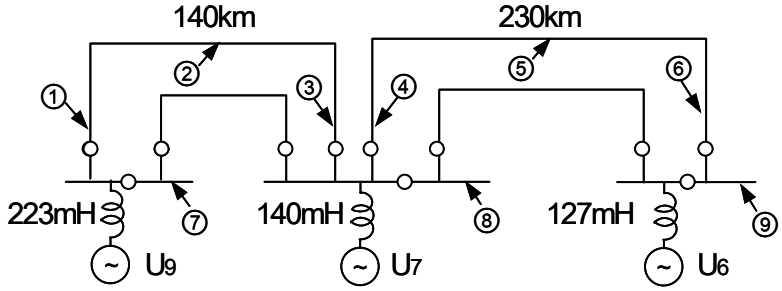

Figure 3.6.6 Analyzed system model for the opening overvoltages

Table 3.6.2 Maximum SFO at the ground fault clearing

	Protection level of SA	Without R	With R		
			500 Ω	750 Ω	1,000 Ω
Maximum SFO at OH-lines	V_{20kA} =1,620 kV	1,640 kV (**1.83 p.u.**)	1,280 kV (**1.42 p.u.**)	1,360 kV (**1.52 p.u.**)	1,440 kV (**1.60 p.u.**)
	V_{20kA} =1,800 kV	1,770 kV (1.97 p.u.)	1,280 kV (1.42 p.u.)	1,380 kV (1.54 p.u.)	1,470 kV (1.64 p.u.)
Maximum SFO at three substations under the above condition	V_{20kA} =1,620 kV	1,280 kV (1.42 p.u.)	1,210 kV (1.35 p.u.)	1,230 kV (1.37 p.u.)	1,250 kV (1.39 p.u.)
	V_{20kA} =1,800 kV	1,390 kV (1.55 p.u.)	1,250 kV (1.39 p.u.)	1,290 kV (1.44 p.u.)	1,310 kV (1.46 p.u.)

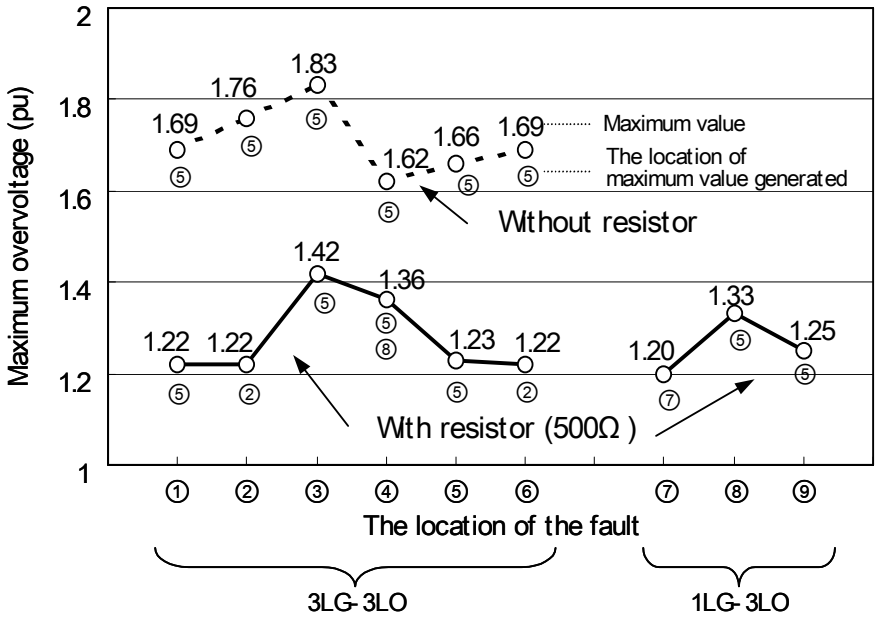

Figure 3.6.7 Relationship between the locations of the fault and maximum SFO

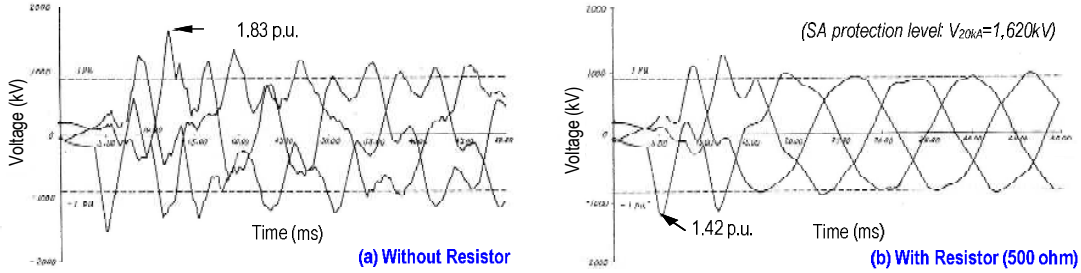

Figure 3.6.8 Waveforms of maximum SFO at the middle of 230km OH-line

Figure 3.6.9 shows the relationship between fault-type/opening-method and maximum SFO for the fault of location 3 in figure 3.6.6. The maximum SFO is generated in case of 3LG fault clearing; without resistor, it would become larger than the level of OH-line design.

The SFO level generally depends on the fault-type and tends to be larger in an order of 1LG <2LG <3LG. The probability of 2LG & 3LG faults is comparatively low (about 10% of the probability of 1LG in UHV systems) suggesting that it may be possible to disregard 2LG & 3LG faults. This would eliminate the need for special requirements to reduce SFO, such as circuit-breakers with opening resistor, however, in the event of a successive fault occurring in a healthy line followed by a fault clearing in another line there could be serious consequence for the whole system. For this reason, in Japan, opening resistors are adopted for line side circuit-breakers.

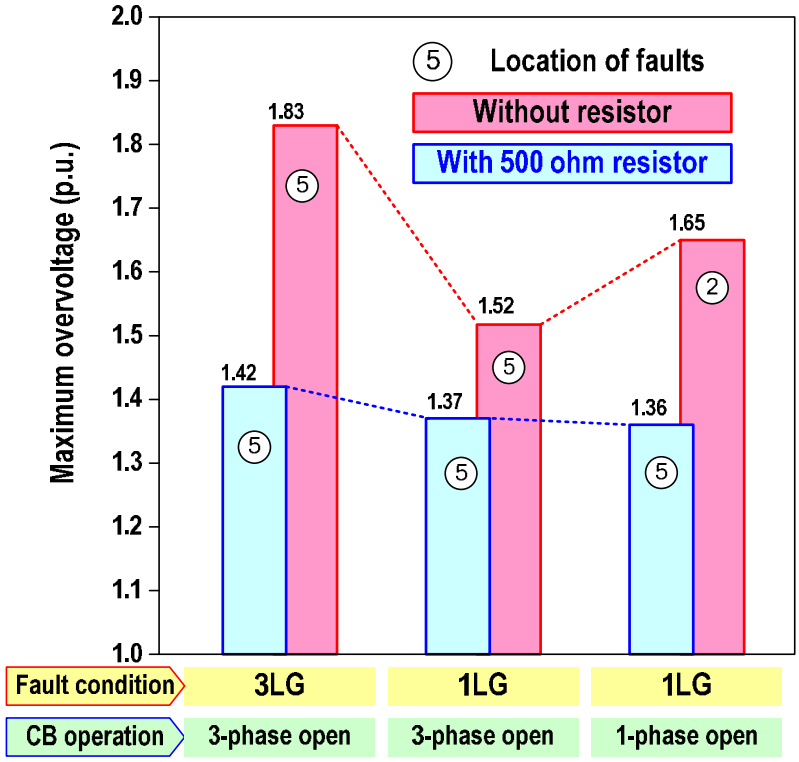

Figure 3.6.9 Maximum SFO for different fault-types and opening-practices

3.6.4 Principal features of CB with opening resistor

The peak value of TRV (U_c) and the rate-of-rise of recovery voltage (RRRV) in case of interruption with an opening resistor have been investigated. First of all the general conditions without opening resistor are reviewed. The impedance of the system in the power frequency region is expressed as equation. (1).

$$Z_{sAC} = \frac{V_{sAC}}{I_{sAC}} \qquad (1)$$

In an 1100kV system with 50 Hz, assuming a short-circuit current of 50kA, the system impedance for T100 and T10 corresponds to 12.7 Ω (40mH) and to 127 Ω (400mH) respectively.

For fast phenomena, such as the initial part of the TRV, the equivalent surge impedance will be used. The equivalent surge impedance Z_{surge} is obtained from equation (2).

$$Z_{surge} = \frac{RRRV}{di/dt} \qquad (2)$$

In the IEC Standard, the RRRV for T100 is specified as 2kV/us and the equivalent surge impedance for T100 becomes

$$Z_{surgeT100} = \frac{2.0}{2\pi \times 50 \times \sqrt{2} \times 50} = 90\Omega, \text{ as } (di/dt) = 2\pi \times 50 \times \sqrt{2} I \quad (50\text{Hz}).$$

For T10 the equivalent surge impedance is much larger with smaller current but higher RRRV:

$$Z_{surgeT10} = \frac{7.0}{2\pi \times 50 \times \sqrt{2} \times 5} = 3150\Omega$$

By putting the opening resistor in parallel to the equivalent network the impedance seen from the breaker terminals can be expressed as Z', as in equation (3).

$$Z' = \frac{Z_s R}{Z_s + R} \qquad (3)$$

Where Z'is the equivalent impedance seen from breaker terminal with Zs being the system impedance and R being the resistance of the opening resistor.

The RRRV at opening of the main contacts is expressed in equation (4)

$$RRRV = Z_{surge}(di/dt) \qquad (4)$$

Here the surge impedance is used. Assuming the opening resistor to be 750 Ω, and Z_{surge} of T100 to be 90 Ω, as given above, the equivalent surge impedance is:

$$Z_{surge} = \frac{90 \times 750}{90 + 750} = 80\Omega$$

and the RRRV is found to be 1.78 kV/μs, which is 89% of the standard value of 2kV/μs (80/90=0.89).

In the case of T10, Z_{surge} may be as large as 3150 Ω leading to:

$$Z_{surge} = \frac{3150 \times 750}{3150 + 750} = 606\Omega$$

For which the RRRV becomes 1.33 kV/μs, which is only 19% of standard value of 7kV/μs (606/3150=0.19).

In conclusion, the application of opening resistors tends to reduce the RRRV for the main contacts to a greater extent for the interruption smaller short-circuit currents (e.g. T10) than for larger currents (e.g. T100).

Near the TRV peak, U_c , the conditions are more complicated.

By inserting resistors into the system just after the main contacts interrupt the current, the transient oscillations are more heavily damped or may even be suppressed. The surge impedance of the TRV region is expressed as Z_{TRV} and the impedance seen from the breaker terminals with opening resistor is Z'_{TRV},

$$Z'_{TRV} = \frac{Z_{TRV} R}{Z_{TRV} + R} = R - \frac{R^2}{Z_{TRV} + R} \qquad (5)$$

From formula (5) it is clear that the larger Z_{TRV} is, the larger Z'_{TRV} is expected to be. On the other hand, for $Z_{TRV} >> R$ (such as for T10), Z'_{TRV} will be slightly below R, while for $Z_{TRV} << R$ (such as for T100), Z'_{TRV} will be slightly below Z_{TRV}. Therefore, the U_c for the T10 duty will be lower than that for the T100 duty.

In order to better understand the entire TRV in the presence of opening resistors an interruption study with a simplified circuit consisting of inductance (L) and capacitance (C) in Figure 3.6.10 has been prepared.

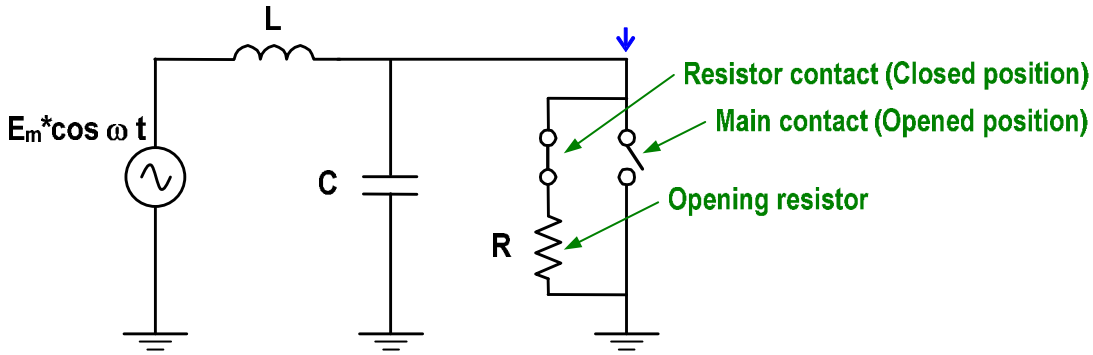

Figure 3.6.10 Simplified circuit to evaluate the effect of opening resistor

The inherent TRV of the system, which means the case without opening resistors, is characterized as follows.

$$V(t) \approx E_m \times (1 - \cos \omega_0 t) \qquad (6)$$

$$RRRV \approx \frac{2E_m}{0.85\pi\sqrt{LC}} \qquad (7)$$

$$Z_{surge} = \frac{RRRV}{di/dt} \approx \frac{2E_m}{0.85\pi\sqrt{LC}} \Big/ \frac{E_m}{L} \approx 0.8 \times Z \qquad (8)$$

Where, $\omega_o = \frac{1}{\sqrt{LC}}$, $Z = \sqrt{L/C}$

In the case with opening resistors, the TRV is obtained as follows.

$$V(t) \approx E_m - E_m \times \exp\left(-\frac{1}{2CR}t\right) \times \cos\left(\sqrt{\frac{1}{LC} - \frac{1}{4C^2R^2}} * t\right) \qquad (9)$$

The amplitude factor k_{af} is

$$k_{af} \approx 1 + \exp\left(\frac{\pi}{\sqrt{4(R/Z)^2 - 1}}\right) \qquad (10)$$

The ratio of the RRRV with and without opening resistors ($RRRV_{ratio}$) is

$$RRRV_{ratio} = \frac{R \times Z_{surge}}{R + Z_{surge}} \times \frac{1}{Z_{surge}} = \frac{R/Z_{surge}}{R/Z_{surge} + 1} \approx \frac{R/Z}{R/Z + 1} \qquad (11)$$

Figure 3.6.11 shows the amplitude factor k_{af} and $RRRV_{ratio}$ calculated as a function of R/Z ($\approx 0.8R/Z_{surge}$). For example, in case of the opening resistor value of 750 Ω, R/Z = 0.8 × 750/3150 = 0.19 for T10 duty, R/Z = 0.8 × 750/90 = 6.7 for T100 duty. Therefore, it can be seen that for small breaking currents such as T10, the TRV is over damped and the RRRV and U_c are reduced considerably by the opening resistors. For large breaking current such as T100, the TRV is oscillatory with higher RRRV and U_c meaning that the effect of TRV reduction due to opening resistor is relatively limited.

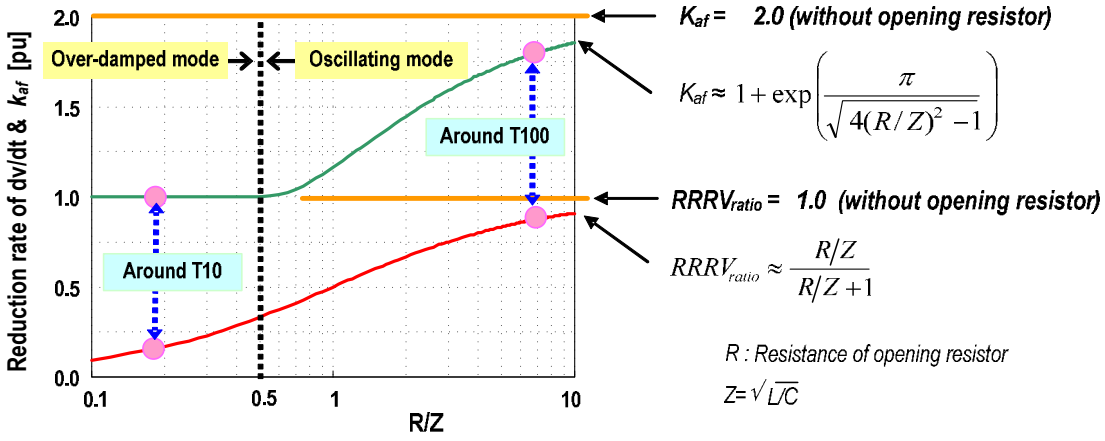

Figure 3.6.11 Effect of opening resistor for amplitude factor (k_{af}) and RRRV

3.6.5 Terminal fault requirements for CB with opening resistor

(a) Main contact

For smaller short-circuit currents, such as T10 and T30, the peak voltage U_c and the RRRV are drastically reduced by the application of opening resistors and the severity of the interruption duty is reduced. The application of opening resistors can also mitigate the severe TRV conditions associated with TLFs and may therefore alleviate the need to apply a highly rated circuit-breaker which might otherwise be necessary to cater for the unmodified TRV conditions.

(b) Auxiliary contact for opening resistor

The application of opening resistors can reduce the current to be interrupted to a few kA, for example, an opening resistor of 750 Ω can reduce the current to around 1 kA, and U_c and RRRV become quite low compared to the case without the opening resistors. As an example (see also figure 3.6.14), an RRRV of 2.3 kV/µs and an associated U_c of 250 kV for the T10 duty can be deduced as follows.

The TLF current is limited through the transformer inductance (0.4 H for 10% of 50 kA at 50 Hz). The response of the transformer to the injected current of about 1 kA (0.444 A/µs) is a damped 1-cos with a time to peak of about 150 µs (t_3 = 130 µs) and an amplitude factor of 0.9×1.7, resulting in a peak value of $0.9 \times 1.7 \times 0.4\,H \times 0.444$ A/µs = 270 kV and a RRRV of 270/130 = 2.0 kV/µs. In addition there is the ramp function across the opening resistor, giving 750Ω × 0.444 A/µs = 0.33 kV/µs and a total value of 2.3 kV/µs.

In the range T30 to T100, U_c is of the order of 1200 kV and the RRRV is approximately 0.5kV/µs, as can be deduced from 0.444 A/µs and 90 Ω +750 Ω for T100 duty, 230 Ω +750 Ω for T60 duty and 750 Ω + 750 Ω for T30 duty. The TRV peak value is slightly above $1\,\text{kA} \times \sqrt{2} \times 750\,\Omega$. (See figure 3.6.15)

3.6.6 Short line fault (SLF) requirements for CB with opening resistor

(a) Main contact

The RRRV for SLF duties in the initial period is quite high. The application of the opening resistor can also reduce the RRRV for SLF effectively.

(b) Auxiliary contact for opening resistor

Similar to the case of terminal fault, the interrupting current becomes small (around 1 kA) and the RRRV also becomes quite small: 0.444 × (450+750) = 0.5 kV/μs.

Figures 3.6.12 through 3.6.15 show typical results of TRV waveforms for these duties.

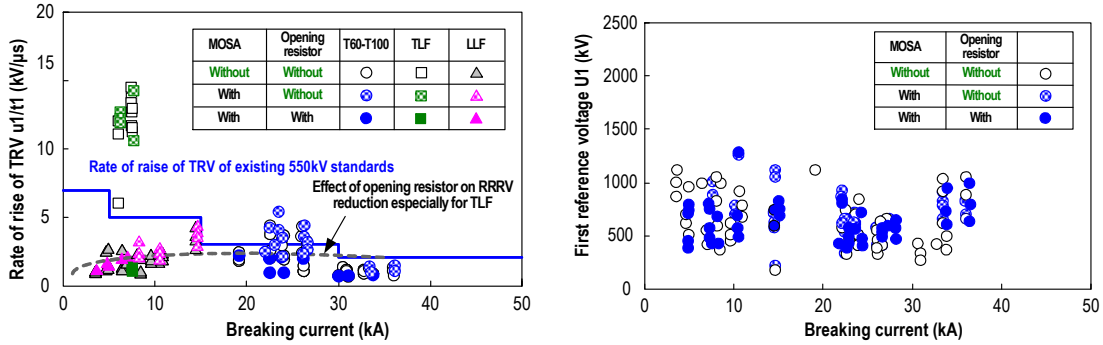

Figures 3.6.12 and 13 Effect of opening resistor for RRRVand first peak value u_1

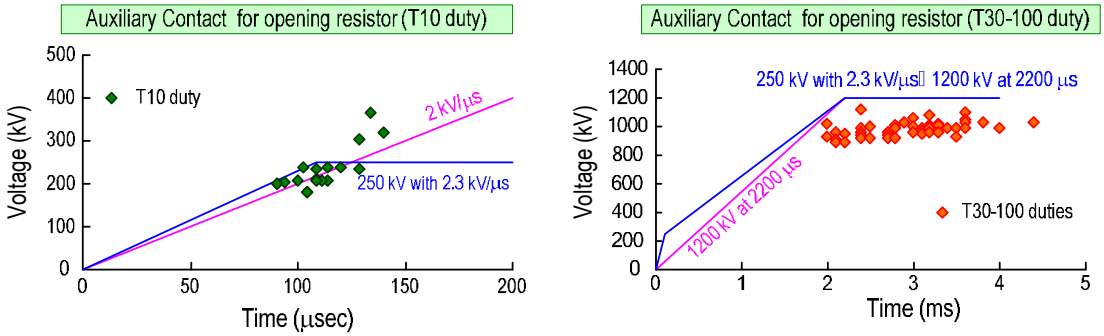

Figures 3.6.14 and 15 TRV plots for auxiliary contact of opening resistor for terminal fault conditions

3.6.7 Long line faults, out-of-phase switching & capacitive current switching requirements for CB with opening resistor

(a) Main contact

For duties where the voltage across the circuit-breaker terminals is defined by the voltages generated at both sides of the breaker, the TRVs tend to be lowered by the application of opening resistors. The voltage across the main contacts before interruption of the auxiliary contacts is expressed as the voltage drop on the resistor

$$V_{resist} = \frac{R}{Z_{line} + Z_{source} + R} V_{system} \qquad (12)$$

Thus the TRV applied to the main contacts is reduced in proportion to the impedance expressed by equation (12).

(b) Auxiliary contact for opening resistor

After the current is transferred into the opening resistors, a phase shift is introduced due to the increased resistive component in the inductive or capacitive current. The more resistive current is, generally speaking, easier to interrupt. On the other hand,

and even though the current is small, the TRV is applied from both sides of the breaker meaning that the TRV requirements for the auxiliary contacts is not always mitigated to the extent of the terminal fault and SLF cases.

3.6.8 LLF requirements for CB with opening resistor

(a) Main contact

Under LLF conditions the system impedance, especially Z_{line}, is high with a small fault current caused by the long line. The TRV will not be suppressed by surge arresters when the voltage at each side of the circuit-breaker is lower than the clipping level of the arresters. The time to the reflection of the travelling wave forwards and backwards across the long distance up to the faulted point is long and the line side transient voltage steadily increases until the moment of reflection. The source side voltage increases (in opposite polarity) during that period and the voltage between the breaker contacts tends to be high.

In case of LLF interruption with an opening resistor, the TRV for the main contacts is reduced because voltage across the resistor decreases according to the equation (12). Also transient oscillations are suppressed by the resistors. All aspects contribute to interruption mitigation.

(b) Auxiliary contact for opening resistor

After the main contacts interrupt the fault current, the resistor is inserted into the circuit resulting in a phase shift due to the increased resistive element. At current zero the voltage is less than the peak, the oscillation becomes smaller and the line side voltage V_{line} is reduced in proportion to R and Z_{line} by the inserted resistors. When the auxiliary contact interrupts the line side voltage oscillates and the source side voltage increases (caused by rather long t_2) but still remains lower than that without opening resistors.

3.6.9 Out-of-phase switching requirements for CB with opening resistor

During out-of-phase interruption a severe TRV is expected due to the voltage oscillation of the source and load sides which cause a large voltage difference across the circuit breaker. As previously explained, the TRV becomes more severe in a switching station with long lines with the same lengths.

According to IEC Standard 62271-100, the specified RRRV for out of phase is 1.54 kV/μs, and the out-of-phase current value is 25%. For a 50kA rating with an equivalent surge impedance of about 280 Ω the application of opening resistors of 750Ω reduces the RRRV 73% of its inherent value.

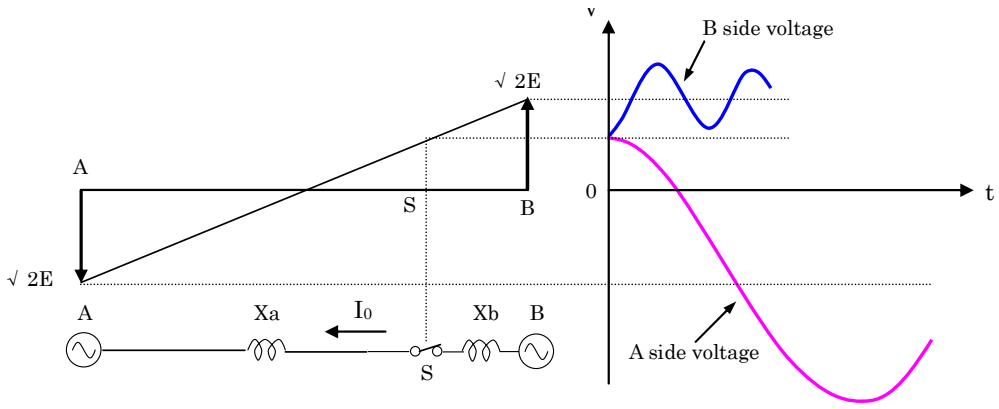

Io =2E*sin(½θ)/ (Xa + Xb)

=2E/ (Xa + Xb) (When θ=180 degree)

Figure 3.6.16 Concept of out-of-phase interruption

In the case without opening resistors, the phase difference between the breaking current and voltage is 90 degree and AC voltage at the moment of interruption is at its peak. At the time of transient voltage peak after interruption, AC component of the voltage has passed its peak. In a network of small short circuit current the frequency of oscillation of TRV tends to be low and therefore the AC component becomes small at the time of TRV peak. This means the TRV peak itself becomes small.

The application of the opening resistor modifies the out-of-phase interruption phenomena as follows (See also figure 3.6.18):

(a) Main contact

The recovery voltage across the contacts V_{main} is

$$V_{main} = \frac{2\sqrt{2}E \times R}{X_a + X_b + R} \qquad (13)$$

So assuming X_a=X_b, R = 600 Ω,

Breaking current: 12.5 kA (= 25% of 50kA), X_a=X_b = 50.8 Ω, V_{main} = 0.86 p.u.

Breaking current: 2.5 kA(= 5% of 50kA), X_a=X_b = 254 Ω, V_{main} = 0.54 p.u.

From this it is clear that the larger the back impedance becomes, the lower the TRV peak is.

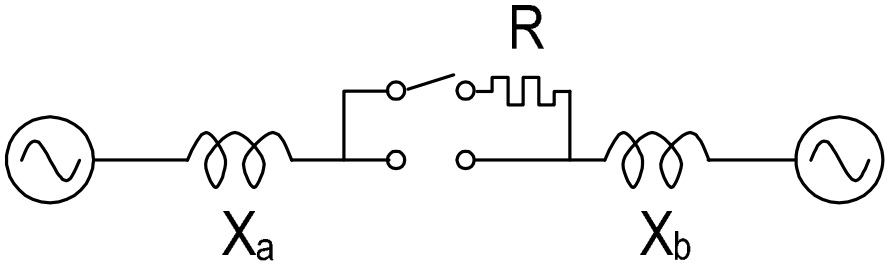

Figure 3.6.17 Simplified circuit of out-of-phase interruption

(b) Auxiliary contact for opening resistor

Insertion of the opening resistor reduces the phase shift between current and voltage to less than 90 degrees and, at the time of current interruption, the AC voltage component is before its peak. This phase shift is determined by the combination of back impedances and resistance of the opening resistor.

With a large back impedance (in other words a network of small short circuit current) the phase shift between current & voltage becomes large and the oscillation peak of the TRV develops slowly and occurs close to the peak of AC component. This may cause a higher peak voltage than the case without opening resistors.

With a small back impedance the phase shift becomes small (approaching zero) and the amplitude of the oscillation also becomes small. The peak of the transient recovery voltage develops quickly and is attenuated by time of the peak of AC component. Through these effects TRV peak is lower than that without opening resistors. (See figure 3.6.18)

Note: Assuming R= 600 Ω and X_a=X_b, the phase shift of current to voltage is 40 deg (2.2 ms) for 2.5 kA, and 9.6 deg (0.5 ms) for 12.5 kA.

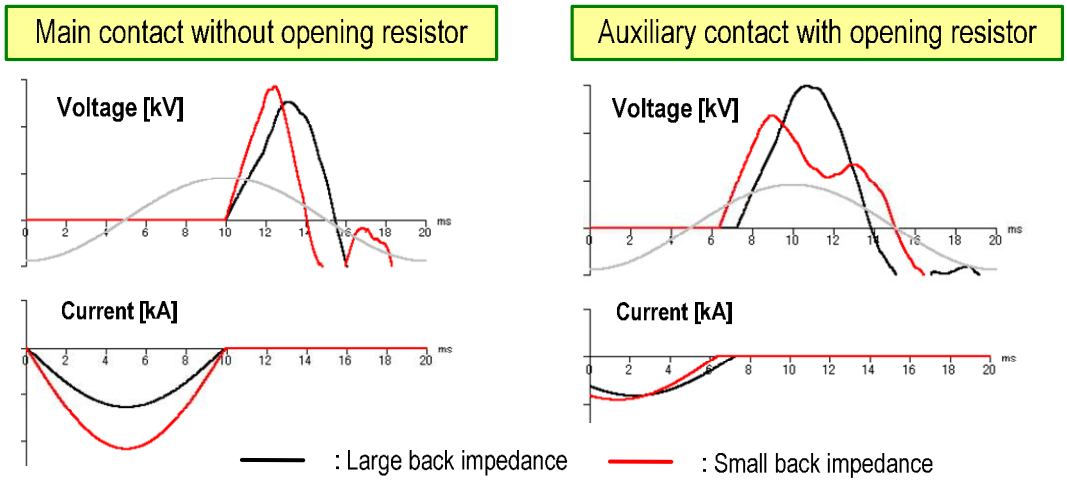

Figure 3.6.18 Effect of back impedance for TRV at out-of-phase interruption

3.6.10 Capacitive current switching requirements for CB with opening resistor

3.6.10.1 General

Figure 3.6.19 shows typical analytical results for capacitive current switching with a CB with opening resistors in the Japanese UHV network. The calculation can provide the following conclusions.

1) The recovery voltage before auxiliary contact interruption is reduced to around the 1/3 of that of the case without opening resistors.

2) After interruption by the auxiliary contacts the recovery voltage does not differ greatly from the case without opening resistors. The amplitude decreases slightly but the RRRV of the initial part becomes higher. The recovery voltage in this time region is applied to the main and auxiliary contacts.

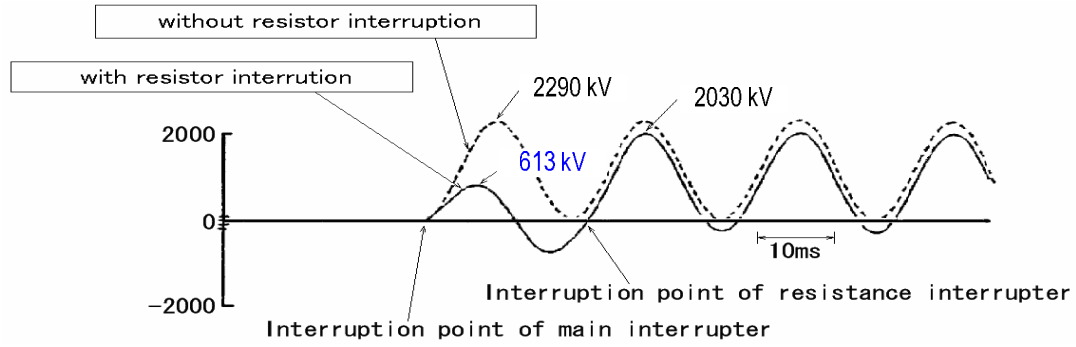

Figure 3.6.19 Effect of opening resistor on main contact for capacitive current switching

Note that, even after the interruption by the auxiliary contact, the capacitive switching duty is still severe since U_c and RRRV are comparable with the case without opening resistors.

3.6.10.2 Phenomena reproduced with simplified circuit

Simplified circuits shown in figure 3.6.11 are used to understand the phenomena. The line side capacitance is given as 3.15 μF, which corresponds to a 210 km long 1100kV transmission line, and an opening resistor of 700 Ω is considered. Network phenomena such as Ferranti effect are not considered in this analysis.

Period 1 is defined to be before interruption by the main contacts. Period 2 is after interruption by the main contacts but before interruption by the auxiliary contacts. Period 3 is after interruption by the auxiliary contacts.

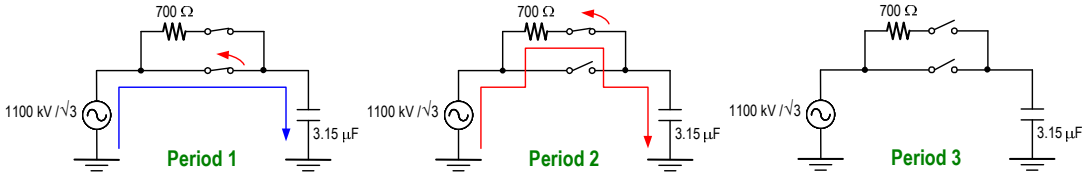

Figure 3.6.20 Simplified circuit of capacitive current interruption with opening resistor

Figures 3.6.12 shows the interrupted currents and the voltages across the main and the auxiliary contacts. Considering the line side voltage in period 2, the phase-shift between the voltages are observed and the amplitude is slightly reduced as compared with the source voltage.

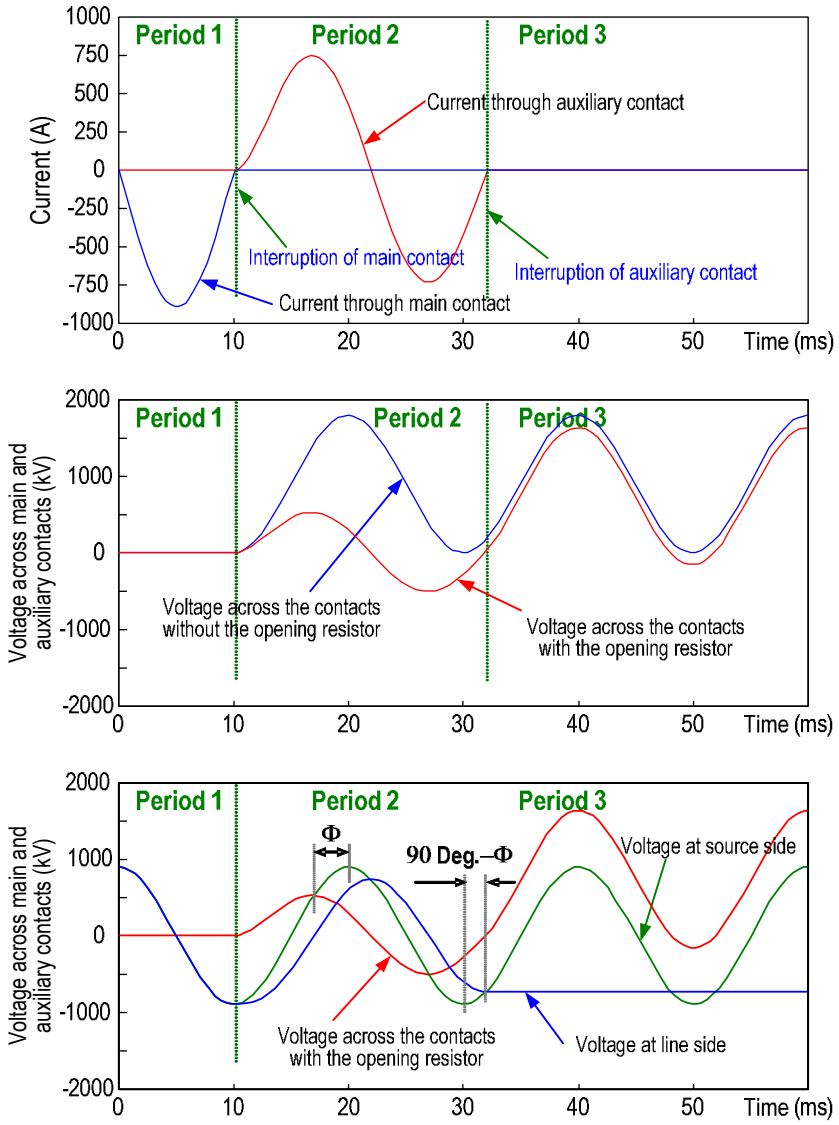

Figure 3.6.21 Typical results for capacitive current interruption in the simplified circuit

With the opening resistor and assuming the source voltage $E_m(t)= -E_m \times \cos\omega t$ (t=0 means t=10ms in figure 3.6.12), the current I(t) for the main contact is expressed as:

$$I(t) = -E_m \times \cos(\omega t + \pi/2) / Z_{LINE} = -\omega C \times E_m \times \cos(\omega t + \pi/2) \quad (14)$$

Where $Z_{LINE} = 1/\omega C$, and C is the line side capacitance.

The interrupting current $I_{RC}(t)$ though the auxiliary contact, considering the initial voltage of the line capacitance as $-E_m$ which is the residual voltage at the instance of the main contact interruption, can be derived as:

$$I_{RC}(t) = (E_m / Z) \times [\cos \varphi \times e^{-t/CR} - \cos(\omega t + \varphi)] \quad (15)$$

Where $Z = \sqrt{(R^2 + (1/\omega C)^2)}$, $\varphi = \tan^{-1}(1/\omega RC)$

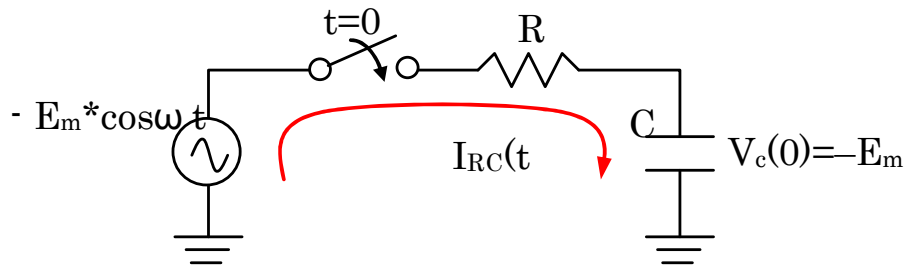

Figure 3.6.22 Equivalent circuit for current transfer to resistor

The recovery voltage V_M (t) of the main contacts before auxiliary contact interruption is,

$$V_M(t) = R \times I_{RC}(t) = E_m \times (R/Z) \times [\cos\varphi \times e^{-t/CR} - \cos(\omega t + \varphi)] \quad (16)$$

In the case without opening resistors (R=∞), this becomes $V_M(t) = E_m \times [1-\cos\omega t]$.

Assuming a source voltage of $1100/\sqrt{3}$ kV_{rms} (E_m=898 kV) and assuming C =3.15 μF, R=700Ω and $Z_{line}=1/\omega$ then:

$C=1/(314 \times 3.15 \times 10^{-6}*) = 1010\ \Omega$,

$Z = \sqrt{[R^2 + Z_{line}^2]} = \sqrt{[700^2 + 1011^2]} = 1230\ \Omega$,

R/Z =700/1230 = 0.57,

$\varphi=\tan^{-1}(1/\omega CR) = \tan^{-1}[1/(314 \times 3.15 \times 10^{-6} \times 700)] = 55.3°$,

$\cos\varphi=\cos 55.3° = 0.57$,

$CR= 3.15 \times 10^{-6} \times 700 = 2.2$ ms

Equation (16) then becomes, $V_M(t) = 0.57E_m \times [0.57\ e^{-t/2.2ms} - \cos(\omega t + 55.3°)]$

Since the peak voltage is generated around $\omega t+55.3° = 180°$, ($\omega t=124.7°$, $t=124.7/360 \times 50= 6.9$ms), the peak value, V_{Mpeak}, is,

$V_{Mpeak} \fallingdotseq 0.57E_m \times [0.57\ e^{-6.9/2.2} - \cos 180°] = 0.584\ E_m\ (= 525kV)$

This corresponds to the peak value of the recovery voltage before the auxiliary contact interruption is reduced to around the 1/3 of that of the case without opening resistor ($2E_m$=1800kV), which corresponds with the result by detailed system analysis.

As for auxiliary contact interruption, the phase angle between source voltage and interrupted current will not 90°, but will be 90°–ϕ due to the insertion of opening resistors. The recovery voltage V_R (t) of auxiliary contacts becomes as follows.

$$V_R(t) = E_m \times [\cos\theta - \cos(\omega t + \theta)] \quad (17)$$

Where $\theta = 90° - \varphi = 90° - \tan^{-1}(1/\omega CR) = \tan^{-1}(\omega CR)$

From equation (17) it can be understood that, as the line length increases, the recovery voltage moves from a 1–cos waveform to a sin one, which means RRRV becomes higher though the peak voltage is reduced.

(a) Main contact

The recovery voltage across the main contacts is the voltage across the opening resistor generated by the current though resistor. Assuming 1000A as the current to be interrupted, with a system impedance of around 635 Ω, the application of opening resistors reduces the TRV peak to around half the value of the situation without the opening resistors.

(b) Auxiliary contact for opening resistor

The phase angle of the current through the opening resistor is shifted from 90° to a value θ (=$\tan^{-1}$(ωCR)), where C is the line side capacitance and R is the value of the opening resistor. The recovery voltage of the auxiliary contacts is determined by the difference between the line side residual voltage at the current zero of the resistor current and the source side recovery voltage of the form cos θ - cos(ωt+ θ). As the line length becomes longer, the residual voltage of cos θ becomes smaller due to larger capacitance of the line and recovery voltage becomes sinusoidal in waveform. A short line with small capacitance will have larger residual voltage and the recovery voltage becomes the so-called 1- cos waveform.

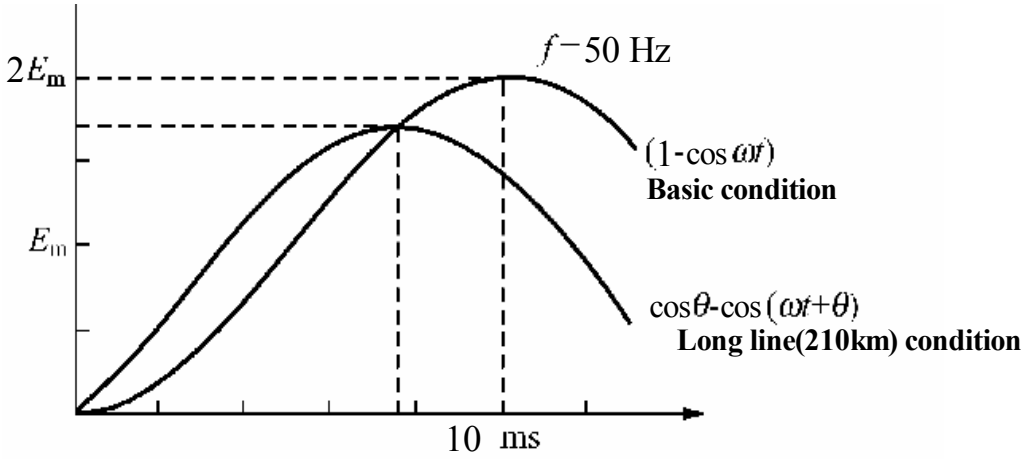

Figure 3.6.23 Waveform of capacitive current for auxiliary contact for opening resistor

3.6.11 Construction, weight, reliability

In comparison to circuit-breakers without opening resistors, those with opening resistors are larger, heavier and more costly. However, by the application of opening resistors, the insulating level of the transmission system, the tower height, the length of insulators, the weight of equipment, the right-of-way requirements, and the number of surge arresters can all be reduced. Hence, the decision whether to apply opening resistors needs to be taken as part of a system wide assessment which includes evaluation of alternative methods to further reduce SFO such as the application of closing resistors, MOSA, opening resistors and TLA (transmission line arresters).

The main drawback of opening resistors is the increased complexity of the circuit-breaker and the additional components involved. Both of these may be expected to

lead to a decrease of reliability and availability and users should ensure that they give due consideration to aspects such as design control, quality control and commissioning control checks. One of the methods to improve and verify the overall reliability of such complex equipment is to apply mechanical operation tests, such as mechanical endurance tests, reliability growth tests, factory acceptance tests and on-site tests, with all relevant parameters monitored.

Utilities should also note that fault clearing surges are generated in the healthy phases of the network at the source side of the circuit breaker, and that successive faults caused by these surges may have significant influence upon the whole system if they are not suppressed. Such risk can be mitigated by the application of opening resistors provided that drawbacks such as mechanical reliability can be overcome and that appropriate quality control of manufacture and installation is achieved.

3.6.12 Requirements for specifications

3.6.12.1 Resistor Value

The values of closing and opening resistors should be taking into account the overvoltages generated by making and/or breaking operations and the insulation design of the transmission system. The resistor values depend on the system aspects such as network configuration, and to which extent the switching surges are to be controlled. In general, in order to control the closing surge level to that of ground fault surges, a resistor value less than 700 Ω is needed. Similarly, for breaking surges, a resistor value of less than 1000 Ω is normally sufficient to ensure suppression to the level of ground fault surges. Whilst smaller resistor values are preferable from an electrical breaking capability perspective, the need to dissipate heat effectively leads to a tendency for smaller physical size (volume). Since the TRV duties with opening resistors in the range 500 to 750 Ω are broadly comparable, resistors in the range 500 and 1000 Ω seem to provide a reasonable compromise between the various factors.

3.6.12.2 Insertion time for resistors

The insertion time for the closing and/or opening resistors should be determined taking into account the switching overvoltages and insulation design of the transmission system. The insertion time of opening resistors should be set to be longer than the maximum arcing time of the main contacts and they should be inserted for fixed period, typically around 30ms, after opening of the main contacts.

3.6.12.3 Making and breaking performance of main contacts

The preliminary specification based on the experiences in Japan is as follows.

For terminal faults, similar duties are applied for T10, T30, T60, and T100a/s. U_c=1385 kV (85-90% of T100 without opening resistors), RRRV = 3 kV/μs (the same as that of T60 without opening resistors)

For Out-of-phase, attention must be paid to the network characteristics which affect U_c as described before. Typical requirement will be such that RRRV = 2 kV/μs and U_c= 2160 kV.

For capacitive current interruption duties, the breaking current is specified to be 1 kA and U_c= 900 kV (72% of peak voltage without opening resistor) with a sin curve and

a 1.4 p.u. (1-cos) curve (corresponds to the recovery voltage after resistor contacts separation).

3.6.12.4 Making and breaking performance of main and auxiliary contacts

The preliminary specification based on the experiences in Japan is as follows.

For terminal faults the same duties are applied for T10, T30, T60, and T100a/s; U_c=1200 kV, RRRV = 0.5 kV/μs.

For Out-of-phase, a breaking current of 2 kA, an RRRV = 2 kV/μs and U_c= 2160 kV are specified. Again attention must be paid to the network characteristics which affect to the U_c.

For capacitive current interruption, waveforms vary depending on the line length and following two duties are specified:

- Breaking current of 1 kA with U_c= 1.4 p.u. and a (1-cos) waveform.
- Breaking current of 0.6 kA with U_c= 1.11 p.u. and a sin waveform (RRRV= 0.34.kV/μs).

3.6.12.5 Thermal requirement for resistor units

Opening resistors need to withstand the thermal stresses caused by the current flowing through the resistors from the moment of current transfer from the main contacts to the end of the insertion period. An example of a realistic specification is the thermal stress during one T100s opening duty followed by one out-of-phase make-break duty with a prospective insertion time for closing of 10ms and for opening of 30ms.

This typical thermal duty is calculated to require heat dissipation of between 128 and 137 MJ, considering some scattering of each parameter. (k_{pp}= 1.1, resistor insertion time for closing = 10±0-4 ms, and resistor insertion time for breaking = 35 ms).

3.6.12.6 Mechanical reliability of the resistor units

Notwithstanding their complexity and large number of parts, the mechanical reliability of the resistors units can be verified by the mechanical endurance tests described in the existing IEC standard. The critical aspects for mechanical reliability will depend upon the specifics of the design, meaning that detailed condition assessment of test object after the tests may provide valuable information regarding long term performance and maintenance.

3.6.12.7 Typical values for specification of opening resistors

Typical values for specifications of opening resistors are shown in table 3.6.3 based on the following assumptions:

Ohmic value of opening/closing resistor: 700 Ω

Insertion period of closing: 10 ms

Insertion period of opening: 30 ms

Duty of opening resistor: Ox1(T100s) + COx1 (out-of-phase)

Table 3.6.3 Example of specifications on main /auxiliary contacts & opening resistors

Duties			Basic specifications	
Main contacts	Short circuit breaking	T10	Breaking current	8 kA
			u_c	1385 kV
			t_3	461 μs
			RRRV	3 kV/μs
		T100s	Breaking current	50 kA
			u_1	990 kV
			RRRV	2 kV/μs
			u_c	1385 kV
			t_2	1485 μs
	SLF	L90	Breaking current	45 kA
			RRRV	8 kV/μs
			Z	450 Ω
			k_{af} (line side)	1.4
	Out-of-phase		Breaking current	12.5 kA
			u_1	1200 kV
			RRRV	2 kV/μs
			u_c	2160 kV
			t_2	1800 μs
	Capacitive current	Sine wave	current	1000 A
			u_c	900 kV
		1-cosine wave	Current	1000 A
			u_c	2515 kV
Resistor contacts	Short circuit breaking		Breaking current	1000 A
			u_1	550 kV
			RRRV	3 kV/μs
			u_c	1200 kV
			t_2	550 μs
	Out-of-phase switching		Breaking current	2000 A
			u_1	1750 kV
			RRRV	2 kV/μs
			u_c	2160 kV
			t_2	1800 μs
	Capacitive current	1-cosine wave	Breaking current	1000 A
			u_c	2515 kV
		Quasi sine wave	Breaking current	600 A
			u_c	2000 kV
			RRRV	0.34 kV/μs
Closing resistors			Insertion period	10 ms
Opening resistors			Insertion period	30 ms
			Thermal duties	128 to 137 MJ

References

[1] CIGRÉ Technical Brochure 362, December 2008, “Technical Requirements for Substation Equipment exceeding 800 kV AC”, CIGRE WG A3.22

[2] CIGRÉ Technical Brochure 400, December 2009, “Technical Requirements for Substations exceeding 800 kV”, CIGRE WG B3.22

[3] Harner (R.), Rodriguez (J.). Transient Recovery Voltages Associated with Power system, Three-phase transformer secondary Faults. IEEE Power Engineering Society (1971-02)

[4] Electra 46, May 1976, pp. 39-66, Contribution to the Study of the Initial Part of the Transient Recovery Voltage, WG 13.01 (Switching Equipment)

[5] H. Hamada, et. al., “Severe Duties on High-Voltage Circuit Breakers Observed in Recent Power Systems”, CIGRE paper 13-103, 2002

[6] WG 13.01, “Surge impedance of overhead lines with bundle conductors during short-line faults”, ELECTRA 17, April 1971

[7] CIGRÉ Technical Brochure 305, October 2006, “Guide for Applivation of IEC 62271-100 and IEC 62271-1, Part II”, CIGRE WG A3.11

4 Equipment Requirements (DS, ES)

4.1 Bus-charging current switching by SF_6-insulated DS

4.1.1 Introduction

Very fast transient overvoltages (VFTO) arise within a GIS whenever there is an instantaneous change in voltage. Most often this change occurs as a result of the opening or closing of a disconnector switch (DS). Other events, such as the operation of a circuit-breaker, the occurrence of a line-to-ground fault or the closing of a grounding switch can also cause VFTO. However, during a DS operation a high number of re-strikes and pre-strikes occur due to the low operating speed of DS compared to a circuit-breaker. Therefore, DS switching is the main source for generating VFTO. The transients are characterized by their short duration and very high frequencies. The rise times are in the range of some ns, with dominant frequency components up to 100 MHz. The generation and propagation of VFT from their original location throughout a GIS can produce internal and external transient overvoltages (see figure 4.1.1). The main concerns are internal overvoltages between the conductor and the enclosure. However, external VFTO can be dangerous for secondary and adjacent equipment. These external transients include transient voltages between the enclosure and ground at GIS-air interfaces, voltages across insulating spacers in the vicinity of GIS current transformers, when they do not have a metallic screen on the outside surface, voltages on the secondary terminals of GIS instrument transformers, radiated electromagnetic fields (EMF) which can be dangerous to adjacent control or relay equipment [1].

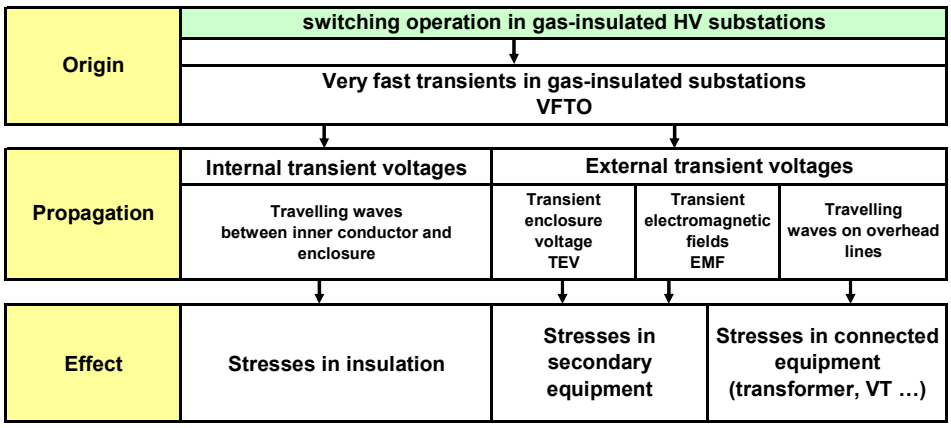

Figure 4.1.1 Classification of VFTO in high voltage GIS substation

As stated above, internal VFTO cause high stress of the insulation system. It has been found that, particularly at 420 kV and higher system voltage levels, disruptive discharges to earth might occur when switching small capacitive currents with gas-insulated metal-enclosed DS, such as energizing or de-energizing unloaded sections of busbar duct or parallel capacitors of CBs [4]. The development of an earth fault by branching of the leader during DS switching depends on parameters such as voltage, gap distance, electrode geometry, contact speed, gas pressure and magnitude and frequency of VFT. A proper design of the DS has shown that in practice earth faults can be eliminated. The geometry of the contact gap can be designed in such a way that the strike occurs where the radial field gradient influencing the branching leader discharge is at a minimum. Screening the strike area with specially designed shielding electrodes and initiating the strike near the axis of the gap are suitable measures [19].

As a conclusion, it was decided to prove the correct design by special switching tests. Annex F of IEC 62271-102 [4] describes the requirements for switching of bus-charging

currents by disconnectors for rated voltages of 72.5 kV and above. Three test duties (TD) are defined:

TD 1: Switching of a very short section of busbar duct. TD 1 is a normal type test and is mandatory for DS. The circuits for DS testing were chosen in such a way that maximum p.u. (per unit) values for VFT peak were generated and it was assumed that they would also be the highest possible in the GIS. According to [4], the test circuit has to be arranged in such a way, that the measured peak voltage to ground without a trapped charge voltage at the load side and 1 p.u. at the source side is higher than 1.4 p.u.. The time to first peak should be less than 500 ns.

TD 2: Switching of parallel capacitors for circuit-breakers under 180° out-of-phase conditions. TD 2 is a special type test to be carried out by agreement between manufacturer and user. A test is required if the circuit-breaker is equipped with parallel capacitors and, clearly, all UHV circuit-breakers consist of two or more breaking units. The maximum VFTO during switching of multiple break CBs under out-of-phase condition is typically in the range of 2.0 p.u. and 2.2 p.u. however the high damping of the grading capacitors results in a lower VFT component.

TD 3: Current-switching capability test. TD 3 is a special type test to be carried out according by agreement between manufacturer and user. It serves only to indicate the current interruption capability of the DS when de-energizing long busbars or other energized parts.

The technical background for the requirements regarding UHV applications for all three test duties is described in the following subchapters. The maximum VFTO in UHV GIS systems without damping measures may reach the level of the LIWV in certain cases. Therefore, it is necessary to design, and maybe to test, considering the VFTO level or to suppress severe VFTO to ensure proper insulation co-ordination. One possible solution for damping of VFTO in GIS is the integration of a switching resistor. This method is a well proven technology. Service experience exists since more than 10 years [12], [16]. When a resistor is used for DS opening and closing, overvoltages can be limited to values such as 1.3 p.u. [17], [18]. Due to a lack of standardization, the background for the requirements of a DS with damping resistor is described in the section 4.1.2.4. Other damping measures, like the suppression of VFTO by magnetic rings, multiple arcs or special methods for the suppression of overvoltages across insulating flanges by using of ZnO arrester elements are under investigation [29], [30].

4.1.2 Background of technical requirements

4.1.2.1 Overview of very fast transient overvoltages (VFTO)

During switching of DS in GIS a varying number of pre-strikes and re-strikes occur, depending of the speed of the switching device. Due to the very fast voltage collapse time of a few nanoseconds at the switching gap, travelling surges are generated in the busbar duct. The multiple reflections and refractions of these surges at impedance discontinuities within the chambers give a rise to complex waveforms, which depend on the disconnector design, the operating conditions and external configurations of the GIS [1].

The maximum value of the VFTO depends on the voltage drop at the DS just before striking and the location considered. Trapped charge remaining on the load side of a DS must be taken into consideration. A voltage drop across the DS of 2 p.u. should be taken into account as the most unfavourable case corresponding to a remaining trapped charge voltage of -1 p.u. on the load side in case of high speed DS or phase opposition conditions. This precondition is mostly used for the calculation of VFTO [5], [12], [7]. For this case the maximum VFTO peak in GIS

has a typical value between 1.5 p.u. and 2.8 p.u.. In some cases a value of 3.05 p.u. is reported [5]. VFTO in GIS are of greater concern at the highest rated voltages, for which the ratio of the basic insulation level to the system voltage is lower [2], [3], [5], [45].

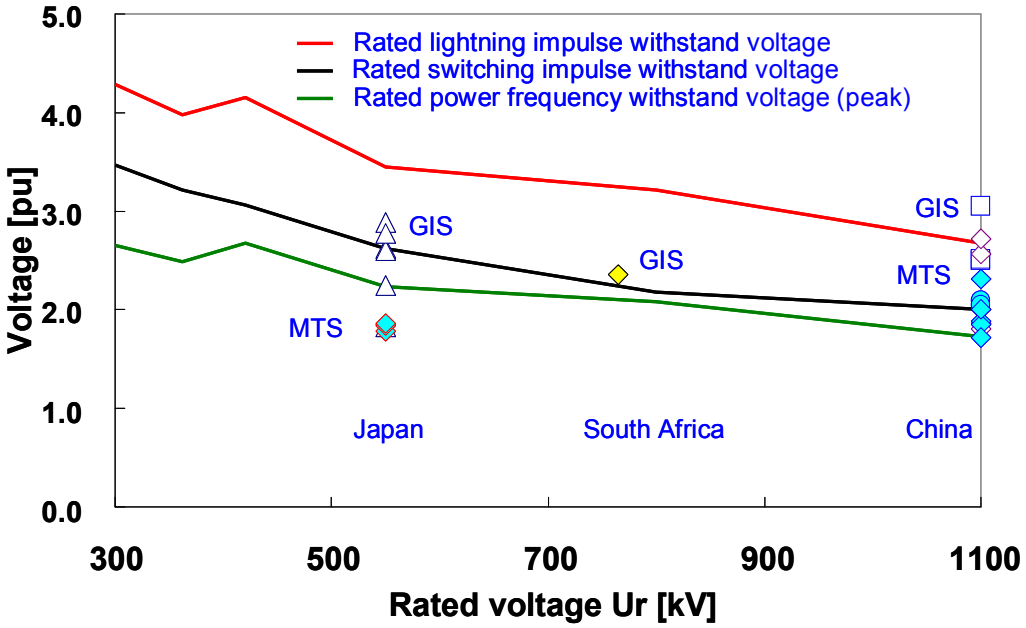

Figure 4.1.2 Dependency of rated withstand voltages and calculated VFTO on rated voltage voltage as per IEC 62271-203 [32], calculated values from [5], [12], [41], [42], [43]

As the rated voltage increases, the difference between the rated lightning impulse withstand voltage (LIWV) and the VFTO decreases, as shown in figure 4.1.2. Figure 4.1.2 shows also the calculation results for different GIS and Hybrid IS (MTS) at different voltage levels [5], [12], [41], [42], [43].

The maximum calculated VFTO in GIS without a DS with damping resistor may reach the insulation level of LIWV. In the case of Hybrid IS a maximum calculated VFTO of 2.2 p.u. is reported, because of the reduced length of busbar sections [5]. This value does not reach the LIWV of the equipment.

As stated above, in GIS the maximum VFTO could reach the LIWV. Therefore, it is necessary to design, and maybe to test, considering the VFTO level or to suppress severe VFTO for the insulation co-ordination. Different approaches are used to determine the necessary measures according to the insulation co-ordination.

4.1.2.2 Japanese approach for VFTO

Because 1100 kV substations would be located in mountainous areas, it was necessary to apply GIS to reduce the substation area as much as possible to meet installation-space constrains, to harmonize with natural environment and to minimize cost. Key requirements for this technology are suppressing various incidents of overvoltage and finding ways to reduce lightning and switching surges [26]. Substation equipment, such as high performance surge arrester, closing and opening resistors for CB, and DS with damping resistor, were developed and the insulation requirements were reduced. As a result, LIWV of GIS was determined as 2250 kV and that of transformer was determined as 1950 kV. By adopting CB with opening and closing resistor, the insulation specifications of all power network

equipment including transmission lines are co-ordinated. Since a UHV transformer is directly connected to GIS, overvoltages occurring during switching of DS or ground switches may directly enter the transformer terminal [25]. Moreover, digital protection and control equipment are located close to the GIS. Therefore, it was very important to take care of the surges transferring into the secondary equipment [11]. The level of these switching overvoltages has to be suppressed as much as possible [22]. To keep VFTO below 1.3 p.u., new DS were provided with 500 Ω resistors for both closing and opening [16], [23], [27].

4.1.2.3 Chinese approach for VFTO

The VFTO of each substation was calculated using the most unfavourable case corresponding to a remaining trapped charge voltage of -1 p.u. The calculated values were compared to the LIWV for the different equipment. For the comparison a co-ordination coefficient (safety factor) was introduced. The co-ordination coefficient was set to 1.15 for the equipment, except for the air insulated busbar in case of Hybrid-IS. The VFTO withstand level is equal to the LIWV divided by the co-ordination factor. If the calculated VFTO level is higher compared to the withstand level, special measures to mitigate the VFTO are required [5].

4.1.2.4 General approach for VFTO

Summarizing the different experiences the following procedure can be proposed, following the general insulation co-ordination approach. The procedure consists of the following three steps.

1. Calculation of VFTO (peak value and rise time)
2. Comparison of calculated VFTO peak values and rise times with VFTO withstand level for the different equipment by using a safety factor k_{VFTO}
3. Definition of measures according to the insulation co-ordination

An explanation of each step of the insulation co-ordination follows.

(First step) Calculation of VFTO

The concept that GIS is a network of interconnected transmission lines can be demonstrated with simulation using travelling wave computer programs or EMTP. The accuracy of a simulation depends on the quality of the model of each individual GIS component. In order to achieve reasonable results, even for time periods of some micro-seconds or for very complex GIS structures, highly accurate models for each internal component and also for external components, connected to the GIS, are necessary. Modelling guidelines are given in [1], [21].

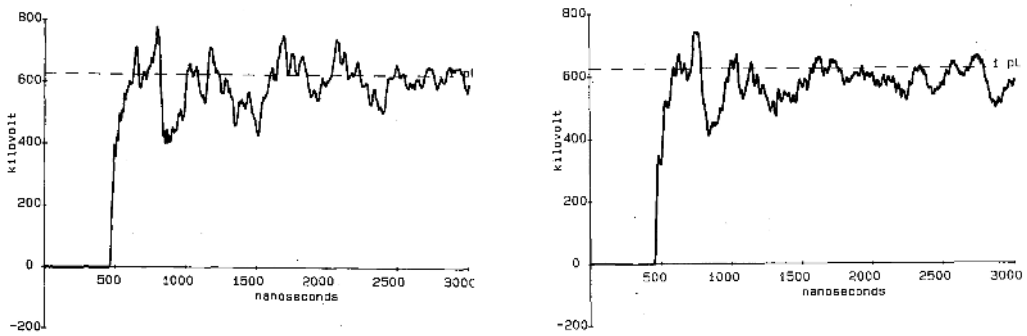

Figure 4.1.3 Measured waveform (left) and calculated waveform (right) for a sample configuration of 765 kV substation [20]

Accurate modelling of each individual GIS component makes it possible to reproduce VFT waveforms with a relatively high precision, especially in short GIS structures or test

equipment. Figure 4.1.3 demonstrates the accuracy of such techniques by comparing a computer simulation with a direct measurement of a transient waveform in an 765 kV GIS [20]. The observed difference in amplitude between measurement and calculation is 5 %, thereby demonstrating the effectiveness of the computer model and calculation procedure. The maximum calculated VFT amplitude in 765 kV GIS was reported as 2.3 p.u. for the worst configuration with a theoretical value of -1 p.u. trapped charge voltage [1].

According to IEC 62271-102 [4], VFT amplitudes of at least 1.4 p.u. are required without pre-charging of the busbar. The VFT amplitude depends on the experimental set-up and the support capacitors on the alternating voltage side. Figure 4.1.4 shows a comparison of simulated and measured VFTO without, and with, dc pre-charging of the busbar. The measured voltage progressions coincide very well with the simulation results as regards VFT amplitude and rise time [8]. During DS switching, VFTO of 2 MV occurs, corresponding to a p.u. value of 2.23 [9]. This value is above the VFTO which occur in real operation of Hybrid IS. The successful test results therefore confirm that no VFT mitigation measures are required for the Hybrid IS design.

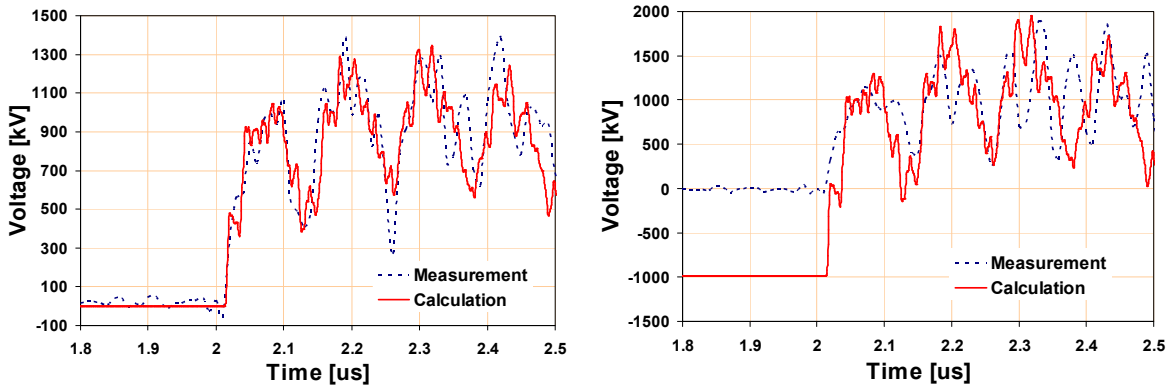

Figure 4.1.4 VFTO calculation and measurement when switching busbars with a GIS disconnector as per IEC 62271-102, Left: without pre-charging, Right: with pre-charging [8]

Because the accuracy of the simulation depends strongly on the quality of the model of each individual GIS component, it is important to verify the simulation results by measurements.

(Second step) Comparison of calculated VFTO peak values and rise times with VFTO withstand level for the different equipment by using a safety factor k_{VFTO}

The basis for the insulation co-ordination is the introduction of a safety factor k_{VFTO}. According to the Chinese approach the safety factor k_{VFTO} was set to 1.15. The insulation withstand strength is equal to LIWV divided by the safety factor [5]. The same safety factor was used for all types of equipment excluding the air-insulated busbar.

GIS and Hybrid IS systems are used for the 1100 kV UHV pilot project in China. The peak value, frequency characteristic and voltage rise time of VFTO under various switching conditions for the substations Jindongnan, Nanyang and Jingmen were calculated and analyzed. The layouts used for the calculation are shown in figures 4.1.5 and 4.1.6.

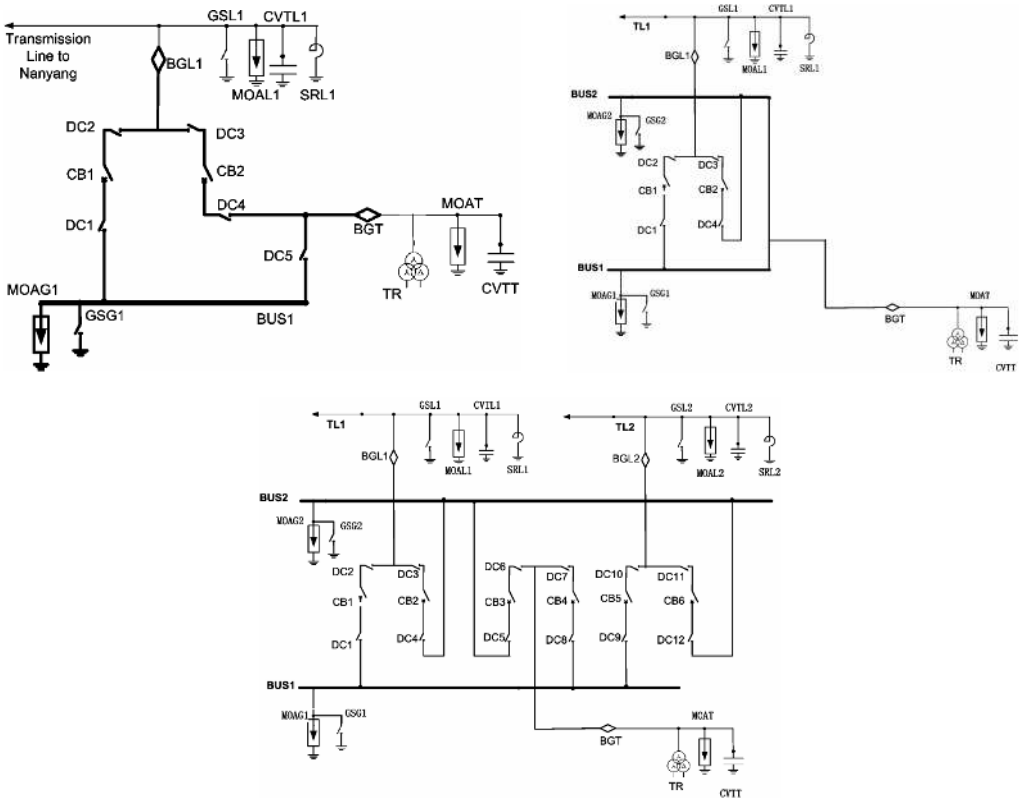

Figure 4.1.5 Layout Jingdongnan GIS substation [5]: single busbar (top left), double busbar (top right), double busbar - future extension (bottom)

The calculation results are summarized in table 4.1.1. As one can see, the peak values of VFTO at Jindongnan GIS can reach 2742 kV (3.05 p.u.) which is higher than the LIWV. In case of GIS, the VFTO inside GIS exceeds the lightning insulation withstand strength. Moreover, the maximum VFTO at GIS bushings is 2295 kV (2.55 p.u.) and exceeds also the lightning insulation withstand strength.

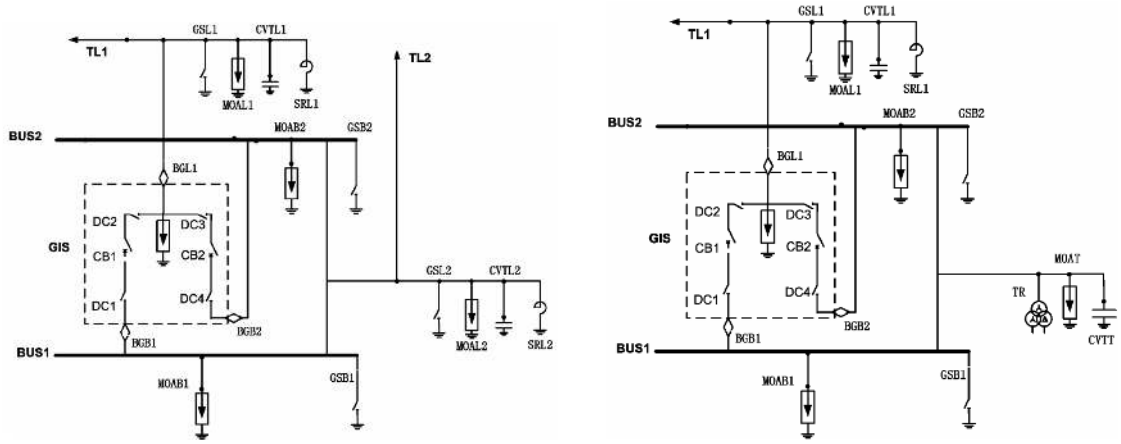

Figure 4.1.6 Layout Hybrid-IS substation [5] from left to right: Nanyang, Jingmen

For Hybrid-IS, the peak values of VFTO at the GIS, bushing, shunt reactor and CVT do not exceed their insulation withstand strength meaning that it is not necessary to mitigate the switching overvoltages. A higher overvoltage was calculated only for the overhead busbar. The maximum overvoltage is 2742 kV (3.05 p.u.) and 2421 kV (2.7 p.u.).

As mentioned above, for the Chinese 1100 kV project a safety factor k_{VFTO} of 1.15 was used. In general, an exact definition of the safety factor cannot be given at the moment. The safety

factor depends on other aspects factors and can be different for the different kinds of equipment. The requirements have to be studied in detail to give recommendations for future applications. The CIGRÉ WG C4.306 "Insulation Co-ordination for UHV AC Systems" will review and discuss insulation co-ordination practice in the UHV AC range taking into account the state-of-the-art technology, with special reference to surge arresters and other mitigation measures. Beside the selection of insulation levels the task of the WG covers also the co-ordination of withstand voltages and safety factors for the equipment.

Generally, the safety factor to be defined is influenced by the breakdown behaviour of the insulating material, the frequency of occurrence and the probability of trapped charge voltages as a basis for the simulation. Moreover, other sources for VFTO and the effects on the different types of equipment have to be considered.

Table 4.1.1 VFTO calculation results for the Chinese 1100 kV project [5], [6]

	Jingdongnan [GIS]						Nanyang [MTS]		Jingmen [MTS]		
	single busbar		double busbar	double busbar future extension	single busbar	double busbar future extension	double busbar	double busbar	double busbar		double busbar
Switching resistor	No	No	No	No	Yes 500 Ohm	Yes 500 Ohm	No	Yes 500 Ohm	No	No	Yes 500 Ohm
Transformer											
BIL [kV]	2250	2250	2250	2250	2250	2250			2250	2250	2250
safety factor	1.15	1.15	1.15	1.15	1.15	1.15			1.15	1.15	1.15
Protection level VFTO [kV]	1957	1957	1957	1957	1957	1957			1957	1957	1957
VFTO[kV]	954	1123	942	1083	905	969			1016	1355	981
VFTO [pu]	**1.06**	**1.25**	**1.05**	**1.21**	**1.01**	**1.08**			**1.13**	**1.51**	**1.09**
VFTO / Protection level	**0.49**	**0.57**	**0.48**	**0.55**	**0.46**	**0.50**			**0.52**	**0.69**	**0.50**
Shunt reactor											
BIL [kV]	2250		2250	2250	2250	2250	2250	2250	2250		2250
safety factor	1.15		1.15	1.15	1.15	1.15	1.15	1.15	1.15		1.15
Protection level VFTO [kV]	1957		1957	1957	1957	1957	1957	1957	1957		1957
VFTO[kV]	1252		1012	1085	982	977	1052	989	1018		943
VFTO [pu]	**1.39**		**1.13**	**1.21**	**1.09**	**1.09**	**1.17**	**1.10**	**1.13**		**1.05**
VFTO / Protection level	**0.64**		**0.52**	**0.55**	**0.50**	**0.50**	**0.54**	**0.51**	**0.52**		**0.48**
GIS											
BIL [kV]	2400	2400	2400	2400	2400	2400	2400	2400	2400	2400	2400
safety factor	1.15	1.15	1.15	1.15	1.15	1.15	1.15	1.15	1.15	1.15	1.15
Protection level VFTO [kV]	2087	2087	2087	2087	2087	2087	2087	2087	2087	2087	2087
VFTO[kV]	2249	1940	2260	2742	1250	1157	1878	1204	1836	1409	1268
VFTO [pu]	**2.50**	**2.16**	**2.52**	**3.05**	**1.39**	**1.29**	**2.09**	**1.34**	**2.04**	**1.57**	**1.41**
VFTO / Protection level	**1.08**	**0.93**	**1.08**	**1.31**	**0.60**	**0.55**	**0.90**	**0.58**	**0.88**	**0.68**	**0.61**
GIS bushing											
BIL [kV]	2400	2400	2400	2400	2400	2400	2400	2400	2400	2400	2400
safety factor	1.15	1.15	1.15	1.15	1.15	1.15	1.15	1.15	1.15	1.15	1.15
Protection level VFTO [kV]	2087	2087	2087	2087	2087	2087	2087	2087	2087	2087	2087
VFTO[kV]	2295	2120	1722	2024	1141	1134	1850	1199	1948	1733	1266
VFTO [pu]	**2.56**	**2.36**	**1.92**	**2.25**	**1.27**	**1.26**	**2.06**	**1.33**	**2.17**	**1.93**	**1.41**
VFTO / Protection level	**1.10**	**1.02**	**0.83**	**0.97**	**0.55**	**0.54**	**0.89**	**0.57**	**0.93**	**0.83**	**0.61**
CVT											
BIL [kV]	2400	2400	2400	2400	2400	2400	2400	2400	2400	2400	2400
safety factor	1.15	1.15	1.15	1.15	1.15	1.15	1.15	1.15	1.15	1.15	1.15
Protection level VFTO [kV]	2087	2087	2087	2087	2087	2087	2087	2087	2087	2087	2087
VFTO[kV]	1233	1499	1015	1093	928	961	1006	966	1041	1302	993
VFTO [pu]	**1.37**	**1.67**	**1.13**	**1.22**	**1.03**	**1.07**	**1.12**	**1.08**	**1.16**	**1.45**	**1.11**
VFTO / Protection level	**0.59**	**0.72**	**0.49**	**0.52**	**0.44**	**0.46**	**0.48**	**0.46**	**0.50**	**0.62**	**0.48**
Overhead busbar											
BIL [kV]							2400	2400	2400	2400	2400
safety factor							1	1	1	1	1
Protection level VFTO [kV]							2400	2400	2400	2400	2400
VFTO[kV]							2742	1306	2421	1482	1314
VFTO [pu]							**3.05**	**1.45**	**2.70**	**1.65**	**1.46**
VFTO / Protection level							**1.14**	**0.54**	**1.01**	**0.62**	**0.55**
Literature	[5]	[6]	[5]	[5]	[5]	[5]	[5]	[5]	[5]	[6]	[5]

4.1.2.5 Trapped charge voltage

(A) Trapped charge voltage behaviour

As mentioned above, trapped charge remaining on the load side of a disconnector must be taken into consideration. Due to the travelling wave behaviour of the VFT, the overvoltages caused by DS show a spatial distribution. Normally the highest overvoltage stress is reached at the open end of the load side. The maximum value of the local VFTO depends on the voltage drop at the DS just before pre-striking and on the location considered. For the calculation of VFT stresses, the trapped charge remaining on the load side of the DS must be taken into consideration. Before disconnecting, all sections within one phase had the same voltage and phase angle. Afterwards the opened section remains at the potential it had at the moment after the last re-strike. The floating section of busbar has therefore been charged to a dc voltage. Since the GIS section has a known capacitance, the dc voltage can expressed as a trapped charge. Figure 4.1.8 shows DS surge mechanism (opening operation). The amplitude of the dc voltage depends on the type of apparatus.

(B) Slow acting DS (e.g. speed lower than 1 m/s)

Switching by a slow acting DS generates numerous re-strikes between the moving and fixed contacts, but 95 % of the trapped charge voltages were limited to 0.5 p.u. with a well designed DS [19]. The trapped charge left when opening a pure capacitive load gives remaining voltages ranging from 0.1 to 0.5 p.u., with a maximum of around 0.3 p.u. This produces values of the voltage across the DS at first strike of 1.1 to 1.5 p.u.

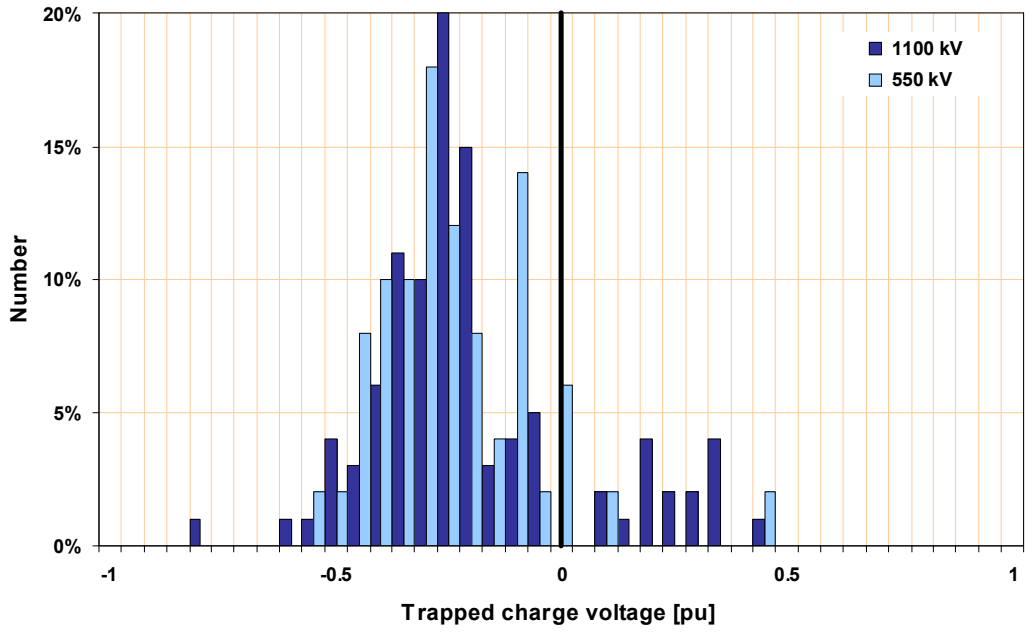

Figure 4.1.7 Measured trapped charge voltage during disconnector switching under laboratory conditions [6]

For a normal DS with a slow speed, the maximum trapped charge reaches 0.6 p.u. resulting in a most unfavourable voltage collapse of 1.6 p.u. Figure 4.1.7 shows an example of measured trapped charge voltages during testing of DS for both applications at 550 kV and 1100 kV [6]. For these cases, the resulting VFTO is in the range of 1.7 p.u. and reaches 2.0 p.u. for very specific cases. Extremely high values of more than 3.0 p.u. have been reported. It can be shown, however, that these values have been derived by calculation using unrealistic simplified simulation models [21]. As mentioned above, the verification of calculated results is important to reach a high accuracy of the simulation.

(C) Fast acting DS (e.g. speed higher than 1 m/s)

Fast operating DS on the other hand can leave trapped charge levels corresponding to 1 p.u. in a non-negligible number of cases [1]. A measurement of the trapped charge voltage for an UHV DS is not available up to now. Based on an evaluation of the voltage during the last re-strike an estimation of the trapped charge behaviour is possible. The principle of the estimation is shown in figure 4.1.8. The breakdown voltage is the measured voltage across the DS before the last re-strike as the sum of the trapped charge voltage at load side before re-strike and the instantaneous source side voltage. Thereby the instantaneous source side voltage is less than 1 p.u.

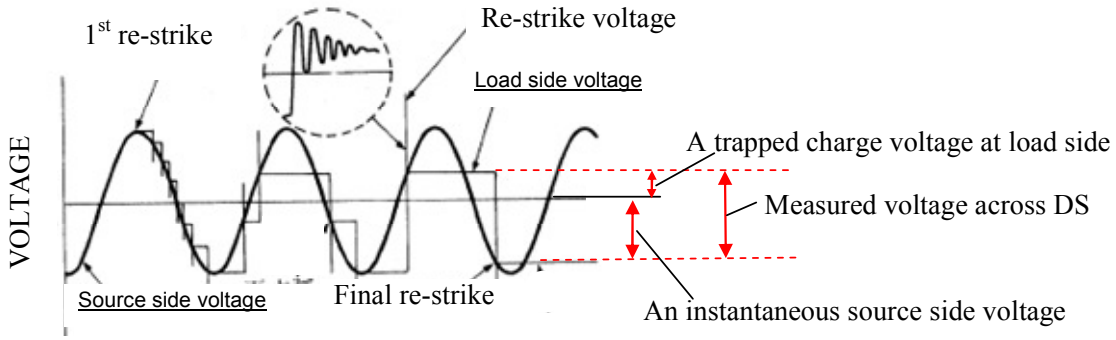

Figure 4.1.8 Principal voltage behaviour during opening of DS

Figure 4.1.9 (left) shows the distribution of the maximum breakdown voltage across the DS during re-striking measured at factory test of a fast acting 550 kV DS during opening operations [44]. The maximum observed breakdown voltage was 1.86 p.u. (1 p.u.= 449 kV). Because the instantaneous source side voltage is less than 1 p.u. the maximum trapped charge voltage before re-strike is higher than 0.86 p.u. Figure 4.1.9 (right) shows the distribution of the maximum breakdown voltage across the DS during re-striking measured at factory test of a fast acting 1100 kV DS during opening operations [17]. During these tests, the power supply voltage was raised to 1.1 p.u. The total number of tests was 400. The maximum observed breakdown voltage was 1.65 p.u. (1 p.u. = 898 kV × 1.1). The maximum trapped charge voltage before re-striking is higher than 0.65 p.u.

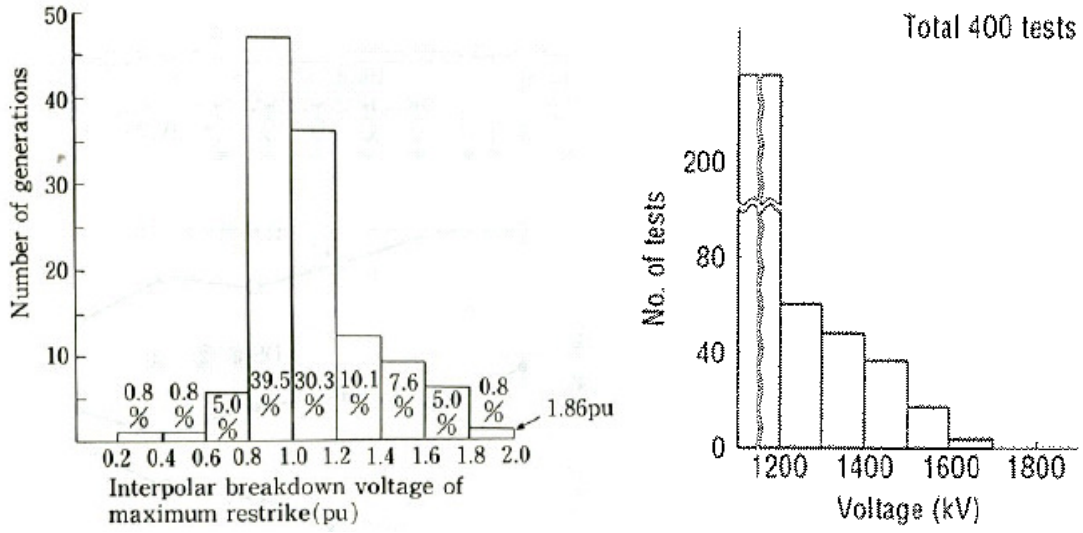

Figure 4.1.9 Maximum breakdown voltage across the DS during re-striking for a 550 kV DS [44] (left) and for a 1100 kV DS [17] (right)

4.1.2.6 Effect of VFTO on equipment

Breakdown caused by VFTO is improbable in a well-designed GIS insulation system during normal operations. However, breakdown values can be reduced by insulation irregularities like edges and fissures. The breakdown probability is very low for low VFTO amplitudes; it increases with the frequency of the oscillations and the degree of the field homogeneity. The VFT stress has been related to the LIWV, which is generally the base for GIS design. For effective insulating systems the VFT stress is covered by it's withstand capability for standard LI (see figure 4.1.10, [19]). Caused by the formative time lag for the breakdown channel, all VFTO breakdown or flashover voltages are above the LIWV. Special attention has to be paid when defects are present. The inhomogeneous fields due to defects give considerably lower breakdown values, with a minimum for LI having a front time of 5 μs. Fixed protrusions on live parts are usually avoided by a proper design, quality control and adequate testing in both the factory and on-site. They can be detected by sensitive diagnostic measurements under ac voltage.

The insulation system of circuit-breakers is not endangered by VFTO generated in adjacent GIS equipment. Ground faults induced by VFTO have been observed in DS operations, as residual leader branches can be activated by enhanced field gradient to ground and by feeding them with GIS-generated VFTO. The development of a ground fault by branching of the leader discharge during a DS operation can be avoided by a proper DS design.

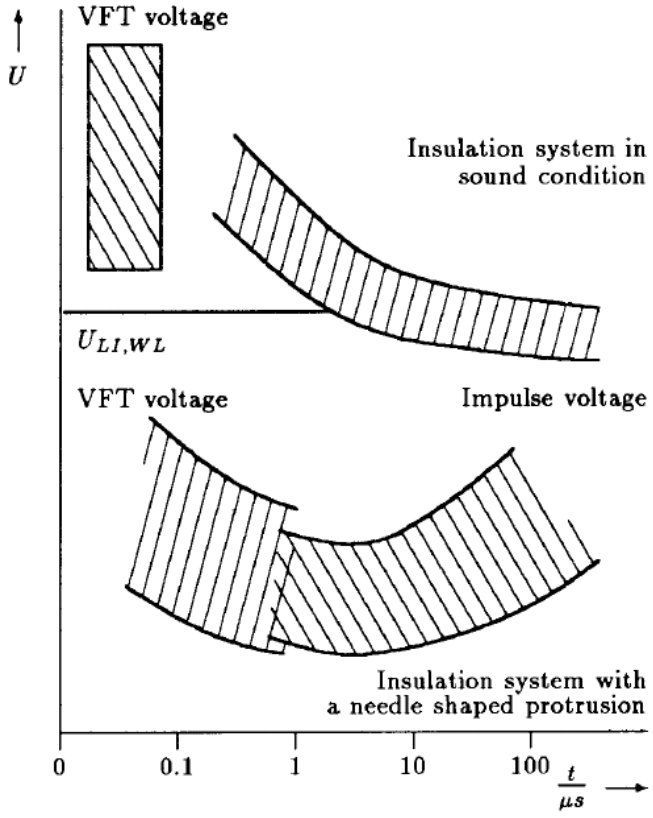

Figure 4.1.10 Principal voltage-time characteristic of SF_6 [19]

SF_6 insulated bushings can be affected as other SF_6 equipment but very few problems have been reported with capacitive graded bushings.

Transformers are either directly connected through SF_6 bushings or indirectly by SF_6–air bushings, overhead lines and air-oil bushings. Directly connected transformers can experience an extremely nonlinear voltage distribution along the high voltage winding, connected to the

oil- SF_6 bushings, due to steep fronted wave impulses. Moreover transient oscillations within the GIS can develop extremely high partial-winding resonance voltages in the transformer winding [25], [24]. When a DS surge passes a bushing, a wave-front time of about 10 ns is extended to about 60 ns. This reduces the voltage generated between turns or sections to 60 % - 80 % of that when a DS surge is applied directly without an air-bushing [25].

Transient Ground Potential Rise (TEV) can cause sparking across insulated flanges and to insulated busbars of CTs, and puncture of insulation which is intended to limit the spread of circulating currents within the enclosure. Moreover, TEV may interfere with secondary equipment or damage sensitive circuits by raising the housing potential if they are directly connected or via cable shields to GIS enclosure by emitting free radiation which may induce currents and voltages in adjacent equipment.

4.1.2.7 Other VFTO sources

VFTO appearing in GIS are caused not only by DS operation. A flashover or breakdown within GIS can also produce VFTO. If the breakdown occurs in an almost homogeneous field, a maximum voltage enhancement factor of 1.7 compared to the applied voltage peak has to be assumed. In case of a breakdown at a defect the voltage collapse time is longer and this leads to a higher damping and a lower enhancement factor of 1.45. Nevertheless, subsequent breakdowns at defects with inhomogeneous field distribution may result. Therefore the breakdown to earth is of special concern during on-site testing. For primary breakdown caused by defects, any subsequent breakdown in a sound system can be avoided by using a test voltage lower than 0.8 LIWV [19]. Nevertheless, subsequent breakdown has to be taken also into account for an earth fault caused by overvoltages during service.

Because of the trapped charge voltage remaining on the busbar, a making operation of an earthing switch can produce VFTO. The maximum VFTO measured during the field test of the 1100 kV GIS in Japan was 1.13 p.u. [11]. The calculated value for a trapped charge voltage was 640 kV. This value is equivalent to the specification for the TRV peak value during electrostatic-induced current switching. However, the VFTO is sufficiently low for the insulation level [16].

CBs may also generate transients in GIS but due to their very fast operation only a few strikes occur. VFTO occur during making of CB and, especially under out-of-phase conditions, the amplitude can reach values up to 2 p.u. However, the internal damping of the VFT influencing the highest frequency components is determined by the spark resistance. Due to the fact that an UHV CB has 2 or 4 breaking interrupter units in series, the VFTO is damped by the multiple arcs and/or the grading capacitors.

A larger number of strikes may occur for the special case of switching of small inductive current during shunt-reactor switching [1]. Re-ignition overvoltages are generated by re-ignitions following an initial interruption. Re-ignitions are provoked when the voltage between the contacts exceeds the dielectric withstand of the contact gap. The rate of rise of a re-ignition overvoltage is between those observed during fast front transients and those of lightning overvoltages [2]. This is lower than the rate of rise observed during DS switching, because UHV CB have two or more interrupter units. The amplitude of a re-ignition overvoltage sometimes becomes higher than that of a chopping overvoltage, when the re-ignition occurs near the crest of the load side oscillation voltage. Therefore the destructive capability of a re-ignition overvoltage on the insulation of a reactor as well as a circuit-breaker must also be considered. The re-ignition behaviour of circuit-breakers depends on the chopping number, design and breaker type. If the re-ignition occurs at the recovery voltage peak, i.e. $u_W = u_0 (1 + k_a)$, the value of the re-ignition overvoltage (k_p) is given by equation 4.1

and can reach values between 1.5 p.u. and 2.5 p.u. [31]. Thereby k_a is the magnitude of the suppression peak overvoltage in p.u. of the crest phase-to-earth voltage.

$$k_p = (1+\beta)\,(1+k_a)\left(\frac{C_S}{C_S+C_L}\right) - k_a \qquad \ldots(4.1)$$

Re-ignition may occasionally be followed by high-frequency arc extinction that could trigger voltage escalation. In South Africa's 800 kV systems, the highest switching and re-ignition overvoltage in a full GIS system were measured as 1.6 p.u. and 1.8 p.u. respectively [2]. The re-ignition overvoltages can be limited or avoided by an opening resistor or controlled switching.

4.1.2.8 External transients

An internally generated VFT propagates throughout the GIS and reaches the bushing where it causes a transient enclosure voltage and a travelling wave that propagates along the overhead transmission line. An explanation about the generation of external transients and some comments on their main characteristics follows [1].

a) Transient enclosure voltages

Transient enclosure voltages (TEV), also known as transient ground potential rise (TGPR), are short duration high voltage transients which appear on the enclosure of the GIS through the coupling of internal transients to enclosure at enclosure discontinuities. The usual location for these voltages is the GIS-overhead line transition at an air bushing, although they can also emerge at other points such as visual inspection ports, insulated spacers for CTs or insulated flanges at GIS/cables interfaces. When an internal wave propagates to the bushing, a portion of the transient is coupled onto the overhead line-to-ground transmission line, and a portion is coupled onto the GIS enclosure-to-ground transmission line. The latter constitutes the TEV. The magnitude varies along the enclosure; it can be in the range of 0.1 to 0.3 p.u., and reaches the highest magnitude near the GIS-air interface. The TEV wave which couples onto the enclosure encounters earthing connections which form transmission line discontinuities and attenuate TEV. Mitigation methods include grounding using low surge impedance, short length leads and the installation of metal-oxide arresters across any insulating spacers.

b) Transients on overhead connections

A portion of the VFT travelling wave incident at a gas-air transition is coupled onto the overhead connection and propagates to other components. This propagation of VFTO on air-insulated lines and busbars is lossy and results in an increase of the VFT rise time. Although transients can have rise times in the range of 10 to 20 ns if the air connection is relatively short. The magnitude of the rise time portion of external transients is generally lower than that of internal VFT. The voltage rate-of-rise can be in the range of 10 - 30 kV/μs, and because of numerous discontinuities the magnitude of VFTO is reduced to about 20 – 40 % of the incident magnitude [1].

However, as VFT occur during normal conditions in GIS and each DS operation can generate tens to hundreds of individual transients, possible aging of the insulation of external components must be considered. These overvoltages can cause stress on adjacent equipment, and resonance phenomena can occur in exposed transformers.

c) Transient electromagnetic fields (EMF)

EMF can cause some stress on secondary equipment, especially on nearby computer-controlled equipment. The frequency depends on the GIS arrangement, but is typically in the range of 10 MHz to 20 MHz.

TEV is a low energy phenomenon, and it is not considered dangerous to humans. The main concern is in the danger of the surprise-shock effect. TEV can also cause interference with or even damage substation control, protection and other secondary equipment, and radiate EMF which may induce voltages and currents within electric circuits.

(Third step) Definition of measures according to the insulation co-ordination

If the calculated amplitude of the VFTO is higher than the insulation withstand strength of the equipment, it is necessary to define measures reducing the risk of failures. There are two possibilities: an increase of the LIWV or a mitigation of VFTO. The first choice is easy to realize, but costly. Nevertheless in some cases this solution has advantages. For the Chinese 1100 kV project this method was used for the air insulated busbar in case of Hybrid-IS [5]. The second choice aims for mitigation of amplitudes of VFTO and finally for a reduction of the effect of VFTO on the equipment. For the different sources of VFTO and for the different equipment many mitigation methods are known. The main techniques which can be used to mitigate the effects are summarized as follow [21]:

The internal damping of the VFT influencing the highest frequency components is determined by the spark resistance. A higher number of arcs reduces the VFTO peak. The main portion of the damping of the VFT occurs by coupling out at the transition to the overhead line. This propagation of VFTO on air-insulated lines and busbars is lossy and results in an increase of the VFT rise time. Therefore, a longer overhead line between GIS and transformer mitigates the VFTO stress at the connected transformer. For instance, a 100 m longer overhead line results in a 10 % lower VFTO peak at the transformer bushing. Normally, transformers can withstand the stress built up by steep front waves. In critical cases, it might be necessary to install varistors to protect tap changers against very high frequency transient oscillations.

The re-ignition overvoltages or overvoltages produced during making of CB can be limited or avoided by a closing and / or opening resistor or by controlled switching.

One possible solution for damping of VFTO generated during DS switching in GIS is the integration of a switching resistor. If a resistor is used for the DS at opening and closing, overvoltage can be limited to values around 1.3 p.u. This mitigation method is described in detail in section 4.1.2.4.

The effect of TEVs on the enclosure can be minimized by a proper design and arrangement of substation mats, by keeping ground leads as short and straight as possible in order to minimize the inductance, by increasing the number of connections to ground, by introducing shielding to prevent internally generated VFT from reaching the outside of the enclosure or by installing voltage limiting varistors where spacers must be employed.

Correct cable connection procedures may minimize interference. The coupling of radiated energy may be reduced by mounting control cables closely along the enclosure supports and other grounded structures, by grounding cable shields at both ends by leads as short as possible or by using optical coupling services. Voltage limiting devices may have to be installed.

Other damping measures like the suppression of VFT by magnetic rings, multiple arcs or special methods for the suppression of overvoltages across insulating flanges by using of ZnO arrester elements are under investigation [29], [30].

4.1.2.9 Out-of-phase switching by DS

The out-of-phase condition is relevant when the DS on the transformer side is required to be closed before synchronizing the system. TD 2 (switching of parallel capacitors for circuit-breakers under 180° out-of-phase condition) is a special type test to be carried out according to the specification by agreement between manufacturer and user, but it is not necessary if the CB is not equipped with parallel capacitors. Generally, UHV CBs consist of at least two interrupters. The voltage distribution depends on the number of interrupting chambers, the capacitances across the contact gap and to earth, and on which side the voltage or voltages are applied. To take optimal advantage of the breaking and making capacity of the individual interrupting chambers, the objective should be the most homogeneous voltage distribution that is possible. This can be achieved if grading capacitors are positioned parallel to each interrupting chamber. Therefore, the TD 2 is recommended as a type test for UHV DS.

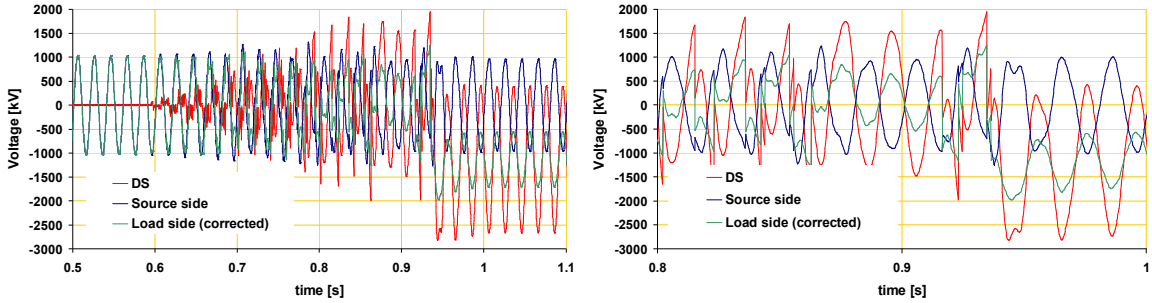

Figure 4.1.11 TD 2 of 1100 kV switching test, typical voltage waveform at source side, load side and across the DS during opening [6], full operation (left), detail of last re-strike (right)

Typical voltage curves for an opening sequence for one 1100 kV DS are shown in figure 4.1.11. The voltage measurements on the busbar with the UHF sensors on both the supply side and load side of the DS were made with capacitive sensors. The measurements with these sensors are not intended to measure dc voltages. They are a pure capacitive divider where the low voltage side is connected to the 1 MΩ input of the oscilloscope. This resistance will decay any dc voltage on the low voltage side. If the transfer function of the sensors is known and if the dc voltage is known at some time during the measurement, it is possible to calculate the dc voltage on the whole curve from the measured signal. The voltage measurement can be simplified to be a capacitive divider with a resistance in parallel to the low voltage capacitor. This will give a transfer function in the frequency domain of the divider. In order to reproduce the input voltage, the measured voltage, could be transformed to the frequency domain and then divided with the transfer function of the capacitive sensors. Figure 4.1.11 shows the corrected voltages according to the calculation procedure.

The maximum VFTO during switching under out-of-phase condition is typically in the range of 2.0 p.u. and 2.2 p.u. However the high damping of the grading capacitors results in a lower VFT component. Therefore, the VFT stress for the equipment is lower compared to TD 1. Nevertheless, the opening of DS under out-of-phase conditions can result in a high power frequency voltage stress across the DS and to ground on the load side of the DS. When the power frequency voltage stress reaches its maximum, the VFTO are mainly decayed.

Opening of DS leads to a remaining dc trapped charge on the busbar between DS and CB. If the last re-strike occurs in the peak of the applied ac source voltage, the remaining trapped charge voltage on the load side is equal to the ac peak value. As discussed in the previous chapter the voltage across the DS just before closing depends on the trapped charge voltage. For the calculation of the voltage stress the trapped charge on the load side must be taken into consideration. Two typical cases are known:

- Case A: Opening of a slow acting DS leads to a remaining trapped charge ranging from 0.1 to 0.5 p.u. A trapped charge voltage of 0.5 p.u. covers 95 % of all cases [19].
- Case B: Opening of a fast operating DS can leave trapped charge levels corresponding to 1 p.u. in a non-negligible number of cases.

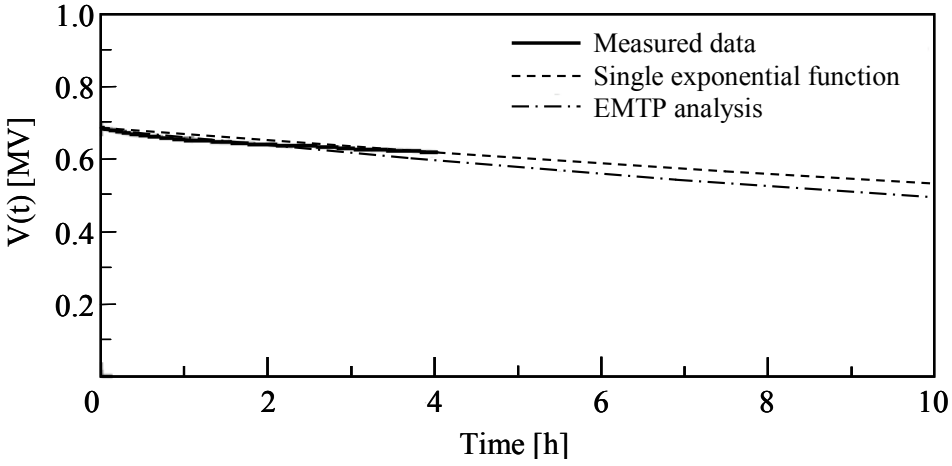

Figure 4.1.12 Decay of trapped charge voltage [11]

Moreover, the voltage stress just before closing is determined by the decay of trapped charges. The decay of the trapped charges in a GIS is strongly dependent on both the trapped charge voltage amplitude and the configuration of insulators. The decay time can be expressed by a time constant τ. The decay time for a single busbar configuration typically has values in the range of several hours up to several days [19]. Gapless surge arresters or inductive transformers connected to the busbar can reduce τ substantially. During the field test of the 1100 kV GIS in Japan the decay time constant was measured and calculated. Figure 4.1.12 shows a good agreement between measurement and calculation. Depending on the design of the CB, the time constant varies from several hours to 66 hours [11]. Due to the high decay time constant, the complete remaining trapped charge must be taken into consideration for the switching operation.

Although the CB would be open, the grading capacitors across the open contacts would allow power frequency coupling. Typically, this voltage can be in the range from 70 – 95 % of the system voltage depending on the load side capacitance. Thus with the system voltage on the other side of the DS the out-of-phase condition can result. The ac voltage on the load side of the DS can be calculated, if the capacitances of the grading capacitors of the CB and the capacitance to ground of the busbar between CB and DS are known. The simulation test circuit and the simulation results are shown in figure 4.1.13 [6]. For the calculation a trapped charge of 1 p.u. was used, according to case B. Figure 4.1.13 shows a simplified test circuit for the simulation of the slow front voltages up to the power frequency, without consideration of VFTO. Typical values for the capacitances of the grading capacitors and of the capacitance to ground for an 1100 kV test circuit were used. In addition, the closing resistor and the closing resistor switch were considered.

The amplitude of the power frequency overvoltage results from the combination of the trapped charge voltage and the coupled voltage from the CB grading capacitors. The voltage across the DS strongly depends on the capacitance to ground of the busbar on the load side and can reach values between 2.5 p.u. and 4 p.u.

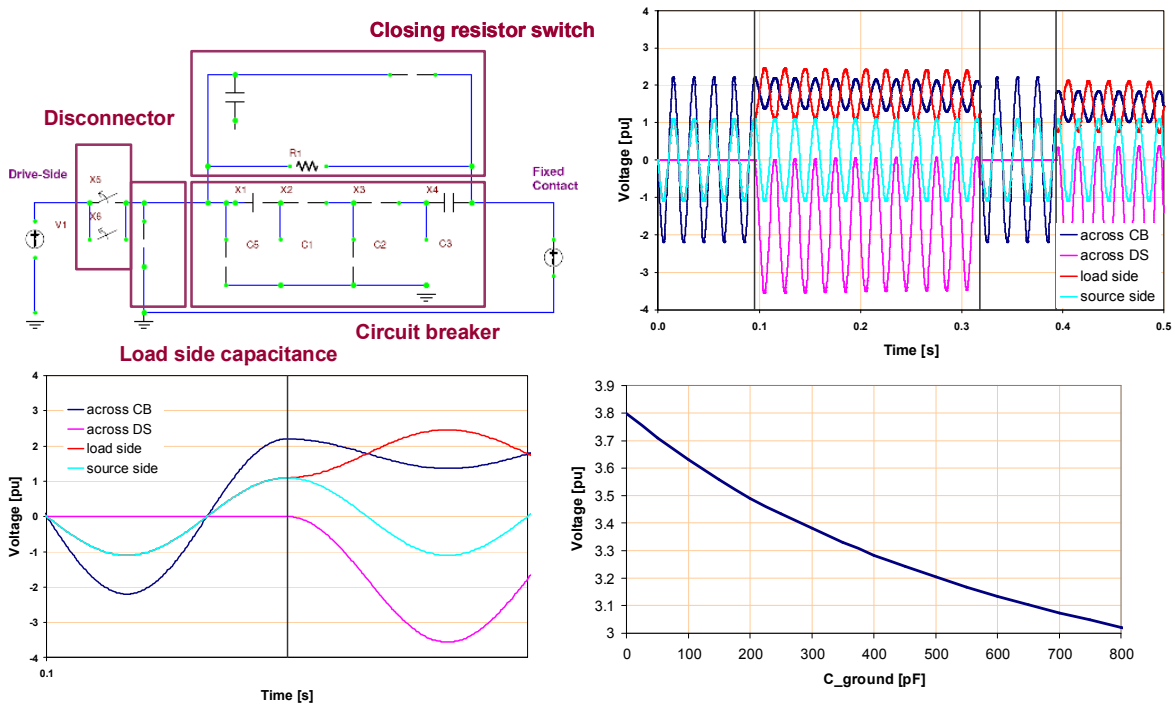

Figure 4.1.13 Simulation test circuit and simulation results for power frequency voltage wave form, from top left to bottom right: test circuit, opening and closing, detail of one opening operation with trapped charge voltage of 1 p.u., influence of load side capacitance [6]

Further analysis results shown in figure 4.1.14 confirm the high voltage across the DS. In this case the maximum voltage across the open DS was 2941 kV, which is equivalent to 3.27 p.u.

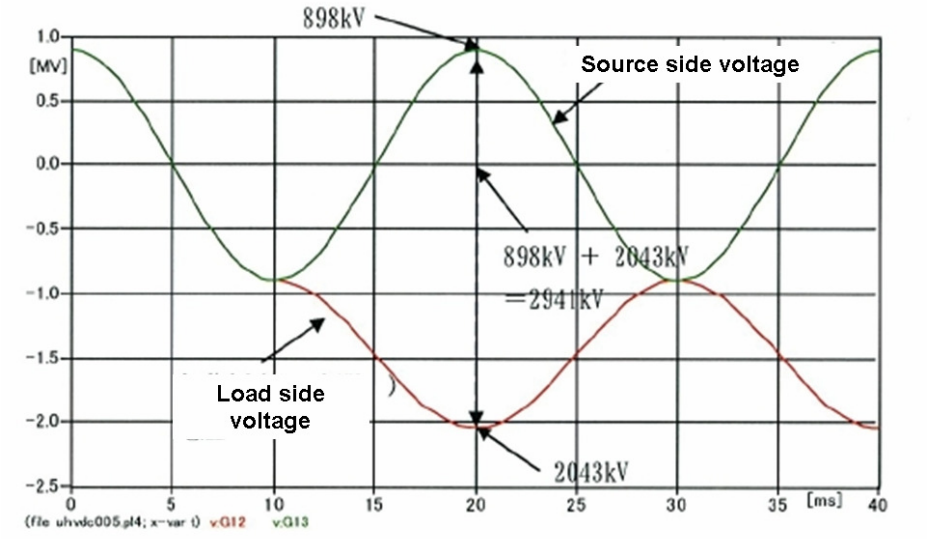

Figure 4.1.14 Measured voltages across the open disconnector (TD 2)

The voltage stress across the open CB can be estimated by using a simple voltage divider, consisting of grading capacitors and a lumped capacitance to ground (See figure 4.1.15). Figure 4.1.15 shows the resulting maximum voltage across the DS as a function of the capacitance to earth (C_{bx}) for a typical circuit-breaker capacitance in the range from 530 pF to 650 pF.

The temporary voltage across the disconnector after opening, assuming the worst case conditions of maximum remaining trapped charge on the busbar, could exceed 3.2 p.u. –

3.8 p.u. prior to a closing operation, assuming a typical capacitance to earth between 150 pF and 300 pF. The theoretical maximum is around 4 p.u.

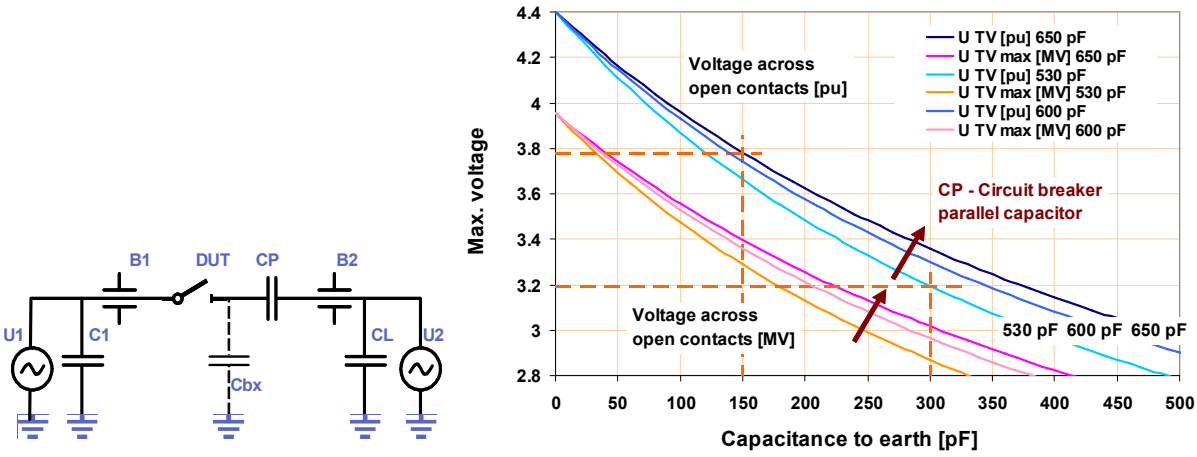

Figure 4.1.15 Simplified simulation test circuit (DUT: tested DS) and calculation result for typical capacitances of 1100 kV CB with trapped charge voltage of 1 p.u. [6]

The temporary overvoltage stress has been related to the LIWV, SIWV and power frequency withstand voltages, which are generally the base for GIS design and the voltage across the disconnector could be higher than the rated voltages. Figure 4.1.16 shows a comparison of the calculated and measured voltages across the disconnector depending on the rated voltage. It can be seen that the voltage across the disconnector at a rated voltage of 1100 kV could be higher than all other rated test voltages. This voltage stress occurs during the switching operation of parallel capacitors for circuit-breakers under 180° out-of-phase condition. The voltage stress occurs for some 10 seconds, 50 times per test.

The amplitude of the temporary power frequency overvoltage, resulting from the combination of the trapped charge voltage and the over coupled voltage from the CB grading capacitors, greatly exceeds that of the rated withstand voltages, for both case A and case B. Figure 4.1.16 shows the comparison of the voltage across the DS and the rated voltages for different voltage levels. For case A, considering a remaining trapped charge voltage of 0.5 p.u. covering 95 % [19] of all cases, only the combined lightning impulse voltage covers the temporary overvoltages during TD 2. Also the temporary voltage to earth at the load side could be higher than the rated voltages (see figure 4.1.16). The maximum temporary overvoltage is again slightly different between these two cases.

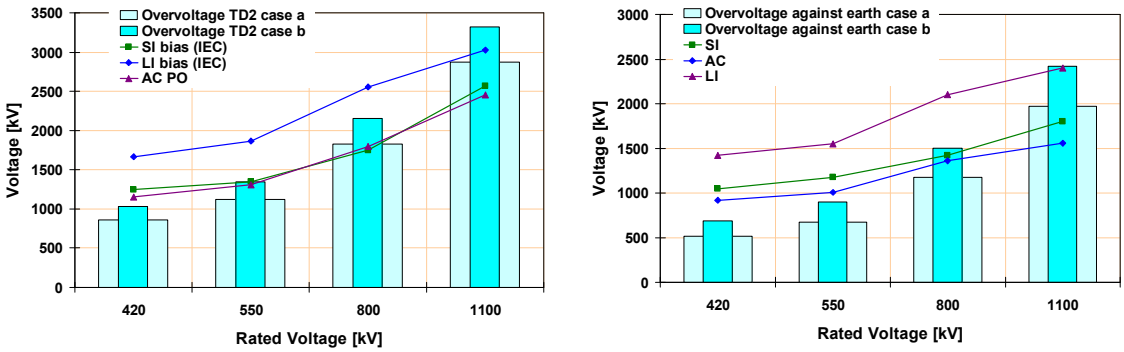

Figure 4.1.16 Power frequency test voltage across the open DS (left) and to earth on the load side (right) in comparison with the rated values (peak values) according to IEC 62271-203 [32]

Switching operations of parallel capacitors for circuit-breakers under 180° out-of-phase conditions are thought to be a special condition occurring only in cases such as that when a generator circuit is directly connected to the UHV network. Hence, for UHV systems, it seems to be rare that TD 2 duty is required for UHV DS. Considering the transient stresses for the grading capacitors and the possible high power frequency voltage across the DS, a test is reasonable and should be carried out according to the specification. It has to be considered that the test arrangement reflects the arrangement in service, especially with regard to the distance between DS and CB being as short as possible.

4.1.2.10 Current switching capability

DS normally have a capacitive current interrupting capability. For air-insulated DS, the interrupting current does not exceeded 2 A for the system operating voltages up to 800 kV. Regarding GIS DS, the interrupting current for test duty (TD) 3 ranges from 0.1 A at 72.5 kV and up to 0.8 A at 800 kV [4]. Extrapolation of specified bus-charging current suggest that the required bus-charging current switching capability of GIS DS at UHV is in the range from 1 A to 1.2 A [2].

The switching current (I), which corresponds to the bus-charging current, can be calculated by using equation 4.2:

$I = \omega C V$, (here C is load capacitance and V is the rated voltage.) …(4.2)

For example, the bus-charging current is specified as 0.5 A for the 1100 kV system in Japan, which corresponds to 2000 pF load side capacitance. The total capacitance consists of the capacitance given by load side bus-duct length and the capacitance of the DS and CB at the load side of the bus coupler bay [3]. For the pilot project in China a bus-charging current of 0.8 A was specified. This value is equal to the requirement according to IEC for 800 kV DS. Table 4.1.2 gives an overview of the requirements regarding bus-charging current and test voltages for making and breaking tests in comparison with the IEC requirement for a rated voltage of 800 kV.

Table 4.1.2 Comparison of requirement for bus-charging current

	IEC 62271-102 Annex F [4]	*Japan (GIS)*	*China (GIS or Hybrid-IS)*
Rated voltage	*800 kV*	*1100 kV*	*1100 kV*
Test voltage	*Ur/√3 = 462 kV*	*Ur/√3 = 635 kV*	*Ur/√3 = 635 kV*
Bus-charging current	*0.8 A*	*0.5 A*	*0.8 A* *2 A (tentative)*

To confirm the requirements, the maximum bus-charging currents for the pilot projects were calculated. The length of busbar in the Jindongnan substation is 96.2 m at the first stage, which corresponds to 4200 pF of load side capacitance The resulting bus-charging current is 0.84 A. This substation is planned to be extended with a busbar up to 420 m at maximum in the future, which corresponds to 19700 pF of load side capacitance and provides the bus-charging current of 3.9 A. Generally, for such cases the adaptation of a load breaker or a CB might be considered. In China it is still under consideration whether to limit the maximum length of the busbar duct to 200 m by installation of bus couplers. However, a tentative value of 2 A was chosen for the specification.

CIGRÉ WG B3.22 has investigated the substation system aspects of UHV networks [3]. Based on the data, the bus-charging current could be calculated according to equation 4.2. The results of the calculations are summarized in table 4.1.3 based on the following capacitances:

- 1100 kV GIS: the average capacitance of busbar is approximately 45 pF/m
- 800 kV AIS: the average capacitance of busbar is approximately 12.7 pF/m
- Load side capacitance at the DS and CB: several hundred pF (800 pF was used for the calculation).

Table 4.1.3 calculation results for bus-charging current

	Longest distance between DS and CB [m]	Busbar capacitance [pF/m]	Capacitance at the CB and DS [pF]	Total capacitance [pF]	Bus-charging current [A]
China 1100 kV GIS*1	11	45	800	1295	0.26
China 1100 kV Hybrid-IS*2	7.6	45	800	1142	0.23
China 1100 kV Hybrid-IS*3	7.1	45	800	1120	0.22
Japan 1100 kV GIS*4	25	45	800	1925	0.38
China 1100kV GIS*5	96.2	*n/a*	*n/a*	4200	0.84
India 800 kV AIS*6	22.6	12.7	800	1087	0.16

*1 China 1100 kV GIS, 2CB scheme [3]
*2 China 1100 kV Hybrid-IS, 1-1/2CB scheme [3]
*3 China 1100 kV Hybrid-IS, 1-1/2CB scheme [3]
*4 Japanese 1100 kV GIS, double busbar scheme [3]
*5 China, pilot project, first stage (Slightly different parameters were used for the calculation)
*6 Indian 800 kV AIS, 1-1/2CB scheme [3]

Figure 4.1.17 shows the load capacitance and the equivalent length of GIS for different voltage levels depending on the specified bus-charging current. The bus charging currents, evaluated based on the existing UHV substation layout, reach a maximum value of 0.84 A. Schemes of future UHV substations with maximum busbar lengths up to 200 m are concluded to be rather exceptional and a bus-charging current of 1 A is sufficient also for future applications.

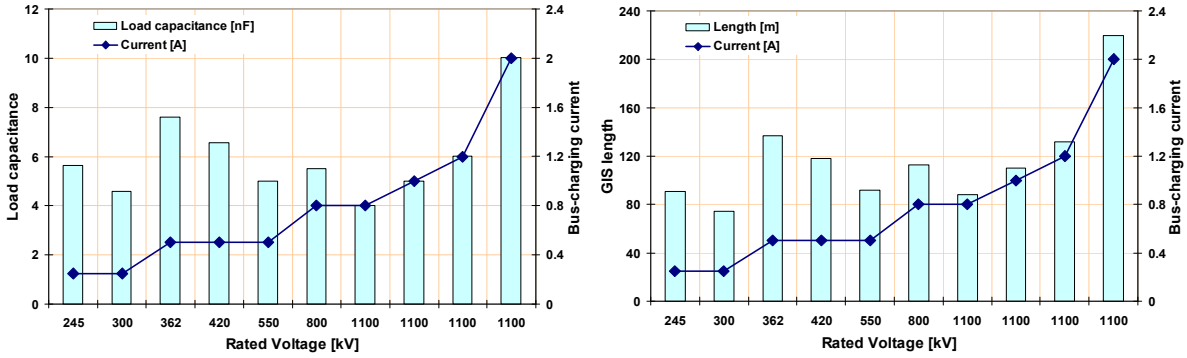

Figure 4.1.17 Dependency of bus-charging current, load capacitance and equivalent busbar length on rated voltage as per IEC 62271-203

TD 3 is a special type test and, for testing, the specific length of the busbar sections is not significant. On the load side a lumped capacitance should be added in order to achieve the specified bus-charging current. For the tests with a required bus-charging current higher than 1 A, lumped capacitors up to 10 nF are needed. In order to reduce resonance effects which can be caused due to high source impedance, connection of a lumped capacitance of any value is acceptable on the source side. The maximum possible capacitance is limited by the capacity of the high voltage test transformer. Testing experiences show that a current-switching capability test with a bus-charging current higher than 1 A using common high voltage transformers is not possible. Unavoidable resonance effects lead to overvoltage in the range of 2 p.u. to 3 p.u. to earth. This voltage stress does not correspond to real service conditions [6].

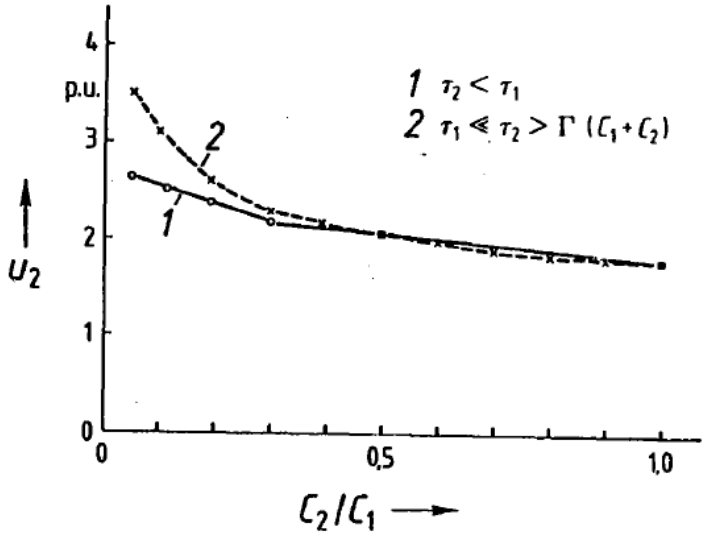

Figure 4.1.18 Maximum VFTO as a function of C_2/C_1 (τ: travel time, Γ :surge impedance)

The VFTO occurring during switching operations must be taken into consideration. The potential reliability of the system decreases with longer load side bus length, since the load side busbar retains the trapped charge and can then be exposed to VFTO by re-strike/ pre-strike of DS. From a probability point of view, longer load side busbars may increases the risk. The maximum value of the VFTO depends on the voltage drop at the DS just before striking and the location considered. The VFTO depends also on the ratio of the capacitances at the load side (C_2) and source side (C_1). A low ratio results in a higher VFTO (See figure 4.1.18). Low ratios are given in practice, if a transformer is placed on the source side of the DS [1]. This behaviour has to be considered.

4.1.3 Disconnectors with damping resistor

One possible solution for damping of VFTO in GIS is the integration of a switching resistor. This method is a well proven technology with service experiences of more than 10 years [12], [16]. When a resistor is used for DS opening and closing, overvoltages can be limited to values such as 1.3 p.u. [17], [18], [23] and it is possible to mitigate external transients caused by DS switching. The reliability of the connected equipments like bushings, power transformers and potential transformers can be increased.

A switching resistor either in parallel or in series is often employed to reduce the amplitude of VFTO generated by DS switching. An introduction to the bus-charging current switching duty for the 1100 kV DS used in Japan and China, the calculation results of VFTO analysis to estimate the effect of DS with damping resistors and the required specifications are described below.

4.1.3.1 Design of DS with damping resistor

Three different types of resistor fitted disconnectors are known. The opening and closing resistor can be positioned in parallel or in series with the switching gap. As shown in figure 4.1.19 the arc commutation method, the series resistor contact method or the parallel resistor contacts method can be used. The arc commutation method is commonly used in today's 1100 kV systems in Japan and China and in the 765 kV system in Korea [13]. The resistor contact method was used in the Italian field test [15].

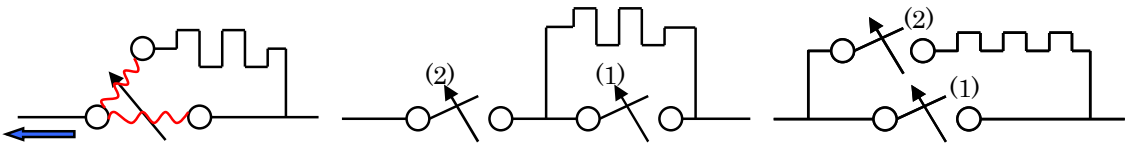

Arc commutation method Series resistor contact method Parallel resistor contact method

Figure 4.1.19 Principles of resistor fitted disconnectors

Generally, the mitigation effect of the damping resistor depends on the values of the resistance. To verify the mitigation effect, calculations were made for a typical 1100 kV substation in Japan. Figure 4.1.20 shows a relation between resistance and VFTO peak for a typical GIS layout with 10 bays and a double busbar scheme. The calculation is based on the assumption that re-striking occurs when the trapped charge voltage at the load side and the voltage at the source side were -1 p.u. and +1 p.u. respectively. Without damping resistor, the VFTO amplitude reaches a value of 2.8 p.u. This exceeds the LIWV according to the insulation co-ordination. In case of integration of a damping resistance higher than 200 Ω, the VFTO amplitude can be suppressed below 1.5 p.u. A damping resistance of more than 1 kΩ mitigates the maximum VFTO amplitude to a level of 1.25 p.u. [17]. Consequently the resistance of the damping resistor can be chosen and defined according to the maximum calculated VFTO and the required mitigation effect. A 110 Ω damping resistor was used in the Italian 1000 kV project. For the Chinese, Japanese and Korean UHV and EHV projects, it was decided to use a 500 Ω damping resistor for mitigation of VFTO [15]. A resistance of 500 Ω limits the maximum VFTO at maximum possible striking voltage across the DS of 1700 kV to 1.3 p.u. [16].

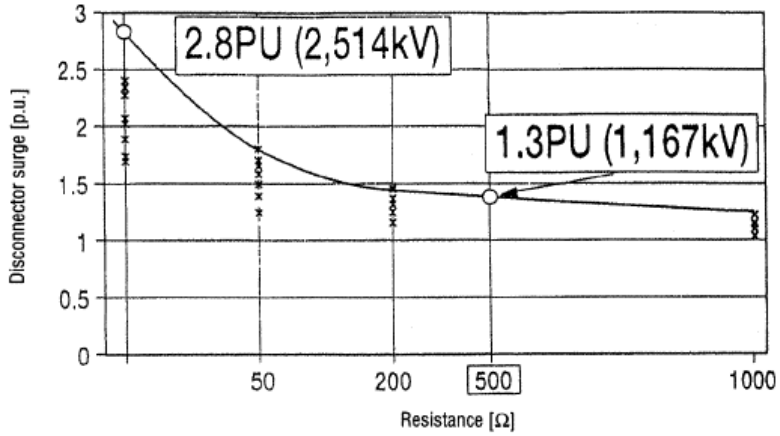

Figure 4.1.20 VFTO in relation to the resistance [26]

An example of a resistor equipped GIS DS structure is shown in figure 4.1.21 which also illustrates the switching process of the disconnector for both opening and closing. At the beginning of the open operation, the moving contact starts to move and separate the main arcing contact S_m on the stationary contact side. The low bus-charging current is interrupted, however, re-striking occurs because of the low dielectric strength at that moment. As the distance between the two electrodes increases, the re-striking arc moves to the part between the arcing electrode S_r of the resistor R_{DS} and the moving contact. At this moment, the damping resistor is inserted in series to the re-striking arc, leading to a suppression of the VFTO. The re-striking repeats. The current is completely interrupted when a sufficient insulating distance is provided. Inserting the resistor into a discharge path, where the gap between electrodes is long and discharge voltage is high, is the principle to suppress the overvoltage [26]. During a close operation the same principle works in reverse.

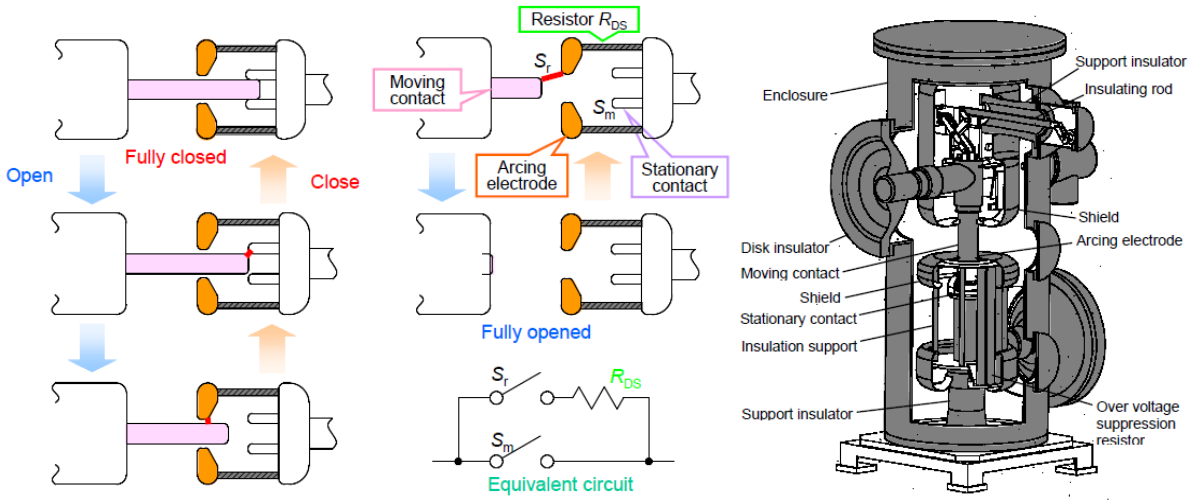

Figure 4.1.21 Working principle and structure of DS with damping resistor [26]

4.1.3.2 Experiences of DS with damping resistor

As mentioned above, the method of VFTO mitigation by using DS with damping resistor has a long tradition in Japan and is used also for the pilot project in China. Therefore the experiences in both countries are described below.

(A) Japanese experiences

To confirm the effect of the damping resistor and to determine the value of the resistance, a VFTO analysis was carried out for a typical substation arrangement. The VFTO was calculated for DS with and without switching resistor [2]. The substation in a double-busbar scheme consists of GIS with 4 feeder bays and 4 transformer bays. The VFTO was calculated using the most unfavourable case corresponding to a trapped charge voltage of -1 p.u. As a consequence, the first pre-strike occurs at a voltage drop across the DS of 2 p.u. Different locations of DS were analyzed: line-side DS, bus-bar side DS of line feeder, bus-tie DS, bus-bar side DS for transformer bay and bus-section DS. The resistor value was varied from 0 Ω to 1000 Ω.

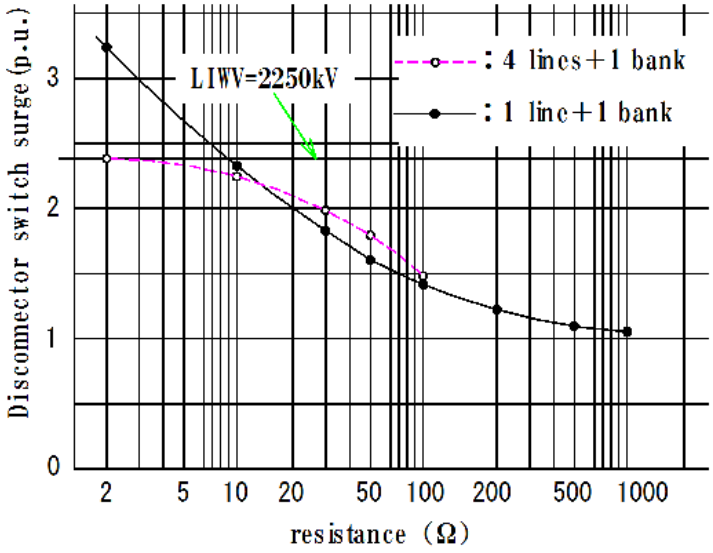

Figure 4.1.22 VFTO in relation to the resistance [2]

The calculation results confirm that the VFTO peak value can be suppressed by using switching resistors. As shown in figure 4.1.22, the calculated maximum VFTO peak without switching resistor was 3.25 p.u. By using a damping resistor of 500 Ω a reduced value of 1.13 p.u. was calculated. The calculated maximum VFTO peak with 1000 Ω resistor was 1.07 p.u. On the other hand, an increasing resistance increases the voltage across the resistor. As a consequence the overall size of DS increases. The resistance of the switching resistor was set to 500 Ω which effectively reduces the overvoltages below 1.3 p.u.

Also field verification tests were performed by connecting the 1100 kV equipment to a 550 kV system. The bus-charging tests were performed under different conditionsand the mitigation effect of the damping resistor was confirmed. The measured maximum VFTO level was lower than 1.2 p.u. TEV was also measured and the maximum peak value was lower than 10 kV. The control and protection systems were not disturbed. Further information is given in [2].

(B) Chinese experiences

The Chinese experiences are mainly based on calculation and analyzing results [7], [5]. GIS and Hybrid-IS are used for the Chinese 1100 kV system. The peak value, frequency characteristic and the rate of rise of VFTO under various switching condition in GIS and Hybrid-IS were analyzed (See figures 4.1.5 and 4.1.6). The VFTO was calculated using the most unfavourable case corresponding to a remaining trapped charge voltage of -1 p.u. The first pre-strike occurs at a voltage drop across the DS of 2 p.u.

As shown in table 4.1.1, the peak values of VFTO at Jindongnan GIS system can reach 3.05 p.u. This value is higher than the protective level. Therefore, it was decided to implement damping countermeasures. By using a DS with a 500 Ω damping resistor, the peak value of VFTO is reduced to 1.29 p.u. for the same configuration.

Beside the amplitude (see table 4.1.1), other factors like the frequency and the rate of rise have to be considered. Directl connected transformers can experience an extremely non-linear voltage distribution along the high voltage winding, connected to the oil-SF_6 bushings, due to steep fronted wave impulses. Moreover transient oscillations within the GIS can develop extremely high partial winding resonance voltages in the transformer winding.

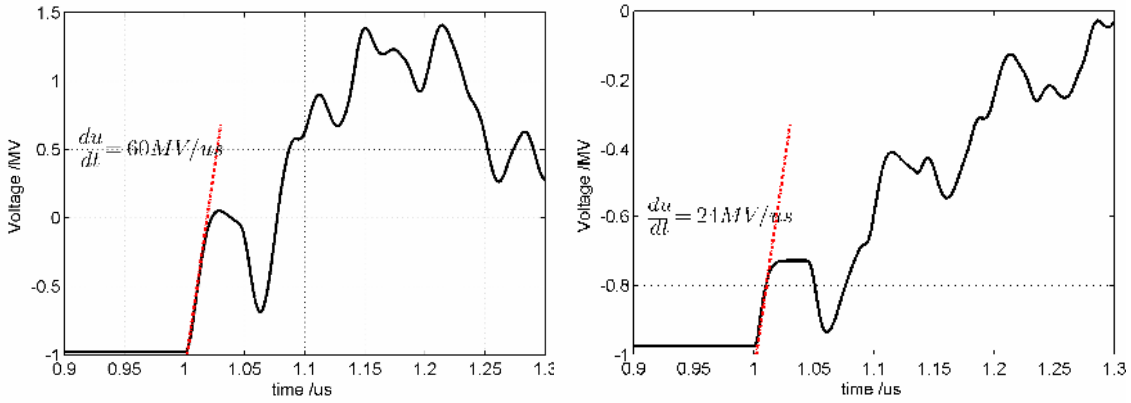

Figure 4.1.23 The rate of rise of VFTO inside the GIS without damping resistor (left) and with 500 Ω damping resistor (right) [5]

The typical waveform of VFTO in GIS is shown in figure 4.1.23. The rate of rise of VFTO reaches up to 60 MV/µs. Both the peak value of VFTO and the rate of rise are reduced by the application of damping resistors. The rate of rise of VFTO inside GIS is reduced from 60 MV/µs to 24 MV/µs. Because of the overhead connection of the transformer the rate of

rise at the transformer is generally lower than the value inside the GIS. Nevertheless, by using a damping resistor, the rate of rise is reduced from 0.9 MV/μs to 0.2 MV/μs.

The frequency spectrum was analyzed and an example is shown in Figure 4.1.24 which shows a clear reduction of the high frequency components due to the application of a damping resistor.

Summarizing, it was decided to use a DS with damping resistor for GIS application. Based on the calculation, a resistance of 100 Ω is sufficient to mitigate the VFTO peak values to below 1500 kV (1.7 p.u.). Considering other effects like withstand voltage and energy consumption capability of the resistor, a damping resistance between 500 Ω and 700 Ω was suggested. However, in Hybrid-IS of Nanyang and Jingmen, the calculation shows that VFTO amplitudes are lower compared to the protective level and a DS with damping resistor is not necessary.

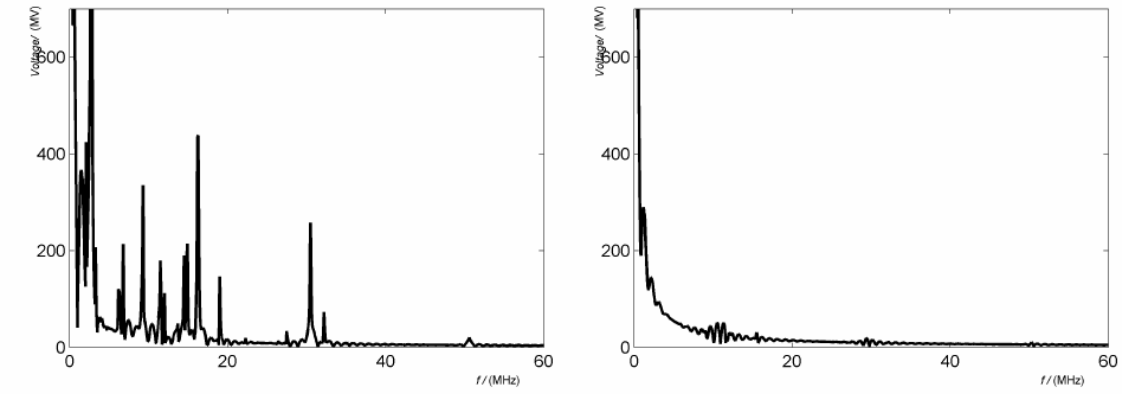

Figure 4.1.24 Frequency spectrum of VFTO inside the GIS without damping resistor (left) and with 500 Ω damping resistor (right) [5]

CIGRÉ WG B3.22 "Technical Requirements for Substation Exceeding 800 kV" has reviewed the UHV substation requirements taking into account the state-of-the-art technology, with reference to mitigation measures [3]. The results regarding the application of mitigation measures can be summarized as follow:

In case of GIS the VFTO amplitude reaches in many cases the LIWV. Therefore it is recommended to mitigate the VFTO generated by DS.

In case of Hybrid-IS the VFTO amplitude is mostly lower than the LIWV. Therefore it is not necessary to reduce the VFTO generated by DS. Nevertheless, the effect of external transients has to be considered.

4.1.3.3 Requirements for the damping resistor

The damping resistor has to withstand the dielectric stress during striking. The highest voltage across the resistor occurs shortly after the first pre-strike during close operation, considering the most unfavourable case corresponding to a remaining trapped charge voltage of -1 p.u. or 1 p.u. The first pre-strike occurs at a voltage drop across the DS of 2 p.u. Therefore, it is necessary to prove the voltage withstanding characteristic and the energy absorption capability of the resistor in case of re-strikes and pre-strikes between the moving contact and the arcing electrode of the resistor. A flashover across the resistor may lead to high VFTO and has to be avoided [16].

(A) Dielectric strength

A higher resistance value leads to a higher voltage stress across the switching resistor [17]. Assuming a first pre-strike at a voltage drop across the DS of 2 p.u., the voltage across the resistor is lower than 2 p.u. The voltage across the damping resistor V_R during striking is approximately given by equation 4.3:

$$V_R = \left(\frac{R}{2\,Z + R} \right) V_0 \qquad \ldots(4.3)$$

Z: Surge impedance of bus duct, R: Resistance of damping resistor, V_0: Voltage across the DS before switching

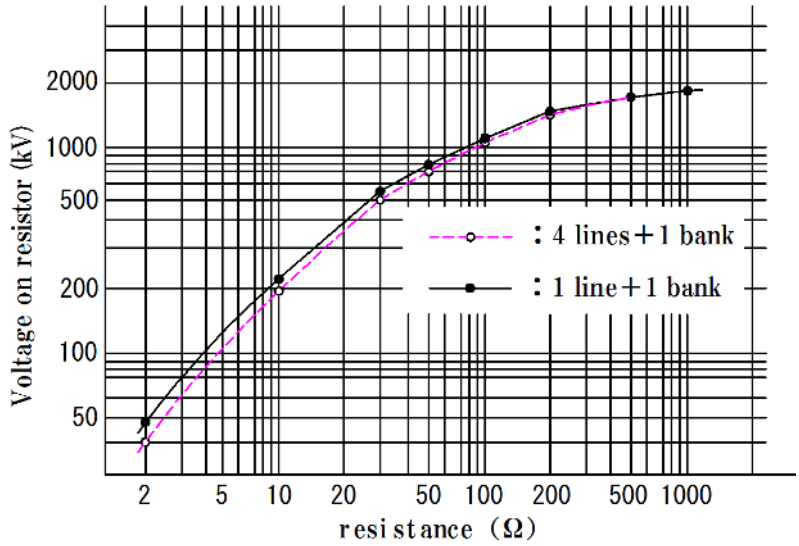

Figure 4.1.25 Calculated voltage across the damping resistor [2]

Figure 4.1.25 shows the calculation result for the voltage across the damping resistor for typical cases, like 4-line feeder and 4-transformer feeder substation [2]. For a 500 Ω resistance the maximum voltage across the resistor is 1700 kV. Therefore, a dielectric withstand voltage for the damping resistor of 1700 kV can be concluded, considering the worst case, if the pre-strike occurs at the peak of the source voltage and a trapped charge voltage of -1 p.u. at the load side.

The rate of rise of the voltage across the resistor could be very high and depends on the set-up and the capacitances on the load and source side. The rate of rise of the voltage across the resistor has to be considered especially during testing.

Another important issue is the decay of the voltage across the DS after re-striking or pre-striking. During striking between the moving contact and the resistor shield, the discharge arc propagates while branching. Disruptive discharges across the damping resistor might occur. This was observed in the initial phases of the DS development. A flashover over the resistor leads to high VFTO amplitudes, comparable with DS without a damping resistor. As a result the connected equipment could be overstressed. Therefore, discharges across the resistor have to be avoided. The development of a fault by branching of the leader during DS switching depends on voltage, gap distance, electrode geometry, contact speed, gas pressure and on the decay time of the voltage across the resistor. The growth of the branching leader speeds up with increasing decay time constant. As a consequence the probability for a flashover across the resistor increases.

If these phenomena are taken into account, it is necessary to adjust the damping of the discharge current through the resistor at the time of striking in the test circuit according to actual systems. The decay time constant of the discharging current through the resistor is

approximately given by the equation C · R, where C is the capacitance at the load side of the DS and R is the resistance of the damping resistor. For the specified values in Japan of 2000 pF and 500 Ω the decay time constant is about 1 µs [17]. A proper design of the DS has shown that in practice such faults can be eliminated. Nevertheless, the design has to be proven by tests. For the test, it is important to consider the maximum load side capacitance as the worst case regarding leader branching.

(B) Energy absorption

VFTO are suppressed by inserting a resistor in series into the circuit as shown in figure 4.1.21. Therefore, energy absorption by the resistor has also to be verified. During the switching a lot of re-strikes or pre-strikes occur. The number of strikes depends strongly on the speed of the moving contact, nevertheless, the absorption energy of each strike must be added to get the whole absorption energy for one operation.

Figure 4.1.26 (left) shows an example for a simulation of the DS open operation. The top row shows the voltage waveform on the source side of the DS, the middle row shows the voltage waveform on the load side of the DS, where a trapped charge voltage remains after each re-striking, and the bottom row shows the cumulative energy applied to the resistor. In this case, the cumulative energy was 14.4 kJ. Figure 4.1.26 (right) shows the results of a switching test. The top row shows the waveform on the load side of the DS and the bottom row shows the cumulative energy absorption for the resistor. These results show almost equal energy values. The switching performance and reliability including energy absorption capability of the resistors was verified, as well analyzed and measured [26].

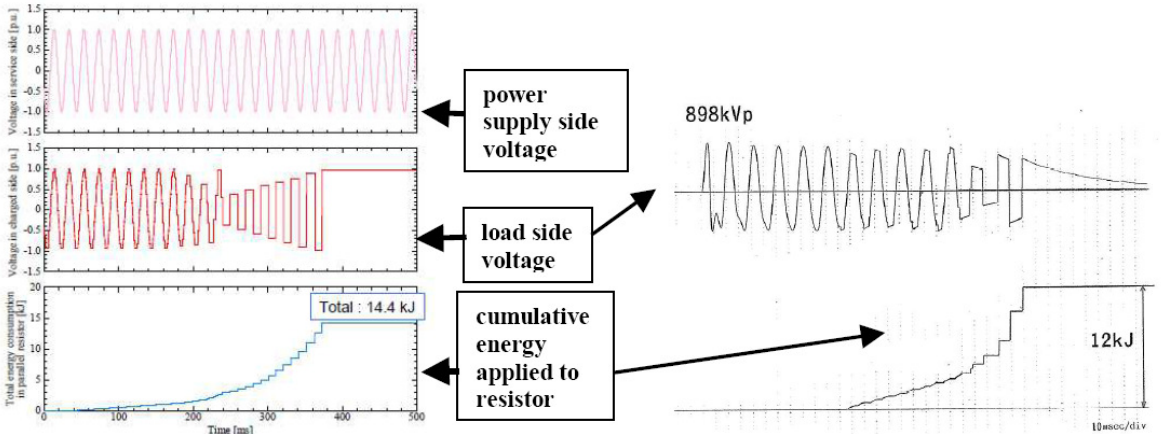

Figure 4.1.26 Energy absorption of damping resistor, calculated (left) and measured (right) [26]

The energy absorption during close operation is generally lower compared to an open operation because of the lower maximum voltage across the DS. The absorption energy E_R of the damping resistor during striking is approximately given by equation 4.4:

$$E_R = \frac{1}{2} C V_0^2 \qquad \ldots(4.4)$$

C: Capacitance at the load side of the DS, V_0: Voltage across DS at the time of striking

The absorption energy depends strongly on the load side capacitance and the voltage across the DS. Taking the bus length at the load side and the capacitance of the open circuit-breaker into account, the capacitance at the load side according to the Japanese requirement was determined as 2000 pF. The required capacity of thermal energy absorption for the resistor was calculated by statistically summing up for one close-open operation containing a high number of strikes during the close and open operation. Figure 4.1.27 shows the calculation

results. According to the Japanese experience, the necessary energy absorption and overvoltage withstand for a 500 Ω resistor were calculated based on the analysis of an actual 4-line, 4-bank substation design considering the most unfavourable case corresponding to a remaining trapped charge voltage of -1 p.u. The required energy absorption for the resistor ranges between 20 kJ and 35 kJ for one close-open operation. The maximum voltage amplitude across the resistor was 1700 kV.

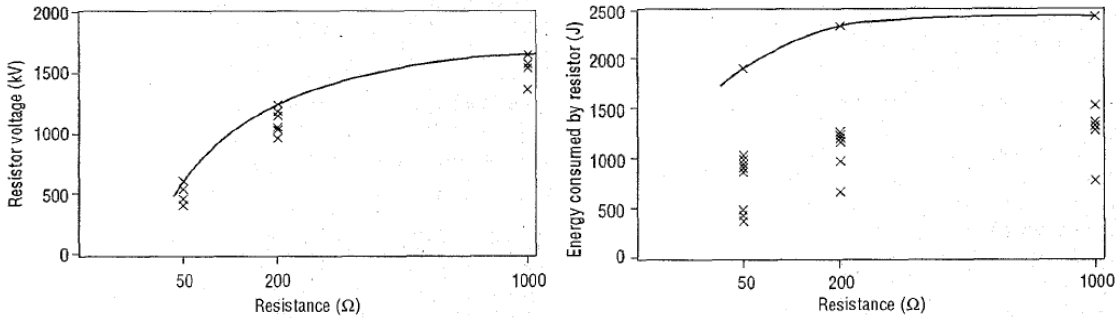

Figure 4.1.27 Resistor voltage and absorption energy of the resistor [26]

Based on the calculation, the requirements for the damping resistor were defined. The requirements are listed in table 4.1.4.

Table 4.1.4 Specification for the damping resistor (Japan)

	Specification
Resistance	500 Ω (2 x 1000 Ω in parallel)
Thermal energy absorption of resistor	20 kJ
Dielectric strength of resistor	1700 kV (2000 times)

The thermal absorption capability of the damping resistor is defined on the basis of withstanding the thermal stress for one close-open operation. The probability of needing to apply more than one close-open operation within some minutes (which corresponds to the thermal time constant of the damping resistor) is considered to be small.

The energy absorption capability of the damping resistor was also calculated for the Chinese project (Jindongnan) [5]. The energy absorbed during one re-striking is related to the capacitance of the load side and the voltage between contacts before striking. The value can reach up to 4.9 kJ. The factors influencing total energy absorbed by the resistor include the speed of the moving contact, gas pressure and the shape of contacts. The calculations indicate that during switching, the energy consumed by the resistor reaches 12.3 kJ in case of a fast acting DS with damping resistor or 24.7 kJ in case of slow acting DS (figure 4.1.28).

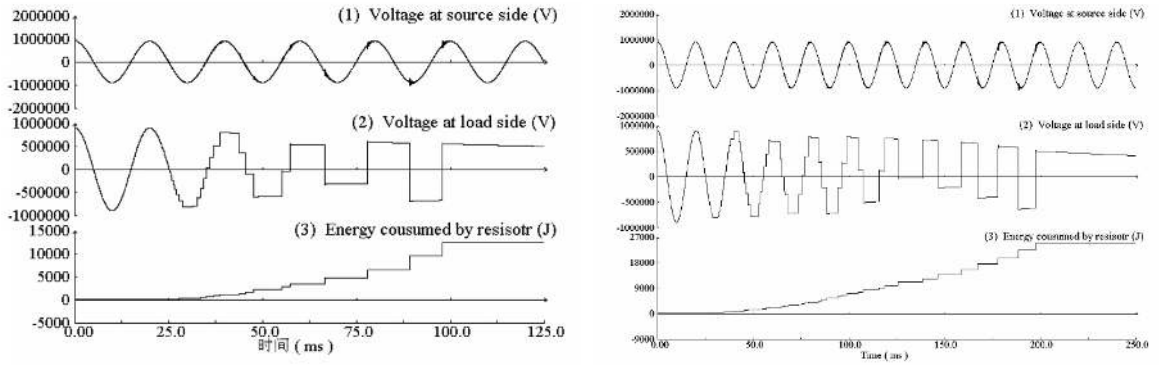

Figure 4.1.28 Absorption energy of the resistor for fast acting (left) and slow acting (right) DS during open operation [5]

4.1.3.4 Testing experience

(A) Bus-charging switching test

Actual verification tests according to the specifications shown in table 4.1.4 such as current interruption and commutation characteristic tests were carried out as factory, laboratory and on-site tests in Japan [37], [38], [39]. Figure 4.1.29 shows the test set-up for the bus-charging current switching test. In order to apply a fast rising voltage to the resistor, a 10 m gas-insulated busbar was installed at each side of the DS. In order to obtain a high voltage across the resistor and a large energy absorption by the resistor, a capacitor with a 15 times larger capacitance compared to the load side was connected to the source side. The testing items according to table 4.1.4 were verified. 400 bus-charging current switching tests (close-open) were carried out. The test voltage was 1.1 p.u and the maximum value across contacts was 1980 kV. Figure 4.1.29 shows the distribution of the re-striking voltage between electrodes. The test results align very well with the calculation results. In order to check the commutation characteristics, photos of the arc between the contacts were taken during the test.

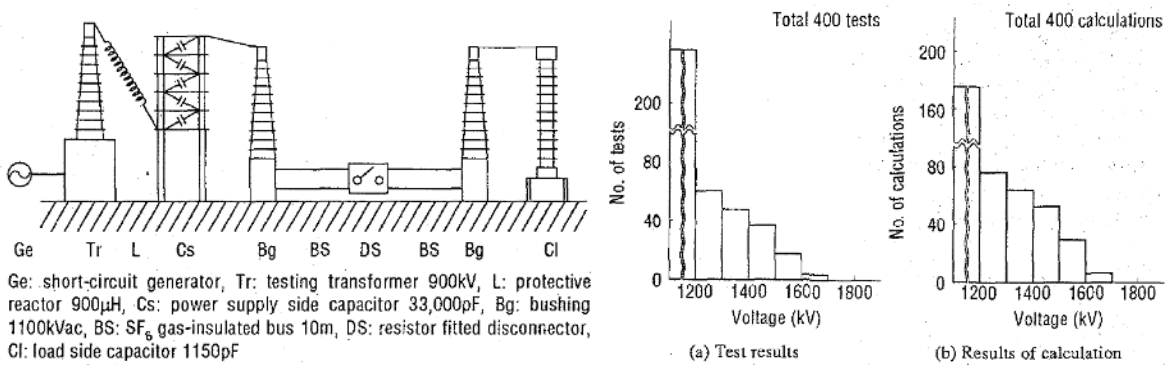

Figure 4.1.29 Test circuit (left) and distributions of maximum values of re-striking inter-electrode voltage (Power supply voltage: 1.1 x 1100 kV/√3) (right) [39]

(B) Multiple surge tests

Multiple surge tests were established as a final development test [40] in order to confirm the thermal energy absorption and dielectric withstand strength of the damping resistor. As mentioned above, the maximum voltage across the resistor is about 1700 kV. However, the last discharge in one close-open operation will not always cause the maximum possible voltage of 1700 kV. To simulate the worst case condition a test was carried out applying a switching impulse voltage from an impulse generator as shown in figure 4.1.30. The moving

contact of the DS with damping resistor was fixed at an intermediate position so that the discharges occurred between the moving contact and the shield of the resistors. The distance between the contacts was fixed so that a flashover occurred at minimum 1700 kV. 2000 switching impulse tests were carried out to confirm the voltage withstand performance of the resistors. The proper function of the DS with damping resistor was proved [16]. The resistor energy absorption was controlled by the capacitors at the source side. During the multiple-surge test the energy was injected by single switching impulses. The thermal energy absorption of the resistor caused by multiple striking during DS switching is around 20 kJ for one close-open operation. The temperature rise of the two resistors was set corresponding to 20 kJ. The resistance was monitored during the whole test. The final result of the test was judged by the proper condition of the resistors after test. During the test no resistor flashover, no resistor short-circuit due to leader branching and no DS ground fault occurred.

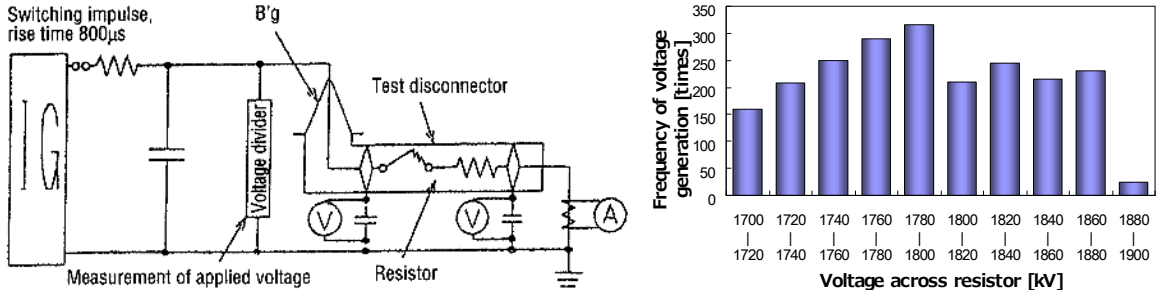

Figure 4.1.30 Test circuit (left) and distributions of maximum values of re-striking inter-electrode voltage (Power supply voltage: 1.1 x 1100 kV/√3) (right) [39]

4.1.4 Recommendations for specifications

4.1.4.1 VFTO

A special topic is the occurrence of VFTO due to the charging and discharging of busbar sections by DS in GIS. The switching causes a large number of re-strikes and pre-strikes which generate high frequency travelling waves in the GIS. Such high frequency voltages may reach amplitudes that could highly stress the insulation of the GIS equipment as well as directly connected equipment such as transformers and shunt reactors. As shown in figure 4.1.2, this phenomenon is more important at UHV than at 800 kV. If the calculated VFTO level is higher than the protective level, special measures to mitigate the VFTO or an increase of the withstand level is required.

The definition of the safety factor has to be studied in detail to give recommendations for future applications. The CIGRÉ WG C4.306 “Insulation Co-ordination for UHV AC Systems” will review and discuss insulation co-ordination practice in the UHV AC range taking into account the state-of-the-art technology, with special reference to surge arresters and other mitigation measures. Beside the selection of insulation levels the task of the WG covers also the co-ordination of withstand voltages and safety factors for the equipment. As an indication the required safety margin depends on both the breakdown and dielectric long-term behaviour of the equipment and the trapped charge behaviour of the DS. A low trapped charge voltage provides an additional safety margin. As a result, the safety factor could be different for equipment (transformer, SF_6 insulation, air insulation) and for different DS designs.

Regarding TD 1, the switching of a very short section of busbar duct, there is no need to change the requirements for test voltages and for the test circuit as given in [4]. The test

circuits for DS testing were chosen in such a way, that maximum p.u. values for VFTO peak were generated.

VFTO amplitudes of at least 1.4 p.u. are required without pre-charging of the busbar. The VFTO amplitude has to be verified by measurements. Moreover it could be recommended to measure also the VFTO amplitude with full trapped charge voltage at the load side. By this, a comparison of calculated stress for the substation equipment with maximum VFTO amplitudes during testing would be possible.

4.1.4.2 Out-of-phase switching

The out-of-phase condition is relevant when the DS on the transformer side is required to be closed before synchronizing system elements, such as generator circuits, which are directly connected to the UHV network. The amplitude of the temporary power frequency overvoltage results from the combination of the trapped charge voltage and the over coupled voltage from the CB grading capacitors. The amplitude of the power frequency overvoltage greatly exceeds that of the rated withstand voltages, especially for high speed DS.

A test should be carried out according to the specification and taking careful consideration of the insulation co-ordination. It has to be confirmed that the test arrangement reflects the arrangement in service. Especially the distance between DS and CB should be as short as possible corresponding to the assembly conditions. There is no need to change the requirements for test voltages and for the test circuit as given in [4].

4.1.4.3 Current switching capability

TD 3 is a special type test to be carried out by agreement between manufacturer and user. There is no need to change the requirements for the test voltages and for the test circuit as given in [4]. The bus-charging current depends on the layout of the substation. The bus-charging currents, evaluated for several existing UHV substation layouts, reach a maximum value of 0.84 A. Schemes of future UHV substations with maximum busbar lengths up to 200 m are concluded to be rather exceptional and a bus-charging current of 1 A is sufficient also for future applications. The required bus-charging current can be lower, if the maximum busbar length is lower. For instance the specified bus-charging current in Japan is 0.5 A. The VFTO occurring during switching operation and its effect to the potential reliability of the system shall be taken into consideration.

4.1.4.4 Special requirements for DS with damping resistor

Table 4.1.5 summarizes additional testing requirements for DS with damping resistor. The requirements are related to three test duties standardized in Annex F of IEC 62271-102 [4], [10]:

TD 1: Switching of a very short section of busbar duct
TD 2: Switching of parallel capacitors for circuit-breakers under 180° out-of-phase conditions
TD 3: Current-switching capability.

The circuit for TD 1 was chosen in such a way that maximum p.u. values for VFTO peak were generated and is also applicable for DS with damping resistor. According to [4], the test circuit has to be arranged in such a way that the measured peak voltage to ground without a trapped charge voltage at the load side and 1 p.u. at the source side is higher than 1.4 p.u. The time to first peak should be less than 500 ns. These values cannot be verified in case of DS with damping resistor, because of the mitigation effect. One verification possibility is an additional test without damping resistor. Another possibility is that the verification can be

done by computer calculation. The calculation for the test with damping resistor can be used to check the validity of the calculation technique.

Attention should be paid to disruptive discharges from phase to earth which are not permitted. In case of DS with damping resistor, attention should be paid also to disruptive discharges across the damping resistor. Discharges across the resistor have to be avoided, because these discharges cause high VFTO stress of the equipment. It is essential that disruptive discharges to earth or across the resistor can be detected properly by adequate measuring or detecting equipment, for instance by a fast transient measurement during the switching operations. The testing requirements for DS with damping resistor are summarized in table 4.1.5.

Table 4.1.5 Testing requirements for DS with damping resistor

Requirements	Arc commutation method	Resistor contacts methods	Relating test duties according to IEC [4]
Thermal energy absorption of resistor	✓	✓	TD 2 and TD 3
Dielectric test of resistor	✓	✓	TD 1 and TD 2
Dielectric test of DS with the resistor	✓	✓	TD 1, TD 2, TD 3
Mechanical reliability		✓	Mechanical Endurance test
Commutation characteristic	✓		TD 1, TD 2, TD 3
Surge suppression effect	✓	✓	TD 1

The requirements for TD 2 and TD 3 according to [4] are applicable also for DS with damping resistor. Attention should be paid to the dielectric withstand capability and the thermal absorption capability of the damping resistor. The specification for damping resistor tests depends on the design, the system configuration and the resistance. Special tests could be carried out according to the specification by agreement between manufacturer and user. Japanese experiences of the DS with damping resistor for the UHV project could be used as a reference. One example is given in table 4.1.4 for a 500 Ω damping resistor and a maximum load side capacitance of 2 nF. In particular, the resistance, the capacitances of load and source side and the speed of the moving contact have a great influence on the dielectric withstand capability and the thermal absorption capability. Therefore, a general specification for these values is not useful. In general, for the determination of the required energy absorption capability one close-open operation has to be considered, except where there is a special specification for higher frequency of switching operations. The specific items for tests with DS with damping resistor are summarized in table 4.1.6. Special requirements regarding the rate of rise of the voltage across the resistor, the energy absorption and the branching behaviour must be taken into account. Especially the maximum load side capacitance, the ratio between load-side and source-side capacitance and the maximum trapped charge voltage according to the actual substation layout have to be considered.

Table 4.1.6 Specific items for tests with DS with damping resistor

Specific items	Individual test	DS test
Thermal energy absorption of resistor	by agreement between manufacturer and user *1	Dielectric tests Bus charging switching test (TD2, TD3)
Dielectric test of resistor	by agreement between manufacturer and user *1	Bus charging switching test (TD1, TD2)
Dielectric test of whole DS with damping resistor	Not applicable	Dielectric tests Bus charging switching test (TD1, TD2, TD3)
Mechanical reliability	Not applicable	Mechanical Endurance test
Commutation characteristic	Not applicable	Bus transfer current switching test Bus charging switching test (TD1, TD2, TD3)

		with arc behaviour monitoring
Surge suppression effect	Not applicable	Bus charging switching test (TD1)

*[1] for example multiple surge tests

4.2 Switching of capacitive currents by AIS disconnectors

Capacitive current interruption with air-insulated disconnectors involves the extinction of free-burning arcs in atmospheric air. Recent research has shown that the arc and its behaviour have a strong dependence on the magnitude of the current and the ratio of the source side capacitance C_S to the load side capacitance C_L [28].

The basic circuit is shown in figure 4.2.1 and in general current interruption is a repetitive break-make event with multiple re-striking. For current magnitudes of 1 A or less, the arc exhibits little or no thermal properties and each re-strike tends to follow a new path, i.e. there is no defined previous arc channel. For currents of 1 A or greater, the arc exhibits thermal properties rising upwards and re-strikes follow the established previous arc channel. If current magnitude alone is considered, at 1 A or less successful interruption is a purely dielectric event dependent only on achieving a contact gap capable of withstanding the recovery voltage; at currents equal to or greater than 1 A it is both a thermal and dielectric event and longer arcing times occur due to added thermal effect.

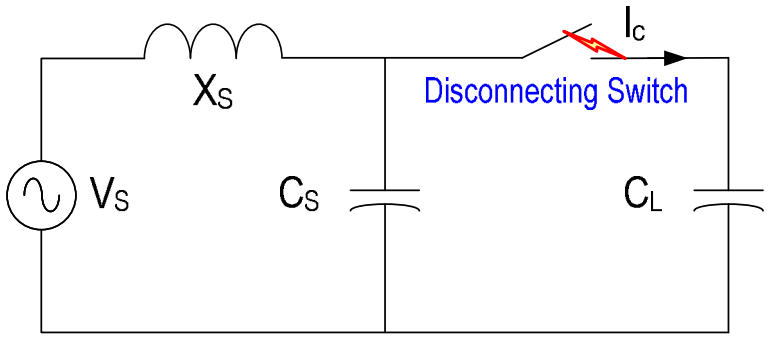

Figure 4.2.1 Basic circuit

The influence of the above-noted capacitance ratio can be explained by reference to figure 4.2.1 and 4.2.2. When a re-strike occurs, the voltages on C_S and C_L will first equalize at U_E and then recover to source voltage U_S but overshooting to produce a re-striking overvoltage as evident in figure 4.2.2. If the ratio C_S/C_L is greater than 1 (Case A in figure 4.2.2), then U_E is close to U_S and the excursion to U_S is low giving a low overvoltage and low energy injected into the arc. If the ratio C_S/C_L is less than 1 (Case B in figure 4.2.2), then U_E is close to the load side trapped charge voltage U_E and the excursion to U_S is high giving a high overvoltage and high energy injected into the arc thereby sustaining it. An unfavourable C_S/C_L ratio therefore means high overvoltages and long arcing times and is a likely occurrence when a length of bus with a connected instrument transformer is switched out. In fact, failures of conventional current transformers have been attributed to disconnector operation.

For air-insulated UHV stations, the maximum capacitive current to be interrupted by disconnectors will depend on the type of instrument transformers to be used. The likelihood of conventional instrument transformers being used is at least debatable and quite probably optical voltage and current transformers will the norm. These devices have negligible charging currents meaning low capacitance values (about that of a post insulator) and hence favourable C_S/C_L ratios.

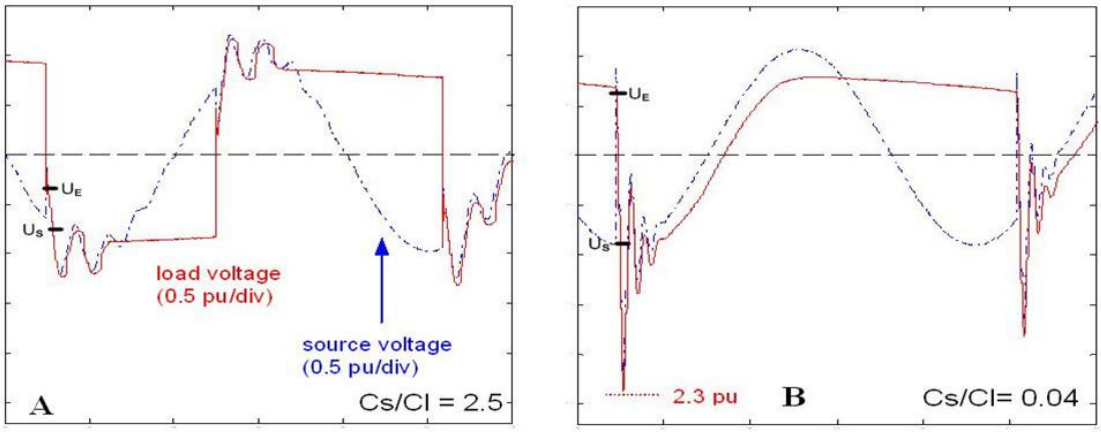

Figure 4.2.2 Re-striking process without overvoltages (A) and with overvoltages (B) at interruption of 2 A capacitive current with disconnector. Load side voltage (solid lines) and source side voltage (dashed lines) are shown. Time: 5 ms/div. 1 p.u. = 245 kV (Traces courtesy of KEMA)

IEC SC 17A Maintenance Team 42 is addressing capacitive current interruption with air-insulated disconnectors and have published Technical Report TR 62271-304. IEC 62271-102 [4] is to be revised to incorporate UHV requirements and a review of the requirements of Annex F with respect to the C_S/C_L ratio influence is recommended.

4.3 Bus-transfer switching by Disconnectors

4.3.1 Introduction

Disconnector bus-transfer current switching ratings are stated in Annex B of IEC 62271-102 [4]. The rated bus-transfer current for both air-insulated and gas-insulated DS is 80 % of the rated current and normally not expected to exceed 1600 A. The rated bus-transfer voltages for DS at 245 kV and above are shown in table 4.3.1. Corresponding loop impedances are simply the bus-transfer voltage divided by the bus-transfer current. Air-insulated DS commonly include commutating contacts to achieve this capability.

Table 4.3.1 Rated bus-transfer voltages for DS [4]

Rated voltage (kV)	Air-insulated disconnectors (V_{rms})	Gas-insulated disconnectors (V_{rms})
245	200	20
300		
362		
420	300	
550		40
800		

4.3.2 Background of technical requirements

4.3.2.1 General requirements

Disconnectors can be used for bus transfer switching (loop switching), e.g. in double busbar or multi-bus arrangements of SF_6 GIS, Hybrid-IS or AIS. A typical switching sequence for the current transfer in a double-bus bar substation is shown in figure 4.3.1. Closing of disconnector No. 2 yields distribution of the load current onto the two parallel paths according

to the relation of the impedances of both sections. Opening of disconnector No. 1 in the third scheme leads to the transfer of the remaining portion of the load current from bus A to bus B.

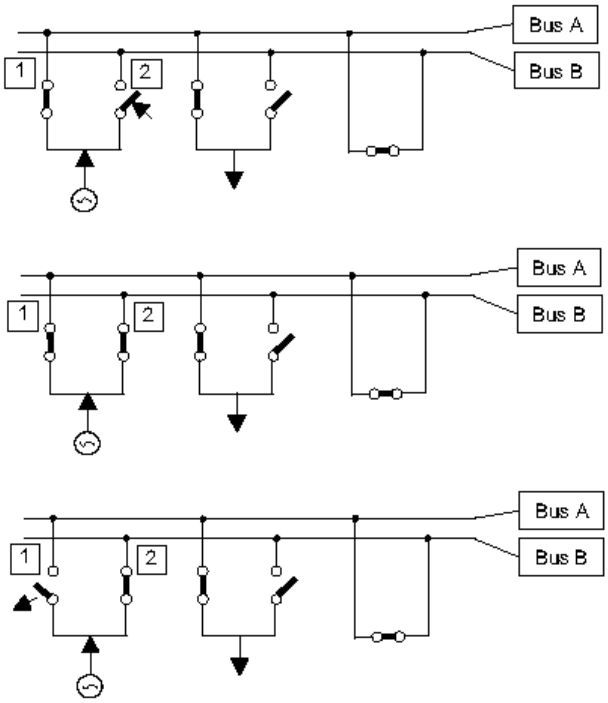

Figure 4.3.1 Principle bus transfer switching sequence in a double-bus bar substation

The stationary voltage V appearing across the terminals of the disconnector after current transfer equals the load current times the impedance of the current carrying path parallel to the open disconnector. Thus, this voltage V is proportional to the load current, power frequency and length of the current carrying loop section between disconnectors No. 1 and No. 2, see equation 4.5.

$$V = I \cdot s\sqrt{R'^2 + (\omega L')^2} \qquad \ldots(4.5)$$

I (A): Bus-transfer current, s (m): Length of current carrying loop, R' (uΩ/m): Resistance, ωL' (uΩ/m): Reactance, ω (s^{-1}): 2 π f, f (Hz): power frequency

4.3.2.2 Specification for the UHV projects

Table 4.3.2 shows the specifications for the current UHV projects.

Table 4.3.2 Requirements for bus-transfer current switching in UHV systems [4]

1100 kV	Japan (GIS)	China (GIS or Hybrid-IS)
Bus-transfer current	8000 A (equal to the rated current)	1600 A
Bus-transfer voltage	300 V_{rms}	400 V_{rms}
TRV requirement	RRRV = 400 V/μs	1-cos, 10 kHz Amplitude factor 1.5

In the past, loop switching with DS has tended to apply to double-busbar layout schemes. Whether such schemes will be used at UHV remains to be established. Also, there is some indication that UHV transmission systems may operate on a constant power flow basis and the present upper of 1600 A bus-transfer current will need to be reviewed. Likewise upper bus-transfer voltages of 300 V and 40 V air-insulated and gas-insulated DS, respectively, should also be reviewed based on the actual circuit layout dimensions.

In Japan, the rated bus-transfer current is equal to the rated current (see table 4.3.2) and it is general practice that the maximum bus-transfer current corresponds to the rated current of the DS. That application is probably unique to utilities in Japan and requires a bus-transfer voltage (recovery voltage) for 1000 kV GIS of 300 V (margin included) at 8000 A. The corresponding TRV has a minimum rate of rise of 400 V/μs again with a margin included. The specification is based on the following calculation. The bus-transfer voltage can be simplified calculated as shown in equation 4.6:

$$V = \omega \cdot L` \cdot s \cdot I \qquad \ldots(4.6)$$

I (A): Bus-transfer current = rated current = 8000 A, s (m): Length of current carrying loop = 250 m,

L` (μH/m): Inductance per meter = 0.42 μH/m, ω (s-1): 2 π f, V (V): 265 V

The TRV can be simplified calculated as shown in equation 4.7:

$$RRRV = \sqrt{2} \cdot \omega \cdot Z \cdot I \qquad \ldots(4.7)$$

I (A): Bus-transfer current = rated current = 8000 A, Z (Ω): Surge impedance = 90 Ω,

ω (s-1): 2 π f, RRRV (V/μs): 320 V/μs

4.3.2.3 Bus-transfer calculation for current UHV projects

The rated bus-transfer current for both air-insulated and gas-insulated disconnectors is 80 % of rated normal current and normally not expected to exceed 1600 A [4]. The bus-transfer current depends on the impedance ratio of long and short circuit of the loop and on the rated current during the switching sequence. Calculations were performed to verify the ratio of long and short circuit of the loop. For the calculation the actual schemes from the 1100 kV systems were used [3]. It should be noted that in a substation built on a 2 CB layout or 1-1/2 CB layout with double busbar, the bus-transfer can be accomplished using a CB to transfer the current (See figure 4.3.2 a-c). Thus, in normal operation conditions, the DS will not be stressed with bus-transfer switching operations. Only in the case of a failure in a CB, bus-transfer switching capability for the DS will be required to disconnect the faulty CB for maintenance. The calculation for these cases was performed only for comparison. Figure 4.3.2 shows the configurations used. The parameters used for the calculation are shown in table 4.3.3.

Table 4.3.3 Electrical parameter used for calculation

	Reactance [μΩ/m]	Inductance [μH/m]	Velocity [m/μs]	Impedance [Ω]
1100 kV GIS busbar (China)	94	0.3	275-300	90
1100 kV AIS busbar (China)	377	1.2	300	360
1100 kV GIS busbar (Japan)	104	0.33	273	90

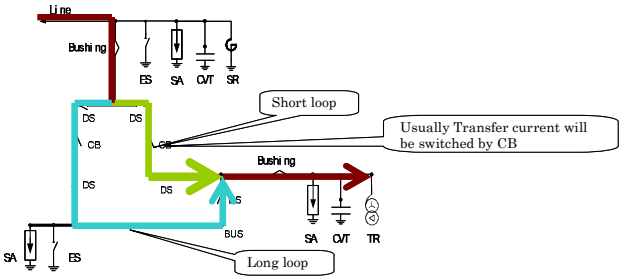

a) China 110 0kV GIS, 2CB layout

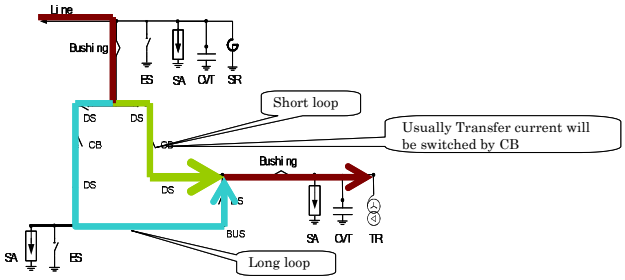

(b) China 1100 kV Hybrid-IS, 1-1/2CB layout

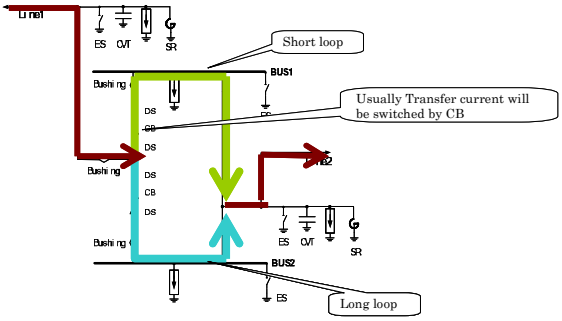

(c) China 1100 kV Hybrid-IS, 1-1/2CB layout

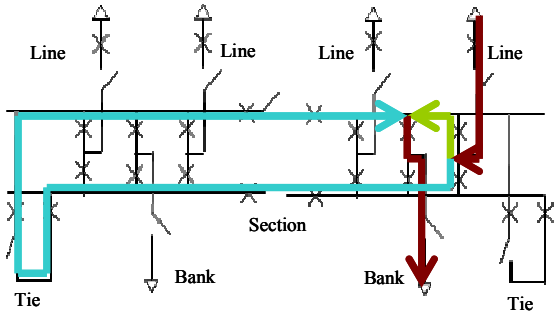

(d) Japan 1100 kV GIS, double busbar layout, busbar coupler farthest away from DS

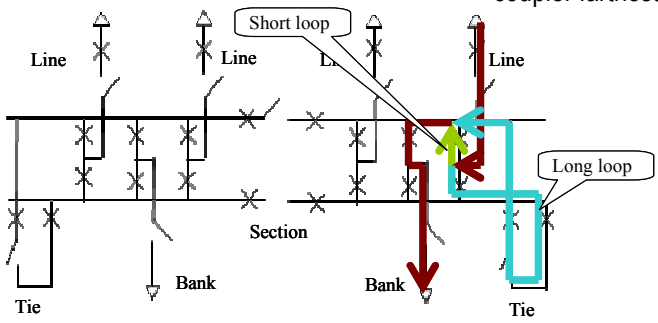

(e) Japan 1100 kV GIS, double busbar layout, busbar coupler near-by the DS

Figures 4.3.2 Bus-transfer current switching, calculated examples according to [3]

Table 4.3.4 shows the calculation results. The ratios, calculated by using actual design, vary between 70 % and 94 %. Considering only the double busbar layout, the ratios vary between 85 % and 94 %. In case of a double busbar configuration two cases were investigated. In case 1, the bus coupler is far away from the switching DS (figure 4.3.2 d) and in case 2 the bus coupler is nearby the switching DS (figure 4.3.2 e).

The typical application for bus-transfer switching is the double busbar layout scheme. Therefore this configuration was investigated more in detail. Two different bus-transfer operations are possible.

Case 1: operation at outgoing/incoming bay (figure 4.3.3)
Case 2: operation at the other bay (figure 4.3.4)

Table 4.3.4 Bus-transfer calculation results

	Figure	Long loop			Short loop			Ratio [%]
		Length [m]		Impedance [Ω]	Length [m]		Impedance [Ω]	
		AIS	GIS	Total	AIS	GIS	Total	
China 1100 kV Full-GIS*1	4.3.3 a	0	84	0.00792	0	36	0.00339	70.0
China 1100 kV Hybrid-IS*2	4.3.3 b	112	78.4	0.04961	30	39.2	0.015	76.8
China 1100 kV Hybrid-IS*3	4.3.3 c	256	36	0.0999	112	36	0.04562	68.7
Japan 1100 kV GIS*4 Bus coupler bay away	4.3.3 d	0	175.9	0.01824	0	10.7	0.00111	94.3
Japan 1100 kV GIS*4 Bus coupler bay nearby	4.3.3 e	0	63.6	0.00659	0	10.7	0.00111	85.6
India 800 kV AIS*5	*n/a*	*n/a*	*n/a*	*n/a*		*n/a*	*n/a*		*n/a*

*1 China 1100 kV GIS, 2CB scheme [3]
*2 China 1100 kV Hybrid-IS, 1-1/2CB scheme [3]
*3 China 1100 kV Hybrid-IS, 1-1/2CB scheme [3]
*4 Japanese 1100 kV GIS, double busbar scheme [3]
*5 Indian 800 kV AIS, 1-1/2CB scheme [3]

1) At initial time power flow route is Line 2 -> Bus1 -> Bank1.
2) Then by the Bus-transfer over at Line 2 bay operation, DS1 is closed. At this moment, there are two power flows in parallel
Line 2 (DS1) -> Bus1 -> Bank1. and,
Line 2 (DS2) -> Bus2 -> Tie 1 -> Bus 2 ->Bank1.
3) Finally by opening operation of DS1, DS1 have to break Bus-transfer current.

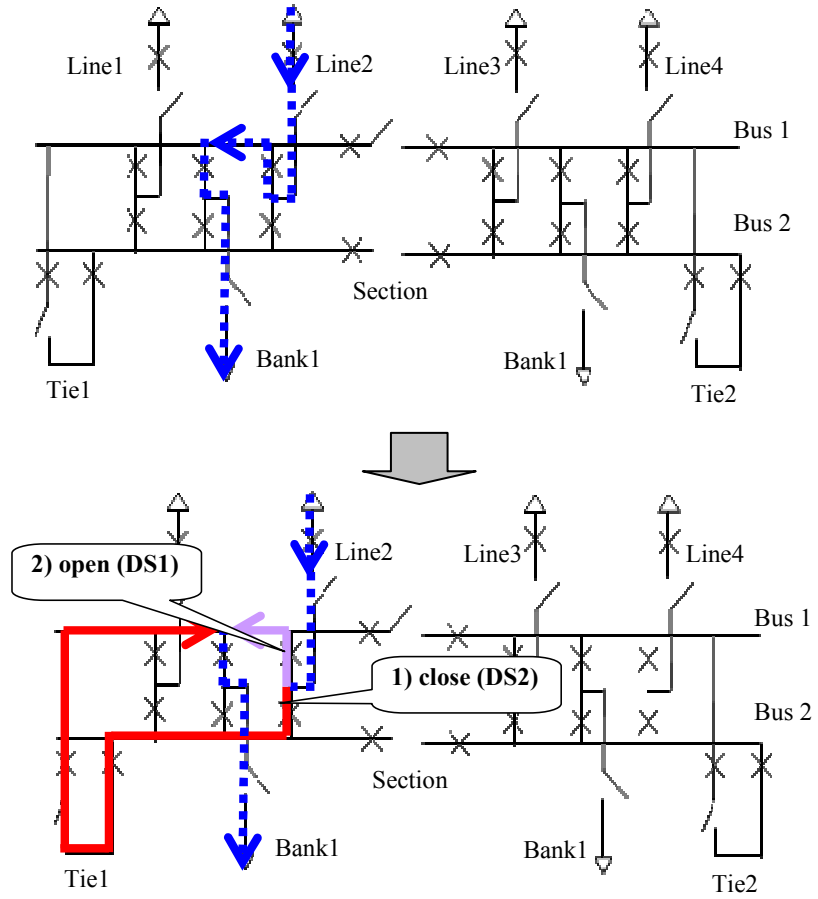

Figure 4.3.3 Bus Bus-transfer current switching, case 1

1) At initial time power flow route is Line 2 -> Bus1 -> Tie 1 ->Bank1.
2) By the bus-transfer over operation at Line 1 bay, both of DS1 and DS2 of Line 1 are closed.
At this moment, there are two power flow in parallel
Line 2 -> Bus1 -> DS1 and DS2 of Line 1 -> Bus2 ->Bank1. and,
Line 2 -> Bus1 -> Tie 1 -> Bus2 ->Bank1.
3) Finally by opening operation of DS1, DS1 have to break Bus-transfer current.

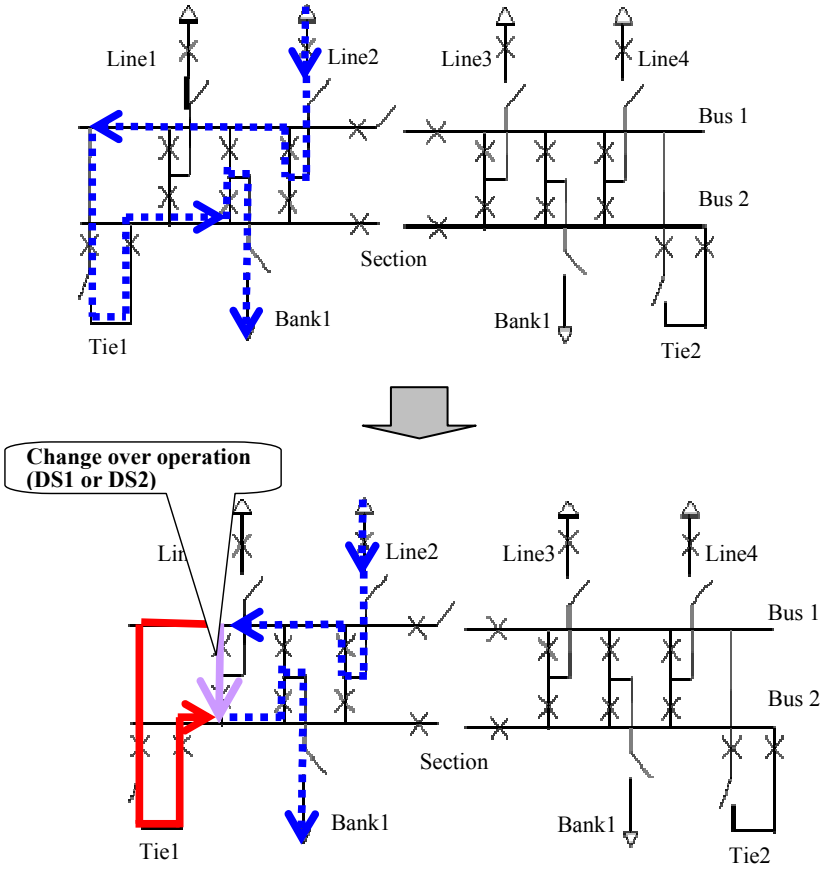

Figure 4.3.4 Bus Bus-transfer current switching, case 2

The model configuration is shown in figure 4.3.5. The arrangement and the length of the busbar are based on the information given in [3].

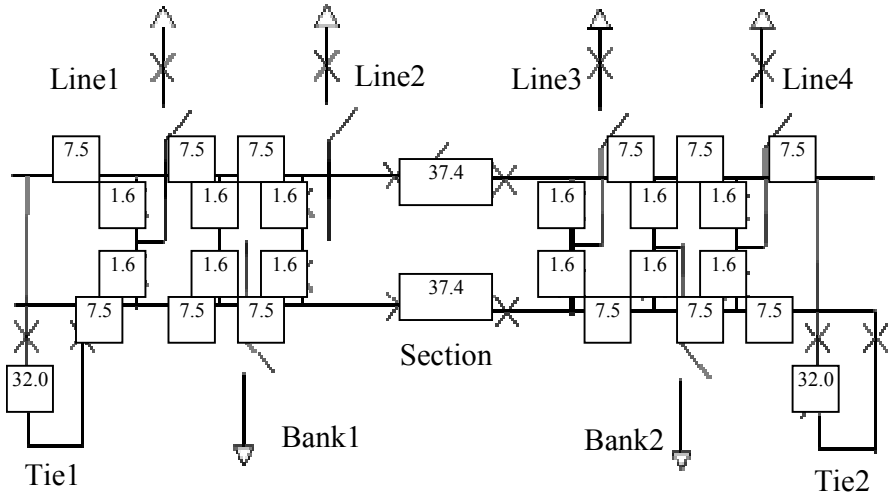

Figure 4.3.5 Model configuration [3]

Table 4.3.5 and table 4.3.6 show the calculated loop length and current distribution ratio for the bus-transfer current for both cases. There are some special cases which can be omitted by considering actual operation condition. These cases are marked as special cases in the tables.

The highest ratio of current distribution is 98 %. By considering these aspects, the most conservative value for bus-transfer current may be equal to the current at the moment of bus-transfer operation. This current may reach the rated current of the bus coupler or the line feeder.

Table 4.3.5 Bus-transfer calculation results – double busbar scheme case 1

Bay of Power flow		Loop length (m)		Ratio	Special cases
From	To (Change Over assumed)	Long loop (via Coupler)	Short loop		
Line 1	Line 2	48.6	1.6	96.8%	
Line 1	Line 3	48.6	1.6	96.8%	*1
Line 1	Line 4	48.6	1.6	96.8%	
Line 1	Bank 1	48.6	1.6	96.8%	
Line 1	Bank 2	48.6	1.6	96.8%	
Line 2	Line 1	63.6	16.6	79.3%	
Line 2	Line 3	78.6	1.6	98.0%	
Line 2	Line 4	78.6	1.6	98.0%	
Line 2	Bank 1	71.1	9.1	88.7%	
Line 2	Bank 2	78.6	1.6	98.0%	
Line 3	Line 1	101	54	65.2%	
Line 3	Line 2	116	39	74.8%	
Line 3	Line 4	153.4	1.6	99.0%	*1
Line 3	Bank 1	108.5	46.5	70.0%	
Line 3	Bank 2	153.4	1.6	99.0%	*1
Line 4	Line 1	116	69	62.7%	
Line 4	Line 2	131	54	70.8%	
Line 4	Line 3	168.4	16.6	91.0%	*1
Line 4	Bank 1	123.5	61.5	66.8%	
Line 4	Bank 2	175.9	9.1	95.1%	*1
Bank 1	Line 1	56.1	9.1	86.0%	
Bank 1	Line 2	63.6	1.6	97.5%	
Bank 1	Line 3	63.6	1.6	97.5%	
Bank 1	Line 4	63.6	1.6	97.5%	
Bank 1	Bank 2	63.6	1.6	97.5%	*2
Bank 2	Line 1	108.5	61.5	63.8%	
Bank 2	Line 2	123.5	46.5	72.6%	
Bank 2	Line 3	160.9	9.1	94.6%	*1
Bank 2	Line 4	168.4	1.6	99.1%	*1
Bank 2	Bank 1	108.5	54	66.8%	*2

*1 Negligible if nearer bus coupler bay is closed

*2 Unusual power flow

Table 4.3.6 Bus-transfer calculation results – double busbar scheme case 2

Bay of Power flow		Change over	Loop length (m)		Ratio	Special cases
From	to		via Coupler	via CO bay		
Line 1	Line 2	Bank 1	39.5	10.7	78.7%	
Line 1	Line 2	Line 3	47	93	33.6%	
Line 1	Line 2	Bank 2	47	108	30.3%	
Line 1	Line 2	Line 4	47	123	27.6%	
Line 1	Line 3	Bank 1	39.5	10.7	78.7%	
Line 1	Line 3	Line 2	47	18.2	72.1%	
Line 1	Line 3	Bank 2	84.5	70.7	54.4%	
Line 1	Line 3	Line 4	84.5	85.7	49.6%	
Line 1	Line 4	Bank 1	39.5	10.7	78.7%	

Bay of Power flow		Change over	Loop length (m)		Ratio	Special cases
From	to		via Coupler	via CO bay		
Line 1	Line 4	Line 2	47	18.2	72.1%	
Line 1	Line 4	Line 3	84.5	55.7	60.3%	
Line 1	Line 4	Bank 2	92	63.2	59.3%	
Line 1	Bank 1	Line 2	39.5	25.7	60.6%	
Line 1	Bank 1	Line 3	39.5	100.7	28.2%	
Line 1	Bank 1	Bank 2	39.5	115.7	25.5%	
Line 1	Bank 1	Line 4	39.5	130.7	23.2%	
Line 1	Bank 2	Bank 1	39.5	10.7	78.7%	
Line 1	Bank 2	Line 2	47	18.2	72.1%	
Line 1	Bank 2	Line 3	84.5	55.7	60.3%	
Line 1	Bank 2	Line 4	92	78.2	54.1%	
Line 2	Line 3	Line 1	32	3.2	90.9%	
Line 2	Line 3	Bank 1	47	3.2	93.6%	
Line 2	Line 3	Bank 2	99.5	55.7	64.1%	
Line 2	Line 3	Line 4	99.5	70.7	58.5%	
Line 2	Line 4	Line 1	32	3.2	90.9%	
Line 2	Line 4	Bank 1	47	3.2	93.6%	
Line 2	Line 4	Bank 2	99.5	40.7	71.0%	
Line 2	Line 4	Line 3	107	48.2	68.9%	
Line 2	Bank 1	Line 1	32	3.2	90.9%	
Line 2	Bank 1	Line 3	54.5	85.7	38.9%	
Line 2	Bank 1	Bank 2	54.5	100.7	35.1%	
Line 2	Bank 1	Line 4	54.5	115.7	32.0%	
Line 2	Bank 2	Line 1	32	3.2	90.9%	
Line 2	Bank 2	Bank 1	47	3.2	93.6%	
Line 2	Bank 2	Line 3	99.5	40.7	71.0%	
Line 2	Bank 2	Line 4	107	63.2	62.9%	
Line 3	Line 4	Line 1	32	3.2	90.9%	*1
Line 3	Line 4	Bank 1	47	3.2	93.6%	*1
Line 3	Line 4	Line 2	62	3.2	95.1%	*1
Line 3	Line 4	Bank 2	144.5	10.7	93.1%	*1
Line 3	Bank 1	Line 1	32	3.2	90.9%	
Line 3	Bank 1	Line 2	54.5	10.7	83.6%	
Line 3	Bank 1	Bank 2	92	63.2	59.3%	
Line 3	Bank 1	Line 4	92	78.2	54.1%	
Line 3	Bank 2	Line 1	32	3.2	90.9%	*1
Line 3	Bank 2	Bank 1	47	3.2	93.6%	*1
Line 3	Bank 2	Line 2	62	3.2	95.1%	*1
Line 3	Bank 2	Line 4	144.5	25.7	84.9%	*1
Line 4	Bank 1	Line 1	32	3.2	90.9%	
Line 4	Bank 1	Line 2	54.5	10.7	83.6%	
Line 4	Bank 1	Line 3	92	48.2	65.6%	
Line 4	Bank 1	Bank 2	99.5	48.2	67.4%	
Line 4	Bank 2	Line 1	32	3.2	90.9%	*1
Line 4	Bank 2	Bank 1	47	3.2	93.6%	*1
Line 4	Bank 2	Line 2	62	3.2	95.1%	*1
Line 4	Bank 2	Line 3	137	3.2	97.7%	*1
Bank 1	Bank 2	Line 1	32	3.2	90.9%	*2
Bank 1	Bank 2	Line 2	47	10.7	81.5%	*2
Bank 1	Bank 2	Line 3	92	48.2	65.6%	*2
Bank 1	Bank 2	Line 4	99.5	70.7	58.5%	*2

*1 Negligible if nearer bus coupler bay is closed, *2 Unusual power flow

4.3.3 Recommendations for specifications

Figure 4.3.6 shows the bus transfer voltage for GIS applications, by using typical values for resistance and reactance. It can be seen that the bus-transfer voltage is linearly increasing with length of current carrying loop. As IEC 62271-102 specifies 1600 A as loop current, these values are given in comparison to 2000 A, 4000 A and 8000 A loop current. The vertical lines indicate what current carrying loop appears between bays with typical distances (20 m x 50 m).

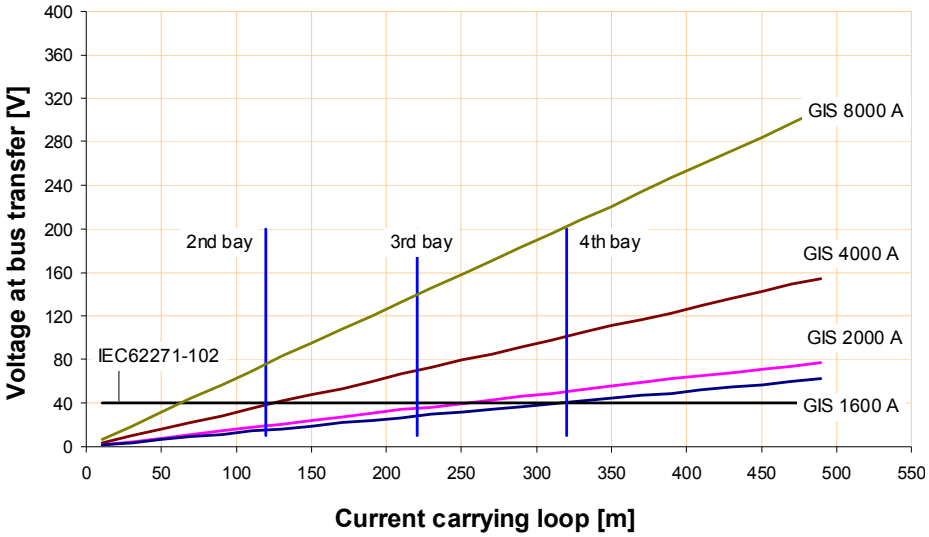

Figure 4.3.6 Bus-transfer voltage as a function of length of GIS current carrying loop (IEC value for 800 kV)

Similar calculations have been conducted for AIS or Hybrid-IS where the busbars will be AIS lines. AIS lines have increased inductance values compared to GIS. Due to higher inductance values, the bus transfer voltage is higher for Hybrid-IS substations, see figure 4.3.7.

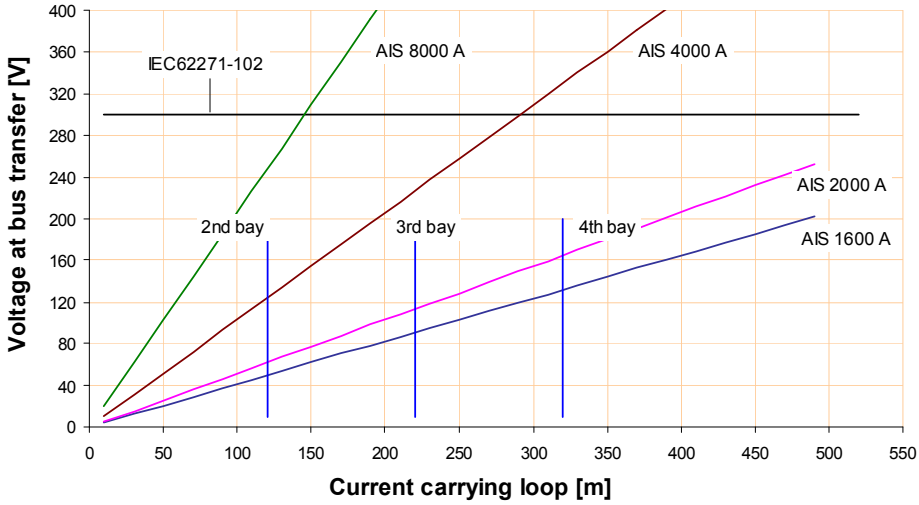

Figure 4.3.7 Bus-transfer voltage as a function of length of AIS / Hybrid-IS current carrying loop (IEC value for 800 kV)

Thus for UHV, the bus-transfer current has to be defined in dependence of the actual current rating. Since the maximum rated current is increased up to 8000 A in the UHV systems, the bus-transfer current should be chosen according to the rated current for the application.

Bus-transfer currents have to be defined in dependence of the actual current ratings, the type of substation and the maximum loop length. As can be learnt from figure 4.3.6 and 4.3.7, for

GIS a bus-transfer voltage of 60 V belongs to 1600 A and of 300 V to 8000 A, while for AIS and Hybrid-IS a voltage of 400 V belongs to 1600 A.

As WG A3.22 has not yet enough information on bus-transfer current and the loop length, any conclusion is too premature. Further investigations are necessary to give recommendations.

4.4 Induced current switching by earthing switches

4.4.1 Introduction

For earthing switches (ES) which are used in transmission circuits operating closely in parallel with other energized transmission circuits, a switching capability is required for the electromagnetically induced current and the electrostatically induced current [4]. In Annex C electromagnetic and electrostatic induced currents and voltages are standardized for 550 kV and 800 kV ES which are designated to be used in circuits with relatively long lines or a high coupling to an adjacent energized circuit (class B earthing switches), (see table 4.4.1).

Table 4.4.1 Induced current and voltage for 550 kV and 800 kV earthing switches (class B) [4]

Rated voltage (kV)	Electromagnetic coupling		Electrostatic coupling	
	Rated induced current (A_{rms})	Rated induced voltage (kV_{rms})	Rated induced current (A_{rms})	Rated induced voltage (kV_{rms})
550	160	20	25	25
800	160	20	25	32

4.4.2 Background of technical requirements

4.4.2.1 General remarks

Earthing switches are used to ground an overhead line. In the closed position, they must withstand the full short-circuit current for the specified duration (typically 1 s or 3 s). For parallel lines, the ES must be able to interrupt the induced current coming from the parallel coupling impedance. This current is of two types: inductive current and capacitive current. The ES will be required to interrupt and establish an inductive current when the ES is operated at one extremity of the de-energized line (parallel with other circuits) where the other extremity in grounded (figure 4.4.1).

The ES will be required to interrupt and establish a capacitive current when the ES is operated at one extremity of the de-energized line (parallel with other circuits) where the other extremity in opened (figure 4.4.2).

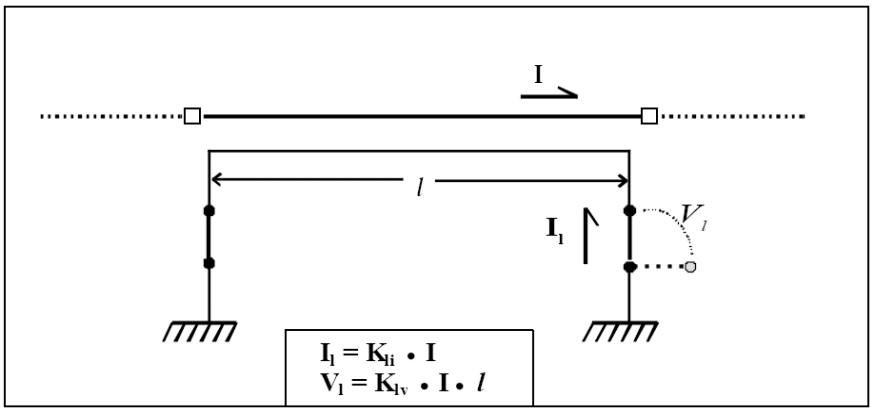

Figure 4.4.1 Electromagnetic Induction (inductive current) from parallel lines

The current induced in a de-energized parallel circuit which is grounded at both ends is function of the current circulating in the energized parallel circuit and the coupling coefficient between the parallel circuits (determined by the geometrical arrangement of the circuits). The induced voltage across the ES in opened position at one end of a circuit with the other end grounded (figure 4.4.1) depends on the amplitude of the current flowing in the energized parallel circuit, on the coupling coefficient (determined by the geometrical arrangement of the circuits) and on the length of the parallel circuits.

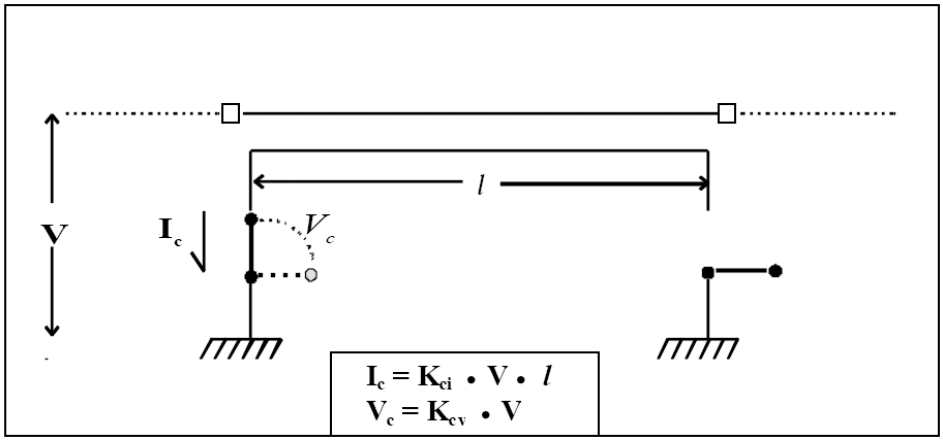

Figure 4.4.2 Electrostatic Induction (Capacitive current) from parallel lines

The capacitive current in a de-energized parallel circuit grounded at one end depends on the voltage of the energized circuit, the coupling coefficient between the circuits (given by the geometrical arrangement) and the length of the parallel circuits (figure 4.4.2). The capacitive voltage induced across an ES in opened position at the end of a circuit with the other end grounded depends on the voltage of the energized circuit and the coupling coefficient between the parallel circuits (figure 4.4.2).

4.4.2.2 Specification for the UHV projects

Hydro-Québec TransÉnergie (HQ) Canada has only single circuit lines at 765 kV. For its 765 kV overhead lines, HQ is using two classes of ES, one which is in line with IEC 62271-102 [4] requirements and a special class with higher requirements.

The coupling coefficients given in figures 4.4.1 and 4.4.2 (K_{li}, K_{lv}, K_{ci}, K_{cv}) have been calculated using EMTP program by simulating the typical OH line configuration. These coefficients are given in table 4.4.2 below.

Table 4.4.2 Coupling coefficients calculated for HQ 765 kV lines

Configurations	K_{li} [A/A]	K_{lv} [V/A/km]	K_{ci} [mA/kV/km]	K_{cv} [V/V]
2 lines, 735 kV 4 conductors / phase	0.026	0.010	0.110	0.024

Using the given coupling coefficients in table 4.4.2, the induced voltages and currents have been calculated for the 765 kV lines and are summarized in table 4.4.3.

Table 4.4.3 Calculated induced currents and voltages for HQ 765 kV lines

Type	Line length (km)	Circulating current I (A)	I_l (A)	V_l (kV)	I_C (A)	V_C (kV)
HQ Class A	80	3000	78	2.4	3.9	10.6
HQ Class B	335	3000	78	10.0	16.3	10.6
IEC Class B 62271-102	*n/a*	*n/a*	*160*	*20.0*	*25.0*	*32.0*

HQ has standardized two classes of ES: class A and class B. Class A is used for short parallel line sections. The values specified by HQ are in conformity with class A of IEC 62271-102. Class B is specified for longer parallel line sections. The HQ values calculated for this class (as shown in table 4.4.3) are much lower than the values defined for class B in IEC 62271-102. Induced current breaking tests were performed at IREQ on different types of ES (using different breaking devices). The results of these tests showed the performance of the different ES breaking devices and allowed HQ to choose the best technical-economical solution to fulfil the requirements for class B. Other devices could meet the requirements of IEC class B but would not be an appropriate choice for HQ. Finally, it was indeed decided that HQ would not adopt IEC values for class B but instead define a special class which is in between class A and class B of IEC.

Moreover, the specifications from TEPCO (Japan), KEPCO (Korea) and China are available and listed in table 4.4.4. Further information is given in [2]. No transmission lines in parallel are installed in China up to now. The future specification was used. More details are given in figures 4.4.3 and 4.4.4.

Table 4.4.4 Summary of calculated induced currents and voltages

	Rated voltage (kV)	Line length (km)	Circulating current I (A_{rms})	Electromagnetic coupling		Electrostatic coupling	
				Rated induced current (A_{rms})	Rated induced voltage (kV_{rms})	Rated induced current (A_{rms})	Rated induced voltage (kV_{rms})
HQ	765	335	3000	78	10.0	16.3	10.6
KEPCO	800	155	8000	1560	122	25	38
TEPCO	1100	*n/a*	8000	1000	70	40	50
CHINA (Future)	1100	327	4000	1134	156	82	63
IEC Class B 62271-102		*n/a*	*n/a*	*160*	*20.0*	*25.0*	*32.0*

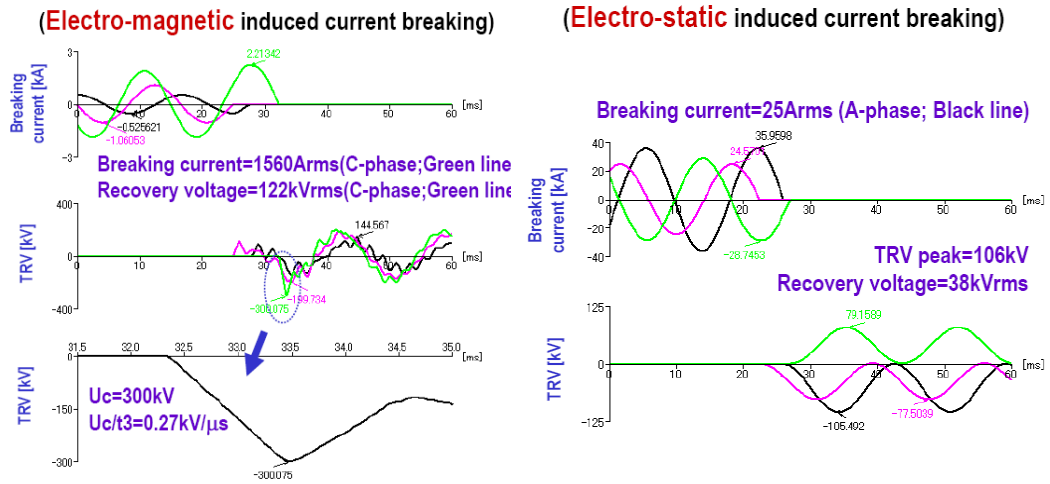

Figure 4.4.3 Analysis Results for Induced Current Switching of 800 kV ES (KEPCO, double circuit tower)

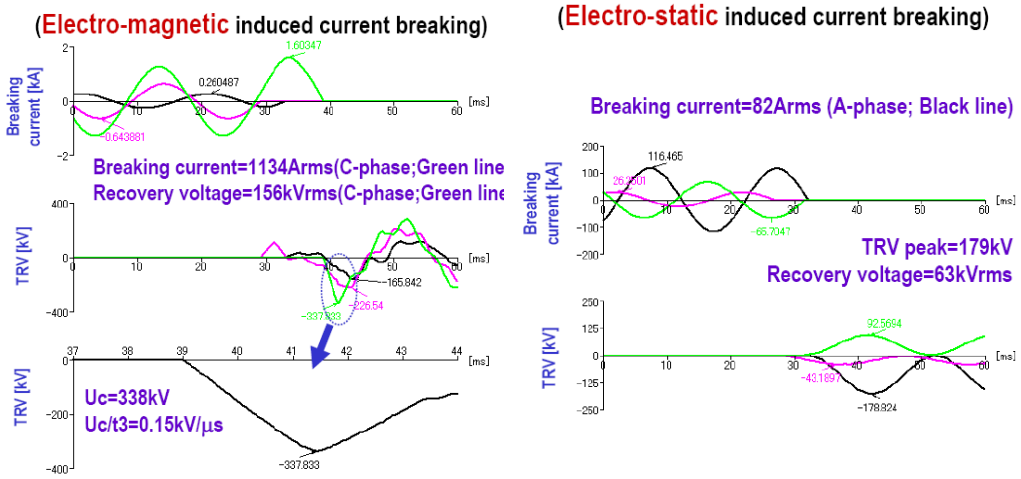

Figure 4.4.4 Analysis Results for Induced Current Switching of 1100 kV ES (CHINA Future: Double-circuit tower)

4.4.2.3 Parameter study

The results of parameter study of electromagnetically induced and electrostatically induced currents switching by earthing switches under the condition of the line length of 125 km, 200 km and 250 km and of a load current from 4000 A to 8000 A are summarized below. For the calculation EMTP-ATP was used instead of the well-known Carson-Pollaczek calculation program. The configuration of the conductors of the transmission line and towers are shown in figure 4.4.5, tables 4.4.5 and 4.4.6

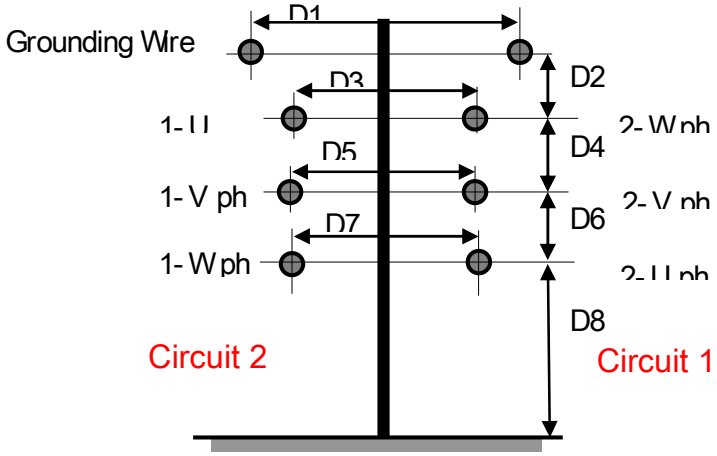

Figure 4.4.5 Analysis model of the tower

Table 4.4.5 Analysis model of the tower

	Tower 1	Tower 2	Tower 3
D1 (m)	38.0	33.0	25.5
D2 (m)	12.5	5.0	6.5
D3 (m)	31.0	30.0	22.5
D4 (m)	17.5	20.0	22.0
D5 (m)	32.0	36.0	28.5
D6 (m)	17.5	20.0	20.0
D7 (m)	33.0	33.0	24.7
D8 (m)	61.5	50.0	50.0

Table 4.4.6 Configuration of conductors of transmission line for calculation

	Overhead grounding wire	Overhead Power line	
Tower	Tower 1, Tower 2, Tower 3	Tower 1	Tower 2, Tower 3
Type and size of lines	OPGW, 500 mm^2 x 2 wires	ACSR, 810 mm^2 x 8 wires	ACSR, 630 mm^2 x 8 wires

Resistance of conductor	0.112 Ω/km	0.0356 Ω/km (per wire)
Relative permittivity	5	1
Rated voltage	1100 kV	
Current for energized line	4000 A, 6000 A, 8000 A	
Transmission line length	125 km, 250 km (Tower 1, Tower 2, Tower 3), 200 km (Tower 1)	

Electromagnetically induced current switching

The calculation was carried out by assuming a 125 km or 250 km un-transposed transmission line and a load current in the range from 4000 A to 8000 A for one operating line with a double transmission line configuration. The other line was in de-energized condition. The calculation for a 200 km un-transported transmission line of tower 1 design was also carried out. The simulation model of EM induced current switching is shown in figure 4.4.6.

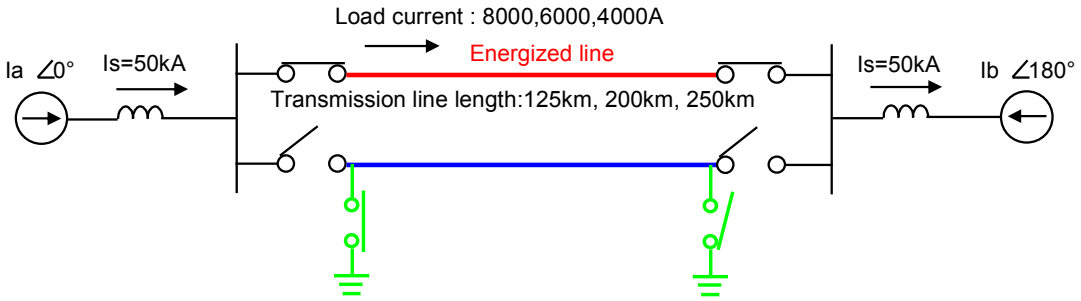

Figure 4.4.6 Simulation model of electromagnetically induced current switching for 1100 kV ES

The maximum current, recovery voltage, and RRRV obtained from the calculation are shown in table 4.4.7, figure 4.4.7 and figure 4.4.8. Typical waveforms of transient recovery voltage are shown in figure 4.4.9.

Table 4.4.7 Results of electromagnetically induced current switching for 1100 kV ES

Line Length[km]	Load Current	EM Induced current			Recovery Voltage			RRRV		
		Tower1	Tower2	Tower3	Tower1	Tower2	Tower3	Tower1	Tower2	Tower3
125	4,000	446	591	732	20.2	28.5	33.9	58.9	81.5	98.2
	6,000	669	887	1,098	30.4	42.7	50.9	88.3	120.8	147.0
	8,000	892	1,182	1,464	40.5	56.9	67.8	117.8	161.1	196.6
200	4,000	446	-	-	32.8	-	-	59.3	-	-
	6,000	669	-	-	49.3	-	-	89.0	-	-
	8,000	892	-	-	65.7	-	-	119.5	-	-
250	4,000	447	599	738	41.5	58.9	70.1	67.8	81.3	93.5
	6,000	671	898	1,108	62.2	88.3	105.1	87.2	121.1	141.0
	8,000	895	1,197	1,477	82.9	117.8	136.3	115.6	161.6	188.1

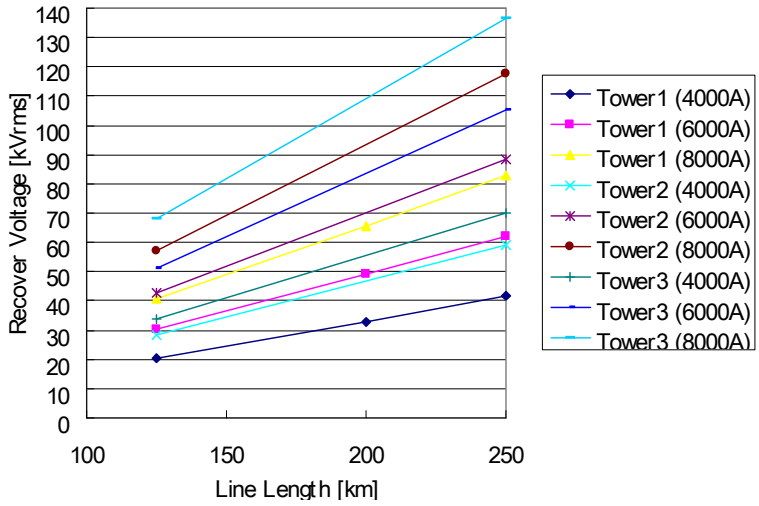

Figure 4.4.7 Relationship between line length and recover voltage

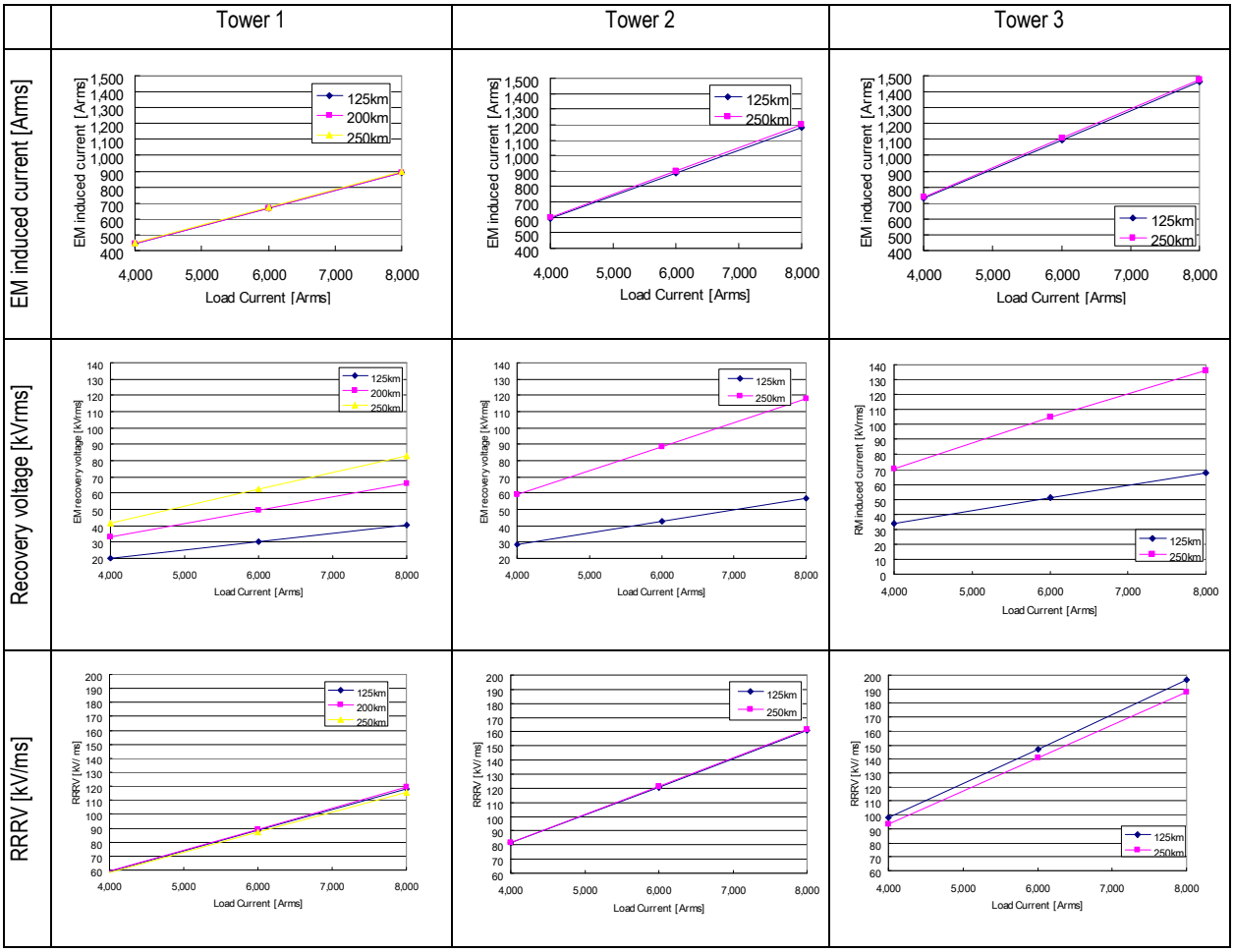

Figure 4.4.8 Results of electromagnetically induced current switching for 1100 kV ES

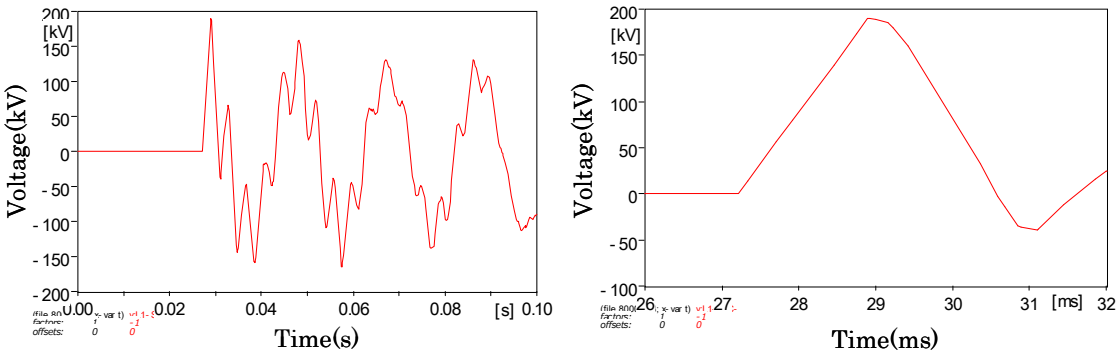

Figure 4.4.9 Typical wave form of recovery voltage of electromagnetically induced current switching (left: overall, right: enlarged)

Electrostatically induced current switching

By using the same configuration and parameters the electrostatically induced currents were calculated. The simulation model of ES induced current switching is shown in figure 4.4.10. The maximum recovery voltages are shown in table 4.4.8.

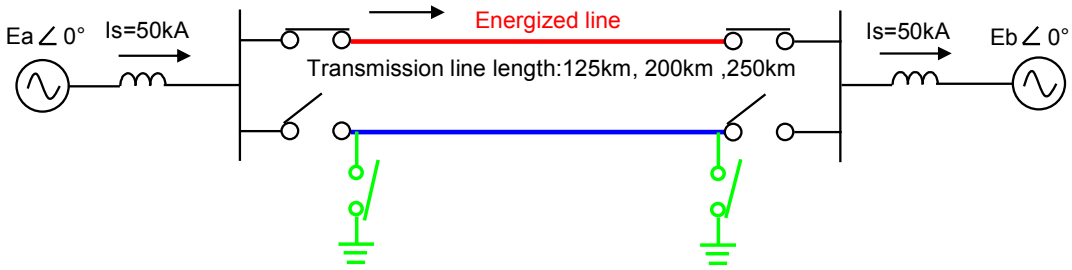

Figure 4.4.10 Simulation model of Electrostatically induced current switching for 1100 kV ES

Table 4.4.8 Results of electrostatically induced current switching for 1100 kV ES

Line length (km)	ES recovery voltage [kVrms]		
	Tower 1	Tower 2	Tower 3
125km	40.3	-	-
250km	40.1	43.5	69.8

4.4.3 Recommendations for specifications

For the UHV ES, the characteristics of the induced current should be estimated individually because of the difference in the conditions, such as the rated current, the configuration of the transmission towers and the length of the parallel transmission lines. As WG A3.22 has not yet enough information on induced voltages and currents on UHV OH-lines, any conclusion is too premature. Further investigations are necessary to give recommendations.

References

[1] CIGRÉ Brochure 35 WG 33/13-09: "Monograph on GIS Very Fast Transients", July 1989

[2] CIGRÉ Brochure 362 WG A3.22: H. Ito (Convenor), A. Janssen (Secretary), J. Amon F., S-W. Bahng, M. C. Bhatnagar, P. Boss, J. Brunke, E. Colombo, R. Diaz, D. Dufournet, Y. Filion, P. C. Fernandez, R. Gorur, A. Gilboulet, J. Jäger, A. Keri, T. Kobayashi, M. Kosakada, E. Kynast, A. Lokhanin, C. van der Merwe, M. de Nigris, V. Rashkes, D. Peelo, B. Richter, H-D. Schlemper, B. Shperling, Y. Shirasaka, R. Smeets, L. Stenström, M. Waldron, A. Wiersma, J-W. Woo, Y. Yamagata, Yao Sili, R. Yeckley, T. Yokota, L. van der Zel: "Technical Requirements for Substation Equipment Exceeding 800 kV - Field experience and technical specifications of Substation equipment up to 1200 kV", December 2008, ISBN : 978-2 85873-049-0

[3] CIGRÉ Brochure WG B3.22: T. Yokota (Convenor), J. Kim (secretary), J. Fan, P. Fitzgerald, M. Ono, F. Gallon, H. Ito, T. Kobayashi, H. Schlemper, Y. Won, R.K. Sarkar, W.Christian, K. Uehara, Y. Shirasaka, K. Sasamori, Z. Lai, A. Amod, U. Krüsi "Technical Requirements for Substation Exceeding 800 kV", to be published in 2009

[4] IEC 62271-102, High-voltage switchgear and controlgear – Part 102: Alternating current disconnectors and earthing switches, First edition 2001-12

[5] Ban Liangeng, Xiang Zutao, Wang Sen, Lin Jiming, Wang Xiaogang, Zheng Bin, Wang Xiaotong: "Estimation of VFTO for GIS and Hybrid-GIS of China 1000 kV UHV pilot project and its suppressing countermeasures"; IEC/CIGRÉ UHV Symposium, Beijing, China, July 18-21, 2007, paper 2-3-4

[6] Riechert, U.; Holaus, W.; Krüsi, U.; Sologuren, D. "Gas-Insulated Switchgear for 1100 kV - Challenges in Development and Testing", CIGRÉ 6th Southern Africa Regional Conference, Joint Colloquium of CIGRÉ Study Committees A2 / A3 / B3, 2009, Somerset West, Western Cape, 17 - 21 August 2009, South Africa

[7] Ban Liangeng, Xiang Zutao, Wang Xiaogang, Lin Jiming, Sun Gang , Zheng Bin: "Research on Very Fast Transient Overvoltage (VFTO) for 1000kV UHV Gas Insulated Station (GIS) of China", 2006 Int. Conference of UHV Power Transmission Technology, Peking, 2006, 27th to 29th Nov 2006, proceedings, pp. 258-262

[8] Riechert, U.; Krüsi, U.; Holaus, W.; Sologuren, D.: "Gasisolierte Schaltanlagen für 1100 kV – Herausforderungen an Entwicklung und Prüfung"; (in German) Stuttgarter Hochspannungssymposium 2008, 05.-06. März 2008, Stuttgart, 2008, Tagungsband, S. 219-234, haka print und medien GmbH, ISBN 978-3-00-024098-0

[9] Holaus, W.; Riechert, U., Sologuren, D.; Krüsi, U.: "Development and Testing of 1100 kV GIS"; The second IEC – CIGRÉ International Symposium on International Standards for UHV Transmission, 29-30 January 2009, New Delhi, India, proceedings pp. 128-141

[10] Ito, H.; Janssen, A.; Dufournet, D.; van der Merwe, Ch.; Filion, Y.; Peelo, D.; Bhatnagar, M. C.; Riechert, U.; Fernandez, P.; Yoshibumi, Y.; Shaowu Wang (On behalf of CIGRÉ WG A3.22) "System Impacts on UHV Substation Equipment"; The second IEC – CIGRÉ International Symposium on International Standards for UHV Transmission, 29-30 January 2009, New Delhi, India, proceedings pp. 95-107

[11] Yamagata, Y.; Nakada, Y.; Murayama, Y.; Hirasawa, K.; Yoshizumi, T.: "Field Test of 1000 kV Gas Insulated Switchgear", CIGRÉ Report 13-209, 38th CIGRÉ Session, Aug. 27 to Sept. 1, 2000, Palais des Congrès de Paris, Paris, France

[12] Hemmi, R.; Shinohara, R.; Kitazumi, Y.; Yatsuzuka, H.; Hirasawa, K.; Yamagiwa, T.: "Evaluation of VFTO (Very Fat Transient Overvoltage) and Its Reduction by Parallel Resistor during Switching Operation of Disconnecting Switch in Future UHV Gas

Insulated Substations", 2006 Int. Conference of UHV Power Transmission Technology, Peking, 2006, 27th to 29th Nov 2006, proceedings, pp. 460-466
[13] Baik, S.D.; Kim, J.H.; Kim, S.H.; Choi, Y.S.; Lee, D.I.; Bang, M.J.: "An Introduction of KEPCO's 765kV AC Transmission System", 2006 Int. Conference of UHV Power Transmission Technology, Peking, 2006, 27th to 29th Nov 2006, proceedings, pp.24-31
[14] Holaus, W.; Krüsi, U.; Sologuren, D.; Riechert, U.; Keller, M.: "Testing of GIS components at 1000 kV rated voltage"; CIGRÉ Report A3-202, 42nd CIGRÉ Session, August 24-August 29, 2008, Palais des Congrès de Paris, Paris, France
[15] Ardito, A.; Colombo, E.; Cova, B.; Giorgi, A.; Manzoni, G.; Paris, L.; Santagostino, G.: "Open aspects and possible alternative technologies following the UHV 1000kV Italian experience", IEC/CIGRÉ UHV Symposium, Beijing, China, July 18-21, 2007, paper 1-1-2
[16] Yamagata, Y., Kobayashi, A.;Yoshizumi, T.; Tsubaki, T.: "Development of 1100 kV GIS – Gas Circuit-breakers, Disconnectors and High Speed Grounding Switches", CIGRÉ Report 13-304, 36th CIGRÉ Session, Aug. 25 to 31, 1996, Palais des Congrès de Paris, Paris, France
[17] Yamagata, Y.; Tanaka, K.; Nishiwaki, S.; Takahashi, N.; Miwa, I.; Komukai, T.; Imai, K.: "Suppression of VFT in 1100 kV GIS by Adopting Resistor-Fitted Disconnector", IEEE Transaction on Power Delivery, Vol.11, No.2, April 1996; pp. 872-880
[18] Yamagata, Y.; Nakada, Y.; Nojima, K., Kosakada, M.; Ozawa, J.; Ishigaki: "Very Fast Transients in 1000kV Gas Insulated Switchgear", IEEE Transmission and Distribution Conference, 1999 IEEE, 11-16 Apr 1999, proceedings, Vol. 2, pp 501 - 508
[19] CIGRÉ Working Group 15.03: "GIS Insulation Properties in Case of VFT and DC Stress", CIGRÉ Report 15-201, 36th CIGRÉ Session, Aug. 25 to 31, 1996, Palais des Congrès de Paris, Paris, France
[20] Fröhlich, K.; Eriksson, A.: "Special phenomena in high-voltage GIS", ABB publication 1004, 1995
[21] Martinez, J.A.; Chowdhuri, P.; Iravani, R.; Keri, A.; Povh, D: "Modelling Guidelines for Very Fast Transients in Gas Insulated Substations", IEEE Special Publication Modelling and Analysis of System Transients using Digital Programs, Prepared by IEEE PES Working Group 15.08.09, 1998
[22] Nakamura, A.; Taniguchi, H.; Yokoyama, A.: "1100 kV AC Transmission Project in Japan", IEC/CIGRÉ UHV Symposium, Beijing, China, July 18-21, 2007, paper 1-2-1
[23] Kobayashi, T.; Ono, M.; Shimomura, T.; Yokota, T.: "Basic design / specifications of GIS for UHV AC and its verification test at site", IEC/CIGRÉ UHV Symposium, Beijing, China, July 18-21, 2007, paper 2-3-3
[24] Yokota, T.; Kim, J.; Fan, J.; Ono, M.; Gallon, F.; Kobayashi, T.; Sarkar, R.K.; Uehara, K.; Sasamori, K.: "Consideration for UHV substation and Recommendation", The second IEC – CIGRÉ International Symposium on International Standards for UHV Transmission, 29-30 January 2009, New Delhi, India, proceedings pp. 119-127
[25] Yamagata, Y.; Okabe, S.: "Utility's experience on design and testing for UHV equipment in Japan", The second IEC – CIGRÉ International Symposium on International Standards for UHV Transmission, 29-30 January 2009, New Delhi, India, proceedings pp. 142-154
[26] Kobayashi, T.; Sun, G.; Yokota, T.; Sasamori, K.; Yamagiwa, T.: "Compactness and High-reliability Technology for UHV Circuit-breakers, disconnectors and earthing switches", The second IEC – CIGRÉ International Symposium on International Standards for UHV Transmission, 29-30 January 2009, New Delhi, India, proceedings pp. 169-177

[27] Kobayashi, A ; Murayama, Y., Ohyama, S.; Kan, M.: “Development and Verification Test of 1100 kV Gas Insulated Switchgear”, 2005 Int. Workshop of UHV Transmission Technology, Peking, April. 25-28, 2005, proceedings, pp. 94-99
[28] Peelo, D.F.; Smeets, R.P.P.; Kuivenhoven, S.; Krone, J.G.: “Capacitive Current Interruption in Atmospheric Air”, CIGRÉ SC A3 & B3 Joint Colloquium, Tokyo, 2005, paper 106
[29] Shimoda, N. ; Taguchi, K.; Nemoto, T.; Kobayashi, M.; Hashimoto, A.; Ozawa, J.; “Suppression of Very Fast Transient Overvoltages across Insulating Flange of 1000 kV GIS”, 11th Int. Symposium on High Voltage Engineering, (ISH`99), London, UK, August 22-27, 1999, Conference Publication No. 467
[30] Weidong, L.; Zhutao, X.; Jiali, Q.: “Simulation Tests of Suppressing VFT in GIS by Magnetic Rings”, Proceedings of the XIVth International Symposium on High Voltage Engineering, Tsinghua University, Beijing, China, August 25-29, 2005, paper J-51
[31] IEC 62271-110, High-voltage switchgear and controlgear – Part 110: Inductive load switching, edition 2.0, 2009-01
[32] IEC 62271-203, High-voltage switchgear and controlgear – Part 203: Gas-insulated metal-enclosed switchgear for rated voltages above 52 kV, edition 1.0, 2003-11
[33] Ji Jiaqin “Analysis of very fast transient overvoltage in GIS”, Journal of tsinghua univeristy, Vol.34 No.1 1994, page 73-82.
[34] Povh, D.; Schmitt, H.; Völcker, O.; Witzmann, R. “Modelling and analysis gridelines for very fast transients”, IEEE Transactions on power delivery, Vol.11, No.4, October 1996, page 2028-20
[35] Ban Liangeng, Lin Jiming, Xiang Zutao, et.al.: “Very fast transient overvoltage analysis for GIS and Hybrid-GIS of China 1000kV UHV pilot project”, Technical Report. China Electric Power Research Institute, Beijing. 2006.
[36] Yanabu, S., Murase, H., et.al.: “Estimation of fast transient overvoltage in gas-insulated substation”, IEEE Transactions on Power Delivery. Vol.5, No.4, 1990.
[37] The Tokyo Electric Power Company, Inc.: “Disconnector Overvoltage Analysis”, Technical Report 2005.
[38] Du Shuchun, Zhang Cuixia, Ge Dong: “Lightning protection for 1000kV UHV AC substation and switching station”, Technical Report, China Electric Power Research Institute, Beijing. 2006.
[39] Yamagata, Y.; Tanaka, K.; Nishiwaki, S. et.al: “Suppression of VFT in 1100kV GIS by adopting resistor-fitted disconnector”, IEEE/PES Summer Meeting 95 SM 499-4 PWRD. 1995, page 534-539
[40] Tanaka, K.; Miwa, I.; Fujiwara, K.; Yokota, T.: “Development of 1000kV Disconnectors (in Japanese)”, IEE of Japan, The technical meeting on Power and Energy div. (Div B), 1994 No.562
[41] Electric Technology Research Association, Rationalization of insulation design, Electric Technology Research Vol. 4, No. 3, 1988
[42] IEEJ, Co-ordination of insulation between very fast transient serge and GIS, Technological report No. 32, 1990
[43] Grandl, J.; Ericsson, A., Meppelink, J.; Merve, C.v.D.: ”Studies of Very Fast Transients (VFT) in a 765 kV Substation“, CIGRÉ Report 33-13, CIGRÉ Session, Aug. 28 to Sept. 3, 1988, Palais des Congrès de Paris, Paris, France
[44] Yanabu, S. et al,: “Estimation of Fast Transient Overvoltage in Gas Insulated Substation”, IEEE 88SM 628-0 (1988)
[45] Riechert, U.; Holaus, W.; Krüsi, U.; Sologuren, D. ”Design and Test of Gas-Insulated Circuit-Breaker and Disconnector for 1100 kV“, 2009 International Conference on UHV Power Transmission, May 20-22, 2009 Beijing, China

5 Equipment Requirements (MOSA)

5.1 Introduction

Relatively detailed technical specifications for arresters have been published for the different UHV projects in Italy, Russia, China, India and Japan. The information has been collected by the WG and the most important requirements for arresters are summarized in Tables 5.1.1 to 5.1.5 [1]. Regarding the project in Italy it must be noted that it was finished before the high-performance arresters of today were available which explains the higher protection level as per Table 5.1.3. This is to some extent also true for the Russian project. Modern gapless Metal Oxide surge arresters were available just before the closing down of this UHV network. In Japan work has been carried out over an extended period with testing and development of high-performance arresters mainly for GIS stations. It is therefore natural that in the Chinese specifications the same protection levels as in Japan are given. However, in China AIS arresters also are considered; adding additional parameters which must be taken into account in the specifications.

In India a higher system voltage is selected; 1200 kV compared to 1100 kV in Japan and China. The protection requirements for the Indian arresters have been varying somewhat over time, reflecting a development and trial phase, but seems now to have been settled and they are set more challenging than for the other projects as shown by Tables 5.1.2 and 5.1.3. Considering that mainly AIS arresters have been discussed for India the stipulated performance data is even more demanding.

Table 5.1.1 Rated and continuous operating voltages specified for arresters [1]

UHV project	Rated voltage, U_r [kV]	p.u. of Um/√3	Continuous operating voltage,U_c [kV]	p.u. of Um/√3	U_c/U_r
Russia			694	1.00	
Japan	826	1.30	635	1.00	0.77
China	828	1.30	638	1.00	0.77
India	850	1.23	723	1.04	0.85
Italy	750	1.24	607	1.00	0.81

Table 5.1.2 Protection levels specified for slow-front overvoltages [1] [2] [3]

UHV project	Co-ordinating current (wave shape 30/60 μs) [kA]	Protection level [kV]	Protection level	
			p.u. of $U_m/\sqrt{3}*\sqrt{2}$	p.u. of U_r
Russia	2.8	1570	1.60	
Japan*	(2)	(1440)	(1.60)	(1.74)
China	2	1460	1.63	1.76
India	2	1500	1.53	1.76

** Co-ordinating current is not officially specified at present. (Calculated value of switching surge by analysis is 1 kA or below.)*

Table 5.1.3 Protection levels specified for fast-front overvoltages [1] [2]

UHV project	Co-ordinating current (wave shape 8/20 μs) [kA]	Protection level [kV]	Protection level	
			p.u. of $U_m/\sqrt{3}*\sqrt{2}$	p.u. of U_r
Russia	15	1764	1.80	
Japan	20	1620	1.80	1.96
China	20	1620	1.80	1.96
India	20	1700	1.74	2.0
Italy	20	1750	2.04	2.33

Table 5.1.4 Energy requirements [1]

UHV project	Energy TOV [MJ]	Energy switching surges [MJ] [kJ/kV(U_r)]	Total energy rating [MJ]
Russia		40	
Japan	55	20 [24]	55
China		20 [24]	40 (2*20)
India	35	10 [12]	55
Italy			17

Table 5.1.5 TOV requirements [1] [2] [3]

UHV project	TOV amplitude (prospective) [p.u.]	TOV duration [seconds]
Russia	1.1 1.3 1.4	1200 3 0.05
Japan	1.5*)	0.55*)
China	1.4	0.35
India	1.4	0.46

**) Approximate values corresponding to the energy absorption of 55 MJ. Note that the amplitude is not prospective but the resulting with the effect of the arrester included.*

The requirements on the industry to deliver the arresters with the specified protection levels, energy and voltage withstand capabilities are in many cases demanding. Significant work is foreseen for standardisation bodies to specify relevant test procedures which can verify performance and provide information regarding acceptable short and long term performance of the arresters.

5.2 Background of technical requirements

The technical requirements reflect a desire for very active use of the arresters to limit overvoltages to the lowest possible levels. In Japan it has also been a clear strategy to use high-performance arresters to limit stresses on the breakers. The insulation levels for equipment are also set lower in Japan, with less margin to arrester protection levels from the detailed insulation co-ordination study, than e.g. in China and India.

In order to obtain low protection levels the arresters are designed utilizing large diameter metal-oxide varistor blocks in several parallel columns. Compared with e.g. 800 kV arresters, approximately 4 times the block area is applied for the UHV arresters. A consequence of these low protection levels is that TOV may be more decisive and may result in high energies. On the other hand, TOV in UHV systems must be controlled carefully but it is notable that, at leat for Japan and India, the stresses under severe TOV conditions have defined the energy ratings.

In Japan, to ensure the high security of the UHV system, a contingency of very severe out-of-phase conditions of a 500kV system connected to the UHV system, which results in load rejection followed by a ground-fault, was considered. This leads to very high TOV amplitudes with a requirement of 55 MJ in arrester energy capability (Table 5.1.5).

In China the given TOV cannot give such high energies and the specified energy requirements are related to switching surges, as is also the case in Russia.

In India a decisive event is given comprising both TOVs as well as switching surges. The calculations indicate that the main energy is due to TOV. The TOV amplitude, 1.4 p.u., is the same as for China but due to relatively lower protection levels in India the energy will be higher.

Regarding energy from switching surges, in some specifications reference is made to IEC line discharge class 5 presumably due to that this is the highest class in the existing standard. However, this equates to approximately 5 to 7.5 kJ/kV rated voltage which generally is much less energy than found stipulated in the specifications to cover the switching events.

5.3 Recommendations for specifications

The recommendations given here take into consideration that the existing IEC standard to some extent does not cover requirements for UHV arresters. Special attention therefore is necessary for certain requirements and in particular regarding how to specify operating duty conditions correctly. The items which are not considered to be fully covered by the existing standard are as follows:

- Arrester classification
- Insulation withstand tests
- Long-duration current impulse withstand – line discharge test parameters
- Switching surge operating duty test
- Test procedures for multi-column arresters
- Short-circuit test
- Voltage grading

5.3.1 Arrester classification

The IEC standard now covers rated voltages up to an including 756 kV. The maximum standardised nominal discharge current is 20 kA and maximum peak current for switching impulse residual voltage test is 2 kA (for 20 kA arresters).

Higher rated voltages in the range up to approximately 900 kV will be required for 1100 to 1200 kV systems but from preliminary studies it seems that a need for higher nominal currents than 2 kA for switching surges and 20 kA for lightning are not necessary. Classifying currents of 2 kA for switching surges and 20 kA for lightning are therefore suitable also for UHV arresters.

5.3.2 Rated voltage and TOV capability

It is recommended not to specify rated voltage exactly, but instead prospective temporary overvoltages with amplitude and duration. The short-circuit impedance seen from the arrester point of installation is also important to specify. High TOV conditions normally occur under weak system conditions with relatively high short circuit impedances. Prospective arrester energy, therefore, may be heavily overestimated if a TOV behind an infinitely low impedance is assumed. A detailed knowledge of the arrester voltage-current characteristics is necessary and this, in general, is only known by the manufacturer. It is therefore better to request that the final performance of the arrester shall be verified in a type test including TOV conditions than try to calculate the energies during a TOV event and then specify this energy to be generally applicable irrespective of arrester make and design. However, preliminary calculations to check relative stresses for different events may be necessary. Preliminary characteristics may also be used to evaluate TOVs for insulation coordination design.

Typically, except if very severe conditions are considered, withstand against TOV amplitudes of 1.3 p.u. to 1.4 p.u. seems to be a realistic requirement. In order to control overvoltages as much as possible arresters are foreseen to be installed at several locations in a UHV station: line entrance, bus, transformers and CB terminals. Hence an opportunity exists to apply different rated voltages for the arresters in the same station. One scenario may be that an

arrester with a lower rated voltage, i.e. a lower TOV capability than the others, is used as a sacrificial arrester in the lower voltage system connected to the UHV system if a severe low-probability TOV does occur in the lower voltage system.

5.3.3 Continuous operating voltage

Voltage grading of arresters becomes more difficult the taller the arresters are. It is therefore very important that the continuous operating voltage is not specified to be higher than necessary. Normally a higher U_c than $U_m/\sqrt{3}$ is not required. If a higher U_c than $U_m/\sqrt{3}$ is used and/or proposed by the manufacturer, a detailed test procedure must be specified to clearly define what is meant with the U_c requirement. Under normal operating conditions, i.e. well below highest ambient temperature and without energy loading equal to rated energy, an arrester may very well be subjected to a voltage in excess of $U_m/\sqrt{3}$ without risking thermal run-away even if the continuous operating temperature of the arrester is well above ambient. However, at a higher ambient temperature and pre-loaded by energy discharges or TOV, the same arrester may not be thermally stable.

5.3.4 Energy capability

Energy requirements arise mainly from switching and TOV events since lightning may not result in decisive energies for UHV arresters due to the very big volume of metal-oxide varistor blocks. Arrester energy from switching events is quite easily calculated. But, as discussed above, TOV energies are more difficult to estimate correctly and therefore TOV requirements, in general, should be specified with prospective amplitudes, durations and equivalent impedance during the event.

Furthermore, the energy requirements should be set from a realistic need and not from the size of the metal-oxide block volume. As discussed earlier the low protection levels targeted, result in a big area and volume of metal-oxide varistor blocks. It could then be tempting to specify energy requirements based on this and not from realistic cases. In UHV systems several other measures to limit switching surges on lines will be used, for example single-phase re-closing and pre-insertion resistors. This will in turn limit the switching surge energy requirements on the arresters.

5.3.5 Insulation withstand

For 10 and 20 kA arresters with rated voltage 200 kV and above the existing IEC standard specifies a lightning impulse withstand voltage of 1.3 times the lightning impulse protection level (LIPL) and a switching impulse withstand voltage of 1.25 times the switching impulse protection level (SIPL). These factors include an altitude correction factor, K_a, of 1.13 as calculated from the formula $K_a = e^{m(H/8150)}$ taking into consideration an altitude of 1000m and with the m-factor set equal to 1. For UHV arresters in AIS the factor for switching impulse withstand voltage should be reconsidered since the m-factor gives a significant reduction for the required withstand voltage levels in the UHV range. If an m-factor of 1 is kept, the requirement for arrester insulation will be higher than for other equipment for which an m-factor is taken into account.

In addition, the standard specifies tests on individual units only. Tests on complete arresters are “under consideration”. Tests on units of arresters and summing up the results on units to obtain the withstand voltage on the complete arrester is questionable for arresters without grading rings and wrong if the arrester is equipped with a grading ring which physically reduces the overall distance phase-to-earth. A linear summation of switching withstand

voltages of units is, in addition, not correct for tall arresters. The insulation requirements for arresters should be verified by tests on complete arresters installed in conditions which are as close as possible to the real conditions and the following is suggested:

- $LIWV = 1.3 \times LIPL$
- $SIWV = 1.17 \times SIPL \left(m - factor = 0.5\right)$

The requirements are considered to be valid up to 1000 m in altitude above sea level.

When the insulation requirements of UHV arresters determined from the above are still higher than that of the protected equipments, it may be reasonable to select the same insulation levels as that of the protected equipments.

5.3.6 Protection levels

For fast-front and slow-front overvoltages protection levels around 1.8 p.u. and 1.6 p.u. defined at 20kA with wave shape 8/20 μs and 2 kA with wave shape 30/60 μs respectively, are realistic values. Even lower levels may be possible if TOVs are limited to below approximately 1.3 p.u. If TOVs are low the decisive factor would be how high a ratio U_c/U_r is possible to be applied on the arrester. This is dependent on arrester design, voltage grading and power losses of the metal-oxide varistors.

5.3.7 Voltage grading

A sufficiently linear voltage grading of an arrester is, of course, more difficult to obtain the taller the arrester is. With only grading rings as a measure to control voltage distribution for AIS arresters, the down-hang and diameter of the rings would be enormous to obtain a sufficiently linear voltage distribution. This would also lead to other problems like e.g. limitations on phase-to-phase clearances. Additional grading capacitors, therefore, are foreseen in many designs. Multiple column metal-oxide varistors improve the self-grading of the arresters but may cause severe thermal problems when block columns are placed in the same housing. One recommended way to check that the voltage grading is sufficient is to measure the temperature on the metal-oxide blocks under steady state conditions when the complete arrester is energized at U_c. When performed single phase in a test laboratory an equivalent installation should be arranged, which could be based on field calculations.

Since normally it is not possible to test a complete UHV arrester at an elevated ambient temperature an average temperature rise above ambient is calculated from the test and added to the specified highest ambient temperature in order to constitute a preheating temperature to be used in an operating duty test.

With respect to possible ageing of the metal-oxide varistors the local highest voltage stress anywhere in the arrester must be considered. This could be determined from accurate field calculations but it could also be assumed that the highest stress anywhere in the arrester must be close to the “knee-point” of the characteristic. Accelerated ageing tests performed on the metal-oxide varistors with a voltage level at, or only a few percent below, the “knee-point” therefore is recommended.

5.3.8 Short-circuit performance

Rated short-circuit currents up to 80 kA_{rms} are given in the IEC standard. This will cover actual fault currents also for UHV arresters. However, the AIS arresters will be extremely tall and comprise several stacks of units in series and possibly also in parallel. An electrical failure of the arrester followed by a high short-circuit current may lead to the whole stack of

insulators collapsing. This would be within acceptable passing criteria according to the standard but it also must be considered what is acceptable in a UHV station. Additional stringent requirements may be more appropriate in this case e.g. to require a mechanical integrity after an overloading and subsequent passage of short-circuit current.

Some manufacturers use SF_6 gas also in AIS arresters. Apart from the concern of long-term leakage of SF_6 and contribution to the green-house effect,t some of the tests in the existing standard will be very difficult to perform with SF_6-filled insulators. In particular for short-circuit current tests the type of gas has a significant effect on the performance. To perform the test with air or nitrogen inside the arrester therefore may not be representative of true performance. This must be considered by the user and the user must state if SF_6 as a filling gas in AIS arresters is acceptable or not. Similarly, the manufacturer must clearly state the type of gas, if any, they use in their AIS arresters.

5.3.9 Mechanical requirements

Due to the size and weight of UHV arresters mechanical requirements may be very demanding; including seismic performance. Static and dynamic loads must be specified and/or possible maximum wind velocity and maximum loads in connectors. The modal difference between porcelain and polymeric designs for AIS applications must be considered. It may also be considered to install polymeric AIS arresters hanging from the bus in the station in order to limit the mechanical stresses.

A seismic verification is considered as necessary for arresters located in seismic active areas. Relevant standards for seismic testing are e.g. IEC 62271-207-2007, IEC 62271-300-2006, IEEE 693-2005 and GB 50260-1996.

5.3.10 Verification tests

It is important to carefully specify important tests which are not covered by the existing IEC standard. The test to verify correct operating duty may be the most important. This test should comprise a verification of thermal recovery after highest specified energy and TOV duty under the most severe ambient conditions and with highest operating voltage applied. Since multiple column arresters normally are not foreseen in the IEC standard but are a “must” for UHV arresters some specific points to consider are discussed below. (In the near future this may be covered by the IEC standard since work is under progress within MT 4 of TC37)

5.3.10.1 Long-duration current impulse tests

The energy capability of 10 and 20 kA arresters is verified by line discharge tests. Five classes 1 to 5 exist which correspond to increasing discharge requirements. For a ratio of 2 between the switching impulse residual voltage and the rated voltage the classes approximately correspond to 1, 2, 3, 4 and 5kJ/kV rated voltage. For lower relative protection levels the energy will be higher e.g. for commonly used protection levels the LDC 5 (line discharge classification) test results in arrester energies in the range 5 to 7.5 kJ/kV rated voltage.

For UHV arresters much higher energies in kJ/kV rated voltage are indicated in the specifications. An extended line discharge classification therefore may be necessary. Even better would be the introduction of a new energy withstand test which is not depending on transmission line parameters but instead having a defined current impulse shape and with specified classes in kJ/kV rated voltage. Specifications for UHV arresters indicate arrester energies for switching surges in the order of 20MJ in single shots. Energy tests with up to 20-30kJ/kV rated voltage, therefore, should be introduced.

However, the energy requirements stated in the specifications should also be critically analyzed. In many applications it may be sufficient with the existing line discharge classes. Transmission line lengths considered for the different UHV projects are as per Table 5.3.1.

Table 5.3.1 Transmission line lengths [2] [4] [5]

UHV project	Line length, [km]
Russia	300-700
Japan	240
China	359
India	450

LDC 5 corresponds to a line length of 480 km and, with the exception of the longest Russian lines, all the UHV lines are within this length. Considering that the lines are compensated and that single-phase re-closing is applied, the energy absorbed by the arresters, will be within the requirements for LDC 5 [2]. The use of pre-insertion resistors will further decrease the arrester duties. However, if the arrester for some reason must withstand a 3-phase re-closing without pre-insertion resistors the energy requirements as per LDC 5 are well exceeded if flashovers along the transmission line do not occur.

5.3.10.2 Switching surge operating duty test – preheating temperature

In IEC an operating duty test is prescribed with preconditioning by current impulses followed by preheating to 60 ºC in a thermally correct model of the arrester. Thereafter thermal stability is checked by application of two line discharges of the relevant line discharge class followed by rated voltage for 10 s and finally maximum continuous operating voltage during at least 30 minutes to prove thermal stability.

The preheating to 60 ºC is intended to cover an ambient temperature of 40 ºC, solar radiation, self heating and some influence of pollution on the arrester housing.

60 ºC in preheating is, in general, sufficient for single column arresters which are used up to 800kV systems and for standard requirements. However, to obtain very low protection levels and meet high energy requirements multi-column arresters with large diameter metal-oxide blocks are necessary at UHV. In addition, highest possible continuous operating voltage in relation to the reference voltage (i.e. the "knee-point") on the voltage-current characteristics is desirable to achieve lowest possible protection levels. The power losses and self-heating of such arresters, therefore, may be significant; particularly for arresters for AIS where SF_6 gas (at high pressure) generally is not used. A new test therefore is necessary for UHV arresters, and indeed for all multicolumn arresters, to establish the correct preheating temperature in the operating duty test or to verify that 60 ºC is sufficient. Before an IEC test procedure is available it is therefore suggested that the average temperature increase above any given ambient is checked on a complete arrester energised at U_c. The temperature above ambient is thereafter added to maximum ambient temperature and shall be used as the preheating temperature in an operating duty test.

5.3.10.3 Requirements for multiple-column arresters

Line discharge tests (or a new energy withstand test) may be performed on single columns, however maximum non-linearity in current sharing between the columns must be taken into account. If the test is performed on test sections with multiple columns the discharge energy must be increased by a factor β_g/β_a where β_g is the guaranteed current sharing factor and β_a is the actual current sharing factor for the test section. If the test is performed on single columns

the energy shall be increased by a factor β_g. Furthermore, a thermal model should contain the highest number of parallel columns which is assembled within one arrester unit housing for the actual design and thermal stability in operating duty tests must be verified on such a section. In IEC 60099-4 it is now stated that a thermal model shall represent a sliced portion of the active part of the arrester being modelled. However, thermal equivalency may not always be possible to obtain for such a model and in particular not for a multi-column design.

5.3.10.4 Grading components

Internal grading capacitors may be used instead of, or as a complement to, grading rings. Similarly grading hoods may be used for both GIS and AIS arresters. The IEC standard lacks tests on grading components and it is stated that "Requirements for internal and external grading components are under consideration". However, operating duty tests should be specified to be performed with the grading components included in the test sections and suitable accelerated ageing tests should be designed for the components. Verifications both before and after the tests should be specified to check for significant changes.

5.3.10.5 Pollution

Pollution on external insulation of a metal-oxide surge arrester may constitute a risk regarding:

a) External flashover

b) Partial heating of the internal active parts

c) Internal partial discharges

However, only a test procedure to check the risk for partial heating of the internal active parts is specified by the existent IEC standard and only for porcelain-housed arresters.

Artificial pollution tests may give some verifications regarding risk of internal partial discharges but in general a long-term test is necessary like the weather ageing test during 1000 or 5000 hours specified for polymer-housed arresters in IEC 60099-4.

Risk of external flashover may be checked by any suitable method used for testing of insulators with respect to pollution.

5.4 Conclusions

A very active use of high-performance arresters to limit overvoltages to lowest possible levels is seen to be one of the most important conditions for the insulation coordination in UHV systems. However, the requirements on the arresters with respect to protection levels, energy and voltage withstand capabilities are demanding for the industry. This in turn shows the importance to develop the standards such that they also consider the arresters for UHV. To some extent it is only to extend the classification system to cover the higher voltage levels but some features are more specific for UHV arresters and need special attention. Items, which are not considered to be fully covered in existing standards, plus a short recommendation for action, are as follows:

(1) Arrester classification

- Existing system must be extended.

(2) Insulation withstand test

- Requirement on SIWV must be in line with requirements for other equipment.

(3) Long-duration current impulse withstand (energy withstand tests)

- The classification system must be extended or, better, a new energy withstand test introduced to cover the much higher energies normally specified for UHV arresters.

(4) Switching surge operating duty test

- Must be reconsidered with respect to, in particular, multi-column arresters.

(5) Test procedures for multi-column arresters

- Energy withstand and thermal tests must be reconsidered with respect to multi-column designs.

(6) Short-circuit and mechanical tests

- The very tall structure of AIS arresters should be considered.

(7) Voltage grading

- Methods to check the voltage grading and the possible components used for grading like external and/or internal grading capacitors should be considered.

(8) Pollution

- It should be further investigated if special test procedures are necessary for surge arresters taking into account other risks than the risk of flashover like heating and internal partial discharges (for design with enclosed gas channel).

References

[1] CIGRÉ Brochure 362 WG A3.22, “Technical Requirements for Substation Equipment Exceeding 800 kV - Field experience and technical specifications of Substation equipment up to 1200 kV”, December 2008, ISBN : 978-2 85873-049-0

6 Equipment Requirements (VT, CT, NCIT)

6.1 Introduction

The technical specifications for UHV voltage and current transformers (VT, CT) including the experience in Japan, Italy and Russia, were obtained from the world survey conducted by CIGRE WG A3.22 [1]-[5]. UHV transmission systems utilize optical capacitive type VTs, which have secondary voltage ranging from $110/\sqrt{3}$ to 100 V, similar to that specified for 800kV VTs. Required accuracy ranges from 0.2 to 1% for measuring applications and 1 to 3% for protection applications.

UHV CTs are either iron core or air core types. The type with an air core is employed in order to avoid iron core saturation caused by increased short-circuit current with large DC time constant. CTs with an iron core have a rated secondary current of 1 A. Secondary voltage of 20 V is specified for CTs with an air core because they have a voltage output, in principle. Required accuracy ranges from 0.2 to 1% for measuring applications and 1% for protection applications. CTs with specified transient characteristics are used for protection applications where the rated short-circuit current is 50 kA.

In conclusions, there do not seem to be any major challenges for VTs and CTs for UHV applications and they can be designed based on the technologies attained for 800 kV systems.

6.2 Background of technical requirements

Conventional CTs and VTs using iron-core have been widely used for measuring and protection devices. However, stand-alone air-core CTs, ECT with Rogowski coil and optical CTs have been proposed instead of conventional CTs to achieve non-saturation, large dynamic range or light weight. On the other hand, amplifier VTs, EVT with capacitive voltage divider and optical VTs have been introduced instead of conventional VT for similar reasons.

As for the conventional CTs, the cross section of iron-core for UHV should be larger in order to prevent the iron-core from saturation as the primary current or the DC component increases. Especially for application to GIS, larger diameter of the CTs is required as the voltage class becomes higher. Therefore, CTs without an iron-core, such as stand-alone air-core CTs, ECT with Rogowski coil and optical CTs, have been developed to be compact and light-weight.

Stand-alone air-core CTs and Rogowski coils use non-magnetic formers instead of an iron-core with the secondary winding wound on it, which principally eliminates the saturation (Figure 6.2.1). However, unlike conventional CTs, their output is a voltage since they detect the induced voltage generated from the magnetic flux passing through the secondary winding. Stand-alone air-core CTs, which have low secondary winding resistance, are directly connected with the protection devices. The output of Rogowski coils for ECT, which generally have high secondary winding resistance, is converted into the digital (optical) output in the vicinity of GIS and transmitted to the protection devices.

Optical CTs using optical fibre or ring glass as a sensor are also proposed using Faraday rotation, which proportionally rotates the plane of polarization depending on the magnetic field caused by the primary current and do not suffer from saturation. However, if the control room is remote from the switchgear and the measuring and protective devices are of the analogue input type, additional amplifiers are required. In such cases economical value of optical CTs is less compelling. Where the associated devices cater for digital input,

particularly using the IEC 61850 protocol, the economical value of optical CTs may be acceptable since the amplifier is not required.

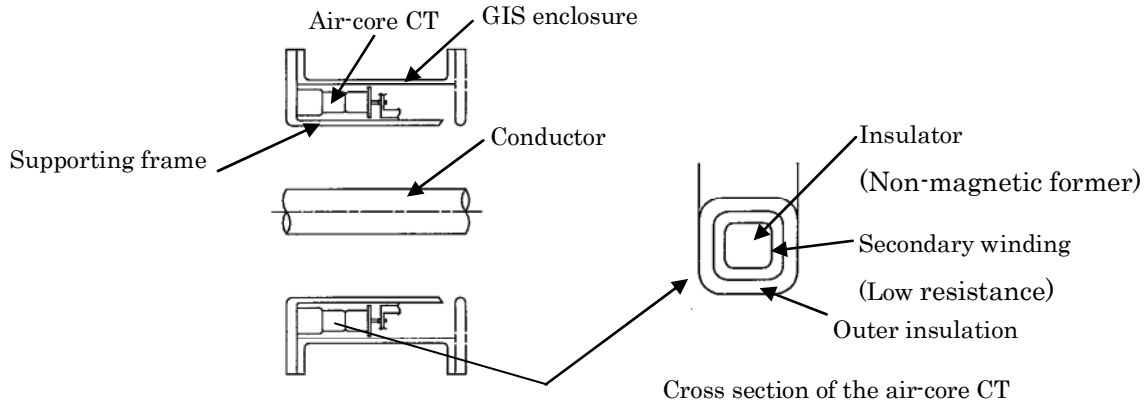

Figure 6.2.1 Configuration of the air-core CT for UHV GIS

As reported at the Second International Symposium on Standards for UHV Transmission in New Delhi, optical CTs are suggested for UHV AC Air Insulated Substations (AIS) because of a good linearity and the reduction of the thermal load caused by dielectric losses in the high voltage insulation. An example of an optical CT is shown in the figure 6.2.2.

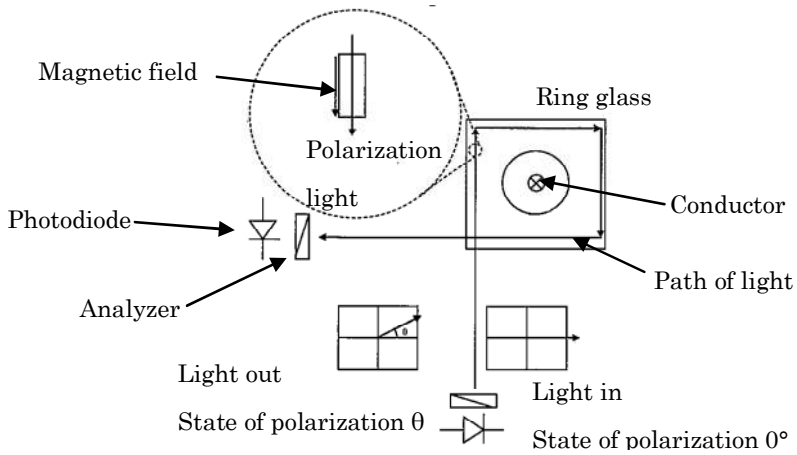

Figure 6.2.2 Configuration of Optical CT

It is expected that an appropriate type will be selected taking account the required performance, applicable equipment or system, and the economical point of view for the application to UHV.

Conventional VTs need a larger iron-core and windings as the system voltage rises higher and amplifier VTs, EVT with capacitive voltage divider and optical VTs have been developed in order to make the equipment more compact and lighter.

The amplifier VTs and EVT with capacitive voltage divider have an intermediate plate between conductor and enclosure of GIS. Capacitance C_1 is formed by conductor and the intermediate plate and capacitance C_2 is formed by the intermediate plate and enclosure. The output voltage is obtained from the voltage divided by C_1 and C_2. The output voltage of the amplifier VTs is connected with the amplifier and transmitted to the measuring and the protection devices. The output voltage of EVT with capacitive voltage divider is converted into the digital (optical) output in the vicinity of GIS and transmitted to the protection devices.

Optical VTs obtain the divided voltage by installing an intermediate plate, as is the case for the amplifier VTs or the EVT with capacitive voltage divider. However, this design converts

the voltage output to an optical output by means of an optical sensor. This optical output fed through an optical fibre into a signal converter in the same location as the measuring and the protection devices are located. Optical VTs also need an amplifier when connected to analogue input devices, as is the case for optical CTs. Figure 6.2.3 shows an optical VT with 4 optical sensors to facilitate multiplexing. The economical disadvantage of providing the amplifier is not such critical issue as for CTs because of the smaller dynamic range required for voltage compared to current where the short-circuit value can be many times higher that the normal, load value.

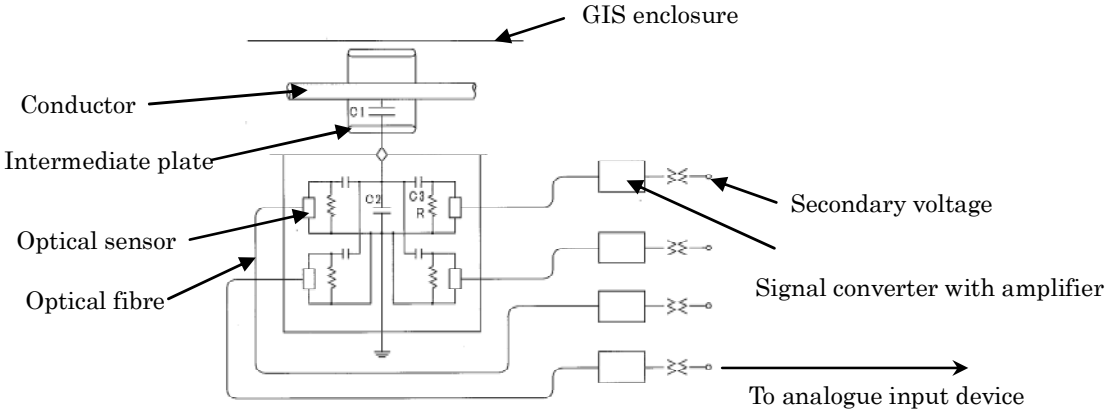

Figure 6.2.3 Configuration of the optical VT for UHV GIS

A further consideration is that amplifier VTs, EVTs with capacitive voltage divider, and optical VTs may have temperature dependencies that affect accuracy of electronic circuits or the optical sensor, resulting in the need to specify temperature characteristics. In these VT's only the intermediate plate part will have different structure depending on the system voltage so the same configuration can be used irrespective of voltage class if the divided voltage is same.

As for the application of these VT's to UHV, it is also expected that an appropriate type will be selected taking account of required performance, applicable equipment or system, and the economical value.

6.3 Recommendations for specifications

Table 6.3.1 shows the structure and features of conventional CTs, stand-alone air-core CTs, ECT with Rogowski coil and optical CTs. Table 6.3.2 shows the structure and features of the conventional VTs, the amplifier VTs, EVTs with capacitive voltage divider and optical VTs.

Table 6.3.1 Comparison of conventional CT, stand-alone air-core CT, ECT with Rogowski coil and optical CT

	Conventional Iron core type	Stand-alone Air core CT	ECT with Rogowski coil	Optical CT
Example of structure	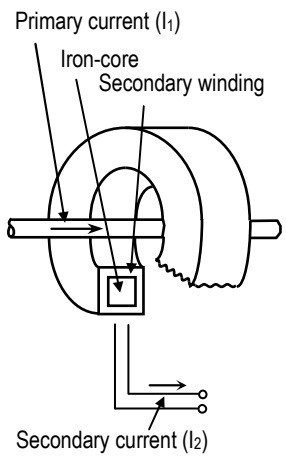	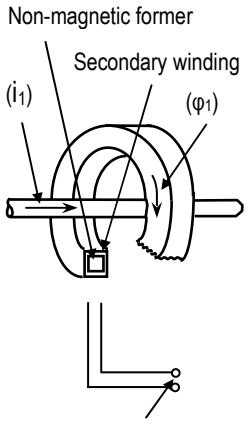	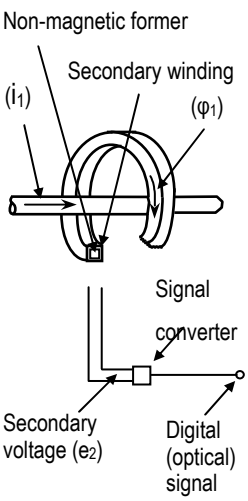	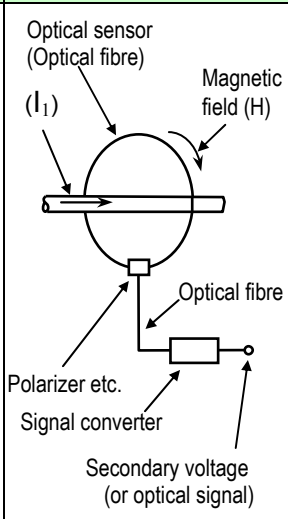
Principal	Secondary current is obtained depending on the turns ratio (primary winding / secondary winding). $I_2 = I_1 \frac{N_1}{N_2}$	Secondary voltage is obtained from the magnetic flux passing through the secondary winding. $e_2 = \frac{d\varphi_1}{dt} = M \frac{di_1}{dt}$ (M: Mutual inductance)	Same as the left column. Secondary voltage is converted to digital (optical) signal in a signal converter with high input impedance located in the vicinity of Rogowski coil.	Optical sensor (optical fibre) is arranged so as to enclose the primary current. The magnetic field generated from the primary current rotates the polarized direction of the light passing through the optical fibre.
Output and secondary connection	Secondary current is transmitted to measuring and protection devices.	Secondary voltage is directly transmitted to protection devices. Air core type is mainly applied for bus-bar protection relay to eliminate the saturation.	The digital (optical) signal is transmitted to measuring and protection devices.	Secondary voltage or optical signal is outputted from a signal processor. An amplifier is required when it is connected to analogue measuring and protection devices.
Accuracy	As the primary current or the d.c. component rises, error increases because of iron-core saturation. Larger cross sectional area of iron-core is required to prevent the iron-core from saturation.	Saturation does not occur even if the primary current or the d.c. component increases.	No saturation. Accuracy mainly depends on the signal converter (linearity, frequency response, temperature dependence).	No saturation. Accuracy mainly depends on the optical sensor or the signal converter (linearity, frequency response, temperature dependence).
Dimension/ Weight	Heavy and large because iron-core is used.	Light because a non-magnetic former is used instead of iron-core.	More light because a non-magnetic former is used instead of iron-core and smaller size of windings.	The lightest because neither iron-core nor windings is used.

Table 6.3.2 Comparison of conventional VT, amplifier VT, EVT with capacitive voltage divider and optical VT

	Conventional VT (Electromagnetic type)	Amplifier VT	EVT with Capacitive voltage divider	Optical VT
Example of structure	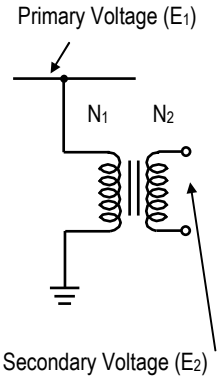	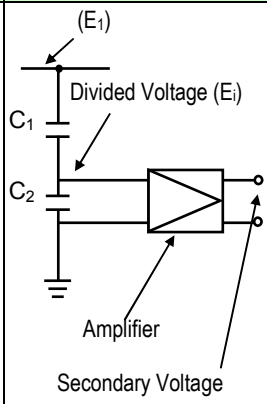	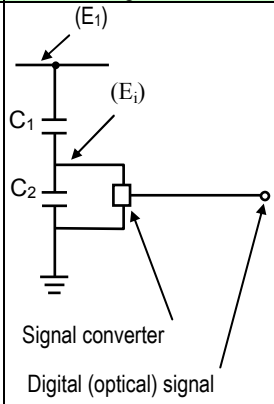	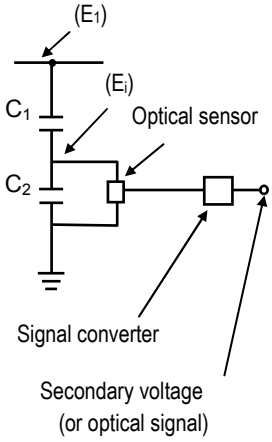
Principal	Secondary voltage is obtained depending on the turns ratio (primary winding/ secondary winding $E_2 = \frac{N_2}{N_1} E_1$	Divided voltage is obtained from voltage divided by C1 and C2 capacitance. The divided voltage is connected with an amplifier. $E_i = \frac{C_1}{C_1+C_2} E_1$	Divided voltage is obtained from voltage divided by C1 and C2 capacitance. It is converted to digital (optical) signal in a signal converter with high input impedance.	Divided voltage is obtained from voltage divided by C1 and C2 capacitor. It is converted to optical signal by the optical sensor, and finally secondary voltage is obtained from an signal converter .
Output and secondary connection	Secondary voltage is transmitted to measuring and protection devices.	Secondary voltage from the amplifier is transmitted to measuring and protection devices.	The digital (optical) signal is transmitted to measuring and protection devices.	Secondary voltage or optical signal is outputted. An amplifier is required when it is connected to analogue input measuring and protection devices.
Accuracy	Larger iron-core is required as voltage becomes higher. Conventional VT might cause ferro-resonance by the iron-core saturation according to operation condition.	No saturation. Accuracy mainly depends on the amplifier (linearity, frequency response, temperature dependence).	No saturation. Accuracy mainly depends on the signal converter. (linearity, frequency response, temperature dependence).	No saturation. Accuracy mainly depends on the optical sensor or the signal converter. (linearity, frequency response, temperature dependence).
Dimension/ Weight	Heavy and large because iron-core and windings are used.	Compact and light. However, larger amplifier is required for analogue larger output burden.	Compact and light. The same signal converter is used irrespective of the primary voltage if the divided voltage is the same.	Compact and light. The same optical sensor and signal converter are used irrespective of the primary voltage if the divided voltage is the same.

References

[1] F. Rahmatian, “DC and Wideband Applications of Optical Voltage and Current Sensors in Electric Power Transmission systems”, CIGRE Session paper A3-301, 2008

[2] J. B. Kim et. Al., “Experience of Non-conventional Instrument Transformer”, J. B. Kim et. Al., “Experience of Non-conventional Instrument Transformer”, CIGRE Session paper A3-304, 2008

[3] J. Schmid et. al., “IEC 61850 Merging Unit for the Universal Connection of Conventional and No-n-conventional Instrument transformers”, CIGRE Session paper A3-306, 2008

[4] L. A. Kojovici, “Innovative Non-conventional Current Transformers for Advanced Substation Designs and Improved Power System Performance”, CIGRE Session paper A3-308, 2008

[5] ICEE 2004 Verification Test of High Accuracy ECT/EVT

7 Factory and Laboratory Testing Experience

7.1 Introduction

7.1.1 Early history of UHV testing

The first testing of UHV substation equipment was in the former USSR, from which very little internationally accessible documentation has emerged. In the 1960s, a 750 kV experimental transmission line was commissioned [1], which enabled commercial operation at that voltage in 1974. This experience led to the decision to start testing at 1150 kV level. Early reports indicate that testing was not performed in factory laboratories, but field studies and tests were carried out in an experimental 1150 kV station [2]. Tests on insulation, switching overvoltage withstand, determination of electrical and mechanical characteristics, measurement of radio interference and audible noise, impact of pollution, impact of high electrical field on humans as well as gaining experience in installation and maintenance were all part of the planned program [3]. Point on wave line switching tests, shunt reactor switching tests and transformer magnetizing current switching have been described in some detail in [2]. After 2 years of commercial operation of the 411 km line at full voltage, the voltage was reduced to 500 kV.

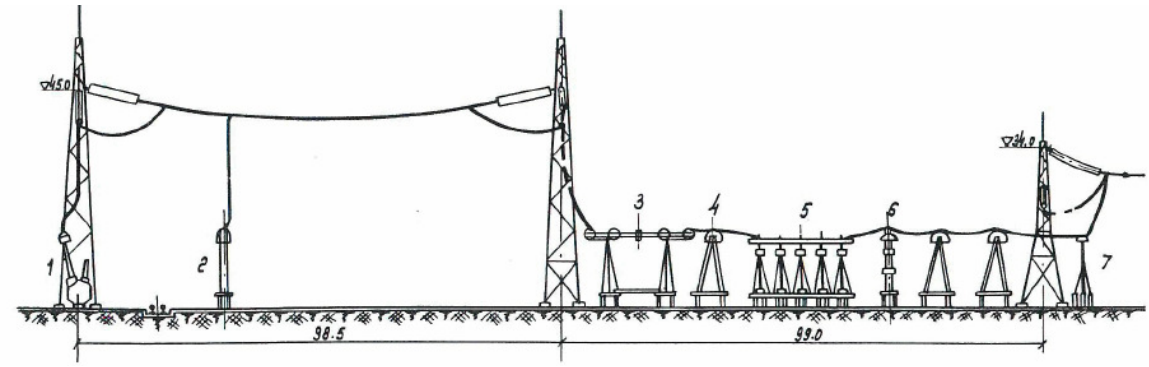

(1) HV transformer, (2) Surge arrester, (3) Disconnector, (4) Current transformer, (5) Circuit breaker, (6) Voltage transformer, (7) Earthing switch

Figure 7.1.1 Layout of USSR 1150 kV testing station

In the 1980s, testing with air insulated or partly GIS-type switchgear systems were carried out at BPA and AEP in the United States and at ENEL's Suvereto substation in Italy, see figure 7.1.2 [4].

Figure 7.1.2 Italian Suvereto UHV testing station

7.1.2 TEPCO project

The first internationally well-documented test-experiences with UHV station equipment are from Japan [5]. In the mid 1990s, all necessary substation equipment was developed and tested separately by three Japanese manufacturers. After extensive testing in the laboratories of the three manufacturers involved in the project, the equipment was installed in the TEPCO Shin Haruna UHV GIS test-station by 1996 (See figure 7.1.3), on a one-manufacturer-per-phase basis for long-term verification. During this period, ample experience in testing was collected, both in manufacturers' laboratories, see figure 7.2.1, independent laboratories and in field pilot/ test-stations. This is described in more detail in the following sections. The Japanese UHV project has led to the development of a wide range of test techniques for arresters, transformers, circuit breakers, high-speed grounding switches, CTs and VTs.

None of the projects initiated in the last century has lead to commercial application at full 1000 - 1100 kV level.

With the advent of the Chinese UHV AC project of State Grid Corporation of China (SGCC), testing of UHV station equipment was reconsidered in various parts of the world: China, Europe, Japan and Korea and this is described in the following.

Figure 7.1.3: Japanese Shin-Haruna UHV test station

7.2 Short-circuit tests for main contacts

Limits of laboratories may prohibit testing of an entire circuit breaker in a single test, especially for UHV making the concept of unit testing (see for definition IEC 62271-100 clause 6.102.4.2), in which only one breaking unit of the breaker is tested with a limited voltage, particularly important. In sections 7.2.2 (AIS) and 7.2.3 (GIS) this aspect is discussed in more detail, using concepts from the informative annex O of IEC 62271-100.

In addition, laboratory limitations may create the need for multi-part testing (see for definition IEC 62271-6.102.4.3). This implies separate and successive testing of parts of selected intervals and parameters of the interruption process that covers the entire process. A clear example of this is the Japanese approach, which will be discussed in section 7.2.4.

7.2.1 Unit testing: general considerations

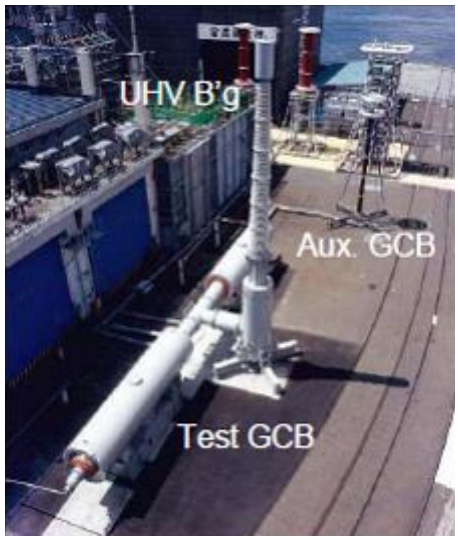

Figure 7.2.1 Impression of full-pole 1100 kV factory testing in the framework of TEPCO project

Circuit breakers for rated voltages higher than 550 kV always consist of multiple interruption chambers (units) in series, because single chambers are not able to withstand the (recovery) voltage at that level. Indeed, even at voltages in the range 245 - 550 kV, breakers may often consist of multiple interruption chambers. Grading capacitors across each interruption chamber usually guarantee an approximately equal share of the voltage is applied to each interruption chamber.

For the E(xtra) and U(ltra) High Voltage levels (245 - 800 kV and ≥ 800 kV respectively), instead of testing the complete pole of a circuit breaker, separate interrupter units are often tested with the appropriate portion of the rated voltage ('unit-testing', or 'half-pole' testing if one pole consists of two interrupter units).

7.2.2 Unit testing of live tank type circuit-breakers

In the case of live tank type circuit-breakers (porcelain or polymer enclosed) having grading capacitors, unit testing is an accepted practise. Special precautions are to taken into account regarding the following stresses:

7.2.2.1 Dielectric stresses

In the absence of grading capacitors, the stray capacitances of the entire breaker in service will determine the distribution of voltage across each chamber. Stray capacitance is not well defined and is determined (in contrast to physically present grading capacitors) by the environment of the breaker. This implies that in testing, care must be taken to include an ample margin in the voltage applied in unit tests. In the case of a graded two-chamber breaker half-pole tests may be carried out with 55% of the total voltage and in the case of the compete absence of grading capacitors this asymmetry of voltage can be much higher. Its value is normally supplied by the manufacturer before the start of a test. It is the duty of the test laboratory to make sure that the physical environment of ungraded breakers is equivalent to the service situation, eg placement of a test breaker too close to wall(s) needs to be avoided since it this would lead to different stray capacitances than in a typical outdoor environment.

7.2.2.2 Mechanical stresses

Typically, for circuit breakers with two arcing chambers for each phase, one operating mechanism and drive system is applied per pole, driving both interrupting units. With half-pole tests, the forces in the operating mechanism and the structure are far less than those encountered during full-pole operation. Therefore, half-pole breaking tests are allowed provided that the other unit carries the same current.

With respect to closing, the symmetrical and asymmetrical 100% short-circuit current making tests have to be carried out anyway in a full-pole configuration. The considerations above also apply to circuit breakers that have a common operating mechanism for the three phases.

7.2.3 Unit testing of metal enclosed (GIS, dead-tank) circuit breakers

In case of unit- (or half pole in case of two units) testing of metal enclosed EHV and UHV circuit-breakers, it is very difficult to correctly represent the mechanical, gas-dynamic, electro-dynamic and dielectric stresses with reference to the full pole conditions. IEC 62271-100 Annex O [6] documents the stresses to be considered for single-phase testing. Some examples of unit testing are given below

7.2.3.1 Dielectric stresses during current interruption

Half-pole tests on metal-enclosed circuit breakers do not represent the correct (full) dielectric stresses between live parts and enclosure, at least for the short-circuit current tests (See figure 7.2.2), since only half the service voltage is between live internal parts and the enclosure.

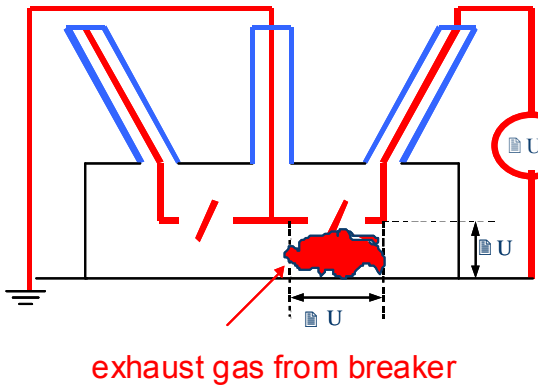

Figure 7.2.2 Half-pole test of metal-enclosed breaker: voltage across interrupter OK, voltage

In testing of metal enclosed circuit breakers with grading capacitors, unit tests may not represent the transient stresses that occur due to unequal dielectric behaviour of the arcing chambers. In unit tests, stresses on grading capacitors (such as occur in pre-strikes) and on the breaker chambers are not represented. This is not trivial since recent work from CIGRE identified grading capacitors as a major contributor to circuit breaker failures [7].

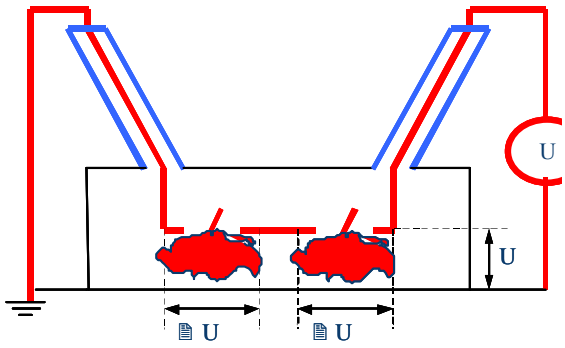

Figure 7.2.3 Full-pole test of metal-enclosed breaker: voltage across interrupters OK, voltage between live parts and enclosure OK

A safety margin of some percent is usually applied in unit testing. This is to cater for an unequal voltage distribution because of an unequal distribution of (stray-) capacitance of the breaker units. Because grading capacitors are normally much larger than these stray capacitances, the unequal voltage distribution is covered by a safety margin of a few percents of voltage above 50% (for a two-chamber breaker).

In case of designs without grading, this small safety margin may no longer be adequate.

It is evident that half-pole tests, without taking into account the afore-mentioned stresses, give inadequate evidence for the correct performance of the test object in service contrary to full-pole tests which verify the voltage between live parts and enclosure (See figure 7.2.3).

7.2.3.2 Gas-dynamic stresses

Depending on the design involved (i.e. combined or separate gas compartments for multiple interrupters), the dynamic gas pressures and gas flows of arcing chambers may mutually affect the gas-dynamic phenomena and thereby interfere with the arc extinction process.

The hot exhaust gases may also deteriorate the dielectric withstand capability of the space surrounding the arcing chambers (between poles, across the chamber, to the enclosure), see figure 7.2.4. With GIS and dead-tank circuit breakers gas dynamic phenomena and the influence of (hot, ionized, contaminated) exhaust gas have to be taken into account with respect to the decision to perform unit- or full-pole tests and with respect to the decision to which side of the circuit breaker the largest dielectric stress has to be applied.

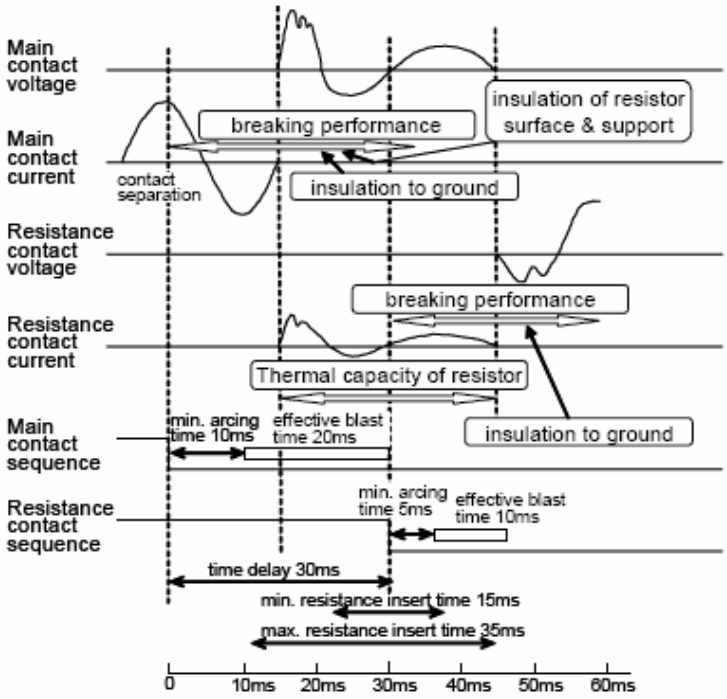

Figure 7.2.4 Phases in the interruption process with Japanese 1100 kV GCB equipped with resistors to be tested with multi-part testing [9]

7.2.3.3 Electro-dynamic stresses

Half-pole tests, where the other breaking unit is not used, as an auxiliary breaker, require an equivalent conducting path for the short-circuit current, simulating correctly its influence on the arc in the unit under test. For the same reason, three-phase tests, as well as single-phase tests, are necessary on three-phase metal-enclosed circuit-breakers, due to the compact design. Also the high-current connections in the direct vicinity of the test object have to be designed with great care, taking into consideration realistic electro-dynamic stresses on the arc and the structure.

7.2.4 Multi-part testing; the Japanese approach

Based on transient network analysis of the (then) projected TEPCO UHV grid, TRV waveform specifications for power testing were determined, adopting the IEC system for test-current values, first-pole-to-clear factor 1.1 and 450 Ω line surge impedance for short-line fault tests [8]. From the results of the network study, "custom-made" TRV parameters for terminal- and out-of-phase fault were defined using 2 or 4 parameters. No attempt was made to include the UHV rating in the IEC standard at that time.

During the equipment specification process for the UHV substations in Japan, in order to rationalize the insulation coordination, application of high-performance surge arresters and circuit breakers with parallel resistors, both for opening and closing were investigated.

In figure 7.2.5, the various stresses and the associated which has to be verified by testing, are outlined.

Compared to the conventional circuit breakers at voltage levels below 550 kV, the 1100 kV, two break, circuit breaker used in Japan has more components in the tank, such as large-volume resistors, two or four resistance interrupters, two main interrupters, and supporting insulators. Thus, it is necessary to check not only the interruption performance between contacts but also the insulation between internal parts and the enclosure when this might be affected by hot gases produced during arcing.

	main interrupter between contacts		main interrupter	main interrupter between poles			resistors and their insulation support
	thermal	dielectric	to ground	hot gas	electro-magnetic	reaction force of puffer	
T10	◎ unit test ◎		△	△	△	△	△
T30	◎	◎	△	△	△	△	△
T60	◎	◎	△	△	△	△	△
T100s	◎ unit test ◎		◎	○ full pole test		○	◎ unit test
T100a	◎ unit test ◎		◎	○ full pole test		○	◎ unit test
SLF	◎ unit test	△	△	△	△	△	△
out-of-phase	△	◎ unit test	△	△	△	△	△
capacitive current	△	◎ unit test	△	△	△	△	△

◎:mandatory ○:verified secondarily △:verified by another test

Figure 7.2.5 Multi-part testing scheme for Japanese UHV circuit breaker considering interacting stresses of main contacts [9]

Due to the presence of the (switchable) resistor in parallel to the main contacts, opening and closing testing must be performed taking account of the interaction between the main breaking unit, resistor and resistor breaker. Japanese sources have always emphasised the importance of taking into account this interaction during testing. Because of this, testing of the "Japanese" UHV breakers followed a multi-part test method. The main reason for not being able to test the breaker in a single-part test is that, due to the presence of the resistor, an adequate voltage across the main interrupter cannot be maintained: the capacitor bank, normally part of a synthetic test installation, loses its voltage due to discharge across this resistor.

The verification of dielectric withstand between live internal parts and enclosure during the interruption process (effect of the hot gasses) is reported as a mandatory full-pole test with 100% of the rated short-circuit breaking current, symmetrical as well as asymmetrical (T100s/a). For the application of TRVs between the contacts, unit (half-pole) tests are considered adequate. In figure 7.2.5, a complete scheme of Japanese testing practice for stresses on the main contacts is given.

In the so-called "modified multi-part method" the following strategy is adopted for testing the main interrupter, the resistor interrupter and the resistor itself individually as well as their combination [10]:

(1) The thermal interruption capability of the main breaker was tested, with resistors installed and with appropriate initial TRV (up to t_1, u_1)

(2) The dielectric interruption capability of the main breaker was tested with the resistor removed

(3) Separate tests for thermal and dielectric withstand of the resistors (incl. out-of-phase conditions). Voltages equivalent to "O" operation of T100s and "CO" operation of out-of phase were applied to the resistors with an "O-t -CO" operating sequence.

(4) Test on the resistor interrupter (See section 7.5 and Annex).

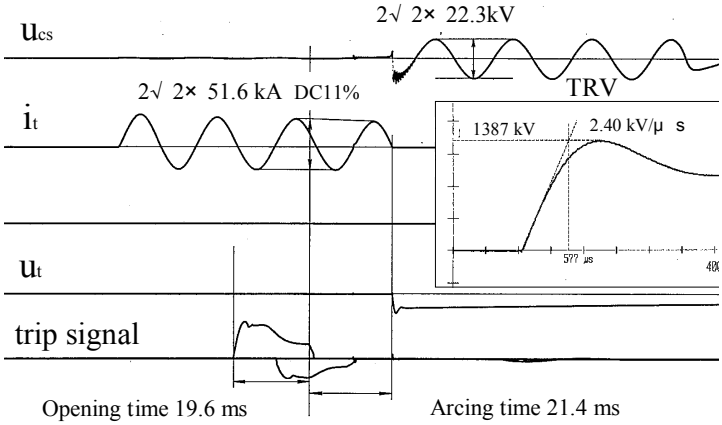

Figure 7.2.6 Demonstration of full-pole T100s test [10]

In figure 7.2.6, the full-pole T100s tests, for verification of the insulation performance to ground during the interruption process, is demonstrated [10]. Here, one breaker is used as a test-object, an identical one as auxiliary breaker. Similar performance was demonstrated with the T100a test duty.

7.2.5 The Chinese approach

In 2008, State Grid Corporation of China (SGCC) commissioned the demonstration Jingdongnan-Nanyang-Jingmen 1100 kV transmission line. Switchgear, using GIS or Hybrid-IS from three different manufacturers was tested at the Xi'an High Voltage Apparatus Research Institute (XIHARI) laboratories. In this case, a number of tests were performed as unit tests, whereas the full-pole test was used to verify insulation during the interruption process.

In at least one case, a circuit breaker with 4 interrupters in series was used in the tests. This called for careful statistical analysis of the voltage distribution across each chamber, taking into account both tolerances in grading capacitors' values as well as geometry and stray capacitances [11], especially since grading capacitors in this design are chosen to be unequal in value. In general, the voltage distribution factor depends on [12]:

(1) Number of interrupters included in the test (half-pole, quarter-pole test)

(2) Presence of a central connection (additional bushing, necessary in case of a unit test)

(3) The application of the voltage (at one side only or at both terminals)

(4) The nature of the test-circuit in the case of more than one voltage application (synthetic) circuit.

Full-pole tests T100s/a were carried out by applying half the specified voltages at opposite polarities to each breaker terminal with the breaker mounted on an insulating platform (See section 7.4), see figure 7.2.7.

Figure 7.2.7 Full-pole testing in China [13]

In this case the moving contact side was connected to the enclosure and the fixed contact side will be subject to the positive polarity of TRV. In this way, 100% TRV will appear across the breaking units and between the fixed contact and enclosure. All other power tests were unit tests.

In addition, Japanese manufacturers carried out additional tests for this project, since the TRV requirements from SGCC are more severe than those from TEPCO. For the Chinese UHV project, Japanese authors expected the UHV breaker to have sufficient margin to break without resistor, to be confirmed by testing [14].

7.2.6 European experience

In Europe, power testing of UHV breakers is reported by KEMA, the Netherlands. By the mid 1990s an initial study was launched on the feasibility and the topologies of future UHV test circuits [15]. In 2002, test-circuits were proposed that would allow full pole testing for 800kV for T100a/s, and making tests and half pole tests for short-line fault [16]. At that time, a solution was proposed, later adopted in China and Korea, to install the breaker on an insulating platform and apply "half" the test voltages at both terminals in opposite polarity. In 2007, full-pole tests were actually performed on 800 kV GIS switchgear, but in a test-circuit where the breaker could remain at ground potential i.e. with no insulating platform [17]. In 2008 full-pole T100a (including arcing time verification), T10 & T30 (including O-CO sequences) tests were realized for 1100 kV switchgear, also with breaker remaining on ground potential [18, 19]. Tests were performed with TRV parameters for 1100 kV extrapolated by taking twice the 550 kV IEC parameters and a first-pole-to-clear factor 1.5. Thereby, T10 values exceeding 2000 kV were reached (See figure 7.2.8). With the TRV parameters, proposed by WG A3.22, this value will cover the 1200 kV rating of T10.

Full pole test T100a		Full pole test T10	
D.C. time constant	120 ms		
First pole to clear factor	1.3	First pole to clear factor	1.5
TRV peak value	1600 kV	TRV peak value	2062 kV
Minimum arcing time	10.3 ms	Minimum arcing time	5.1 ms

Figure 7.2.8 Full-pole 1100 / 1200 kV testing in the Netherlands [19]

7.2.7 Korean experience

In Korea, 800 kV full-pole T100a/s tests are reported by KERI laboratories [20], in accordance with IEC TRV parameters. Two types of breakers were tested, one with a single operating mechanism (for the two breaks) and one with a double mechanism. As per the Chinese practice, the (deadtank) breaker was raised in potential during the test (See figure 7.2.9).

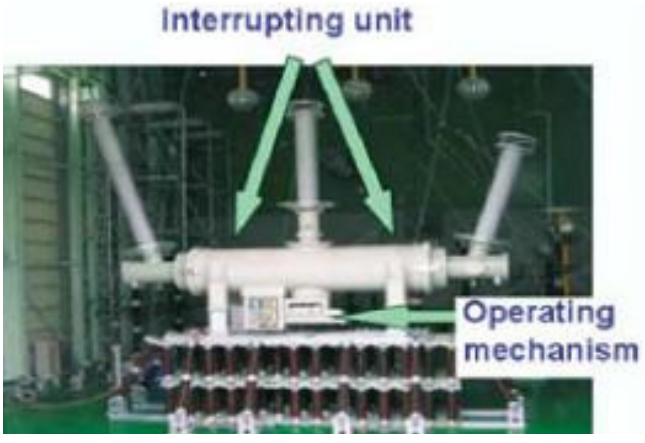

Figure 7.2.9 800 kV full-pole testing in Korea

7.2.8 Test current issues

7.2.8.1 Arc voltage

A key point in UHV testing is the necessity to have test current supplied at the highest possible voltage. This is because of the interaction of the arc voltage with the circuit which may cause test-current deformation [21].

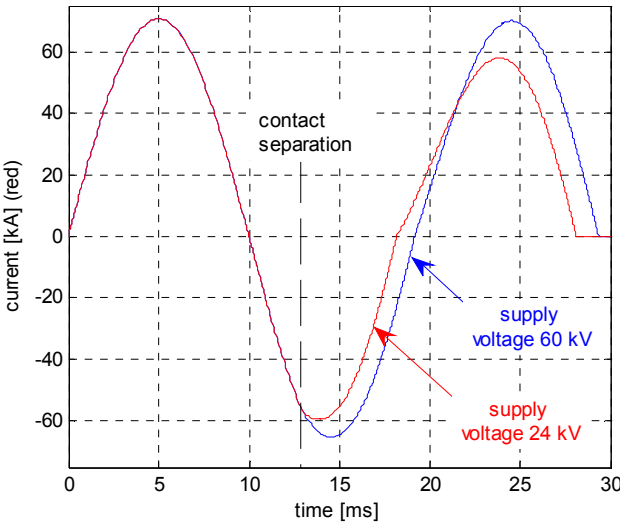

Figure 7.2.10 Comparison of 50 kA test-current with 24 kV of supply voltage (red) and 60 kV supply voltage (blue) in UHV synthetic test-circuit with 8 breaker chambers totalling 12 kV of arc voltage

Since, in synthetic circuits for UHV, two breakers must be placed in series an unusually large number of arcs is involved. In an actual UHV test case, the breaker under test was a metal enclosed, chamber breaker and an 1100 kV 4 chamber live-tank circuit breaker was installed as an auxiliary breaker. This implies 8 arcs in series, totalling at least approx. 14 -18 kV of arcing voltage. This voltage is counteracting the supply voltage, leaving much lower current-driving voltage available than in the situation without arcs. This effect is illustrated in figure 7.2.10, showing a test-current of 50 kA in a circuit with 8 arcs in series (modelled with a Cassie arc model creating 1.5 kV of arc voltage for each arc) with adequate supply voltage of 60 kV. Also, in red, a current with an (insufficient) supply voltage of 24 kV is shown. Lack of regard for this effect seriously influences the power frequency wave-shape from the moment both breakers are arcing, and reduces the energy in the arcing chambers. This often leads to an unacceptable distortion of current, as can be seen clearly in figure 7.2.10.

7.2.8.2 DC time constant

In UHV systems much a higher DC time constant (such as 150 ms) than the standard (45 ms) is estimated due to lower resistive loss of the lines and the high capacity of generator connections nearby. Due to test facility limitations it is difficult to adjust the DC time constant of the test circuit to such high values. One approach to overcome this issue is described by Japanese authors [9]. In this approach, the arc energy supplied to the contact system when interrupting current was analyzed and compared with the arc energy with a DC time constant of 70 ms in the 550 kV - 63 kA one-break circuit-breaker, with a contact system very similar to the UHV breakers. By this "equivalent arc energy method", it was calculated that the combination of current / time constant (63 kA / 70 ms) led to higher input than 50 kA / 150 ms. Equivalence of arc energy (1.8 MJ) is found to be 58.2 kA / 70 ms. Hence, from arc energy point of view, testing with 58.2 kA / 70 ms is equivalent to 50 kA / 150 ms.

7.2.8.3 Superimposed high-frequency current

During the Japanese project it was recognized that, as a result of a phase-to-ground fault, high-frequency (HF) current is superimposed on the power frequency current, and persists until current zero due to the small damping in the UHV system [22]. This leads to a higher than expected value of di/dt at current zero. Japanese authors report testing of a 50 kA breaker with a di/dt, corresponding to 63 kA [9]. This is achieved with a synthetic current injection scheme, creating the proper increased di/dt at current zero, while keeping the power frequency

current as the rated value (See figure 7.2.11). The effect of the HF current on TRV was found to be strongly reduced thanks to the parallel resistors.

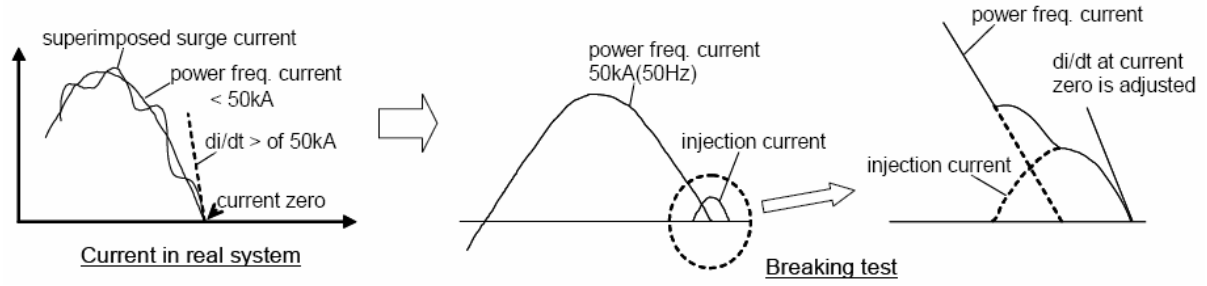

Figure 7.2.11 High-frequency currents lead to higher di/dt at current zero than power frequency current [9]

7.2.8.4 Short-line fault tests

Short-line fault tests prove the thermal interruption capability of circuit breakers. Since the correct rate-of-rise of the initial TRV is critical, especially for circuit-breakers for AIS, synthetic current injection circuits should be chosen as the correct solution (as opposed to voltage injection circuits). (ITRV is estimated as 90 Ω for GIS technology and 300 Ω for AIS technology. See the section 3.1.2.4)

This test can be carried out as a unit test, since it is not the aim of this test to verify the internal dielectric withstand of GIS (IEC 62771-100 O.3.2). In unit tests with GIS breakers, an additional bushing must be mounted and care must be taken that its capacitance does not increase the time delay beyond the acceptable limits.

For breakers with rate voltages of 800 kV and below, IEC 62271-100 accepts omission of the ITRV (initial TRV) test if the line side TRV has a time delay less than 100 ns (IEC 62271-100 6.109.3). For circuit-breakers in UHV systems, an immediately rising line-side TRV may no longer be assumed to cover the busbar generated ITRV, since OH line surge impedance is proposed to decrease from 450 Ω to 330 Ω. The need for ITRV test circuits and the topology of the test circuits have to be investigated in the near future, as these circuits are not yet available.

7.2.9 Making tests

The making test as part of T100s/a should be performed full-pole in order to represent the correct stresses on the mechanism. At present, however, no such tests have been demonstrated. Authors of [12] propose the following possible solutions:

(1) Reduce the gas pressure to maintain the correct duration of the pre-strike arc
(2) Perform half-pole tests by short-circuiting one half of the breaker (which leads to incorrect stress on the mechanism)
(3) The use of one or more fuse wires between the contacts (not allowed in IEC 62271-100),

The stated preference is to reduce the gas pressure.

Authors of [23] report availability of an 1100 kV full-pole synthetic making circuit but cannot show experience as yet.

7.3 Short-circuit tests for auxiliary contacts

Ample test experience exists in Japan, where resistor interrupters has have been installed and tested.

	main interrupter between contacts		main interrupter	main interrupter between poles		
	thermal	dielectric	to ground	hot gas	electro-magnetic	reaction force of puffer
T10	◎ unit test ◎		△	△	△	△
out-of-phase	△	◎	○	◎ full pole test	○	○
capacitive current	△	◎ unit test	△	△	△	△

Figure 7.3.1 Multi-part testing scheme for Japanese UHV circuit breaker stresses of resistor interrupter contacts [9]. (Symbols as in figure 7.2.5)

Separate specifications for the resistor interrupter were defined for the TEPCO project [5]. For testing the resistance interrupter, also in this case a multi-part testing approach was chosen, as summarized in figure 7.3.1. The out-of-phase switching is identified as the most severe condition, and testing on a full-pole basis is recommended. In separate tests, thermal stresses of the resistor elements are applied, taking into account the full rated sequence of the breaker: O (as T100s) - t - CO (as out-of-phase).

7.3.1 Line charging tests

For metal-enclosed breakers, line charging current switching tests (interruption of capacitive current of unloaded OH lines) should preferably be performed on a full-pole basis (IEC 62271-100 O.3.3.2) due to the presence of dc voltages and the possible formation of space charges on parts of the insulation.

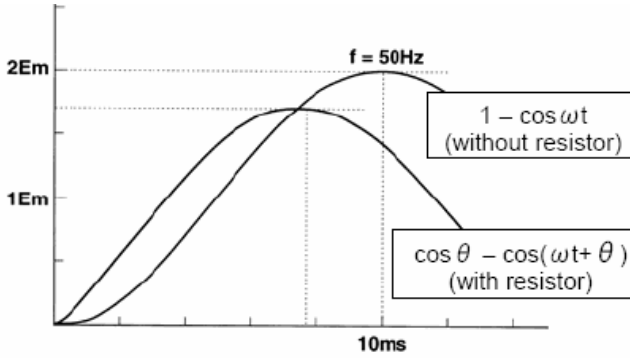

Figure 7.3.2 Influence of resistor on the recovery voltage in line charging current switching tests [9]

Unit test are only acceptable if the electrical field to enclosure at one terminal is equal to the field strength to enclosure at full-pole testing. This requirement can be met by:

(1) Raising the complete enclosure to the proper voltage;

(2) Performing half-pole testing with ac and dc voltages combined at one terminal with the other terminal earthed;

1100 kV line charging current interruption test experience is reported from Japan [9]. Line charging tests were performed on circuit-breakers including resistor interrupters on a half-pole basis. Due to the presence of resistor, the 1-cos capacitive recovery waveform is modified to become a more or less sinusoidal wave-shape, with higher rate-of-rise but lower amplitude (See figure 7.3.2). Test-specifications indicate a peak voltage of 2515 kV both for the main contacts and for the resistor interrupter contacts [8]. From Chinese sources, several studies have been published on line charging current switching tests [24 - 28]. Half-pole test results are reported in [29].

Korean sources report 800 kV capacitive testing using a half-pole synthetic capacitive switching method by which correct stresses between contacts and between phase and enclosure are claimed [20].

7.4 Testing methods for the application of high TRV

7.4.1 Full-pole test circuits

For UHV power switching tests two test circuits are typically in use (See figure 7.4.1).

(1) The "platform" method (in use in China and Korea), by which the tested breaker is installed on an elevated platform and voltages are supplied to both terminals in phase opposition.

(2) The "ground" method (in use in Japan and in the Netherlands), by which the tested breaker remains on the ground and voltage is applied to one terminal only.

In both methods, two synthetic circuits are used and, by proper timing and circuit tuning, 4 parameter TRV's, as required by IEC 62271-100 can be realized. An example is given in figure 7.4.2

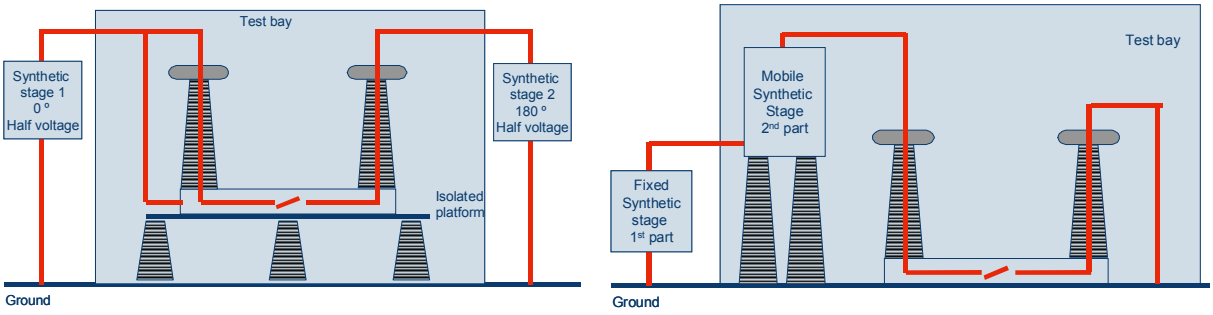

Figure 7.4.1 Principle circuits for UHV testing; Left: "Platform" method, right: "Ground" method

The relative advantages of each method are summarized in the table below.

Table 7.4.1 Comparison of test methods between platform and ground method

Advantages of "platform" method	Advantages of "ground" method
Auxiliary breakers (2) for only half the rated voltage	Only one auxiliary breaker (for full voltage)
Voltage measurements (2) with smaller dividers	One voltage measurement (for full TRV)
Smaller dielectric stresses to laboratory components	No need to build an isolated platform
Smaller test-hall can be used (dielectrically)	No problems with mechanical stability
Current injection can be applied	Most realistic test condition with service situation
	No problem with auxiliary power supply and controls

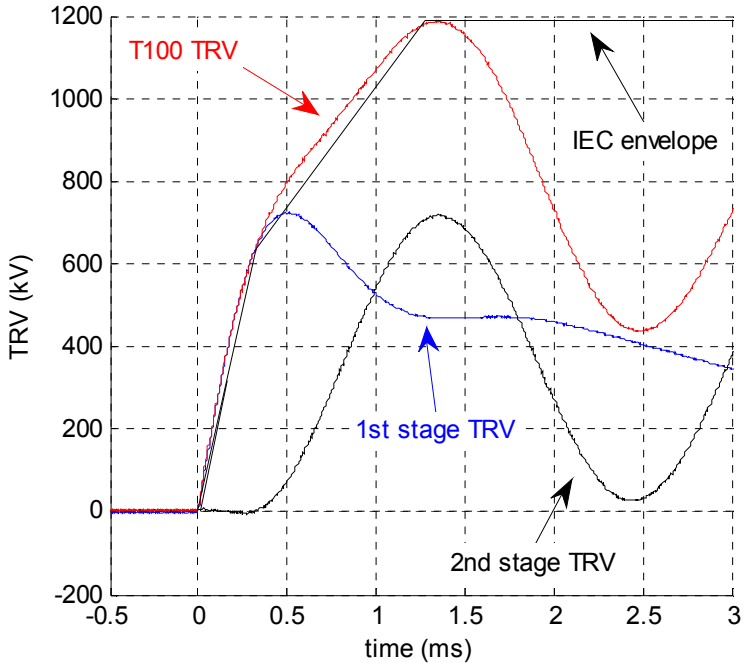

Figure 7.4.2 Oscillogram (from test) of double stage synthetic 4 parameter TRV for 800 kV circuit breakers with IEC envelope [18]

In table 7.4.2, detailed test circuits are summarized for the test laboratories that have demonstrated 1100 / 800 kV tests on a full-pole basis. [17].

Table 7.4.2: Realized test-circuits for full-pole tests of UHV circuit breakers

Japan: T100 circuit (ground method) [10]. Full voltage application at one terminal, other terminal grounded. Test breaker grounded. T100s peak voltage reported: 1387 kV [10]	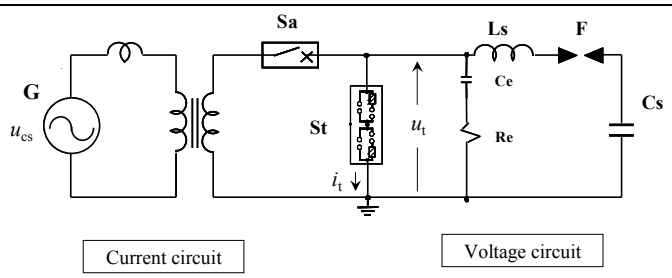
China: T100 circuit [30] (platform method). Test breaker at half the tested voltage; half voltage application in phase opposition at both terminals. T100s peak voltage reported: 1653 kV [13]	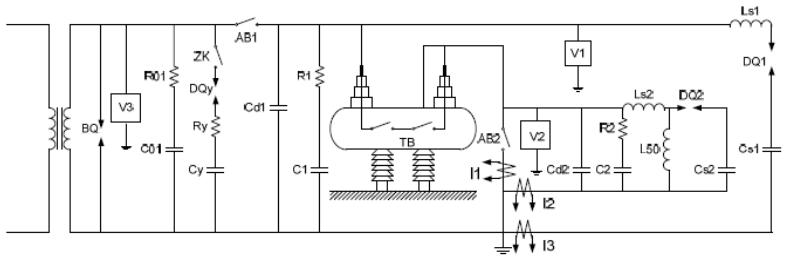
Netherlands: T100 circuit [23] (ground method). Test breaker TO at ground potential. Full voltage application at one terminal, other terminal grounded. T10 peak voltage reported: 2060 kV [23]	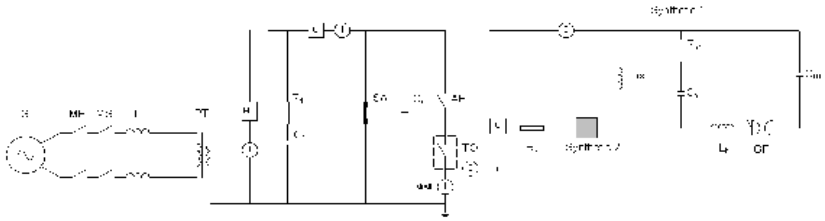
Korea: T100 circuit for 800 kV (platform method) [31]. Test breaker at half the tested voltage; half voltage application in phase opposition at both terminals. T100s peak voltage reported: 1189 kV [20]	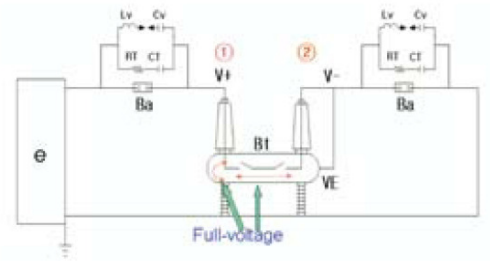

Recently, various alternative circuits, partially applied in the nineties for the TEPCO project have been proposed for UHV testing by Japanese authors [32]. In section 7.10 a detailed description is presented on testing UHV gas circuit breakers, including representation of the stress to the (opening) resistor unit and its interrupter, based on experience from the TEPCO project

7.4.2 RV test

Challenges still remain in the development of high-power testing of UHV circuit-breakers such as achieving the correct ac recovery voltage (RV) after interruption and the proper representation of transient stresses in unit tests. Regarding the former, special tests can be carried out by applying an ac or dc voltage to the enclosure and applying the TRV in opposite polarity to the breaker terminals, with the breaker on an insulating platform (Figure 7.4.3). By increasing the test peak value to the RV peak value, 100 % TRV and RV will appear between fixed contact and enclosure [33] and a positive test result will confirm the interruption capability.

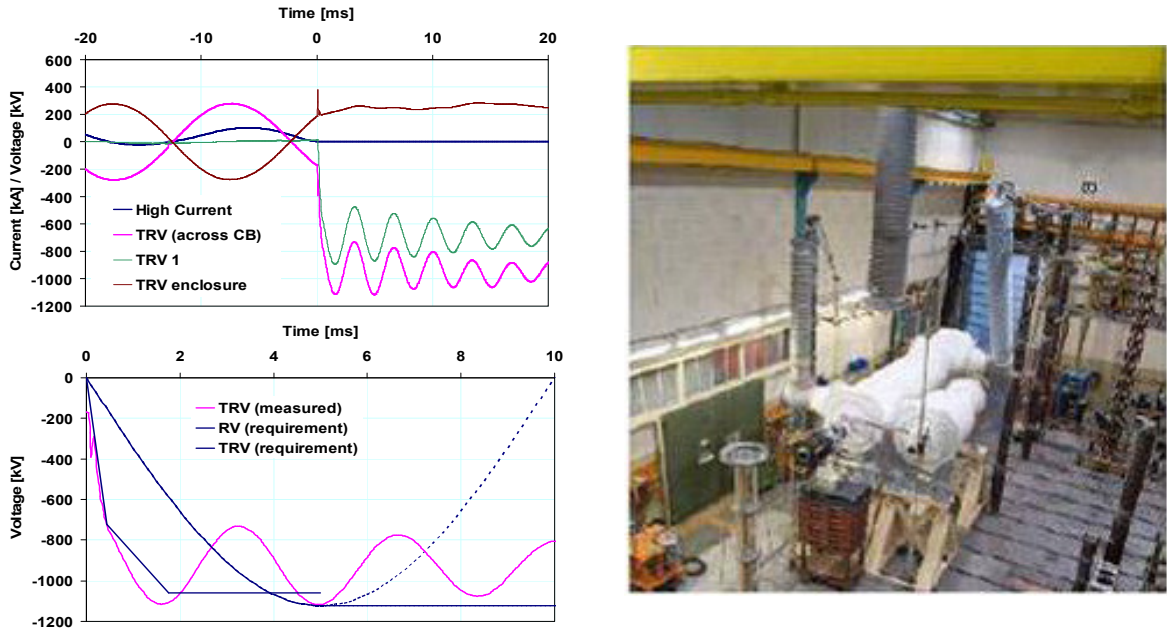

Figure 7.4.3 Full pole tests, required and prospective TRV and RV for terminal fault T100a (left) test set-up (right)

7.5 Remaining challenges in UHV power testing

The following challenges still remain in the development of high-power testing of UHV circuit breakers:

(1) There is a lack of testing experiences regarding the correct application of ac recovery voltage after interruption (as required by IEC 62271-101).

(2) Full-pole capacitive current interruption has not yet been demonstrated although synthetic circuits have been described [24 - 28]. For 1100/1200 kV very large ac voltage stresses will have to be produced and a major problem will be the decay of recovery voltage.

(3) Fully satisfactory making tests have not yet been demonstrated. Spark gaps for full voltage are necessary in full-pole synthetic making. The application of fuse wire to promote pre-arcing for circuit-breakers is not accepted and the acceptability of using reduced gas pressure is under discussion.

(4) Measurement can be problem in "ground" method test-circuits due to the very high-voltages involved and their low-switching frequency content for which standard commercial voltage dividers are not available.

(5) Insufficient voltage at the output of the current source in synthetic testing may pose problems but can be overcome by using several generators and/or suitable short-circuit test transformers in series.

(6) Synthetic testing with voltage / current injection. In order to represent the thermal interruption stresses adequately during synthetic short-line fault testing, current injection must be used in order to get the best representation of the initial rising part of the TRV. However, for the highest voltages, current injection cannot be applied due to fundamental limitations of the method [34]. For dielectric aspects of TRV withstand voltage injection is acceptable.

(7) No tests have been performed yet with the proposed reduced line surge impedance and the increased busbar surge impedance (with respect to the present standardized values in IEC). Hence, realistic ITRV testing remains to be demonstrated.

7.6 Switching tests for disconnecting switch, earthing switch and high-speed earthing switch

7.6.1 Disconnector

7.6.1.1 Bus-charging tests

Tests on bus-charging current switching capability of 1100 GIS disconnectors in STRI labs in Sweden are reported in [35, 36]. The aim of this test is to demonstrate that the switching arc remains between the disconnector contacts. Due to the slow switching process, a large number of successive breakdown and recovery events can be observed, manifesting themselves as very fast transient overvoltages (VFTO) inside the GIS, which can only be monitored with special UHF sensors. Full scale measurements report VFTO of some 2000 kV, with rise time of a few tens of ns [11], see figure 7.6.1. When switching capacitive current, the focus is on VFT overvoltages in particular. In addition to the requirements for the disconnector, the overvoltages that occur represent a major challenge in relation to the EMC of the measurement and control equipment. Figure 7.6.2 gives an impression of the test set-up.

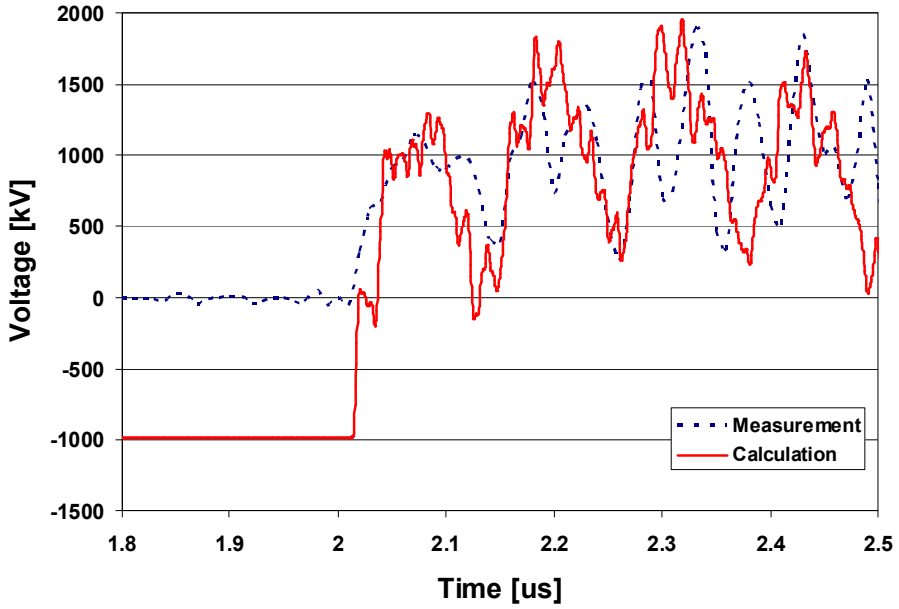

Figure 7.6.1 VFTOs when switching busbars with a 1100 kV GIS disconnectors as per IEC 62271-102 [11]

Figure 7.6.2 Test pole for bus-charging switching tests [11]

IEC 62271-102 Annex F defines three test-duties of which, TD2 (switching of parallel capacitor current under full out-of-phase condition) needs particular attention. The authors of [35] conclude that, in the UHV case, the voltage across the disconnector during switching is temporarily higher than the rated dielectrical test voltages, due to the trapped charge on the grading capacitor. Values between 3 and 4 p.u. are reported, depending on the capacitance to ground during testing with full AC voltage on both sides of the disconnector [35].

Regarding TD3 of IEC 62271-102 Annex F (capacitive current switching capability tests) it was concluded by the authors of [36], based on full-scale testing with 2 A, that "*a current-switching capability test with a bus-charging current higher than 1 A and using common high voltage transformers is not possible. Unavoidable resonance effects lead to overvoltage in the range of 2 p.u. to 3 p.u. This voltage stress does not correspond to real service conditions*". The authors recommend to check if such a condition is a typical electrical network condition and to re-discuss the test values and the test procedure for switching of bus-charging currents by disconnectors.

Japanese sources report 2.8 p.u. [5] (also exceeding LIWV) which can be limited to 1.3 p.u. by an internal resistor. Testing is reported to verify the absence of flashover to the enclosure, and the voltage and energy withstand of the resistor and disconnector [5]. Impulse generators were used to produce discharges in the disconnector and create conditions that are identical to the most severe conditions of switching.

7.6.2 Bus transfer tests

Testing is reported by Japanese authors [5] based on the TEPCO project specification for loop switching of 8000 A, with 300 V recovery voltage and rate of rise of 500 V/μs.

Detailed calculations for the Chinese SGCC project, taking into account the long busbar length and the associated high values of the induced voltages against which the disconnector must transfer the load current, can be found in [37].

Various tests on air-insulated 1100 kV disconnectors are reported in [38].

7.6.3 Earthing switch

No specific testing is reported yet. For the making tests, the discussion of the possibility to use a fuse wire for the initiation of the pre-strike arc is still going on, but as yet, this method remains allowed in the soon-to-be-revised IEC 62271-102 (in contrast to making tests with circuit breakers). Also, proposals on using reduced gas pressure have been published [39].

7.6.4 High-speed grounding (earthing) switch (HSGS, HSES)

High-speed earthing switches need to interrupt both electromagnetic and electrostatic induced currents and, as observed in some cases, need to be able to cater for an absence of current zeros that may last for almost 100 ms. Test experience of UHV equipment is available from Japan [40] ad the authors report testing of the following conditions for 40 (Case A) and 200 (Case B) km transmission lines:

(1) Interruption of electromagnetic induced current of up to 7 kA (A), with 640 kV TRV peak (B) and with RRRV = 1.15 kV/μs (A).

(2) Interruption of electrostatically induced current of up to 1.2 kA (B) with 900 kV for TRV peak (B)

(3) Interruption of current having delayed current zero, starting at around 17 kA, and decaying to zero in around 90 ms (See figure 7.6.3). Very special test-circuits are described in [5, 40].

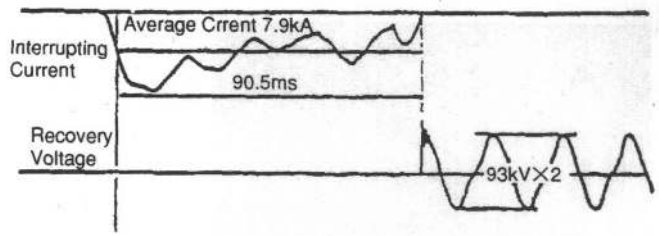

Figure 7.6.3 Oscillogram of tests on HSGS current interruption without current zero [40]

A more detailed description of the experiences from Japan [41, 42] are presented in the following sections.

7.6.4.1 Operation of HSGS

HSGS (HSES) used in Japan has a puffer interrupting chamber with a hydraulic operating mechanism. To ensure the interrupting capability for an arcing time of 80 ms, the dead volume in the puffer cylinder was increased to allow SF_6 gas of the required pressure to be continuously supplied between contacts, even after the movable contact reached its full-stroke. The devices were specified to be free of re-ignitions and re-strikes during interruption of electrostatic induced currents such that no surges are generated during normal operation. During the interruption of electromagnetically induced currents re-ignitions may occur if the arcing time is sufficiently short. The TRV peak value for electromagnetic induced current interruption is 640 kV, which will be transferred to the ground side in case of re-ignition. This needs effective measures to lower the transient surge voltages generated in the grounding circuit to a safe level.

7.6.4.2 Laboratory tests

(a) Voltage surge tests

Figure 7.6.4 shows a HSGS under test with the GIS simulated by connection of a 13m busbar and a transmission line simulated by coupling a capacitor to the bushing. The grounding system was simulated by a mesh system of copper wires positioned at 2 m intervals and further by a main mesh system having copper plates laid at a larger spacing. The induced voltages were measured at various points with low voltages and also directly measured at the

insulated terminal with high voltages. The results showed that a combination of 4 grounding plates arranged radially could lower the induced voltages to one-tenth of the voltage compared with a single grounding plate. For 640 kV on the main circuit, a voltage of 15.8 kV, 25 MHz, is generated at the terminal with a damping time constant as low as several 100 μs.

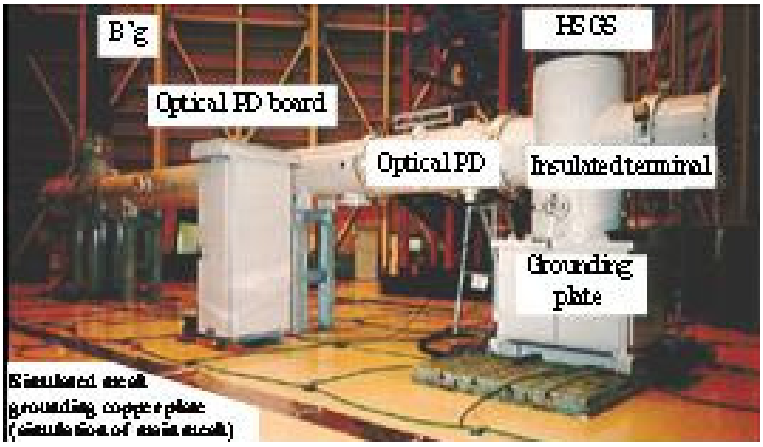

Figure 7.6.4 Surge voltage measurements in the grounding system

(b) Electrostatically induced current interruption test

Figure 7.6.5 shows the circuit for the electrostatic induced current interruption test with HSGS and also a test oscillogram. In the circuit diagram, the circuit part to the left of the HSGS is the current source and to the right side is the voltage source.

A current with delayed current zero is generated by feeding an oscillating current from a pre-charged capacitor C_v via reactor L_3 to the HSGS. CB2 is closed at the peak current and feeds the electromagnetic energy at L_3 as a current to the HSGS via reactor L_2. A small capacitive current is fed beforehand from the voltage source. When the arcing time of the HSGS reaches 80ms, CB2 opens causing a current zero, and then CB3 and HSGS are opened simultaneously, causing a (1 – cos) type TRV to appear across the HSGS.

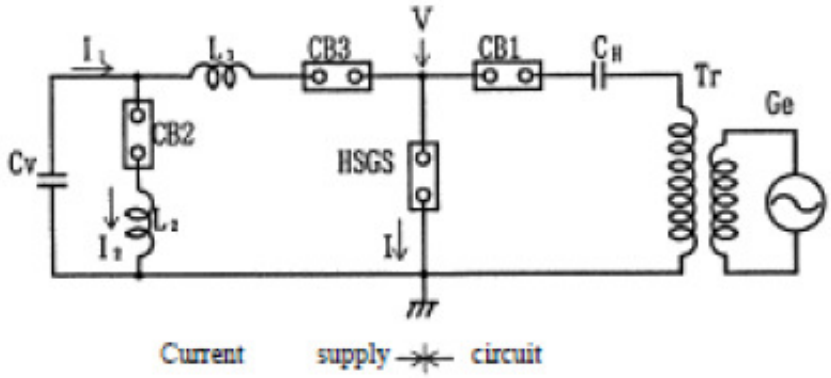

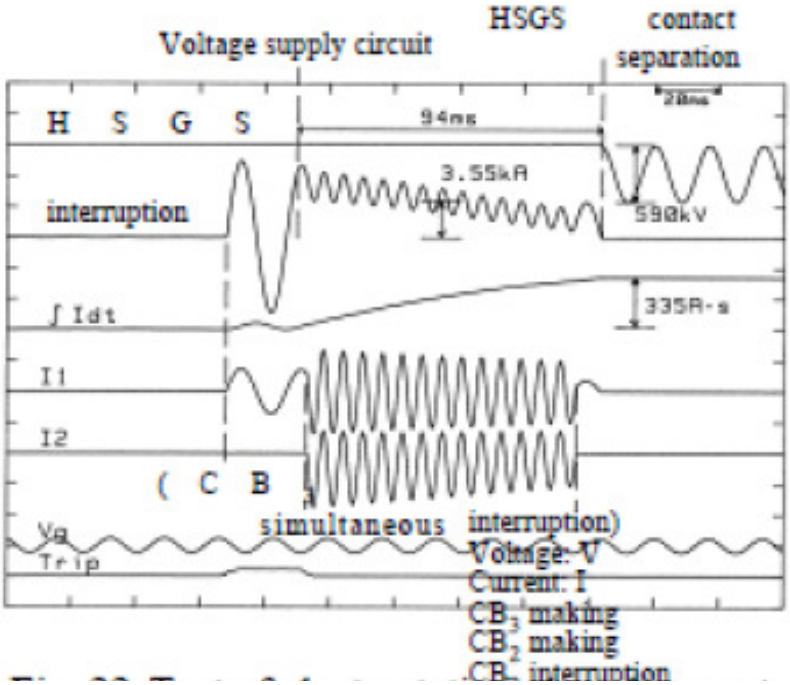

Figure 7.6.5 Test of electrostatically induced current interruption with delayed current zero

(c) Electromagnetically induced current interruption test

Figure 7.6.6 shows the circuit for the electromagnetically induced current interruption test and a test oscillogram. Two short-circuit generators G_1 and G_2 are operated synchronously with G1 supplying current i_1, containing the DC component.

When the current reaches its peak value, the auxiliary circuit breaker, Sh, is closed to superimpose current i_2 on i_1 with a phase angle difference of 180 degree. When Sh interrupts, a current lacking current zeros, i_p , is fed to the HSGS for 80 ms. The remaining current is i_1 and a current zero is created permitting interruption. As the TRV at the G1 side is adjusted to the specified waveform, the conditions during the interruption process can be made the same as in a direct test.

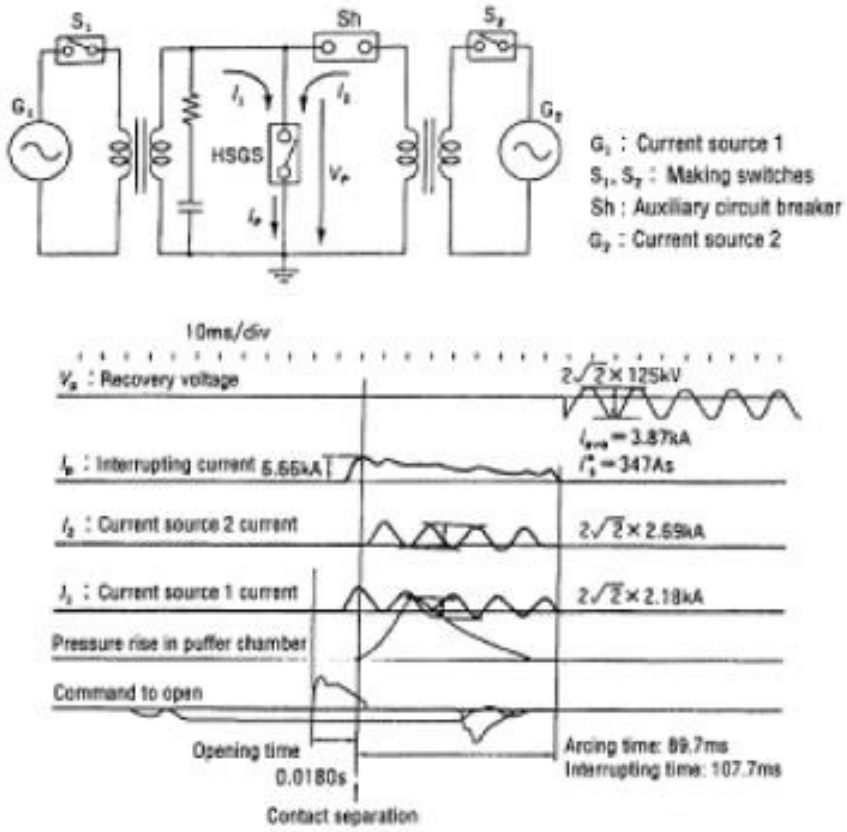

Figure 7.6.6 Test of electromagnetically induced current interruption with delayed current zero

7.6.4.3 Field test

(a) Measurement set up

Two circuits have been used, one of which is shown in figure 7.6.7. In the test, DS1 and GCB were left open.

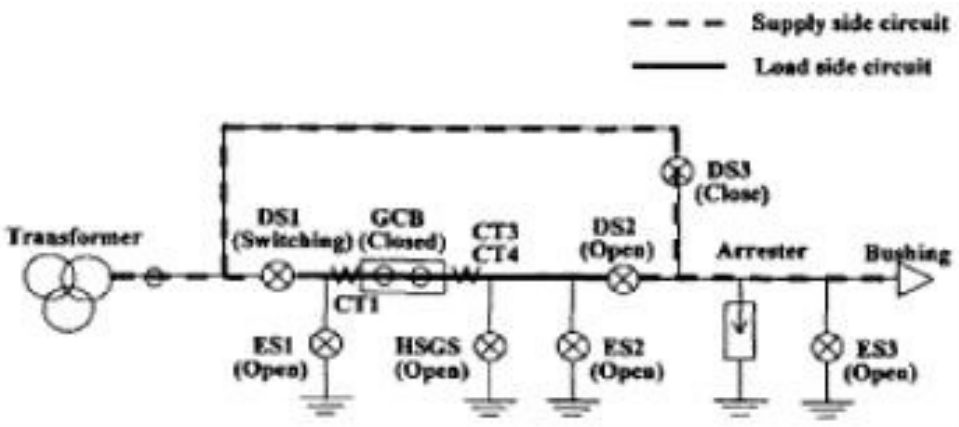

Figure 7.6.7 Field test circuit

In one circuit (circuit-A), a residual voltage was applied to a long section from the HSGS to the bushing and to DS3 by opening the DS3. In the other circuit (circuit-B), a residual voltage was applied to a short section from the HSGS to DS2 by opening the DS2. VFTOs generated by closing of the HSGS were measured. Measurement of VFTO in the high-voltage circuit was by means of the same capacitance divider used to measure DS surges.

VFTOs were measured at HSGS, DSl, and bushing. The potentials of the HSGS grounded terminal and the tank at the HSGS grounded terminal were also measured using an electro-optical conversion transmission system. In the field, the maximum inter-electrode flashover voltage when closing and re-opening the HSGS is 640 kV [42]. In the test, as another item for evaluating the surge level when a ground fault at a normal operating voltage was simulated, the residual high-voltage circuit voltage was set as close to 898 kV(=l p.u.) as possible. The maximum residual voltages for the phases were 820 kV, 883 kV and 805 kV.

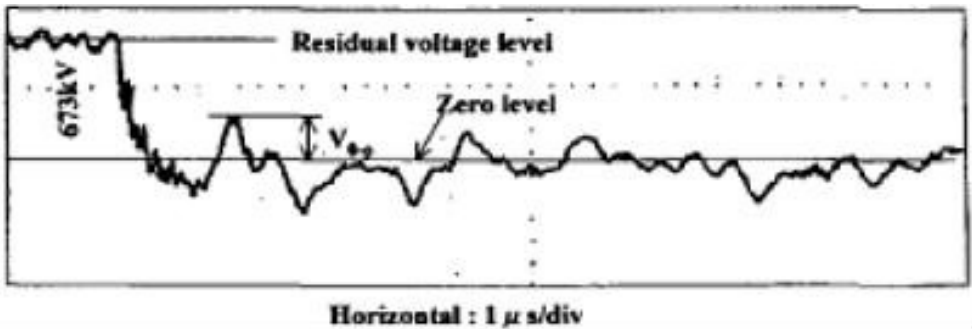

Figure 7.6.8 Voltage measurement of high-voltage circuit (C phase of HSGS)

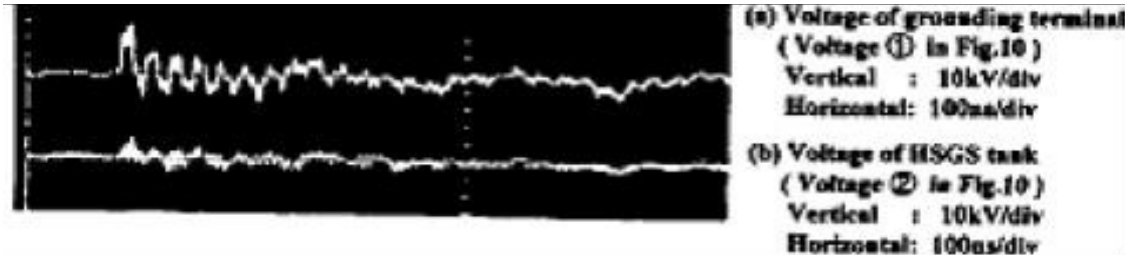

Figure 7.6.9 Voltage measurement of grounded circuit (C phase, residual voltage: 673 kV)

(b) Results

Figure 7.6.8 shows a measured waveform of a surge voltage in the high-voltage circuit in circuit-A. Figure 7.6.9 shows the waveforms, measured simultaneously with figure 7.6.8, of voltages at the grounded terminal. In the voltage waveform in the high-voltage circuit of the HSGS, a higher-frequency component of approximately 38 MHz is superimposed on the basic frequency component of 5.15 MHz at the initial part. This initial higher frequency component agrees with the frequency component of the surge voltage in the HSGS grounding circuit. Its duration is about 300 ns, which is comparable to that of the surge at the grounding terminal. From these results, the higher frequency component superimposed on the surge waveform in the high-voltage circuit can be presumed to be a frequency related to the grounding circuit.

(c) Summary of HSGS field tests

(1) In the high-voltage circuit, the maximum surge voltage was lower than 1.1 p.u.

(2) At the HSGS grounded circuit terminal, the maximum surge voltage was 6.32 kV_{peak}, which is as low as 32 % of the insulation terminals withstand voltage. This verified the effect of the low-inductance grounding structure of the grounded terminal.

(3) In the protective and control components, the maximum surge voltage found was lower than the lightning impulse test voltage of the terminals.

The voltages generated were nearly proportional to the residual DC voltages. Figure 7.6.10 shows the relationship between grounding circuit surge voltage and residual DC voltage. This is probably because the voltage generated in the grounding circuit contains only high-

frequency component around 38 MHz determined by the grounding circuit. Both grounded terminal and HSGS enclosure voltages saturated in the high voltage range above 500 kV.

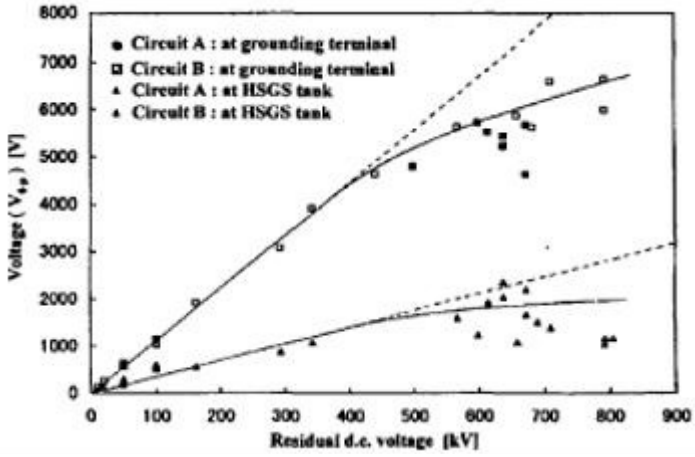

Figure 7.6.10 Relation between residual DC voltage and generated voltage (C phase grounding circuit)

7.7 Dielectric tests for circuit breaker, disconnecting switch, earthing switch and high-speed earthing switch

Technical requirements for dielectric testing of equipment in the UHV range have been developed by individual users, manufacturers and laboratories, such that there is only limited worldwide standardization. A review of the present state-of-the-art and problems that emerged during dielectric testing of UHV equipment when compared to the applicable international standards is under consideration by CIGRE WG D1.36, in order to identify areas of commonality and of divergence and to address technical “best practice”.

Special requirements and standardization for dielectric testing of UHV equipment will result from the ongoing clarification process on the related challenges and pending aspects, a summary of which is presented hereunder.

7.7.1 The challenges

UHV equipments present testing problems due to their relatively huge dimensions in comparison to those of test laboratories making the test room size a genuine limitation for dielectric testing of components’ external insulation. Considering AIS equipment specifically, challenges include the space available for the indoor test room, the ability to perform withstand tests under wet conditions, partial discharge or RIV tests, the verification of performance under contaminated conditions and the ability to properly represent other electrical-environmental stresses [43].

For GIS, tests under combined alternating and switching impulse voltages require a certain minimum distance between bushings and between live parts and walls these distances already exceed the limits of most high-voltage laboratories for the UHV range. The size of the test objects substantially increases the capacitance of the test circuit and a high-performance high-voltage transformer must also be available.

7.7.2 The pending aspects

Problems emerged during dielectric tests of UHV equipment concern the overshoot of lightning impulse voltage, the over-coupling of combined voltages, the background noise

level of PD measurement and the applicability of non-conventional PD measurement methods (UHF).

Particular considerations that have been reported [12] are as follows:

(1) Impulse generators are usually not designed for the dimensions of UHV test objects meaning that lightning impulse peak voltages may overshoot by 7% to 10%. It is proposed that the third edition of IEC 60060-1 will accept this situation however specific requirements for UHV testing are under consideration by IEC TC42.

(2) UHF-PD measurement allows very sensitive detection & localization of a PD source by means of a time-of-flight measurement providing that sufficient field sensors are integrated into the component. One apparent drawback of the UHF measurement is that the signal cannot be unambiguously correlated to the apparent charge from the PD source, so calibration as in accordance with IEC 60270. However, a so-called 'sensitivity verification' of the UHF sensors is possible

(3) Combined voltage tests performed across open isolating distances and open switching devices require the application of alternating voltage on one side and of impulse voltage on the other. In the case of UHV components, the relatively high switchgear capacitance causes over-coupling of the impulse voltage on the alternating voltage transformer during the combined voltage tests. The voltage drop can be compensated by a voltage increase or the over-coupling can be reduced by additional lumped capacitances on the alternating voltage side.

(4) The simple extrapolation of insulation distances and atmospheric correction factors from EHV to UHV cannot be technically justified and additional research on UHV insulation will be necessary to improve size solutions and specific standardization.

Investigations are under way to determine the breakdown behaviour of SF_6, the voltage linearity of measurement systems (for LI, SI, AC, DC) and the most appropriate calibration methods for greater than 1 MV.

Chinese simulation studies are presented in [44].

7.7.3 Experience of high-voltage testing of 1100 kV circuit breakers

7.7.3.1 German experience [19]

Power testing of a circuit breaker for a system voltage of 1100 kV has been performed in the Netherlands as described in section 7.2.6 and dielectric testing has been performed at the German test institute FGH. This has demonstrated that, whilst challenges remain, solutions for testing at the UHV level have been found based on available test facilities.

UHV metal enclosed circuit breakers with four interrupter units, for use in dead tank or GIS installations have been developed based on existing 550 kV designs, and having insulation levels according to the specification for the Chinese 1100 kV system.

The following voltage values have been used to prove the dielectric withstand capabilities to earth and across the open circuit breaker:

Power-frequency withstand voltage	to earth	1100 kV
	across open CB	1180 kV + 320 kV
Lightning impulse withstand voltage	to earth	2400 kV
	across open CB	2400 kV + 630 kV
Switching impulse withstand voltage	to earth	1800 kV
	across open CB	1675 kV + 900 kV

Figure 7.7.1 Test set up for dielectric test of circuit-breaker 1100 kV in Germany [19]

The test voltages to ground are also appropriate for 1200 kV systems. The voltages across the open circuit breaker have to be carried out as combined voltage test with one component related to the system voltage. According to the standardized test voltages for the lower voltage levels, the lightning impulse voltage across the open breaker has to be combined with 70 % of the power-frequency voltage line-to-ground (630 kV) and the switching impulse with 100 % line-to-ground voltage (900 kV). Because of the relation to the system voltage the test results cannot be transferred directly to a 1200 kV system. For this case the experience and the knowledge concerning the withstand capability of the breaker units from the application in 550 kV systems provide confidence that the performance for a 1200 kV system will be met also.

To overcome test facility limitations regarding high voltage testing, half-pole testing can be an appropriate solution to demonstrate the withstand capability of the complete breaker. Since the breaker is symmetrically designed testing of only two units will prove the correct line to earth withstand voltages whilst optimising the space required in the laboratory.

Concerning the withstand capability across the open breaker, the voltage distribution has to be calculated and the test voltage can be reduced accordingly. Examples of such calculations are given in [45].

(a) Partial discharge measurement

Reduction in size of the test object may also overcome problems associated with testing outdoors where partial discharge measurement according to the conventional PD measurement of IEC 60270is not possible. The availability of suitable high-voltage test halls with screened walls will be much higher with the reduced size of the test object.

(b) Overshoot of lightning impulse voltage shape

Due to the size of the complete test circuit, and the inductances included in the loops of the connecting wires, an oscillation of the lightning impulse test voltage cannot be avoided. An overshoot of 10 % above the double exponential impulse curve 1.2/50 µs was recorded (See figure 7.7.2 impulse shapes). To reduce the overshoot an increase in front time would have been necessary. It was decided to keep the front time within the tolerances given by IEC and accept the relative overshoot magnitude not exceeding 10%. The relevant Technical Committees could propose other specification.

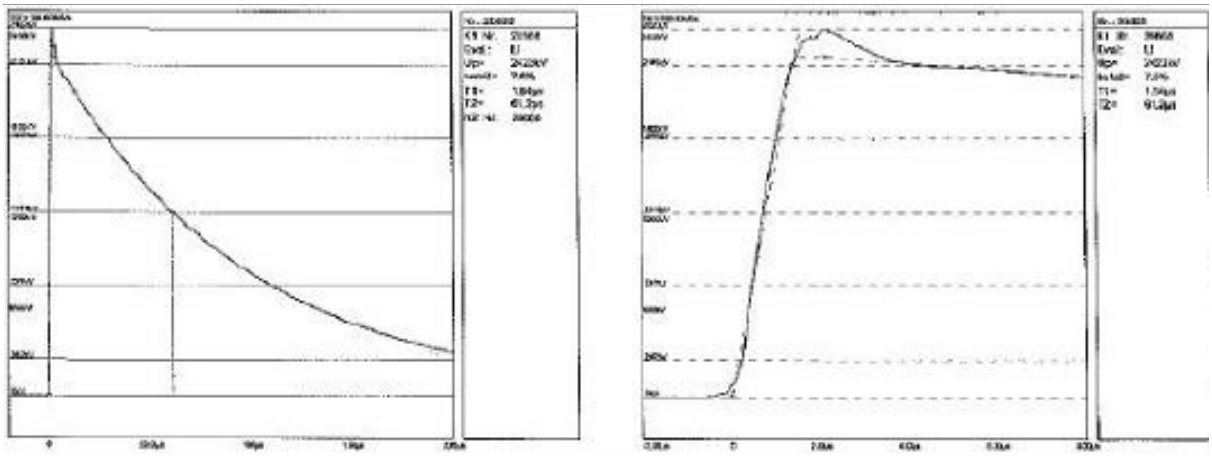

Figure 7.7.2 Impulse shapes of lightning impulse test on UHV circuit breaker [19]

7.7.3.2 Chinese/Swiss experience [46]

The development and type tests were carried out at XIHARI Laboratories in China (See figure 7.7.3), with the parameters shown below. Furthermore, PD measurements and lightning impulse voltage tests up to 3 MV were performed [11].

Power-frequency withstand voltage	to earth	1100 kV
	across open CB	1100 kV + 635 kV
Lightning impulse withstand voltage	to earth	2400 kV
	across open CB	2400 kV + 900 kV
Switching impulse withstand voltage	to earth	1800 kV
	across open CB	1675 kV + 900 kV

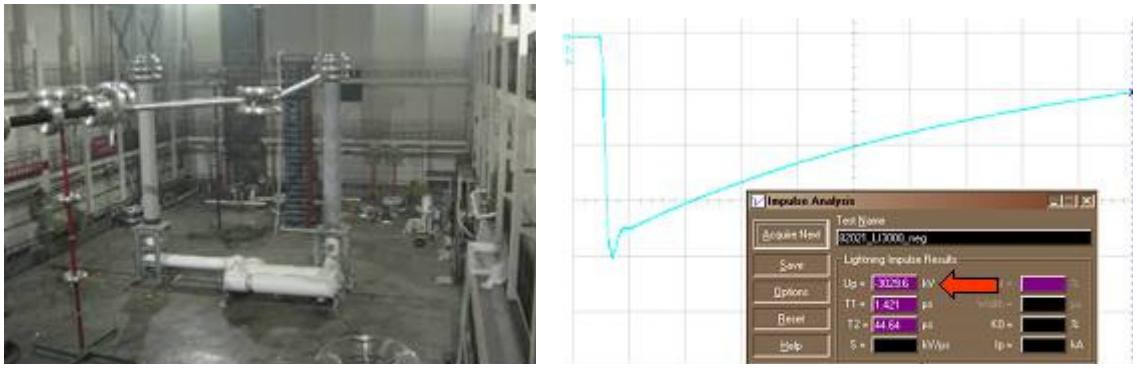

Figure 7.7.3 Impulse shapes of lightning impulse test on UHV circuit breaker and test set-up

The test pole for dielectric type tests has a capacitance of about 3 nF and that transformer's power limit only allows a relatively low value of the coupling capacitor of 0.35 nF.

Due to external interference from the test systems and corona, this set-up results in a background noise level of approximately 7 pC at 1000 kV. To achieve high sensitivity for the laboratory measurements, non-conventional PD measurement like acoustic and UHF PD measurement methods were also used as the measuring procedure for type tests in addition to the conventional PD measurements.

Impulse generators are not usually designed for the dimensions of 1100 kV GIS test objects. As a result of the large dimension and the associated inductance of the test circuit, overshoots of 7% to 10% occur around lightning impulse voltage peak which is above the limit given in IEC 60060. For SF_6 insulated systems, compensation of the lightning impulse voltage according to the recent revision of IEC 60060-1 is considered correct also for larger overshoots. Since testing with existing impulse generators will have to continue in the future, the recommendation is that the requirement for dielectric type tests at 1100 kV should be taken into account in the standardization and CIGRÉ WG D1.36 is currently working on this topic.

Combined voltage tests are conducted on the open isolating and contact gaps where alternating voltage is applied on one side and an impulse voltage on the other. The high breaker capacitance causes over-coupling of the impulse voltage on the alternating voltage transformer during the combined voltage tests. The voltage drop must be compensated by an increase of either AC or LI voltage. The over-coupling can be reduced by additional support capacitors of several nF on the AC side however the support capacitance value is restricted by the power limit of the transformer. During 1100 kV type tests, maximum over-coupling of 20% of the impulse voltage has occurred and compensation measures have been required on either side. Inevitably, compensation on the impulse voltage side stresses the earth insulation beyond the rated values and compensation on the alternating voltage side leads to very long AC loads close to the rated short-time power frequency withstand voltage. Combined tests with low voltage losses require alternating voltage transformers with currents from 3 A to 4 A on the high-voltage side. In this case too, the special requirements for 1100 kV must be discussed in connection with standardization.

7.7.3.3 Japanese experience [44]

Dielectric type testing of UHV GCB for the SGCC project incorporates a combined voltage test which applies the power-frequency voltage (AC voltage) to both terminals across the open switching device for 1 minute. The AC-AC combined test voltages are 635 kV_{rms} for one terminal and 1100 kV_{rms} for the other terminal at reversed phase.

Figure 7.7.4 Set up for UHV dielectric tests in Japan [47]

This AC-AC combined voltage test procedure presents three key problems as follows:

(1) Two AC voltage sources are needed whereas high-voltage testing laboratories have only one large scale testing transformer in a testing room.

(2) Since UHV GCB with two breaks have grading capacitors across the breaks, large current flows through the capacitors in the test circuit. One source voltage influences the other source voltage greatly due to the capacitors making it difficult to control the applied voltages individually.

(3) A large power supply is needed due to the current through the grading capacitors of UHV GCB.

These problems are solved by the following methods:

(1) The laboratory has already installed a testing transformer of rated voltage 2300 kV in a testing room and another testing transformer of rated voltage 900 kV was transferred into the same testing room. The AC-AC combined voltage test setup is shown in figure 7.7.4.

(2) The AC-AC combined voltage test was carried out using a first AC voltage source circuit in which the current becomes a minimum due to the resonant nature of the circuit. The second AC voltage source was arranged to ensure that the change of impedance is low. By optimizing the composition of these circuits the mutual influences on each AC source voltage became very small and each AC voltage control was made possible.

(3) A suitable generator in the high power laboratory was used to supply both AC voltage sources catering for the large power requirement. An AC voltage of 1100 kV_{rms} + 635 kV_{rms} under out-of-phase conditions was applied across the terminals of UHV GCB for 1 minute with a phase difference between AC voltages applied across terminals of about 176 degree.

7.7.4 Transient stress calculation for individual chambers

Unit tests of metal enclosed circuit breakers with grading capacitors may not represent the transient stresses that occur in the real case due to unequal dielectric behaviour of the arcing chambers. Stresses on grading capacitors, such as due to the occurrence of pre-strikes, are not represented well during unit tests and the frequency-dependent voltage distribution was calculated by using real grading capacitors containing both inductance and resistance values. As an example, the dynamic behaviour shown in figure 7.7.5 is obtained.

By way of clarification, the voltage stress for individual interrupting chambers for an impulse voltage stress with a rise time of 400 ns is shown. In summary, it has been established that the individual interrupting chambers are not overstressed even when subject to VFT overvoltage stresses. For verification, the CB was used as test device for switching of bus-charging current by DS [33]. The circuit breaker in the open position was used in order to have the proper capacitive current during testing and VFTO in the range of 2 MV were measured. The perfect behaviour of the grading capacitors during the DS switching tests confirms the calculation results and dielectric capability of the grading capacitors.

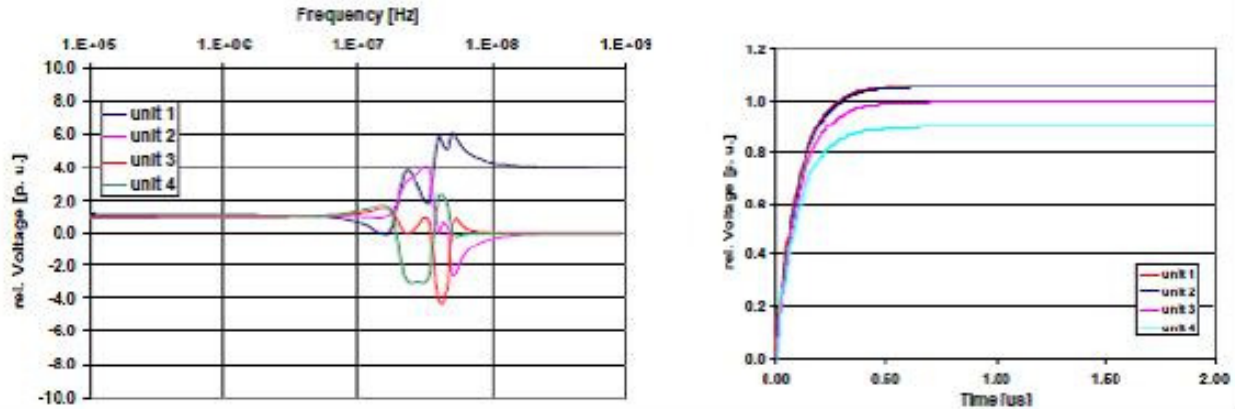

Figure 7.7.5 Voltage stress for individual interrupter chambers, in relation to one quarter of the total voltage with voltage stress from one side, frequency-dependent (left) and for impulse stress with a rise time of 400 ns (right)

7.8 Tests for MOSA

7.8.1 The challenges

Arresters in UHV systems are used to ensure insulation protection levels which are extremely low compared with those for the EHV range and below. Typically, the switching impulse withstand voltage level is only 2 p.u. and the lightning impulse withstand voltage level is 2.5-2.7 p.u. As a consequence, issues such as the dielectric requirements and tests on the arrester housing, the energy handling capability, the protective distance and the mechanical and thermal stresses require special considerations [48].

7.8.2 The pending aspects

From a specification and testing point of view the existing standards and application guidelines for surge arresters do not cover all requirements for UHV applications, and need to be revised. Due to the very low protection levels employed, surge arresters for UHV applications are very sensitive to temporary overvoltages which determines the energy discharge capability [19].

In particular, the operating test duties, the insulation withstand tests of the arrester housing, the mechanical tests for the different possible designs, the voltage distribution during tests, the pollution performance and the tests on complete arresters are subjects still under consideration by IEC technical committees TC 37 (surge arresters) and TC 28 (insulation coordination).

Test improvements are needed when dealing with the following features:

(1) The clearance to ground, as well as the geometry of the grading system have strong impacts on the dielectric strength and the performance under SI voltages at UHV levels. A test on the complete housing assembly is considered to be mandatory for UHV applications.

(2) The energy related aspects, such as the energy handling capability for MO-arresters, and the appropriate test procedures require review. In a typical UHV system the required specific value of energy handling capability is at least 25 kJ/kV of rated voltage. This can be catered for by having multiple (typically three to five) MO columns in parallel but the energy rating cannot be tested according to the arrester standard IEC 60099-4. An operating duty test according to line discharge class 5 will inject only 50 %-25 % of the required energy meaning that the test procedure for UHV arresters has to be adapted accordingly. For instance, energy could be injected by more than two long duration current impulses (subject under discussion by CIGRE WG A3.17).

(3) The effect of the surge arrester active parts on the electrical behaviour of the insulator housing (e.g. voltage grading or unbalance, radial field stress, internal partial discharge activity, etc) as well as on the thermal behaviour (e.g. heat exchange capability, influence of ambient temperature, solar radiation, etc.). This subject is under discussion by CIGRE WG A3.21.

(4) The mechanical requirements which, due to the huge size of UHV arresters, are very demanding, especially under seismic conditions;

(5) The performance under short-circuit. Arresters will often be installed in close proximity to other equipment in order to achieve effective protection but this makes it particularly important that any possible arrester failure occurs in a “controlled” way.

7.9 Mechanical tests for circuit breakers

The UHV circuit-breakers considered are equipped with a main contact system for fault current interruption and an auxiliary interrupter for interruption of the current in the parallel resistor. To confirm that proper opening and closing synchronicity of both interrupters is maintained over the entire operating temperature range specific tests have been performed [49]. The breaker was placed in a large environment controlled testing room and operated at temperatures from -30°C to +60°C. The opening and closing times during the opening operation of the interrupters were confirmed to remain within the stable range of 32-33 ms thereby confirming that the hydraulic delay circuitry is immune to temperature-induced variations in the viscosity of the hydraulic fluid.

7.10 Japanese approach to multi-part testing of UHV-GCB with opening resistor [32]

7.10.1 Part 1: Thermal interruption verification for main interrupter

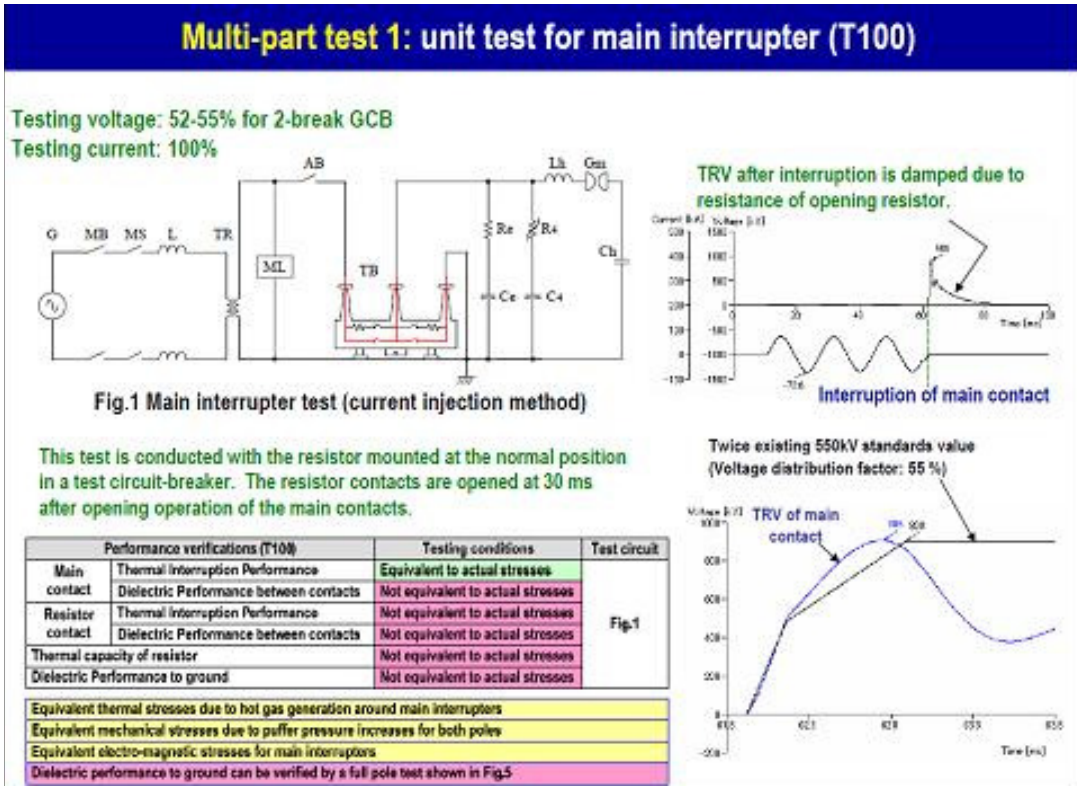

Figure 7.10.1 Short-circuit test T100 for main interrupter to verify thermal interruption performance

7.10.2 Part-2: Dielectric interruption verification for main interrupter

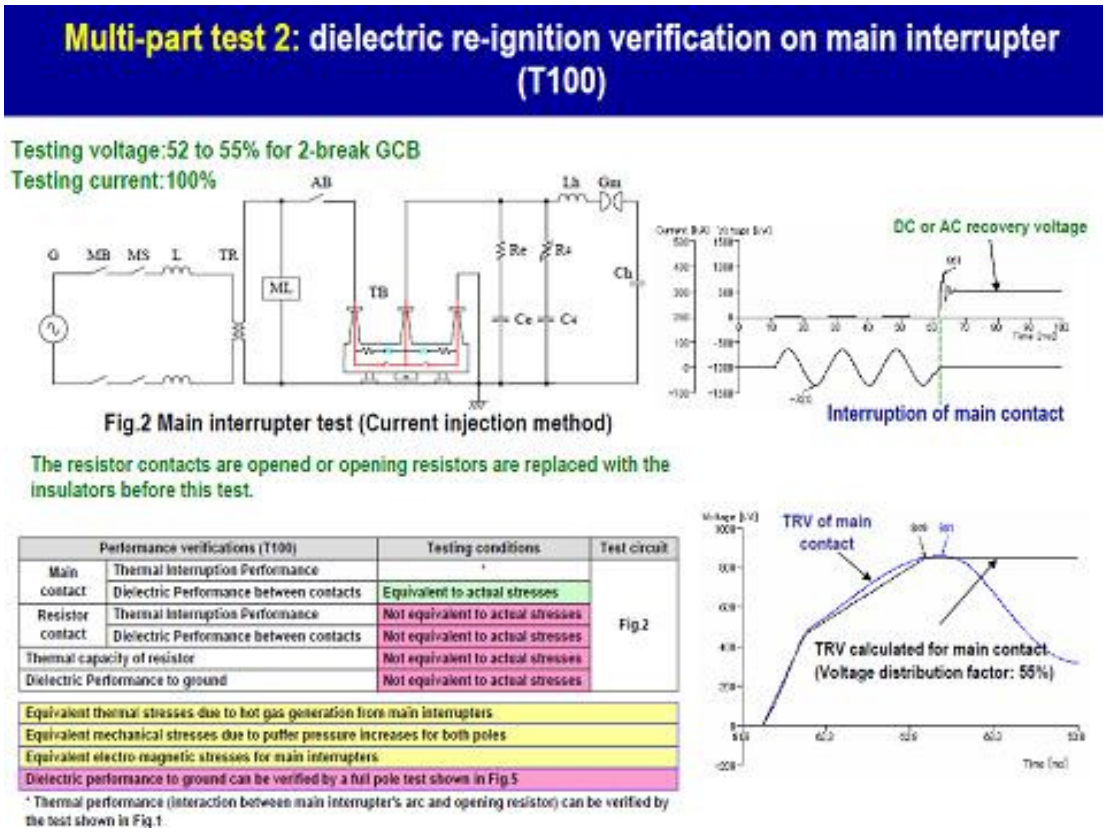

Figure 7.10.2 Short-circuit test T100 for main interrupter to verify dielectric interruption performance

7.10.3 Part-3: Thermal & Dielectric interruption verification for resistor interrupter

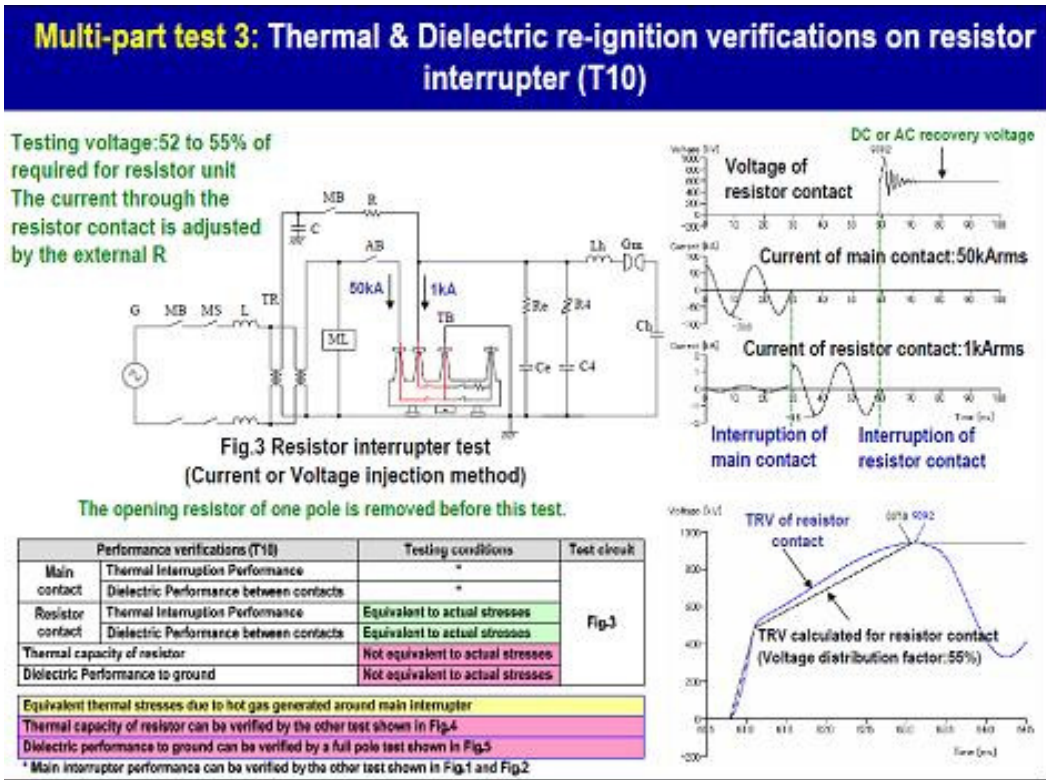

Performance verifications (T10)		Testing conditions	Test circuit
Main contact	Thermal Interruption Performance	*	Fig.1
	Dielectric Performance between contacts	*	
Resistor contact	Thermal Interruption Performance	Equivalent to actual stresses	
	Dielectric Performance between contacts	Equivalent to actual stresses	
Thermal capacity of resistor		Not equivalent to actual stresses	
Dielectric Performance to ground		Not equivalent to actual stresses	

Figure 7.10.3 Short-circuit test T10 for resistor interrupter to verify thermal and dielectric interruption performance

7.10.4 Part-4 Thermal capacity verification for resistor unit

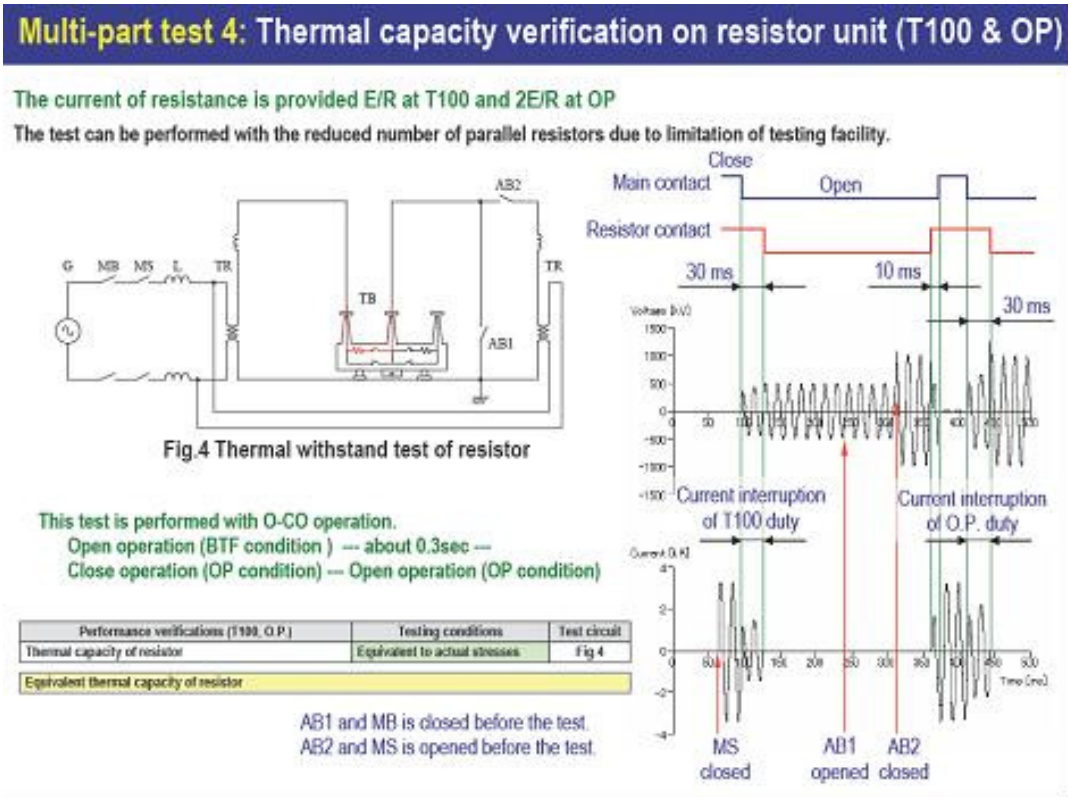

Figure 7.10.4 Short-circuit test T100 for resistor interrupter to verify thermal capacity

7.10.5 Part-5 Full-pole tests for dielectric withstand between life parts and tank

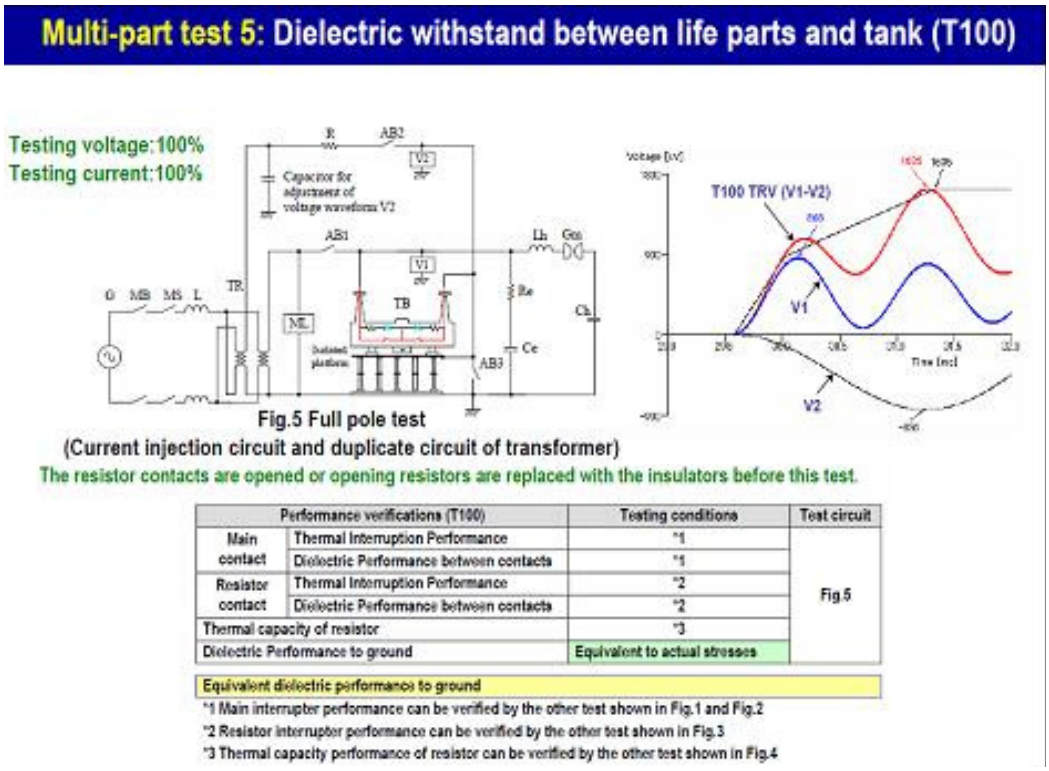

Figure 7.10.5 Short-circuit test T100 for main interrupter to verify dielectric withstand to the tank

7.10.6 T10 and T100 simulation

(a) T10 simulation

For the evaluation of stresses, an EMTP simulation has been performed using a source voltage of 1100 kV, a breaking current of the main contact of 5 kA and a breaking current of about 1 kA for the resistor interrupter. For the TRV of the main contact the rate of rise of recovery voltage (RRRV) is 7 kV/μs. The corresponding amplitude factor is defined as 1.7 and a 700 Ω opening and closing resistor is used. The opening resistor in combination with the surge impedance will lead to a strongly damped system reaction meaning that the opening resistor also decreases the TRV peak value. In the figure, the TRV after resistor interruption is shown. The presence of the opening resistor results in a reduction in phase angle between the source voltage and the simulated current and therefore the voltage at the current zero crossing will decrease as well.

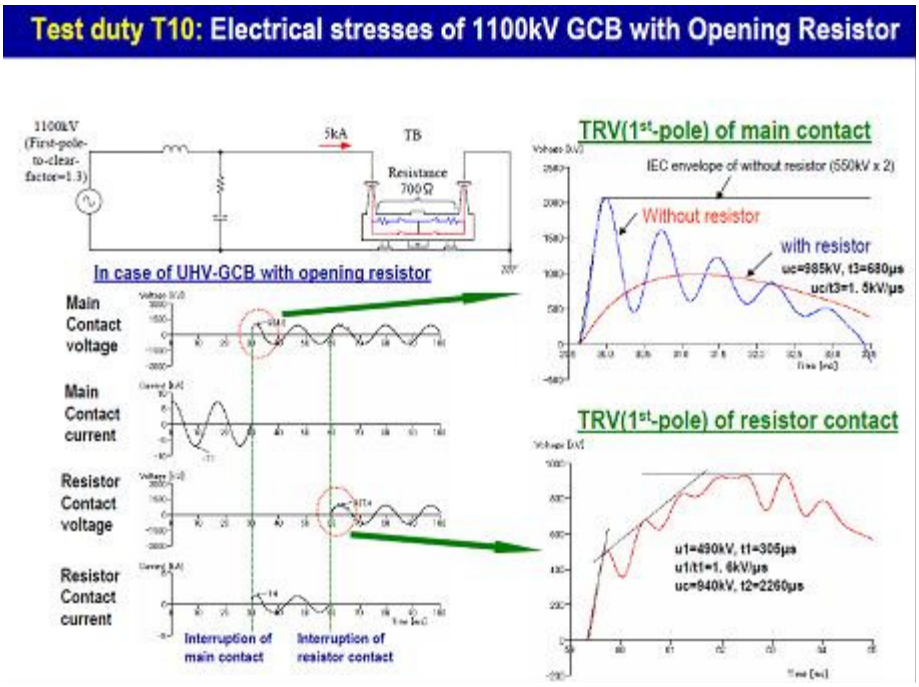

Figure 7.10.6 TRV requirements (T10) for main and resistor interrupters

(b) T100 simulation

The breaking current of the main contact is 50 kA and the breaking current of the resistor contact is about 1 kA. For the 4 parameter TRV of the main contact, the RRRV is 2kV/μs and the corresponding amplitude factor is defined as 1.4. The effect of the interrupting resistor on the peak amplitude of the TRV is smaller than in the T10 case since the surge impedance correlates with smaller applied inductance of a T100 duty and hence the ratio of the surge impedance and the closing resistor decreases.

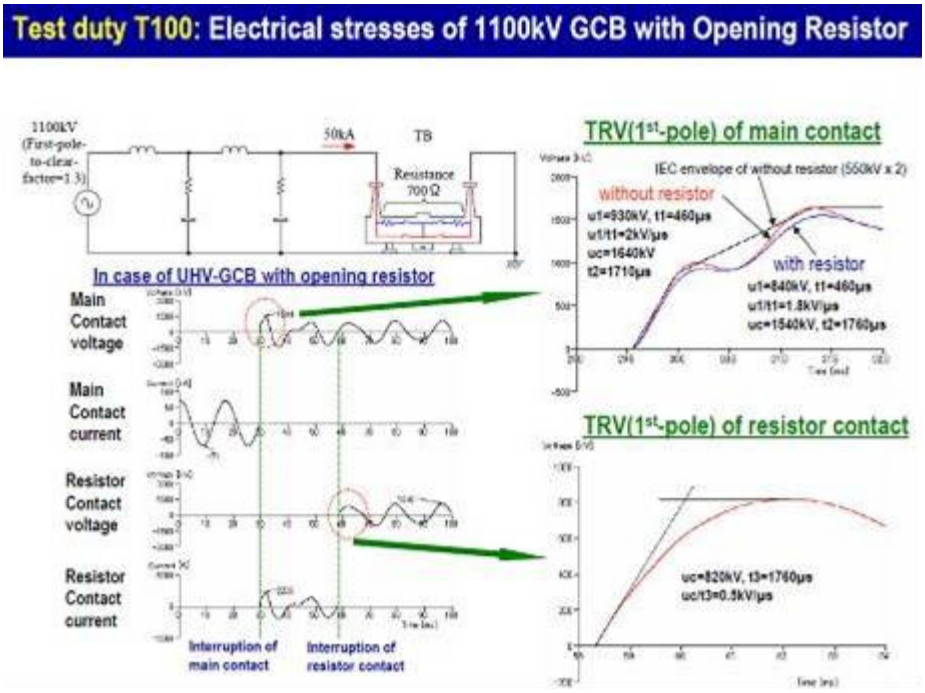

Figure 7.10.7 TRV requirements (T100) for main interrupter with opening resistor

Table 7.10.1 shows the TRV and breaking current results in the case of the T10 and T100 duties. It can be observed that the influence of an opening resistor is small for a T100 duty compared to a T10 duty. For the resistor contacts, the phase difference between the breaking current and voltage of a T100 duty is small and therefore the rate of rise of TRV is also low

Table 7.10.1 TRV and breaking current results in the case of T10 and T100 duties

Test duty	TRV parameters	Without resistor	With resistor	
		Main contact	Main contact	Resistor contact
T10	u1	-	-	490
	t1	-	-	310
	u1/t1,uc/t3	7	1.5	1.6
	uc	2070	985	937
	t3	295	680	2260
Breaking current		5	5	0.9
T100	u1	930	840	-
	t1	460	460	-
	u1/t1,uc/t3	2	1.8	0.5
	uc	1640	1540	820
	t3	1710	1760	1760
Breaking current		50	50	0.9

7.11 Conclusions

In the various UHV projects testing of substation component has played a central role in the development. Certification has not been an issue to date because of the absence of standards, and test parameters have been chosen to be in accordance with the local conditions of the relevant networks (estimated by simulation) in which the equipment was to be applied.

Due to the high power and high voltage required, the development of test circuits and test methods has presented major challenges to laboratories, especially in those situations where unit testing (with reduced voltage) cannot properly represent the full service situation. In those situations, full stresses have to be applied during testing.

(a) Circuit breakers.

The first large scale test experience is related to the Japanese UHV TEPCO project. An elaborate scheme was applied in three Japanese laboratories for part-testing of the current interrupting capability including stresses on both main arcing and auxiliary contacts. In this approach, both unit- and full-pole tests were carried out. An update on possible and (partly) proven part test schemes and circuits is described.

The second strong driver for development of UHV testing was the SGCC 1100 kV project in China. Various tests were carried out in laboratories in China and Europe, including full-pole tests of complete circuit-breakers mounted on an isolating platform as well as at ground potential. TRVs in excess of 2 MV were demonstrated. Several open issues still exist, such as capacitive/inductive current interruption, the application of adequate recovery voltage for a sufficiently long period and making tests.

(b) Disconnectors

Full scale disconnector switching (bus charging) tests have been reported recently showing very large value of VFTO. The main issue is the size of the object and the very severe requirements of the measurement system regarding its ultra high frequency response.

(c) High-speed earthing switches

Circuits and test methods (in laboratory and field) have been described and applied during the TEPCO project. The specialty here is the production of test current with delayed current zero.

(d) Dielectric tests

Recent experiences in Europe, China and Japan is described. The challenges are in the dimensions of the test object, as well as in the overshoot of the LI test-voltage and adequate PD measurement. It has been described that in case of unit tests, adequate stresses have to be verified by calculation.

(e) MOSA

Because of the very low protection level (as compared to temporary over-voltages), the verification of the energy handling capability is of special concern. Also, the large size is a challenge. No specific UHV test experience is published yet.

References

[1] Akopian et al., "750 kV Experimental-industrial transmission line Konakovo Electric Power Station", paper 413, CIGRE Conf. 1964

[2] N.N. Beliakov. V.A. Verskov, G.K. Vishniakov, A.N. Komarov, V.S. Rashkes, Yu. A. Yakub, "1150 kV Experimental Installation at the Bely Rast Substation", paper 23-02, CIGRE Conf. 1976

[3] I.M. Bortnik, N.N. Belyakov, A.F. Djakov, M.I. Horoshev, V.V. Ilynichin, I.I. Kartashev, O.A. Nitikin, V.S. Rashkes, N.N. Tikhodeyev, O.V. Volkova, "1200 kV Transmission Line in the USSR. The first results of operation", paper 38-09, CIGRE Conf., 1988.

[4] B.A. Cauzillo, R. Conti, P. Nicolini, L. Gianuzzi, "Suvereto 1000 kV pilot plant: Results of the research and plant design characteristics", paper 38-15, CIGRE Conf. 1988

[5] Y.Yamagata, A. Kobayashi, T. Yoshizumi, T. Tsubaki, "Development of 1100 kV GIS - Gas Circuit Breakers, Disconnectors and High-Speed Grounding Switches", CIGRE Conf., paper 13-304, Paris 1996

[6] IEC 62271-100 High-Voltage Switchgear and Controlgear Part 100: Alternating-Current Circuit-Breakers ed. 2.0, 2008.

[7] M. Runde et al. (CIGRE WG A3.18), "Service experience with voltage grading capacitors", Paper A3-207, CIGRE Conf., 2006

[8] M. Tanabe, Y. Yamagata, S. Yanabu, A. Kobayashi, T. Marutani, T. Yoshizumi, M. Ohno, K. Hirasawa, "Interruption duties and test specifications of 1100 kV gas circuit breaker and its development for future UHV power transmission systems in Japan", Report 1.2 CIGRE SC 13 Colloquium, Florianopolis, 1995

[9] T. Kawamura, E. Haginomori, Y. Goda, T. Sawada, N. Nakajima, H. Kawano, "Making and Breaking Tests of 1100 kV Circuit-Breakers", IEC/CIGRE UHV Symp., Beijing, 18-21 July 2007

[10] Uchii, Miyake, Toyoda, Kosakada, "Modified multi-part test method for 1100 kV GCB with opening resistors", Prep. Contr. CIGRE Conf., Paris 2008 and A3-08(WG22)166

[11] U. Riechert, "Gas-insulated switchgear for 1100 kV - challenges in development and testing", Stuttgarter Hochspanniugssymposium, Tagesband S.219-234, Haka Print und Medien GmbH, ISBN 978-3-00-024098-0, Stuttgart, März 5-6, 2008 A3-08(WG22)190

[12] W. Holaus, U. Krüsi, D. Sologuren, U. Riechert, M. Keller, "Testing of GIS components at 1000 kV rated voltage", CIGRE Conf., paper A3-202, Paris 2008

[13] Xihari test laboratory authors, "High Power Tests for UHV Circuit Breaker", A3-08(WG22)083, 2008

[14] H. Kawano, T. Yokota, H. Ishizuka, H. Sato, Y. Murayama, H.S. Mo, "Effects of Resistor Switching in UHV Systems and Their Testing Methods", Int. Conf. on UHV Power Transmission, Beijing, 2006

[15] B. Sheng, "A New Synthetic Test Circuit for UHV Circuit Breakers", Ph.D. Thesis, Delft University, 1995, ISBN 90-407-1210-7

[16] Janssen A.L.J., te Paske L.H., Knol P., Smeets R.P.P, A. Shin., "Limitations of High-Power Testing Methods for EHV and UHV Circuit Breakers", paper 13.105 CIGRE Conf. 2002

[17] R.P.P. Smeets, S. Kuivenhoven, A.B. Hofstee, P. Knol, "Testing of UHV circuit breakers", CIGRE Conf., paper A3-206, Paris 2008

[18] R.P.P. Smeets, P. Knol, A.B. Hofstee, S. Kuivenhoven, P. Leufkens, "Power Testing of 1100 - 1200 kV Circuit Breakers", GridTech Conf., January 29-30, 2009, India Power Grid, New Delhi

[19] R. Göhler, D. Helbig, L.R. Jaenicke, E. Kynast, G. Lingner, B. Raeth, J. Schmid, G. Srinivas, N. Trapp, "1200 kV AC subsations: Full-scale products and integrated solutions", 2nd IEC/CIGRE UHV Symp., Delhi, 29-30 Jan 2009

[20] S.J. Park, I.S. Choi, Y.H. Lee, M.H. Kim, Y.S. Kim, H.D. Yoon, "Full-pole test results for dead-tank gas circuit breaker rated 800 kV, 50 kA, 50 Hz, SWICON Conf., Mumbai 2007

[21] L. van der Sluis, B. Sheng, "The Influence of the Arc Voltage in Synthetic Test Circuits", IEEE Trans. Power Del., vol. 10 no.1, pp.274-279, 1995

[22] K. Ikebe, T. Shimomura, I. Iyoda, "Simulation Technology for 1000 kV Power Systems", 1000 kV Power Systems Edition, Mitsubishi Electric Advance, pp 23 - 25, vol. 77, Dec. 1996

[23] R.P.P. Smeets, "Power testing of UHV switchgear at KEMA", A3-08(WG22)205

[24] Xihari authors, "The direct test method of 1100 kV GCB about LC1 and LC2", A3-08(WG22)084, 2008

[25] W. Du, S.-L. Yao, P. Li, S. Hong, "Study on high-power test techniques for UHV circuit breaker", IEC/CIGRE UHV Symposium, Beijing, 18-21 July 2007

[26] S. Huang, S.-Li. Yao, H. Zhang, P. Li, E. Tian, W. Du, "Study on test method of line charging current switching for UHV circuit breaker", IEC/CIGRE UHV Symposium, Beijing, 18-21 July 2007

[27] S. Huang, S.-L. Yao, H. Zhang, P. Li, W. Du, H. Li, "Study on Test method of clearing energized current for 1100 kV Circuit-Breaker", Int. Conf. on UHV Power Transmission, Beijing, 2006

[28] W. Du, S.-L. Yao, P. Li, S. Hong, "Study on high-power test techniques for UHV circuit breaker", IEC/CIGRE UHV Symposium, Beijing, 18-21 July 2007

[29] Xihari authors, "High power tests for UHV circuit breaker", A3-08(WG22)083

[30] S.-L. Yao, W. Du, "High-Power testing for 1100 kV circuit-breaker", presentation WGA3.22 Beijing, 2008

[31] K. Kim, Y.H. Lee, J.K. Jung, K.Y. Kweon, W.P. Song, D.S. Kim, "Design of the Circuit-Breaker for 1100 kV Gas Insulated Stwitchgear", Int. Conf. on UHV Power Transmission, Beijing, 2006

[32] H. Ito, A3-09(WG22)083 UHV testing methods with opening resistor

[33] U. Riechert, et al., "Gas-Insulated Switchgear for 1100 kV – Chanlleges in Development and Testing ", CIGRE 6 th South Africa Regional Conference, 2009

[34] L. van der Sluis, G.C. Damstra, H.W. Kempen, W.A. van der Linden, "Synthetic Test Methods: Experience and Future Developments", paper 13-203, CIGRE Conference 1992

[35] U. Riechert, "Switching of bus-charging currents by disconnectors, test duty 2: switching of parallel capacitors for circuit breakers under 180 out-of-phase condition", A3-08(WG22)188, 2008

[36] U. Riechert, "Switching of bus-charging currents by disconnectors, test duty 3: current switching capability test", A3-08(WG22)189, 2008

[37] U. Riechert, "Bus Transfer Current Switching", A3(WG22)187, 2008

[38] C. Le Postec, D. Chatrefou, F. Dainin, R. Piccoli, E. Kutlu, "Development in Testing and HV substation equipment - UHV AIS Switchgear modules", CIGRE Conf., paper A3-204, Paris 2008

[39] R.P.P. Smeets, A.G.A. Lathouwers, "Calculation methods as an aid in HV earthing switch testing", Q2-4, prepared contribution CIGRE Conference 2008

[40] Y. Yamagata, E. Zaima, T. Marutani, H. Yamamoto, Y. Ikeda, K. Suzuki, M. Ohno, Y. Ohsita, "Specifications and development of high-speed grounding switch (HSGS) for use in future 1000 kV transmission lines of Japan", Report 1.3 CIGRE SC 13 Colloquium, Florianopolis, 1995

[41] Y. Yamagata, Y. Nakada, K. Nojima, M. Kosakada, J. Ozawa, I. Ishigaki, “Very Fast transients in 1000kV Gas Insulated Switchgear”, IEEE T&D 1999

[42] Y. Yamagata, A. Kobayashi, T. Yoshizumi, T. Tsubaki, ”Development of 1,100kV GIS - Gas Circuit Breakers Disconnectors and High-Speed Grounding Switches –“, CIGRÉ Session 1996, 13-304

[43] G. Aldrovandi, L. Bergonzi, E. Colombo, G. Cordioli, E. D’Adda, M. de Nigris, F. Dianin, F. Gatti, A. Pigini, “Testing challenges for UHV equipment”, IEC/CIGRE UHV Symposium Beijing, 2007, paper 4.1

[44] L. Zhong, "Simulation Research on Combined Voltage Test Techniques for UHV switchgear", Int. Conf. on High-Voltage Engineering and Application, ICHVE 2008, Chongqing, 2008

[45] CIGRE WG A3.18 “Operating environment of voltage grading capacitors applied to high voltage circuit-breakers”, Technical Brochure No 368, 2009

[46] U. Riechert, "Experiences with Type Testing of GIS for 1100 kV", prepared contribution A3 PS2 Q2 O2 Riechert, CIGRE Conference 2008

[47] T. Uchii, "AC-AC Combined Voltage Test for UHV Gas Circuit Breaker", Prepared Contribution A3 PS2 Q2 O2 Uchii, CIGRE Conference 2008

[48] B. Richter, M. de Nigris, V. Hinrichsen on behalf of CIGRE WG A3.17, CIGRE WG A3.21 and IEC TC 37 MT4, “MO-surge arresters for systems above 550 kV - Experience and challenges for the future”, IEC/CIGRE UHV Symposium paper 2.5.1 Beijing, 2007

[49] T. Yonezawa, T. Sugiyama, M. Hikada, "Development of a 1000 kV SF6 Gas Circuit Breaker", 1000 kV Power Systems Edition, Mitsubishi Electric Advance, pp 10 - 13, vol. 77, Dec. 1996

8 Field testing experience and on-site tests

8.1 Introduction

After installation, and before being put into service, GIS must be tested in order to check the correct operation and the dielectric integrity of the equipment. These tests and verifications according to [1] comprise

- Dielectric tests on the main circuits
- Dielectric tests on auxiliary circuits
- Measurement of the resistance of the main circuit
- Gas tightness tests
- Checks and verifications
- Gas quality verifications

However, major challenges for the testing of a UHV GIS or MTS are posed by the limited testing possibilities, in particular for dielectric tests on the main circuits.

On-site testing of GIS is an important step during commissioning of a new GIS. This test assures correct erection and verifies that no defects are within the GIS which might lead to a major failure during operation. Various methods can be performed depending on rated voltage level and GIS type and design. Experience of on-site testing with different waveforms and procedures have shown which method is suitable to detect major defects within a GIS.

According to [1] one of the following test procedures for UHV applications should be chosen:

(1) Procedure A (recommended for 170 kV and below):

- Power-frequency voltage test for duration of 1 min at the value specified in Table 8.1.1, Column 2

(2) Procedure B (recommended for 245 kV and above):

- Power-frequency voltage test for duration of 1 min at the value specified in Table 8.1.1, Column 2
- Partial discharge (PD) measurements according to [1, table 106], however with Upre-stress = Uds of table 8.1.1, Column 2

(3) Procedure C (recommended for 245 kV and above, alternative to procedure B):

- Power-frequency voltage test for duration of 1 min at the value specified in Table 8.1.1, Column 2
- Lightning impulse tests with three impulses of each polarity and with the value specified in Table 8.1.1, Column 4

Figure 8.1.1 shows the test voltages according to [1], together with the calculated test voltage for 1100 kV / 1200 kV. For the calculation the following rated voltages according to [2] were used:

Rated switching impulse withstand voltage U_s = 1800 kV

Rated lightning impulse withstand voltage U_p = 2400 kV

Table 8.1.1 On-site test voltages for 800 kV [1, table 107] and approximation for UHV

Rated voltage for equipment U_r, kV (r.m.s. value)	On-site short-duration power-frequency withstand voltage U_{ds}, kV (r.m.s. value)	On-site switching impulse withstand voltage U_{ss}, kV (peak value)	On-site lightning impulse withstand voltage U_{ps}, kV (peak value)
(1)	(2) (see Note 1)	(3)	(4)
800	760	1140	1680
1100 / 1200	865	1440	1920

NOTE 1) Values of column (2) are only applicable for SF_6 insulation or when SF_6 is a major part of the gas mixture. For other insulation refer to Tables 1 and 2 of IEC 60694 (now IEC 62271-1), applying a factor 0.8 on column (2).

NOTE 2) The on-site test voltages have been calculated as follows:

U_{ds} (on-site test value) = U_p×0.45×0.8 (column 2)
U_{ss} (on-site test value) = U_s×0.8 (column 3)
U_{ps} (on-site test value) = U_p×0.8 (column 4)

All values have been rounded up to the next higher modus 5 kV.

NOTE 3) If other insulation levels than the preferred values of Tables 102 and 103 (e.g. the lower insulation levels of Tables 1 and 2 in IEC 60694) are specified, then the on-site test voltage should be calculated according to Note 2.

In certain circumstances, for technical or practical reasons, dielectric tests on-site may be carried out with reduced voltage values. Details are given in clause C.3 of [1].

8.2 On site test procedure

Existing standards define no single technique or procedure which has to be used for on-site testing. Agreement between manufacture and customer must be reached with regard to which testing procedure and which kinds of test voltage or combination of test voltages have to be applied. It has been common practice for nearly 30 years to carry out ac high voltage tests by resonant test systems with variable frequencies. IEC 62271-203 [1] defines a test frequency range between 10 Hz to 300 Hz and typically frequencies above 80 Hz are applied for testing including voltage transformers. Extensive experience with the application of resonant test systems, in combination with sensitive partial discharge measurements, have proved their successful application.

Typical PD causing defects, which might be produced during transportation or erecting, are protrusions, free moving particles, floating parts or cracks in spacers. Due to the different physical behaviour of the defects under HV ac stress, LI or switching operations, it is impossible to find all defects by withstand testing of only one waveform. Table 8.2.1 gives an overview of the effectiveness of the various applied HV voltage waveforms to detect the different defects [3]. As shown the application of PD measurement enables the detection of all kind of serious defects during ac voltage testing.

Table 8.2.1 Effectiveness of on-site tests on GIS defects with different test procedures [3]

Defect	High AC	Low AC With PD	High AC With PD	LI	SI
Sharp protrusions fixed on live parts			less effective	effective	
Round protrusions fixed on live parts (Assembly faults)	less effective		effective	effective	effective
Particles on spacers	less effective / effective		less effective / effective	effective	less effective
Cracks in spacers	less effective / effective	less effective	effective	less effective	less effective
Free partides	effective	effective	effective		less effective
Parts floating	less effective	effective	effective		
Left foreign bodies	effective	less effective	effective	effective	less effective

To detect partial discharges in GIS the following main PD measuring methods are in use [4]:

1. Conventional measuring systems based on the IEC 60270,
2. UHF measuring systems using narrowband or wideband filter detection in a frequency range up to several GHz,
3. Acoustic measurements, mainly for PD location, using externally mounted acoustic sensors which detect the acoustic signals emitted by a PD.

The conventional method is of limited use because of technical limitations. For partial discharge detection on-site, the electrical VHF/UHF and the acoustic method can be used in GIS. These methods are less sensitive to noise than the conventional measurement and can also be used for partial discharge monitoring in service. The UHF technique, which needs special couplers, is very sensitive and can also locate the PD source. As couplers, special build-in sensors can be used or external sensors can be applied if the substation has suitable access windows. Different kinds of sensors are shown in figure 8.2.1 [5]. By means of appropriate design, the sensor can have almost the same sensitivity or divider ratio over a wide frequency range. Sensitive UHF sensors can form the basis of a practicable PD measurement system however, in a similar way, acoustic sensors can have high sensitivity and and good local resolution for PD detection.

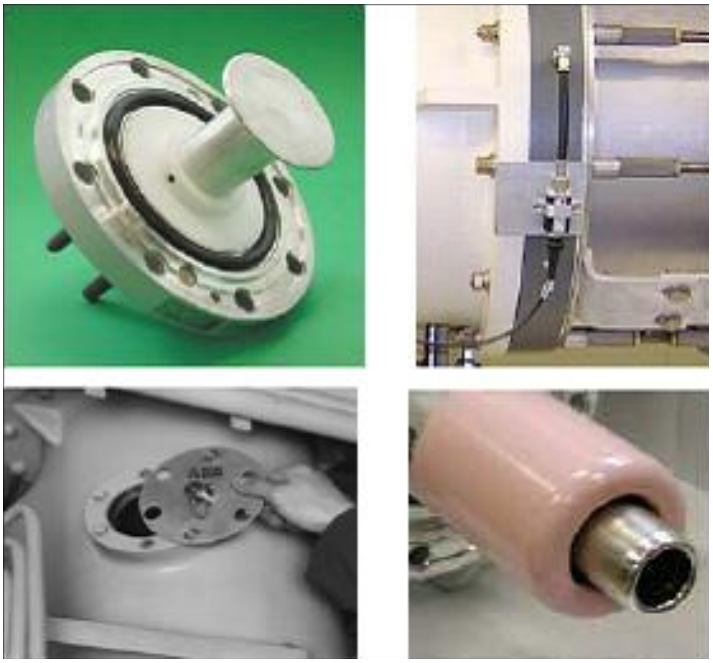

Figure 8.2.1 Different types of PD couplers for GIS [5]

In contrast to the conventional method, the UHF/VHF and the acoustic methods cannot be readily calibrated to establish a clear correlation between the apparent charge and the display on the PD measurement system. This perceived disadvantage of the UHF method is of limited criticality since interpretation of UHF is more related to aspects such as the overall number of pulses, the pulses per half-wave and the phase relation of the PD pulses relative to the applied high voltage. These are independent of the bandwidth of the measurement system used and the absolute magnitude of the partial discharge amplitude. In this respect the PRPD patterns appear the same, independent of whether or not they were obtained using the conventional method, the UHF method or with acoustic methods. To compare the sensitivity of different UHF/VHF or acoustic couplers a CIGRÉ brochure was published which describes in detail

the sensitivity check of such sensors [6]. As this document is nearly 10 years old, CIGRE working group D1.25 was established in 2008 to review the document.

For GIS, PD measurements in the UHF range, i.e. frequencies above 300 MHz and up to 2 GHz, special designed capacitive couplers are suitable and have been proven for testing GIS on-site. In principle two types of UHF PD detection techniques can be used, the narrow band technique with a bandwidth around 5 MHz and the wide band technique using a bandwidth up to 2 GHz. In older substations, without fixed couplers, only mobile window sensors can be used. A comparison with internal sensors shows that with appropriate size of the window sensors similar sensitivities to a conventional UHF sensor can be achieved [7].

Different procedures and methods can be applied for location of PD sources. Sectionalizing and the electrical time-of-flight measurements are the most practical procedures and are typical for the UHF PD measurement method. These techniques are also applicable for acoustic measurements. More detailed information is given in [8, 9]. The very fast electric pulse, of rise time below 1ns, emitted by a PD source, propagates in all directions along the GIS bus duct. It arrives at couplers which might be located on both sides of the PD source. By the time-of-flight technique the time difference between the two wave fronts arriving at both couplers can indicate the location of the PD source (See figure 8.2.2). The time difference is typically in the tens of nanoseconds range, so a fast digital oscilloscope has to be applied for measurements.

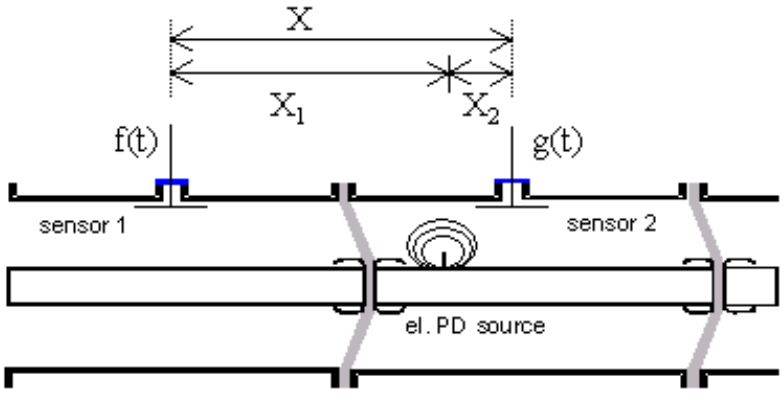

Figure 8.2.2 Time-of-flight location [9]

Testing GIS on-site with an ac resonant test system with variable frequency (ACRF) is nowadays a common practice up to 1100 kV and two main technical realizations are possible.

Completely metal-enclosed, SF_6-insulated HV reactors, which can be directly coupled to the GIS, achieve a high PD sensitivity with low background noise. These require the lowest space and no additional safety requirements. Today, the maximum test voltage for this system is about 740 kV meaning that oil-insulated modular reactors are also used. This test system cannot be directly coupled to the GIS and the HV has to be supplied via a bushing to the GIS. The inductance of the reactors can be well adapted to the test object capacitance by series and parallel connection of reactor modules. Test voltages in the range up to 800 kV can be realized.

8.2.1 Chinese experiences

For the on-site test a 1200 kV test transformer was used (Figure 8.2.3). The HV was supplied via a bushing to the MTS. The typical test sequence, consisting of a conditioning phase and

the withstand test voltage test for 1 min is given in figure 8.2.3. For the pilot project the test procedure was slightly changed as follows:

- Conditioning phase 10 min, 635 kV (1.0 p.u.)
- Conditioning phase 5 min, 760 kV (1.2 p.u.)
- High voltage test 1 min, 880 kV (0.8 x Rated short-duration power-frequency withstand voltage Ud)
- PD measurement 30 min, 700 kV (1.1 p.u.)

For the PD measurement, both the UHV and the acoustic techniques were used. The combination of both PD measurement techniques is very powerful to detect, locate and interpret PD events and to distinguish them from signals not originating from harmful defects. The first step of sensitivity verification of the couplers was performed during the HV tests in the laboratory [10]. The results were used for optimal placement for the couplers. The sensitivity verification can be checked on-site on the same sensors as follows:

An artificial pulse is applied to the selected sensor. If this pulse can now be measured at the neighbouring sensor, two conclusions can be drawn: first of all, the sensitivity of the sensor is confirmed and secondly, the signal corresponds to a PD source with approx. 5 pC (+/- 30 %) amplitude.

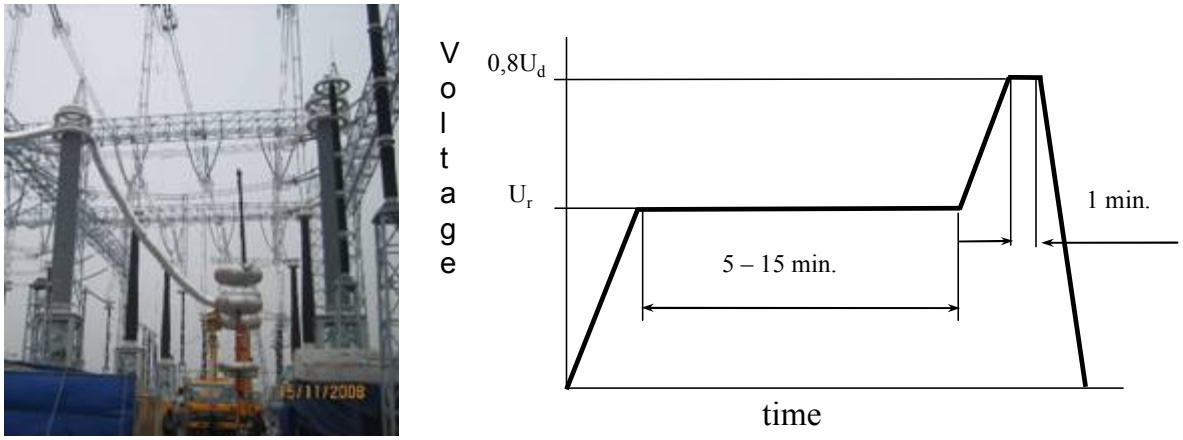

Figure 8.2.3 On-site HV test set-up (left) and typical test procedure (right)

8.2.2 Korean experiences

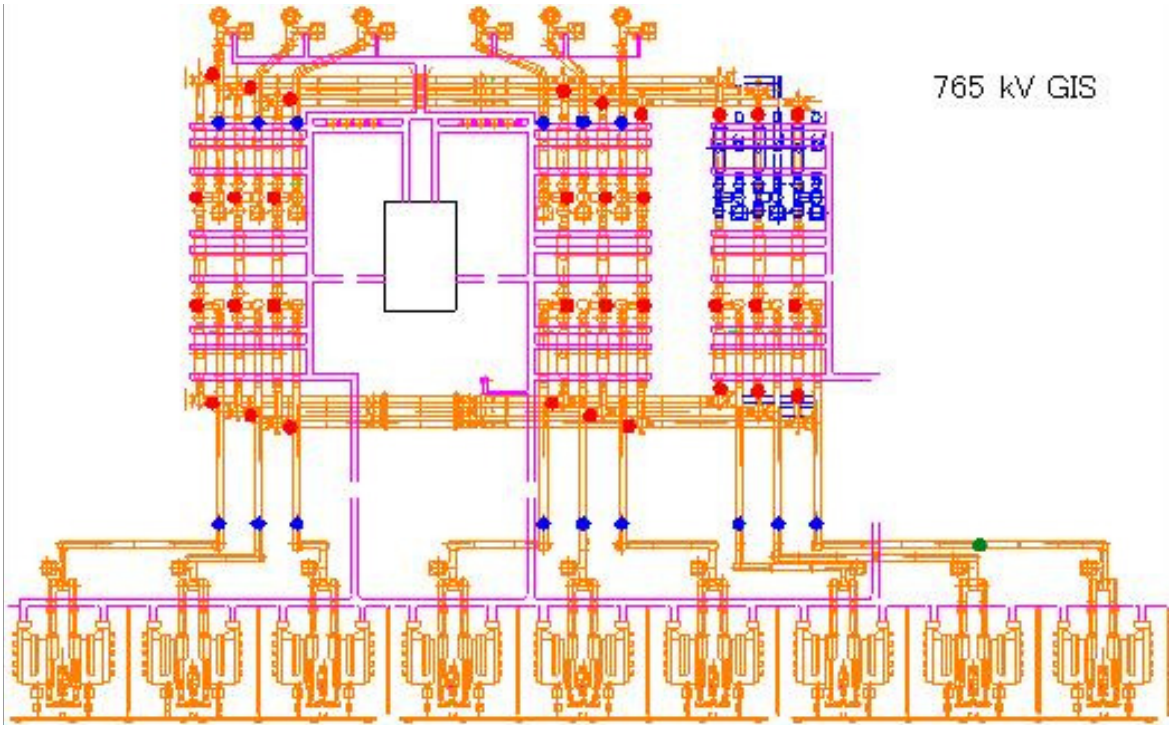

Figure 8.2.4 Sensor locations in KEPCO 800kV GIS

UHF PD diagnostics have been chosen for on-line monitoring and commissioning tests for the 800 kV and 362 kV GIS in 765 kV substations of KEPCO to detect defects and prevent failures. The sensitivity of internal or external (barrier) sensors was first tested according to the Korean standard KSC3700: Electromagnetic partial discharge measuring devices [12]. Propagation losses of the UHF PD signal in the GIS were measured for each type of components such as GIL, DS, CB, HSDS etc. Optimal sensor locations have obtained by using the spectral sensitivity data of sensors and propagation losses of GIS components. Figure 8.2.4 shows the sensor location for the 800 kV GIS, based on the investigation results [11]. At the time of the GIS installation, the required PD sensitivity was 10 pC according to IEC. The sensors were placed according to the specification. The later required sensitivity of 5 pC was achieved by placement of additional external sensors.

By using the on-line PD monitoring system, several PD signals were monitored during the no-load energizing period of the GIS. The signals were further monitored. By intensive field measurements and analysis the exact location and the type of the PD signal was identified. Figure 8.2.5 shows one of the PD signals captured during the initial energizing period of one 800 kV GIS. The PD signal was identified as a free moving particle and located. By cleaning of the located area inside the GIS the PD source was removed.

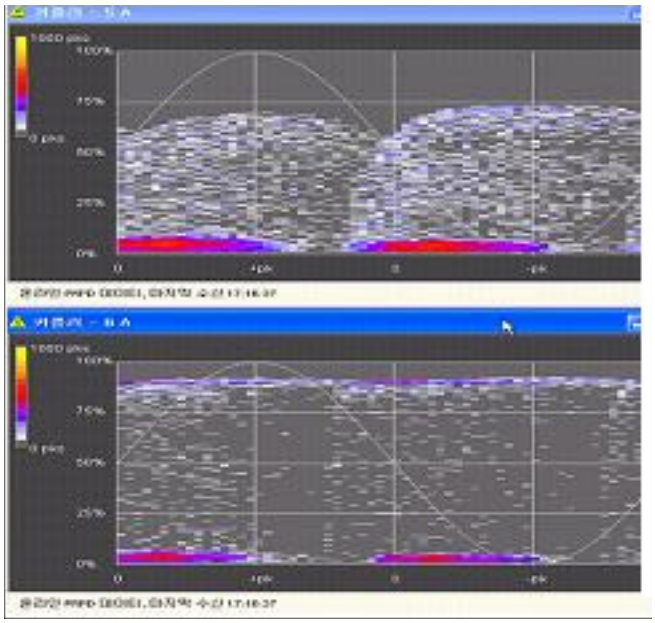

Figure 8.2.5 PRPD pattern of free moving particle

To locate the exact position of the PD signal source, time-of-flight method was applied using both internal and external sensors.

Table 8.2.1 shows an overview of the experiences of on-line UHF PD diagnostic and monitoring systems in Korea.

Table 8.2.1 On-line UHF PD diagnostic and monitoring systems for 800 kV substations, in service in Korea

765 kV substation	Manufacturer	Sensor type	Diagnostic system type	Note
Sin Ansung	A	Barrier type	On-line	Retrofit
Sin Seosan	A	Barrier type	On-line	Retrofit
Sin Gapyong	A	Internal type	On-line	
SinTaebaek	B	Internal type	On-line	
Dangjin Switch yard	A	Barrier type	On-line (NB)	Retrofit

8.3 Recommendations for high-voltage on-site testing

Considering the importance of UHV substations, a high voltage on-site test following the procedure B [13] seems a preferable solution. For technical and practical reasons, dielectric tests for UHV GIS on site are carried out with the reduced voltage values. Typical test voltages for power-frequency and lightning impulse withstand are approximately 80 % of the rated test voltages. For partial discharge detection on-site, the electrical VHF/UHF and the acoustic method can be used in the UHV range, which is less sensitive to noise as compared with the conventional measurement.

8.4 Japanese experiences on TEPCO 1100kV projects - Field tests

8.4.1 Overview

In order to prepare future UHV transmission systems, TEPCO started an 1100kV project in early 1990's. Various UHV substation equipment was developed and installed in the UHV testing station (550kV Shin-Haruna substation). Full-scale field tests have been carried out since May 1996. Figures 8.4.1 and 8.4.2 show the configuration of the UHV testing station and a photograph is shown in figure 8.4.3. The testing station has one three-phase power transformer bank and one bay of GIS with the control and protection systems. Each single-

phase transformer has two split units and one on-load voltage regulator is equipped with each unit, enabling a current flow through the coil by using tap-voltage difference between same-phase tanks. The GIS has an additional loop circuit with a power current transformer. The test currents of up to 10,000 A can be achieved by a reverse excitation of the power current transformer. The tables 8.4.1 and 8.4.2 summarize the accumulated durations of long-term verification tests and the testing items.

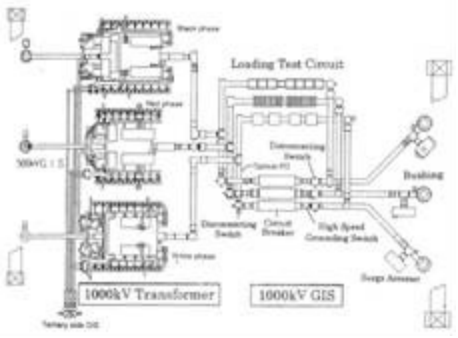

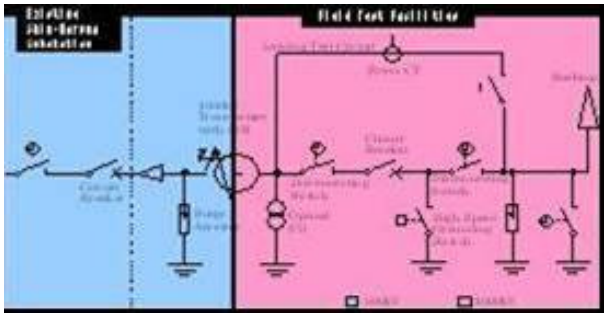

Figure 8.4.1 Configuration of UHV Field test, Figure 8.4.2 Single line diagram of UHV field test site

Figure 8.4.3 TEPCO UHV testing station

Table 8.4.1 Operation records (as per August 2007)

Testing durations	Hours
Cumulated operation duration at UHV field test site	60,456
Current carrying duration through GISs	9,995
Current carrying duration through transformers using the tap-voltage difference	7,918

Table 8.4.2 Field test items

		Testing Items
Transformer	Common	Long-term energizing and current carrying
	Periodical inspection	Dissolved gas analysis, insulation oil characteristics measurement
		Leakage current measurement at neutral terminal
		Noise, vibration measurement
	Inrush test	
GIS	Common	Long-term energizing / loop current carrying, temperature and thermal behaviour measurement
	Periodical measurement	Partial discharge, surge arrester leakage current
		Operating characteristics
		Optical PD accuracy
	Surge measurement	DS operating surge
		HSGS making surge
		Transient response of grounding system
		Residual DC voltage damping characteristics
	Surge arrester's temperature and thermal behaviour	
	Gas bushing vibration test	

8.4.2 Long-term voltage energizing and loop current carrying test

The total energized duration reached more than 60,000 hours at the end of 2007 with loop currents up to 10,000A being conducted and switched periodically. Dielectric as well as thermal stresses were imposed onto the insulators and the equipment. The main circuit resistance was stable and neither harmful decomposition products in SF_6 gas nor partial discharge were detected during the tests.

8.4.3 Periodic measurement of operating characteristics

Due to the design & construction of 1100kV GCBs the operating mechanism requires larger drive force than for lower voltage units. The GCB is equipped with a resistor for both closing and opening meaning that operating mechanism becomes relatively complicated.

The operating times after long idle times (an interval of some months) and during frequent operation (20 time successive operations) were measured. Delays of several milliseconds in opening time were observed for a circuit breaker at first operation after some months idle time due to a lack of margin of control valve for the hydraulic operating mechanism. The design was improved by adjusting the balance of drive force against friction and, following implementation, the measured characteristics have been stable.

Regarding the application of synchronous switching, any variation of closing and opening time is important and hence the operating characteristics were studied, even though the 1100kV GCB is not intended to apply for synchronous switching. Figure 8.4.4 shows an example of the closing time measured at ambient temperatures ranging from 0 to 22℃ and at idle times up to 226 days. A line in figure 8.4.4 (a) is an average closing time against the ambient temperature during successive operations. Figure 8.4.4 (b) shows an increase of closing time from the average operating time due to longer idle time. When the compensation for closing time dependence on temperature is considered, an increase of closing time tends to

saturate at less than 2.5ms. The long-term reliability of the operating characteristics has been assured.

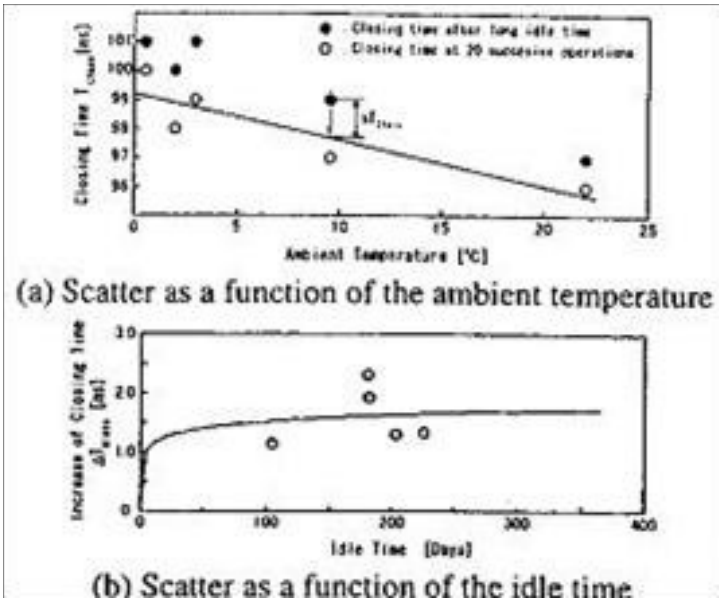

Figure 8.4.4 Closing time characteristics of 1000kV CB

8.4.4 Measurement of residual DC voltage in GIS

DC voltage distribution on the insulators changes with AC voltage application and in 1100kV GIS higher levels of the residual DC charge remain in the GIS after DS opening making it worthwhile to investigate the DC withstand performance. The residual DC voltages in the GIS after opening operations and their decaying characteristics at both terminals of CB were measured using the circuit shown in the case (1) in figure 8.4.5.

A typical measured result is shown in figure 8.4.6. Two calculated results are also shown in figure 8.4.6. The first one is a fitted single-exponential curve and the second one is a result of EMTP analysis. If the decaying characteristic is represented by a single exponential function, the time constant is evaluated from several hours to 66 hours at maximum, depending on the difference of the design. The equivalent circuit of the two-break CB and adjacent equipment for EMTP analysis is as shown in figure 8.4.7.

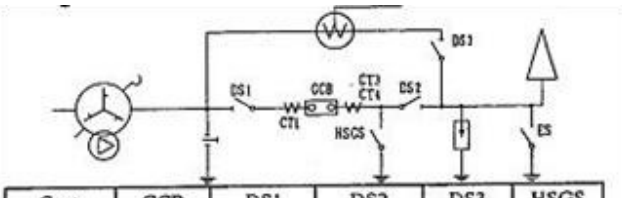

Case	GCB	DS1	DS2	DS3	HSGS
(1) step 1	open	closed	opening	closed	open
(1) step 2	open	opening	open	closed	open
(2)-1	open	closed	operating	closed	open
(2)-2	closed	open	operating	closed	open
(2)-3	open	operating	open	closed	open
(2)-4	closed	operating	open	open	open
(3)-1	open	closed	closed	open	closing
(3)-2	open	closed	open	closed	closing

ESs are opened in any measuring circuit.
Case(1):Residual voltage measurement
Case(2):DS surge measurement
Case(3):HSGS making surge measurement

Figure 8.4.5 Switching operations for respective measurements

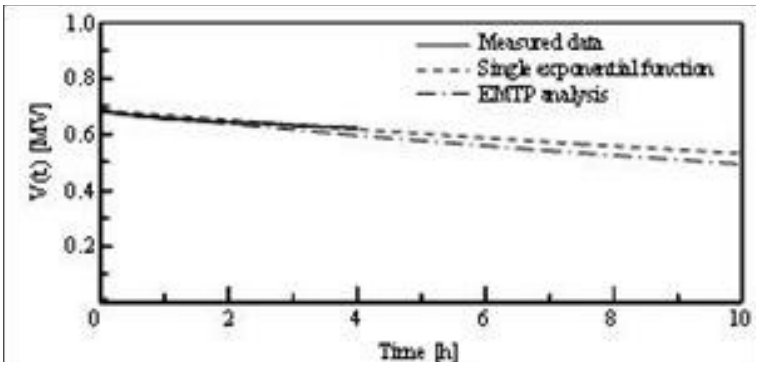

Figure 8.4.6 Typical residual voltage decaying waveform

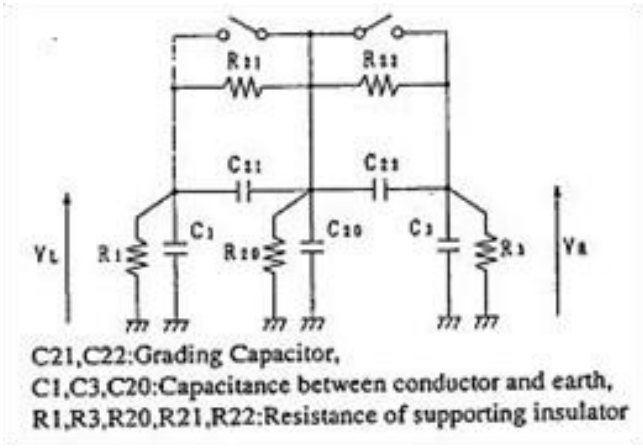

Figure 8.4.7 Equivalent circuit for EMTP analysis

There are two ways of discharging the DC. One is directly to earth through insulators and the other is through insulators across the contacts. It was observed that DC voltage remains between phase to earth and across the contacts of CB for a relatively long period meaning that it might be necessary to specify a DC withstand voltage for CBs used in GIS.

After two-year energizing, an internal inspection for CB, DS and HSGS was carried out to check the condition of equipment and no problems were observed.

8.4.5 Surge tests

Insulation coordination was deliberately investigated and established for the UHV system. As a result, lightning impulse withstand voltage (LIWV) for the 1100 kV GIS is reduced to 2250 kV_p (2.5 p.u., 1 p.u.=898 kV_p=1100 kVx√2/3) by applying high performance surge arresters and resistor switching methods. LIWV on 550 kV system in Japan is at the level from 1425 kV_p to 1800 kV_p (3.17 p.u. to 4 p.u., $1p.u. = 449kV_p = 550kV \times \sqrt{2}/3$). In addition, digital protection and control panels for UHV equipment are located close to GIS and it is very important to mitigate the effect of surges transferring into the secondary low voltage circuits. For these reasons, the very fast transient overvoltage (VFTO) in GIS at switching of DS, HSGS, 550kV GCB at transformer secondary side and the electo-magnetic interference (EMI) on secondary circuits were measured.

8.4.5.1 DS surge tests [15]

The 1100kV DS employs a resistor of 500 Ω to reduce the switching surge level to below 1.3 p.u.[16]. DS surge measurements were carried out to check if the surge suppressing effect worked as expected. Case (2) in figure 8.4.5 shows a measuring circuit and figure 8.4.8 shows

a single observed waveform from amongst many hundreds of operations. The maximum voltage across the contacts before re-strike was 2 p.u. and there were neither voltage overshoots nor fast-rising oscillating waves even though these are the general features of DS re-striking surge. The maximum surge observed during measurement was 1.20 p.u. The energy absorbed by the resistor was less than 20 kJ as expected and the resistor switching is considered to work effectively.

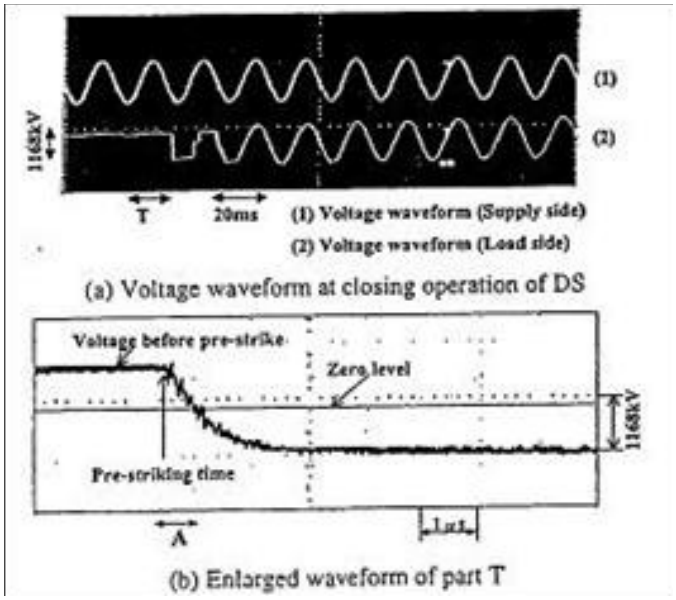

Figure 8.4.8 DS surge waveforms

EMI on secondary low voltage circuits was examined when main-circuit surges transferred through current transformers (CT). Figure 8.4.9 shows the voltage waveform observed at the secondary circuits of CT at both terminals of the CB. Figure 8.4.9 (a) shows the main circuit surge, enlarged waveform of part A in figure 8.4.9 (b). Figure 8.4.9 (b) shows a voltage of secondary circuit at CT1 on the operating DS side of the CB. It was observed that only high-frequency components on the main circuit affected the CT secondary circuit. Though the amplitude at the CT terminal exceeded 7kVp, the insulation of the equipment was assured by V-t characteristics as the shape of the surge wavefront was steep. Figure 8.4.9 (c) and (d) show the voltage of the secondary circuit of CT3 installed at the load side of the CB. Figure 8.4.9 (c) is at the CT terminal; Figure 8.4.9 (d) at the interface panel terminal. The highest level observed at the interface panel and the relay panels was $200V_p$, which was not considered excessive. Even though values in excess of $7kV_p$ were observed at CT terminals, this surge rapidly attenuated as it travel in secondary cable.

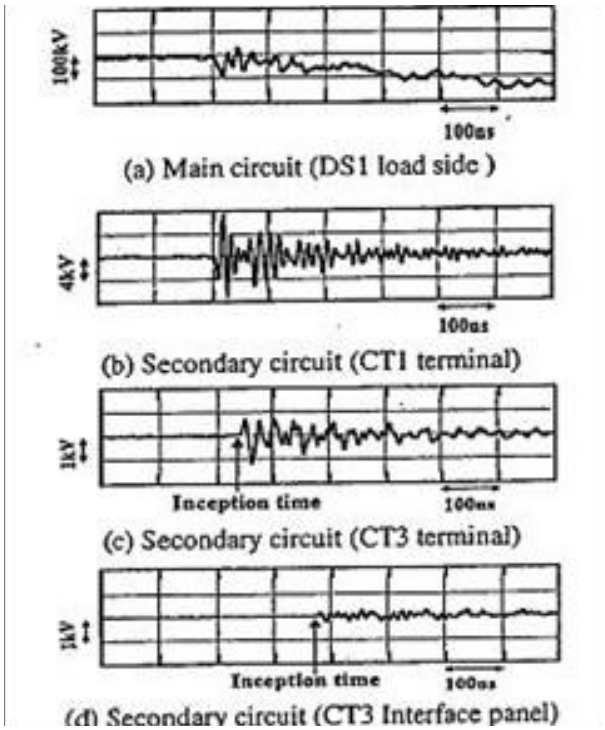

Figure 8.4.9 DS surge waveforms at CT secondary circuit

8.4.5.2 HSGS making surge tests [15]

In the case of a transmission line fault in the 1100kV system, the secondary arc at the arc-horn of a transmission tower is sustained longer than in 550kV systems. High-speed grounding switches (HSGS) are employed to extinguish the arc early and to complete high-speed re-closing successfully. The operating sequence during re-closing is as follows:

1) Open the CBs at both sides on the faulted phase (fault cleared).

2) Close the HSGSs on both sides of the phase concerned (Secondary arc extinguished).

3) Open the HSGSs,

4) Re-close the CBs.

When the HSGS re-ignites at a time shorter than the minimum arcing time, the discharge voltage across the contacts becomes 640 kV_p at maximum corresponding to the TRV peak value for an inductive current interruption. Furthermore, when a grounding fault occurs in the 1100 kV GIS, transient overvoltages may cause mal-operation of the protective relays. In this sense the HSGS making surge was measured. A DC residual voltage was maintained by DS opening operation following which a making operation of HSGS was done. Figure 8.4.10 shows typical surge waveform on the main circuit at the grounding terminal and at the enclosure of HSGS. These are measured when the residual voltage was 673 kV_p (0.75 p.u.). The waveform on the main circuit shows that a high-frequency component of approximately 40 MHz was superimposed on the main frequency component of several MHz at the initial part of the waveform. The maximum surge, $V_{o\text{-}p}$ in figure 8.4.10 (a), appeared approximately 300 ns later than the making instant where the initial high-frequency component attenuated.

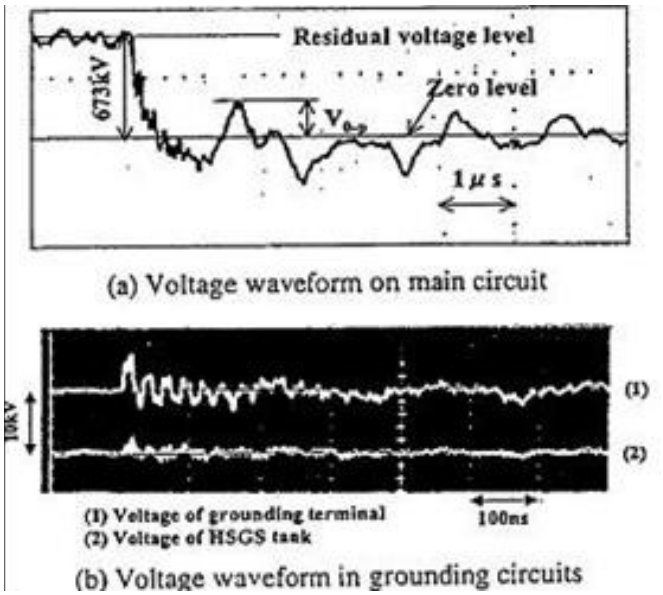

Figure 8.4.10 HSGS making surge level

The maximum residual voltage on the main circuit before making was 0.98 p.u. In general, the surge voltage generated on the main circuit was lower than the residual voltage. However, the maximum voltage recorded was 1.13 p.u. due to a reflection at the open end. The frequency of the HSGS making surge is similar to that of the DS but with much lower amplitude meaning that the HSGS surge does not threaten the insulation of the main circuit.

Maximum EMI levels at protection and control panels were 1200 V_p at a frequency of approximately 50 MHz. This voltage value is much lower than the specified value (7 kV_p) and no mal-operation was observed.

8.4.6 Transformer inrush current and transfer surge measurement

Inrush current might cause mal-operation of transformer protective relay and voltage fluctuation of 500 kV system (the secondary side of the power transformer), and also might affect the transformer itself. Inrush current due to CB closing with and without closing resistor was measured as a function of the phase angle.

An air-blast breaker at the 500 kV side with a closing resistor insertion characteristics of 1000 Ω for 10 ms was used for closing field tests. The maximum inrush current observed was 5920A_p without closing resistor and 550A_p with closing resistor. There was no mal-operation of protective relay system and it was confirmed that inrush current can be calculated precisely by providing the transformer ϕ-i characteristics, residual magnetic flux in core, and closing-phase angle [13][14].

After opening the transformer circuit, the residual magnetic flux (which strongly affects inrush current level), was measured by using low voltage excitation method. The maximum residual flux was about 40 % of the rated value, though the value of 80 % was conventionally used based on the property of the magnetic core material. When the CB is opened, the voltage is de-energized nearly at its voltage peak, and it slowly oscillates to finally reach zero after damping rapidly and reversing polarity with core saturation as shown in Figure 8.4.11. It was clarified that the residual flux reduction phenomenon occurs in this process [15].

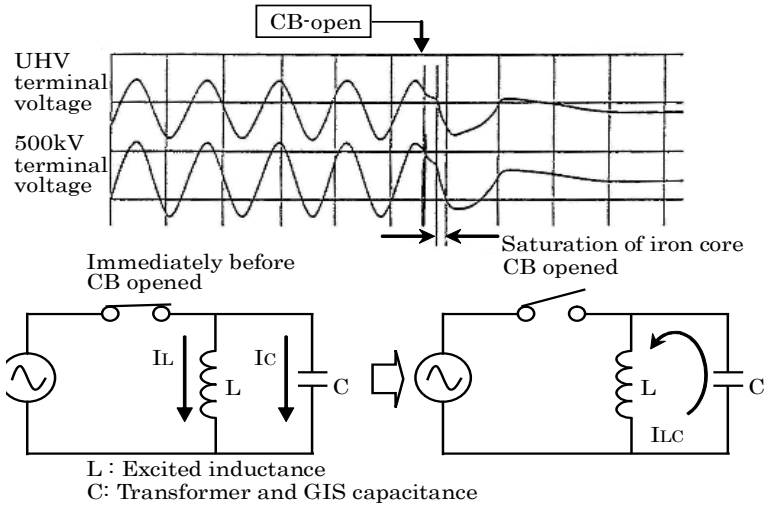

Figure 8.4.11 Voltage waveform after transformer circuit opened

As a part of the test the making phase angle for the first pole was measured and figure 8.4.12 shows the results. The figure shows the making phase angle concentrated around the voltage peaks (90°, 270°), where the inrush current can be suppressed in the case of small residual flux in a transformer core. It is notable that this CB has a relatively small rate of decrease of dielectric strength (RDDS).

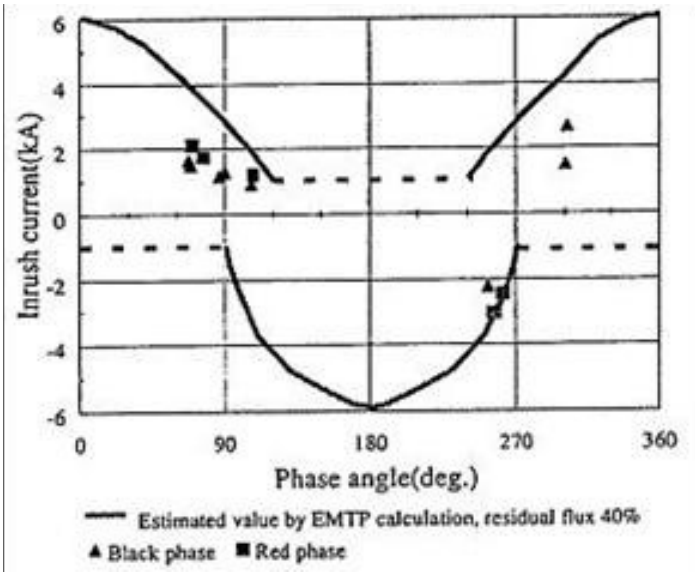

Figure 8.4.12 Making phase angle of first pole and caused inrush current

8.4.7 Effect and reliability of UHV MOSA

In field tests, comparatively high transferred surge voltages from the 550kV to the UHV side were observed, and with MOSA operating effectively, these surge voltages were limited to less than the SIPL level of MOSA (about 1.6 p.u.). Table 8.4.3 summarizes the maximum voltage surges generated by switching.

Table.8.4.3 maximum switching surge on main circuit

Switching at 1000kV side			Transfer surge by 500kV side circuit breaker making	
GCB switching*	DS switching	HSGS making	with resistor	without resistor
1.10pu	1.20pu	1.13pu	1.40pu	1.57pu

* Only capacitive current within GIS was switched

Since the protection level of UHV MOSAs is relatively low, they have also operated due to lightning on the 550kV transmission lines. Figure 8.4.13 shows these field operation data plotted on the V-I characteristics of a UHV MOSA that was drawn based on the type test data. Examples of these measured waveforms are shown in figures 8.4.14 and 8.4.15 [16] [17].

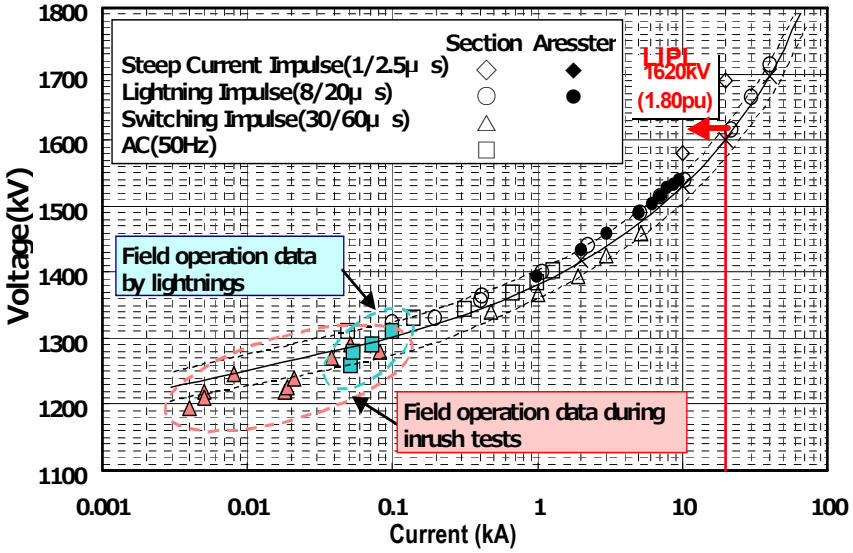

Figure 8.4.13 Field operation data of UHV MOSA

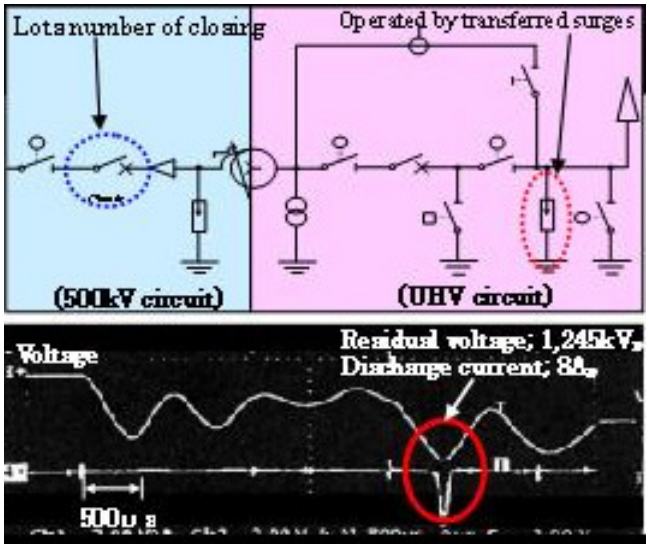

Figure 8.4.14 Test circuit and measured waveform at UHV MOSA terminal in inrush current test

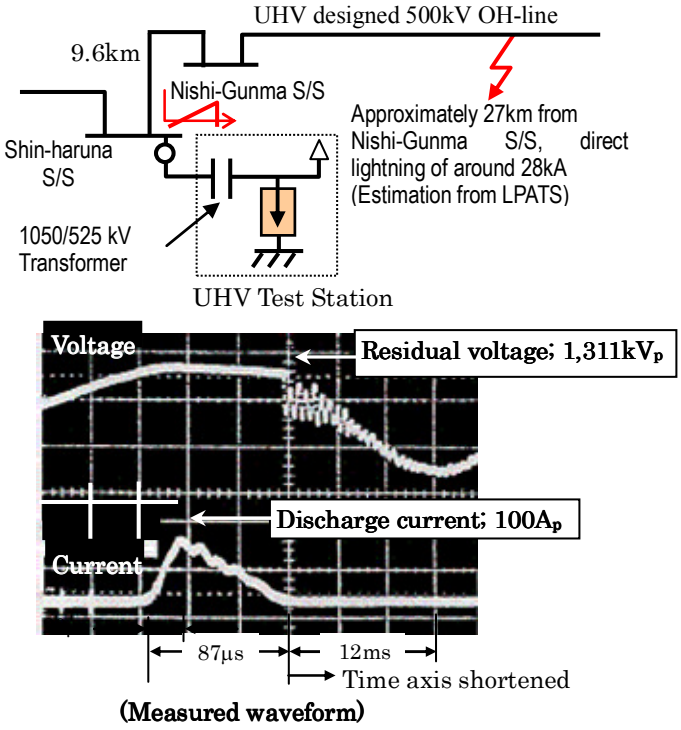

Figure 8.4.15 UHV MOSA operation by lightning in 500kV network (August 3, 1997)

So called "high-grade" MOSAs are a key technology for the insulation co-ordination of UHV systems. As demonstrated by field test, these MOSAs operate along the V-I characteristics and perform with good sensitivity even in the range of small discharge current such as 10 - 100 A. Their long-term reliability has been confirmed because the leakage currents are almost constant and stable as shown in figure 8.4.16 [16]-[20].

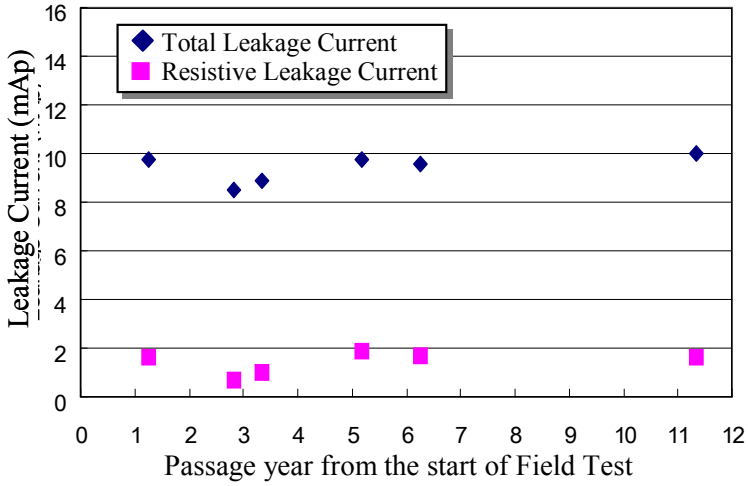

Figure 8.4.16 Measured values of leakage current of UHV MOSA

8.4.8 Conclusion

Field verification of 1100kV GIS has been conducted for more than four years. The test results indicate that new technologies applied for 1100kV GIS have been verified and the system coordination, including VFTO, has aligned well with the studies undertaken in advance. Controlled switching application to transformer energisation was also investigated at the field test site. All the field data has been satisfied and the reliability of 1100kV GIS has been assured. The long term field tests have provided valuable field experience for the

commercial UHV substation. Further field verifications are being continued focusing on long-term voltage application. For the planned UHV systems, a variety of detailed analyses were made to determine the specifications of 1100kV substation equipment in accordance with the technical requirements.

8.5 Chinese experience gained through 1100 kV pilot project

8.5.1 UHV pilot project overview

1100kV Jindongnan - Nanyang - Jingmen UHV AC pilot project is the first challenge of Chinese UHV development. The UHV transmission line starts from Jindongnan substation in Shanxi province, extends to Nanyang switching station in Henan province and terminates in Jingmen substation in Hubei province. The whole transmission line is single-circuit with the length of 639.8 km. The nominal system voltage is 1000 kV and the maximum operating voltage is 1100 kV. Figure 8.5.1 shows the UHV AC pilot project.

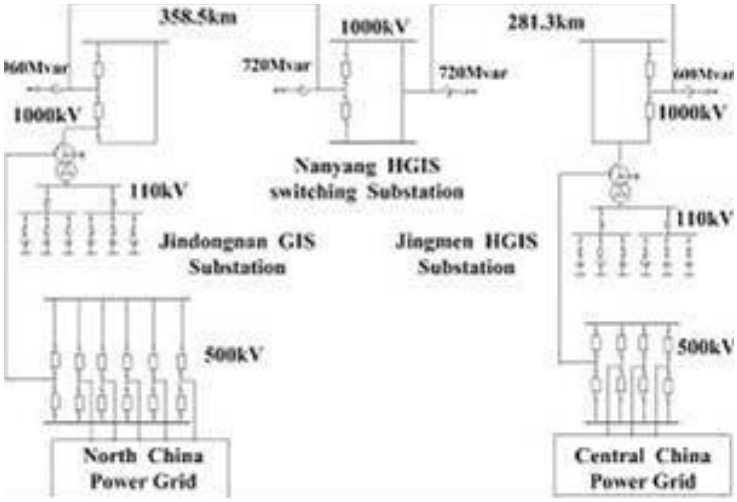

Figure 8.5.1 Main connection of 1000kV UHV AC pilot project

8.5.2 Research on commissioning tests

UHV AC transmission projects have distinctive features such as ultra high voltage insulation, long electricity transmission distance and huge electrical capacity meaning that higher equipment performance and reliability are required. Various commissioning tests have been carried out before the UHV project was put into commercial operation. For example, voltage-raising experiments were performed to confirm the insulation performance of UHV equipment and power control experiments were done to verify the effectiveness of the power control system that can limit the power fluctuations caused by 550 kV lines. An artificial grounding fault experiment was also performed to check the validity of the relay protection systems. Among the various experience obtained during the Chinese UHV commissioning tests, some experiments related to switching equipment are described.

8.5.3 Equipment switching experiments

(a) Switching no-load transformer on 500 kV side

During 24 switching operations on transformers no significant voltage disturbance was observed. Table 8.5.1 shows typical measurements of inrush exciting current and overvoltage for both primary and secondary sides caused by transformer energisation. These results are

within a permissible range. Figure 8.5.2 shows typical waveforms measured at Jindongnan substation.

Table 8.5.1 Results of UHV transformer energisation

Substation	Maximum overvoltage		Maximum exciting current (A)
	550 kV	1100 kV	
Jindongnan	1.48 p.u.	1.54 p.u.	3426
Jingmen	1.26 p.u.	1.43 p.u.	4816

1 p.u.=898 kV for 1100 kV and 449 kV for 550 kV ratings

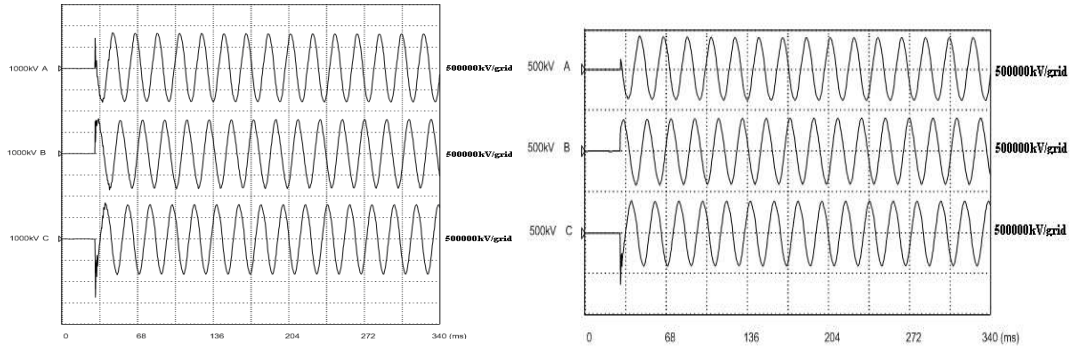

(a) Voltage measured at 1100 kV primary side, (b) Voltage measured at 550 kV secondary side

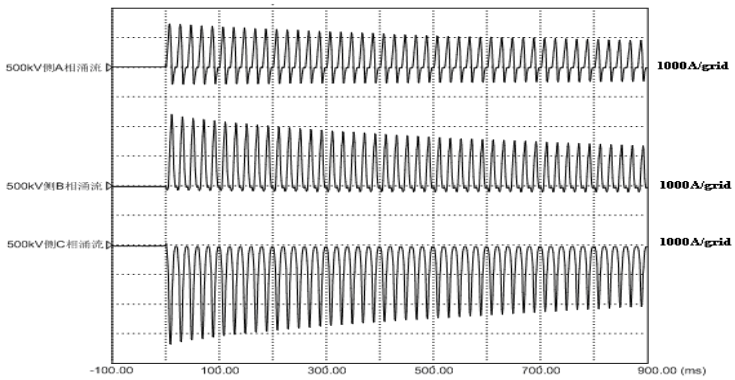

(c) Inrush current measured at 550kV secondary side

Figures 8.5.2 Typical measurement of switching overvoltage and inrush current

Figures 8.5.3 and 8.5.4 show typical results when the reactors and capacitors were energized and de-energised. The maximum switching overvoltage was 166 kV in case of 110 kV reactor energisations at Jindongnan and Jingmen substations. The overvoltage was 171 kV in case of 110 kV capacitor energisations at Jindongnan and Jingmen substations. These results are lower than the standard insulation levels.

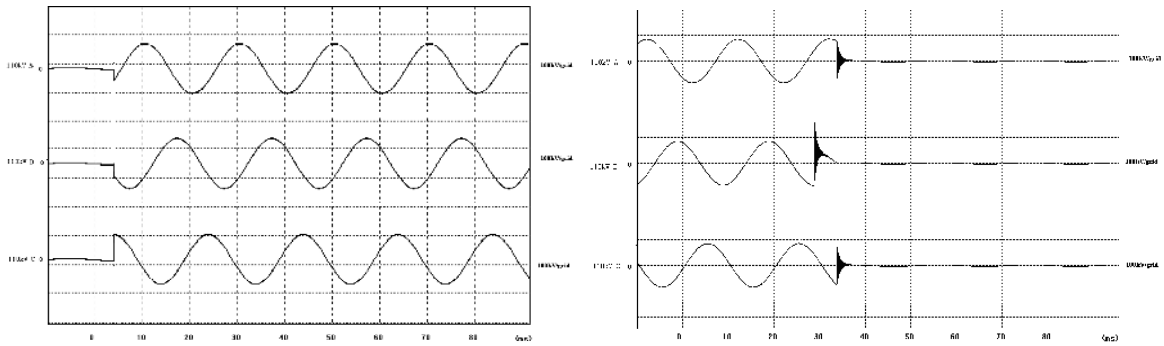

Figure 8.5.3 Typical waveforms in case of 110 kV reactors closing and opening

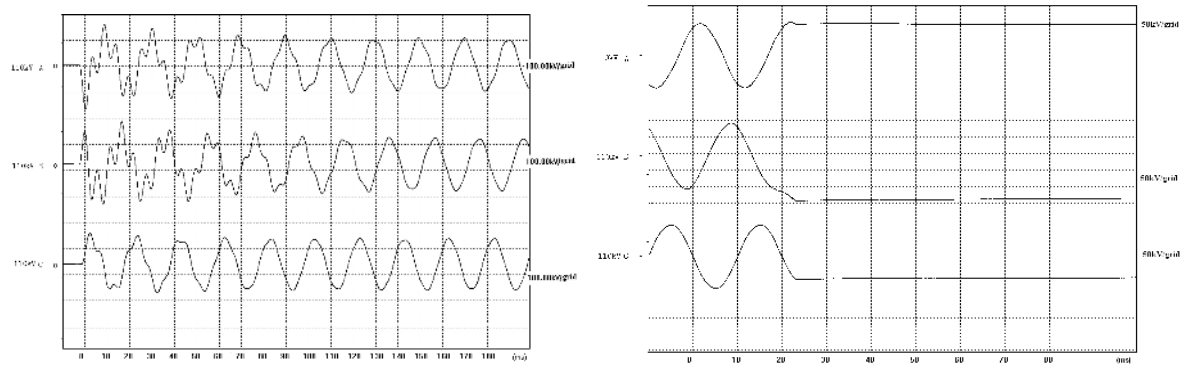

Figure 8.5.4 Typical waveforms in case of 110 kV capacitors closing and opening

(b) Switch no-load transmission line switching

The largest phase-to-ground overvoltage measured is 1.25 p.u. on the busbar side and 1.26 p.u. on the line side, respectively. Both results are lower than the specified insulation level. Figure 8.5.5 shows typical voltage waveforms.

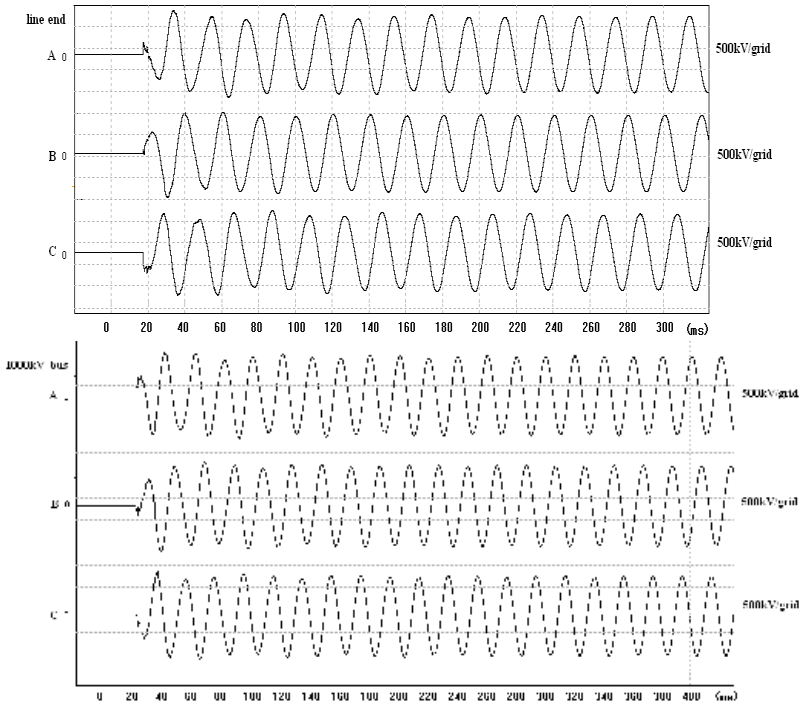

Figure 8.5.5 Typical waveforms in case of Nanyang-Jingmen line energisation at Nanyang station

(c) Artificial single-phase grounding fault experiment

UHV AC power system employs the single-phase re-closing scheme in order to ensure reliable and stable transmission. The success of single-phase re-closing depends on how quickly the secondary arc is extinguished on the UHV line after an occurrence of a ground fault. Based on calculations and experimental demonstrations, SGCC decide to apply two full transpositions to UHV lines with high-voltage four legged shunt reactor with neutral point grounded through a small reactor. These measures can reduce secondary arc extinction time and recovery voltage. Artificial single-phase groundings tests were conducted to verify the effectiveness of single-phase re-closing at Jindongnan-Nanyang and Nanyang-Jingmen transmission lines. The secondary arc extinction time was 118 ms on Jindongnan-Nanyang line and 42 ms on Nanyang-Jingmen line. No re-ignition is observed after secondary arc

extinguishing. Four legged shunt reactor with the neutral reactor can effectively extinguish the secondary arc. The pilot project's re-closing time is chosen between 0.7 to 1 s.

8.5.4 Conclusions

The successful construction of UHV AC pilot project in China demonstrates major technical breakthrough on UHV AC key technology and equipment. The project has great significance in ensuring the reliability of Chinese electric power supply and also promoting the researches and applications of UHV transmission technology in the world.

(1) In the voltage-raising experiments, all equipment was demonstrated to withstand the UHV dielectric requirements.

(2) During the experiments, UHV transformers, circuit breakers, UHV transmission lines, shunt reactors and low-voltage compensation devices were demonstrated to withstand the switching impulse tests.

(3) The validity of the relay protection systems was confirmed by artificial grounding fault experiments

(4) Electromagnetic environment tests were confirmed to meet the requirements of the Chinese State Environmental Protection Agency.

References

[1] IEC 62271-203, High-voltage switchgear and controlgear – Part 203: Gas-insulated metal-enclosed switchgear for rated voltages above 52 kV, edition 1.0, 2003-11

[2] Zaima, E.; Neumann, C.: “Insulation Coordination for UHV AC Systems based on Surge Arrester Application (CIGRE C4.306)”; The second IEC – CIGRÉ International Symposium on International Standards for UHV Transmission, 29-30 January 2009, New Delhi, India, proceedings pp. 108-118

[3] Cigré JWG 33/23.12: “Insulation Co-Ordination of GIS: Return of Experience, Onsite Tests and Diagnostic Techniques”, ELECTRA, No. 176, 1998

[4] Cigré TB WG D1.33.05 : “HV Test and PD Measuring Technique on Site”, to be published in 2009

[5] Riechert, U.; Đurđić, A.; Kudoke, M.; Stanek, M., “Monitoring and Diagnostics of Gas-Insulated Switchgear – Development Trends and Range of Applications”, ETG Fachtagung Diagnostik elektrischer Betriebsmittel 2006, 19.-20. September 2006, Kassel, 2006, ETG-Fachbericht 104, 2006, S. 161-166, VDE VERLAG GMBH, Berlin und Offenbach, ISBN 978-3-8007-2977-7

[6] CIGRE TF 15/33.03.05: “PD detection system for GIS: Sensitivity verification for the UHF method and the acoustic method”, ELECTRA, No. 183 (1999)

[7] Neuhold, S.; Heizmann, Th.; Bräunlich, R.; Koechli; D.; Riechert, U.; Dehne, Ch., “Experiences with UHF PD detection in GIS using external capacitive sensors on windows and disk-insulators”, 15th Int. Symposium on High Voltage Engineering, (ISH`2007), August 27-31, 2007, Ljubljana, Slovenia, paper T7-480

[8] CIGRE TB 297: “Practical aspects of the Detection and Localization of PD in Power Cables”, 2006

[9] Hoek, St.; Bornowski, M.; Tenbohlen, St.; Strehl, Th.; Riechert, U., “Partial Discharge Detection and Localisation in Gas-Insulated Switchgears”, Stuttgarter Hochspannungs-symposium 2008, 05.-06. März 2008, Stuttgart, 2008, Tagungsband, S. 211-218, haka print und medien GmbH, ISBN 978-3-00-024098-0

[10] Riechert, U.; Krüsi, U.; Holaus, W.; Sologuren, D.: “Gasisolierte Schaltanlagen für 1100 kV – Herausforderungen an Entwicklung und Prüfung”; (in German) Stuttgarter Hochspannungssymposium 2008, 05.-06. März 2008, Stuttgart, 2008, Tagungsband, S. 219-234, haka print und medien GmbH, ISBN 978-3-00-024098-0

[11] K. Park, et-al., “Measurement of ultra-high frequency (UHF) partial discharge sensor sensitivity and partial-discharge (PD) signal losses in the 800 kV gas-insulated substation (GIS) ”, In JJ Smit (Ed.), ISH 2003 Proceedings of the 13th international symposium on high voltage engineering (pp. 1-4). Rotterdam: Millpress. 2003

[12] S. Goo, et-al., “Sensitivity Determination Method of On-line UHF Partial Discharge Monitoring System for Gas Insulated Switchgear”, Condition Monitoring and Diagnosis, 2006, CMD 2006, International Conference on condition monitoring, 2006

[13] Y.Yamagata et. al., “Field test of 1000kV gas insulated switchgear,” CIGRE 2000 Paris Session SC13-209

[14] Y. Yamagata, et. Al., “Development and Field Test of 1000kV 3000MVA Transformer” CIGRE Paris Session 1998, SC12-303

[15] Y. Yamagata et. al., ”Very Fast Transients in 1000kV Gas Insulated Switchgear,” IEEE Transmission and Distribution Conf., 1998

[16] Y. Yamagata et. al., ”Suppression of VFT in 1100kV GIS by Adopting Resistor – fitted disconnector,” IEEE Tr. On PWRD vol.11, No.2 April 1996

[17] Egawa et al. , “Field Verification Test of 1000kV Substation Equipment”, Beijing Electric Power Conf. on Transmission and Distribution 1997

[18] T. Kawamura, et .al., “Development and long term tests for UHV, 3000MVA Transformer in Japan” IEC/CIGRE UHV Symposium Beijing 2007, Session 2-6-5

[19] Y. Yamagata, “Verification of the reliability of UHV MOSA”, prepared contribution A3, PS2, Q2.3 Yamagata, CIGRE Conference 2008

[20] Y. Yamagata, et. Al., “Utility’s experience on UHV substation equipment in Japan”, Beijing 2009 International Conference on UHV Transmission Technology, UHV09-FP049

9 Conclusions

Following publication of the first Technical Brochure by WG A3.22 (Technical Requirements for Substation Equipment exceeding 800 kV AC: Technical Brochure 362) it was clear that a number of technical topics are particularly challenging in the UHV range and that, in many cases, simple extrapolation of assumptions from lower voltages is not appropriate. Several distinctive phenomena have been identified including a prominent Ferranti effect, large DC time constant in the fault currents, severe TRVs and slow front overvoltages, possible risk of prolonged secondary arc extinction and a lower first-pole-to-clear factor.

The international experts have continued further investigations on these specific topics and have summarized the recommendations from the deeper studies in this second Technical Brochure. The aim of the second Technical Brochure is to collect and provide available background information for the international specifications of UHV equipment. The main results from investigations of several topics are summarized as follows;

Insulation Coordination

UHV technology is characterized by a need to minimise the sizes, weights, costs and environmental impacts of the OH-lines and substations and hence to develop projects which are feasible from an economic, societal and technical point of view. The UHV voltages presently standardized by IEC are some 50% higher than those for system voltages of the 800 kV class, however since insulation strength per metre decreases with the length of the air gap (particularly for switching impulses under wet conditions) simple extrapolation of the dielectric requirements would lead to disproportionately large structures. By means of the application of a number of new technologies and new analysis techniques, utilities are able to reduce the dielectric requirements to values that lead to much smaller structures. This results in insulation levels that are not far from the levels applied at the 800 kV class. In Japan the towers of the UHV OH-lines are only 77% of the size that would be necessary if insulation levels would have been extrapolated directly from the lower voltage classes.

Technologies used to reduce the insulation levels include “high performance” surge arresters that show a steeper curvature than conventional arresters and therefore a lower ratio between LIPL/SIPL and COV (Continuous Operating Voltage). In addition by applying multi-column arresters and/or a number of arresters in parallel, the ratio can be further decreased.

Switchable shunt reactors, fast protection schemes, single-phase auto-re-closing (SPAR), three-phase auto-re-closing (TPAR) and 4-legged shunt reactors are applied to achieve stable power supply when a fault occurs on the lines. Closing resistors are used to control slow front overvoltage (SFO) due to closing and re-closing of OH-lines. With respect to SFO generated in the healthy lines at the source side of the CB when clearing a fault, it depends on the fault conditions and tends to be larger in multi-phase line faults to ground such as 2LG, 3LG. Although the probability of the occurrence of these faults is comparatively low in the UHV systems, opening resistors are used to reduce the opening SFO for the purpose of avoiding successive breakdowns that may affect the availability of the whole system.

In future, SFO reduction might be possible by the application of transmission line arresters (TLA), and/or controlled switching. Shielding of OH-lines, improved earth return conditions and other countermeasures against back-flashover lead to a better lightning withstand performance. When necessary, damping resistors in GIS disconnectors, will reduce the amplitude of VFTO-phenomena, that otherwise may exceed the LIWV of the switchgear.

By advanced calculation and simulation techniques utilities are able to get an overview of many potentially difficult situations and select combinations of events and conditions that

have to be considered, or not, or with reduced margins. By such a systematic approach transparency is offered with respect to the utility's risk policy.

Transient Recovery Voltages (TRV)

One of the most important findings for UHV networks is that the surge impedance of the OH-lines is far less than 450 Ω; the value presently specified in the IEC Standard 62271-100. The surge impedance plays a role in the first, steep part of the TRV for terminal faults, short-line faults and out-of-phase conditions. Due to the application of heavy multi-conductor bundles, that will not fully contract before current interruption under short-circuit conditions, the surge impedance of UHV OH-lines is close to 300 Ω, for the first as well as the last clearing pole. The transient phenomena are very fast, so that surge impedances for frequencies in the kHz range are of interest and the recommended value for the surge impedance of UHV OH-lines is 330 Ω. By means of the value of 330 Ω and information available on the minimum number of OH-lines and equipment in an UHV substation, recommendations for the parameters that define the first part of the TRV envelope have been given such as to keep RRRV, u_1 (in p.u.), td and t_{dL} for UHV identical to the values as specified for the test duties T100, T60, T30, T10 and SLF at lower rated voltages.

Differences in the parameters to define the TRV envelope occur around the peak value and the time to peak which are influenced by the low damping of the travelling waves (due to the heavy sub-conductor bundles and low number of refractions), by the physical dimensions of the UHV network and by the large contribution of power transformers to the short-circuit currents. These aspects lead respectively to a higher amplitude factor k_{af}, a lower ratio between t_2 and t_1 (corresponding to the second and first knee-point in the TRV envelope) and a lower first-pole-to-clear factor k_{pp}.

From simulations it is clear that MOSAs have a reducing impact on the peak values of the TRV. By means of the equivalent surge impedance seen by the circuit-breaker's clearing pole and the number of MOSAs connected at the source side of the circuit-breaker (i.e. present at the substation) the intersection point with the surge arrester characteristic(s) can be determined, giving the clipping level. In case of UHV, more MOSAs are applied than the number of OH-line circuits and the surge arrester characteristic becomes flatter. Therefore the intersection point will anyway be lower than SIPL at 2 kA.

In case of breaker terminal faults, to be at the safe side, SIPL could be taken as the clipping level for TRV peak values, but the problem is that SIPLs are not standardized internationally and that they differ from country to country and even between utilities. The effect of all these considerations is a recommendation to adapt the TRV parameters as given in Table 9.1. Note that t_1 and t_3 are directly influenced by the reduced k_{pp}.

Table 9.1 UHV TRV requirements in relation to 800 kV requirements

UHV	RRRV	k_{pp}	k_{af}	t_2	t_3
T100	2	1.3 -> 1.2	1.4 -> 1.5	$4*t_1$ -> $3*t_{1\circ}$	
T60	3	1.3 -> 1.2	1.5	$6*t_1$ -> $4.5*t_{1\circ}$	
T30	5	1.3 -> 1.2	1.54		t_3 -> $t_{3\circ}$
T10	7	1.3 -> 1.2	1.76		t_3 -> $t_{3\circ}$
TLF	(°)	1.5 -> 1.2	0.9*1.7		(°)

$t_{1\circ}$ and $t_{3\circ}$ are based on k_{pp}=1.2, (°)= $6 \times \sqrt{U_r} / I^{0.21}$

The given recommendations cover long line faults as well as transformer limited faults (TLF). In the latter case the rate of rise (steepness) of the TRV (RRRV) and the time to peak (t_3) are determined by the transformer impedance and its equivalent surge capacitance, which is recommended to be specified as a fixed value of 9 nF.

Although most UHV substations are foreseen to be erected as a GIS substation or a mixed technology substation, WG A3.22 paid also attention to AIS substations, where the very initial part of the TRV (ITRV) is influenced by travelling waves inside the substation itself. Such ITRV conditions at 100% of the rated short-circuit current may be regarded as covered by the short-line fault test duty at 90% of the rated short-circuit current, when no time delay is applied at the line side. Such a conclusion applies for terminal faults, as the busbar surge impedance is 300 Ω or less, while the line surge impedance is specified to be 330 Ω. Other faults, not covered by the IEC Standard, will show travelling waves at both sides of the circuit-breaker and, thus, higher values of the ITRV, at least up to 0.3 to 0.4 μs.

With respect to capacitive current switching conditions, especially unloaded line switching, the studies reveal that the voltage factors to define the peak value of the TRV can be kept similar to those for lower rated voltages (i.e. 1.2 under normal conditions and 1.4 under earth fault conditions). Though the initial part shows to be more severe due to the Ferranti-effect, thus leading possibly result in larger arcing times and less dielectric stress to the circuit-breaker.

Opening and closing resistors

Opening and/or closing resistors may be applied to a circuit breaker in order to reduce switching overvoltages. Examples of the effects and the specification of opening resistors are elaborated. However, no specific recommendations for the resistor value and its thermal capacity can be given, so that standardization, for the moment, is out of question. The effects of opening resistors on terminal faults, long line faults, short-line faults, out-of-phase switching and capacitive switching are addressed.

In the Technical Brochure attention is paid to type test methods for UHV circuit-breakers, equipped with opening resistors. Closing resistors are well known and widely applied, so that not much text is devoted to closing resistors.

Disconnector and earthing switches

The ratings for disconnectors and earthing switches applied in UHV systems show to be higher than those applied at lower voltages. The specified currents and related voltages for the bus-transfer duty and bus-charging current switching duty are relatively high. Bus-transfer currents have to be defined in dependence of the actual current ratings, the type of substation and the maximum loop length. A bus transfer voltage of 80 V belongs to 1600 A and of 300 V to 8000 A, while for AIS and MTS a voltage of 400 V belongs to 1600 A as well as 4000 A.

In Annex C of IEC 62271-102, electromagnetic and electrostatic induced currents and voltages are standardized for 550 kV and 800 kV earthing switches, which are designated to be used in circuits with relatively long lines or a high coupling to an adjacent energized circuit (class B earthing switches). As WG A3.22 has not yet enough information on induced voltages and currents on UHV OH-lines, any conclusion is too premature.

A special topic is the occurrence of VFTO (very fast transient overvoltages) due to the charging and discharging of busbar sections by disconnectors in GIS. These switching operations cause a large number of restrikes and prestrikes, respectively, with high frequency responses by the travelling waves in the GIS, up to tens of MHz. Depending on the trapped charge, the high frequency voltages may reach amplitudes that could endanger the insulation

of the GIS equipments as well as directly connected equipment, such as transformers and shunt reactors. The statistical distribution of the trapped charges shows that VFTO is less severe for the slow acting disconnectors than that for the fast acting disconnectors. This phenomenon is a larger problem at UHV than at 800 kV. In the case of necessity, a counter measure is the application of a pre-insertion resistor to the disconnectors.

Secondary arc extinction and High Speed Grounding Switches (HSGS)

Dedicated switchgear is used to ensure secondary arc extinction. When SPAR is used, most utilities apply 4-legged shunt reactors to limit the secondary arc current, so that it will extinguish within a reasonable short time (mostly within 1 second). Some utilities apply HSGS (High Speed Grounding Switches) to by-pass the secondary arc during a short time (typically 0.5 s) in order to extinguish it. Such solutions are used for UHV, 800 kV and lower voltages. These options depend on line length, whether double circuit OH lines are utilized, whether the lines are transposed, on the dynamic stability requirements and on the combination of line faults to be covered.

Standardization of the HSGS is now ongoing within the IEC where the term HSES (high speed earthing switch) is used. Other switchgear for the special switching scheme of a healthy phase shunt reactor is yet to be addressed.

Metal-Oxide Surge Arresters (MOSA)

A very active use of “high performance” surge arresters to limit overvoltages to the lowest possible levels is seen to be one of the most important conditions for the insulation coordination in UHV systems. However, the requirements placed upon the arresters with respect to protection levels, energy and voltage withstand capabilities are demanding for the industry. This in turn shows the importance to develop the standards such that they also consider the arresters for UHV. To some extent it is only to extend the classification system to cover the higher voltage levels but some features are more specific for UHV arresters and need special attention. Items, which are not considered to be fully covered in existing standards are insulation withstand test, long duration current impulse withstand tests, switching surge operating duty test and energy withstand test for multi-column arresters, short-circuit and mechanical tests for the very tall structures, voltage grading check methods taking into consideration the internal and external grading components and better pollution tests suitable for long polymeric housings for UHV MOSA.

In close co-operation with IEC, CIGRÉ WG A3.25 will conduct further investigations to support the specification of MOSA for UHV applications.

Instrument transformers

Conventional instrument transformers for UHV-AIS have large drawbacks, mainly from the point of view of size and weight. Non-conventional instrument transformers (NCIT) are more likely to be applied, for AIS as well as GIS and MTS substations. Some examples are given in the Technical Brochure. Short overviews give the physics and merits of several solutions. The chapter on NCIT is kept short as other WGs within SC A3 are dealing with this topic, with a wider scope than UHV applications alone.